MITOCHONDRIA AT THE CROSSROADS OF IMMUNITY AND INFLAMMATORY TISSUE DAMAGE

EDITED BY: Edecio Cunha-Neto, Christophe Chevillard and
Pedro Manoel Mendes Moraes Vieira
PUBLISHED IN: Frontiers in Immunology

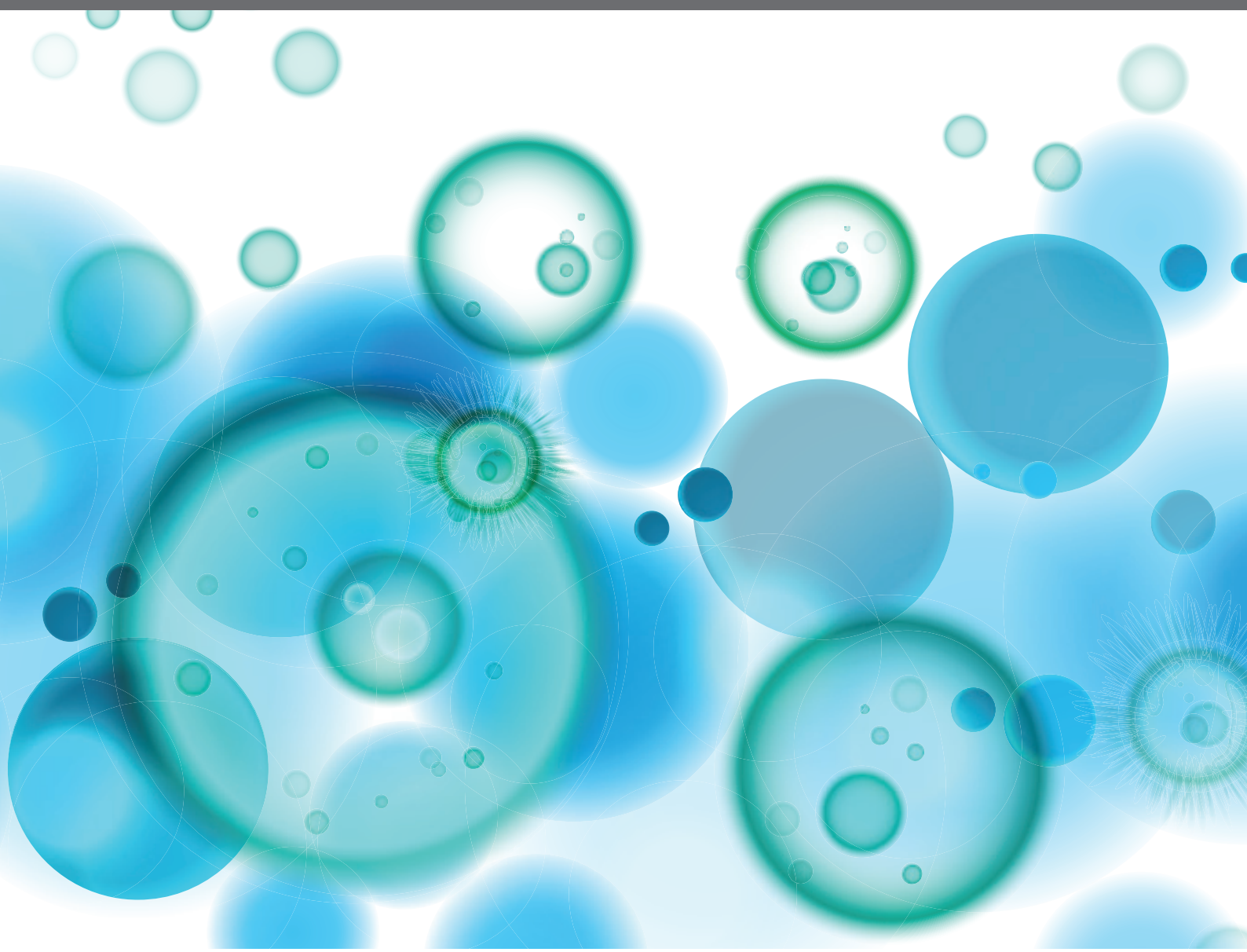

frontiers Research Topics

frontiers

ISSN 1664-8714
ISBN 978-2-88974-093-2
DOI 10.3389/978-2-88974-093-2

About Frontiers

Frontiers is more than just an open-access publisher of scholarly articles: it is a pioneering approach to the world of academia, radically improving the way scholarly research is managed. The grand vision of Frontiers is a world where all people have an equal opportunity to seek, share and generate knowledge. Frontiers provides immediate and permanent online open access to all its publications, but this alone is not enough to realize our grand goals.

Frontiers Journal Series

The Frontiers Journal Series is a multi-tier and interdisciplinary set of open-access, online journals, promising a paradigm shift from the current review, selection and dissemination processes in academic publishing. All Frontiers journals are driven by researchers for researchers; therefore, they constitute a service to the scholarly community. At the same time, the Frontiers Journal Series operates on a revolutionary invention, the tiered publishing system, initially addressing specific communities of scholars, and gradually climbing up to broader public understanding, thus serving the interests of the lay society, too.

Dedication to Quality

Each Frontiers article is a landmark of the highest quality, thanks to genuinely collaborative interactions between authors and review editors, who include some of the world's best academicians. Research must be certified by peers before entering a stream of knowledge that may eventually reach the public - and shape society; therefore, Frontiers only applies the most rigorous and unbiased reviews.
Frontiers revolutionizes research publishing by freely delivering the most outstanding research, evaluated with no bias from both the academic and social point of view. By applying the most advanced information technologies, Frontiers is catapulting scholarly publishing into a new generation.

What are Frontiers Research Topics?

Frontiers Research Topics are very popular trademarks of the Frontiers Journals Series: they are collections of at least ten articles, all centered on a particular subject. With their unique mix of varied contributions from Original Research to Review Articles, Frontiers Research Topics unify the most influential researchers, the latest key findings and historical advances in a hot research area! Find out more on how to host your own Frontiers Research Topic or contribute to one as an author by contacting the Frontiers Editorial Office: frontiersin.org/about/contact

MITOCHONDRIA AT THE CROSSROADS OF IMMUNITY AND INFLAMMATORY TISSUE DAMAGE

Topic Editors:
Edecio Cunha-Neto, University of São Paulo, Brazil
Christophe Chevillard, TAGC Theories and Approaches of Genomic Complexity, France
Pedro Manoel Mendes Moraes Vieira, State University of Campinass, Brazil

Citation: Cunha-Neto, E., Chevillard, C., Vieira, P. M. M. M., eds. (2022). Mitochondria at the Crossroads of Immunity and Inflammatory Tissue Damage. Lausanne: Frontiers Media SA. doi: 10.3389/978-2-88974-093-2

Table of Contents

frontiers in Immunology

EDITORIAL
published: 30 November 2021
doi: 10.3389/fimmu.2021.810787

Editorial: Mitochondria at the Crossroads of Immunity and Inflammatory Tissue Damage

João Paulo Silva Nunes[1,2,3,4], *Pedro M. Moraes-Vieira*[5*], *Christophe Chevillard*[4*] *and Edecio Cunha-Neto*[1,2,3*]

[1] Laboratory of Immunology, Heart Institute (InCor), School of Medicine, University of São Paulo, São Paulo, Brazil, [2] Division of Clinical Immunology and Allergy, School of Medicine, University of São Paulo, São Paulo, Brazil, [3] Institute for Investigation in Immunology (iii), Instituto Nacional de Ciência e Tecnologia (INCT), São Paulo, Brazil, [4] INSERM, UMR_1090, Aix Marseille Université, TAGC Theories and Approaches of Genomic Complexity, Institut MarMaRa, Marseille, France, [5] Department of Genetics, Evolution, Microbiology and Immunology, Institute of Biology, Experimental Medicine Research Cluster (EMRC), and Obesity and Comorbidities Research Center (OCRC), University of Campinas, Campinas, Brazil

Keywords: tissue damage, mitochondria, immunity, inflammation, Chagas

Editorial on the Research Topic

Mitochondria at the Crossroads of Immunity and Inflammatory Tissue Damage

OPEN ACCESS

Edited and reviewed by:
Francesca Granucci,
University of Milano-Bicocca, Italy

***Correspondence:**
Pedro M. Moraes-Vieira
pmvieira@unicamp.br
Christophe Chevillard
christophe.chevillard@univ-amu.fr
Edecio Cunha-Neto
edecunha@gmail.com

Specialty section:
This article was submitted to Molecular Innate Immunity, a section of the journal Frontiers in Immunology

Received: *07 November 2021*
Accepted: *15 November 2021*
Published: *30 November 2021*

Citation:
Nunes JPS, Moraes-Vieira PM, Chevillard C and Cunha-Neto E (2021) Editorial: Mitochondria at the Crossroads of Immunity and Inflammatory Tissue Damage. Front. Immunol. 12:810787. doi: 10.3389/fimmu.2021.810787

Once activated, immune cells significantly increase their energy metabolism demand through the central metabolic pathways of glycolysis and respiration. Different immune cell subsets depend on distinct energy metabolism pathways. In addition to energy production, upon inflammatory stimuli, immune cells increase the biosynthesis of membranes and organelles (for phagocytosis and motility), post-translational and epigenetic modifications (for example, supply of acetate and lactate for histone modification), free radical production, and the increased production of effector cytokines and chemokines. Mitochondria are the central organelles of metabolic reactions and regulation, and the main source of ATP and pathways for biosynthesis of macromolecules. In addition to being a central metabolism hub, they play a critical part in regulated cell death, reactive oxygen species signaling, calcium homeostasis and cell differentiation potential. Systemic, environmental, nutritional, microbiome-related and tissue-derived cues shape mitochondria through fission/fusion and mitochondrial quality control, which orchestrates how mitochondria will ultimately function and their energetic and metabolic coupling. A dysfunction in any of these processes can trigger severe disease, including chronic inflammation and neurodegeneration. Thus, it is relevant to understand how mitochondria regulation is connected to adaptive metabolism and functional output in immune and tissue-resident stromal cells in a cytokine-rich inflammatory milieu, both in physiological and pathological states. In this Research Topic, authors presented new insights of the involvement between mitochondria, oxidative stress, immune response, neurological and skeletal joint disease and regulation of circadian clock. Also, novel molecular mechanisms linking mitochondria to disease, as well as mitochondria-targeted therapies are covered by the authors.

Paul et al. assessed whether the neutrophil-to-lymphocyte ratio (NRL) is a good biomarker to assess the immune status of astronauts. They found that astronauts had higher granulocyte-to-lymphocyte (GLR) and *in vivo* and *in vitro* experiments performed in microgravity simulation revealed that microgravity increased NRL in rodents, as well imbalanced the redox processes and elevated the myeloperoxidase expression. They showed that antioxidant therapy (N-acetyl cysteine)

ameliorated these effects. Also, mCAT (mitochondrial catalase) transgenic mice had reduced oxidative stress response compared to wild type. To authors, limiting ROS-drive inflammation is thus important to keep homeostatic immunity during long-term missions in space.

Wolff et al. explored the link between the circadian clock, cellular metabolism and the immune metabolic function of microglia. They reported that stimulation of microglia with SR9011, agonist of nuclear receptor Rev-erbα (involved in molecular clock and cell metabolism), disturbed the expression of metabolic and clock-related genes, decreased phagocytic activity and impaired mitochondrial respiration and ATP production. Their study provides new insights in intrinsic clock and immunometabolism of microglia. In line with this, Wang et al. also investigated the relationship between circadian clock and microglial immunometabolism. Their data revealed dysregulated expression of inflammatory and metabolic associated genes in the microglia cells of Bmal1$^{-/-}$ mice. Bmal1 is the core transcript factor that regulates the circadian clock. Wang et al.'s data suggest that Bmal1 is a key regulator of microglial immune response and cellular metabolism.

The review of Fairley et al. summarized recent data regarding mitochondrial regulation of the microglial immunometabolism in Alzheimer's disease (AD). They described the coordination of mitochondria in the microglial innate immunity along with nutritional, genetic and aging factors of Alzheimer's disease. Also, they reviewed how microglial metabolism reprogramming with exercise, ketone body, mTOR and TSPO targeted-therapeutics can ameliorate AD. de Oliveira et al. discussed the importance of mitochondrial dynamics, such as mitophagy, ER-mitochondria communication and production of reactive oxygen species during neuroinflammation. They described the correlation of these mitochondrial dynamics with amelioration or worsening of central nervous system disease such as Parkinson's and Alzheimer's disease.

Wu et al. investigated the role of mitochondria, NLRP3 inflammasome and mitophagy in chronic intermittent hypoxia (CHI)-elicited neuroinflammation. Their *in vitro* and *in vivo* data revealed a damaging relationship of NLRP3, Parkin-dependent mitophagy and hypoxia. Authors suggest that NRLP3 knockout or pharmacological blockade can be a therapeutic strategy for CHI-elicited neuroinflammation, such as obstructive sleep apnea. Bu et al. investigated if dysfunction of mitophagy is associated with innate antiviral immunity. They described that Parkin is a negative regulator of innate immunity by facilitating degradation of RIG-I and MDA5 through K48-linked polyubiquitination of RIG-I and MDA5. Parkin is pointed by the authors as a potential therapeutic target for the control of viral infection.

In line with viral infection, Seo et al. indicated that the post-translational modification O-GlcNAcylation of the mitochondrial antiviral signaling proteins (MAVS) is important to regulate the host defense against RNA viruses. They performed experiments that revealed a heavily enriched region of O-GlcNAcylated serine in MAVS and that this modification disrupted MAVS aggregation, thus preventing MAVS-mediated activation and RLR signaling, suppressing IRF3 activation and consequently the production of type I interferon, such as IFN-β.

Teixeira et al. performed proteomic studies on myocardium tissue of patients with Chagas disease cardiomyopathy (CCC). They identified a higher frequency of dysregulated proteins involved in mitochondrial energy metabolism, cardiac remodeling and oxidative stress in CCC patients compared to patients with ischemic (IC) and idiopathic dilated cardiomyopathy (IDC). This dysregulation affected important pathways for heart function, such as fatty acid oxidation and transmembrane potential of mitochondria. Nunes et al. showed that *in vitro* stimulation of cardiomyocytes with IFN-γ and TNF-α caused increased oxidative and nitrosative stress, decreased ATP production and dependency of fatty acid oxidation, recapitulating the pathologic phenotype observed in the myocardium tissue of CCC patients. In addition, authors showed that agonists of the mitochondrial protective molecules AMPK, SIRT1 and NRF2 can ameliorate mitochondrial function of cytokine-treated cardiomyocytes. These results are relevant for several cardiac conditions where IFN-γ plays a role, like myocardial aging, myocardial infarction and anthracycline cancer chemotherapy-associated cardiopathy.

Silwal et al. discussed the double-edged behavior of mitochondrial superoxide in host defense and inflammation during infection. They pointed out that despite controlled mtROS production being essential for an efficient immune response, uncontrolled production can lead to mitochondrial damage and disease. They described the host's mechanisms that can ameliorate mtROS generation and also how pathogens can modulate mtROS production for their own benefit. Choudhuri et al. reviewed how mitochondria health and dysfunction can influence macrophages immune response. They discussed, for example, how mitochondrial dynamics and energetics participate in the macrophage response to pathogens, the metabolic switch from oxidative phosphorylation to glycolysis, metabolic regulation and apoptosis. Like previous authors, they suggest that therapeutic strategies targeting mitochondria might be useful to control pathogenic effects of intracellular pathogens.

Yi et al. suggested that the key glycolysis enzyme Pyruvate kinase M2 (PKM2) can be a therapeutic target to treat sepsis and other inflammatory diseases. They showed that a PKM2 small-molecule agonist TEPP-46 can enhance macrophage endotoxin tolerance, increase tolerance to LPS, lethal endotoxemia and sepsis in mice. Also, TEPP-46 enhanced mitochondrial biogenesis through the key regulator PGC-1α.

Early et al. reviewed the crosstalk of mitochondria and skeletal joint diseases, such as rheumatoid arthritis and osteoarthritis. They described the central involvement of mitochondria in mechanical tissue damage, fluid-flow in bone and cartilage cells and hydrostatic pressure.

Finally, Chelombitko et al. reviewed the roles of mitochondria in the activation of mast cells through FcεRI (Fc epsilon RI receptor). They compiled data reporting that alterations in mitochondrial membrane potential, calcium influx and reactive oxygen species have a fundamental role in the FcεRI-dependent mast cells activation. Also, it is discussed that the PDH complex

and activation of the transcription factors STAT3 and MITF are direct modulators of the mitochondrial activity of mast cells.

In summary, the articles in this Research Topic provided an outlook at the intricacies of mitochondrial and metabolic involvement in key antimicrobial and inflammatory pathways and diseases and paved the way for mitochondrial processes as therapeutic targets in infectious and inflammatory diseases.

AUTHOR CONTRIBUTIONS

All authors listed have made a substantial, direct, and intellectual contribution to the work and approved it for publication.

FUNDING

This work was supported by the Institut National de la Santé et de la Recherche Médicale (INSERM); the Aix-Marseille University (grant number: AMIDEX "International_2018" MITOMUTCHAGAS); the French Agency for Research (Agence Nationale de la Recherche-ANR (grant numbers: "Br-Fr-Chagas", "landscardio"); the CNPq (Brazilian Council for Scientific and Technological Development); and the FAPESP (São Paulo State Research Funding Agency Brazil (grant numbers: 2013/50302-3, 2014/50890-5, 2015/15626-8, 2019/25973-8, 2019/19435-3); the National Institutes of Health/USA (grant numbers: 2 P50 AI098461-02 and 2U19AI098461-06). This work was founded by the Inserm Cross-Cutting Project GOLD. This project has received funding from the Excellence Initiative of Aix-Marseille University - A*Midex a French "Investissements d'Avenir programme"- Institute MarMaRa AMX-19-IET-007. JPSN was a recipient of a MarMaRa fellowship.

Conflict of Interest: The authors declare that the research was conducted in the absence of any commercial or financial relationships that could be construed as a potential conflict of interest.

Publisher's Note: All claims expressed in this article are solely those of the authors and do not necessarily represent those of their affiliated organizations, or those of the publisher, the editors and the reviewers. Any product that may be evaluated in this article, or claim that may be made by its manufacturer, is not guaranteed or endorsed by the publisher.

frontiers in Immunology

MINI REVIEW
published: 14 August 2020
doi: 10.3389/fimmu.2020.01649

Mitochondrial Reactive Oxygen Species: Double-Edged Weapon in Host Defense and Pathological Inflammation During Infection

Prashanta Silwal[1,2], *Jin Kyung Kim*[1,2], *Young Jae Kim*[1,2] *and Eun-Kyeong Jo*[1,2]*

[1] Department of Microbiology, Chungnam National University School of Medicine, Daejeon, South Korea, [2] Infection Control Convergence Research Center, Chungnam National University School of Medicine, Daejeon, South Korea

Mitochondria are inevitable sources for the generation of mitochondrial reactive oxygen species (mtROS) due to their fundamental roles in respiration. mtROS were reported to be bactericidal weapons with an innate effector function during infection. However, the controlled generation of mtROS is vital for the induction of efficient immune responses because excessive production of mtROS with mitochondrial damage leads to sustained inflammation, resulting in pathological outcomes such as sepsis. Here, we discuss the beneficial and detrimental roles of mtROS in the innate immune system during bacterial, viral, and fungal infections. Recent evidence suggests that several pathogens have evolved multiple strategies to modulate mtROS for their own benefit. We are just beginning to understand the mechanisms by which mtROS generation is regulated and how mtROS affect protective and pathological responses during infection. Several agents/small molecules that prevent the uncontrolled production of mtROS are known to be beneficial in the maintenance of tissue homeostasis during sepsis. mtROS-targeted approaches need to be incorporated into preventive and therapeutic strategies against a variety of infections.

Keywords: mitochondrial ROS, infection, inflammation, immunity, host defense

OPEN ACCESS

Edited by:
Pedro Manoel Mendes Moraes Vieira, Campinas State University, Brazil

Reviewed by:
Cristina Carvalho, University of Coimbra, Portugal
Cristiane Naffah De Souza, University of São Paulo, Brazil
Angela Castoldi, University of São Paulo, Brazil

***Correspondence:**
Eun-Kyeong Jo
hayoungj@cnu.ac.kr

Specialty section:
This article was submitted to Molecular Innate Immunity, a section of the journal Frontiers in Immunology

Received: *22 April 2020*
Accepted: *19 June 2020*
Published: *14 August 2020*

Citation:
Silwal P, Kim JK, Kim YJ and Jo E-K (2020) Mitochondrial Reactive Oxygen Species: Double-Edged Weapon in Host Defense and Pathological Inflammation During Infection. Front. Immunol. 11:1649. doi: 10.3389/fimmu.2020.01649

INTRODUCTION

Mitochondria are essential organelles for the generation of reactive oxygen species (ROS) through respiration and function as a crucial signaling platform for various biological responses, including metabolism, innate immunity, and inflammation (1). Innate immune cells such as macrophages and neutrophils produce and employ mitochondrial reactive oxygen species (mtROS) as direct antimicrobial agents in host defense to combat pathogens (2). Accumulating evidence has revealed more complex molecular functions of mtROS in the activation of nucleoside oligomerization domain-, leucine-rich repeat-, and pyrin domain-containing protein 3 (NLRP3) inflammasomes and the regulation of innate signaling pathways triggered by numerous pattern-recognition receptor engagement (3, 4). Indeed, mtROS are critically required for innate host defense as effectors through their toxic action against pathogens. However, uncontrolled regulation of mtROS may lead to chronic inflammation and pathologies during infection (5, 6).

In this review, we discuss recent advances in our understanding of the protective role of mtROS associated with host-defensive signaling pathways involved in actions against pathogens during infection. We further highlight how pathogens evade mtROS-dependent antimicrobial responses or enhance mtROS-mediated pathological inflammation. In addition, we review the detrimental functions of mtROS when they are produced in excess in damaged cells and tissues during infection. We also introduce the idea that several agents/approaches evolved to modulate mtROS in the maintenance of tissue homeostasis in the context of sepsis. An understanding of the collective actions of mtROS in innate immune functions represents a new frontier in the development of novel therapeutic strategies against acute and chronic infections.

Protective Functions of mtROS in the Activation of the Host Defense

mtROS in Innate Immune Signaling

A decade ago, strong evidence indicated that mtROS provide antimicrobial responses in the context of innate immunity. Numerous studies showed that the maximal bactericidal activity in innate immune cells depended on mtROS generation. Toll-like receptor (TLR; TLRs 1, 2, and 4) signaling triggers the recruitment of mitochondria to the phagosomes and augments mtROS generation to enhance macrophage bactericidal activity (7). Additional studies showed that the mammalian STE20-like protein kinase-1/2 (MST1/2) were required for ROS production through mitochondrial trafficking to the phagosomes, and that they promoted TLR-mediated assembly of the tumor necrosis factor receptor-associated factor 6 (TRAF6), an evolutionarily conserved signaling intermediate in Toll pathway (ECSIT) complex, thus enhancing antibacterial killing and inflammatory signaling in macrophages (7–9). Importantly, ECSIT plays a role in the assembly and activity of respiratory complex-I of the electron transport chain (ETC) to produce mtROS in macrophages after TLR4 stimulation (10). In neutrophils, mtROS mediates the functional responses such as oxidative burst, degranulation and apoptosis (11), as well as NETosis induced by Ca^{2+} ionophore where mitochondrial permeability transition pore (mPTP) is critically involved in mtROS production (12). These studies suggest the role for mtROS in the regulation of different aspects of innate immune responses in macrophages and neutrophils against pathogenic stimuli.

mtROS in Antibacterial and Antiparasitic Defense

Several other studies showed the role of mtROS as the antimicrobial components in the innate defense against bacterial infection. Early studies showed that Th1 cytokine interferon (IFN)-γ signaling activated transcriptional activation of the mitochondrial respiratory chain machinery through the nuclear receptor estrogen-related receptor α (ERRα; NR3B1), which is required for mtROS generation to promote clearance of *Listeria monocytogenes* (13). A more recent study revealed that ERRα is essentially required for antimicrobial host defense against *Mycobacterium tuberculosis* (Mtb) infection through autophagy activation, although whether mtROS was implicated in the activation of xenophagy, a selective autophagy-targeting pathogen (14), was not clarified (15). As mtROS play key roles in the maintenance of cellular homeostasis, such as autophagy (16, 17), additional studies are warranted to elucidate the roles of mtROS in the activation of xenophagy in the context of the innate immune defense. Although relatively uncharacterized in the function of mtROS in terms of antiparasitic defense, mtROS contributed to upregulating the intracellular clearance of *Leishmania donovani*, an intracellular parasite (18, 19).

Although there are some debates, the metabolic sensor 5' AMP-activated protein kinase (AMPK) inhibits the generation of mtROS, whereas hypoxia-inducible factor (HIF)-1α upregulates mtROS production. Mutual regulation between AMPK and HIF-1α is required to maintain mtROS at the optimal level, thereby promoting the innate defense against several pathogenic bacteria (20, 21). HIF-1α and the mammalian target of the rapamycin (mTOR) pathway are critical for driving an immunometabolic signaling toward glycolysis during infection (22, 23). The mTOR-mediated aerobic glycolysis in human monocytes ($CD14^{+}CD16^{-}$) results in the accumulation of ROS and inflammatory signaling to activate monocyte function (23). However, mTOR inhibition upregulates mtROS production and NLRP3 inflammasome activation to suppress the replication of *Trypanosoma cruzi* in macrophages (24). More investigation into the paradoxical function of mTOR signaling is required for a better understanding of its role in the coordination of immunometabolism and mtROS-related host defense. Metformin, a widely used antidiabetic drug, was beneficial in the clearance of *Legionella pneumophila* infection through AMPK signaling activation and mtROS generation (25). Metformin-mediated antibacterial effects were ameliorated by glutathione treatment, suggesting a protective role of mtROS in improving antibacterial immunity against *L. pneumophila* pneumonia (25). In addition, it should be noted that ERRα is regulated at the downstream of AMPK to enhance antimycobacterial immunity and plays a crucial role in the activation of autophagy (15). Therefore, a delicate control of immunometabolic shifting between aerobic glycolysis (HIF-1α/mTOR-mediated) and mitochondrial respiration (AMPK mediated) may affect the innate effector functions, at least partly through the regulation of mtROS generation.

Moreover, macrophage recognition of live bacteria led to a transient shift in the mitochondrial respiratory system and destabilization of the ETC complex I but increased the activity of complex II, which was essential for the antimicrobial response (26). During live bacterial sensing in macrophages, nicotinamide adenine dinucleotide phosphate (NADPH) oxidase-mediated ROS, in cooperation with mtROS, play essential roles in the early induction of ETC adaptations (26). In this regard, mtROS, which are derived from several respiratory complexes (complexes I, II, and III) (27, 28), may contribute to the different aspects of antimicrobial and inflammatory function, and further investigation of their specific roles depending on differential sources and cell types is warranted.

mtROS in Antiviral Signaling

Early studies highlighted the function of mtROS in the amplification of mitochondrial antiviral signaling (MAVS)

and RIG-I-like receptor (RLR)-mediated antiviral responses (29). During infection with influenza A virus (IAV), both mitochondrial and dual oxidase (Doux) 2-generated ROS were essential for the antiviral host defense in normal human nasal epithelial (NHNE) cells. Notably, the induction of the IFN-λ gene and protein expression, which was mediated through ROS, contributed to the suppression of IAV viral titers (30). Another study showed that mtROS generation was required for IAV-induced signal transducer and activator of transcription (STAT) phosphorylation and IFN-stimulated gene expression, which promoted antiviral responses in NHNE cells (31). Scavenging mtROS led to the attenuation of innate immune responses to IAV and increased viral titers in nasal epithelial cells (30, 31). These findings suggest that mtROS play a crucial role in the induction of antiviral immune defense against IAV infection.

A recent study identified tetrachlorodibenzo-p-dioxin (TCDD)-inducible poly(ADP ribose) polymerase (TIPARP), a zinc finger antiviral protein (ZAP), as a pattern-recognition receptor for the RNA of Sindbis virus (32), a positive-sense single-stranded RNA virus belonging to the genus Alphavirus in the family Togaviridae (33). TIPARP was found to protect mice against lethal Sindbis virus infection through promotion of antiviral responses. It was noted that TIPARP redistribution from the nucleus to the cytoplasm during infection is mediated through mtROS-dependent oxidization of the nuclear pore and mitochondrial damage (32). This cytoplasmic accumulation of TIPARP, which is triggered by mtROS, seems to favor the persistence of TIPARP localization in the cytosol to mediate antiviral response in the host cells (32). In addition to TIPARP, there are several zinc finger domain-containing protein family members that participate in the inhibition of viral replication, particularly in HIV-1 and flavivirus infections (34, 35). The role of mtROS in most zinc finger domain-containing family members should be characterized in a future study.

mtROS also cooperate with several innate effectors/pathways in macrophages and/or other immune cells during infection. mtROS participate in the activation of the NLRP3 inflammasome, which plays a crucial function in the innate immune defense against numerous pathogens (3, 4). Indeed, mtROS activation serves as an important second signal to trigger NLRP3 inflammasome activation, which leads not only to the host defense against diverse bacterial, viral, and fungal infections but also to pathophysiological responses when uncontrolled or dysregulated (3). Elucidating the potential mechanisms of the coordinated mtROS generation could help develop further knowledge on host defense through appropriate activation of NLRP3 inflammasome complex during infections by various pathogens.

Autophagy, an intracellular homeostatic process during stress conditions (14), contributes to regulating the production of mtROS during viral infection. Previous studies showed that mtROS generation, accompanied by dysfunctional mitochondria, was upregulated to promote RLR-mediated mitochondrial antiviral signaling protein (MAVS/IPS-1) signaling and resistance to vesicular stomatitis virus infection in ATG5-deficient primary mouse embryonic fibroblasts (MEF) cells and macrophages (29). During Sendai virus infection, mitochondrial COX5B, the ETS component of the cytochrome *c* oxidase complex subunit, can interact with MAVS and ATG5 and contributes to the balance in MAVS-mediated antiviral signaling (36). Mechanistically, MAVS activation results in the expression of COX5B, which, in turn, downregulates MAVS-mediated antiviral signaling through the inhibition of mtROS. These data suggest a link between the mitochondrial ETS system and MAVS-mediated antiviral signaling through the modulation of ROS (36). A recent study also showed that Parkin, a key player in mitophagy, plays an inhibitory role in antiviral immunity through controlling the mtROS-NLRP3 inflammasome during viral infection. Parkin deficiency amplifies antiviral inflammation by enhancing mtROS to activate the NLRP3 inflammasome, thereby enhancing viral clearance in macrophages and dendritic cells (37). Taken together, these studies highlight the role of mtROS in the balanced regulation of the autophagy–inflammasome axis, which is crucial for the innate host defense. The protective roles of mtROS in antimicrobial innate immune defense are summarized in **Figure 1A**.

Pathogens Modulate mtROS to Promote Pathogenesis and Virulence

Bacteria, Fungi, and Parasites Regulate Host mtROS for Their Own Benefits

Several studies showed that pathogens and their components are able to evade host immune system or augment pathological inflammation through modulation of mitochondrial oxidative stresses for their own benefits. A recent study showed that the outer membrane protein 34 (Omp34) of *Acinetobacter baumannii*, a Gram-negative opportunistic pathogen, triggers mtROS generation, leading to the hyper-activation of NLRP3 inflammasome and pyroptosis during infection (38). In addition, *Escherichia coli* O157:H7 can induce severe inflammation through damage of mitochondria and mtROS, which triggered NLRP3 inflammasome activation; this was ameliorated by quercetin *via* prevention of ROS and autophagy activation (39). Moreover, *Aspergillus* protease stimulation of lung epithelial cells (A549 cells) upregulated mRNAs of a variety of inflammatory cytokines and intercellular adhesion molecule (ICAM)-1 through mtROS (40), suggesting the role of mtROS as a therapeutic target for fungal inflammation.

In *Pseudomonas aeruginosa* infection, pyocyanin is an important virulence factor through which mtROS mediate cell apoptosis through the induction of mitochondrial acid sphingomyelinase in neutrophils (41). In addition, pyocyanin can trigger natural killer (NK) cell apoptosis through mitochondrial damage and intracellular calcium release (42). Although the exact role for mtROS was not described in this study, intracellular ROS, generated by the NADPH oxidase, was not involved in NK cell death (42). As mitochondrial damage results in the excessive mtROS production in numerous pathological conditions (43), future studies will clarify the role for mtROS in immune cell death during *P. aeruginosa* infection.

Early studies showed that the intracellular parasite *Leishmania donovani* targets and stabilizes host transcriptional factor SREBP2 to regulate macrophage cholesterol and inhibit

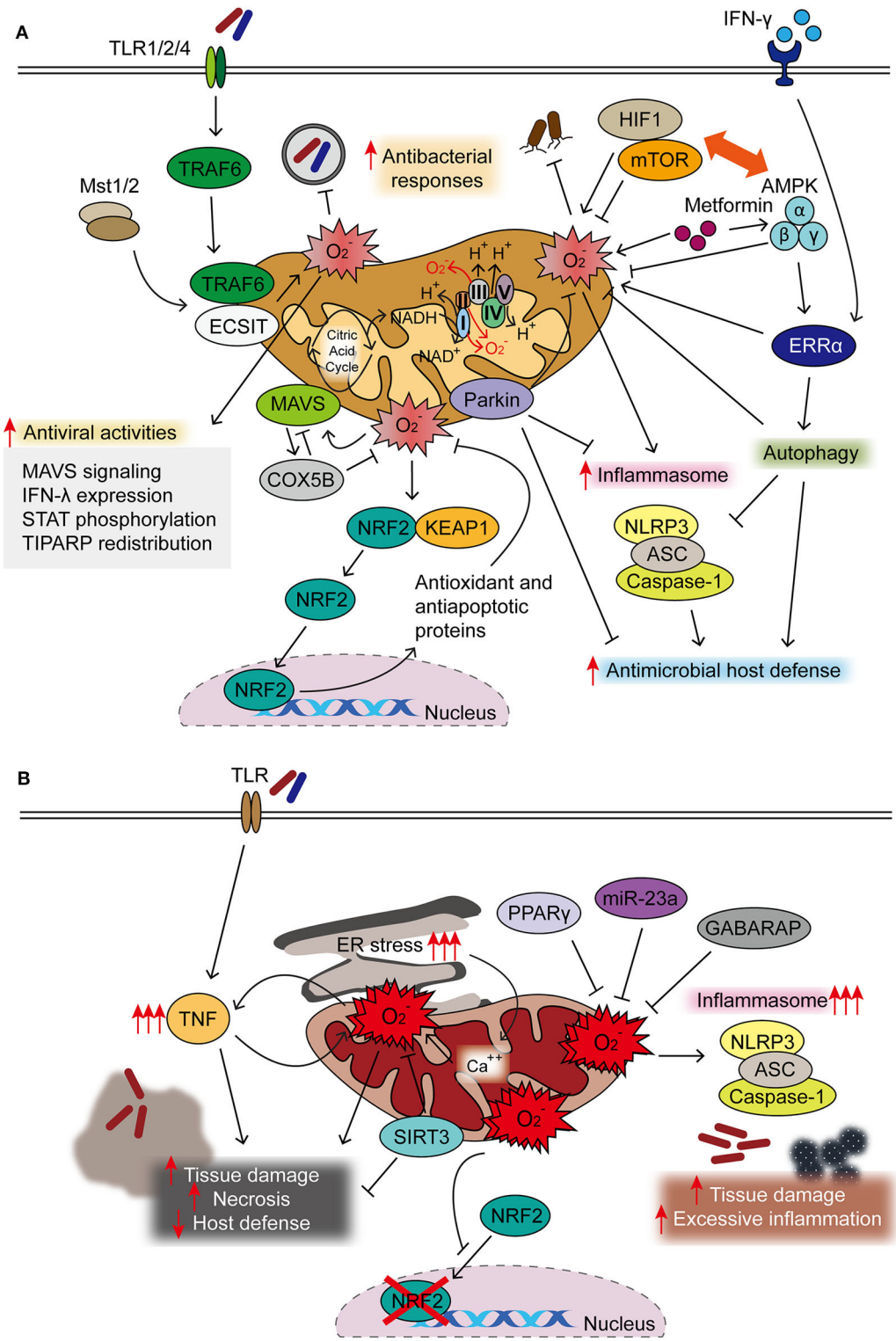

FIGURE 1 | Protective and detrimental roles of mitochondrial reactive oxygen species (mtROS) during infection. **(A)** Majority of mtROS are generated by oxidative phosphorylation (OXPHOS) complexes I and III in macrophages activated through TLR signaling, interferon (IFN)-γ, and microbial infection. Both Mst1 and Mst2 promoted Toll-like receptor (TLR)-mediated assembly of the tumor necrosis factor receptor-associated factor 6–evolutionarily conserved signaling intermediate in Toll pathway (TRAF6-ECSIT) complex, to enhance antibacterial killing effects through mtROS. IFN-γ signaling activates estrogen-related receptor α (ERRα) to enhance antimicrobial clearance through mtROS generation. mtROS are closely related to the pathways of autophagy and inflammasome, both essential in the maintenance

(Continued)

FIGURE 1 | of cellular homeostasis and activation of innate host defense. 5′ AMP-activated protein kinase (AMPK) inhibits, but hypoxia-inducible factor (HIF)-1α enhances, the generation of mtROS, thereby influencing innate defense against several pathogenic bacteria. HIF-1α/mTOR signaling drives aerobic glycolysis and reactive oxygen species (ROS) generation; mTOR inhibition leads to the enhancement of mtROS to promote host defense against *Trypanosoma cruzi* infection. AMPK activation by metformin is beneficial in the clearance of intracellular bacterial infection through phosphorylation of AMPK and mtROS generation. In addition, AMPK is the upstream kinase for ERRα-mediated antimicrobial responses during *Mycobacterium tuberculosis* (Mtb) infection. During oxidative stress, NRF2 translocates to the nucleus after dissociation from Keap1 to induce the expression of protective antioxidant genes. Mitochondrial antiviral signaling (MAVS) activation results in the expression of COX5B, which inhibit the mtROS to block the MAVS-mediated antiviral signaling. mtROS involvement in antiviral responses is described in the text in details. **(B)** Uncontrolled mtROS production leads to excessive inflammatory responses, tissue damage, and necrosis, thus detrimental to host defense. Dysregulated activation of NLRP3 inflammasome results in tissue damage and pathological inflammation through mitochondrial dysfunction and mtROS generation. Several host factors [sirtuin 3 (SIRT3), miR-23a, and peroxisome proliferator-activated receptor gamma (PPARγ)] are negative regulators for controlling excessive mtROS generation, thereby coordinating antimicrobial host defense. Excessive ROS production blocks the nuclear translocation and activity of NRF2. The accumulation of mtROS, which is also mediated by sustained endoplasmic reticulum (ER) stress, is detrimental to host defense.

microbicidal mtROS production, thereby favoring parasite persistence (18). In another study, *L. donovani* infection induced the upregulation of uncoupling protein 2 (UCP2) to inhibit mtROS generation, thereby attenuating host Th1-biased immune response and parasitic clearance (19). These data support the idea that several pathogens may alter the host gene program and/or immune metabolism to up- or downregulate mtROS production, thereby inhibiting host cell death and/or facilitating parasite survival.

Bacterial pathogens can also inhibit potentially harmful oxidative radicals for their own survival. In human gingival epithelial cells, *Porphyromonas gingivalis* can circumvent the hypochlorous acid (HOCl)-mediated antimicrobial clearance system through the activation of host glutathione synthesis pathways (44). *Porphyromonas gingivalis* nucleoside-diphosphate kinase (Ndk) was found to act as an effector, inhibiting antimicrobial signaling activities by extracellular adenosine triphosphate-induced ROS production, thus leading to pathogen persistence in gingival epithelial cells (45). Overall, the data suggest that several microbial pathogens evade or inhibit the host-defensive mtROS pathway and bactericidal free radicals (**Table 1**). Future experimental data are needed to elucidate the mechanisms by which each pathogen modulates the components/pathways of the host mtROS production system.

Viruses Manipulate Host mtROS for Pathogenesis

Numerous viruses co-opt host mitochondrial functions and mtROS to favor their pathogenesis and virulence (**Table 1**). A recent study showed that respiratory syncytial virus infection resulted in the impairment of mitochondrial respiration, loss of mitochondrial membrane potential, and increased mtROS, which promoted and favored viral replication in the cells (47). In addition, human immunodeficiency virus (HIV) can suppress or enhance mtROS generation in both productive and non-productive stages for its own benefit. Productive HIV infection in human astrocytes led to the attenuation of mtROS production and dissipation of matrix metalloproteinases, thereby making the virus resistant to cell death, whereas non-productive HIV infection induced mitochondrial damage and inflammasome-induced cell death (48). Mechanistically, productive HIV infection increased the mitophagy to resist cell death, whereas non-productive HIV infection enhanced the pyroptosis of astrocytes through NLRP3-mediated gasdermin D pathway activation (48). Thus, HIV co-opts mtROS and mitochondrial damage in both productive and non-productive infection to drive viral pathogenesis in HIV-associated neurodegenerative diseases (48). In addition, IAV can also circumvent antiviral responses and favor viral replication through NADPH oxidase 2-mediated endogenous ROS generation (50–52). Additional studies are warranted to reveal how a variety of viruses manipulate mtROS in relation to pathological inflammation, thereby enhancing their virulence and pathogenesis.

Detrimental Roles of mtROS During Infection and Sepsis

mtROS in the Amplification of Pathological Responses During Infection

Uncontrolled ROS production is thought to lead to necrosis, thereby resulting in hyper-inflammation and tissue damage (53). Tumor necrosis factor (TNF) is an essential cytokine for the maintenance of host defense during human tuberculosis (TB), as patients with rheumatoid arthritis often develop TB reactivation during anti-TNF therapy (54). In the pathogenesis of TB, mtROS production due to hyper-TNF responses plays a detrimental role, inducing host cell-programmed necrosis and the propagation of mycobacteria into the extracellular milieu (54). In a recent study, sirtuin 3 was shown to be critically involved in the host defense against Mtb infection through the control of exaggerated proinflammatory responses and neutrophil infiltration (55). These protective effects were mediated through the sirtuin 3-dependent inhibition of mitochondrial dysfunction and excessive mtROS generation in macrophages during Mtb infection (55). During infection with *E. coli* O157:H7, a pathogen that causes serious gastrointestinal infection, mitochondrial dysfunction and oxidative stress were associated with excessive inflammation and host damage (39). In addition, exaggerated production of mtROS results in fungus-mediated pathological inflammation in airway epithelial cells (40) and *T. cruzi*-mediated cardiomyopathy in Chagas disease (46). Also, mtROS inhibition suppressed respiratory syncytial virus replication and virus-mediated lung inflammation (47). These data suggest the pathogenic role of mtROS during infections of various pathogens.

As mtROS affect the number of phagocytes during infection, blockade of mtROS or superoxide dismutase functions in beneficial roles through the prevention of cell death in several

TABLE 1 | Pathogen-mediated modulation of mtROS.

Pathogens	Study model	mtROS	Consequences	Mechanism of action	References
Bacteria					
A. baumannii	RAW264.7 cells	↑	Induction of pyroptosis and apoptosis	Activation of NLRP3 inflammasome	(38)
E. coli O157:H7	Human colonic epithelial Caco-2 cells	↑	Induction of severe inflammation	Excessive ROS production from damaged mitochondria leading to NLRP3 inflammasome activation, which is inhibited by quercetin	(39)
P. aeruginosa	Primary murine neutrophils, HL-60 cells	↑	Neutrophil death	Pyocyanin-induced activation of neutrophil death through mitochondrial acid sphingomyelinase	(41)
P. gingivalis	Human primary gingival epithelial cells	↓	Increased bacterial survival and persistence	Inhibition of eATP/NOX2-ROS-antibacterial pathway	(44)
	Human primary gingival epithelial cells	↓	Increased bacterial survival and persistence	Upregulation of the antioxidant glutathione responses to inhibit eATP-induced cytosolic and mtROS	(45)
Parasite					
L. donovani	Murine peritoneal macrophages, *in vivo*	↓	Facilitation of parasite entry and survival	SREBP2-dependent upregulation of UCP2, a mitochondrial inner membrane protein, suppresses mtROS generation	(18)
	RAW264.7 cells, murine splenic macrophages, *in vivo*	↓	Establishment of infection; anti-inflammatory immune responses	Upregulation of UCP2 suppresses mtROS; Inactivation of MAPK to ameliorate a Th1-biased immune responses	(19)
T. cruzi	C2C12 cell line, human cardiac myocytes, HeLa, *in vivo*	↑	Heart failure in chagasic cardiomyopathy (CCM)	Excessive ROS-dependent inhibition in the nuclear translocation and activity of NFE2L2 (Nrf2) and induction of fibrotic gene expression	(46)
Virus					
RSV	A549 cells, vero cells, BCi-NS1 cells, pBECs	↑	Facilitation of viral infection	RSV induces mitochondrial redistribution, impairs mitochondrial respiration, loss of mitochondrial membrane potential	(47)
HIV	Human astrocytes	PI, ↓; NPI, ↑	PI, astrocyte survival; NPI, Pyroptosis	PI, increased autophagic flux and activation of mitophagy; NPI, NLRP3-caspase-1-GSDMD pathway activation	(48)
IAV	*In vivo*; murine alveolar macrophages and neutrophils	↑	Exacerbation of viral pathogenesis	The mechanisms of IAV-mediated induction of mitoROS are not described; mitoTEMPO alleviates lung inflammation and attenuates the death of neutrophils and macrophages.	(49)
	NHNE cells	↑	Restriction of IAV replication	Production of IFN-λ *via* mitochondrial and Duox2-grenerated ROS	(30)
	NHNE cells	↑	Inhibition of IAV viral titer	STAT phosphorylation and induction of IFN-stimulated genes	(31)

eATP, extracellular adenosine triphosphate; $P2X_7$, purinergic receptor; NADPH, nicotinamide adenine dinucleotide phosphate; NOX2, NADPH oxidase 2; NLRP3, NLR family Pyrin domain-containing 3; SREBP2, sterol regulatory element binding protein 2; UCP2, uncoupling protein 2; MAPK, mitogen-activated protein kinase; NFE2L2 (Nrf2), nuclear factor erythroid 2-related factor 2; RSV, respiratory syncytial virus; pBEC, primary human bronchial epithelial cells; HIV, human immunodeficiency virus; PI, productively infected; NPI, nonproductively infected; GSDMD, gasdermin D; IAV, influenza A virus; NHNE, normal human nasal epithelial cells; IFN, interferon; Duox2, dual oxidase 2; STAT, signal transducer and activator of transcription; ↑, increase; ↓, decrease.

severe infections. Previous studies showed that either Sod2 deficiency or MitoTEMPO, a scavenger of mtROS, treatment increased neutrophil numbers and reduced the bacterial burden during *P. aeruginosa* infection in zebrafish models (56). Moreover, recent studies showed that IAV-mediated exacerbation of viral pathogenesis is ameliorated by scavenging mitoROS (49). During IAV infection, the local delivery of MitoTEMPO significantly inhibited viral titers and mortality in mice infected with IAV (Hkx31, H3N2) and attenuated apoptotic and necrotic neutrophils/macrophages in lung tissues during infection (49). These data suggest the pathological effects of mtROS that promote harmful inflammation and cell death during severe pathogenic infection and support the potential use of mtROS scavengers as host-directed adjuvant therapies.

Host Factors and Mechanisms That Ameliorate mtROS Generation During Infection

There are several reports suggesting the mechanisms by which mtROS generation is controlled in the host cells during infection. Previous studies have shown that microRNA-23a is essential for the maintenance of mitochondrial integrity and restriction of mtROS through the targeting of PPIF, the gatekeeper of mitochondria permeability transition pores, thereby blocking excessive necrosis and liver damage in *L. monocytogenes* infection

(53). In rotavirus infection, the accumulation of mtROS is mediated by sustained endoplasmic reticulum (ER) stress and the release of calcium from the ER to the mitochondria, which further contributes to viral inflammation (57). Furthermore, the inhibition of mtROS, at least partly through peroxisome proliferator-activated receptor gamma (PPARγ) activation, played a beneficial role in the reduction of rotavirus infection (58). These data encourage us to target mtROS as a therapeutic strategy for viral infections by alleviation of virus-mediated ER stress and inflammatory responses (57, 58).

There is emerging interest in the role of nuclear factor erythroid 2-related factor 2 (NFE2L2)/Nrf2, a master regulator of antioxidant and anti-apoptosis system (59, 60), in the regulation of mitochondrial homeostatic functions in a variety of physiological and pathological conditions including infection (60, 61). During *P. aeruginosa* infection, the non-histone nuclear protein HMGN2 contributes to the cell-autonomous immune defense through the clearance of pyocyanin-mediated intracellular oxidative stress *via* elevation of the Nrf2-mediated antioxidant gene (62). In *T. cruzi* infection, mtROS production was increased *in vivo* and *in vitro*, resulting in the inhibition of nuclear translocation of Nrf2 and antioxidant gene expression (46). Preserving Nrf2 activity was beneficial for maintenance of cardiac function in heart failure of infectious etiologies (46). Together, these findings highlight the mechanisms by which mtROS accumulation and mitochondrial damage are mediated, although a large body of mechanism has not been well-defined, in a variety of infections. The actions of known host factors to regulate mtROS in the context of infection are illustrated in **Figure 1**.

Detrimental Roles of mtROS During Sepsis

Relatively well-characterized functions of mtROS generation have been shown in the human and animal model of sepsis. In patients with sepsis, mitochondrial function and antioxidant defenses appear to have important roles in the protection against multi-organ failure through the control of harmful excessive ROS production (63, 64). In sepsis-induced acute kidney injury, mitochondrial alteration and ROS production contributed to pathology, which was ameliorated by SIRT3, a NAD(+)-dependent deacetylase (65). In a study, mesenchymal stromal cells showed beneficial effects on experimental sepsis through the inhibition of macrophage NLRP3 inflammasome activation *via* suppression of mtROS (66). A recent genetic study showed that a specific mtDNA mutation (T6459C) might be associated with genetic susceptibility to sepsis, as the mutation group showed increased ROS levels and apoptosis (67). GABA type A receptor-associated protein (GABARAP) deficiency led to increased susceptibility to sepsis through the enhancement of mtROS and proinflammatory cytokine expression with NLRP3 inflammasome activation (68). Furthermore, blockade of the NOTCH pathway inhibited mtROS generation through the suppression of glucose oxidation, thereby attenuating hepatic macrophage M1 shifting, which reduced the lethality of endotoxin-mediated fulminant hepatitis (69). These data suggest that understanding the molecular mechanisms by which host factors target mtROS generation can contribute to the development of potential therapeutic strategies against sepsis.

Given the role of mtROS in the pathogenesis of sepsis, targeted delivery of antioxidants to mitochondria has been suggested as a potential therapeutic strategy against sepsis (63). Glucocorticoids, which are widely used anti-inflammatory drugs, control endotoxin-mediated inflammation and sepsis by inhibiting mitochondrial calcium homeostasis and the production of mtROS (70). Stefin B, an endogenous cysteine cathepsin inhibitor, was found to be essential for the control of LPS-induced sepsis through the stabilization of mitochondrial membrane potential and amelioration of mtROS generation (71). In a cecal ligation and puncture mouse model of sepsis, synthetic antioxidant lignan secoisolariciresinol diglucoside (SDG; LGM2605) alleviated septic cardiac dysfunction. Mechanistically, LGM2605 improved cardiac function by protecting cardiac mitochondrial function and inhibiting ROS accumulation (72). Furthermore, maresin 1, a metabolite of the omega-3 fatty acid, had significant inhibitory effects on mtROS generation but increased ATP content and the mtDNA copy number, thereby showing a protective role against sepsis (73). Taken together, these data suggest that the agents and small molecules involved in the control of mitochondrial dysfunction could attenuate pathological responses during sepsis through the amelioration of mtROS. Future studies for the pharmacological approaches targeting mtROS may develop potentially promising strategies to increase survival and treatment efficacy of sepsis.

CONCLUSION

The past several years have provided us with increasing evidence of the means by which the mtROS signaling pathway affects innate immunity during infection. mtROS generation *via* pathogen infection may bring together the intracellular autophagy, immune, and metabolic pathways to guide and shape the effector response. mtROS-mediated antiviral signaling is linked partially to MAVS and STAT signaling, leading to the antiviral host defense. In addition, mtROS is a crucial signal for bactericidal responses and NLRP3 inflammasome activation to enhance antibacterial responses. Nevertheless, our current knowledge is limited on how mtROS activates antibacterial or antiviral responses, and how mtROS are implicated in the inflammatory signaling pathways under different pathogenic stimuli. Further studies to understand molecular mechanisms will shed new light on the impacts of the mtROS signaling network on distinct innate effector functions and/or for driving pathological inflammatory responses during infection.

Moreover, a variety of pathogens modulate, escape, or enhance mtROS production for their own benefit, although our understanding of the underlying mechanisms remains limited. In the future, elucidating how pathogens interact with host-defensive machineries of mtROS system should help to assess the pathogenesis and/or defensive pathways in the context of infection. As mtROS generation is interconnected with the immunometabolic status in macrophages, it would be extremely interesting to investigate how mtROS crosstalk with the AMPK-mTOR pathway during infection. Further exploiting the host-defensive mechanisms for repressing pathological mtROS production and function is a crucial next step in developing therapeutic application. Although accumulating

data have provided extensive evidence that mtROS contribute to inflammation-induced pathology during sepsis, therapeutic outcomes have been limited in the use of mtROS modulators in clinical settings.

Many of the yin-and-yang aspects of mtROS signaling remain unknown in terms of infection. Answers to the above questions will provide exciting new opportunities for therapeutic approaches to many diverse infections.

AUTHOR CONTRIBUTIONS

E-KJ: designed. E-KJ, PS, JK, and YK wrote and reviewed the manuscript. PS: summarized the table. JK and YK prepared the figure. All authors read and approved the final version of the review.

FUNDING

This work was supported by the National Research Foundation of Korea (NRF) grant funded by the Korea government (MSIT) (Grand nos. 2017R1A5A2015385 and 2019R1A2C1087686), under the framework of international cooperation program managed by National Research Foundation of Korea (Grant no. 2015K2A2A6002008), and by Chungnam National University Hospital Research Fund, 2019.

ACKNOWLEDGMENTS

We are indebted to current and past members of our laboratory for discussions and investigations that contributed to this article. We thank H-W Suh for critical reading of the paper.

REFERENCES

1. Sandhir R, Halder A, Sunkaria A. Mitochondria as a centrally positioned hub in the innate immune response. *Biochim Biophys Acta Mol Basis Dis.* (2017) 1863:1090–7. doi: 10.1016/j.bbadis.2016.10.020
2. Stocks CJ, Schembri MA, Sweet MJ, Kapetanovic R. For when bacterial infections persist: toll-like receptor-inducible direct antimicrobial pathways in macrophages. *J Leukoc Biol.* (2018) 103:35–51. doi: 10.1002/JLB.4RI0917-358R
3. Abais JM, Xia M, Zhang Y, Boini KM, Li PL. Redox regulation of NLRP3 inflammasomes: ROS as trigger or effector? *Antioxid Redox Signal.* (2015) 22:1111–29. doi: 10.1089/ars.2014.5994
4. Harijith A, Ebenezer DL, Natarajan V. Reactive oxygen species at the crossroads of inflammasome and inflammation. *Front Physiol.* (2014) 5:352. doi: 10.3389/fphys.2014.00352
5. To EE, O'Leary JJ, O'Neill LAJ, Vlahos R, Bozinovski S, Porter CJH, et al. Spatial properties of reactive oxygen species govern pathogen-specific immune system responses. *Antioxid Redox Signal.* (2020) 32:982–92. doi: 10.1089/ars.2020.8027
6. Chen Y, Zhou Z, Min W. Mitochondria, oxidative stress and innate immunity. *Front Physiol.* (2018) 9:1487. doi: 10.3389/fphys.2018.01487
7. West AP, Brodsky IE, Rahner C, Woo DK, Erdjument-Bromage H, Tempst P, et al. TLR signalling augments macrophage bactericidal activity through mitochondrial ROS. *Nature.* (2011) 472:476–80. doi: 10.1038/nature09973
8. Geng J, Sun X, Wang P, Zhang S, Wang X, Wu H, et al. Kinases Mst1 and Mst2 positively regulate phagocytic induction of reactive oxygen species and bactericidal activity. *Nat Immunol.* (2015) 16:1142–52. doi: 10.1038/ni.3268
9. Wi SM, Moon G, Kim J, Kim ST, Shim JH, Chun E, et al. TAK1-ECSIT-TRAF6 complex plays a key role in the TLR4 signal to activate NF-kappaB. *J Biol Chem.* (2014) 289:35205–14. doi: 10.1074/jbc.M114.597187
10. Carneiro FRG, Lepelley A, Seeley JJ, Hayden MS, Ghosh S. An essential role for ECSIT in mitochondrial complex I assembly and mitophagy in macrophages. *Cell Rep.* (2018) 22:2654–66. doi: 10.1016/j.celrep.2018.02.051
11. Vorobjeva N, Prikhodko A, Galkin I, Pletjushkina O, Zinovkin R, Sud'ina G, et al. Mitochondrial reactive oxygen species are involved in chemoattractant-induced oxidative burst and degranulation of human neutrophils *in vitro*. *Eur J Cell Biol.* (2017) 96:254–65. doi: 10.1016/j.ejcb.2017.03.003
12. Vorobjeva N, Galkin I, Pletjushkina O, Golyshev S, Zinovkin R, Prikhodko A, et al. Mitochondrial permeability transition pore is involved in oxidative burst and NETosis of human neutrophils. *Biochim Biophys Acta Mol Basis Dis.* (2020) 1866:165664. doi: 10.1016/j.bbadis.2020.165664
13. Sonoda J, Laganiere J, Mehl IR, Barish GD, Chong LW, Li X, et al. Nuclear receptor ERR alpha and coactivator PGC-1 beta are effectors of IFN-gamma-induced host defense. *Genes Dev.* (2007) 21:1909–20. doi: 10.1101/gad.1553007
14. Yu L, Chen Y, Tooze SA. Autophagy pathway: cellular and molecular mechanisms. *Autophagy.* (2018) 14:207–15. doi: 10.1080/15548627.2017.1378838
15. Kim SY, Yang CS, Lee HM, Kim JK, Kim YS, Kim YR, et al. ESRRA (estrogen-related receptor alpha) is a key coordinator of transcriptional and post-translational activation of autophagy to promote innate host defense. *Autophagy.* (2018) 14:152–68. doi: 10.1080/15548627.2017.1339001
16. Scherz-Shouval R, Elazar Z. ROS, mitochondria and the regulation of autophagy. *Trends Cell Biol.* (2007) 17:422–7. doi: 10.1016/j.tcb.2007.07.009
17. Roca-Agujetas V, de Dios C, Leston L, Mari M, Morales A, Colell A. Recent insights into the mitochondrial role in autophagy and its regulation by oxidative stress. *Oxid Med Cell Longev.* (2019) 2019:3809308. doi: 10.1155/2019/3809308
18. Mukherjee M, Basu Ball W, Das PK. Leishmania donovani activates SREBP2 to modulate macrophage membrane cholesterol and mitochondrial oxidants for establishment of infection. *Int J Biochem Cell Biol.* (2014) 55:196–208. doi: 10.1016/j.biocel.2014.08.019
19. Basu Ball W, Kar S, Mukherjee M, Chande AG, Mukhopadhyaya R, Das PK. Uncoupling protein 2 negatively regulates mitochondrial reactive oxygen species generation and induces phosphatase-mediated anti-inflammatory response in experimental visceral leishmaniasis. *J Immunol.* (2011) 187:1322–32. doi: 10.4049/jimmunol.1004237
20. Hwang AB, Ryu EA, Artan M, Chang HW, Kabir MH, Nam HJ, et al. Feedback regulation via AMPK and HIF-1 mediates ROS-dependent longevity in Caenorhabditis elegans. *Proc Natl Acad Sci USA.* (2014) 111:E4458–67. doi: 10.1073/pnas.1411199111
21. Kwon S, Kim EJE, Lee SV. Mitochondria-mediated defense mechanisms against pathogens in Caenorhabditis elegans. *BMB Rep.* (2018) 51:274–9. doi: 10.5483/BMBRep.2018.51.6.111
22. Goncalves SM, Duarte-Oliveira C, Campos CF, Aimanianda V, Ter Horst R, Leite L, et al. Phagosomal removal of fungal melanin reprograms macrophage metabolism to promote antifungal immunity. *Nat Commun.* (2020) 11:2282. doi: 10.1038/s41467-020-16120-z
23. Lee MKS, Al-Sharea A, Shihata WA, Bertuzzo Veiga C, Cooney OD, Fleetwood AJ, et al. Glycolysis is required for LPS-induced activation and adhesion of human CD14(+)CD16(-) monocytes. *Front Immunol.* (2019) 10:2054. doi: 10.3389/fimmu.2019.02054
24. Rojas Marquez JD, Ana Y, Baigorri RE, Stempin CC, Cerban FM. Mammalian target of rapamycin inhibition in *Trypanosoma cruzi*-infected macrophages leads to an intracellular profile that is detrimental for infection. *Front Immunol.* (2018) 9:313. doi: 10.3389/fimmu.2018.00313
25. Kajiwara C, Kusaka Y, Kimura S, Yamaguchi T, Nanjo Y, Ishii Y, et al. Metformin mediates protection against Legionella pneumonia through activation of AMPK and mitochondrial reactive oxygen species. *J Immunol.* (2018) 200:623–31. doi: 10.4049/jimmunol.1700474

26. Garaude J, Acin-Perez R, Martinez-Cano S, Enamorado M, Ugolini M, Nistal-Villan E, et al. Mitochondrial respiratory-chain adaptations in macrophages contribute to antibacterial host defense. *Nat Immunol.* (2016) 17:1037–45. doi: 10.1038/ni.3509
27. Scialo F, Fernandez-Ayala DJ, Sanz A. Role of mitochondrial reverse electron transport in ROS signaling: potential roles in health and disease. *Front Physiol.* (2017) 8:428. doi: 10.3389/fphys.2017.00428
28. Sena LA, Chandel NS. Physiological roles of mitochondrial reactive oxygen species. *Mol Cell.* (2012) 48:158–67. doi: 10.1016/j.molcel.2012.09.025
29. Tal MC, Sasai M, Lee HK, Yordy B, Shadel GS, Iwasaki A. Absence of autophagy results in reactive oxygen species-dependent amplification of RLR signaling. *Proc Natl Acad Sci USA.* (2009) 106:2770–5. doi: 10.1073/pnas.0807694106
30. Kim HJ, Kim CH, Ryu JH, Kim MJ, Park CY, Lee JM, et al. Reactive oxygen species induce antiviral innate immune response through IFN-lambda regulation in human nasal epithelial cells. *Am J Respir Cell Mol Biol.* (2013) 49:855–65. doi: 10.1165/rcmb.2013-0003OC
31. Kim S, Kim MJ, Park DY, Chung HJ, Kim CH, Yoon JH, et al. Mitochondrial reactive oxygen species modulate innate immune response to influenza A virus in human nasal epithelium. *Antiviral Res.* (2015) 119:78–83. doi: 10.1016/j.antiviral.2015.04.011
32. Kozaki T, Komano J, Kanbayashi D, Takahama M, Misawa T, Satoh T, et al. Mitochondrial damage elicits a TCDD-inducible poly(ADP-ribose) polymerase-mediated antiviral response. *Proc Natl Acad Sci USA.* (2017) 114:2681–6. doi: 10.1073/pnas.1621508114
33. Jose J, Snyder JE, Kuhn RJ. A structural and functional perspective of alphavirus replication and assembly. *Future Microbiol.* (2009) 4:837–56. doi: 10.2217/fmb.09.59
34. Maeda M, Sawa H, Tobiume M, Tokunaga K, Hasegawa H, Ichinohe T, et al. Tristetraprolin inhibits HIV-1 production by binding to genomic RNA. *Microbes Infect.* (2006) 8:2647–56. doi: 10.1016/j.micinf.2006.07.010
35. Lin RJ, Chien HL, Lin SY, Chang BL, Yu HP, Tang WC, et al. MCPIP1 ribonuclease exhibits broad-spectrum antiviral effects through viral RNA binding and degradation. *Nucleic Acids Res.* (2013) 41:3314–26. doi: 10.1093/nar/gkt019
36. Zhao Y, Sun X, Nie X, Sun L, Tang TS, Chen D, et al. COX5B regulates MAVS-mediated antiviral signaling through interaction with ATG5 and repressing ROS production. *PLoS Pathog.* (2012) 8:e1003086. doi: 10.1371/journal.ppat.1003086
37. Li J, Ma C, Long F, Yang D, Liu X, Hu Y, et al. Parkin impairs antiviral immunity by suppressing the mitochondrial reactive oxygen species-Nlrp3 axis and antiviral inflammation. *iScience.* (2019) 16:468–84. doi: 10.1016/j.isci.2019.06.008
38. An Z, Su J. Acinetobacter baumannii outer membrane protein 34 elicits NLRP3 inflammasome activation via mitochondria-derived reactive oxygen species in RAW264.7 macrophages. *Microbes Infect.* (2019) 21:143–53. doi: 10.1016/j.micinf.2018.10.005
39. Xue Y, Du M, Zhu MJ. Quercetin suppresses NLRP3 inflammasome activation in epithelial cells triggered by *Escherichia coli* O157:H7. *Free Radic Biol Med.* (2017) 108:760–9. doi: 10.1016/j.freeradbiomed.2017.05.003
40. Kim YH, Lee SH. Mitochondrial reactive oxygen species regulate fungal protease-induced inflammatory responses. *Toxicology.* (2017) 378:86–94. doi: 10.1016/j.tox.2017.01.008
41. Manago A, Becker KA, Carpinteiro A, Wilker B, Soddemann M, Seitz AP, et al. Pseudomonas aeruginosa pyocyanin induces neutrophil death via mitochondrial reactive oxygen species and mitochondrial acid sphingomyelinase. *Antioxid Redox Signal.* (2015) 22:1097–110. doi: 10.1089/ars.2014.5979
42. Li T, Huang X, Yuan Z, Wang L, Chen M, Su F, et al. Pyocyanin induces NK92 cell apoptosis via mitochondrial damage and elevated intracellular Ca(2). *Innate Immun.* (2019) 25:3–12. doi: 10.1177/1753425918809860
43. Zorov DB, Juhaszova M, Sollott SJ. Mitochondrial reactive oxygen species (ROS) and ROS-induced ROS release. *Physiol Rev.* (2014) 94:909–50. doi: 10.1152/physrev.00026.2013
44. Roberts JS, Atanasova KR, Lee J, Diamond G, Deguzman J, Hee Choi C, et al. Opportunistic pathogen *Porphyromonas gingivalis* modulates danger signal ATP-mediated antibacterial NOX2 pathways in primary epithelial cells. *Front Cell Infect Microbiol.* (2017) 7:291. doi: 10.3389/fcimb.2017.00291
45. Choi CH, Spooner R, DeGuzman J, Koutouzis T, Ojcius DM, Yilmaz O. Porphyromonas gingivalis-nucleoside-diphosphate-kinase inhibits ATP-induced reactive-oxygen-species via P2X7 receptor/NADPH-oxidase signalling and contributes to persistence. *Cell Microbiol.* (2013) 15:961–76. doi: 10.1111/cmi.12089
46. Wen JJ, Porter C, Garg NJ. Inhibition of NFE2L2-antioxidant response element pathway by mitochondrial reactive oxygen species contributes to development of cardiomyopathy and left ventricular dysfunction in chagas disease. *Antioxid Redox Signal.* (2017) 27:550–66. doi: 10.1089/ars.2016.6831
47. Hu M, Schulze KE, Ghildyal R, Henstridge DC, Kolanowski JL, New EJ, et al. Respiratory syncytial virus co-opts host mitochondrial function to favour infectious virus production. *Elife.* (2019) 8:e42448. doi: 10.7554/eLife.42448
48. Ojeda DS, Grasso D, Urquiza J, Till A, Vaccaro MI, Quarleri J. Cell death is counteracted by mitophagy in hiv-productively infected astrocytes but is promoted by inflammasome activation among non-productively infected cells. *Front Immunol.* (2018) 9:2633. doi: 10.3389/fimmu.2018.02633
49. To EE, Erlich JR, Liong F, Luong R, Liong S, Esaq F, et al. Mitochondrial reactive oxygen species contribute to pathological inflammation during influenza A virus infection in mice. *Antioxid Redox Signal.* (2020) 32:929–42. doi: 10.1089/ars.2019.7727
50. Erlich JR, To EE, Liong S, Brooks R, Vlahos R, O'Leary JJ, et al. Targeting evolutionary conserved oxidative stress and immunometabolic pathways for the treatment of respiratory infectious diseases. *Antioxid Redox Signal.* (2020) 32:993–1013. doi: 10.1089/ars.2020.8028
51. To EE, Vlahos R, Luong R, Halls ML, Reading PC, King PT, et al. Endosomal NOX2 oxidase exacerbates virus pathogenicity and is a target for antiviral therapy. *Nat Commun.* (2017) 8:69. doi: 10.1038/s41467-017-00057-x
52. Vlahos R, Stambas J, Bozinovski S, Broughton BR, Drummond GR, Selemidis S. Inhibition of Nox2 oxidase activity ameliorates influenza A virus-induced lung inflammation. *PLoS Pathog.* (2011) 7:e1001271. doi: 10.1371/journal.ppat.1001271
53. Zhang B, Liu SQ, Li C, Lykken E, Jiang S, Wong E, et al. MicroRNA-23a curbs necrosis during early T cell activation by enforcing intracellular reactive oxygen species equilibrium. *Immunity.* (2016) 44:568–81. doi: 10.1016/j.immuni.2016.01.007
54. Roca FJ, Ramakrishnan L. TNF dually mediates resistance and susceptibility to mycobacteria via mitochondrial reactive oxygen species. *Cell.* (2013) 153:521–34. doi: 10.1016/j.cell.2013.03.022
55. Kim TS, Jin YB, Kim YS, Kim S, Kim JK, Lee HM, et al. SIRT3 promotes antimycobacterial defenses by coordinating mitochondrial and autophagic functions. *Autophagy.* (2019) 15:1356–75. doi: 10.1080/15548627.2019.1582743
56. Peterman EM, Sullivan C, Goody MF, Rodriguez-Nunez I, Yoder JA, Kim CH. Neutralization of mitochondrial superoxide by superoxide dismutase 2 promotes bacterial clearance and regulates phagocyte numbers in zebrafish. *Infect Immun.* (2015) 83:430–40. doi: 10.1128/IAI.02245-14
57. Guerrero CA, Acosta O. Inflammatory and oxidative stress in rotavirus infection. *World J Virol.* (2016) 5:38–62. doi: 10.5501/wjv.v5.i2.38
58. Gomez D, Munoz N, Guerrero R, Acosta O, Guerrero CA. PPARgamma agonists as an anti-inflammatory treatment inhibiting rotavirus infection of small intestinal villi. *PPAR Res.* (2016) 2016:4049373. doi: 10.1155/2016/4049373
59. Kobayashi A, Kang MI, Okawa H, Ohtsuji M, Zenke Y, Chiba T, et al. Oxidative stress sensor Keap1 functions as an adaptor for Cul3-based E3 ligase to regulate proteasomal degradation of Nrf2. *Mol Cell Biol.* (2004) 24:7130–9. doi: 10.1128/MCB.24.16.7130-7139.2004
60. Kasai S, Shimizu S, Tatara Y, Mimura J, Itoh K. Regulation of Nrf2 by mitochondrial reactive oxygen species in physiology and pathology. *Biomolecules.* (2020) 10:320. doi: 10.3390/biom10020320
61. Soares MP, Ribeiro AM. Nrf2 as a master regulator of tissue damage control and disease tolerance to infection. *Biochem Soc Trans.* (2015) 43:663–8. doi: 10.1042/BST20150054
62. Liu K, Wang X, Sha K, Zhang F, Xiong F, Wang X, et al. Nuclear protein HMGN2 attenuates pyocyanin-induced oxidative stress via Nrf2 signaling and inhibits Pseudomonas aeruginosa internalization in A549 cells. *Free Radic Biol Med.* (2017) 108:404–17. doi: 10.1016/j.freeradbiomed.2017.04.007

63. Rocha M, Herance R, Rovira S, Hernandez-Mijares A, Victor VM. Mitochondrial dysfunction and antioxidant therapy in sepsis. *Infect Disord Drug Targets.* (2012) 12:161–78. doi: 10.2174/187152612800100189
64. Karlsson M, Hara N, Morata S, Sjovall F, Kilbaugh T, Hansson MJ, et al. Diverse and tissue-specific mitochondrial respiratory response in a mouse model of sepsis-induced multiple organ failure. *Shock.* (2016) 45:404–10. doi: 10.1097/SHK.0000000000000525
65. Zhao WY, Zhang L, Sui MX, Zhu YH, Zeng L. Protective effects of sirtuin 3 in a murine model of sepsis-induced acute kidney injury. *Sci Rep.* (2016) 6:33201. doi: 10.1038/srep33201
66. Li S, Wu H, Han D, Ma S, Fan W, Wang Y, et al. A novel mechanism of mesenchymal stromal cell-mediated protection against sepsis: restricting inflammasome activation in macrophages by increasing mitophagy and decreasing mitochondrial ROS. *Oxid Med Cell Longev.* (2018) 2018:3537609. doi: 10.1155/2018/3537609
67. Shen X, Han G, Li S, Song Y, Shen H, Zhai Y, et al. Association between the T6459C point mutation of the mitochondrial MT-CO1 gene and susceptibility to sepsis among Chinese Han people. *J Cell Mol Med.* (2018) 22:5257–64. doi: 10.1111/jcmm.13746
68. Zhang Z, Xu X, Ma J, Wu J, Wang Y, Zhou R, et al. Gene deletion of Gabarap enhances Nlrp3 inflammasome-dependent inflammatory responses. *J Immunol.* (2013) 190:3517–24. doi: 10.4049/jimmunol.1202628
69. Xu J, Chi F, Guo T, Punj V, Lee WN, French SW, et al. NOTCH reprograms mitochondrial metabolism for proinflammatory macrophage activation. *J Clin Invest.* (2015) 125:1579–90. doi: 10.1172/JCI76468
70. Kasahara E, Inoue M. Cross-talk between HPA-axis-increased glucocorticoids and mitochondrial stress determines immune responses and clinical manifestations of patients with sepsis. *Redox Rep.* (2015) 20:1–10. doi: 10.1179/1351000214Y.0000000107
71. Maher K, Jeric Kokelj B, Butinar M, Mikhaylov G, Mancek-Keber M, Stoka V, et al. A role for stefin B (cystatin B) in inflammation and endotoxemia. *J Biol Chem.* (2014) 289:31736–50. doi: 10.1074/jbc.M114.609396
72. Kokkinaki D, Hoffman M, Kalliora C, Kyriazis ID, Maning J, Lucchese AM, et al. Chemically synthesized Secoisolariciresinol diglucoside (LGM2605) improves mitochondrial function in cardiac myocytes and alleviates septic cardiomyopathy. *J Mol Cell Cardiol.* (2019) 127:232–45. doi: 10.1016/j.yjmcc.2018.12.016
73. Gu J, Luo L, Wang Q, Yan S, Lin J, Li D, et al. Maresin 1 attenuates mitochondrial dysfunction through the ALX/cAMP/ROS pathway in the cecal ligation and puncture mouse model and sepsis patients. *Lab Invest.* (2018) 98:715–33. doi: 10.1038/s41374-018-0031-x

Conflict of Interest: The authors declare that the research was conducted in the absence of any commercial or financial relationships that could be construed as a potential conflict of interest.

frontiers in Immunology

ORIGINAL RESEARCH
published: 02 September 2020
doi: 10.3389/fimmu.2020.01926

The Ubiquitin E3 Ligase Parkin Inhibits Innate Antiviral Immunity Through K48-Linked Polyubiquitination of RIG-I and MDA5

Lang Bu[1], Huan Wang[2], Panpan Hou[1], Shuting Guo[3], Miao He[1], Jingshu Xiao[1], Ping Li[1], Yongheng Zhong[1], Penghui Jia[1], Yuanyuan Cao[4], Guanzhan Liang[1], Chenwei Yang[1], Lang Chen[3], Deyin Guo[1] and Chun-Mei Li[1]**

[1] MOE Key Laboratory of Tropical Disease Control, the Infection and Immunity Center (TIIC), School of Medicine, Sun Yat-sen University, Shenzhen, China, [2] Institute of Precision Medicine, The First Affiliated Hospital, Sun Yat-sen University, Guangzhou, China, [3] Department of Immunology, School of Basic Medical Sciences, Wuhan University, Wuhan, China, [4] School of Basic Medical Sciences, Anhui Medical University, Hefei, China

OPEN ACCESS

Edited by:
Edecio Cunha-Neto,
University of São Paulo, Brazil

Reviewed by:
Hiroyuki Oshiumi,
Kumamoto University, Japan
Caroline Jefferies,
Cedars Sinai Medical Center,
United States

***Correspondence:**
Deyin Guo
guodeyin@mail.sysu.edu.cn
Chun-Mei Li
lichm8@mail.sysu.edu.cn

Specialty section:
This article was submitted to Molecular Innate Immunity, a section of the journal Frontiers in Immunology

Received: 08 April 2020
Accepted: 17 July 2020
Published: 02 September 2020

Citation:
Bu L, Wang H, Hou P, Guo S, He M, Xiao J, Li P, Zhong Y, Jia P, Cao Y, Liang G, Yang C, Chen L, Guo D and Li C-M (2020) The Ubiquitin E3 Ligase Parkin Inhibits Innate Antiviral Immunity Through K48-Linked Polyubiquitination of RIG-I and MDA5. Front. Immunol. 11:1926. doi: 10.3389/fimmu.2020.01926

Innate immunity is the first-line defense against antiviral or antimicrobial infection. RIG-I and MDA5, which mediate the recognition of pathogen-derived nucleic acids, are essential for production of type I interferons (IFN). Here, we identified mitochondrion depolarization inducer carbonyl cyanide 3-chlorophenylhydrazone (CCCP) inhibited the response and antiviral activity of type I IFN during viral infection. Furthermore, we found that the PTEN-induced putative kinase 1 (PINK1) and the E3 ubiquitin-protein ligase Parkin mediated mitophagy, thus negatively regulating the activation of RIG-I and MDA5. Parkin directly interacted with and catalyzed the K48-linked polyubiquitination and subsequent degradation of RIG-I and MDA5. Thus, we demonstrate that Parkin limits RLR-triggered innate immunity activation, suggesting Parkin as a potential therapeutic target for the control of viral infection.

Keywords: parkin, mitophagy, polyubiquitination, RIG-I, MDA5, innate immunity

INTRODUCTION

The self- vs. non-self-recognition by the innate immune system has been first reported by Charles Alderson Janeway in 1989 (1). Janeway proposed that the so-called pathogen-associated molecular patterns (PAMPs), which are conserved structures in microorganisms, were recognized as non-self by a germline-encoded pattern-recognition receptor (PRR) system (1). Recent evidences indicate that PRRs are also responsible for recognizing the damage-associated molecular patterns (DAMPs) released from damaged cells. Till now, different classes of PRRs have been reported, including Toll-like receptors (TLRs), nucleotide oligomerization domain (NOD)-like receptors (NLRs), C-type lectin receptors (CLRs), and retinoic acid-inducible gene I (RIG-I)-like receptors (RLRs) (2–6).

The RLR family comprises three members: RIG-I, MDA5, and laboratory of genetics and physiology 2 (LGP2). MDA5 and RIG-I both bind to dsRNA (7). They all have a DExD/H box RNA helicase domain that can detect viral RNA and a C-terminal RNA binding domain (CTD). Both RIG-I and MDA5 contain two caspase activation and recruitment domains (CARDs) in N-terminal region, whereas LGP2 lacks the CARD domains. When the RIG-I or MDA5 recognizes the viral dsRNA, it exposes the N-terminal CARD domains,

which interact with the CARD domain of the mitochondrial antiviral signaling protein (MAVS) (8). And then MAVS activates the IKKε and TBK1, which promote the activation of IFN-regulatory factors (IRFs) and nuclear factor-κB (NF-κB) (9). NF-κB and IRFs translocate into the nucleus, where they activate the innate immunity and promote the expression of pro-inflammatory cytokines and type I IFNs (10).

Mitophagy is a special type of mitochondrial autophagy, which can remove damaged or depolarized mitochondria (11, 12). Cells maintain energy balance and resist oxidative stress by regulating the movement, distribution, and clearance of mitochondria (13). Parkinson's disease (PD) is one of the most common neurodegenerative diseases. Although the pathogenesis of PD is still unclear, more and more evidences show that mitochondrial dysfunction is one of the molecular pathogenesis of PD (11, 14). Familial PD can be induced by the mutations of the PTEN-induced putative kinase 1 (PINK1) and E3 ubiquitin-protein ligase Parkin, both of which maintain mitochondrial health by regulating mitochondrial dynamics and quality control (15–17). In normal mitochondria, PINK1 contains a mitochondrial targeting sequence and is transferred from the outer mitochondrial membrane (OMM) to the inner mitochondrial membrane (IMM), where it is cleaved by the protease presenilin-associated rhomboid-like protein (PARL) and degraded by the proteasome 26S subsequently (18, 19). When mitochondria get damaged and depolarized, PINK1 cannot be processed by PARL and stabilized on the OMM. Then, PINK1 can phosphorylate itself and enhance its own activation (20). Furthermore, PINK1 phosphorylates ubiquitin on Ser65, and then Ub-pSer65 binds to Parkin (21). Then Parkin can be phosphorylated by PINK1 on its Ser65, leading to its full activation (22). Once activated, Parkin conjugates ubiquitin chains on OMM proteins and recruits several substrates in mitochondria, such as mitofusin 2 (Mfn2), voltage-dependent anion-selective channel protein (VDAC), and dynamin-1-like protein (DRP1) (23–26). Mitophagy receptors containing a LIR (LC3 interacting region) motif can be recruited by OMM proteins to interact with the LC3 anchored in the membrane of autophagosome. These ubiquitin chains bind to autophagic cargo receptors such as optineurin (OPTN) and sequestosome 1 (SQSTM1, also known as p62), which act in concert with the general autophagy mechanism to capture damaged mitochondria in the autophagosomal double-membrane (27, 28). The fusion with lysosomes facilitates the degradation of mitochondria by lysosomal hydrolases (29). The degradation of mitochondria by this process is referred to as PINK1/Parkin-dependent mitophagy. Mitochondria plays the pivotal role in the innate immune signaling pathway, and mitophagy is a key regulatory mechanism to limit excessive inflammation and maintain tissue homeostasis (30).

In this study, we demonstrated that mitochondria depolarization inducer carbonyl cyanide 3-chlorophenylhydrazone (CCCP) inhibited the antiviral responses and the activity of type I IFN during viral infection. Moreover, we identified that a mitophagy associated protein, the E3 ubiquitin ligase Parkin, was a negative regulator of innate immunity. PINK1 and Parkin mediated mitophagy, which negatively regulated the response of type I IFN. Overall, Parkin interacted with and promoted the K48-linked polyubiquitination of RIG-I and MDA5. Thus Parkin-mediated K48-linked polyubiquitination facilitates the degradation of RIG-I and MDA5.

RESULTS

Mitochondrial Uncoupler CCCP Inhibits Type I IFN Responses

In order to study the possible regulatory effects of mitophagy on innate immunity, we first tested the effect of the carbonyl cyanide 3-chlorophenylhydrazone (CCCP) on mitochondria depolarization. The results showed that Parkin expressed diffusely in the cytoplasm in CCCP untreated cells, while in CCCP treated cells, it was recruited to puncta that co-localized with mitochondria, as monitored by GFP-mito (a mitochondrion-targeted green fluorescent protein) (**Figure 1A**). In order to reveal, the roles of mitophagy in innate immunity and antiviral responses, we first observed whether mitochondrial uncoupler CCCP inhibited type I IFN responses during viral infection. Luciferase assays showed that CCCP inhibited the SeV-induced activation of *IFNB1* promoter reporter and interferon-stimulating regulatory element (ISRE) promoter reporter containing IRF3-responsive positive regulatory domains (PRD) III and I, but did not inhibit the activation of NF-κB promoter reporter (**Figure 1B**). These results showed that CCCP inhibited the activation of IFN-β luciferase through IRF3 instead of NF-κB. To confirm the function of CCCP in IFN-β signaling, we detected the expression of *IFNB1* and the transcription of IRF3-dependent genes such as *ISG15* and *IFIT1* mRNA. We observed CCCP decreased the expression of these genes in a dose- and time-dependent manner in HEK293 and Raw264.7 cells (**Figures 1C,D** and **Supplementary Figures 1A,B**). Furthermore, CCCP could decrease the expression of the interferon-regulating genes such as *Ifnb1*, *Isg15*, and *Ifit1* in BMDCs (**Supplementary Figure 1C**). Then we investigated which step of activation of IFN-β can be influenced by CCCP, the results of which indicated that CCCP inhibited the *IFNB1* promoter reporter induced by upstream activators, including RIG-I-N, MDA5-N, MAVS, and TBK1 (**Figure 1E**). Similarly, CCCP decreased the expression of SeV-induced RIG-I, MDA5, MAVS, and the phosphorylation of TBK1 and IRF3 (**Figure 1F**). All together, these data demonstrate that CCCP can inhibit SeV-induced interferon responses.

E3 Ubiquitin Ligase Parkin Negatively Regulates the Responses and Antiviral Immunity of Type I IFN

CCCP can promote the recruitment of Parkin to mitochondria, which eventually leads to mitophagy mediated by PINK1/Parkin. As PINK1 has been identified as a positive regulator for RLR signaling (31), we investigated the effects of Parkin in RLR-induced IFN-β signaling. Parkin was transfected into HEK293 cells, and the results suggested that Parkin could reduce SeV-induced activation of *IFNB1* promoter reporter and ISRE

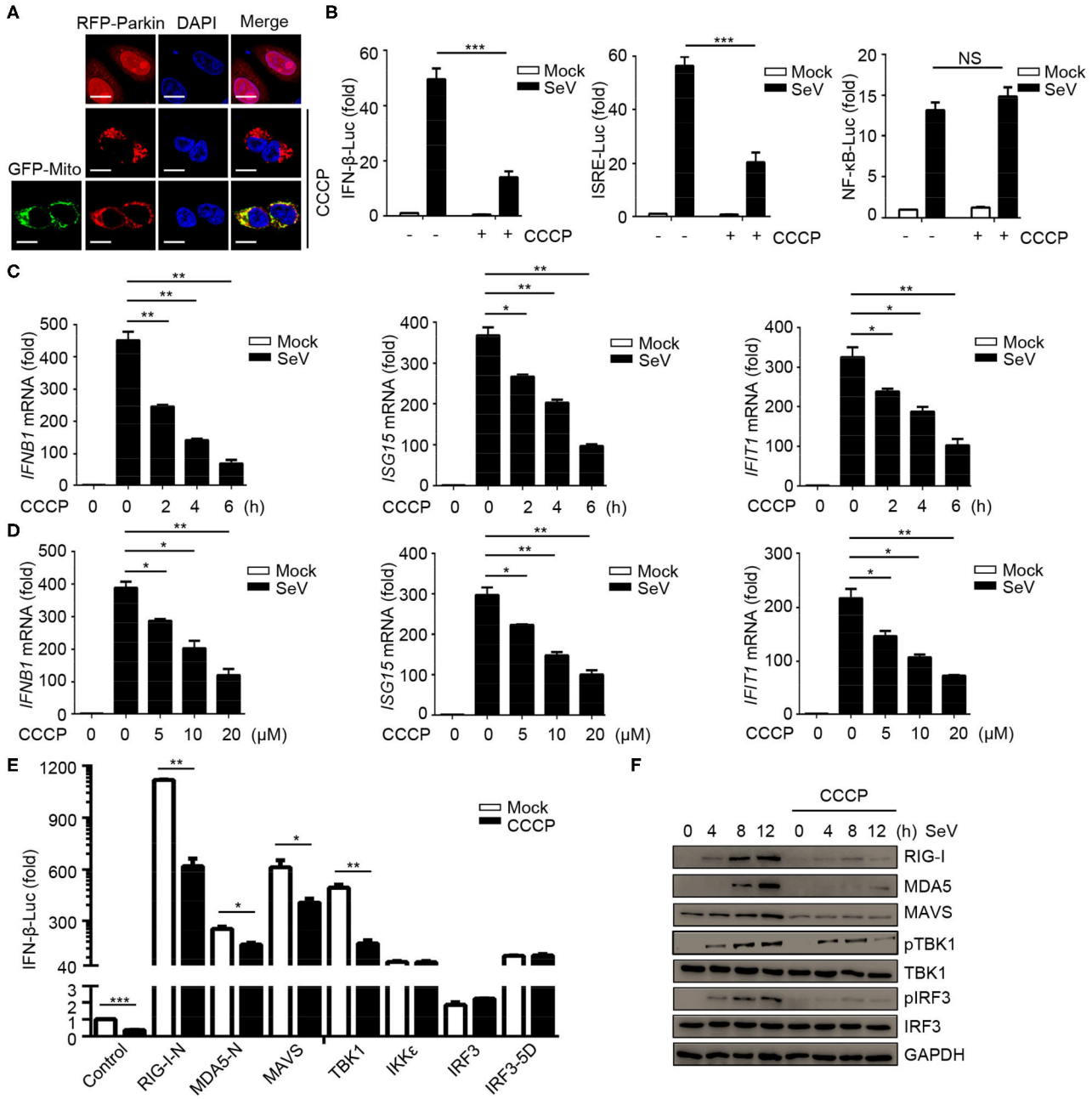

FIGURE 1 | Mitochondrial uncoupler CCCP inhibits type I IFN responses. **(A)** 293T cells were transfected with RFP-Parkin alone or together with GFP-Mito, 24 h post-transfection, the cells were untreated or treated with CCCP (10 μM) for 6 h and subjected to IF analysis. Scale bar is 10 μm. **(B)** HEK293 cells were transfected with a luciferase reporter of the IFN-β promoter, ISRE promoter, and NF-κB promoter. 24 h post-transfection, the cells were untreated or treated with CCCP (10 μM) for 2 h, then left unstimulated or stimulated with SeV for 10 h, and luciferase assays were performed. **(C)** HEK293 cells were untreated or treated with CCCP (10 μM) for different times, unstimulated or stimulated with SeV for 10 h. Then quantitative RT-PCR analysis of *IFNB1*, *ISG15*, and *IFIT1* mRNA. **(D)** HEK293 cells were untreated or treated with different concentrations of CCCP for 2 h, then unstimulated or stimulated with SeV for 10 h, and subjected to quantitative RT-PCR analysis. **(E)** HEK293 cells were co-transfected with IFN-β luciferase reporter and RIG-I-N, MDA5-N, MAVS, TBK1, IKKε, IRF3, or IRF3-5D for 24 h, then untreated or treated with CCCP (10 μM) for 12 h, and subjected to luciferase assays. **(F)** HEK293 cells were untreated or treated with CCCP (10 μM) for 2 h, then unstimulated or stimulated with SeV for different times, and the whole cell extracts were subjected to IB analysis. The data represent the average of three independent experiments and were analyzed by unpaired *t*-test. All data represent the mean ± S.D. $^{*}p < 0.05$, $^{**}p < 0.01$, and $^{***}p < 0.001$.

promoter reporter, instead of the NF-κB-responsive promoter reporter (**Figure 2A**). The expression of *IFNB1*, *ISG15*, and *IFIT1* mRNA were decreased in HEK293 cells transfected with Parkin upon infection with SeV (**Figure 2B**). Consistently, knockdown of Parkin could increase the expression of *IFNB1*, *ISG15*, and *IFIT1* mRNA in THP1, A549, and THP1 differentiated

macrophages (**Figure 2C** and **Supplementary Figures 2A,B**). We then investigated which step of activation of IFN-β can be influenced by Parkin, and the results indicated that Parkin inhibited the activity of *IFNB1* promoter reporter induced by upstream activators, including RIG-I-N, MDA5-N, MAVS, and TBK1 (**Figure 2D**). Similarly, overexpression of Parkin decreased the expression of SeV-induced RIG-I, MDA5, MAVS, and the phosphorylation of TBK1 and IRF3 (**Figure 2E**). Additionally, knockdown of Parkin increased the expression of SeV-induced RIG-I, MDA5, MAVS, and the phosphorylation of TBK1 and IRF3 in HEK293 and A549 cells (**Figure 2F** and **Supplementary Figure 2C**). Moreover, overexpression of Parkin increased the level of VSV-GFP and VSV titers in HEK293 cells while knockdown of Parkin decreased the level of VSV-GFP and VSV titers (**Figures 2G,H**). In summary, our results conclude that E3 ubiquitin ligase Parkin negatively regulates RLR-mediated IFN-β signaling.

Parkin Promotes the Inhibition of CCCP on Innate Immunity

The above results have shown that CCCP and Parkin could inhibit the response of type I IFN. To confirm whether CCCP can inhibit the innate immunity-associated mitophagy mediated by PINK1/Parkin, we carried out a series of experiments. Luciferase assays revealed that Parkin could promote the inhibition of CCCP on SeV-induced activation of an *IFNB1* promoter reporter and ISRE promoter reporter (**Figure 3A**). Likewise, Parkin could increase the inhibitory effect of CCCP on the expression of *IFNB1*, *ISG15*, and *IFIT1* mRNA in HEK293 cells (**Figure 3B**). As a mitochondrial antiviral signaling protein, MAVS functions as a critical adaptor of the RLR signaling pathway. It has been reported that human parainfluenza virus type 3 (HPIV3)-mediated mitophagy inhibits the type I IFN response through MAVS (32). Parkin can also interact with MAVS and accumulate unanchored linear polyubiquitin chains on MAVS (33). In our study, we found that overexpression or knockdown of Parkin could change the expression of endogenous RIG-I and MDA5 but could not affect the protein level of endogenous MAVS (**Figures 2E,F**). Furthermore, CCCP did not affect the localization of MAVS on mitochondria (**Supplementary Figure 3A**). Therefore, our data indicate that Parkin affects innate immunity mainly through RIG-I and MDA5. CCCP and Parkin could both reduce the expression of exogenous RIG-I and MDA5. Notably, Parkin could increase the inhibitory effect of CCCP on the expression of exogenous RIG-I and MDA5 (**Figure 3C**). Nevertheless, siRNA-mediated knockdown of Parkin decreased the inhibition of CCCP on SeV-induced activation of an *IFNB1* promoter reporter and ISRE promoter reporter in HEK293 cells (**Figure 3D**). Similarly, knockdown of Parkin could decrease the inhibition of CCCP on the expression of *IFNB1*, *ISG15*, and *IFIT1* mRNA in HEK293 cells (**Figure 3E**). Also, knockdown of Parkin could decrease the inhibitory effect of CCCP on the expression of exogenous RIG-I and MDA5 (**Figure 3F**). These data suggest that the inhibitory effect of CCCP on innate immunity can be enhanced by Parkin.

Mitophagy Mediated by PINK1/Parkin Negatively Regulates the Responses and Antiviral Immunity of Type I IFN

To assess the relevance of mitophagy in innate immunity, we expressed PINK1 and Parkin alone or together, and evaluated the effect of mitophagy mediated by PINK1/Parkin on innate immunity. The results indicated that the single expression of PINK1 or Parkin expressed diffusely in the cells, and co-expression of PINK1 and Parkin could be recruited and co-localized with GFP-Mito (a mitochondrial marker) and accumulated in distinct puncta adjacent to damaged and incomplete mitochondria, an indicator of mitophagy (**Figure 4A**). Luciferase assays showed that PINK1 and Parkin could inhibit SeV-induced activation of an *IFNB1* promoter reporter and ISRE promoter reporter (**Figure 4B**). In addition, PINK1 and Parkin could reduce the expression of *IFNB1*, *ISG15*, and *IFIT1* mRNA in HEK293 cells (**Figure 4C**). We also observed that PINK1 and Parkin could reduce the expression of exogenous RIG-I and MDA5, and degrade the mitochondrial outer membrane protein TOM20 and the mitochondrial matrix protein HSPD1, an indication of mitophagy (**Figure 4D**). The proteasome inhibitor MG-132 and autophagy inhibitor bafilomycin A1 (BafA1) could reduce the inhibition of PINK1 and Parkin on RIG-I and MDA5 (**Figure 4E**). Furthermore, autophagy inhibitor BafA1 could reduce the inhibition of PINK1 and Parkin on the expression of *IFNB1*, *ISG15*, and *IFIT1* mRNA in HEK293 cells (**Figure 4F**). Moreover, overexpression of PINK1 and Parkin increased the level of VSV-GFP and VSV titers in HEK293 cells (**Figures 4G,H**). Collectively, these data suggest that mitophagy mediated by PINK1/Parkin can suppress the antiviral immune responses.

Parkin Interacts With RIG-I and MDA5

Next, we sought to determine the molecular mechanisms of mitophagy mediated by PINK1/Parkin decreasing type I interferon signaling. The co-immunoprecipitation assays showed that Parkin could interacted with RIG-I, and CCCP could promote the interaction (**Figure 5A**). We also found the interaction between Parkin and MDA5, and CCCP could also promote the interaction (**Figure 5B**). In addition, we did not observe the interaction between PINK1 and RIG-I or MDA5 in 293T cells treated with CCCP (**Figure 5C**). Furthermore, we found that endogenous interaction between Parkin and RIG-I or MDA5 in HEK293 cells stimulated with SeV (**Figure 5D**). Under a microscope, we observed the colocalization of Parkin and RIG-I or MDA5, and CCCP could promote their colocalization on mitochondria (**Figures 5E,F**). Moreover, PINK1 could promote the colocalization of Parkin and RIG-I or MDA5 (**Figure 5G**). These results indicate that Parkin interacts with RIG-I and MDA5, and the interaction can be enhanced by CCCP.

Parkin Increases K48-Linked Polyubiquitination of RIG-I and MDA5

To investigate whether Parkin regulates the polyubiquitination of RIG-I and MDA5 through its E3 ligase activity, we designed

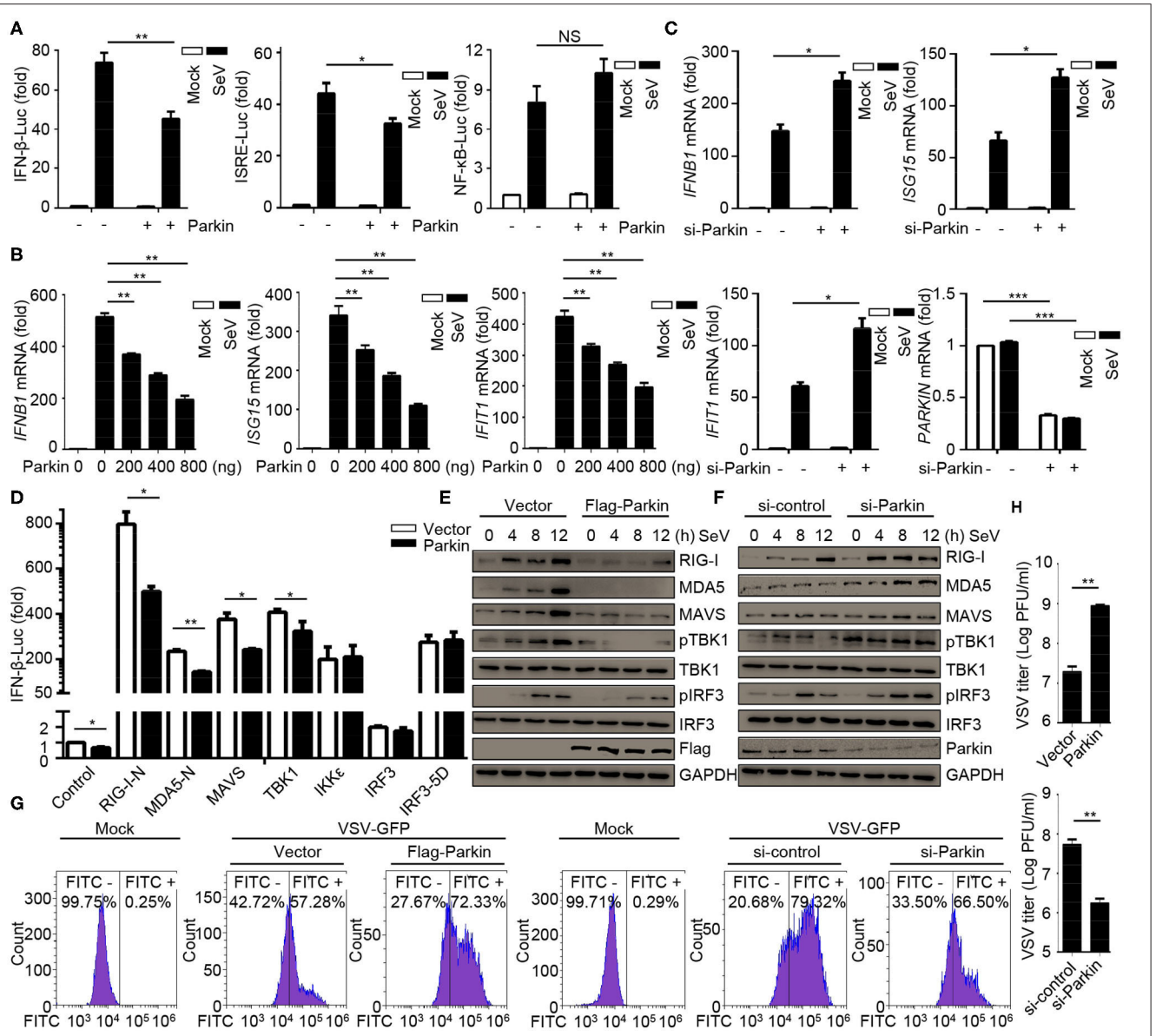

FIGURE 2 | E3 ubiquitin-protein ligase Parkin inhibits type I IFN responses. **(A)** HEK293 cells were co-transfected with vector or Parkin and IFN-β, ISRE, or NF-κB luciferase reporter for 24 h, then unstimulated or stimulated with SeV for 10 h, and subjected to luciferase assays. **(B)** HEK293 cells were transfected with vector or different quality of Parkin for 24 h, then unstimulated or stimulated with SeV for 10 h, and subjected to quantitative RT-PCR analysis. **(C)** PMA-differentiated THP1 cells were transfected with si-control or si-Parkin for 48 h, then unstimulated or stimulated with SeV for 10 h, and subjected to quantitative RT-PCR analysis. **(D)** Vector or Parkin were co-transfected with IFN-β luciferase reporter and RIG-I-N, MDA5-N, MAVS, TBK1, IKKε, IRF3, or IRF3-5D for 24 h in HEK293 cells, then subjected to luciferase assays. **(E)** HEK293 cells were transfected with vector or Flag-Parkin for 24 h, then unstimulated or stimulated with SeV for different times, and the whole cell extracts were subjected to IB analysis. **(F)** HEK293 cells were transfected with si-control or si-Parkin for 48 h, then unstimulated or stimulated with SeV for different times, and the whole cell extracts were subjected to IB analysis. **(G)** HEK293 cells were transfected with vector or Parkin for 24 h, or transfected with si-control or si-Parkin for 48 h, then cells were infected with or without VSV-GFP (MOI = 0.01), and then cells were subjected to flow cytometer assays. **(H)** HEK293 cells were transfected with vector or Parkin for 24 h, or transfected with si-control or si-Parkin for 48 h, then cells were infected with VSV-GFP (MOI = 0.01), and the supernatants were subjected to VSV plaque assays. The data represent the average of three independent experiments and were analyzed by unpaired *t*-test. All data represent the mean ± S.D. $^{*}p < 0.05$, $^{**}p < 0.01$, and $^{***}p < 0.001$.

a series of experiments. We found that Parkin and CCCP could both increase the polyubiquitination of RIG-I or MDA5, and Parkin could increase the CCCP-mediated polyubiquitination of RIG-I or MDA5 in the presence of MG-132 and BafA1 (**Figure 6A**). K63-linked polyubiquitination is required for the activation of RIG-I and MDA5 upon viral infection and K48-linked polyubiquitination is indicated for the degradation of RIG-I and MDA5. To further investigate the type of

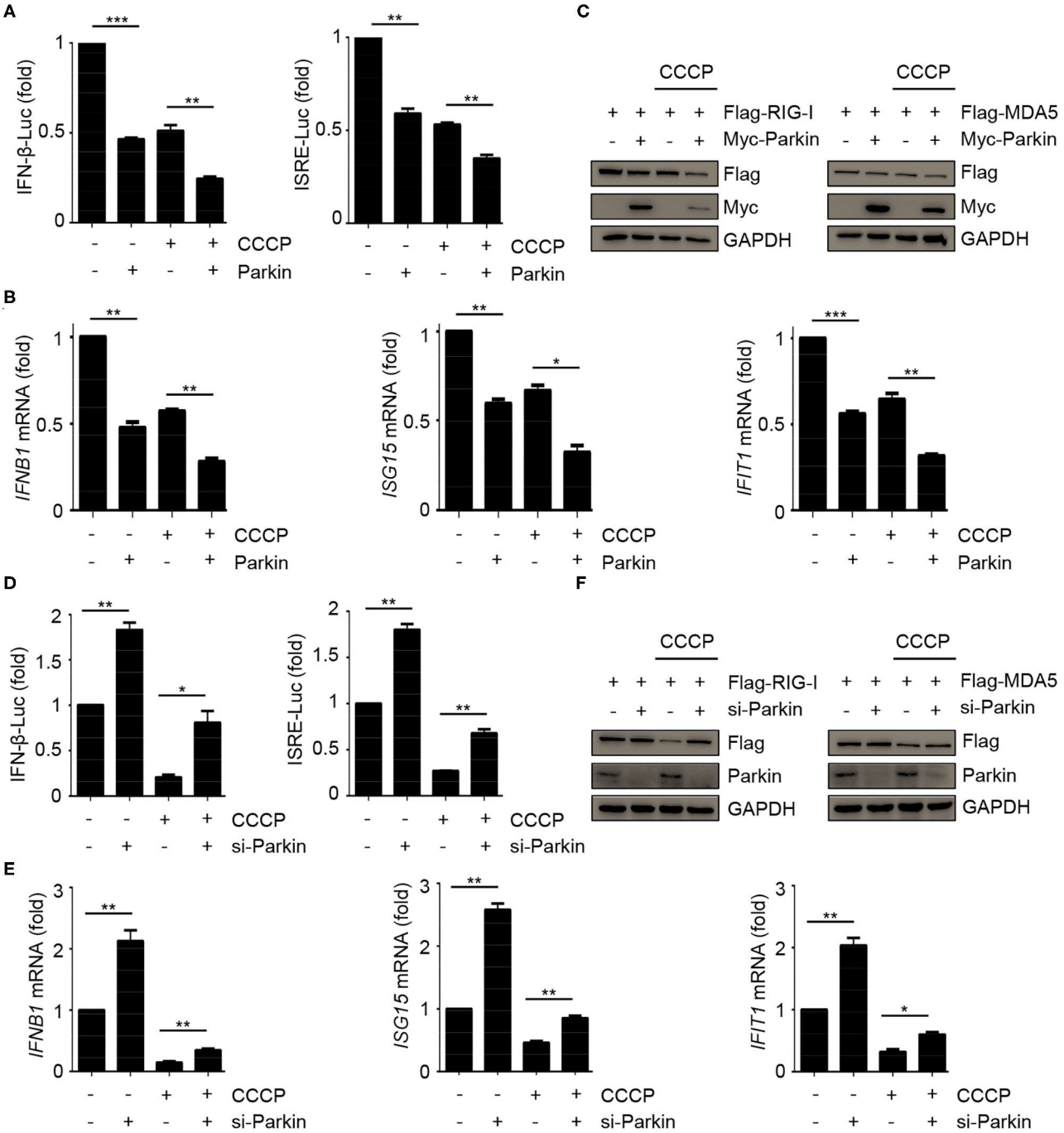

FIGURE 3 | Parkin promotes the inhibition of CCCP on innate immunity. **(A)** HEK293 cells were co-transfected with vector or Parkin and IFN-β or ISRE luciferase reporter for 24 h, untreated or treated with CCCP (10 μM) for 2 h, then stimulated with SeV for 10 h, and subjected to luciferase assays. **(B)** HEK293 cells were transfected with vector or Parkin for 24 h, untreated or treated with CCCP (10 μM) for 2 h, then stimulated with SeV for 10 h, and subjected to quantitative RT-PCR analysis. **(C)** 293T cells were co-transfected with Flag-RIG-I or Flag-MDA5 and vector or Myc-Parkin for 24 h, untreated or treated with CCCP (10 μM) for 12 h, and the whole cell extracts were subjected to IB analysis. **(D)** HEK293 cells were co-transfected with si-control or si-Parkin and IFN-β or ISRE luciferase reporter for 48 h, untreated, or treated with CCCP (10 μM) for 2 h, then stimulated with SeV for 10 h, and subjected to luciferase assays. **(E)** HEK293 cells were si-control or si-Parkin for 48 h, untreated or treated with CCCP (10 μM) for 2 h, then stimulated with SeV for 10 h, and subjected to quantitative RT-PCR analysis. **(F)** 293T cells were co-transfected with Flag-RIG-I or Flag-MDA5 and si-control or si-Parkin for 48 h, untreated or treated with CCCP (10 μM) for 12 h, and the whole cell extracts were subjected to IB analysis. The data represent the average of three independent experiments and were analyzed by unpaired *t*-test. All data represent the mean ± S.D. $^{*}p < 0.05$, $^{**}p < 0.01$, and $^{***}p < 0.001$.

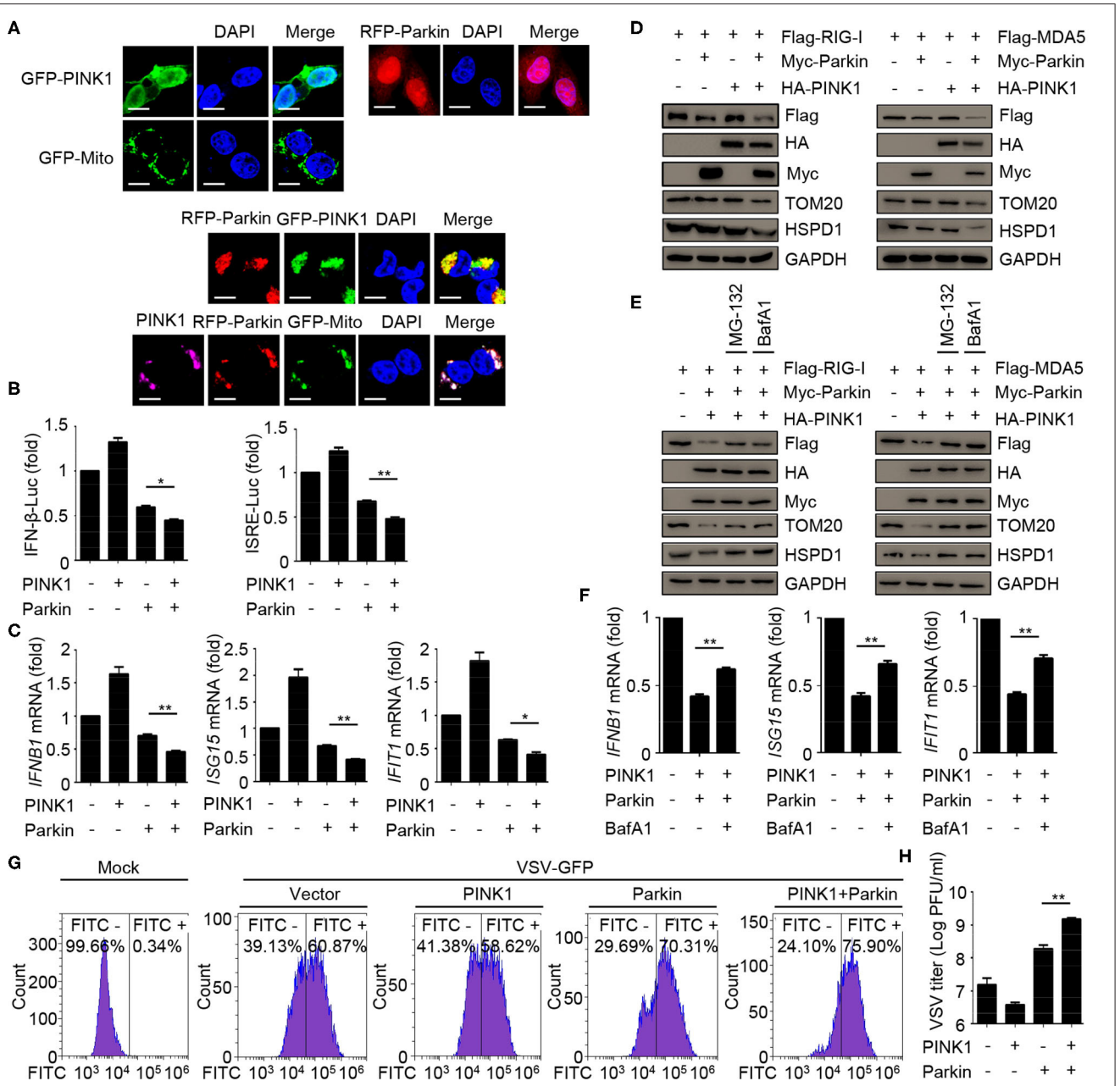

FIGURE 4 | Mitophagy mediated by PINK1/Parkin negatively regulates the type I IFN responses. **(A)** 293T cells were transfected with PINK1, Parkin, and GFP-Mito alone or together for 24 h, and then subjected to IF assays. Scale bar is 10 μm. **(B)** HEK293 cells were transfected with PINK1 or Parkin alone or together with IFN-β or ISRE luciferase reporter, 24 h post-transfection, stimulated with SeV for 10 h, and subjected to luciferase assays. **(C)** HEK293 cells were transfected with PINK1 or Parkin alone or together, 24 h post-transfection, stimulated with SeV for 10 h, and subjected to quantitative RT-PCR analysis. **(D)** Flag-RIG-I or Flag-MDA5 were co-transfected with HA-PINK1 or Myc-Parkin in 293T cells for 24 h, and the whole cell extracts were subjected to IB analysis. **(E)** Flag-RIG-I or Flag-MDA5 were co-transfected with vector or HA-PINK1 and Myc-Parkin in 293T cells for 24 h, and untreated or treated with MG-132 (10 μM) or BafA1 (200 nM) for 8 h. The whole cell extracts were subjected to IB analysis. **(F)** HEK293 cells were transfected with vector or PINK1 and Parkin, 24 h post-transfection, stimulated with SeV for 10 h in the absence or presence of BafA1 (200 nM), and subjected to quantitative RT-PCR analysis. **(G)** HEK293 cells were transfected with PINK1 and Parkin alone or together for 24 h, then cells were infected with VSV-GFP (MOI = 0.01), and then cells were subjected to flow cytometer assays. **(H)** HEK293 cells were transfected with PINK1 and Parkin alone or together for 24 h, then cells were infected with VSV-GFP (MOI = 0.01), and the supernatants were subjected to VSV plaque assays. The data represent the average of three independent experiments and were analyzed by unpaired *t*-test. All data represent the mean ± S.D. $^{*}p < 0.05$, and $^{**}p < 0.01$.

Parkin-mediated polyubiquitination of RIG-I or MDA5, we used vectors expressing HA-Ubiquitin-K48, which contain arginine to replace all lysine residues except lysine at position 48. It was revealed by immunoprecipitation experiments that Parkin and CCCP could both increase the K48-linked polyubiquitination of RIG-I or MDA5, and Parkin could

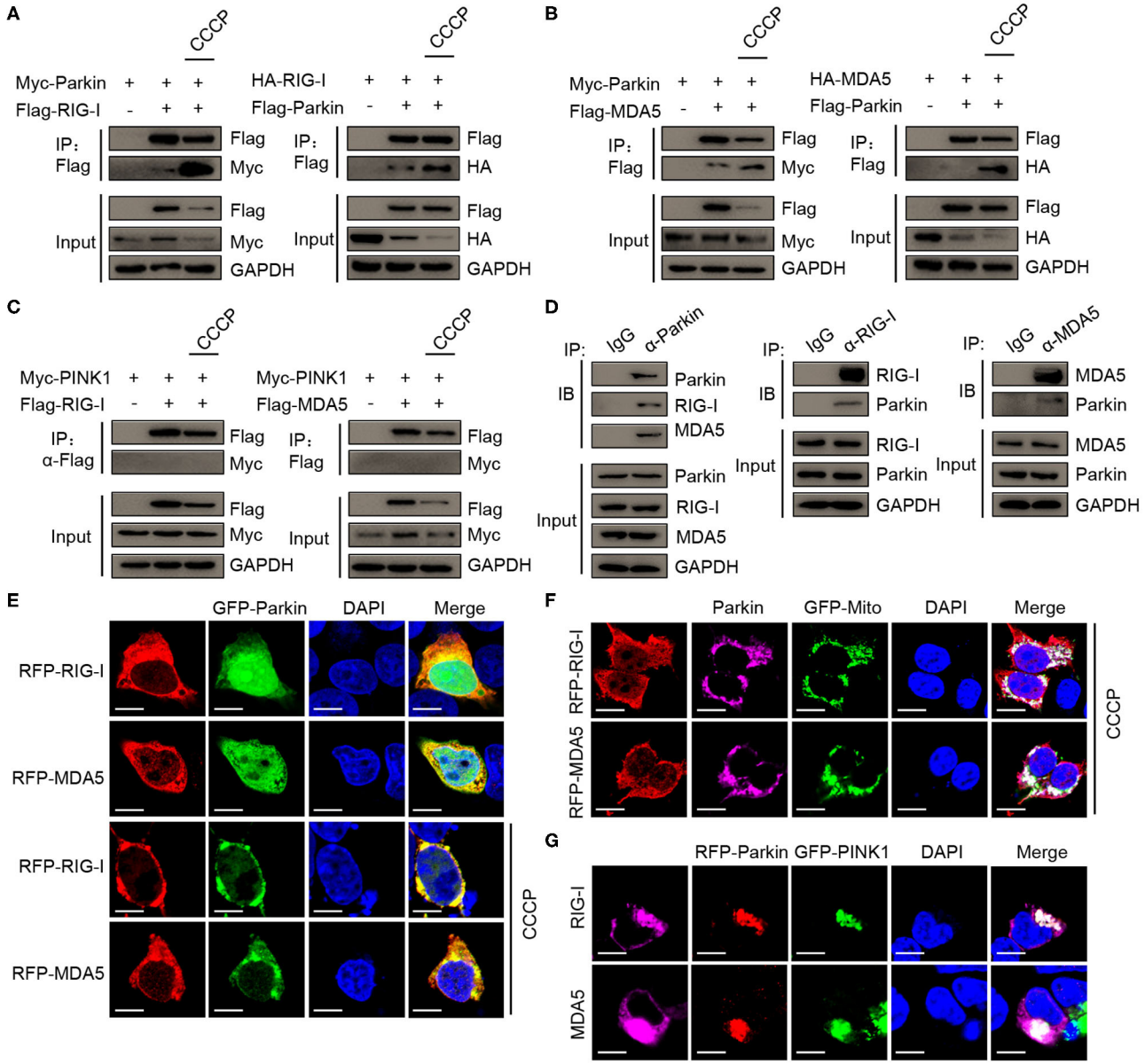

FIGURE 5 | CCCP promotes the interaction between Parkin and RIG-I or MDA5 on mitochondria. **(A)** 293T cells were co-transfected with Myc-Parkin and vector or Flag-RIG-I, or co-transfected with HA-RIG-I and vector or Flag-Parkin. 24 h post-transfection, untreated or treated with CCCP (10 μM) for 12 h, and then subjected to IP and IB analysis. **(B)** 293T cells were co-transfected with Myc-Parkin and vector or Flag-MDA5, or co-transfected with HA-MDA5 and vector or Flag-Parkin. 24 h post-transfection, untreated, or treated with CCCP (10 μM) for 12 h, and then subjected to IP and IB analysis. **(C)** 293T cells were co-transfected with Myc-PINK1 and vector, Flag-RIG-I, or Flag-MDA5. 24 h post-transfection, untreated or treated with CCCP (10 μM) for 12 h, and then subjected to IP and IB analysis. **(D)** HEK293 cells were stimulated with SeV for 10 h, and then whole cell lysates were collected, immunoprecipitated with indicated antibodies and subjected to IB analysis. **(E)** 293T cells were co-transfected with GFP-Parkin and RFP-RIG-I, or RFP-MDA5. 24 h post-transfection, untreated, or treated with CCCP (10 μM) for 6 h, and then subjected to IF analysis. Scale bar is 10 μm. **(F)** Parkin and GFP-Mito were co-transfected with RFP-RIG-I or RFP-MDA5 for 24 h in 293T cell, treated with CCCP (10 μM) for 6 h, and then subjected to IF analysis. Scale bar is 10 μm. **(G)** GFP-PINK1 and RFP-Parkin were co-transfected with RIG-I or MDA5 for 24 h in 293T cells, then subjected to IF analysis. Scale bar is 10 μm.

increase CCCP-mediated K48-Ubiquitination of RIG-I or MDA5 in the presence of MG-132 and BafA1 (**Figure 6B**). In addition, siRNA-mediated knockdown of Parkin substantially attenuated RIG-I or MDA5 polyubiquitination in 293T cells transfected with HA-Ubiquitin or HA-Ubiquitin-K48 in the presence of MG-132 and BafA1 (**Figures 6C,D**). In summary, our results depict the molecular mechanism that Parkin and CCCP promote K48-linked polyubiquitination of RIG-I and MDA5, and Parkin could increase the effect of CCCP.

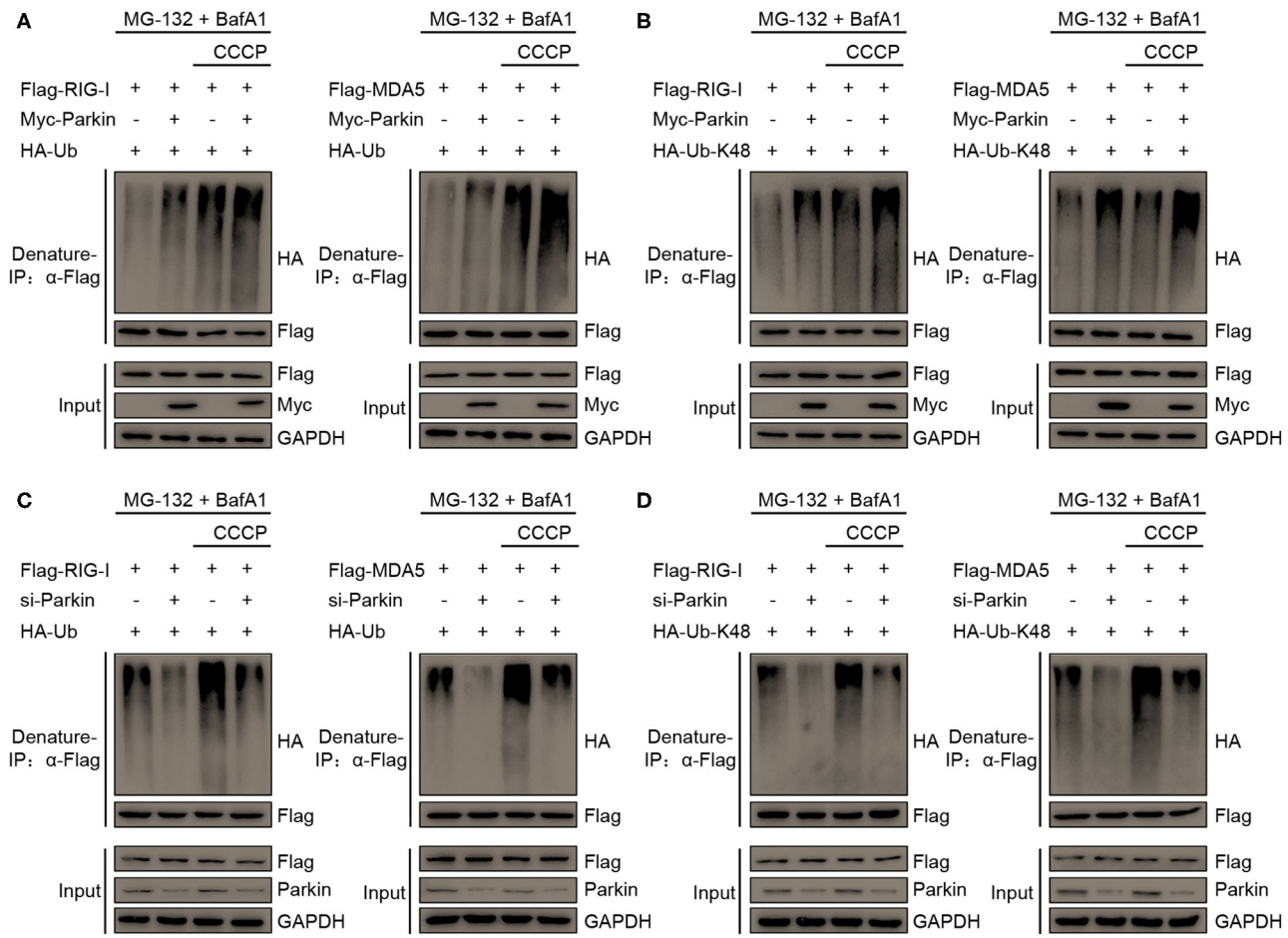

FIGURE 6 | Parkin catalyzes the K48-linked polyubiquitination of RIG-I and MDA5. **(A)** HA-Ubiquitin and Flag-RIG-I or Flag-MDA5 were co-transfected with vector or Myc-Parkin in 293T cells. 24 h post-transfection, untreated or treated with CCCP (10 μM) for 12 h in the presence of MG-132 (10 μM) and BafA1 (200 nM) at the last 8 h, and then subjected to denature-IP and IB analysis. **(B)** HA-Ubiquitin-K48 and Flag-RIG-I or Flag-MDA5 were co-transfected with vector or Myc-Parkin in 293T cells. 24 h post-transfection, untreated or treated with CCCP (10 μM) for 12 h in the presence of MG-132 (10 μM) and BafA1 (200 nM) at the last 8 h, and then subjected to denature-IP and IB analysis. **(C)** HA-Ubiquitin and Flag-RIG-I or Flag-MDA5 were co-transfected with si-control or si-Parkin in 293T cells. 48 h post-transfection, untreated or treated with CCCP (10 μM) for 12 h in the presence of MG-132 (10 μM) and BafA1 (200 nM) at the last 8 h, and then subjected to denature-IP and IB analysis. **(D)** HA-Ubiquitin-K48 and Flag-RIG-I or Flag-MDA5 were co-transfected with si-control or si-Parkin in 293T cells. 48 h post-transfection, untreated or treated with CCCP (10 μM) for 12 h in the presence of MG-132 (10 μM) and BafA1 (200 nM) at the last 8 h, and then subjected to denature-IP and IB analysis.

DISCUSSION

Evidence accumulated during the last few years has convincingly revealed that the immune system is excessively activated in the brains of patients with Parkinson's disease (34). Moreover, the latest researches show that Parkinson's disease may be related to the overactivation of patients' autoimmune response (35). There are a set of pro-inflammatory cytokines including IL-6, TNF, IL-1β, and IFN-γ in the serum of patients with Parkinson's disease (36). What's more, familial Parkinson's disease can be induced by the mutations of PINK1 and Parkin, which leads to mitophagy dysfunction. The dysfunction of mitophagy may excessively activate the immune system of Parkinson's disease (37). Here, we provided several lines of evidence to demonstrate that mitophagy induced by CCCP negatively regulates the innate antiviral immunity.

As a special autophagy pathway, mitophagy mediates the clearance of damaged mitochondria by lysosomes, which plays an important role in mitochondrial quality control (38). In addition, mitochondrial stress can lead to the release of damage-associated molecular patterns (DAMPs), which can activate innate immunity. Furthermore, mitochondrial DNA (mtDNA) can be recognized by the cGAS/STING-dependent DNA sensing pathway, which initiates the innate immunity (39). Mitochondrial double-stranded RNA engages an MDA5-driven antiviral signaling pathway that triggers the response of type I interferon (40). Mitochondrial apoptosis is mediated by BAK and BAX, which triggers the release of mitochondrial DNA, and

apoptotic caspases suppresses the production of type I interferon (41–43). Mitophagy is a form of selective autophagy, PINK1 and Parkin are the two key molecules in the regulation of mitophagy (28, 44). These studies suggest that PINK1 and Parkin mediated mitophagy can mitigate inflammation and autoimmune disease (36, 45, 46). When neurodegenerative diseases occur in the central nervous system, mitochondrial DNA can activate the innate immunity and cause neuroinflammation (47). Type I IFN contribute to the inflammatory response during normal aging and in age-related neurodegenerative disorders (48–51). In our study, we found that PINK1 and Parkin mediated mitophagy can inhibit the response and antiviral immunity of type I IFN, and these results may suggest that loss of functional PINK1 and Parkin may increase IFN production and drive the pathology of neurodegeneration.

Recognition of the RNA by endosomal and cytosolic sensors is a central element in the detection of virus by the innate immune system. The RNA sensors RIG-I and MDA5 recognize the dsRNA and activate the innate antiviral immunity subsequently (52). According to recent reports, polyubiquitination regulates the activation of RIG-I and MDA5 so as to avoid their sustained activation. It has been identified that several E3 ligases promote K48-linked ubiquitination of RIG-I and MDA5, including RNF125, Siglec-G, TRIM40, and STUB1 (53–56). Here, we demonstrate that Parkin served as a specific regulator of RIG-I-mediated and MDA5-mediated innate antiviral immunity through direct conjugation of K48-linked polyubiquitin chains to RIG-I and MDA5. Therefore, Parkin may inhibit the innate immunity by enhancing the degradation of RIG-I and MDA5.

In summary, we have identified an E3 ubiquitin ligase, Parkin, as a negative regulator of RIG-I and MDA5. Parkin interacted with RIG-I and MDA5, and then catalyzed the K48-linked polyubiquitination of RIG-I and MDA5, which facilitated the degradation of RIG-I and MDA5 and prevented excessive activation of innate antiviral immunity.

MATERIALS AND METHODS

Cell Culture and Viruses

293T, HEK293, Raw264.7, A549, and VERO cells were maintained in DMEM medium (Hyclone) supplemented with 10% heat-inactivated fetal bovine serum (FBS, Gibco) and cultured at 37°C in a 5% CO_2 incubator. BMDCs were isolated from mouse tibia and femur as described previously (57). THP-1 cells were maintained in 1640 medium (Hyclone) supplemented with 10% heat-inactivated fetal bovine serum (FBS, Gibco) and cultured at 37°C in a 5% CO_2 incubator. THP-1 cells were differentiated to macrophages for 48 h with 50 ng/ml phorbol myristate acetate (PMA). Sendai virus (SeV) and vesicular stomatitis virus (VSV) carrying a GFP reporter gene (VSV-GFP) were kindly provided by Dr Hong-Bing Shu.

Reagents and Antibodies

The chemical reagents used in this study were listed as follows: CCCP (C2759), MG-132 (M8699), PMA (P1585), and bafilomycin A1 (B1793) were purchased from Sigma. Anti-Parkin antibody (4211), anti-RIG-I (3743) antibody, anti-MDA5 (5321) antibody, anti-MAVS (24930) antibody, anti-pTBK1-Ser172 (5483) antibody, anti-TBK1 (38066) antibody, anti-pIRF3-Ser396 (29047) antibody, anti-IRF3 (11904) antibody, anti-TOM20 (42406) antibody, anti-HSPD1 (12165) antibody, and anti-GAPDH (5174) were purchased from Cell Signaling Technology. Mouse anti-HA antibody (H3663), rabbit anti-HA antibody (H6908), mouse anti-Myc antibody (SAB2702192), rabbit anti-Myc antibody (C3956), mouse anti-Flag antibody (F3165), and rabbit anti-Flag antibody (F7425) were purchased from Sigma. Anti-Flag M2 Affinity Gel (A2220) were purchased from Millipore. Goat anti-rabbit Alexa Fluor Plus 647 (A32733) were purchased from Invitrogen.

Plasmids

pEF-Flag-RIG-I, pEF-Flag-MDA5, pEF-Flag-MAVS, pEF-Flag-MDA5-N, pEF-Flag-RIG-I-N, pEF-Flag-TBK1, pEF-Flag-IKKε, pEF-Flag-IRF3, pEF-Flag-IRF3-5D, pRK-HA-RIG-I, and pRK-HA-MDA5 have described previously (58). pRK5-HA-Parkin (#17613) and pCMVTNT-PINK1-N-myc (#13313) were purchased from Addgene. pEF-Flag-Parkin, pEF-Myc-Parkin, pEF-Myc-PINK1, pRK-HA-PINK1, pEGFP-Parkin, pDs-Red-Parkin, pEGFP-PINK1, pDs-Red-MAVS, pDs-Red-RIG-I, and pDs-Red-MDA5 are constructed according to the manufacturer's standard procedures. GFP-Mito plasmid was purchased from Invitrogen (catalog number: V822-20). HA-Ub, HA-Ub-K48 have described previously (57).

RNA Interference Assay

Human Parkin-specific siRNA and control siRNA were obtained from Ribobio, the siRNA sequence used in this study are as following: si-Parkin 5′-GGAGUGCAGUGCCGUAUUU-3′. These siRNA duplexes were transfected into cells using RNAi MAX (Invitrogen) according to the manufacturer's protocol.

Quantitative Real-Time PCR

Total RNA was isolated from HEK293 or Raw264.7 cells using TRIzol reagent (Invitrogen) and then was reverse transcribed into cDNA using PrimeScript RT reagent kit with gDNA Eraser (Takara) according to the manufacturer's instructions. An ABI 7300 Detection System (Applied Biosystems) and a SYBR RT-PCR kit (Takara) were used to amplify the reverse-transcription products of different samples for quantitative RT-PCR analysis. The RT-PCR primer of Parkin is given as following: Parkin forward, 5′-GTGTTTGTCAGGTTCAACTCCA-3′ and Parkin reverse, 5′-GAAAATCACACGCAACTGGTC-3′. Other primer sequences were as reported in our previous work (58).

Luciferase Assay

HEK293 cells (2×10^5) were seeded on 24-well-plates and transfected with a mixture of renilla luciferase plasmid and IFN-β, ISRE, or NF-κB luciferase reporter plasmid together with indicated expression plasmids or empty control plasmid. After 24–36 h of transfection, luciferase activity was measured with a dual-luciferase reporter assay system according to the manufacturer's instructions (Promega). By calculating the ratio of firefly luciferase activity to renilla luciferase activity, data were normalized for transfection efficiency.

Flow Cytometry

HEK293 cells were seeded and transfected with plasmids or siRNA for 48 h, then infected with VSV-GFP for 2 h. Then cells were washed three times with PBS and added fresh medium for 24 h, cells were immediately analyzed by the flow cytometer (BD FACSAria III, BD).

VSV Plaque Assay

HEK293 cells were seeded and transfected with plasmids or siRNA for 48 h, then infected with VSV-GFP for 2 h. Then cells were washed three times with PBS and added fresh medium for 24 h, collected supernatants, and diluted to infect VERO cells seeded on 24-well-plates. Two hours later, supernatants were removed, and methylcellulose was added. Three days later, cells were stained with crystal violet (0.2%) overnight. The results were averaged and multiplied by the dilution factor to calculate the viral titer as PFU/ml.

Immunofluorescence (IF) Assay

293T cells (3×10^4) were seeded in chamber slides and transfected with plasmids for 24 h. Then the cells were fixed with 4% formaldehyde for 10 min and permeabilized with 0.1% Triton X-100 for 10 min. Then cells were blocked with 5% BSA for 30 min. The samples were incubated with primary antibodies overnight at 4°C. Next, cells were incubated with appropriate second antibodies for 1 h at 37°C, then conducted with 4,6-diamidino-2-phenylindole (DAPI) for 5 min. The confocal images were captured using Zeiss LSM780 microscope.

Immunoprecipitation (IP) and Immunoblotting (IB) Analysis

For immunoprecipitation experiments, 293T cells (5×10^6) were seeded on 10-cm dishes, then transfected with a total of 12 μg appropriate plasmids. After 24 h, cells were lysed with lysis buffer (50 mM Tris-HCl (pH 7.6), 150 mM NaCl, 10 mM NaF, 2 mM EGTA, 2 mM DTT, 1 mM Na_3VO_4, and 0.5% Triton-X-100 and 1× Cocktail). Then immunoprecipitated with 30 μL anti-Flag agarose (Millipore) at 4°C overnight. Beads were washed four times with RIPA buffer, and immunoprecipitates were eluted with 2× SDS loading buffer by boiling for 5 min and subjected to IB analysis. For immunoblotting experiments, cells were washed and lysed in RIPA buffer, cell extracts were centrifugated at 12,000 rpm for 10 min, then mixed with 5× SDS loading buffer and boiled for 5 min. Samples were resolved on 10% SDS-PAGE gels and subjected to western blotting that was performed according to the instructions as indicated.

In vivo Ubiquitination Assay

Whole cells were lysed with lysis buffer (100 μl) and the supernatants were denatured at 100°C for 5 min in the presence of 1% SDS by lysates. The denatured lysates were diluted with lysis buffer until the concentration of SDS was reduced < 0.1% followed by immunoprecipitation (denature-IP) with the indicated antibodies. The immunoprecipitants were subject to immunoblot analysis.

Statistical Analysis

The data were shown as the mean ± standard deviation (mean ± SD) from at least three independent experiments. The statistical significance of the difference between any two samples was evaluated by Student's *t*-test using GraphPad Prism for Windows version 5.0 (GraphPad Software, USA). The values of $p < 0.05$ were considered statistically significant.

DATA AVAILABILITY STATEMENT

All datasets generated for this study are included in the article/**Supplementary Material**.

AUTHOR CONTRIBUTIONS

DG, C-ML, and LB conceived and designed the experiments. LB carried out the experiments and analyzed data. HW, PH, SG, MH, JX, PL, YZ, PJ, YC, GL, and CY assisted with the experiments. LC assisted with experimental design. DG, LB, and HW wrote the manuscript. All authors commented on the manuscript.

FUNDING

This work was supported by the National Natural Science Foundation of China (grant #81620108020), Guangdong Zhujiang Talents Program (to DG), Shenzhen Science and Technology Program (Grant No. KQTD20180411143323605), and National Ten-thousand Talents Program (to DG).

ACKNOWLEDGMENTS

We thank Dr. Hong-Bing Shu (Wuhan University, China) for providing SeV and VSV.

SUPPLEMENTARY MATERIAL

The Supplementary Material for this article can be found online at: https://www.frontiersin.org/articles/10.3389/fimmu.2020.01926/full#supplementary-material

REFERENCES

1. Janeway CA Jr. Approaching the asymptote? Evolution and revolution in immunology. *Cold Spring Harb Symp Quant Biol.* (1989) 54(Pt 1):1–13. doi: 10.1101/SQB.1989.054.01.003
2. Honda K, Taniguchi T. IRFs: master regulators of signalling by Toll-like receptors and cytosolic pattern-recognition receptors. *Nat Rev Immunol.* (2006) 6:644–58. doi: 10.1038/nri1900
3. Inohara N, Chamaillard M, McDonald C, Nunez G. NOD-LRR proteins: role in host-microbial interactions and inflammatory disease. *Annu Rev Biochem.* (2005) 74:355–83. doi: 10.1146/annurev.biochem.74.082803.133347
4. Medzhitov R. Recognition of microorganisms and activation of the immune response. *Nature.* (2007) 449:819–26. doi: 10.1038/nature06246

5. Meylan E, Tschopp J, Karin M. Intracellular pattern recognition receptors in the host response. *Nature.* (2006) 442:39–44. doi: 10.1038/nature04946
6. Ting JP, Kastner DL, Hoffman HM. CATERPILLERs, pyrin and hereditary immunological disorders. *Nat Rev Immunol.* (2006) 6:183–95. doi: 10.1038/nri1788
7. Peisley A, Wu B, Yao H, Walz T, Hur S. RIG-I forms signaling-competent filaments in an ATP-dependent, ubiquitin-independent manner. *Mol Cell.* (2013) 51:573–83. doi: 10.1016/j.molcel.2013.07.024
8. Hou F, Sun L, Zheng H, Skaug B, Jiang QX, Chen ZJ. MAVS forms functional prion-like aggregates to activate and propagate antiviral innate immune response. *Cell.* (2011) 146:448–61. doi: 10.1016/j.cell.2011.06.041
9. Cui J, Zhu L, Xia X, Wang HY, Legras X, Hong J, et al. NLRC5 negatively regulates the NF-kappaB and type I interferon signaling pathways. *Cell.* (2010) 141:483–96. doi: 10.1016/j.cell.2010.03.040
10. Cai X, Chen ZJ. Prion-like polymerization as a signaling mechanism. *Trends Immunol.* (2014) 35:622–30. doi: 10.1016/j.it.2014.10.003
11. Youle RJ, Narendra DP. Mechanisms of mitophagy. *Nat Rev Mol Cell Biol.* (2011) 12:9–14. doi: 10.1038/nrm3028
12. Ashrafi G, Schwarz TL. The pathways of mitophagy for quality control and clearance of mitochondria. *Cell Death Differ.* (2013) 20:31–42. doi: 10.1038/cdd.2012.81
13. Xie X, Zhang D, Zhao B, Lu MK, You M, Condorelli G, et al. IkappaB kinase epsilon and TANK-binding kinase 1 activate AKT by direct phosphorylation. *Proc Natl Acad Sci U S A.* (2011) 108:6474–9. doi: 10.1073/pnas.1016132108
14. Whitworth AJ, Pallanck LJ. The PINK1/Parkin pathway: a mitochondrial quality control system? *J Bioenerg Biomembr.* (2009) 41:499–503. doi: 10.1007/s10863-009-9253-3
15. Kitada T, Asakawa S, Hattori N, Matsumine H, Yamamura Y, Minoshima S, et al. Mutations in the parkin gene cause autosomal recessive juvenile parkinsonism. *Nature.* (1998) 392:605–8. doi: 10.1038/33416
16. Valente EM, Abou-Sleiman PM, Caputo V, Muqit MM, Harvey K, Gispert S, et al. Hereditary early-onset Parkinson's disease caused by mutations in PINK1. *Science.* (2004) 304:1158–60. doi: 10.1126/science.1096284
17. Narendra DP, Youle RJ. Targeting mitochondrial dysfunction: role for PINK1 and Parkin in mitochondrial quality control. *Antioxid Redox Signal.* (2011) 14:1929–38. doi: 10.1089/ars.2010.3799
18. Jin SM, Lazarou M, Wang C, Kane LA, Narendra DP, Youle RJ. Mitochondrial membrane potential regulates PINK1 import and proteolytic destabilization by PARL. *J Cell Biol.* (2010) 191:933–42. doi: 10.1083/jcb.201008084
19. Yamano K, Youle RJ. PINK1 is degraded through the N-end rule pathway. *Autophagy.* (2013) 9:1758–69. doi: 10.4161/auto.24633
20. Villa E, Marchetti S, Ricci JE. No Parkin Zone: Mitophagy without Parkin. *Trends Cell Biol.* (2018) 28:882–95. doi: 10.1016/j.tcb.2018.07.004
21. Koyano F, Okatsu K, Kosako H, Tamura Y, Go E, Kimura M, et al. Ubiquitin is phosphorylated by PINK1 to activate parkin. *Nature.* (2014) 510:162–6. doi: 10.1038/nature13392
22. Kumar A, Aguirre JD, Condos TE, Martinez-Torres RJ, Chaugule VK, Toth R, et al. Disruption of the autoinhibited state primes the E3 ligase parkin for activation and catalysis. *EMBO J.* (2015) 34:2506–21. doi: 10.15252/embj.201592337
23. McLelland GL, Goiran T, Yi W, Dorval G, Chen CX, Lauinger ND, et al. Mfn2 ubiquitination by PINK1/parkin gates the p97-dependent release of ER from mitochondria to drive mitophagy. *Elife.* (2018) 7:e32866. doi: 10.7554/eLife.32866
24. Geisler S, Holmstrom KM, Skujat D, Fiesel FC, Rothfuss OC, Kahle PJ, et al. PINK1/Parkin-mediated mitophagy is dependent on VDAC1 and p62/SQSTM1. *Nat Cell Biol.* (2010) 12:119–31. doi: 10.1038/ncb2012
25. Kageyama Y, Hoshijima M, Seo K, Bedja D, Sysa-Shah P, Andrabi SA, et al. Parkin-independent mitophagy requires Drp1 and maintains the integrity of mammalian heart and brain. *EMBO J.* (2014) 33:2798–813. doi: 10.15252/embj.201488658
26. Wang L, Cho YL, Tang Y, Wang J, Park JE, Wu Y, et al. PTEN-L is a novel protein phosphatase for ubiquitin dephosphorylation to inhibit PINK1-Parkin-mediated mitophagy. *Cell Res.* (2018) 28:787–802. doi: 10.1038/s41422-018-0056-0
27. Matsumoto G, Wada K, Okuno M, Kurosawa M, Nukina N. Serine 403 phosphorylation of p62/SQSTM1 regulates selective autophagic clearance of ubiquitinated proteins. *Mol Cell.* (2011) 44:279–89. doi: 10.1016/j.molcel.2011.07.039
28. Harper JW, Ordureau A, Heo JM. Building and decoding ubiquitin chains for mitophagy. *Nat Rev Mol Cell Biol.* (2018) 19:93–108. doi: 10.1038/nrm.2017.129
29. Tsuboyama K, Koyama-Honda I, Sakamaki Y, Koike M, Morishita H, Mizushima N. The ATG conjugation systems are important for degradation of the inner autophagosomal membrane. *Science.* (2016) 354:1036–41. doi: 10.1126/science.aaf6136
30. Gkikas I, Palikaras K, Tavernarakis N. The role of mitophagy in innate immunity. *Front Immunol.* (2018) 9:1283. doi: 10.3389/fimmu.2018.01283
31. Zhou J, Yang R, Zhang Z, Liu Q, Zhang Y, Wang Q, et al. Mitochondrial protein PINK1 positively regulates RLR signaling. *Front Immunol.* (2019) 10:1069. doi: 10.3389/fimmu.2019.01069
32. Ding B, Zhang L, Li Z, Zhong Y, Tang Q, Qin Y, et al. The matrix protein of human parainfluenza virus type 3 induces mitophagy that suppresses interferon responses. *Cell Host Microbe.* (2017) 21:538–47.e4. doi: 10.1016/j.chom.2017.03.004
33. Khan M, Syed GH, Kim SJ, Siddiqui A. Hepatitis B virus-induced parkin-dependent recruitment of linear ubiquitin assembly complex (LUBAC) to mitochondria and attenuation of innate immunity. *PLoS Pathog.* (2016) 12:e1005693. doi: 10.1371/journal.ppat.1005693
34. Grozdanov V, Bousset L, Hoffmeister M, Bliederhaeuser C, Meier C, Madiona K, et al. Increased immune activation by pathologic alpha-synuclein in Parkinson's disease. *Ann Neurol.* (2019) 86:593–606. doi: 10.1002/ana.25557
35. Matheoud D, Sugiura A, Bellemare-Pelletier A, Laplante A, Rondeau C, Chemali M, et al. Parkinson's disease-related proteins PINK1 and parkin repress mitochondrial antigen presentation. *Cell.* (2016) 166:314–27. doi: 10.1016/j.cell.2016.05.039
36. Sliter DA, Martinez J, Hao L, Chen X, Sun N, Fischer TD, et al. Parkin and PINK1 mitigate STING-induced inflammation. *Nature.* (2018) 561:258–62. doi: 10.1038/s41586-018-0448-9
37. Heo JM, Ordureau A, Paulo JA, Rinehart J, Harper JW. The PINK1-PARKIN mitochondrial ubiquitylation pathway drives a program of OPTN/NDP52 recruitment and TBK1 activation to promote mitophagy. *Mol Cell.* (2015) 60:7–20. doi: 10.1016/j.molcel.2015.08.016
38. Bingol B, Tea JS, Phu L, Reichelt M, Bakalarski CE, Song Q, et al. The mitochondrial deubiquitinase USP30 opposes parkin-mediated mitophagy. *Nature.* (2014) 510:370–5. doi: 10.1038/nature13418
39. West AP, Khoury-Hanold W, Staron M, Tal MC, Pineda CM, Lang SM, et al. Mitochondrial DNA stress primes the antiviral innate immune response. *Nature.* (2015) 520:553–7. doi: 10.1038/nature14156
40. Dhir A, Dhir S, Borowski LS, Jimenez L, Teitell M, Rotig A, et al. Mitochondrial double-stranded RNA triggers antiviral signalling in humans. *Nature.* (2018) 560:238–42. doi: 10.1038/s41586-018-0363-0
41. Rongvaux A, Jackson R, Harman CC, Li T, West AP, de Zoete MR, et al. Apoptotic caspases prevent the induction of type I interferons by mitochondrial DNA. *Cell.* (2014) 159:1563–77. doi: 10.1016/j.cell.2014.11.037
42. White MJ, McArthur K, Metcalf D, Lane RM, Cambier JC, Herold MJ, et al. Apoptotic caspases suppress mtDNA-induced STING-mediated type I IFN production. *Cell.* (2014) 159:1549–62. doi: 10.1016/j.cell.2014.11.036
43. McArthur K, Whitehead LW, Heddleston JM, Li L, Padman BS, Oorschot V, et al. BAK/BAX macropores facilitate mitochondrial herniation and mtDNA efflux during apoptosis. *Science.* (2018) 359:eaao6047. doi: 10.1126/science.aao6047
44. Lazarou M, Sliter DA, Kane LA, Sarraf SA, Wang C, Burman JL, et al. The ubiquitin kinase PINK1 recruits autophagy receptors to induce mitophagy. *Nature.* (2015) 524:309–14. doi: 10.1038/nature14893
45. Xu Y, Shen J, Ran Z. Emerging views of mitophagy in immunity and autoimmune diseases. *Autophagy.* (2020) 16:3–17. doi: 10.1080/15548627.2019.1603547
46. Cho DH, Kim JK, Jo EK. Mitophagy and innate immunity in infection. *Mol Cells.* (2020) 43:10–22. doi: 10.14348/molcells.2020.2329
47. Chin AC. Neuroinflammation and the cGAS-STING pathway. *J Neurophysiol.* (2019) 121:1087–91. doi: 10.1152/jn.00848.2018
48. Barrett JP, Henry RJ, Shirey KA, Doran SJ, Makarevich OD, Ritzel RM, et al. Interferon-beta plays a detrimental role in experimental traumatic brain injury by enhancing neuroinflammation that

drives chronic neurodegeneration. *J Neurosci.* (2020) 40:2357–70. doi: 10.1523/JNEUROSCI.2516-19.2020
49. Baruch K, Deczkowska A, David E, Castellano JM, Miller O, Kertser A, et al. Aging-induced type I interferon response at the choroid plexus negatively affects brain function. *Science.* (2014) 346:89–93. doi: 10.1126/science.1252945
50. Taylor JM, Minter MR, Newman AG, Zhang M, Adlard PA, Crack PJ. Type-1 interferon signaling mediates neuro-inflammatory events in models of Alzheimer's disease. *Neurobiol Aging.* (2014) 35:1012–23. doi: 10.1016/j.neurobiolaging.2013.10.089
51. Roy ER, Wang B, Wan YW, Chiu G, Cole A, Yin Z, et al. Type I interferon response drives neuroinflammation and synapse loss in Alzheimer disease. *J Clin Invest.* (2020) 130:1912–30. doi: 10.1172/JCI133737
52. Yoneyama M, Fujita T. Structural mechanism of RNA recognition by the RIG-I-like receptors. *Immunity.* (2008) 29:178–81. doi: 10.1016/j.immuni.2008.07.009
53. Arimoto K, Takahashi H, Hishiki T, Konishi H, Fujita T, Shimotohno K. Negative regulation of the RIG-I signaling by the ubiquitin ligase RNF125. *Proc Natl Acad Sci U S A.* (2007) 104:7500–5. doi: 10.1073/pnas.0611551104
54. Chen W, Han C, Xie B, Hu X, Yu Q, Shi L, et al. Induction of Siglec-G by RNA viruses inhibits the innate immune response by promoting RIG-I degradation. *Cell.* (2013) 152:467–78. doi: 10.1016/j.cell.2013.01.011
55. Zhao C, Jia M, Song H, Yu Z, Wang W, Li Q, et al. The E3 ubiquitin ligase TRIM40 attenuates antiviral immune responses by targeting MDA5 and RIG-I. *Cell Rep.* (2017) 21:1613–23. doi: 10.1016/j.celrep.2017.10.020
56. Zhou P, Ding X, Wan X, Liu L, Yuan X, Zhang W, et al. MLL5 suppresses antiviral innate immune response by facilitating STUB1-mediated RIG-I degradation. *Nat Commun.* (2018) 9:1243. doi: 10.1038/s41467-018-03563-8
57. Ma Y, Yuan S, Tian X, Lin S, Wei S, Hu T, et al. ABIN1 inhibits HDAC1 ubiquitination and protects it from both proteasome- and lysozyme-dependent degradation. *J Cell Biochem.* (2018) 119:3030–43. doi: 10.1002/jcb.26428
58. Li S, Zhu M, Pan R, Fang T, Cao YY, Chen S, et al. The tumor suppressor PTEN has a critical role in antiviral innate immunity. *Nat Immunol.* (2016) 17:241–9. doi: 10.1038/ni.3311

Conflict of Interest: The authors declare that the research was conducted in the absence of any commercial or financial relationships that could be construed as a potential conflict of interest.

frontiers in Immunology

ORIGINAL RESEARCH
published: 25 September 2020
doi: 10.3389/fimmu.2020.550145

The Effect of Rev-erbα Agonist SR9011 on the Immune Response and Cell Metabolism of Microglia

Samantha E. C. Wolff[1,2,3], Xiao-Lan Wang[1,2,4], Han Jiao[3], Jia Sun[3], Andries Kalsbeek[1,2,5], Chun-Xia Yi[1,2,5] and Yuanqing Gao[3]**

[1] Department of Endocrinology and Metabolism, Amsterdam University Medical Centers, University of Amsterdam, Amsterdam, Netherlands, [2] Laboratory of Endocrinology, Amsterdam University Medical Centers, Amsterdam Gastroenterology & Metabolism, University of Amsterdam, Amsterdam, Netherlands, [3] Key Laboratory of Cardiovascular and Cerebrovascular Medicine, School of Pharmacy, Nanjing Medical University, Nanjing, China, [4] Laboratoire de Neuroscience Cognitives et Adaptatives, Université de Strasbourg, Strasbourg, France, [5] Netherlands Institute for Neuroscience, Royal Netherlands Academy of Arts and Sciences, Amsterdam, Netherlands

OPEN ACCESS

Edited by:
Pedro Manoel Mendes Moraes Vieira, Campinas State University, Brazil

Reviewed by:
Jennifer Lee, Beth Israel Deaconess Medical Center and Harvard Medical School, United States
Huatao Chen, Northwest A&F University, China

***Correspondence:**
Yuanqing Gao
yuanqinggao@njmu.edu.cn
Chun-Xia Yi
c.yi@amsterdamumc.nl; c.yi@amc.uva.nl

Specialty section:
This article was submitted to Inflammation, a section of the journal Frontiers in Immunology

Received: *09 April 2020*
Accepted: *04 September 2020*
Published: *25 September 2020*

Citation:
Wolff SEC, Wang X-L, Jiao H, Sun J, Kalsbeek A, Yi C-X and Gao Y (2020) The Effect of Rev-erbα Agonist SR9011 on the Immune Response and Cell Metabolism of Microglia. Front. Immunol. 11:550145. doi: 10.3389/fimmu.2020.550145

Microglia are the immune cells of the brain. Hyperactivation of microglia contributes to the pathology of metabolic and neuroinflammatory diseases. Evidence has emerged that links the circadian clock, cellular metabolism, and immune activity in microglia. Rev-erb nuclear receptors are known for their regulatory role in both the molecular clock and cell metabolism, and have recently been found to play an important role in neuroinflammation. The Rev-erbα agonist SR9011 disrupts circadian rhythm by altering intracellular clock machinery. However, the exact role of Rev-erbα in microglial immunometabolism remains to be elucidated. In the current study, we explored whether SR9011 also had such a detrimental impact on microglial immunometabolic functions. Primary microglia were isolated from 1–3 days old Sprague-Dawley rat pups. The expression of clock genes, cytokines and metabolic genes was evaluated using RT-PCR and rhythmic expression was analyzed. Phagocytic activity was determined by the uptake capacity of fluorescent microspheres. Mitochondria function was evaluated by measuring oxygen consumption rate and extracellular acidification rate. We found that key cytokines and metabolic genes are rhythmically expressed in microglia. SR9011 disturbed rhythmic expression of clock genes in microglia. Pro-inflammatory cytokine expression was attenuated by SR9011 during an immune challenge by TNFα, while expression of the anti-inflammatory cytokine *Il10* was stimulated. Moreover, SR9011 decreased phagocytic activity, mitochondrial respiration, ATP production, and metabolic gene expression. Our study highlights the link between the intrinsic clock and immunometabolism of microglia. We show that Rev-erbα is implicated in both metabolic homeostasis and the inflammatory responses in microglia, which has important implications for the treatment of metabolic and neuroinflammatory diseases.

Keywords: clock genes, Innate immunity, microglia, immunometabolism, neuroinflammation, cytokines, phagocytosis

INTRODUCTION

The circadian brain clock orchestrates physiological and metabolic processes to prepare the body for environmental changes and to optimize energy metabolism (1). Cells in peripheral tissues, including metabolic tissues such as liver, pancreas, and kidney, also display rhythms in activity that are regulated by an intrinsic clock machinery. Since metabolic events are tightly regulated by the circadian clock, disruptions of the circadian timing system can result in metabolic dysfunctions and contribute to obesity and type 2 diabetes (2–10). Thus, the intracellular clock system is tightly involved in the control of metabolic rhythms that are essential for metabolic homeostasis.

The nuclear receptor reverse viral erythroblastosis oncogene product alpha (Rev-erbα) plays a crucial role in both the molecular clock of the circadian timing system and the regulation of metabolism. Rev-erbα stabilizes circadian rhythms by inhibiting the expression of the core clock genes brain and muscle ARNT-Like 1 (*Bmal1)* and circadian locomotor output cycles kaput (*Clock*) (11–13). The known endogenous ligand of Rev-erbα is heme, which plays an important role in mitochondrial respiration, and is required for the repressive activity of Rev-erbα/β on target genes (14–17). Additionally, nuclear receptors are sensors for dietary lipids and lipid-soluble hormones, thus rhythmic expression of Rev-erbα/β is also involved in regulating metabolic processes in a circadian manner (18, 19). Intriguingly, a recent Rev-erbα knock-out study proposed an important role for Rev-erbα in regulating neuroinflammation (20). In previous research, Rev-erbα agonists (GSK4112 and SR9011), and antagonists (SR8278) have provided us with insights about the function of Rev-erbα (21–24). For example, systemic administration of the Rev-erbα agonist SR9011 altered clock genes expression and disrupted the circadian behavior of mice leading to loss of locomotor activity during the active phase (dark phase), while vehicle administration caused no disruption (23). These results show that Rev-erb nuclear receptors have profound effects on circadian rhythm, metabolism and neuroinflammation, and possibly are eligible targets for treating metabolic diseases.

Recent research has demonstrated that a high fat, high sugar diet is associated with chronic activation of microglia, also known as microgliosis, which contributes to disturbed energy homeostasis and diet-induced obesity (DIO) (25–29). Additionally, our group recently reported that microglia activity shows a clear day/night rhythm when animals are fed a regular diet, but this rhythm is disrupted in DIO (30, 31). These findings suggest that the daily microglial rhythm is important for its normal activity and disturbance may result in metabolic diseases. However, little is known about the mechanism behind the intrinsic clock and the function of microglia. There is also a complex interplay between metabolic processes and immune responses, known as immunometabolism, in which metabolic reprogramming underlies the inflammatory state of microglia (32, 33). Therefore, considering the important role of Rev-erbα in the molecular clock machinery, neuroinflammation, and metabolism, in the current study we used the Rev-erbα agonist SR9011 to investigate the role of Rev-erbα in microglial immunometabolism.

MATERIALS AND METHODS

Primary Microglia Culture

Primary microglia cultures were prepared from brains of newborn, male Sprague Dawley rat pups (1–3 days old; Nanjing Medical University, China). After removal of the meninges, the brains were dissected and homogenized. Tissue lysates were centrifuged and suspended in Dulbecco's modified Eagle's medium (DMEM; Gibco, United States; C11885500BT) containing 1 *g*/L D-Glucose, L-Glutamine, 110 mg/L sodium pyruvate, and supplemented with 10% Fetal Bovine Serum (FBS; Gibco, United States; 10099141) and 1% Penicillin/Streptomycin (Gibco, United States; 15140122). Mixed glia cells were plated at a density of one brain per T75 flask or three brains per T175 flask, and incubated at 37°C in a humid atmosphere with 5% CO2. Culture medium was refreshed every 3 days. After the astrocyte layer reached confluency (8–14 days), the microglial cells were collected by shaking the flasks 150 rpm/min for 1 h at 37°C. Cells were seeded in 96-well plates (30k–50k cells/well) for the 3-(4,5-dimethylthiazol-2-yl)-5-(3-carboxymethoxyphenyl)-2-(4-sulfophenyl)-2H-tetrazolium (MTS) assay, 12-well plates (250k–300k cells/well) for qPCR experiments, or coverslipped in a 24-well plate (100k–150k cells/well) for phagocytosis experiments, or the Seahorse XF96 Cell Culture Microplate (Agilent, United States; 50k cells/well) for Seahorse experiments. For palmitic acid study, the palmitic – BSA solution was prepared 5:1 molar ratio palmitate: BSA in Krebs ringer buffer. All plates were coated with poly-L-lysine hydrobromide (MDBio, China). Dexamethasone (Sigma-Aldrich, United States; D4902), SR9011 (Sigma-Aldrich, United States; SML2067), DMSO (MDBio, China; D015), Fatty acids free BSA (Sigma A7030), Sodium Palmitate (Sigma-Aldrich, United States; P9767), TNFα (Peprotech, United States; 315-01A), and 0.1% BSA (Beyotime, China; ST023) were used to treat the cells during the experiments.

Cell Viability Assay

Cell viability was determined with the CellTiter 96 Aqueous assay (Promega, United States; G3582). Cells were treated with dexamethasone for 2 h, followed by a 24-h treatment with 5 μM SR9011 (or DMSO for control). Afterward, MTS solution was added followed by incubation for 3 h at 37°C, and the absorbance at 490 nm was measured on a SpectraMax M2 microplate reader (Molecular Devices).

Real-Time PCR

For gene expression analysis, total RNA was extracted from primary microglia using the RNAeasy^{TM} kit (Beyotime, China; R0026) according to the manufacturer's protocol. RNA concentration was measured with the NanoDrop Onec Spectrophotometer (Thermo Scientific, United States) and reverse transcribed into cDNA using the HiScript II qRT Supermix (Vazyme Biotech; R222-01). Gene expression levels of *Bmal1, Clock, Nr1d1 (Rev-erbα), Per2, Cry1, Il1*β*, Il4 Il6,*

Il10, Tnfα, Ccl2, Gm-csf, Tgfβ, CD36, CD68, Cpt1, Pdk1, Hk2, Fasn, Glut5, and *Hprt* (housekeeping gene; see **Supplementary Table 1** for primer sequences) were measured using real-time quantitative PCR on a QuantStudio 5 (Applied Biosystems Thermo Scientific), using the AceQ qPCR SYBR Green Master Mix (Vazyme Biotech; Q131-02). Gene expression levels were normalized to the housekeeping gene. Primers were designed using the Basic Local Alignment Search Tool (BLAST) from the National Center for Biotechnology Information (NCBI) and purchased from GeneRay Biotech.

Phagocytosis Assay

After treatment with SR9011 or DMSO for 12 h, microglia were incubated with 0.05% fluorescent latex microspheres (Sigma, United States; L1030-1 ml) in DMEM containing 0.25% FBS for 1 h. Subsequently, the cells were fixed with 4% paraformaldehyde for 30 min and a fluorescence staining of microglia was performed with Rabbit Anti-Iba1 (Wako, Japan; 019-19741) and the nuclei were counterstained with 4',6-diamidino-2-phenylindole (DAPI; Bioprox, France). Images were captured with an Olympus BX53F microscope equipped with an Olympus U-HGLGPS light source, and analyzed with ImageJ software (version 1.48). The relative fluorescent intensity of the beads was determined by dividing the total fluorescent intensity of the beads by the number of DAPI-stained nuclei.

Cellular Bioenergetics

Microglia were treated with 5 μM SR9011 or DMSO for 4 h prior to placement in the Seahorse XFe96 Analyzer (Agilent, United States). During the run, oxygen consumption rate (OCR), and extracellular acidification rate (ECAR) were measured and the wells were injected with modulators from the Agilent Seahorse XF Mito Stress Kit to determine parameters of mitochondrial function. After measuring basal levels of OCR and ECAR, oligomycin was injected to block ATP synthase, which decreases mitochondrial respiration. The second injection was carbonyl cyanide-4 (trifluoromethoxy) phenylhydrazone (FCCP), which disrupts the mitochondrial membrane potential and maximizes oxygen consumption. The third injection was a mixture of rotenone and antimycin A, which block complex I and III (respectively) and shut down mitochondrial respiration. Lastly, 2-deoxy-D-glucose (2-DG) was added to inhibit glycolysis, leading to a decrease in ECAR. Cellular respiration, mitochondrial respiration, cellular acidification, maximum substrate utilization, and maximum glycolytic capacity were calculated as previously described (34). ATP production was calculated from mitochondrial respiration by using a phosphate/oxygen ratio of 2.3 (35). After the measurements, cells were fixed with 4% paraformaldehyde and attached cells were quantified using a crystal violet assay by measuring absorbance at 590 nm with a SpectraMax M2 microplate reader (Molecular Devices). Data obtained from the Seahorse XF96 Analyzer was normalized to cell quantity per well.

Statistical Analyses

All results are expressed as mean ± SEM. Statistical analysis was performed using Graph-Pad PRISM (version 7.00), ImageJ software (version 1.48), and JTK_Cycle software (36). Two-way ANOVA and Bonferroni's *post hoc* test was used to assess the SR9011 effects on clock genes within 24 h after synchronization. Unpaired *t*-tests were used to evaluate the differences between DMSO and SR9011 groups in the rest of the study. ImageJ software was used for the analysis of phagocytosis assays. JTK_Cycle software (36) was used to identify rhythmic components in circadian PCR data.

RESULTS

Rhythmic Expression of Cytokines and Metabolic Genes in Microglia

The intrinsic clock machinery is present in microglia with clock genes being rhythmically expressed (30, 37). It has been well documented that cytokines and metabolic genes exhibit rhythmic expression (23, 38). To confirm whether cytokines and metabolic genes were also temporally regulated in primary microglia, we investigated the expression of three key pro-inflammatory cytokines – interleukin-1 beta (*Il1*β), interleukin-6 (*Il6*), and tumor necrosis factor-alpha (*Tnf*α), as well as three important metabolic genes – carnitine palmitoyltransferase 1 (*Cpt1*), hexokinase 2 (*Hk2*), and pyruvate dehydrogenase kinase 1 (*Pdk1*). Primary microglia were synchronized by 10 nM dexamethasone for 2 h as reported before (39) and cultured for 0, 6, 12, 18, or 24 h before being harvested. Gene expression of the cytokines and metabolic genes was determined over these time points [time post-synchronization, from now on referred to as "Time (T)" in hours] and rhythmicity was analyzed by JTK_Cycle software (**Figure 1**). *Tnfα, Il6, Pdk1,* and *Cpt1* showed a clear rhythmic expression, while *Il1*β and *Hk2* were not rhythmically expressed (**Figure 1**). The acrophase of the curves was estimated at T6, for *Il6, Pdk1* and *Cpt1*, and T12 for *Tnf*α. These data show that *Il6, Tnfα, Pdk1,* and *Cpt1* expression are likely orchestrated by the circadian timing system in primary microglia.

SR9011 Disrupts Clock Gene Rhythmicity in Microglia

We first determined whether SR9011 enhances Rev-erbα activity and disrupts the clock machinery in primary microglia. For this, we performed a dose-response study with 1, 5, 10, and 50 μM SR9011 (data not shown) and decided to use 5 μM for this study. To test the efficiency of SR9011, we first analyzed the effects of SR9011 on Rev-erb targets *Serpine1*, *Cyp7a1*, and *Srebf1* and found significant reductions in their expression compared to control, which confirms that SR9011 acts through Rev-erb (**Supplementary Figure 1**). When using SR9011 as a pretreatment before synchronization with dexamethasone, we found that the effect of SR9011 pretreatment did not persist after removing SR9011 from the culture (**Supplementary Figure 2** and **Supplementary Table 2**), contrary to the result from Nakazato et al. (39). Therefore, the following design was used in this study: primary rat microglia were exposed to dexamethasone for 2 h to synchronize the cells, followed by treatment with

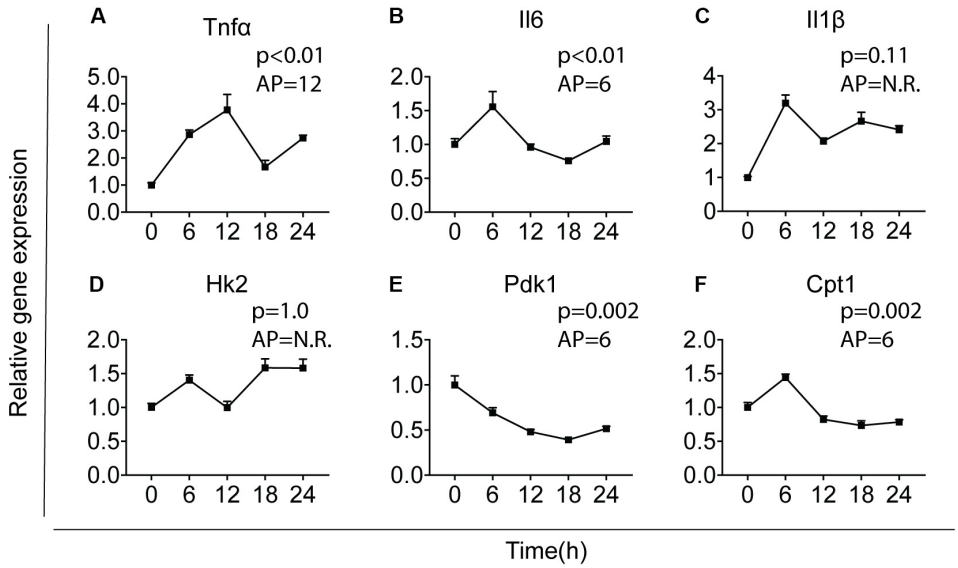

FIGURE 1 | Major cytokines and metabolic genes are rhythmically expressed in microglia. Relative gene expression of major cytokines and metabolic genes was measured in primary microglia. After synchronization by dexamethasone for 2 h, cells were cultured and harvested at the indicated post-synchronization time points (T; $n = 6$ per group, per time point). Rhythmic expression is signified by a p-value of less than 0.05 and can be found for *Tnf* **(A)**, *Il6* **(B)**, *Pdk1* **(E)**, and *Cpt1* **(F)**. The expression of *Il1* **(C)** and *Hk2* **(D)** was not rhythmic. The acrophase of the curve is not relevant (N.R.) if data does not fit a curve. Data are presented as means ± SEM and statistical significance was determined using JTK_Cycle software.

5 μm SR9011 or DMSO for 0, 6, 12, 18, or 24 h. Rhythmic expression of *Bmal1*, *Clock*, period 2 (*Per2),* cryptochrome 1 (*Cry1),* period 1 (*Per1)* and nuclear receptor subfamily 1 group d member 1 (*Nr1d1* or *Rev-erb*α) was found in primary microglia treated with DMSO, as evaluated with Two-way ANOVA (**Table 1**) and JTK_Cycle Software (**Figure 2** and **Table 2**). SR9011 exerted an inhibitory effect on *Bmal1* and *Per2* expression, as analyzed by Two way ANOVA (**Table 1**). An interactive effect of SR9011 and Time was found on *Bmal1*, *Clock*, and *Nr1d1* (=*Rev-erb*α, see **Table 1**). The impact of SR9011 at each time point was analyzed by multiple comparison (**Figures 2A–F**). Notably, SR9011 disrupted the rhythmic expression of *Bmal1* and *Clock*, and caused a shift in the acrophase of *Per2* rhythm, as analyzed by JTK_Cycle (**Table 2**). SR9011 in combination with dexamethasone had no impact on cell viability (**Figure 2G**), indicating that a decrease in gene expression could not be attributed to cell death. These results show that SR9011 disrupted the rhythm of clock gene expression, pertaining to both amplitude and phase depending on the clock gene, which means that rhythmic expression of clock gene expression became non-rhythmic after adding SR9011. SR9011 had the strongest impact on *Bmal1* and *Clock*, while the effect on *Per2* and *Cry1* was less potent. This is probably due to the direct inhibitory effect of Rev-erbα on the BMAL1 and CLOCK complex, which indirectly influences *Per2* and *Cry1* expression.

TABLE 1 | Two-way ANOVA assessment of effect of Time, SR9011, and Interaction in clock genes in primary microglia with SR9011.

Genes	Two-way ANOVA analysis		
	p-value		
	Interaction	**Time**	**SR9011**
Bmal1	**0.0195**	**<0.0001**	**0.0370**
Clock	**0.0251**	**<0.0001**	0.0659
Cry1	0.1234	**<0.0001**	0.0907
Per1	0.5030	**<0.0001**	0.3939
Per2	0.0648	**<0.0001**	**0.0489**
Nr1d1	**0.0003**	**<0.0001**	0.4462

SR9011, Time and Interaction effects were evaluated in primary microglia for clock genes after treated with DMSO or SR9011. SR9011 has significant impact on Bmal1 and Per2, and has interaction effect with time on Bmal1, Clock, and Nr1d1.

SR9011 Alters Cytokine Expression in Microglia

Cytokine secretion constitutes an essential part of microglial immune function. Rev-erbα has very recently been reported to regulate neuroinflammation (20). To evaluate the role of Rev-erbα in regulating cytokine expression, we stimulated the cells with TNFα to resemble an immune challenge and analyzed the effect of SR9011. Primary microglia were exposed to 5 μM SR9011 (or DMSO for control) for 12 h, followed by 100 ng/ml TNFα treatment (or BSA for control) for 12 h in combination with SR9011 or DMSO. TNFα significantly increased the expression of the pro-inflammatory cytokines tumor necrosis factor-alpha (*Tnfα)*, interleukin-6 (*Il6)*, interleukin-1 beta (*Il1*β), and C-C Motif Chemokine Ligand (*Ccl2*; **Figures 3A–E**). TNFα also significantly increased the regulatory cytokine granulocyte-macrophage colony-stimulating factor (*Gm-csf*; **Figure 3F**). In all

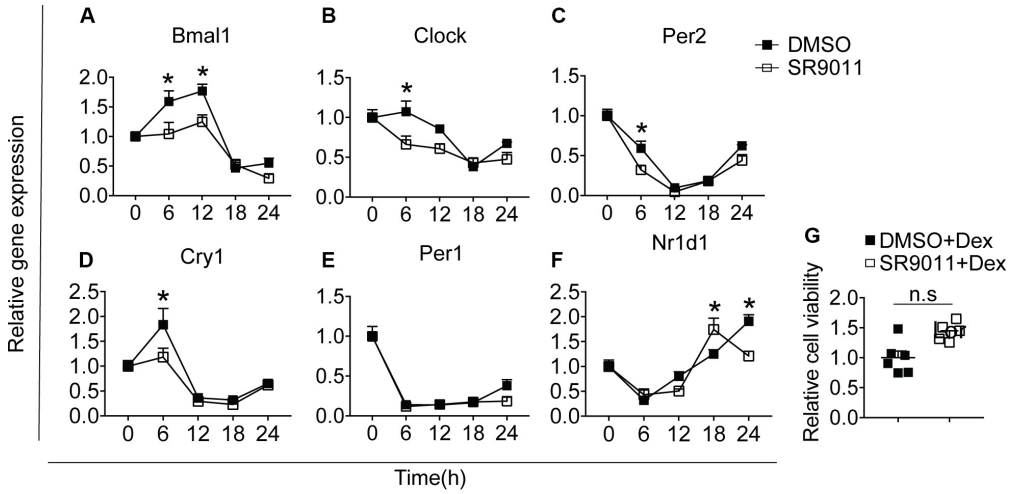

FIGURE 2 | SR9011 disrupts clock gene expression in microglia. Rhythmic and relative gene expression of clock genes in primary microglia. Cells were treated with dexamethasone for 2 h followed by SR9011 or DMSO and were harvested at the indicated time points (n = 4 per group, per time point). **(A–F)** Clock gene expression is altered by SR9011 treatment compared to DMSO (control). SR9011 disrupted the rhythmic expression of *Bmal1* and *Clock*, and caused a shift in the acrophase of *Per2* rhythm, as analyzed by JTK_Cycle. **(G)** Cell viability of primary microglia was not affected by the 24-h SR9011 treatment with dexamethasone. Data are presented as means ± SEM. $p < 0.05$* vs. DMSO group was determined using Two-way ANOVA followed by Bonferroni's *post hoc* test and multiple comparison.

cases, the increase in gene expression by TNFα treatment was attenuated after treatment with SR9011. Different results were found for anti-inflammatory cytokines. TNFα had no effect on the regulatory cytokine transforming growth factor-beta (*Tgf*β) expression, however, SR9011 treatment decreased *Tgf*β expression (**Figure 3G**). No changes were found in interleukin-4 (*Il4)* expression (**Figure 3H**). Interestingly, while TNFα had no effect on the expression of anti-inflammatory cytokine interleukin-10 (*Il10)*, SR9011 stimulated the expression of *Il10* (**Figure 3I**). These results suggest that SR9011 attenuates the pro-inflammatory response in primary microglia in the context of an immune challenge, while stimulating the expression of the anti-inflammatory cytokine *Il10*.

SR9011 Attenuated Palmitic Acid Induced Inflammatory Response in Microglia

To further test whether SR9011 has a potential therapeutic effect for overnutrition-induced neuroinflammation, we stimulated the microglia with palmitic acid (PA) to resemble a pro-inflammatory stimulus on high-fat diet feeding. Primary microglia were exposed to 5 μM SR9011 (or DMSO for control) for 12 h, followed by 50 μM palmitic acid (or BSA for control) for 12 h in combination with SR9011 or DMSO. Palmitic acid significantly increased the expression of pro-inflammatory cytokines *Il6* and *Il1*β. which were attenuated by SR9011 (**Figures 4A,B**). Palmitic acid also significantly stimulated *Gm-csf* expression, while SR9011 had a profound inhibitory effect on *Gm-csf* expression (**Figure 4C**). *Tnf*α and *Ccl2* expression was not enhanced by palmitic acid treatment (**Figures 4D,E**), which is a slightly different outcome compared to the TNFα stimulus. In addition, palmitic acid treatment exerted impacts on the expression of core clock genes *Nr1d1* and *Per1* after 12h incubation (**Supplementary Figure 3**), which indicates palmitic acid treatment might also influence circadian rhythms. This is consistent with our previous observation that circadian rhythms of microglia are disrupted in DIO animals (30). Thus, these data suggest that SR9011 attenuates the pro-inflammatory response in primary microglia upon palmitic acid treatment, which may be beneficial for DIO-induced neuroinflammation.

SR9011 Decreases Phagocytosis in Microglia

One of the main neuroprotective functions of microglia is phagocytosis, so we evaluated the effect of SR9011 on phagocytic activity. Primary microglia were treated with 5 μM SR9011 (or DMSO) for 12 h and subsequently exposed to 0.05% fluorescent

TABLE 2 | JTK_Cycle analysis of clock genes in primary microglia with SR9011.

Gene	DMSO		SR9011	
	***P*-value**	**Acrophase**	***P*-value**	**Acrophase**
Bmal1	**0.0053**	9	0.0980	N.R.
Clock	**0.0293**	9	1	N.R.
Cry1	**<0.0001**	6	**0.0006**	6
Per1	**<0.0001**	0	**0.0293**	0
Per2	**<0.0001**	3	**<0.0001**	0
Nr1d1	**0.0364**	21	**<0.0001**	21

Clock genes rhythmicity in microglia treated with SR9011 are analyzed by JTK_Cycle software. All the clock genes were rhythmically expressed in primary microglia treated with DMSO, signified by a p-value of less than 0.05. SR9011 disrupted the rhythmic expression of Bmal1 and Clock. The acrophase of the curve is not relevant (N.R.) when data does not fit a curve.

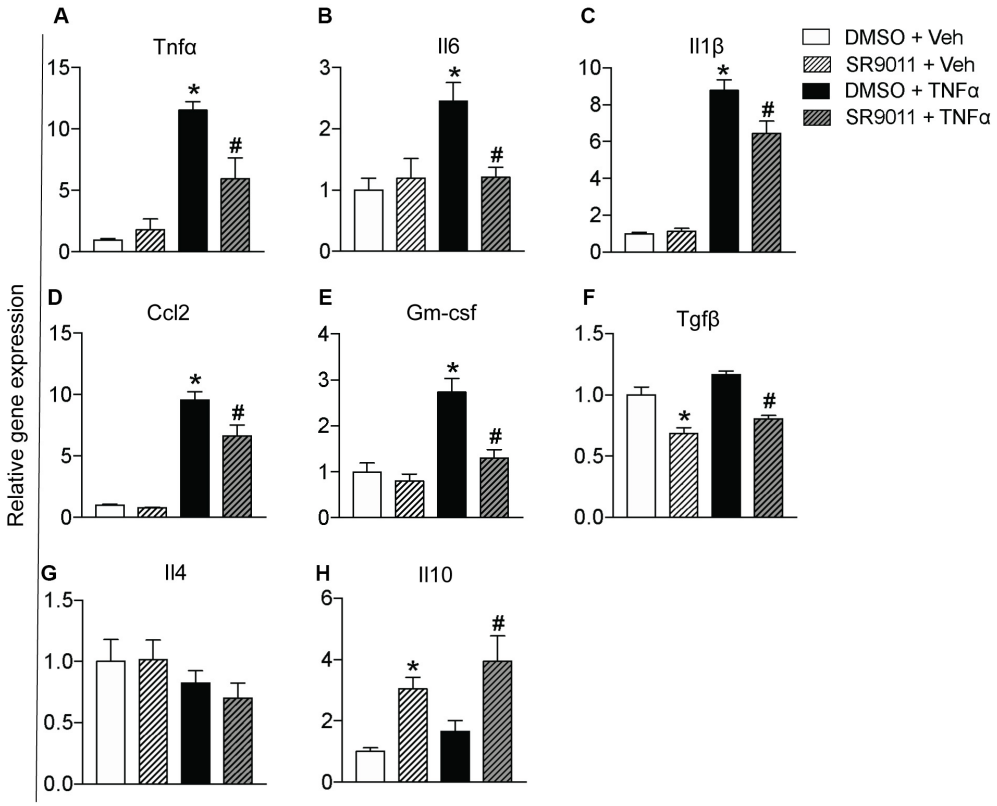

FIGURE 3 | The effect of SR9011 on cytokine expression in microglia. Relative gene expression of cytokines in primary microglia treated with SR9011 or DMSO for 12 h followed by TNFα or BSA treatment for 12 h (n = 6 per group). This figure shows the effect of TNFα and SR9011 on pro-inflammatory cytokine expression **(A–E)**, regulatory cytokine expression **(F)**, and anti-inflammatory cytokine expression **(G–H)**. TNFα increases the gene expression of *Tnfα, Il6, Il1β, Ccl2,* and *Gm-csf*. SR9011 attenuates the expression of *Tnfα*, *Il6*, *Il1β*, *Ccl2*, and *Gm-csf* compared to treatment with TNFα alone. Conversely, SR9011 increases *Il10* expression after TNFα stimulation. Data are presented as means ± SEM and statistical significance was determined using Unpaired t-test in all experiments. $p < 0.05^{*}$ vs DMSO + BSA and $p < 0.05^{\#}$ vs DMSO + TNFα.

beads for 1 h. A fluorescence staining was performed for IBA1 (microglia marker) and DAPI, after which the intensity of fluorescent beads per cell was determined (**Figure 5A**). The uptake of fluorescent beads was decreased in primary microglia treated with SR9011 (**Figure 5B**). Additionally, the expression of cluster of differentiation 68 (*CD68*), a phagocytic marker, was decreased in primary microglia that were starved for 6 h (0% FBS) and subsequently treated with 5 μM SR9011 for 12 h (**Figure 5C**). The purity of the cultures was tested by staining primary microglia with IBA1 and DAPI and a microglia purity of 98.81% was determined (data not shown). These results indicate that SR9011 decreases phagocytic activity, meaning that Rev-erbα plays an inhibitory role in regulating phagocytosis.

SR9011 Inhibits Mitochondrial Respiration and Metabolic Gene Expression in Microglia

Major metabolic genes are expressed in a rhythmic manner in microglia, as shown in **Figure 1**. We evaluated metabolism after disrupting the intrinsic microglial clock with SR9011. Primary microglia were treated with 5 μM SR9011 (or DMSO) for 12 h after which cellular respiration and ECAR were measured using the Seahorse XFe96 Analyzer to evaluate mitochondrial respiration and glycolysis. The raw data of OCR and ECAR are shown in **Figures 6A,B**. Cellular respiration was significantly decreased by SR9011, which was mainly attributed to less ATP-linked mitochondrial respiration, while the H^{+} proton leak remained unchanged (**Figures 6C,D**). Consequently, ATP production was greatly reduced (**Figure 6E**). Furthermore, maximum substrate oxidation was decreased after SR9011 treatment (**Figure 6F**). No changes were found in cellular acidification (glycolysis) and maximum glycolytic capacity (**Figures 6G,H**). These results indicate that SR9011 decreases ATP production by inhibiting oxidative phosphorylation. This mitochondrial dysfunction is not compensated with glycolysis. Furthermore, SR9011 inhibits the expression of *Hk2*, *Pdk1,* and *Cpt1* (**Figures 6I–K**), which are key enzymes involved in substrate utilization by the citric acid cycle. Taken together, these results suggest an overall decrease in cellular metabolism caused by activation of Rev-erbα by SR9011. Thus, Rev-erbα is a potent inhibitor of cell metabolism in primary microglia.

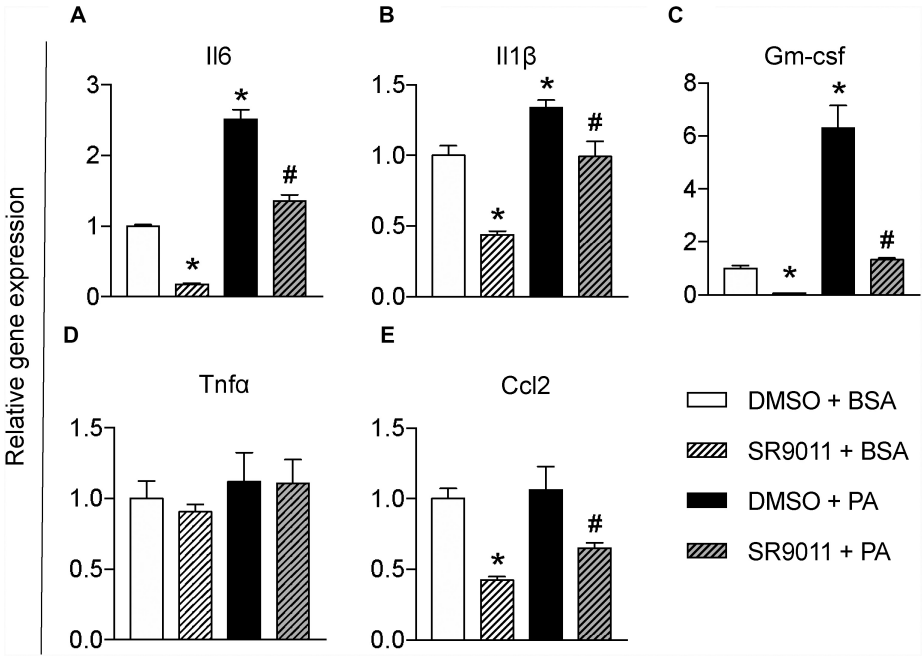

FIGURE 4 | The effect of SR9011 on palmitic acid induced inflammatory responses in microglia. Relative gene expression of cytokines in primary microglia treated with SR9011 or DMSO for 12 h followed by 50 μM palmitic acid or BSA treatment for 12 h (n = 4 per group). Palmitic acid treatment increases *Il6* **(A)**, *Il1β* **(B)**, and *Gm-csf* **(C)**, which are inhibited by SR9011. Palmitic acid treatment has no profound effect on the expression of *Tnfα* **(D)** and *Ccl2* **(E)**, while SR9011 decreased *Ccl2* expression with and without palmitic acid treatment **(E)**. $p < 0.05^{*}$ vs DMSO + BSA and $p < 0.05^{\#}$ vs DMSO + PA.

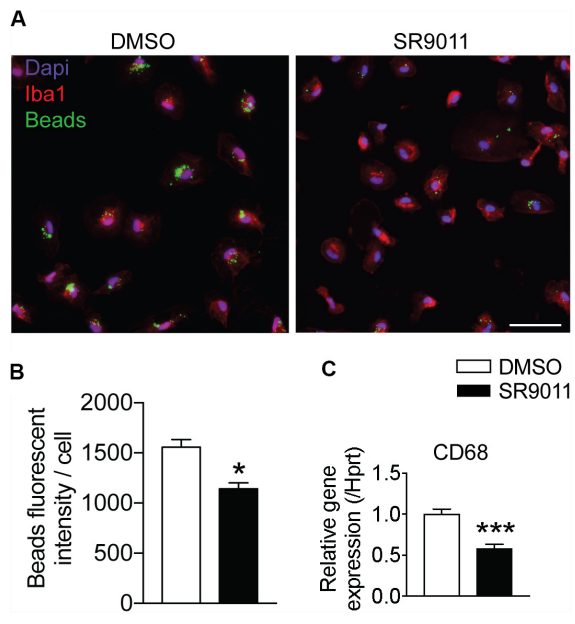

FIGURE 5 | SR9011 decreased phagocytic activity in primary microglia. **(A)** The uptake of fluorescent beads by primary microglia treated with DMSO or SR9011. **(B)** Primary microglia treated with SR9011 exhibit decreased phagocytic activity (n = 15). **(C)** The expression of phagocytic marker *CD68* is decreased in primary microglia treated with SR9011 for 12 h (n = 6). Data are presented as means ± SEM and statistical significance was determined using Unpaired t-test in all experiments. $p < 0.05^{*}$ and $p < 0.001^{***}$ vs. DMSO.

DISCUSSION

The aim of the current study was to determine the role of Rev-erbα in microglial immunometabolism. We show that key cytokine and metabolic genes are rhythmically expressed in primary microglia. Activation of Rev-erbα with SR9011 disrupted the intrinsic microglial clock and attenuated the phagocytosis and the pro-inflammatory response. SR9011 also decreased mitochondrial respiration and metabolic gene expression in microglia. These findings shed new light on the link between the circadian clock, cell metabolism and immune function in microglia and identify Rev-erbα as a possible important therapeutic target for treatment of neuroinflammatory diseases.

The rhythmic expression of major cytokines and metabolic genes in primary microglia observed in the current study supports our previous idea that *in vivo* the intrinsic clock is coupled with cellular metabolism (30). Such rhythmicity of cytokines may have physiological relevance *in vivo* – we reported before that microglia activity displays a day and night difference and is accompanied by a change in TNFα expression in the medial basal hypothalamus, which in turn affected the mitochondria function of nearby neurons (31). A growing body of literature reports that an obesogenic diet is associated with constant activation of microglia, leading to chronic hypothalamic inflammation, which contributes to the pathology observed (26, 27, 31, 40). We also reported that microglial circadian rhythmicity is disrupted in DIO animals (27). In this study, we found that SR9011 prevents the microglia pro-inflammatory

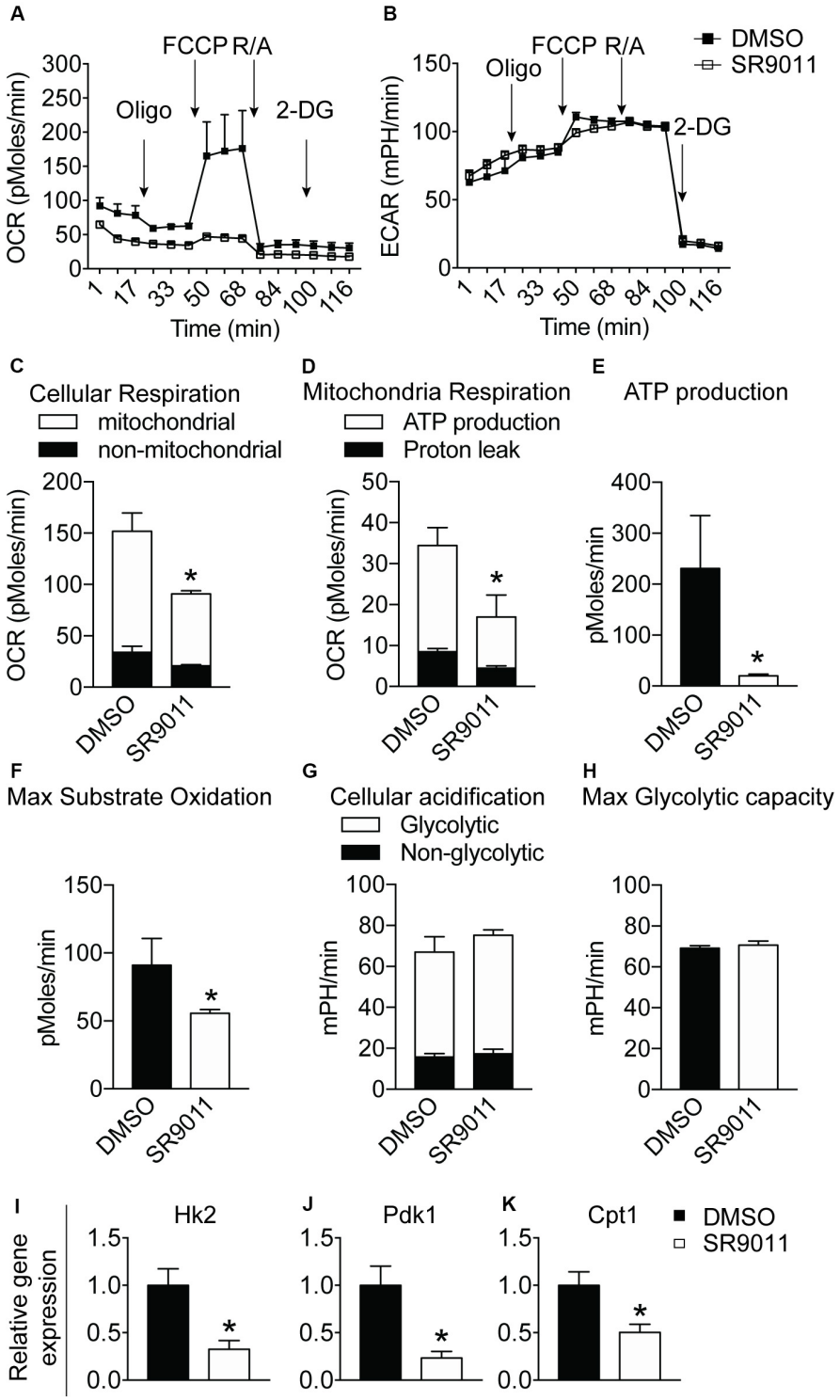

FIGURE 6 | The effect of SR9011 on cellular metabolism in primary microglia. Cellular bioenergetics and metabolic gene expression in primary microglia after SR9011 treatment (n = 4 per group). **(A, B)** Overview of OCR **(A)** and ECAR **(B)** of primary microglia treated with DMSO or SR9011 for 12 h. Indicated are the times on which oligomycin, FCCP, rotenone/antimycin A (R/A) and 2DG were administered. **(C–H)** SR9011 decreased cellular respiration **(C)**, which was caused by a decline in ATP-linked mitochondrial respiration **(D)**. Consequently, ATP production was significantly decreased in response to SR9011 **(E)**. SR9011 also caused a decrease in maximum substrate oxidation **(F)**. No changes were found in cellular acidification **(G)** and maximum glycolytic capacity **(H)**. **(I–K)** SR9011 decreased the expression of metabolic genes *Hk2* **(I)**, *Pdk1* **(J)**, and *Cpt1* **(K)** in primary microglia treated by dexamethasone for 2 h and SR9011 for 6 h. Data are presented as means ± SEM and statistical significance was determined using Unpaired t-test in all experiments. $p < 0.05$*.

responses usually observed during an inflammatory challenge and an obesogenic metabolic challenge. The mechanism behind the metabolic improvements observed in DIO mice can partially be explained by the mitigating effect of SR9011 on hyperactive microglia, thereby attenuating inflammation. This finding can have major implications for reducing microgliosis caused by obesity or neuroinflammatory diseases. A better *ex vivo* experimental setting to mimic the *in vivo* situation under a chronic high-fat diet challenge would be helpful to further elucidate these mechanisms.

The current study examined the immune function of microglia upon SR9011-associated Rev-erbα activation. Similar topics have been discussed before. In studies on knock-out mice or mice pharmacologically administered with SR9011, microglia activation and *Il6* expression was downregulated upon LPS exposure (39, 41). In another Rev-erbα deletion study, mice displayed microgliosis, increased CD68, and neuroinflammation in the hippocampus (20). Consistent with these results, we enhanced Rev-erbα activity with SR9011 and found a decreased pro-inflammatory response and phagocytosis. A recent study describes a regulatory role of Bmal1 in macrophage motility and phagocytosis (42), which may indicate a possible interplay between Rev-erb and Bmal1 in the regulation of phagocytosis in microglia – an interesting topic for future research. Additionally, SR9011 stimulated the expression of the anti-inflammatory cytokine *Il10*. This suggests Rev-erbα not only inhibits pro-inflammatory cytokines, but also promotes the anti-inflammatory response. Moreover, to more accurately mimic microglia's immune response, we used TNFα as an innate immune challenge, which is more physiologically relevant compared to lipopolysaccharide (LPS) used in the studies mentioned above. These findings suggest that the molecular clock components Bmal1 and Rev-erbα are closely related to the microglial immune response, and that Rev-erbα activity can regulate the inflammatory state in microglia under physiological and pathological conditions.

Rev-erbα nuclear receptors were reported to regulate metabolic homeostasis in cancer cells, hepatic cells and hepatoma cells (17, 18, 43). The findings of the current study show that Rev-erbα nuclear receptors regulate cell metabolism in primary microglia, the innate immune cells, as evidenced by the decrease in mitochondrial respiration and ATP production, as well as the decreased expression of rate-limiting enzymes such as *Cpt1*, *Pdk1*, and *Hk2* in response to SR9011. Our study dissected how the Rev-erbα-associated clock machinery interacts with immunometabolism in microglia. It is generally assumed that immune function is tightly linked to cell metabolism due to the metabolic demand of an inflammatory response (44). One explanation for the decline in energy metabolism is that it is a consequential phenomenon caused by less energy demand due to the attenuated pro-inflammatory response. Another possibility is a direct effect of Rev-erbα on cellular metabolism. Rev-erbα nuclear receptors, when bound to their ligand, repress the transcription of not only clock genes like *Bmal1*, but also repress metabolic genes and are involved in mitochondrial respiration (14, 15, 45, 46). The inflammatory response of microglia also involves metabolic reprogramming, which also might explain the attenuation of pro-inflammatory cytokines (32, 33). Another speculation would be that the intrinsic molecular clock orchestrates both microglial metabolism and immune response, and that it can also change the activation state of microglia. The latter would mean that SR9011-induced enhanced Rev-erbα activity is associated with disturbed microglial circadian rhythms, which consequently changed the cellular metabolism and immune response. Indeed, the *in vivo* situation might be far more complicated, because it is unknown what occurs first in the development of metabolic disorders: the disrupted circadian rhythmicity, the alterations in intracellular metabolism, the changes in immune response, or any other unknown factors. In our opinion, the disrupted circadian rhythmicity is very likely to be the driving force of the other two. In addition, the appropriate immune response of microglia is required to defend the CNS under normal conditions, so attenuated pro-inflammatory responses might not be always beneficial for the body. Further research is needed to elucidate the causal relation among the intracellular clock, cellular metabolism and immune response in microglia under physiological condition and metabolic challenges. It is interesting to note that SR9009, a REV-ERB agonist similar to SR9011, has been reported to exert Rev-erbα independent side-effects on cell proliferation and metabolism (47). Whether SR9011 has the same side-effects is currently unknown, and requires further research.

Future research should also investigate the significance of the microglial intrinsic clock *in vivo*. It is likely that the exact consequences of disturbing the microglial clock depend on the brain regions involved. Microgliosis in the hypothalamus is associated with metabolic disorders, while microglia in other brain regions will have other functions, depending on the micro-environment. On the other hand, the role of Rev-erbα should also be investigated in other immune cells and their related immune-diseases.

CONCLUSION

Our study demonstrates that disturbing circadian rhythmicity by SR9011-induced Rev-erbα activation attenuates pro-inflammatory cytokine expression and reduces cellular metabolism in microglia. In addition, expression of the anti-inflammatory cytokine *Il10* is stimulated, emphasizing the mitigating effect of Rev-erbα activation on the pro-inflammatory response. The findings of this study identify an interconnected role of Rev-erbα in the circadian rhythmicity, cell metabolism and inflammatory response of microglia and may have important implications for the employment of Rev-erbα as a potential therapeutic target for the treatment of neuroinflammatory diseases, however, further studies are required to achieve this goal.

DATA AVAILABILITY STATEMENT

The datasets presented in this study can be found in online repositories. The names of the repository/repositories and accession number(s) can be found in the article/**Supplementary Material**.

ETHICS STATEMENT

The experiments were approved by the Animal Care and Use Committee of Nanjing Medical University, and the experiments were performed according to the Guide for the Care and Use of Laboratory Animals of China.

AUTHOR CONTRIBUTIONS

SW, JS, HJ, and YG performed the experiments. C-XY and YG designed the study. SW, X-LW, and AK analyzed the data and wrote the manuscript. All authors read and approved the final manuscript.

FUNDING

This work was funded by the international student fellowship from Amsterdam Gastroenterology & Metabolism (AG&M), grants from the National Natural Science Foundation of China 81873654 and 31800971, and Jiangsu Province Science Foundation for Youths BK20180684, the Department of Cardiovascular and Cerebrovascular Medicine, Nanjing Medical University (YG Lab); and AMC fellowship, Amsterdam University Medical Center (2014; C-XY lab); and the doctoral fellowship from the 'NeuroTime" Erasmus+ Program (X-LW).

ACKNOWLEDGMENTS

We thank AG&M for granting SW the international student fellowship to conduct this valuable research at Nanjing Medical University under the supervision of YG.

SUPPLEMENTARY MATERIAL

The Supplementary Material for this article can be found online at: https://www.frontiersin.org/articles/10.3389/fimmu.2020.550145/full#supplementary-material

REFERENCES

1. Kalsbeek A, Palm IF, La Fleur SE, Scheer FAJL, Perreau-Lenz S, Ruiter M, et al. SCN outputs and the hypothalamic balance of life. *J Biol Rhythms*. (2006) 21:458–69. doi: 10.1177/0748730406293854
2. Boden G, Chen X, Polansky M. Disruption of circadian insulin secretion is associated with reduced glucose uptake in first-degree relatives of patients with type 2 diabetes. *Diabetes*. (1999) 48:2182–8. doi: 10.2337/diabetes.48.11.2182
3. Depner CM, Stothard ER, Wright KP. Metabolic consequences of sleep and circadian disorders. *Curr Diab Rep*. (2014) 14:507. doi: 10.1007/s11892-014-0507-z
4. McGinnis GR, Young ME. Circadian regulation of metabolic homeostasis: causes and consequences. *Nat Sci Sleep*. (2016) 8:163–80. doi: 10.2147/NSS.S78946
5. Turek FW, Joshu C, Kohsaka A, Lin E, Ivanova G, McDearmon E, et al. Obesity and metabolic syndrome in circadian clock mutant nice. *Science*. (2005) 308:1043–5. doi: 10.1126/science.1108750
6. Ma D, Liu T, Chang L, Rui C, Xiao Y, Li S, et al. The liver clock controls cholesterol homeostasis through trib1 protein-mediated regulation of PCSK9/Low density lipoprotein receptor (LDLR) axis. *J Biol Chem*. (2015) 290:31003–12. doi: 10.1074/jbc.M115.685982
7. Marcheva B, Ramsey KM, Buhr ED, Kobayashi Y, Su H, Ko CH, et al. Disruption of the clock components CLOCK and BMAL1 leads to hypoinsulinaemia and diabetes. *Nature*. (2010) 466:627–31. doi: 10.1038/nature09253
8. Inoue I, Shinoda Y, Ikeda M, Hayashi K, Kanazawa K, Nomura M, et al. CLOCK/BMAL1 is involved in lipid metabolism via transactivation of the peroxisome proliferator-activated receptor (PPAR) response element. *J Atheroscler Thromb*. (2005) 12:169–74. doi: 10.5551/jat.12.169
9. Sato F, Kohsaka A, Bhawal UK, Muragaki Y. Potential roles of dec and bmal1 genes in interconnecting circadian clock and energy metabolism. *Int J Mol Sci*. (2018) 19:781. doi: 10.3390/ijms19030781
10. Shimba S, Ogawa T, Hitosugi S, Ichihashi Y, Nakadaira Y, Kobayashi M, et al. Deficient of a clock gene, brain and muscle arnt-like protein-1 (BMAL1), induces dyslipidemia and ectopic fat formation. *PLoS One*. (2011) 6:e25231. doi: 10.1371/journal.pone.0025231
11. Crumbley C, Burris TP. Direct regulation of CLOCK expression by REV-ERB. *PLoS One*. (2011) 6:e17290. doi: 10.1371/journal.pone.0017290
12. Gaucher J, Montellier E, Sassone-Corsi P. Molecular cogs: interplay between circadian clock and cell cycle. *Trends Cell Biol*. (2018) 28:368–79. doi: 10.1016/j.tcb.2018.01.006
13. Preitner N, Damiola F, Lopez-Molina L, Zakany J, Duboule D, Albrecht U, et al. The orphan nuclear receptor REV-ERBα controls circadian transcription within the positive limb of the mammalian circadian oscillator. *Cell*. (2002) 110:251–60. doi: 10.1016/S0092-8674(02)00825-5
14. Padmanaban G, Venkateswar V, Rangarajan PN. Haem as a multifunctional regulator. *Trends Biochem Sci*. (1989) 14:492–6. doi: 10.1016/0968-0004(89)90182-5
15. Raghuram S, Stayrook KR, Huang P, Rogers PM, Nosie AK, McClure DB, et al. Identification of heme as the ligand for the orphan nuclear receptors REV-ERBα and REV-ERBβ. *Nat Struct Mol Biol*. (2007) 14:1207–13. doi: 10.1038/nsmb1344
16. Wu N, Yin L, Hanniman EA, Joshi S, Lazar MA. Negative feedback maintenance of heme homeostasis by its receptor, Rev-erbα. *Genes Dev*. (2009) 23:2201–9. doi: 10.1101/gad.1825809
17. Yin L, Wu N, Curtin JC, Qatanani M, Szwergold NR, Reid RA, et al. Rev-erbα, a heme sensor that coordinates metabolic and circadian pathways. *Science*. (2007) 318:1786–9. doi: 10.1126/science.1150179
18. Duez H, Staels B. Rev-erbα gives a time cue to metabolism. *FEBS Lett*. (2008) 582:19–25. doi: 10.1016/j.febslet.2007.08.032
19. Yang X, Downes M, Yu RT, Bookout AL, He W, Straume M, et al. Nuclear receptor expression links the circadian clock to metabolism. *Cell*. (2006) 126:801–10. doi: 10.1016/j.cell.2006.06.050
20. Griffin P, Dimitry JM, Sheehan PW, Lananna BV, Guo C, Robinette ML, et al. Circadian clock protein Rev-erbα regulates neuroinflammation. *Proc Natl Acad Sci USA*. (2019) 116:5102–7. doi: 10.1073/pnas.1812405116
21. Grant D, Yin L, Collins JL, Parks DJ, Orband-Miller LA, Wisely GB, et al. GSK4112, a small molecule chemical probe for the cell biology of the nuclear heme receptor rev-erbα. *ACS Chem Biol*. (2010) 5:925–32. doi: 10.1021/cb100141y
22. Chen H, Chu G, Zhao L, Yamauchi N, Shigeyoshi Y, Hashimoto S, et al. Rev-erbα regulates circadian rhythms and StAR expression in rat granulosa cells as identified by the agonist GSK4112. *Biochem Biophys Res Commun*. (2012) 420:374–9. doi: 10.1016/j.bbrc.2012.02.164
23. Solt LA, Wang Y, Banerjee S, Hughes T, Kojetin DJ, Lundasen T, et al. Regulation of circadian behaviour and metabolism by synthetic REV-ERB agonists. *Nature*. (2012) 485:62–8. doi: 10.1038/nature11030
24. Kojetin D, Wang Y, Kamenecka TM, Burris TP. Identification of SR8278, a synthetic antagonist of the nuclear heme receptor REV-ERB. *ACS Chem Biol*. (2011) 6:131–4. doi: 10.1021/cb1002575
25. Dragano NRV, Solon C, Ramalho AF, de Moura RF, Razolli DS, Christiansen E, et al. Polyunsaturated fatty acid receptors, GPR40 and GPR120, are expressed

in the hypothalamus and control energy homeostasis and inflammation. *J Neuroinflammation*. (2017) 14:91. doi: 10.1186/s12974-017-0869-7
26. Gao Y, Bielohuby M, Fleming T, Grabner GF, Foppen E, Bernhard W, et al. Dietary sugars, not lipids, drive hypothalamic inflammation. *Mol Metab*. (2017) 6:897–908. doi: 10.1016/j.molmet.2017.06.008
27. Maldonado-Ruiz R, Montalvo-Martínez L, Fuentes-Mera L, Camacho A. Microglia activation due to obesity programs metabolic failure leading to type two diabetes. *Nutr Diabetes*. (2017) 7:e254. doi: 10.1038/nutd.2017.10
28. Paolicelli RC, Angiari S. Microglia immunometabolism: from metabolic disorders to single cell metabolism. *Semin Cell Dev Biol*. (2019) 94:129–37. doi: 10.1016/j.semcdb.2019.03.012
29. Valdearcos M, Robblee MM, Benjamin DI, Nomura DK, Xu AW, Koliwad SK. Microglia dictate the impact of saturated fat consumption on hypothalamic inflammation and neuronal function. *Cell Rep*. (2014) 9:2124–38. doi: 10.1016/j.celrep.2014.11.018
30. Milanova IV, Kalsbeek MJT, Wang XL, Korpel NL, Stenvers DJ, Wolff SEC, et al. Diet-induced obesity disturbs microglial immunometabolism in a time-of-day manner. *Front Endocrinol*. (2019) 10:424. doi: 10.3389/fendo.2019.00424
31. Yi CX, Walter M, Gao Y, Pitra S, Legutko B, Kälin S, et al. TNFα drives mitochondrial stress in POMC neurons in obesity. *Nat Commun*. (2017) 8:15143. doi: 10.1038/ncomms15143
32. Orihuela R, McPherson CA, Harry GJ. Microglial M1/M2 polarization and metabolic states. *Br J Pharmacol*. (2016) 173:649–65. doi: 10.1111/bph.13139
33. Wang A, Luan HH, Medzhitov R. An evolutionary perspective on immunometabolism. *Science*. (2019) 363:eaar3932. doi: 10.1126/science.aar3932
34. Keuper M, Jastroch M, Yi CX, Fischer-Posovszky P, Wabitsch M, Tschöp MH, et al. Spare mitochondrial respiratory capacity permits human adipocytes to maintain ATP homeostasis under hypoglycemic conditions. *FASEB J*. (2014) 28:761–70. doi: 10.1096/fj.13-238725
35. Brand M. The efficiency and plasticity of mitochondrial energy transduction. *Biochem Soc Trans*. (2005) 33(Pt 5):897–904. doi: 10.1042/BST20050897
36. Hughes ME, Hogenesch JB, Kornacker K. JTK-CYCLE an efficient nonparametric algorithm for detecting rhythmic components in genome-scale data sets. *J Biol Rhythms*. (2010) 25:372–80. doi: 10.1177/0748730410379711
37. Nakazato R, Takarada T, Yamamoto T, Hotta S, Hinoi E, Yoneda Y. Selective upregulation of Per1 mRNA expression by ATP through activation of P2X7 purinergic receptors expressed in microglial cells. *J Pharmacol Sci*. (2011) 116:350–61. doi: 10.1254/jphs.11069FP
38. Logan RW, Sarkar DK. Circadian nature of immune function. *Mol Cell Endocrinol*. (2012) 349:82–90. doi: 10.1016/j.mce.2011.06.039
39. Nakazato R, Hotta S, Yamada D, Kou M, Nakamura S, Takahata Y, et al. The intrinsic microglial clock system regulates interleukin-6 expression. *Glia*. (2017) 65:198–208. doi: 10.1002/glia.23087
40. Gao Y, Ottaway N, Schriever SC, Legutko B, García-Cáceres C, de la Fuente E, et al. Hormones and diet, but not body weight, control hypothalamic microglial activity. *Glia*. (2014) 62:17–25. doi: 10.1002/glia.22580
41. Guo D, Zhu Y, Sun H, Xu X, Zhang S, Hao Z, et al. Pharmacological activation of REV-ERBα represses LPS-induced microglial activation through the NF-κB pathway. *Acta Pharmacol Sin*. (2019) 40:26–34. doi: 10.1038/s41401-018-0064-0
42. Kitchen GB, Cunningham PS, Poolman TM, Iqbal M, Maidstone R, Baxter M, et al. The clock gene Bmal1 inhibits macrophage motility, phagocytosis, and impairs defense against pneumonia. *Proc Natl Acad Sci USA*. (2020) 117:1543–51. doi: 10.1073/pnas.1915932117
43. Sulli G, Rommel A, Wang X, Kolar MJ, Puca F, Saghatelian A, et al. Pharmacological activation of REV-ERBs is lethal in cancer and oncogene-induced senescence. *Nature*. (2018) 553:351–5. doi: 10.1038/nature25170
44. Borst K, Schwabenland M, Prinz M. Microglia metabolism in health and disease. *Neurochem Int*. (2019) 130:104331. doi: 10.1016/j.neuint.2018.11.006
45. Bugge A, Feng D, Everett LJ, Briggs ER, Mullican SE, Wang F, et al. Rev-erbα and Rev-erbβ coordinately protect the circadian clock and normal metabolic function. *Genes Dev*. (2012) 26:657–67. doi: 10.1101/gad.186858.112
46. Everett LJ, Lazar MA. Nuclear receptor Rev-erbα: up, down, and all around. *Trends Endocrinol Metab*. (2014) 25:586–92. doi: 10.1016/j.tem.2014.06.011
47. Dierickx P, Emmett MJ, Jiang C, Uehara K, Liu M, Adlanmerini M, et al. SR9009 has REV-ERB–independent effects on cell proliferation and metabolism. *Proc Natl Acad Sci USA*. (2019) 16:12147–52. doi: 10.1073/pnas.1904226116

Conflict of Interest: The authors declare that the research was conducted in the absence of any commercial or financial relationships that could be construed as a potential conflict of interest.

frontiers in Immunology

REVIEW
published: 16 October 2020
doi: 10.3389/fimmu.2020.584210

The Role Played by Mitochondria in FcεRI-Dependent Mast Cell Activation

Maria A. Chelombitko[1], Boris V. Chernyak[1], Artem V. Fedorov[2], Roman A. Zinovkin[1,3], Ehud Razin[4] and Lakhsmi Bhargavi Paruchuru[4]**

[1] Belozersky Institute of Physico-Chemical Biology, Lomonosov Moscow State University, Moscow, Russia, [2] Department of Cell Biology and Histology, Biology Faculty, Lomonosov Moscow State University, Moscow, Russia, [3] Institute of Molecular Medicine, I.M. Sechenov First Moscow State Medical University, Moscow, Russia, [4] Department of Biochemistry and Molecular Biology, School of Medicine, Hebrew University of Jerusalem, Jerusalem, Israel

OPEN ACCESS

Edited by:
Pedro Manoel Mendes Moraes Vieira, Campinas State University, Brazil

Reviewed by:
Petr Draber, Institute of Molecular Genetics (ASCR), Czechia
Claudia Gonzalez, National Polytechnic Institute of Mexico (CINVESTAV), Mexico
Julie Ann Gosse, University of Maine, United States

***Correspondence:**
Maria A. Chelombitko
chelombitko@mail.bio.msu.ru
Lakhsmi Bhargavi Paruchuru
bhargavi.lakshmi@mail.huji.ac.il

Specialty section:
This article was submitted to Molecular Innate Immunity, a section of the journal Frontiers in Immunology

Received: 16 July 2020
Accepted: 20 August 2020
Published: 16 October 2020

Citation:
Chelombitko MA, Chernyak BV, Fedorov AV, Zinovkin RA, Razin E and Paruchuru LB (2020) The Role Played by Mitochondria in FcεRI-Dependent Mast Cell Activation. Front. Immunol. 11:584210. doi: 10.3389/fimmu.2020.584210

Mast cells play a key role in the regulation of innate and adaptive immunity and are involved in pathogenesis of many inflammatory and allergic diseases. The most studied mechanism of mast cell activation is mediated by the interaction of antigens with immunoglobulin E (IgE) and a subsequent binding with the high-affinity receptor Fc epsilon RI (FcεRI). Increasing evidences indicated that mitochondria are actively involved in the FcεRI-dependent activation of this type of cells. Here, we discuss changes in energy metabolism and mitochondrial dynamics during IgE-antigen stimulation of mast cells. We reviewed the recent data with regards to the role played by mitochondrial membrane potential, mitochondrial calcium ions (Ca^{2+}) influx and reactive oxygen species (ROS) in mast cell FcεRI-dependent activation. Additionally, in the present review we have discussed the crucial role played by the pyruvate dehydrogenase (PDH) complex, transcription factors signal transducer and activator of transcription 3 (STAT3) and microphthalmia-associated transcription factor (MITF) in the development and function of mast cells. These two transcription factors besides their nuclear localization were also found to translocate in to the mitochondria and functions as direct modulators of mitochondrial activity. Studying the role played by mast cell mitochondria following their activation is essential for expanding our basic knowledge about mast cell physiological functions and would help to design mitochondria-targeted anti-allergic and anti-inflammatory drugs.

Keywords: mast cell, mitochondria, FcεRI-dependent activation, IgE, allergy

INTRODUCTION

Mitochondria are semi-autonomous double-membrane-bound organelles of an endosymbiotic origin with various compartments for operating the metabolic reactions including the citric acid cycle, oxidative phosphorylation (OXPHOS) and fatty acid β-oxidation. These reactions lead to the increase in the synthesis of ATP and also certain metabolites being generated. Furthermore, mitochondria produce ROS, accumulate Ca^{2+}, and contribute to the programmed cell death and cell signaling regulation (1).

Increasing evidences suggests a strong correlation between cellular metabolism and mitochondrial morphology. For example, elongated mitochondria has contributed to a high level of OXPHOS activity and attenuated when the mitochondria was fragmented showing the impact of morphology (2, 3). It is well-known that when immune cells are activated their metabolism shifts from anabolism to catabolism and different immune cells employ different mechanisms of metabolic reprogramming enabling the optimized coordination between energetic and biosynthetic processes (3–6). Effector T cells and pro-inflammatory M1-macrophages predominantly employ anaerobic glycolysis which takes place in the cytoplasm, whereas regulatory T cell and anti-inflammatory M2-macrophages employ OXPHOS and fatty acid β-oxidation through mitochondria. This kind of alternative mechanism signifies the regulatory function of the mitochondrial morphology in these cells, where the mitochondria in effector T cells and M1-macrophages are fragmented while they were elongated in regulatory T cells and M2-macrophages (4, 5, 7). Moreover, immune cell activation is equally linked to the mitochondrial dynamics with in the cell. For example, antigen-induced activation of T cells is accompanied by fragmentation of mitochondria and their translocation to the immune synapse area (4, 5, 7). Mitochondrial fragmentation and translocation to the cell leading edge is necessary for migration of T cells (4, 8) and neutrophils (9). Efferocytosis of apoptotic cells by macrophages requires mitochondrial fragmentation as well (4).

The role played by mast cells in the development of inflammatory and allergic diseases is well-known (10, 11). Mast cell functions are mediated through a wide spectrum of biologically active compounds being secreted and regulated by various mechanisms. The most studied mechanism of mast cell activation is mediated by the interaction of antigens with immunoglobulin E (IgE) and a subsequent binding with the high-affinity receptor FcεRI. This event triggers FcεRI-dependent signaling which makes the mast cells secreting mediators such as histamine, proteoglycans, neutral proteases, and various cytokines. First, the preformed mediators are released from secretory granules via a degranulation process afterwards newly synthesized mediators such as cytokines and eicosanoids are being released to the extracellular environment for inducing inflammation (12, 13).

Mitochondria are actively involved in the FcεRI-dependent mast cell activation. Antigen-mediated mast cell stimulation is accompanied by mitochondrial fragmentation and their translocation to the site of exocytosis of secretory granules via secretion of mitochondrial components (14, 15). The OXPHOS process serves as an important step for mast cell degranulation and cytokine synthesis. The uncoupling of OXPHOS inhibits the FcεRI-dependent mast cell activation, however, the mechanisms that mediate this process is not fully understood (16–19). Mitochondria play an important role in regulating the cytosolic Ca^{2+} level which is critical for mast cell activation as they are able to accumulate Ca^{2+} (20–23). Mitochondrial ROS are also involved in activating mast cell (24, 25). Special attention should be given to the transcription factors STAT3 and MITF which play an important role in the development and function of mast cells. A small pool of these transcription factors reside in the mitochondria and modulate the mitochondrial activity independently as proteins other than regulating the expression of nuclear target genes (26–29).

Further investigation of the functions of mitochondria in mast cell activation is essential as it would expand our basic knowledge about mast cell physiology and could help in designing new anti-allergic and anti-inflammatory drugs.

THE FCεRI-DEPENDENT MAST CELL ACTIVATION

Mast cells represent an important cell population of the connective tissue that maintains its homeostasis and is involved in innate as well as adaptive immunity responses (12). The role played by these type of immune cells in the pathogenesis of various inflammatory and allergic diseases is well-documented (10). The strongest association of excessive mast cell activation and the severity of symptom manifestation were observed during arthritis, bronchial asthma, allergic rhinitis, and atopic dermatitis (11). Mast cell functions are mediated through the secretion of a wide spectrum of biologically active compounds. Mediators could be divided into two categories: the preformed mediators and the newly synthesized mediators. Mast cells

Abbreviations: ANT, adenine nucleotide translocase; Ap4A, diadenosine tetraphosphate; ATP, adenosine triphosphate; BMMCs, bone marrow–derived mast cells; Ca^{2+}, calcium ions; CaMK, calmodulin-dependent protein kinase; CRAC, calcium release-activated channels; DAG, diacylglycerol; DNP, 2,4-dinitrophenol; Doc2α, double C2; Drp1, dynamin related protein 1; Erk1/2, extracellular signal-regulated kinase; ITAM, (Ig) α immunoreceptor tyrosine–based activation; ETC, electron transport chain; FAD, flavin adenine dinucleotide; $FADH_2$, FAD dihydrogen; FCCP, carbonyl cyanide-4-(trifluoromethoxy)phenylhydrazone; FcεRI, high-affinity IgE receptor; Gab2, Grb2-associeted binder 1; HINT1, histidine triad nucleotide-binding protein 1; IgE, immunoglobulin E; IKK, IκB kinase; IL-6, Interlukin 6; IL-8, Interlukin 8; IP_3, inositol trisphosphate; IP_3R, inositol trisphosphate receptor; IκB, inhibitor of nuclear factor kappa B; JNK, c-Jun N-terminal kinases; LAD2, laboratory of allergic diseases 2; LAT, linker for activation of T cells; LysRS, lysyl-tRNA synthetase; M2PK, M2 pyruvate kinase; MAPK, mitogen-activated protein kinase; MCU, mitochondrial calcium uniporter; mDivi-1, mitochondrial division inhibitor 1; Mfn1, mitofusin1; Mfn2, mitofusin2; MITF, microphthalmia associated transcription factor; MLCK, myosin light chain kinase; mPTP, mitochondrial permeability transition pore; NAD, nicotinamide adenine dinucleotide; NADH, NAD hydrogen; NEMO, NF-κB essential modulator; NFAT, nuclear factors of activated T cell; NF-kB, nuclear factor- kappaB; NOX4, NADH oxidase; NTAL, non-T cell activation linker; OPA1, dynamin-like 120 kDa; Orai1, calcium release-activated calcium channel protein 1; OXPHOS, oxidative phosphorylation; p66shc, proteins having Src homology 2; PDC, pyruvate dehydrogenase complex; PDH, pyruvate dehydrogenase; PDH E1α, pyruvate dehydrogenase E1α subunit; PGC-1 α, peroxisome proliferator–activated receptor γ coactivator 1 α; PINK1, phosphatase and tensin homolog induced kinase 1; PIP_2, phosphatidylinositol 4,5-bisphosphate; PKC, protein kinase C; PLCγ, phospholipase Cγ; RBL-2H3, rat basophilic leukemia; ROS, reactive oxygen species; SERCA, sarco/endoplasmic reticulum Ca^{2+}-ATPase; siRNA, small interfering ribonucleic acid (RNA); SNARE, soluble NSF attachment protein receptor; STAT3, signal transducer and activator of transcription 3; STIM1, stromal interaction molecule 1; Syk, spleen tyrosine kinase; TFEB, transcription factor EB; Th2, T-helper type 2; TNFα, tumor necrosis factor alpha; TRPC, Ca^{2+} transporters transient receptor potential canonical; TRPML1, mucolipin 1 TRP or MCOLN1 channel; UCP2, uncoupling protein 2; Uqcrfs1, ubiquinol-cytochrome C reductase, Rieske iron-sulfur polypeptide 1; VDAC, voltage-dependent anion channels.

secretory granules contain lysosomal proteins such as β-hexosaminidase mediators (such as histamine and serotonin), glycosaminoglycans (such as heparin and chondroitin sulfates) and enzymes (such as tryptase and chymase). The second group of mediators include metabolites of arachidonic acid, cytokines, chemokines, and growth factors are synthesized only upon mast cell stimulation (12, 13, 30, 31). There are two subpopulations of mast cells—mucosal mast cells, which are characterized by the presence of tryptase without chymase and mast cells of the connective tissue that contain both enzymes. Mucosal mast cells contain low levels of histamine, but produce many cysteinyl leukotrienes (LTC4, LTD4, LTE4, LTF4). Granules in these type of mast cells are characterized by their presence of chondroitin sulfate. In turn, connective tissue mast cells are characterized by higher content of histamine and secretes high levels of prostaglandin D2 while their granules contain heparin instead of chondroitin sulfate (32, 33). However, mast cells from different tissues are highly heterogeneous in the expression of both granules and enzymes needed for their secretion according to the studies on transcriptome analysis of bone marrow–derived mast cells (BMMCs) (34).

The mechanism of FcεRI-dependent mast cell activation is well-documented in number of reviews (12, 20, 35, 36). Interaction of the antigen-IgE complex with the FcεRI receptors induces their aggregation and phosphorylation of tyrosine residues in the (Ig) α immunoreceptor tyrosine–based activation motif (ITAM) regions of β- and γ-chains by the Lyn kinase. These regions bind to the spleen tyrosine kinase (Syk) which phosphorylates the transmembrane adaptor molecule linker for activation of T cells (LAT). LAT phosphorylation activates phospholipase Cγ (PLCγ) that catalyzes the hydrolysis of phosphatidylinositol (4,5)-bisphosphate (PIP_2) in the plasma membrane. Inositol trisphosphate (IP_3) and diacylglycerol (DAG) generated during hydrolysis of PIP_2 will induce the release of Ca^{2+} from intracellular stores into the cytosol and activation of the protein kinase C (PKC) thus causing the degranulation of mast cell. Also, LAT activates the small GTPase RAS which in turn stimulates mitogen-activated protein kinase (MAPK) signaling leading to cytokine production and activates phospholipase A2 (PLA2) which regulates the synthesis of eicosanoids (12, 20, 35). Crosslinking of FcεRI receptors also activates Src-family kinase Fyn which is essential for mast cell degranulation along with cytokine and leukotriene production. Fyn kinase initiates complementary signals required for IgE-dependent mast cell degranulation and when there is a Fyn deficiency, an impaired FcεRI-dependent gene expression with a defective eicosanoid and cytokine production was resulted in mast cells. With the help of the adapter protein non-T cell activation linker (NTAL) Fyn phosphorylates Grb2-associeted binder 1 (Gab2) thus activating phosphatidylinositol 3 kinase (PI3K) (36, 37). Activated PI3K phosphorylates PIP_2 and produces phosphatidylinositol (3,4,5)-trisphosphate (PIP_3) which subsequently activates the 3-phosphoinositide-dependent protein kinase-1 (PDK1), RAC-alpha serine/threonine-protein kinase (Akt) and Bruton's tyrosine kinase (Btk) kinases (37, 38).

THE ROLE PLAYED BY MITOCHONDRIA IN THE FCεRI-DEPENDENT MAST CELL ACTIVATION

The Energy Metabolism

For quite a long time, mitochondria were thought to exert only the bioenergetic function by uptaking the substrate from cytosol and their catabolic conversion using fatty acid oxidation or the citric acid cycle (Krebs cycle) thus causing the reduction of nicotinamide adenine dinucleotide (NAD) and flavin adenine dinucleotide (FAD). Further oxidation of NAD hydrogen (NADH) and FAD dihydogen ($FADH_2$) by the electron transport chain (ETC) is linked to a proton electrochemical potential generation across the inner mitochondrial membrane. The energy of this electrochemical potential is harnessed by the ATP-synthase to produce ATP. In addition to ATP production, mitochondria are involved in the biosynthesis of pyrimidines, certain fatty acids, heme, ROS production and maintenance of Ca^{2+} homeostasis (1).

Adequate ATP levels in mast cells have been shown to be essential for FcεRI-dependent activation of mast cells. ATP production and oxygen consumption was increased during antigen-induced activation (26). Apparently, both glycolysis and OXPHOS could be the source of ATP in mast cells (6). FcεRI-dependent stimulation of the rat basophilic leukemia RBL-2H3 mast cells was shown to induce phosphorylation and inactivation of the M2 pyruvate kinase (M2PK) which is involved in the terminal reaction of glycolysis and pyruvate production (39).

Using a Seahorse cell metabolism analyzer, the antigen-induced stimulation of mast cells derived from the murine bone marrow has been shown to rapidly stimulate the glycolysis (40). Glycolysis suppression by dichloroacetate that inhibits the kinase of pyruvate dehydrogenase and ETC complex I inhibition by rotenone abated both degranulation and cytokine production. The competitive inhibitor of glycolysis 2-deoxyglucose also diminished both degranulation and production of cytokines upon antigen-dependent mast cell activation. However, the suppressing fatty acid oxidation by etomoxir which inhibits carnitine palmitoyltransferase-1 had no effects (40). It should be noted that mast cell sensitization only with IgE prior to antigen-induced stimulation elevates the glycolytic capacity (40). Our own data demonstrated that inhibition of glycolysis doesn't affect FcεRI-dependent degranulation of RBL-2H3 and bone marrow-derived mast cells. This indicated that the major part of the energy for degranulation is derived from mitochondrial ATP (26).

The PDH complex serves as a gatekeeper in the metabolism of pyruvate in order to maintain glucose homeostasis during the fed and fasting states. Important mast cell functions such as degranulation and cytokine secretion were found to be regulated by mitochondrial PDH. This is based on our findings that in IgE-antigen activated RBL-2H3 cells and BMMCS, serine 293 dephosphorylated PDH levels were significantly reduced, indicating the active state of this complex. Furthermore, CPI-613, a small molecule selective inhibitor of PDH, which is now in phase 2 of clinical studies for cancer treatment has

severely impaired mitochondrial ATP production. This inhibitor treatment led to a 50% decrease in mast cell degranulation and completely abolished the tumor necrosis factor alpha (TNFα) secretion in RBL-2H3 cells. This effect was not a result of apoptosis as no cleaved caspase 3 was observed and was due to PDH inactivation where a significant increase in PDH phosphorylation levels indicates a decrease in the complex's activity. Moreover, the knockdown of PDH using small interfering ribonucleic acid (RNA) (siRNA) has also replicated the degranulation results. PDH depletion has greatly effected interleukin 6 (IL-6) and TNF-α levels than degranulation values which indicates a strong correlation between the loss of mitochondrial ATP and cytokine secretion during mast cell exocytosis. These findings were extended to human cord blood-derived mast cells also where both degranulation and IL-6 secretion were abolished by CPI-613, providing a future potential target for allergic diseases research (28).

The antigen-dependent stimulation of mast cell was shown to effect the extracellular signal-regulated kinase (Erk1/2) dependent phosphorylation of mitochondrial STAT3 thus causing an increase in OXPHOS activity. Inhibition of STAT3 activity has attenuated both degranulation and cytokine secretion in mast cells (26, 29). Thus, FcεRI-dependent mast cell stimulation requires both activities of glycolysis and OXPHOS.

The Mitochondrial Membrane Potential

The mitochondrial membrane potential ($\delta\Psi m$) plays an important role in the regulation of FcεRI-mediated mast cell degranulation. $\Delta\Psi m$ is generated by ETC proton pumps (complexes I, III, and IV). Along with the proton gradient, $\Delta\Psi m$ forms the proton electrochemical transmembrane potential (or the proton-motive force) used for ATP synthesis (41, 42). $\Delta\Psi m$ is a driving force for the transporting various substrates in mitochondria and for Ca^{2+} accumulation. High $\Delta\Psi m$ can induce NAD reduction (so-called reverse electron transport) that is the key contributor to mitochondrial ROS production (41–43). Membrane potential plays an important role in signal transduction and regulates the mitochondrial structural dynamics. Decreased $\Delta\Psi m$ is accompanied by fragmentation of the elongated mitochondria (41, 42). A significant decline of mitochondrial potential is associated with mitochondrial dysfunction. It activates the mitochondrial quality control systems including the phosphatase and tensin homolog induced kinase 1(PINK1)-parkin pathway which induces selective autophagy of defective mitochondria (mitophagy). At high $\Delta\Psi m$ PINK1 undergoes degradation, while $\Delta\Psi m$ is reduced, PINK1 accumulates on the outer surface of the mitochondria and recruits parkin ubiquitin ligase that ubiquitinylates PINK1 leading to mitophagy induction (41–43). $\Delta\Psi m$ decrease due to OXPHOS uncoupling attenuates mast cell activation. The uncoupler carbonyl cyanide m-chlorophenyl hydrazone (CCCP) inhibits the antigen-induced secretion of β-hexosaminidase in rat mast cell line RBL-2H3 (16). Mitochondrial respiration inhibitors such as ETC complex I inhibitor rotenone, complex III inhibitor antimycin A, and the uncoupler carbonyl cyanide-4-(trifluoromethoxy)phenylhydrazone (FCCP) suppress IgE-mediated degranulation of murine bone marrow mast cells and RBL-2H3 cells. This suggests that this process may depend on a high ATP level. However, antimycin A and FCCP (but not rotenone) promoted degranulation in the absence of extracellular Ca^{2+} via a rapid decrease of $\Delta\Psi m$. Mitochondrial depolarization enhanced IgE-mediated Ca^{2+} release from mitochondria and intracellular stores. This can imply that uncouplers affect mast cell degranulation both via a decreased ATP level and an increased release of mitochondrial Ca^{2+} (17).

Many natural and synthetic compounds possess an uncoupling activity along with the uncouplers widely used in experimental work. The antibacterial and antifungal agent triclosan has an uncoupling activity. Triclosan brings about a decline in $\Delta\Psi m$ and ATP production and promotes mitochondrial fragmentation and ROS generation in unstimulated RBL-2H3 cells. Upon mast cell stimulation, triclosan inhibits microtubule polymerization and mitochondrial translocation to the plasma membrane and suppresses the entry of extracellular Ca^{2+} through the plasma membrane. The inhibited mitochondrial translocation might prevent the activation of calcium release-activated channels (CRAC) which plays a crucial role in Ca^{2+} from the extracellular environment indicates thattriclosan attenuates FcεRI-dependent mast cell degranulation (18, 19).

It is worth noting that some uncouplers can act as mast cell activators. In our recent study, we have shown that degranulation of RBL-2H3 mast cells is stimulated by usnic acid which is a secondary messenger in lichens and has an uncoupling activity. Usnic acid appears to act not only as a protonophore uncoupler but also as a calcium ionophore. Similar to calcium ionophore A23187, usnic acid elevated the intracellular Ca^{2+} level in RBL-2H3 cells acting as a trigger for degranulation (44). Thus, $\Delta\Psi m$ plays an important role in mast cell function, most likely due to its role in Ca^{2+} transport across the mitochondrial membrane.

Calcium Signaling

All stages of FcεRI-dependent mast cell activation including their degranulation, biosynthesis of eicosanoids and cytokine production are Ca^{2+}-dependent (20–23, 45). Antigen-induced mast cell stimulation activates phosphoinositide phospholipase C (PLCγ) which catalyzes phosphatidylinositol 4,5-bisphosphate (PIP_2) hydrolysis in the plasma membrane. Inositol trisphosphate (IP_3) induces Ca^{2+} release from the endoplasmic reticulum through inositol trisphosphate receptor (IP_3R) channels into the cytosol (20–23, 45). Mitochondria and endoplasmic reticulum can strongly interact with each other via special contacts called mitochondria-associated membranes (MAMs) (22) with their membranes that are spaced 10–50 nm apart. Ca^{2+} released from endoplasmic reticulum penetrates into mitochondria through the potential-dependent porin voltage-dependent anion channels (VDAC) localized at the outer mitochondrial membrane following mitochondrial calcium uniporter (MCU) at the inner mitochondrial membrane (22, 45). ATP-dependent Ca^{2+} pumps sarco/endoplasmic reticulum Ca2+-ATPase (SERCA) restore the Ca^{2+} pool in endoplasmic reticulum (22). The downregulation of the MCU transporter has been shown to impair FcεRI-dependent mast cell degranulation (21). An increased level of mitochondrial

Ca^{2+} enhances OXPHOS and promotes ATP production and ROS generation. Importantly, Ca^{2+} release from mitochondria, mediated by Na^+/Ca^{2+}-exchanger and to a lesser extent by H^+/Ca^{2+}-exchanger, is important for maintaining of Ca^{2+} oscillations in the cytosol and preventing the mitochondrial Ca^{2+} overload (20–23, 45). Excessive accumulation of Ca^{2+} in mitochondria promotes the opening of the non-selective mitochondrial permeability transition pore (mPTP) which is essential for a rapid Ca^{2+} release from mitochondria. The mPTP complex most likely comprises ATP-synthase (F0F1), adenine nucleotide translocase (ANT) and cyclophilin D from the mitochondrial matrix (46). Both decreased $\Delta\Psi m$ and oxidative stress significantly increases the probability of mPTP opening which plays an important role in mast cell activation. This is supported by the fact that atractyloside and bongkrekic acid (the agonist and antagonist of mPTP, respectively) enhanced and suppressed FcεRI-mediated intracellular Ca^{2+} release in mast cells, respectively. Bongkrekic acid abolished the elevated antigen-induced mast cell degranulation which was observed in the absence of intracellular Ca^{2+} upon treatment with antimycin A or FCCP (17).

It is known that mPTP opening can be reversible and facilitate the long-term Ca^{2+} oscillations in the cytoplasm. Meanwhile, prolonged mPTP opening results in reduced ATP production and increased ROS generation, mitochondrial swelling, disruption of the outer mitochondrial membrane, and release of proapoptotic factors from the mitochondrial intermembrane space into the cytoplasm (47).

Transient Ca^{2+} oscillations triggered by Ca^{2+} release from the intracellular stores are incapable of maintaining the degranulation of antigen-stimulated mast cells in the absence of the extracellular Ca^{2+} influx. Mast cell activation requires Ca^{2+} influx by store-operated entry (SOCE). SOCE is activated by Ca^{2+} depletion in the endoplasmic reticulum and subsequent influx of extracellular Ca^{2+}. The loss of Ca^{2+} binding to EF-hand motifs in a luminal domain of Ca^{2+} sensor stromal interaction molecule 1 (STIM1) results in its oligomerization and redistribution to regions of the endoplasmic reticulum proximal to the plasma membrane where it interacts with pore-forming subunits of calcium release-activated channel (Orai1/CRACM1) forming an active CRAC (20, 48). Besides CRAC some transient receptor potential canonical (TRPC) TRPCs can participate in Ca^{2+} influx in FcεRI-dependent mast cell activation. For example, mast cell Fyn kinase regulates expression of TRPC1. Fyn null mast cells demonstrate a decreased expression of TRPC1, impaired Ca^{2+} influx and cortical F-actin depolymerization (a key step for granule-plasma membrane fusion) has resulted in a decreased degranulation (49). TRPC5 in RBL-2H3 cells associates with STIM1 and Orai1, enhances entry of Ca^{2+} and degranulation (50). The results obtained on the studies of non-mast cells suggest that interaction between STIM1 and Orai1 can be mediated by microtubule-directed reorganization of endoplasmic reticulum and establishment of contacts between the endoplasmic reticulum and the plasma membrane (51–53).

Mitochondria appears to play an important role in SOCE. Trafficking of STIM1 to endoplasmic reticulum-plasma membrane junctions and subsequent activation of CRAC in rat basophilic leukemia cells RBL-1 and HEK293 cells was impaired following the mitochondrial depolarization (54). The mitochondrial Ca^{2+} current was shown to be necessary for STIM1 oligomerization and activation in HeLa cells (55). Two steps elevation in mitochondrial Ca^{2+} concentration was shown in antigen-activated RBL-2H3 mast cells. The first is Ca^{2+} entry to mitochondria derived from the Ca^{2+} release from the endoplasmic reticulum. The second step is Ca^{2+} influx mediated by STIM1-Orai1. Inhibition of mitochondrial ETC complex I and III by rotenone and antimycin A, respectively, diminished mitochondrial Ca^{2+} uptake and inhibited antigen-induced degranulation (56). Mitochondrial Ca^{2+} uptake can maintain an active state of CRAC channels along with activation of OXPHOS and STIM1. Studies on T-lymphocytes have demonstrated that increased Ca^{2+} levels will lead to CRAC inactivation and the mitochondrial Ca^{2+} uptake in the vicinity of CRAC prevents their inactivation (8). Another mechanism that maintains the extracellular Ca^{2+} influx was demonstrated on HEK293T and RBL-2H3 cells, where the activity of mitochondrial Na^+/Ca^{2+}-exchanger has interfered the ROS-dependent Orai1 inactivation (57).

When intracellular Ca^{2+} in mast cells is elevated, it activates Ca^{2+}-binding protein calmodulin which in turn stimulates calmodulin-dependent protein kinase (CaMK), myosin light chain kinase (MLCK), and phosphatase calcineurin (47). The importance of CaMK and MLCK activation for secretory granule exocytosis was demonstrated in the RBL-2H3 mast cells (58). Calcineurin promotes mitochondrial fragmentation and induces nuclear translocation of the transcription factors such as transcription factor EB (TFEB), nuclear factors of activated T cell (NFAT) and nuclear factor- kappaB (NF-kB) which are involved in autophagy and mitochondrial biogenesis as well as secretion of pro-inflammatory cytokines (59, 60). The activation of transcription factor NFAT, which regulates the expression of pro-inflammatory cytokines associated with the Th2-dependent immune response, strongly depends on calcineurin. The inhibited calcineurin activity reduces the secretion of both preformed and synthesized mediators. It should be noted that calcineurin inhibitors are used for therapy of atopic dermatitis and some other allergic diseases. NFAT has been shown to regulate mast cell degranulation affecting the activity of kinases protein kinase C (PKC), p38, and Erk (59, 60).

The soluble NSF attachment proteins receptor (SNARE) protein complex plays a crucial role in fusing the secretory granules with each other and with the plasma membrane. Some proteins required for its proper function are Ca^{2+}-sensitive. Such proteins include Munc13-4, synaptotagmin II, and double C2 (Doc2α) (61–63).

Mitochondrial ROS

We have already discussed the role played by ROS in mast cell activation (25) and the present review focuses on the possible role of the mitochondrial ROS in mast cell activation.

Most mitochondrial ROS arise from ETC function (by complexes I and III, NADH dehydrogenase and cytochrome bc1 complex, respectively). Mitochondrial ROS generation depends on many factors: oxygen level, respiration rates,

Ca^{2+} levels, and $\Delta\Psi m$. For example, high $\Delta\Psi m$ may boost ROS production. Mitochondrial ROS can be generated as byproducts of dehydrogenase activity in the mitochondrial matrix, the proteins having Src homology 2 (p66shc) in the intermembrane space, monoamine oxidase at the outer mitochondrial membrane, and NADH oxidase (NOX4) at the inner mitochondrial membrane. Mitochondria have an efficient antioxidant system. It includes thiol-containing peptide glutathione, thioredoxins and glutaredoxins, glutathione reductases, thioredoxin peroxidases (peroxiredoxins), and superoxide reductases (64–66).

Histamine production and mast cell degranulation were shown to be attenuated by uncoupling protein 2 (UCP2), the protein of the inner mitochondrial membrane that regulates ROS generation (24). Our previous data indicated that mitochondria-targeted antioxidant SkQ1 abrogates the antigen-dependent degranulation of RBL-2H3 mast cells (67), which implies that mitochondrial ROS contribute to mast cell activation. As it will be discussed below in the part "Mitochondrial dynamics," mast cell degranulation is accompanied by the mitochondrial fragmentation and its translocation to the plasma membrane. Preventing mitochondrial fragmentation suppresses mast cell degranulation (14). Mitochondrial ROS seem to be a vital regulator of mitochondrial fragmentation. The mitochondria-targeted antioxidants MitoQ (68–70) and SkQ1 (71) can inhibit mitochondrial fragmentation induced by uncoupling agents and oxidative stress in many cell cultures. The protective effect of the mitochondria-targeted antioxidants appears to be mediated by modulation of the activity or localization of dynamin-like proteins Drp1 and OPA1 (66, 69), as well as by regulation of the expression of genes that control mitochondrial dynamics (70, 72).

Probably, mitochondrial ROS can regulate exocytosis of mast cells by acting on Ca^{2+} channels in secretory granules. The main lysosomal Ca^{2+} channel mucolipin-1 (MCOLN1/TRPML1) is localized in the secretory lysosomes of NK cells related to secretory granules (73) and can be directly activated by mitochondrial ROS (61, 74, 75). Ca^{2+} release via TRPML1 leads to lysosomal fission (76) and calcineurin-dependent translocation of the nuclear transcription factor TFEB which stimulates lysosome exocytosis, autophagy, and lysosome biogenesis (61, 74, 75). The key role of mucolipin-1 in the regulation of granule exocytosis was demonstrated in experiments in which the pharmacological inhibition of phosphoinositide kinase PIKfyve, which stimulates the opening of the mucolipin-1 channel, inhibited exocytosis in mouse bone marrow-derived mast cells during FcεRI-dependent activation (77).

The results obtained from the studies of various cell types suggest that mitochondrial ROS can also affect antigen-dependent mast cell activation by modifying activities of MAPK and transcription factors NF-κB and NFAT. Stimulating the mitochondrial ROS production by antimycin A induces Erk1/2 phosphorylation and interleukin 8 (IL-8) secretion by polymorphonuclear leukocytes from human peripheral blood (78). There is evidence indicating that mitochondrial ROS are involved in activating P38 MAPK (79, 80) and c-Jun N-terminal kinases (JNK) (81). Mitochondria-targeted antioxidants can inhibit the phosphorylation of all three mentioned kinases (81–83).

Mitochondrial ROS can stimulate NF-κB signaling by activating the kinase (IKK) of the inhibitor of NF-κB (IκB), which promotes its proteasome degradation and induces nuclear translocation of NF-κB (81, 84). Mitochondrial ROS-dependent activation of IKK can be mediated by several mechanisms, including the formation of intermolecular disulfide bonds in NF-κB essential modulator (NEMO), a component of the IKK complex (85).

The activity of another important transcription factor, NFAT, also depends on mitochondrial ROS. It has been shown that NFAT nuclear translocation is abolished in T cells deficient in the mitochondrial ubiquinol-cytochrome C reductase subunit, the Riske iron-sulfur protein (Uqcrfs1), which is involved in the generation of ROS (86).

Figure 1 shows schematically possible function of mitochondrial ROS in the antigen-dependent mast cell stimulation.

The Mitochondrial Dynamics

The research evidences indicates that mitochondrial reticulum is a highly dynamic structure. Depending on the cell requirements, mitochondria can both alter their localization using the cytoskeleton and modulates their morphology by fusion and fragmentation. Mitochondrial fusion is regulated by the GTPases mitofusin1 (Mfn1) and mitofusin2 (Mfn2) at the outer mitochondrial membrane and by OPA1 at the inner mitochondrial membrane. Mitochondrial fragmentation is mediated mainly by the GTPase Drp1 which is localized in the cytosol is being inactive (2, 3).

Inhibiting Drp1 activity by mitochondrial division inhibitor 1 (mDivi-1) or downregulation of Drp1 expression using siRNA suppresses mitochondrial fragmentation and translocation, attenuates mast cell degranulation but does not affect *de novo* biosynthesis of mediators. The translocation of mitochondria to the plasma membrane was observed in the mast cells isolated from the skin of atopic dermatitis patients. Furthermore, Drp1 and calcineurin were upregulated in the skin of those patients (14). The number of cristae in mitochondria of RBL-2H3 mast cells was found to increase upon the antigen-induced stimulation (87). Generally, the number of cristae increases as OXPHOS activity enhances (7). Furthermore, IgE-dependent stimulation of laboratory of allergic diseases 2 (LAD2) mast cells was shown to be accompanied by secretion of mitochondrial particles, mitochondrial DNA, and ATP in the absence of cell death (15).

Drp1 activity depends on its phosphorylation on Ser616 and Ser637. Dephosphorylation of Drp1 on Ser637 by Ca^{2+}-dependent phosphatase calcineurin promotes the recruitment of Drp1 to the mitochondrial surface. Drp1 activation requires phosphorylation on Ser616 which is executed by various MAPK kinases including Erk1/2 (2). Calcineurin activation occurs in response to an increased intracellular Ca^{2+}. Apart from Drp1 activation, calcineurin triggers nuclear translocation of transcription factors TFEB, NFAT, and NF-kB involved in the biogenesis of mitochondria and lysosomes, autophagy, and secretion of pro-inflammatory cytokines. Activation of the NFAT transcription factor that regulates the expression

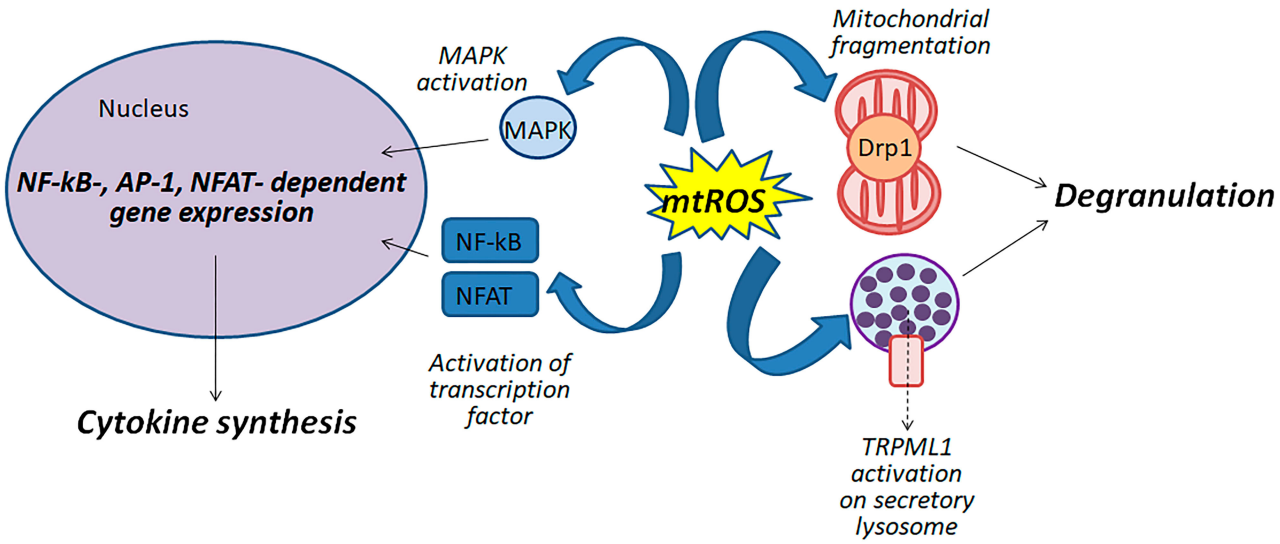

FIGURE 1 | Mitochondrial ROS (mtROS) can be involved in the activation of mast cells by various mechanisms: (i) participating in the fragmentation of mitochondria; (ii) regulating degranulation by stimulation of Ca^{2+}-channels TRPML1 localized to secretory lysosomes; (iii) affecting the activity of MAP kinases and transcription factors NF-κB and NFAT.

of the pro-inflammatory cytokines involved in T helper type 2 (Th2) dependent immune response strongly depends on calcineurin (60).

The role of the Drp1-dependent reorganization of mitochondrial reticulum in T cell activation is well-studied. Mitochondrial fragmentation that occurs during the differentiation of effector T cells is accompanied by a disassembly of ETC complexes and reducing OXPHOS activity (7). Upon T cell activation, mitochondria are translocated to the area of the immunological synapse. Mitochondrial Ca^{2+} uptake interferes with Ca^{2+}-dependent inactivation of CRAC channels and thus facilitates the increased and stabilized extracellular Ca^{2+} influx (88). The Erk1/2-dependent phosphorylation of Drp1 and the subsequent mitochondrial fragmentation were shown to be necessary for the T cell migration as it requires local ATP production at the cell leading edge and activation of the motor protein myosin (89, 90).

Notably, that Drp1 can exert functions distinct from the regulation of mitochondrial fragmentation. Drp1 has been shown to be involved in postsynaptic endocytosis in neurons (91). Drp1 was also shown to be involved in the pore formation for exocytosis of thrombocyte granules (92).

These data suggest that Drp1-mediated mitochondrial fragmentation upon antigen-induced mast cell stimulation can regulate degranulation by maintaining Ca^{2+} homeostasis and the local ATP production. At the same time, the effects of Drp1 on mast cell degranulation may be associated not only with the influence of Drp1 on mitochondrial fragmentation but also with its direct role in the exocytosis.

The Mitochondrial STAT3 and MITF

It's important to discuss the issue of two transcription factors, STAT3 and MITF, which have a small pool localized in mast cell mitochondria. The transcriptional switch induced by these proteins allows the cells to shift their metabolism rapidly in response to altered conditions.

FcεRI-dependent mast cell activation is accompanied by Erk1/2-dependent phosphorylation of STAT3 on Ser727 and its translocation to mitochondria. This affects the ETC complex III activity and elevates ATP production, but the influence on the activity of complexes I and II cannot be ruled out. The selective small-molecule inhibitor of STAT3 Stattic and the mitochondria-targeted inhibitors Mitocur-1 and Mitocur-3 (the curcumin conjugated with the triphenylphosphonium lipophilic cations) suppress both degranulation and cytokine production by mast cells *in vitro* and *in vivo* (26, 29).

Mitochondrial STAT3 can modulate mast cell activation affecting ETC activity, ROS production, Ca^{2+} homeostasis, and mitophagy. Rotenone-induced mitochondrial ROS mediate phosphorylation of STAT3 on Ser727 and its subsequent translocation to mitochondria. In its turn, mitochondrial STAT3 facilitates ATP production affecting predominantly the activity of ETC complexes I and II and decreases ROS generation. Therefore, STAT3 senses and regulates ROS levels (27, 93). Mitochondrial STAT has been also shown to bind to the mPTP component cyclophilin D and prevent its opening which can be one of the crucial mechanisms of ROS generation inhibition (94). Furthermore, mitochondrial STAT3 was shown to increase the mitochondrial and intracellular levels of Ca^{2+} (27). There is also evidence indicating that mitochondrial STAT3 inhibits mitophagy (95).

Pyruvate dehydrogenase complex (PDC) is the main regulator of Kreb's cycle and it's a complex made up of 3 subunits including pyruvate dehydrogenase PDH (2 subunits E1α, β), dihydrolipoamide acetyltransferase (E2) and dihydrolipoamide dehydrogenase (E3). For the conversion of pyruvate to acetyl-CoA, an activated dephosphorylated PDC catalyzes the oxidative decarboxylation step, thus regulating the citric acid cycle

inside mitochondria. For the mast cell function during FcεRI-dependent activation an increase in OXPHOS activity and ATP production was observed (26). MITF whose major function is to regulate the differentiation of melanocytes and osteoclasts (96) was also found in mast cells (97). The studies on lysyl-tRNA synthetase (LysRS), diadenosine tetraphosphate (Ap4A), histidine triad nucleotide-binding protein 1 (HINT1) in FcεRI-dependent stimulated mast cells highlights the transcriptional activity of MITF in mast cells and describes the LysRS-Ap4A-HINT-MITF signaling pathway (98, 99). Interestingly, peroxisome proliferator–activated receptor γ coactivator 1 α (PGC-1 α) an important coactivator for regulating OXPHOS genes for maintaining the mitochondrial biogenesis was found to be regulated by MITF (100) in melanoma cells. Most recently MITF as a protein was found to be partially localized in the mitochondria and found to interact with pyruvate dehydrogenase E1α subunit (PDH E1α) in mast cells. Allergic stimulation has activated the PDH thus causing its detachment from MITF in IgE-DNP treated RBL-2H3 cells and bone marrow–derived mast cell. Also an impaired degranulation, ATP production, oxygen consumption and the reduction of TNFα and IL-6 cytokines with CPI-613 (PDC inhibitor) treatment

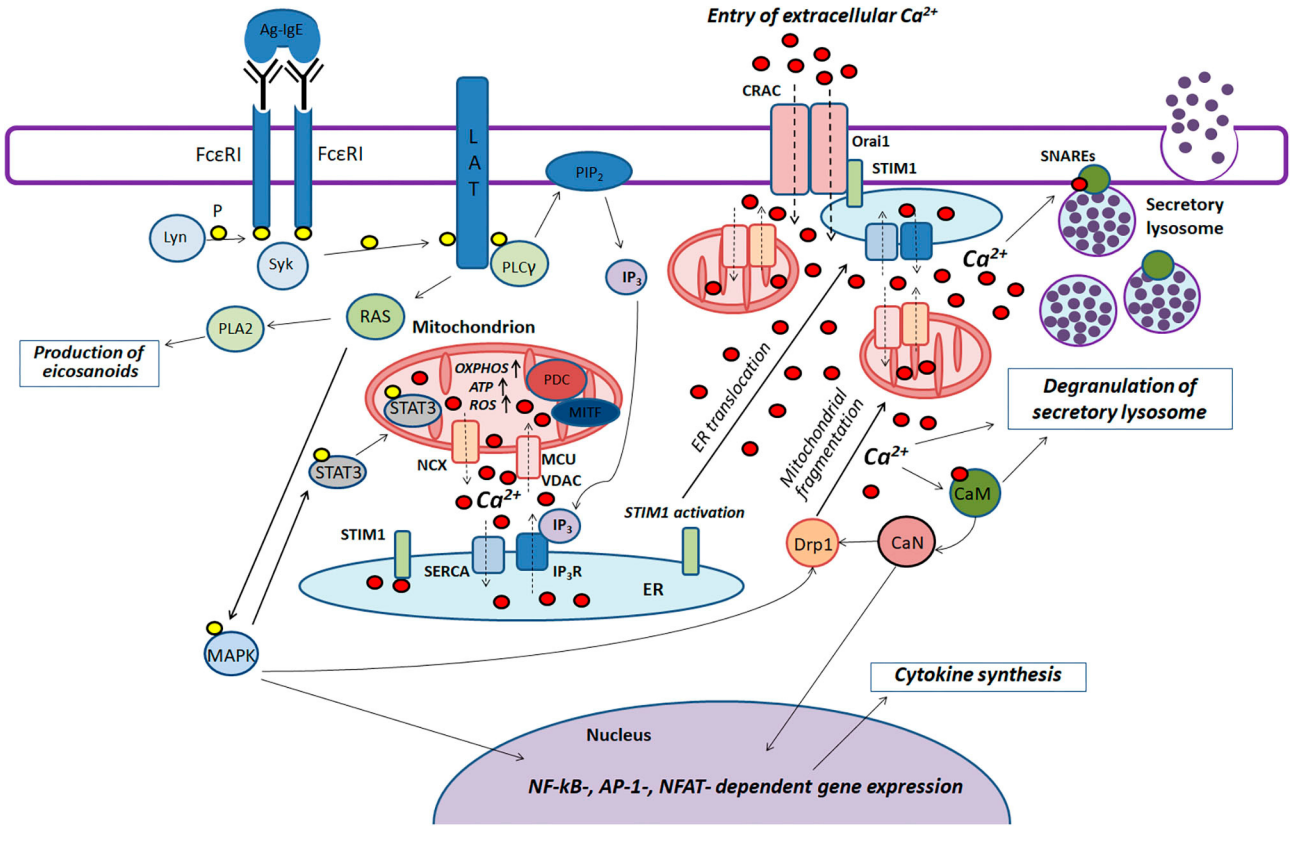

FIGURE 2 | The role played by mitochondria in the antigen-dependent mast cell stimulation. Binding of the antigen complex to IgE (Ag-IgE) causes aggregation of FcεRI receptors and recruits the Lyn kinase which phosphorylates (P) ITAM regions of FcεRI with subsequent recruitment of the Syk kinase. This kinase activates the adapter molecule LAT that further stimulates phospholipase PLCγ and small GTPase RAS. PLCγ hydrolyzes PIP_2 with the production of IP_3 and DAG. IP_3 causes Ca^{2+} release from endoplasmic reticulum (ER) through IP_3R channels. Mitochondria interact with ER and uptake the released Ca^{2+} via the potential-dependent transporter system VDAC-MCU. In mitochondria, Ca^{2+} enhances OXPHOS and ROS and ATP production. Local Ca^{2+} oscillations occur due to the activity of the mitochondrial Na^{+}/Ca^{2+}-exchanger (NCX) and SERCA pumps localized in ER. Ca^{2+} release from ER causes activation and oligomerization of the calcium sensor STIM1. After the microtubule-dependent ER translocation to the plasma membrane, STIM1 binds to the pore-forming subunits of CRAC Orai1. This maintains the current of the intracellular Ca^{2+}. The activated GTPase RAS stimulates phospholipase PLA2 and activates MAPK signaling cascade leading to the biosynthesis of eicosanoids and cytokine production. Furthermore, MAPK kinase Erk1/2 induces phosphorylation of the transcription factor STAT3 and its translocation to mitochondria. There it enhances OXPHOS and ATP production but prevents excessive ROS generation and mitophagy. A pyruvate dehydrogenase complex (PDC) regulating mitochondrial MITF along with STAT3 could also play a potential role in regulating the antigen-induced stimulation of mast cells. An elevated level of intracellular Ca^{2+} activates calmodulin (CaM) followed by stimulation of the phosphatase calcineurin (CaN) which together with MAPK kinases induces Drp1-dependent mitochondrial fragmentation along. Fragmented mitochondria are translocated to the plasma membrane. Suppression of fragmentation or translocation of mitochondria attenuates the antigen-dependent mast cell degranulation. The main function of mitochondria seems to be as following: they maintain intracellular Ca^{2+} current preventing of Ca^{2+}- and ROS-dependent inactivation of the CRAC channels. The accumulation of the intracellular Ca^{2+} is also important for activating certain proteins that play an important role in SNARE complex function which is necessary for fusion of the secretory lysosomes with each other and with the plasma membrane.

in cord blood–derived mast cell explains the importance of PDH complex during mast cells function. A decreased PDH activity with MITF overexpression in bone marrow–derived mast cell and RBL-2H3 cells indicates the importance of protein interactions in mitochondria. Also, MITF was found to associate with phosphorylated PDH after CPI-613 treatment clearly emphasizes the regulatory role of MITF for maintaining the PDH activity during allergic stimulus (28). However, the mitochondrial MITF localization and function other than regulating the PDC activity during allergic activation remains unclear.

CONCLUSION AND FUTURE DIRECTIONS

Mast cells play an important role in the pathogenesis of various inflammatory and allergic diseases. Mitochondria are actively involved in many stages of FcεRI-dependent mast cell activation. Based on literature data summarized in this review we try to present scheme of the function of mitochondria in the antigen-dependent mast cell stimulation (**Figure 2**).

Investigation of the functions of mitochondria in mast cell activation is essential as it would expand the basic knowledge about mast cell physiology and would help to design new anti-allergic and anti-inflammatory drugs targeted to mitochondria. The data summarized in the review indicate the promising potential of uncouplers, mitochondria-targeted antioxidants, and Drp1 and STAT3 inhibitors to reduce FcεRI-activation of mast cells. However, a wealth of information was obtained solely from *in vitro* studies of mast cell degranulation without estimation of cytokines and eicosanoids secretion. There is an urgent need for *in vivo* research to investigate the therapeutic potential of the drugs targeted to mitochondria.

AUTHOR CONTRIBUTIONS

All authors contributed to manuscript designing, writing, and editing and reviewed the final version of this article.

FUNDING

This work was funded by RFBR and MOST according to the research project No. 19-54-06003.

ACKNOWLEDGMENTS

We would like to thank Pletjushkina O. Y. and Galkin I. I. (A.N. Belozersky Institute of Physico-Chemical Biology, Lomonosov Moscow State University) for helpful comments.

REFERENCES

1. Skulachev VP, Bogachev AV, Kasparinsky FO. *Principles of Bioenergetics*. Berlin; Heidelberg: Springer Science & Business Media (2012).
2. Mishra P, Chan DC. Metabolic regulation of mitochondrial dynamics. *J Cell Biol*. (2016) 212:379–87. doi: 10.1083/jcb.201511036
3. Rambold AS, Pearce EL. Mitochondrial dynamics at the interface of immune cell metabolism and function. *Trends Immunol*. (2018) 39:6–18. doi: 10.1016/j.it.2017.08.006
4. Angajala A, Lim S, Phillips JB, Kim J-H, Yates C, You Z, et al. Diverse roles of mitochondria in immune responses: novel insights into immuno-metabolism. *Front Immunol*. (2018) 9:1605. doi: 10.3389/fimmu.2018.01605
5. Breda CN de S, Davanzo GG, Basso PJ, Saraiva Câmara NO, Moraes-Vieira PMM. Mitochondria as central hub of the immune system. *Redox Biol*. (2019) 26:101255. doi: 10.1016/j.redox.2019.101255
6. Michaeloudes C, Bhavsar PK, Mumby S, Xu B, Hui CKM, Chung KF, et al. Role of metabolic reprogramming in pulmonary innate immunity and its impact on lung diseases. *J Innate Immun*. (2020) 12:31–46. doi: 10.1159/000504344
7. Buck MD, O'Sullivan D, Klein Geltink RI, Curtis JD, Chang C-H, Sanin DE, et al. Mitochondrial dynamics controls T cell fate through metabolic programming. *Cell*. (2016) 166:63–76. doi: 10.1016/j.cell.2016.05.035
8. Desdín-Micó G, Soto-Heredero G, Mittelbrunn M. Mitochondrial activity in T cells. *Mitochondrion*. (2018) 41:51–7. doi: 10.1016/j.mito.2017.10.006
9. Zheng X, Chen M, Meng X, Chu X, Cai C, Zou F. Phosphorylation of dynamin-related protein 1 at Ser616 regulates mitochondrial fission and is involved in mitochondrial calcium uniporter-mediated neutrophil polarization and chemotaxis. *Mol Immunol*. (2017) 87:23–32. doi: 10.1016/j.molimm.2017.03.019
10. Sismanopoulos N, Delivanis D-A, Alysandratos K-D, Angelidou A, Therianou A, Kalogeromitros D, et al. Mast cells in allergic and inflammatory diseases. *Curr Pharm Des*. (2012) 18:2261–77. doi: 10.2174/138161212800165997
11. Theoharides TC, Alysandratos K-D, Angelidou A, Delivanis D-A, Sismanopoulos N, Zhang B, et al. Mast cells and inflammation. *Biochim Biophys Acta*. (2012) 1822:21–33. doi: 10.1016/j.bbadis.2010.12.014
12. da Silva EZM, Jamur MC, Oliver C. Mast cell function: a new vision of an old cell. *J Histochem Cytochem*. (2014) 62:698–738. doi: 10.1369/0022155414545334
13. Krystel-Whittemore M, Dileepan KN, Wood JG. Mast cell: a multi-functional master cell. *Front Immunol*. (2016) 6:620. doi: 10.3389/fimmu.2015.00620
14. Zhang B, Alysandratos K-D, Angelidou A, Asadi S, Sismanopoulos N, Delivanis D-A, et al. Human mast cell degranulation and preformed TNF secretion require mitochondrial translocation to exocytosis sites: relevance to atopic dermatitis. *J Allergy Clin Immunol*. (2011) 127:1522–31.e8. doi: 10.1016/j.jaci.2011.02.005
15. Zhang B, Asadi S, Weng Z, Sismanopoulos N, Theoharides TC. Stimulated human mast cells secrete mitochondrial components that have autocrine and paracrine inflammatory actions. *PLoS ONE*. (2012) 7:e49767. doi: 10.1371/journal.pone.0049767
16. Mohr FC, Fewtrell C. The relative contributions of extracellular and intracellular calcium to secretion from tumor mast cells. Multiple effects of the proton ionophore carbonyl cyanide m-chlorophenylhydrazone. *J Biol Chem*. (1987) 262:10638–43.
17. Suzuki Y, Yoshimaru T, Inoue T, Ra C. Mitochondrial Ca^{2+} flux is a critical determinant of the Ca^{2+} dependence of mast cell degranulation. *J Leukoc Biol*. (2006) 79:508–18. doi: 10.1189/jlb.0705412
18. Weatherly LM, Shim J, Hashmi HN, Kennedy RH, Hess ST, Gosse JA. Antimicrobial agent triclosan is a proton ionophore uncoupler of mitochondria in living rat and human mast cells and in primary human keratinocytes. *J Appl Toxicol*. (2016) 36:777–89. doi: 10.1002/jat.3209
19. Weatherly LM, Nelson AJ, Shim J, Riitano AM, Gerson ED, Hart AJ, et al. Antimicrobial agent triclosan disrupts mitochondrial structure, revealed by super-resolution microscopy, and inhibits mast cell signaling via calcium modulation. *Toxicol Appl Pharmacol*. (2018) 349:39–54. doi: 10.1016/j.taap.2018.04.005

20. Ma H-T, Beaven MA. Regulators of Ca^{2+} signaling in mast cells: potential targets for treatment of mast cell-related diseases? *Adv Exp Med Biol*. (2011) 716:62–90. doi: 10.1007/978-1-4419-9533-9_5
21. Furuno T, Shinkai N, Inoh Y, Nakanishi M. Impaired expression of the mitochondrial calcium uniporter suppresses mast cell degranulation. *Mol Cell Biochem*. (2015) 410:215–21. doi: 10.1007/s11010-015-2554-4
22. Marchi S, Patergnani S, Missiroli S, Morciano G, Rimessi A, Wieckowski MR, et al. Mitochondrial and endoplasmic reticulum calcium homeostasis and cell death. *Cell Calcium*. (2018) 69:62–72. doi: 10.1016/j.ceca.2017.05.003
23. Trebak M, Kinet J-P. Calcium signalling in T cells. *Nat Rev Immunol*. (2019) 19:154–69. doi: 10.1038/s41577-018-0110-7
24. Tagen M, Elorza A, Kempuraj D, Boucher W, Kepley CL, Shirihai OS, et al. Mitochondrial uncoupling protein 2 inhibits mast cell activation and reduces histamine content. *J Immunol*. (2009) 183:6313–9. doi: 10.4049/jimmunol.0803422
25. Chelombitko MA, Averina OA, Vasilyeva TV, Pletiushkina OY, Popova EN, Fedorov AV, et al. Mitochondria-targeted antioxidant SkQ1 (10-(6'-plastoquinonyl)decyltriphenylphosphonium bromide) inhibits mast cell degranulation *in vivo* and *in vitro*. *Biochemistry*. (2017) 82:1493–503. doi: 10.1134/S0006297917120082
26. Erlich TH, Yagil Z, Kay G, Peretz A, Migalovich-Sheikhet H, Tshori S, et al. Mitochondrial STAT3 plays a major role in IgE-antigen–mediated mast cell exocytosis. *J Allergy Clin Immunol*. (2014) 134:460–9.e10. doi: 10.1016/j.jaci.2013.12.1075
27. Yang R, Rincon M. Mitochondrial Stat3, the need for design thinking. *Int J Biol Sci*. (2016) 12:532–44. doi: 10.7150/ijbs.15153
28. Sharkia I, Erlich TH, Landolina N, Assayag M, Motzik A, Rachmin I, et al. Pyruvate dehydrogenase has a major role in mast cell function, and its activity is regulated by mitochondrial microphthalmia transcription factor. *J Allergy Clin Immunol*. (2017) 140:204–14.e8. doi: 10.1016/j.jaci.2016.09.047
29. Erlich TH, Sharkia I, Landolina N, Assayag M, Goldberger O, Berkman N, et al. Modulation of allergic responses by mitochondrial STAT3 inhibitors. *Allergy*. (2018) 73:2160–71. doi: 10.1111/all.13467
30. Wernersson S, Pejler G. Mast cell secretory granules: armed for battle. *Nat Rev Immunol*. (2014) 14:478–94. doi: 10.1038/nri3690
31. Pejler G, Hu Frisk JM, Sjöström D, Paivandy A, Öhrvik H. Acidic pH is essential for maintaining mast cell secretory granule homeostasis. *Cell Death Dis*. (2017) 8:e2785. doi: 10.1038/cddis.2017.206
32. Razin E, Mencia-Huerta JM, Stevens RL, Lewis RA, Liu FT, Corey E, et al. IgE-mediated release of leukotriene C4, chondroitin sulfate E proteoglycan, beta-hexosaminidase, and histamine from cultured bone marrow-derived mouse mast cells. *J Exp Med*. (1983) 157:189–201. doi: 10.1084/jem.157.1.189
33. Moon TC, St Laurent CD, Morris KE, Marcet C, Yoshimura T, Sekar Y, et al. Advances in mast cell biology: new understanding of heterogeneity and function. *Mucosal Immunol*. (2010) 3:111–28. doi: 10.1038/mi.2009.136
34. Akula S, Paivandy A, Fu Z, Thorpe M, Pejler G, Hellman L, et al. Quantitative in-depth analysis of the mouse mast cell transcriptome reveals organ-specific mast cell heterogeneity. *Cells*. (2020) 9:211. doi: 10.3390/cells9010211
35. Elieh Ali Komi D, Wöhrl S, Bielory L. Mast cell biology at molecular level: a comprehensive review. *Clin Rev Allergy Immunol*. (2020) 58:342–65. doi: 10.1007/s12016-019-08769-2
36. Parravicini V, Gadina M, Kovarova M, Odom S, Gonzalez-Espinosa C, Furumoto Y, et al. Fyn kinase initiates complementary signals required for IgE-dependent mast cell degranulation. *Nat Immunol*. (2002) 3:741–8. doi: 10.1038/ni817
37. Sibilano R, Frossi B, Pucillo CE. Mast cell activation: a complex interplay of positive and negative signaling pathways. *Eur J Immunol*. (2014) 44:2558–66. doi: 10.1002/eji.201444546
38. Kim MS, Rådinger M, Gilfillan AM. The multiple roles of phosphoinositide 3-kinase in mast cell biology. *Trends Immunol*. (2008) 29:493–501. doi: 10.1016/j.it.2008.07.004
39. Ryu H, Walker JKL, Kim S, Koo N, Barak LS, Noguchi T, et al. Regulation of M2-type pyruvate kinase mediated by the high-affinity IgE receptors is required for mast cell degranulation. *Br J Pharmacol*. (2008) 154:1035–46. doi: 10.1038/bjp.2008.148
40. Phong B, Avery L, Menk AV, Delgoffe GM, Kane LP. Cutting edge: murine mast cells rapidly modulate metabolic pathways essential for distinct effector functions. *J Immunol*. (2017) 198:640–4. doi: 10.4049/jimmunol.1601150
41. Perry SW, Norman JP, Barbieri J, Brown EB, Gelbard HA. Mitochondrial membrane potential probes and the proton gradient: a practical usage guide. *Biotechniques*. (2011) 50:98–115. doi: 10.2144/000113610
42. Zorova LD, Popkov VA, Plotnikov EY, Silachev DN, Pevzner IB, Jankauskas SS, et al. Mitochondrial membrane potential. *Anal Biochem*. (2018) 552:50–9. doi: 10.1016/j.ab.2017.07.009
43. Brookes PS, Yoon Y, Robotham JL, Anders MW, Sheu S-S. Calcium, ATP, and ROS: a mitochondrial love-hate triangle. *Am J Physiol Cell Physiol*. (2004) 287:C817–33. doi: 10.1152/ajpcell.00139.2004
44. Chelombitko MA, Firsov AM, Kotova EA, Rokitskaya TI, Khailova LS, Popova LB, et al. Usnic acid as calcium ionophore and mast cells stimulator. *Biochim Biophys Acta Biomembr*. (2020) 1862:183303. doi: 10.1016/j.bbamem.2020.183303
45. Rizzuto R, De Stefani D, Raffaello A, Mammucari C. Mitochondria as sensors and regulators of calcium signalling. *Nat Rev Mol Cell Biol*. (2012) 13:566–78. doi: 10.1038/nrm3412
46. Bernardi P, Rasola A, Forte M, Lippe G. The mitochondrial permeability transition pore: channel formation by F-ATP synthase, integration in signal transduction, and role in pathophysiology. *Physiol Rev*. (2015) 95:1111–55. doi: 10.1152/physrev.00001.2015
47. Bohovych I, Khalimonchuk O. Sending out an SOS: mitochondria as a signaling hub. *Front Cell Dev Biol*. (2016) 4:109. doi: 10.3389/fcell.2016.00109
48. Holowka D, Calloway N, Cohen R, Gadi D, Lee J, Smith NL, et al. Roles for Ca^{2+} mobilization and its regulation in mast cell functions. *Front Immunol*. (2012) 3:104. doi: 10.3389/fimmu.2012.00104
49. Suzuki R, Liu X, Olivera A, Aguiniga L, Yamashita Y, Blank U, et al. Loss of TRPC1-mediated Ca^{2+} influx contributes to impaired degranulation in Fyn-deficient mouse bone marrow-derived mast cells. *J Leukoc Biol*. (2010) 88:863–75. doi: 10.1189/jlb.0510253
50. Ma HT, Peng Z, Hiragun T, Iwaki S, Gilfillan AM, Beaven MA. Canonical transient receptor potential 5 channel in conjunction with Orai1 and STIM1 allows Sr^{2+} entry, optimal influx of Ca^{2+}, and degranulation in a rat mast cell line. *J Immunol*. (2008) 180:2233–9. doi: 10.4049/jimmunol.180.4.2233
51. Smyth JT, DeHaven WI, Bird GS, Putney JW Jr. Role of the microtubule cytoskeleton in the function of the store-operated Ca^{2+} channel activator STIM1. *J Cell Sci*. (2007) 120:3762–71. doi: 10.1242/jcs.015735
52. Wu S, Chen H, Alexeyev MF, King JA, Moore TM, Stevens T, et al. Microtubule motors regulate ISOC activation necessary to increase endothelial cell permeability. *J Biol Chem*. (2007) 282:34801–8. doi: 10.1074/jbc.M704522200
53. Shen WW, Frieden M, Demaurex N. Remodelling of the endoplasmic reticulum during store-operated calcium entry. *Biol Cell*. (2011) 103:365–80. doi: 10.1042/BC20100152
54. Singaravelu K, Nelson C, Bakowski D, de Brito OM, Ng SW, Capite JD, et al. Mitofusin 2 regulates STIM1 migration from the Ca^{2+} store to the plasma membrane in cells with depolarized mitochondria. *J Biol Chem*. (2011) 286:12189–201. doi: 10.1074/jbc.M110.174029
55. Deak AT, Blass S, Khan MJ, Groschner LN, Waldeck-Weiermair M, Hallström S, et al. IP3-mediated STIM1 oligomerization requires intact mitochondrial Ca^{2+} uptake. *J Cell Sci*. (2014) 127:2944–55. doi: 10.1242/jcs.149807
56. Takekawa M, Furuno T, Hirashima N, Nakanishi M. Mitochondria take up Ca^{2+} in two steps dependently on store-operated Ca^{2+} entry in mast cells. *Biol Pharm Bull*. (2012) 35:1354–60. doi: 10.1248/bpb.b110576
57. Nissim TB, Zhang X, Elazar A, Roy S, Stolwijk JA, Zhou Y, et al. Mitochondria control store-operated Ca^{2+} entry through Na and redox signals. *EMBO J*. (2017) 36:797–815. doi: 10.15252/embj.201592481
58. Funaba M. Degranulation in RBL-2H3 cells: regulation by calmodulin pathway. *Cell Biol Int*. (2003) 27:879–85. doi: 10.1016/S1065-6995(03)00177-X
59. Bornhövd EC, Burgdorf WHC, Wollenberg A. Immunomodulatory macrolactams for topical treatment of inflammatory skin diseases. *Curr Opin Investig Drugs*. (2002) 3:708–12.
60. Ma Z, Jiao Z. Mast cells as targets of pimecrolimus. *Curr Pharm Des*. (2011) 17:3823–9. doi: 10.2174/138161211798357827
61. Settembre C, Fraldi A, Medina DL, Ballabio A. Signals from the lysosome: a control centre for cellular clearance and energy metabolism. *Nat Rev Mol Cell Biol*. (2013) 14:283–96. doi: 10.1038/nrm3565

62. Woo SS, James DJ, Martin TFJ. Munc13-4 functions as a Ca^{2+} sensor for homotypic secretory granule fusion to generate endosomal exocytic vacuoles. *Mol Biol Cell*. (2017) 28:792–808. doi: 10.1091/mbc.e16-08-0617
63. Klein O, Sagi-Eisenberg R. Anaphylactic degranulation of mast cells: focus on compound exocytosis. *J Immunol Res*. (2019) 2019:9542656. doi: 10.1155/2019/9542656
64. Zorov DB, Juhaszova M, Sollott SJ. Mitochondrial reactive oxygen species (ROS) and ROS-induced ROS release. *Physiol Rev*. (2014) 94:909–50. doi: 10.1152/physrev.00026.2013
65. Shanmugasundaram K, Nayak BK, Friedrichs WE, Kaushik D, Rodriguez R, Block K. NOX4 functions as a mitochondrial energetic sensor coupling cancer metabolic reprogramming to drug resistance. *Nat Commun*. (2017) 8:997. doi: 10.1038/s41467-017-01106-1
66. Forrester SJ, Kikuchi DS, Hernandes MS, Xu Q, Griendling KK. Reactive oxygen species in metabolic and inflammatory signaling. *Circ Res*. (2018) 122:877–902. doi: 10.1161/CIRCRESAHA.117.311401
67. Chelombitko MA, Fedorov AV, Ilyinskaya OP, Zinovkin RA, Chernyak BV. Role of reactive oxygen species in mast cell degranulation. *Biochemistry*. (2016) 81:1564–77. doi: 10.1134/S000629791612018X
68. Pletjushkina OY, Lyamzaev KG, Popova EN, Nepryakhina OK, Ivanova OY, Domnina LV, et al. Effect of oxidative stress on dynamics of mitochondrial reticulum. *Biochim Biophys Acta*. (2006) 1757:518–24. doi: 10.1016/j.bbabio.2006.03.018
69. Solesio ME, Prime TA, Logan A, Murphy MP, Del Mar Arroyo-Jimenez M, Jordán J, et al. The mitochondria-targeted anti-oxidant MitoQ reduces aspects of mitochondrial fission in the 6-OHDA cell model of Parkinson's disease. *Biochim Biophys Acta*. (2013) 1832:174–82. doi: 10.1016/j.bbadis.2012.07.009
70. Yin X, Manczak M, Reddy PH. Mitochondria-targeted molecules MitoQ and SS31 reduce mutant huntingtin-induced mitochondrial toxicity and synaptic damage in Huntington's disease. *Hum Mol Genet*. (2016) 25:1739–53. doi: 10.1093/hmg/ddw045
71. Rogov AG, Goleva TN, Trendeleva TA, Ovchenkova AP, Aliverdieva DA, Zvyagilskaya RA. New data on effects of SkQ1 and SkQT1 on rat liver mitochondria and yeast cells. *Biochemistry*. (2018) 83:552–61. doi: 10.1134/S0006297918050085
72. Xiao L, Xu X, Zhang F, Wang M, Xu Y, Tang D, et al. The mitochondria-targeted antioxidant MitoQ ameliorated tubular injury mediated by mitophagy in diabetic kidney disease via Nrf2/PINK1. *Redox Biol*. (2017) 11:297–311. doi: 10.1016/j.redox.2016.12.022
73. Clement D, Goodridge JP, Grimm C, Patel S, Malmberg KJ. TRP channels as interior designers: remodeling the endolysosomal compartment in natural killer cells. *Front Immunol*. (2020) 11:753. doi: 10.3389/fimmu.2020.00753
74. Zhang X, Cheng X, Yu L, Yang J, Calvo R, Patnaik S, et al. MCOLN1 is a ROS sensor in lysosomes that regulates autophagy. *Nat Commun*. (2016) 7:12109. doi: 10.1038/ncomms12109
75. Di Paola S, Medina DL. TRPML1-/TFEB-dependent regulation of lysosomal exocytosis. *Methods Mol Biol*. (2019) 1925:143–44. doi: 10.1007/978-1-4939-9018-4_12
76. Goodridge JP, Jacobs B, Saetersmoen ML, Clement D, Clancy T, Skarpen E, et al. TRPML1-mediated modulation of dense-core granules tunes functional potential in NK cells. *bioRxiv [Preprint]*. (2018) 305862. doi: 10.1101/305862
77. Shaik GM, Dráberová L, Heneberg P, Dráber P. Vacuolin-1-modulated exocytosis and cell resealing in mast cells. *Cell Signal*. (2009) 21:1337–45 doi: 10.1016/j.cellsig.2009.04.001
78. Sundqvist M, Christenson K, Björnsdottir H, Osla V, Karlsson A, Dahlgren C, et al. Elevated mitochondrial reactive oxygen species and cellular redox imbalance in human NADPH-oxidase-deficient phagocytes. *Front Immunol*. (2017) 8:1828. doi: 10.3389/fimmu.2017.01828
79. Emerling BM, Platanias LC, Black E, Nebreda AR, Davis RJ, Chandel NS. Mitochondrial reactive oxygen species activation of p38 mitogen-activated protein kinase is required for hypoxia signaling. *Mol Cell Biol*. (2005) 25:4853–62. doi: 10.1128/MCB.25.12.4853-4862.2005
80. Wang C, Shao L, Pan C, Ye J, Ding Z, Wu J, et al. Elevated level of mitochondrial reactive oxygen species via fatty acid β-oxidation in cancer stem cells promotes cancer metastasis by inducing epithelial–mesenchymal transition. *Stem Cell Res Ther*. (2019) 10:175. doi: 10.1186/s13287-019-1265-2
81. Park J, Min J-S, Kim B, Chae U-B, Yun JW, Choi M-S, et al. Mitochondrial ROS govern the LPS-induced pro-inflammatory response in microglia cells by regulating MAPK and NF-κB pathways. *Neurosci Lett*. (2015) 584:191–196. doi: 10.1016/j.neulet.2014.10.016
82. Rehman H, Liu Q, Krishnasamy Y, Shi Z. The mitochondria-targeted antioxidant MitoQ attenuates liver fibrosis in mice. *J Physiol*. (2016) 8:14–27.
83. Shagieva G, Domnina L, Makarevich O, Chernyak B, Skulachev V, Dugina V. Depletion of mitochondrial reactive oxygen species downregulates epithelial-to-mesenchymal transition in cervical cancer cells. *Oncotarget*. (2017) 8:4901. doi: 10.18632/oncotarget.13612
84. Zinovkin RA, Romaschenko VP, Galkin II, Zakharova VV, Pletjushkina OY, Chernyak BV, et al. Role of mitochondrial reactive oxygen species in age-related inflammatory activation of endothelium. *Aging*. (2014) 6:661–74. doi: 10.18632/aging.100685
85. Herb M, Gluschko A, Wiegmann K, Farid A, Wolf A, Utermöhlen O, et al. Mitochondrial reactive oxygen species enable proinflammatory signaling through disulfide linkage of NEMO. *Sci Signal*. (2019) 12:eaar5926. doi: 10.1126/scisignal.aar5926
86. Sena LA, Li S, Jairaman A, Prakriya M, Ezponda T, Hildeman DA, et al. Mitochondria are required for antigen-specific T cell activation through reactive oxygen species signaling. *Immunity*. (2013) 38:225–36. doi: 10.1016/j.immuni.2012.10.020
87. Chen H-Y, Chiang DM-L, Lin Z-J, Hsieh C-C, Yin G-C, Chun Weng I, et al. Nanoimaging granule dynamics and subcellular structures in activated mast cells using soft X-ray tomography. *Sci Rep*. (2017) 7:40458. doi: 10.1038/srep40458
88. Quintana A, Schwindling C, Wenning AS, Becherer U, Rettig J, Schwarz EC, et al. T cell activation requires mitochondrial translocation to the immunological synapse. *Proc Natl Acad Sci USA*. (2007) 104:14418–23. doi: 10.1073/pnas.0703126104
89. Baixauli F, Martín-Cófreces NB, Morlino G, Carrasco YR, Calabia-Linares C, Veiga E, et al. The mitochondrial fission factor dynamin-related protein 1 modulates T-cell receptor signalling at the immune synapse. *EMBO J*. (2011) 30:1238–50. doi: 10.1038/emboj.2011.25
90. Simula L, Pacella I, Colamatteo A, Procaccini C, Cancila V, Bordi M, et al. Drp1 Controls effective T cell immune-surveillance by regulating T cell migration, proliferation, and cMyc-dependent metabolic reprogramming. *Cell Rep*. (2018) 25:3059–73.e10. doi: 10.1016/j.celrep.2018.11.018
91. Itoh K, Murata D, Kato T, Yamada T, Araki Y, Saito A, et al. Brain-specific Drp1 regulates postsynaptic endocytosis and dendrite formation independently of mitochondrial division. *eLife*. (2019) 8:e44739. doi: 10.7554/eLife.44739
92. Koseoglu S, Dilks JR, Peters CG, Fitch-Tewfik JL, Fadel NA, Jasuja R, et al. Dynamin-related protein-1 controls fusion pore dynamics during platelet granule exocytosis. *Arterioscl Thromb Vasc Biol*. (2013) 33:481–8. doi: 10.1161/ATVBAHA.112.255737
93. Mohammed F, Gorla M, Bisoyi V, Tammineni P, Sepuri NBV. Rotenone-induced reactive oxygen species signal the recruitment of STAT3 to mitochondria. *FEBS Lett*. (2020) 594:1403–12. doi: 10.1002/1873-3468.13741
94. Meier JA, Hyun M, Cantwell M, Raza A, Mertens C, Raje V, et al. Stress-induced dynamic regulation of mitochondrial STAT3 and its association with cyclophilin D reduce mitochondrial ROS production. *Sci Signal*. (2017) 10:472. doi: 10.1126/scisignal.aag2588
95. You L, Wang Z, Li H, Shou J, Jing Z, Xie J, et al. The role of STAT3 in autophagy. *Autophagy*. (2015) 11:729–39. doi: 10.1080/15548627.2015.1017192
96. Hershey CL, Fisher DE. Mitf and Tfe3: members of a b-HLH-ZIP transcription factor family essential for osteoclast development and function. *Bone*. (2004) 34:689–96. doi: 10.1016/j.bone.2003.08.014
97. Lee Y-N, Nechushtan H, Figov N, Razin E. The function of Lysyl-tRNA synthetase and Ap4A as signaling regulators of MITF activity in FcεRI-activated mast cells. *Immunity*. (2004) 20:145–51. doi: 10.1016/S1074-7613(04)00020-2
98. Carmi-Levy I, Yannay-Cohen N, Kay G, Razin E, Nechushtan H. Diadenosine tetraphosphate hydrolase is part of the

transcriptional regulation network in immunologically activated mast cells. *Mol Cell Biol*. (2008) 28:5777–84. doi: 10.1128/MCB.00106-08

99. Yannay-Cohen N, Carmi-Levy I, Kay G, Yang CM, Han JM, Michael Kemeny D, et al. LysRS serves as a key signaling molecule in the immune response by regulating gene expression. *Mol Cell*. (2009) 34:603–11. doi: 10.1016/j.molcel.2009.05.019
100. Haq R, Shoag J, Andreu-Perez P, Yokoyama S, Edelman H, Rowe GC, et al. Oncogenic BRAF regulates oxidative metabolism via PGC1α and MITF. *Cancer Cell*. (2013) 23:302–15. doi: 10.1016/j.ccr.2013.02.003

Conflict of Interest: The authors declare that the research was conducted in the absence of any commercial or financial relationships that could be construed as a potential conflict of interest.

frontiers in Immunology

CORRECTION
published: 11 December 2020
doi: 10.3389/fimmu.2020.620293

Corrigendum: The Role Played by Mitochondria in FcεRI-Dependent Mast Cell Activation

Maria A. Chelombitko[1], Boris V. Chernyak[1], Artem V. Fedorov[2], Roman A. Zinovkin[1,3], Ehud Razin[4] and Lakhsmi Bhargavi Paruchuru[4]**

[1] Belozersky Institute of Physico-Chemical Biology, Lomonosov Moscow State University, Moscow, Russia, [2] Department of Cell Biology and Histology, Biology Faculty, Lomonosov Moscow State University, Moscow, Russia, [3] Institute of Molecular Medicine, I.M. Sechenov First Moscow State Medical University, Moscow, Russia, [4] Department of Biochemistry and Molecular Biology, School of Medicine, Hebrew University of Jerusalem, Jerusalem, Israel

OPEN ACCESS

Edited and reviewed by:
Pedro Manoel Mendes Moraes Vieira, Campinas State University, Brazil

***Correspondence:**
Maria A. Chelombitko
chelombitko@mail.bio.msu.ru
Lakhsmi Bhargavi Paruchuru
bhargavi.lakshmi@mail.huji.ac.il

Specialty section:
This article was submitted to Molecular Innate Immunity, a section of the journal Frontiers in Immunology

Received: *22 October 2020*
Accepted: *10 November 2020*
Published: *11 December 2020*

Citation:
Chelombitko MA, Chernyak BV, Fedorov AV, Zinovkin RA, Razin E and Paruchuru LB (2020) Corrigendum: The Role Played by Mitochondria in FcεRI-Dependent Mast Cell Activation. Front. Immunol. 11:620293. doi: 10.3389/fimmu.2020.620293

Keywords: mast cell, mitochondria, FcεRI-dependent activation, IgE, allergy

A Corrigendum on

The Role Played by Mitochondria in FcεRI-Dependent Mast Cell Activation
By Chelombitko MA, Chernyak BV, Fedorov AV, Zinovkin RA, Razin E and Paruchuru LB (2020). Front. Immunol. 11:584210. doi: 10.3389/fimmu.2020.584210

In the original article, there was an error. The statement that mitochondrial ROS inhibit the activity of NEMO is wrong. Mitochondrial ROS are crucial for the activation of the IKK-NEMO complex.

A correction has been made to the section **The Role Played by Mitochondria in the FcεRI-Dependent Mast Cell Activation,** subsection **Mitochondrial ROS**, paragraph 6. The correct paragraph appears below.

Mitochondrial ROS can stimulate NF-κB signaling by activating the kinase (IKK) of the inhibitor of NF-κB (IκB), which promotes its proteasome degradation and induces nuclear translocation of NF-κB (81, 84). Mitochondrial ROS-dependent activation of IKK can be mediated by several mechanisms, including the formation of intermolecular disulfide bonds in NF-κB essential modulator (NEMO), a component of the IKK complex (85).

The authors apologize for this error and state that this does not change the scientific conclusions of the article in any way. The original article has been updated.

REFERENCES

81. Park J, Min J-S, Kim B, Chae U-B, Yun JW, Choi M-S, et al. Mitochondrial ROS govern the LPS-induced pro-inflammatory response in microglia cells by regulating MAPK and NF-κB pathways. *Neurosci Lett.* (2015) 584:191–196. doi: 10.1016/j.neulet.2014.10.016
84. Zinovkin RA, Romaschenko VP, Galkin II, Zakharova VV, Pletjushkina OY, Chernyak BV, et al. Role of mitochondrial reactive oxygen species in age-related inflammatory activation of endothelium. *Aging.* (2014) 6:661–74. doi: 10.18632/aging.100685
85. Herb M, Gluschko A, Wiegmann K, Farid A, Wolf A, Utermöhlen O, et al. Mitochondrial reactive oxygen species enable proinflammatory signaling through disulfide linkage of NEMO. *Sci Signal.* (2019) 12:eaar5926. doi: 10.1126/scisignal.aar5926

frontiers in Immunology

ORIGINAL RESEARCH
published: 02 November 2020
doi: 10.3389/fimmu.2020.564950

Neutrophil-to-Lymphocyte Ratio: A Biomarker to Monitor the Immune Status of Astronauts

*Amber M. Paul[1,2], Siddhita D. Mhatre[1,3,4], Egle Cekanaviciute[1], Ann-Sofie Schreurs[1], Candice G. T. Tahimic[1,3,5], Ruth K. Globus[1], Sulekha Anand[6], Brian E. Crucian[7] and Sharmila Bhattacharya[1]**

[1] Space Biosciences Division, NASA Ames Research Center, Moffett Field, CA, United States, [2] Universities Space Research Association, Columbia, MD, United States, [3] COSMIAC Research Center, University of New Mexico, Albuquerque, NM, United States, [4] KBR, Houston, TX, United States, [5] Department of Biology, University of North Florida, Jacksonville, FL, United States, [6] Department of Biological Sciences, San Jose State University, San Jose, CA, United States, [7] Biomedical Research and Environmental Sciences Division, NASA Johnson Science Center, Houston, TX, United States

OPEN ACCESS

Edited by:
Edecio Cunha-Neto,
University of São Paulo, Brazil

Reviewed by:
Luz Pamela Blanco,
National Institutes of Health (NIH), United States
Katherine R. Martin,
Walter and Eliza Hall Institute of Medical Research, Australia

***Correspondence:**
Sharmila Bhattacharya
Sharmila.Bhattacharya@nasa.gov

Specialty section:
This article was submitted to Inflammation, a section of the journal Frontiers in Immunology

Received: 23 May 2020
Accepted: 12 October 2020
Published: 02 November 2020

Citation:
Paul AM, Mhatre SD, Cekanaviciute E, Schreurs A-S, Tahimic CGT, Globus RK, Anand S, Crucian BE and Bhattacharya S (2020) Neutrophil-to-Lymphocyte Ratio: A Biomarker to Monitor the Immune Status of Astronauts. Front. Immunol. 11:564950. doi: 10.3389/fimmu.2020.564950

A comprehensive understanding of spaceflight factors involved in immune dysfunction and the evaluation of biomarkers to assess in-flight astronaut health are essential goals for NASA. An elevated neutrophil-to-lymphocyte ratio (NLR) is a potential biomarker candidate, as leukocyte differentials are altered during spaceflight. In the reduced gravity environment of space, rodents and astronauts displayed elevated NLR and granulocyte-to-lymphocyte ratios (GLR), respectively. To simulate microgravity using two well-established ground-based models, we cultured human whole blood-leukocytes in high-aspect rotating wall vessels (HARV-RWV) and used hindlimb unloaded (HU) mice. Both HARV-RWV simulation of leukocytes and HU-exposed mice showed elevated NLR profiles comparable to spaceflight exposed samples. To assess mechanisms involved, we found the simulated microgravity HARV-RWV model resulted in an imbalance of redox processes and activation of myeloperoxidase-producing inflammatory neutrophils, while antioxidant treatment reversed these effects. In the simulated microgravity HU model, mitochondrial catalase-transgenic mice that have reduced oxidative stress responses showed reduced neutrophil counts, NLR, and a dampened release of selective inflammatory cytokines compared to wildtype HU mice, suggesting simulated microgravity induced oxidative stress responses that triggered inflammation. In brief, both spaceflight and simulated microgravity models caused elevated NLR, indicating this as a potential biomarker for future in-flight immune health monitoring.

Keywords: neutrophils, spaceflight, simulated microgravity, NLR, inflammation, oxidative stress response

INTRODUCTION

Spaceflight can pose novel challenges to the health of astronauts. For instance, physiological aging occurs significantly faster as a result of spaceflight, when measured by muscle wasting, loss of bone density, and immune dysfunction (1, 2). Processes regulated by redox imbalance may contribute to these adverse outcomes (3–9). Redox imbalance results from a disproportionate increase in reactive

oxygen species (ROS) produced by the mitochondria (10) compared to antioxidants in the cell. Elevated ROS is also a product of the oxidative burst response of neutrophils (11). In response to stimuli, terminally differentiated neutrophils in circulation become activated and engage the oxidative burst response, producing inflammatory mediators (11). If left unchecked, elevated ROS can cause cellular damage that potentiates inflammation both on Earth and during spaceflight (4, 12). Therefore, it is necessary to maintain tight regulation of the oxidative burst response to limit inflammation (13) and regulate immunity during prolonged spaceflight.

Neutrophils are granulocytes that constitute approximately 50–70% of the total leukocyte population in humans. Neutrophils are the first responders to infection or injury and are typically short-lived in blood circulation under homeostatic conditions (14, 15). Lymphocytes are an important group of white blood cells involved in both innate and adaptive immunity. They constitute 20–50% of total leukocytes in circulation and consist of natural killer, natural killer T cells, innate lymphoid cells, T cells, and B cells (16, 17). On Earth, elevated neutrophil-to-lymphocyte ratio (NLR) is a useful biomarker to measure subclinical inflammation in humans (18). Chronic, persistent inflammation can be a major pre-existing cause of disease development (19, 20) and can be monitored by the expression of blood-based biomarkers. For example, elevated NLR predicts poor prognosis in some cancers (21–24), positively correlates with age (25), and reflects chronic stress in mice (26). Although, elevated human NLR (>3.53) (27) has been implicated in clinical settings to identify heightened inflammation (18), this biomarker has not yet been recognized for spaceflight-induced inflammation. Spaceflight raises circulating white blood cell (WBC) counts, primarily granulocytes, may reduce lymphocyte counts (12, 28, 29), and impairs immune cell functions (6, 12, 30, 31). Although, the spaceflight environment elevates circulating blood granulocytes counts in astronauts (29), the underlying molecular mechanisms remain elusive. Currently, there are no well-established biomarkers for astronauts on long-duration, deep space missions, where medical intervention will be limited. Thus, identifying biomarkers to monitor in-flight astronaut health and developing countermeasures that reverse these adverse outcomes are necessary for successful future missions to the lunar surface and Mars. Therefore, we propose that an elevated NLR may be a useful prognostic indicator or diagnostic biomarker to assess astronaut immune status during long-duration missions.

To test this, we analyzed both spaceflight-treated, and ground-based simulated microgravity-treated, samples to determine if NLR was elevated. Analyses of complete blood count (CBC) leukocyte differentials revealed spaceflight caused a progressive increase of granulocyte-to-lymphocyte (GLR) in astronauts and NLR in rodents. To simulate microgravity using established methods, human leukocytes were cultured in high-aspect rotating wall vessels (HARV-RWV) *in vitro* and mice were hindlimb unloaded (HU) *in vivo* (32, 33). HARV-RWV is a bioreactor allowing 3D-spatial freedom for cells and can model microgravity. It has two unique aspects similar to the spaceflight-associated microgravity environment, (1) a state of constant suspension, and (2) a quiescent surrounding without any shear or turbulent forces. Previous studies have determined leukocyte responses utilizing HARV-RWV produce similar responses as leukocytes cultured post-landing or *ex vivo* in flight (34–42). Hindlimb unloading (HU) is a ground-based model mimicking spaceflight-associated microgravity in rodents. The hindlimbs of rodents are elevated to produce 30–40 degree head-down tilt, inducing a cephalad fluid shift and preventing weightbearing of hindlimbs (43). The HU model can lead to immune, bone, and musculoskeletal alterations, some of which have also been observed in International Space Station (ISS) crew (44, 45). In our study, functional outputs of neutrophils in response to simulated microgravity (sμg) revealed elevated ROS and proinflammatory myeloperoxidase (MPO) expression in activated neutrophils. Interestingly, this effect could be mitigated with antioxidant treatment. Furthermore, sμg HU *wildtype* (*Wt*) mice displayed elevated neutrophils, NLR and marginal inflammation, which was dampened in mitochondrial catalase (*mCAT*) transgenic mice, known to show reduced oxidative stress responses. Our findings demonstrated that, albeit distinct mechanisms, both sμg models (*in vitro* HARV-RWV and *in vivo* HU), displayed elevated oxidative stress and NLR, that could be mitigated by antioxidants. Therefore, modifying mechanisms involved in ROS-driven inflammation (46) may provide a promising avenue to limit chronic inflammation and maintain homeostatic immunity during long-duration missions.

MATERIALS AND METHODS

Mouse and Human Ethics

Deidentified, human buffy coat samples from healthy donors were obtained from Blood Centers of America, Oklahoma Blood Institute, and isolated on-site at NASA Ames. The use of human samples was approved by NASA Ames Institutional Review Board (IRB, 201791646CTO-02, HR-357, and HR-358) with informed consent from each blood donor. Astronaut and rodent CBC data sets were approved for use by the electronic (e)IRB/Life Sciences Data Archive (LSDA) advisory board (#11028), sourced from previous publications (29, 47, 48). All mice were purchased from Jackson Laboratories and were housed in the Animal Care Facility at Ames Research Center. Hindlimb unloading and subsequent blood isolation procedures were performed following NASA Ames Research Center Institutional Animal Care and Use Committee protocol (IACUC, NAS-17-001-Y2).

Cell Culture

Human whole blood samples were separated using centrifuge gradient Ficoll-paque Plus (Thermo Fisher Scientific) and the lymphocyte/monocyte layer and granulocyte/top red blood cell (RBC) layers were collected. Cells were RBC-lysed with 1XRBC lysis buffer (Thermo Fisher Scientific) and resuspended (5×10^5 cells/ml) in RPMI containing 10% fetal bovine serum (FBS) and

1% Penicillin/Streptomycin (Pen/Strep, Thermo Fisher Scientific) for subsequent assays.

In Vitro Simulated Microgravity of Leukocytes Using HARV-RWV

3D high-aspect rotating wall vessels (HARV-RWV, Synthecon) were used to simulate microgravity with low-shear, hydrodynamic fluid flow and omni-directional gravitational force on suspended cells in rotating free-fall (34, 49–51). To optimize the measurement of oxidative stress from granulocytes in human leukocytes, suspended cells were cultured at 5×10^5 cells/ml in 10 ml and rotated at 20 revolutions per minute (RPM) in a parallel-to-ground axis to simulate microgravity (sμg, omnidirectional g-force) for 20 h and controls were plated in upright T-25 flasks (1 g, unidirectional g-force). Following incubation, 1 ml of sample was collected, SYTOX™ live/dead dye-Red (Thermo Fisher Scientific) was added to the sample and cells were immediately acquired on a BD FACSMelody™. Stained cells were considered dead, and cells that did not stain were considered live and were reported. For neutrophil differential experiments with antioxidant treatment, *N*-acetyl cysteine (NAC, 1 mM) was added to WBC (5×10^5 cells/ml) and cultured in HARV-RWV for 20 h, followed by flow cytometric analyses.

Mouse Blood Collections

Blood was collected from the vena cava on the day of euthanasia and RBC were lysed using 1XRBC lysis buffer (Thermo Fisher Scientific). Remaining WBC were fixed (2% PFA), washed in PBS, labeled with leukocyte subset markers, and analyzed by flow cytometric analyses.

Flow Cytometry Staining and Methods

Mouse and human blood samples were isolated, as described above, and single-cell suspensions were generated for flow cytometry acquisition. Debris was gated off and forward scatter (FSC-A) and side scatter (SSC-A) profiled granulocyte, monocyte, and lymphocyte populations were measured. Mouse antibodies, including anti-CD45, anti-Ly6g, and anti-CD11b, and human antibodies, including anti-CD66b, anti-CD16, anti-MPO, CellROX™, SYTOX™ live/dead stain, and active Caspase 3/7 were used to label multiple leukocyte subsets, and measure ROS formation and cellular viability. All antibodies and dyes were purchased from Thermo Fisher Scientific. Unstained and single-color compensation controls were used for all flow cytometric experiments, with a minimum of 30,000 events collected/sample. All acquisitions were performed using a S3 Cell Sorter (Bio-Rad) or a BD FACSMelody™ (BD biosciences), and FlowJo (version 10.5.3) was used for data analysis.

Quantitative PCR (qPCR)

Total RNA was extracted from cells using Trizol reagent (Thermo Fisher Scientific) and converted to cDNA using iSCRIPT cDNA synthesis kit (Bio-Rad). All assays were performed using iQ SYBR Green Supermix (Bio-Rad). An ABI 7500 Real-Time PCR (Applied Biosystems) was used and threshold cycle values that were ≥35 cycles were excluded from the results. Primers were designed using BLAST and purchased from IDT with the following sequences: mouse *β-Actin* forward 5'-AGAGGGAAATCGTGCGTGAC-3' and reverse 5'-CAATAGTGATGATGACCTGGCCGT-3', *Myeloperoxidase* (*Mpo)* forward 5'-ACCTACCCCAGTACCGATCC-3' and reverse 5'-AACTCTCCAGCTGGCAAAAA-3', *NADPH oxidase* (*Nox-2*, *gp91^{phox}*, *Cybb*) forward 5'-ACTCCTTGGAGCACTGG-3' and reverse 5'-GTTCCTGTCCAGTTGTCTTCG-3', and *Il-1β* forward 5'-CCAAAGAAGAAGATGGAAAAGCG-3' and reverse 5'-GGTGCTGATGTACCAGTTGGG-3'.

Mice and Hindlimb Unloading

All mice handling and experiments were performed according to the pre-approved NASA Ames Institutional Animal Care and Use Committee (IACUC). Mice were generated for experiments by breeding male, hemizygous *mCAT* mice [male B6.Cg-Tg (CAG-OTC/CAT) 4033Prab/J strain] (52, 53) with female *wildtype* (*Wt)* mice (*C57BL/6NJ*) (Jackson Laboratories, Bar Harbor, ME). *C57BL/6NJ Wt* mice were used as controls. DNA was purified from tail snips using RedExtract-N-Amp (Sigma, St. Louis, MO) followed by genotyping using forward 5'-CTGAGGATCCTGTTAAACAATGC-3' and reverse 5'-CTATCTGTTCAACCTCAGCAAAG-3' (54) primers for the *mCAT* gene. For HU experiments, female mice were acclimated to their assigned cages three days prior to the onset of HU. Animals were 16-weeks of age at the beginning of HU. For the 14-day HU study, *C57BL/6NJ Wt* female mice were assigned to one of two treatments: normally loaded (NL) controls, singly housed in standard vivarium cages or HU. For the 30-day HU experiment, mice were assigned to one of four groups: *Wt*/NL, *Wt*/HU, *mCAT*/NL, or *mCAT*/HU. In both 14- and 30-day HU studies, mice were housed under 12 h light and 12 h dark cycle conditions and provided cotton nestlets (Ancare, NES3600) as enrichment. Nestlets were refreshed daily. Ambient temperature ranged from 23.3 to 25.6°C. Body weights were monitored every 2–3 days throughout the experiment. Blood draws were performed at euthanasia on days 14 or 30 (32).

Statistical Analyses

Data were compared with either paired or unpaired, nonparametric or parametric analyses, or with one- or two-way ANOVA using GraphPad Prism software (version 6.0). A $p < 0.05$ was considered statistically significant. All statistical analyses were supported by a trained statistician.

RESULTS

Spaceflight Elevates NLR and GLR

Peripheral WBC data from previously space-flown rodent and astronaut experiments were re-analyzed to determine the contribution of spaceflight to NLR and GLR immune profile shifts. In rodents (47, 48), spaceflight increased NLR after 14 days in-flight and immediately post-landing (**Figure 1A**). Later post-flight (2–8 days after landing, R+2 to R+8), NLR decreased relative to flight (F14) and landing (R+0) values, suggesting a re-adaptation response to Earth's 1 gravity (1 g) (**Figure 1A**). Retrospective GLR data were not recorded for this spaceflight mission. Human WBC data (29) were re-analyzed and GLR was

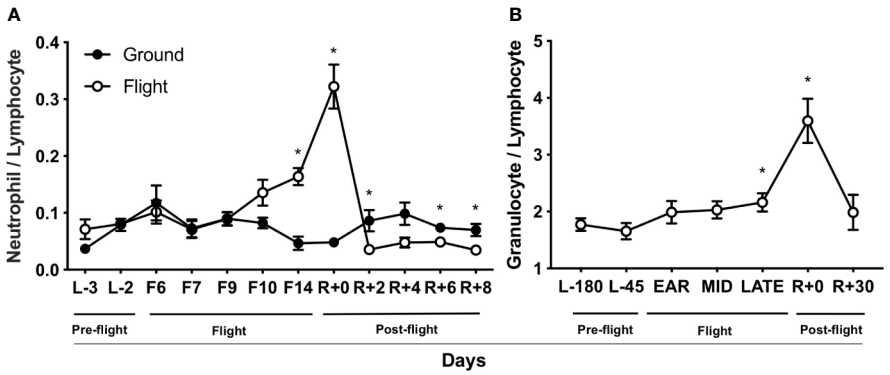

FIGURE 1 | Spaceflight elevates NLR and GLR. **(A)** Rodent NLR from Space Life Sciences (SLS)-2 mission (47, 48) (n = 5–15). **(B)** Human GLR from published data (29) (n = 23). L, launch; F, flight; R, return on Earth denoted in days. "Ear"ly, day 14 in-flight; "mid," days 60–120 in-flight; and "late," day 180. A non-parametric, unpaired Mann-Whitney test compared ground controls with in-flight samples at each timepoint in rodent data set and a parametric, paired Student's *t*-test compared to L-180 days was performed in human data set, a * indicates $p < 0.05$. Error bars denote standard error of mean.

elevated after 180 days on-orbit (late) and in samples collected within 2–3 hours post-landing (R+0) (**Figure 1B**). Later post-flight (30-day, R+30), GLR recovered to pre-flight baseline levels (L-180). Retrospective NLR data were not recorded for this mission. Thus, a progressive increase in NLR and GLR occurred in-flight and immediately post-landing in rodents and humans, suggesting NLR may be a useful biomarker to monitor astronaut immune status.

HARV-RWV sμg Elevates NLR in Human Leukocytes *In Vitro*

Due to the constraints of conducting spaceflight experiments, we further confirmed these results using an *in vitro* sμg model. For this, human WBC were cultured in HARV-RWV sμg for 20 h. Flow cytometry showed sμg increased granulocyte percentage (%) and absolute counts, reduced lymphocyte and monocyte %, and although not statistically significant, a reduced trend in absolute counts (forward scatter area, FSC-A *versus* side scatter area, SSC-A) (**Figures 2A, B**, and **Figure S1A**), and increased GLR (**Figure 2C**). To determine if altered GLR was due to elevated survival of granulocytes or increased death of lymphocytes, active Caspase 3/7 staining was performed, which indicated elevated lymphocyte apoptosis in sμg **(Figures 2D, E)**. To characterize human neutrophil populations within the WBC pool following sμg, cell surface markers $CD66b^+$ and $CD16^+$ were used (55–58), which displayed elevated neutrophils (**Figure 2F**) and elevated NLR (**Figure 2G**). Collectively, these findings confirm the utility of NLR as a biomarker to monitor astronaut immune status.

HARV-RWV sμg Elevates ROS and Activates Neutrophils, While the Antioxidant *N*-Acetyl Cysteine Ameliorates This Effect

Elevated percentage and absolute count of granulocytes within WBC (**Figures 2A, B**, and **Figure S1A**) were observed in sμg, with no difference in apoptosis (**Figures 2D, E**). Elevated percentage of neutrophils within WBC (**Figure 2F**) were also observed in sμg. Since mature granulocytes, including neutrophils, in blood are non-proliferating, terminally differentiated cells, elevated percentages may be due to differential light scatter properties, indicative of cellular activation. CD66b not only serves as a marker for human neutrophils, but its cell surface expression level per cell is also elevated in activated neutrophils (58, 59). Therefore, we sought to determine if sμg can activate neutrophils. We found sμg resulted in elevated cell surface receptor median fluorescence intensity (MFI) expression of CD66b per granulocyte, with no difference in CD16 MFI (**Figures 3A, B**), suggesting neutrophil activation during sμg. We further confirmed neutrophil activation by uncovering elevated cell surface receptor CD11b median fluorescence intensity (MFI) within $CD16^+CD66b^+$ granulocytes (**Figures S1B, C**). Activated neutrophils also express elevated reactive oxygen species (ROS) and myeloperoxidase (MPO) during the oxidative burst response (11, 60–62). Furthermore, spaceflight and analog models on Earth (4–9, 63) can promote redox imbalance, triggering cellular damage and persistent inflammation (12). We found ROS (*via* mean fluorescence intensity, or MFI) per granulocyte and MPO (mean fluorescence intensity, MFI) per neutrophil, were both elevated in sμg, collectively suggesting sμg caused neutrophil activation (**Figures 3C, E**).

N-acetyl cysteine (NAC) is an antioxidant that scavenges free radicals, promotes glutathione biosynthesis, and decreases mitochondrial membrane depolarization (64). To assess the effects of NAC on neutrophil activation we cultured WBCs in the presence or absence of NAC (1 mM) under sμg for 20 h. The results showed reduced expression of MPO in the presence of NAC (**Figures 3D, E**), suggesting antioxidant treatment ameliorates sμg induced neutrophil activation, thus serving as a promising countermeasure to suppress spaceflight-induced inflammation.

Hindlimb Unloading (14-day) sμg Increases Circulating Blood Neutrophils and Elevates NLR *In Vivo*

To test the effects of sμg on immunity in an *in vivo* model (32), blood was collected from *wildtype* HU (*Wt*/HU) mice following

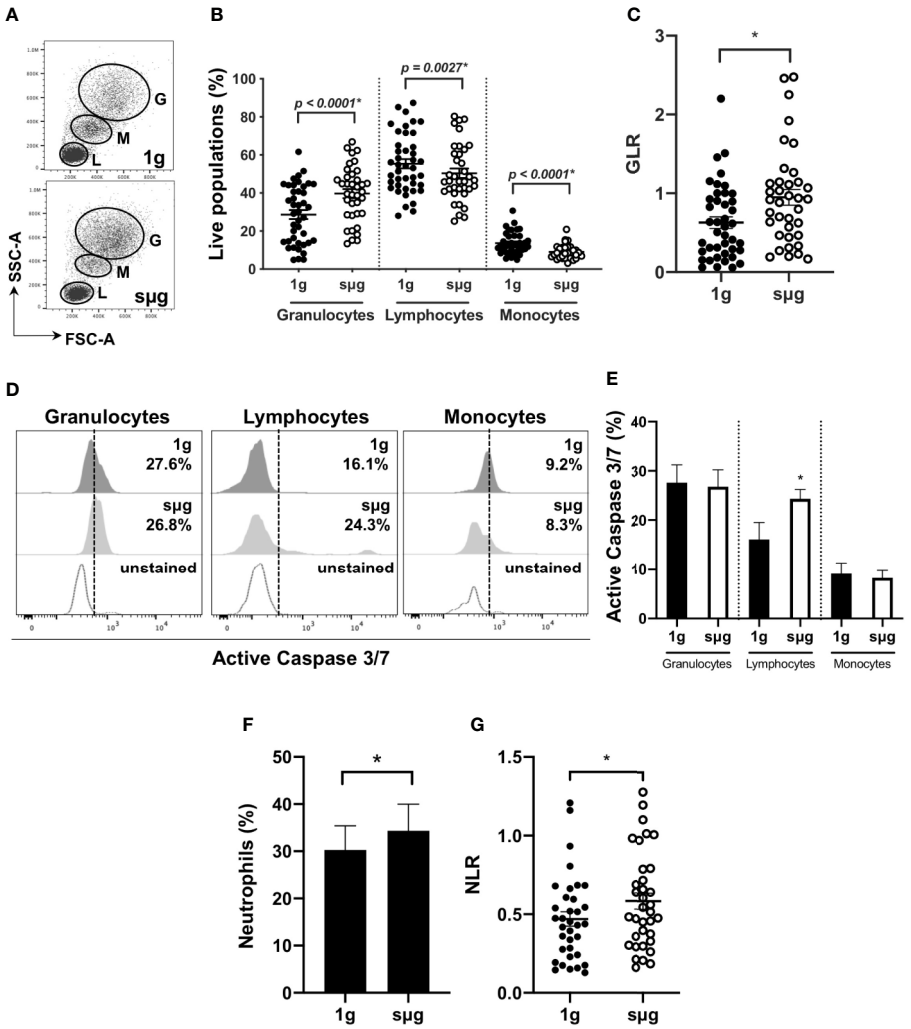

FIGURE 2 | HARV-RWV sμg elevates GLR and NLR. **(A)** Flow scatter plot: G, Granulocyte; M, Monocyte; L, Lymphocytes. **(B)** Percent (%) live population of each cell type (n = 37–42). **(C)** GLR based on % population of each cell type (n = 37–42). **(D)** Representative flow histogram plots of active Caspase 3/7 within each population type. **(E)** Percent (%) active Caspase 3/7 fluorescence within all events per leukocyte population (n = 10). **(F)** Bar graph of neutrophils ($CD66b^{+}CD16^{+}$) within WBC post-20 h incubation at 1 g and sμg (n = 28). **(G)** Total NLR (n = 28). All experiments were repeated at least twice. A non-parametric, Wilcoxon matched pairs signed rank test compared to 1 g was performed for sμg leukocyte differential analyses and GLR/NLR determination. A * indicates $p < 0.05$ and error bars denote standard error of mean.

14 days of HU. Cells were immunoprofiled to determine neutrophil counts and NLR in circulating blood. Ly6g is a ubiquitous cell surface marker in mice used to distinguish eosinophils/myeloid-derived suppressor cells ($Ly6g^{low}$) from neutrophils ($Ly6g^{high}$) (65) (**Figure 4A**). Compared to normally loaded (NL) controls, no difference was observed in eosinophil/myeloid-derived suppressor cell % (**Figure 4B**) and absolute counts (**Figure S2A**) populations, while increased % (**Figure 4C**) and absolute counts (**Figure S2B**) of neutrophils were observed in HU. No difference in lymphocyte % (**Figure 4D**) or absolute counts (**Figure S2C**) were noted in the *in vivo* HU model, in contrast with the reduced lymphocytes % observed *in vitro* HARV-RWV sμg-treated leukocytes (**Figure 2B**) with increased apoptosis of lymphocytes. No significant differences were observed with monocyte % or absolute counts (**Figures S2D, E**). However, significantly elevated NLR was observed following 14 days of HU (**Figure 4E**). Therefore, HU (14-day) displayed elevated NLR values as observed previously with rodents and humans in spaceflight and sμg experiments, confirming elevated NLR in multiple reduced gravity models, albeit produced *via* potentially different mechanisms.

Prolonged Hindlimb Unloading (30-day) sμg Results in Elevated Blood Neutrophil Persistence and NLR, While This Effect is Mitigated in *mCAT* Mice

Elevated neutrophil numbers and persistence in blood circulation result in tissue damage and impaired immune

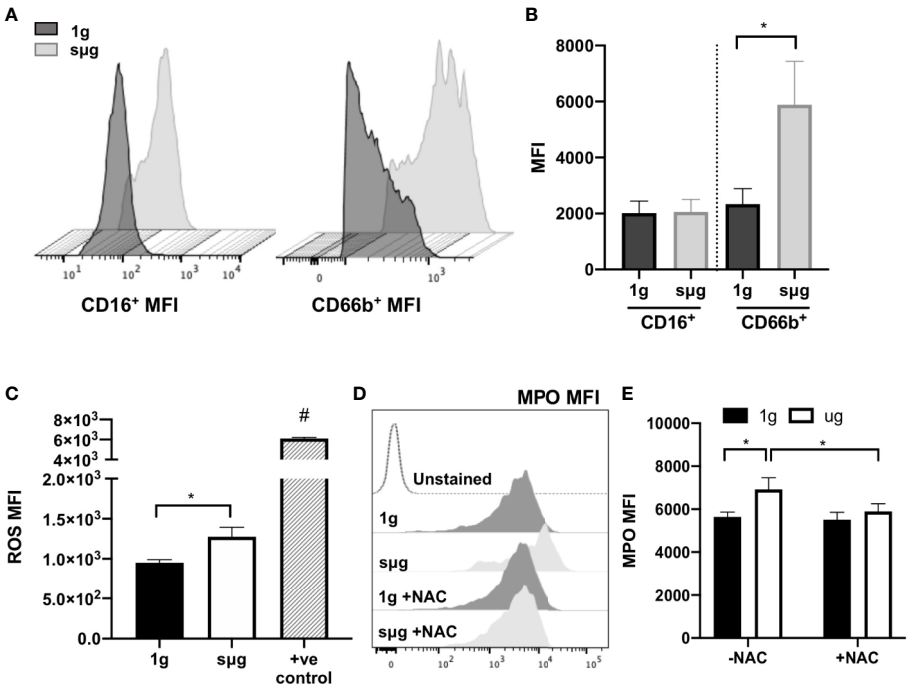

FIGURE 3 | HARV-RWV sμg activates neutrophils to produce ROS and MPO, while antioxidant treatment ameliorates this effect. **(A)** Representative $CD16^+$ and $CD66b^+$ median fluorescence intensity (MFI) histograms. **(B)** Median fluorescence intensity (MFI) cell surface expression of $CD16^+$ and $CD66b^+$ per granulocyte (n = 32). **(C)** CellROX measurement of mean fluorescence intensity (MFI) of ROS per granulocyte (n = 10). Positive controls (+ve control) included a 30-min incubation with the ROS-inducer *tert*-Butyl hydroperoxide (TBHP, 400 μM) (n = 2). **(D)** Representative flow histogram plot of MPO mean fluorescence intensity (MFI). **(E)** MPO MFI per neutrophil ($CD66b^+CD16^+$) in the presence or absence of the antioxidant, *N*-acetyl cysteine (NAC, 1 mM, n = 10–24). All experiments were repeated at least twice. A non-parametric, Wilcoxon matched pairs signed rank test compared to 1g or control groups, a * indicates $p < 0.05$, a # indicates the positive control with a $p<0.05$ compared to 1g. Error bars denote standard error of mean.

responses (66). HU also induces redox imbalance (8). Therefore, we compared the effects of prolonged HU (30-day) in *Wt* mice with transgenic mice expressing human mitochondrial *catalase (mCAT)* (54). Catalase is an antioxidant enzyme that converts reactive hydrogen peroxide into non-reactive water and oxygen, a cellular antioxidant mechanism that restores redox balance. Comparable to 14-day HU, 30-day HU in *Wt* mice resulted in elevated neutrophils, no significant difference in lymphocytes, and an elevated NLR, while these results were mitigated in *mCAT*/HU mice (**Figures 5A–C** and **Figure S3**). Oxidative stress and inflammatory gene expression in *Wt* and *mCAT* mice were assessed by qPCR. Compared to *Wt*/NL controls, *Mpo* ($p = 0.0240$*) was increased in *Wt*/HU (**Figure 5D**), while a non-significant elevation in *NADPH oxidase-2* (*Nox-2*, $p = 0.6411$) and *Il-1β* ($p = 0.1349$) were also observed (**Figures 5E, F**). On the other hand, *mCAT*/HU mice partially mitigated some of these effects (**Figures 5D–F**). Collectively, prolonged HU (30-days) induced persistent NLR, oxidative stress and marginal inflammation, while *catalase* overexpression mitigated some of these outcomes.

Collectively, our findings demonstrated that, through potentially different mechanisms, both spaceflight and multiple sμg models elevated NLR, ROS, and MPO inflammation, while antioxidants mitigated some of these outcomes. Therefore, elevated NLR may be a suitable prognostic biomarker to monitor astronaut immune status and inflammation during long-duration missions.

DISCUSSION

Spaceflight causes immune dysfunction that can lead to health risks for astronauts. Health risks that arise from immune dysfunction are complex and include an inability to defend against pathogens, altered tolerance to self-antigens resulting in potential autoimmunity development, chronic inflammation, and immune senescence. Therefore, mitigation during spaceflight will likely require selective targeting of specific immune cell types and/or developmental stages. Elevated NLR may be a prospective biomarker candidate to identify immune deviations that can cause disease. Currently, elevated NLR is used as a clinical biomarker to detect sub-clinical inflammation in humans and predicts poor prognosis in cancer (18). In this study, a spike in GLR in humans and NLR in rodents was observed at landing and elevated GLR and NLR were observed during spaceflight (**Figure 1**). In humans, GLR was elevated at 180-days in-flight,

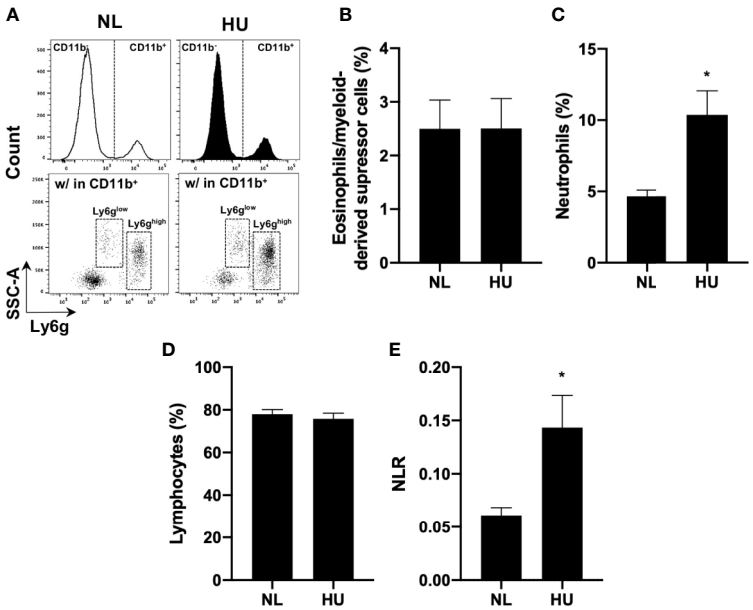

FIGURE 4 | 14-day HU sμg increases number of circulating blood neutrophils and elevates NLR. Blood from HU and NL (14-day) *Wt* mice. **(A)** Representative flow cytometric gating scheme for Ly6g^{low} (eosinophils/myeloid-derived suppressor cells) (65) and Ly6g^{high} (neutrophils) within CD11b^{+}/CD45^{+} myeloid cells and CD11b^{-}/CD45^{+} lymphocytes. % of eosinophils/myeloid-derived suppressor cells **(B)**, neutrophils **(C),** and lymphocytes **(D)**. **(E)** NLR deduced from neutrophils (Ly6g^{high} CD11b^{+}/CD45^{+} events) to lymphocytes (CD11b^{-}/CD45^{+} events) (n = 7). A non-parametric, unpaired Mann-Whitney test compared to NL controls was performed, a * indicates $p < 0.05$. Error bars denote standard error of mean.

suggesting prolonged exposure to spaceflight caused leukocyte differential changes. This change in immune differentials may be in response to elevated inflammation experienced in-flight (4, 6, 12), since elevated, chronic inflammation is often coupled with immune dysfunction and disease development (13, 19, 20, 67–70). Therefore, monitoring distinct biomarkers, such as elevated NLR, can determine when countermeasures can intervene to avert immune dysfunction, promote immune recovery, and prevent disease development.

Elevated numbers of granulocytes and neutrophils were observed *in vitro* following 20 h of HARV-RWV modeled microgravity in human peripheral blood (**Figure 2** and **Figure S1**). However, since mature neutrophils are terminally differentiated in blood circulation, i.e., banded or segmented neutrophils, we estimate that this increased percentage is due to increased scatter properties indicative of cellular activation. Indeed, elevated cell surface expression of CD66b and CD11b per granulocyte, which are activation markers for neutrophils (58, 59), were increased in sμg (**Figure 3** and **Figure S1**). Further studies revealed elevated ROS and MPO expression (**Figure 3**), confirming HARV-RWV sμg resulted in granulocytes, and in particular, neutrophil activation. Physiological effects of elevated active granulocytes or neutrophils in circulation intensifies sterile inflammation (70–72), promotes edema, and non-specific tissue damage (73), and can threaten astronaut health if not adequately controlled. Interestingly, MPO gene expression (**Figure 5D**) was elevated in HU, suggesting immature neutrophil entry into blood circulation, compared to neutrophil activation observed *in vitro* in the HARV-RWV. MPO gene synthesis only occurs in bone marrow early in neutrophil development, i.e. immature neutrophils (myeloblasts, promyelocytes, and myelocytes). MPO gene expression ends once neutrophils differentiate into metamyelocytes (74) and synthesized MPO protein is packaged into granules released during neutrophil activation (75). Typically, immature neutrophils are not released into blood circulation unless the body is in a diseased or inflammatory state (74, 75). However, since MPO gene expression was elevated in HU mice blood, this suggests the potential for myelocyte/immature neutrophil infiltration and may also serve as a biomarker for elevated inflammation during spaceflight. To our knowledge no measurements have been recorded for elevated immature neutrophils in blood circulation in-flight; however, elevated neutrophils were identified in blood from 9 of 16 astronauts at landing (6, 76, 77). As compared to the rodent spaceflight results (in-flight day 14), elevated neutrophils were also observed at days 14 and 30 of HU in mice (**Figures 4C** and **5A**), suggesting the physical effects of fluid-shifting experienced during spaceflight and HU may stimulate the release of neutrophils into circulation; however this requires further investigation.

Indeed, elevated MPO during sμg may contribute to immune dysfunction. MPO catalyzes hydrogen peroxide into reactive intermediates that can damage proteins, lipids, and DNA (67). Excess MPO impairs phagocytic function (67–69) and triggers neutrophil degranulation, causing inflammatory tissue damage (78) in cardiovascular disease (62, 67, 79). Pathologically this is relevant during spaceflight, as cardiovascular disease is a

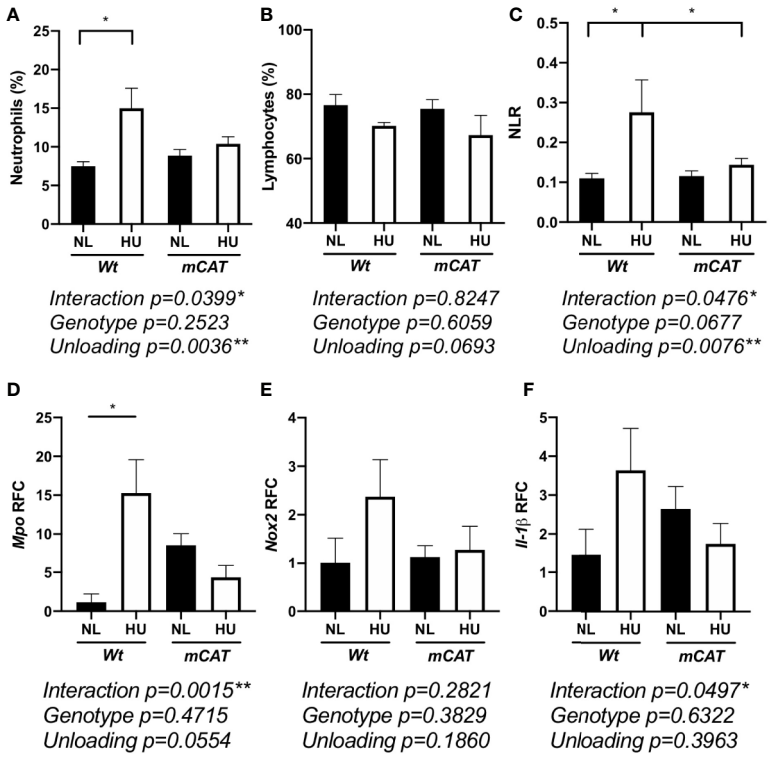

FIGURE 5 | 30-day HU sμg results in elevated blood neutrophil persistence and NLR with this effect mitigated in *mCAT* mice. Blood from HU (30-day) *Wt* and *mCAT* mice. % neutrophils (Ly6g^{high} CD11b^{+}/CD45^{+} events) **(A)**, lymphocytes (CD11b^{-}/CD45^{+}) **(B)**, and NLR **(C)** from NL and HU mice (n = 5–8). qPCR relative fold change (RFC) of *Mpo* **(D)**, *Nox-2* **(E)**, and *Il-1β* **(F)** in blood collected from *Wt* and *mCAT*, NL and HU mice (30-day, n = 3–8). A two-way ANOVA and a non-parametric, Dunn's multiple comparisons test was performed between groups, a * indicates $p < 0.05$. Error bars denote standard error of mean.

prominent risk factor associated with returned astronauts (80). Furthermore, elevated NLR is currently used as a predictor of cardiovascular disease risk on Earth (81), thereby highlighting the clinical relevance of monitoring NLR during spaceflight. Neutrophil oxidative burst responses and elevated ROS can induce cellular death (82), including lymphocyte apoptosis (83), and suppression of T lymphocyte function (84). HARV-RWV sμg induced ROS in granulocytes, indicating HARV-RWV sμg activated granulocytes and triggered the oxidative burst response. Thus HARV-RWV sμg can serve as a valuable model to study ROS-induced inflammation (72, 85). Indeed, redox imbalance occurs in humans and cell cultures exposed to spaceflight (4–6) and *in vitro* ground-based sμg models (8, 9, 86). The cause of elevated ROS in sμg may be due to: (1) cell death factors or other unknown stimulators of the oxidative burst response, (2) a mechanosensitive stress receptor in phagocytes that triggers redox imbalance (87), and/or (3) a combination of these effects. In our study, HARV-RWV sμg induced active Caspase 3/7 expression in lymphocyte populations (**Figure 2D**), indicating lymphocyte apoptosis and shifting of immune differentials to favor higher NLR and GLR. Further analyses of our *in vivo* HU studies revealed no difference in lymphocyte percent or absolute count populations (**Figures 4** and **5**, and **Figures S2** and **3**) compared to HARV-RWV sμg studies, suggesting elevated lymphocyte recovery or unknown ROS-quenching mechanisms that limit lymphocyte apoptosis, both of which require further studies.

Therefore, the two sμg models, HARV-RWV and HU, displayed different mechanisms towards generating an elevated NLR. The HARV-RWV microgravity model appears to display robust lymphocyte turnover, i.e. elevated lymphocyte apoptosis, and most likely immune function that may differ from astronauts in-flight. However, this does not rule out that lymphocyte apoptosis does not occur *in vivo* HU, as turnover of lymphocytes to replace loss most likely occurs, albeit apoptosis may occur at a slower rate than *in vitro* HARV-RWV. Furthermore, ROS concentration within each sμg model may be drastically different. For example, ROS levels in HARV-RWV may be much higher in the absence of *in vivo* ROS quenchers compared to 14- or 30-day HU, which would affect the rate of lymphocyte apoptosis (88, 89). Indeed, concentration and exposure time of ROS determines cellular responses. Homeostatic levels of ROS can promote cell survival, while elevated ROS (oxidative stress) can induce cellular death (82). In line with this, the timeline of measurements of lymphocyte counts (20 h HARV-RWV *versus* 14- and 30-days HU) differ between the two models; therefore direct comparisons cannot be assumed. Finally, the HARV-RWV model cultured human blood samples, which have different leukocyte percentages compared to

mice leukocytes in the HU model; therefore the kinetics of apoptosis across the two microgravity models would also be affected. Crucian et al. showed there is an elevation of granulocytes in blood circulation, while no differences are observed in lymphocyte absolute counts, suggesting lymphocytes may not undergo apoptosis in spaceflight; rather there may be release of more granulocytes into blood circulation (29). Controversially however, multiple reports have indicated lymphocytes and lymphocyte-like cell lines undergo apoptosis during spaceflight/microgravity conditions (36–42), albeit measurements were either reported post-landing or from *ex vivo* cell cultures in flight. In fact, the role of apoptosis in lymphocyte depression (ROALD) experiment that was part of the BIO-4 mission and comprised of ESA, Energia, and NASA agencies, was performed with the goal to understand how microgravity affects lymphocyte apoptosis. The results showed after 48 h on-board the ISS *ex vivo* cultures of lymphocytes displayed increased DNA fragmentation, PARP protein expression, and elevated p53 expression, compared to ground controls (36). Due to this, we believe the *in vivo* HU microgravity model, although having its own limitations, may be a better representative ground-based model for spaceflight. Nonetheless, additional studies are required to better understand the degree of lymphocyte turnover during *in vivo* HU that is comparable to spaceflight.

Monocytes were significantly reduced following HARV-RWV (**Figure 2B**); however no differences were observed in HU mice (**Figures S2D, E**), further indicating the variability between the two simulated microgravity models. Yet, inconsistency with these cell types in terms of population differentials have also been noted across spaceflight literature (77, 90, 91), which may be a factor of sampling timepoints. However, consensus suggests phagocytic function of monocytes following spaceflight is impaired (92, 93). Phagocytic impairment of monocytes can directly affect clearance of neutrophils from circulation, inflammation resolution (94), and can impact NLR. Therefore, further research into the function and distribution of monocytes following simulated microgravity are currently underway.

Transgenic mice expressing the human antioxidant gene *catalase* reversed HU-induced elevation of NLR and dampened inflammatory gene expression (**Figure 5**), suggesting redox imbalance caused leukocyte differential changes. In line with this, mice deficient in apolipoprotein E (ApoE), a protein with antioxidant activity, display elevated ROS expression and activated neutrophils (95). In our study, HARV-RWV sμg of human leukocytes induced neutrophil activation that was reversed in the presence of the antioxidant NAC (**Figure 3D**), further suggesting antioxidants can suppress inflammation. Indeed, *in vivo* NAC treatment successfully ameliorated acetic acid-induced colitis by reversing pro-inflammatory mediators TNF-α, IL-6, and MPO in rats (96). Collectively, these results indicate antioxidants as viable countermeasures to regulate spaceflight-induced inflammation and immune dysfunction.

Clinically, elevated NLR (>3.53) (27) is a prognostic indicator for cancer development, cardiovascular disease, inflammation, and infectious conditions (18, 21–23, 25), but no NLR standard has been established for astronaut immunity. Our results revealed elevated GLR in astronauts at landing (GLR = 3.6, **Figure 1B**), compared to clinically relevant GLR (>2.24) (97), may result in biological significance for astronaut health. Although restoration to normal GLR occurred at landing on Earth, landing on the lunar surface and/or Mars, where gravity is less than Earth's, may pose a significant risk to astronaut immune recovery. Therefore, monitoring and developing countermeasures to mitigate elevated NLR, GLR, and inflammatory neutrophil phenotypes for future long-duration and long-distance space travel are essential for mission success.

In summary, we identified increased GLR and NLR in both human and rodent spaceflight samples and ground simulations of microgravity. Our results *in vitro* indicated that leukocytes shift in favor of elevated activated inflammatory neutrophils, which may amplify disease development *in vivo*. Further, antioxidants may be useful countermeasures to ameliorate these outcomes in sμg, as NAC treatment inhibited activated inflammatory human neutrophils in HARV-RWV and *catalase* partially mitigated elevated NLR in HU mice. Based on these findings, we suggest monitoring both in-flight and landing NLR to assess astronaut immune status. We further advocate the investigation of antioxidants as future countermeasures to mitigate immune deviations, including elevated NLR and inflammation, to safeguard astronaut health on future missions.

DATA AVAILABILITY STATEMENT

The data analyzed in this study are subject to the following licenses/restrictions: NASA Life Sciences Data Archive (LSDA) is an active repository for astronaut health datasets. Requests for dataset access is required. Requests to access these datasets should be directed to https://lsda.jsc.nasa.gov.

ETHICS STATEMENT

The studies involving human participants were reviewed and approved by NASA Ames Institutional Review Board (IRB, 201791646CTO-02, HR-357 and HR-358) with informed consent from each blood donor. Astronaut and rodent CBC data sets were approved for use by the electronic (e)IRB/Life Sciences Data Archive (LSDA) advisory board (#11028). The patients/participants provided their written informed consent to participate in this study. The animal study was reviewed and approved by NASA Ames Research Center Institutional Animal Care and Use Committee (IACUC, NAS-17-001-Y2).

AUTHOR CONTRIBUTIONS

AMP conceived/performed majority of the experiments and wrote/prepared the manuscript. SDM performed experiments and contributed to manuscript preparation. EC provided human blood samples and edited the manuscript. A-SS, CGTT, and RKG performed the HU animal experiments, provided mouse blood samples, and edited the manuscript. SA assisted with statistical testing and edited the manuscript. RG, BEC, and SB

edited the manuscript and provided intellectual advice. SB provided funding for the study. BEC provided human LSDA-sourced data sets and edited the manuscript. All authors contributed to the article and approved the submitted version.

FUNDING

This work was supported in part by Universities Space Research Association (USRA) and NASA's Space Biology Program post-doctoral fellowship (to AMP) and NASA's Space Biology Grant # NNX15AB42G (to SB).

ACKNOWLEDGMENTS

We thank Dr. John Hogan for use of the S3 Cell Sorter and Dr. Brian Crucian for providing raw data sets of Life Sciences Data Archive (LSDA) sourced astronaut data.

SUPPLEMENTARY MATERIAL

The Supplementary Material for this article can be found online at: https://www.frontiersin.org/articles/10.3389/fimmu.2020.564950/full#supplementary-material

REFERENCES

1. Demontis GC, Germani MM, Caiani EG, Barravecchia I, Passino C, Angeloni D. Human Pathophysiological Adaptations to the Space Environment. *Front Physiol* (2017) 8:547. doi: 10.3389/fphys.2017.00547
2. Vernikos J, Schneider VS. Space, gravity and the physiology of aging: parallel or convergent disciplines? A mini-review. *Gerontology* (2010) 56(2):157–66. doi: 10.1159/000252852
3. Liguori I, Russo G, Curcio F, Bulli G, Aran L, Della-Morte D, et al. Oxidative stress, aging, and diseases. *Clin Interv Aging* (2018) 13:757–72. doi: 10.2147/CIA.S158513
4. Garrett-Bakelman FE, Darshi M, Green SJ, Gur RC, Lin L, Macias BR, et al. The NASA Twins Study: A multidimensional analysis of a year-long human spaceflight. *Science* (2019) 364(6436):eaau8650. doi: 10.1126/science.aau8650.
5. Versari S, Longinotti G, Barenghi L, Maier JA, Bradamante S. The challenging environment on board the International Space Station affects endothelial cell function by triggering oxidative stress through thioredoxin interacting protein overexpression: the ESA-SPHINX experiment. *FASEB J* (2013) 27(11):4466–75. doi: 10.1096/fj.13-229195
6. Buchheim JI, Matzel S, Rykova M, Vassilieva G, Ponomarev S, Nichiporuk I, et al. Stress Related Shift Toward Inflammaging in Cosmonauts After Long-Duration Space Flight. *Front Physiol* (2019) 10:85. doi: 10.3389/fphys.2019.00085
7. Tauber S, Christoffel S, Thiel CS, Ullrich O. Transcriptional Homeostasis of Oxidative Stress-Related Pathways in Altered Gravity. *Int J Mol Sci* (2018) 19(9):2814–39. doi: 10.3390/ijms19092814
8. Lawler JM, Song W, Demaree SR. Hindlimb unloading increases oxidative stress and disrupts antioxidant capacity in skeletal muscle. *Free Radic Biol Med* (2003) 35(1):9–16. doi: 10.1016/S0891-5849(03)00186-2
9. Mao XW, Nishiyama NC, Pecaut MJ, Campbell-Beachler M, Gifford P, Haynes KE, et al. Simulated Microgravity and Low-Dose/Low-Dose-Rate Radiation Induces Oxidative Damage in the Mouse Brain. *Radiat Res* (2016) 185(6):647–57. doi: 10.1667/RR14267.1
10. Liu Y, Fiskum G, Schubert D. Generation of reactive oxygen species by the mitochondrial electron transport chain. *J Neurochem* (2002) 80(5):780–7. doi: 10.1046/j.0022-3042.2002.00744.x
11. Nguyen GT, Green ER, Mecsas J. Neutrophils to the ROScue: Mechanisms of NADPH Oxidase Activation and Bacterial Resistance. *Front Cell Infect Microbiol* (2017) 7:373. doi: 10.3389/fcimb.2017.00373
12. Crucian BE, Chouker A, Simpson RJ, Mehta S, Marshall G, Smith SM, et al. Immune System Dysregulation During Spaceflight: Potential Countermeasures for Deep Space Exploration Missions. *Front Immunol* (2018) 9:1437. doi: 10.3389/fimmu.2018.01437
13. Vernon PJ, Schaub LJ, Dallelucca JJ, Pusateri AE, Sheppard FR. Rapid Detection of Neutrophil Oxidative Burst Capacity is Predictive of Whole Blood Cytokine Responses. *PloS One* (2015) 10(12):e0146105. doi: 10.1371/journal.pone.0146105
14. Kolaczkowska E, Kubes P. Neutrophil recruitment and function in health and inflammation. *Nat Rev Immunol* (2013) 13(3):159–75. doi: 10.1038/nri3399
15. Paul AM, Acharya D, Duty L, Thompson EA, Le L, Stokic DS, et al. Osteopontin facilitates West Nile virus neuroinvasion via neutrophil "Trojan horse" transport. *Sci Rep* (2017) 7(1):4722. doi: 10.1038/s41598-017-04839-7
16. Larosa DF, Orange JS. 1. Lymphocytes. *J Allergy Clin Immunol* (2008) 121(2 Suppl):S364–9; quiz S412. doi: 10.1016/j.jaci.2007.06.016
17. Adams NM, Grassmann S, Sun JC. Clonal expansion of innate and adaptive lymphocytes. *Nat Rev Immunol* (2020) 20:694–707. doi: 10.1038/s41577-020-0307-4
18. Isaac V, Wu CY, Huang CT, Baune BT, Tseng CL, McLachlan CS. Elevated neutrophil to lymphocyte ratio predicts mortality in medical inpatients with multiple chronic conditions. *Med (Baltimore)* (2016) 95(23):e3832. doi: 10.1097/MD.0000000000003832
19. Kunnumakkara AB, Sailo BL, Banik K, Harsha C, Prasad S, Gupta SC, et al. Chronic diseases, inflammation, and spices: how are they linked? *J Transl Med* (2018) 16(1):14. doi: 10.1186/s12967-018-1381-2
20. Chen L, Deng H, Cui H, Fang J, Zuo Z, Deng J, et al. Inflammatory responses and inflammation-associated diseases in organs. *Oncotarget* (2018) 9(6):7204–18. doi: 10.18632/oncotarget.23208
21. Akinci Ozyurek B, Sahin Ozdemirel T, Buyukyaylaci Ozden S, Erdogan Y, Kaplan B, Kaplan T. Prognostic Value of the Neutrophil to Lymphocyte Ratio (NLR) in Lung Cancer Cases. *Asian Pac J Cancer Prev* (2017) 18(5):1417–21. doi: 10.22034/APJCP.2017.18.5.1417
22. McNamara MG, Templeton AJ, Maganti M, Walter T, Horgan AM, McKeever L, et al. Neutrophil/lymphocyte ratio as a prognostic factor in biliary tract cancer. *Eur J Cancer* (2014) 50(9):1581–9. doi: 10.1016/j.ejca.2014.02.015
23. Guthrie GJ, Charles KA, Roxburgh CS, Horgan PG, McMillan DC, Clarke SJ. The systemic inflammation-based neutrophil-lymphocyte ratio: experience in patients with cancer. *Crit Rev Oncol Hematol* (2013) 88(1):218–30. doi: 10.1016/j.critrevonc.2013.03.010
24. Liu H, Tabuchi T, Takemura A, Kasuga T, Motohashi G, Hiraishi K, et al. The granulocyte/lymphocyte ratio as an independent predictor of tumour growth, metastasis and progression: Its clinical applications. *Mol Med Rep* (2008) 1(5):699–704. doi: 10.3892/mmr_00000016
25. Li J, Chen Q, Luo X, Hong J, Pan K, Lin X, et al. Neutrophil-to-Lymphocyte Ratio Positively Correlates to Age in Healthy Population. *J Clin Lab Anal* (2015) 29(6):437–43. doi: 10.1002/jcla.21791
26. Hickman DL. Evaluation of the neutrophil:lymphocyte ratio as an indicator of chronic distress in the laboratory mouse. *Lab Anim (NY)* (2017) 46(7):303–7. doi: 10.1038/laban.1298
27. Forget P, Khalifa C, Defour JP, Latinne D, Van Pel MC, De Kock M. What is the normal value of the neutrophil-to-lymphocyte ratio? *BMC Res Notes* (2017) 10(1):12. doi: 10.1186/s13104-016-2335-5
28. Crucian BE, Stowe RP, Pierson DL, Sams CF. Immune system dysregulation following short- vs long-duration spaceflight. *Aviat Space Environ Med* (2008) 79(9):835–43. doi: 10.3357/ASEM.2276.2008
29. Crucian B, Stowe RP, Mehta S, Quiriarte H, Pierson D, Sams C. Alterations in adaptive immunity persist during long-duration spaceflight. *NPJ Microgravity* (2015) 1:15013. doi: 10.1038/npjmgrav.2015.13
30. Sanada F, Taniyama Y, Muratsu J, Otsu R, Shimizu H, Rakugi H, et al. Source of Chronic Inflammation in Aging. *Front Cardiovasc Med* (2018) 5:12. doi: 10.3389/fcvm.2018.00012

31. Schroder AK, Rink L. Neutrophil immunity of the elderly. *Mech Ageing Dev* (2003) 124(4):419–25. doi: 10.1016/S0047-6374(03)00017-4
32. Globus RK, Morey-Holton E. Hindlimb unloading: rodent analog for microgravity. *J Appl Physiol (1985)* (2016) 120(10):1196–206. doi: 10.1152/japplphysiol.00997.2015
33. Hammond TG, Hammond JM. Optimized suspension culture: the rotating-wall vessel. *Am J Physiol Renal Physiol* (2001) 281(1):F12–25. doi: 10.1152/ajprenal.2001.281.1.F12
34. Pellis NR, Goodwin TJ, Risin D, McIntyre BW, Pizzini RP, Cooper D, et al. Changes in gravity inhibit lymphocyte locomotion through type I collagen. *In Vitro Cell Dev Biol Anim* (1997) 33(5):398–405. doi: 10.1007/s11626-997-0012-7
35. Cooper D, Pellis NR. Suppressed PHA activation of T lymphocytes in simulated microgravity is restored by direct activation of protein kinase C. *J Leukoc Biol* (1998) 63(5):550–62. doi: 10.1002/jlb.63.5.550
36. Battista N, Meloni MA, Bari M, Mastrangelo N, Galleri G, Rapino C, et al. 5-Lipoxygenase-dependent apoptosis of human lymphocytes in the International Space Station: data from the ROALD experiment. *FASEB J* (2012) 26(5):1791–8. doi: 10.1096/fj.11-199406
37. Cubano LA, Lewis ML. Fas/APO-1 protein is increased in spaceflown lymphocytes (Jurkat). *Exp Gerontol* (2000) 35(3):389–400. doi: 10.1016/S0531-5565(00)00090-5
38. Gridley DS, Slater JM, Luo-Owen X, Rizvi A, Chapes SK, Stodieck LS, et al. Spaceflight effects on T lymphocyte distribution, function and gene expression. *J Appl Physiol (1985)* (2009) 106(1):194–202. doi: 10.1152/japplphysiol.91126.2008
39. Lewis ML, Reynolds JL, Cubano LA, Hatton JP, Lawless BD, Piepmeier EH. Spaceflight alters microtubules and increases apoptosis in human lymphocytes (Jurkat). *FASEB J* (1998) 12(11):1007–18. doi: 10.1096/fasebj.12.11.1007
40. Moreno-Villanueva M, Feiveson AH, Krieger S, Kay Brinda A, von Scheven G, Bürkle A, et al. Synergistic Effects of Weightlessness, Isoproterenol, and Radiation on DNA Damage Response and Cytokine Production in Immune Cells. *Int J Mol Sci* (2018) 19(11):3689–12. doi: 10.3390/ijms19113689
41. Novoselova EG, Lunin SM, Khrenov MO, Parfenyuk SB, Novoselova TV, Shenkman BS, et al. Changes in immune cell signalling, apoptosis and stress response functions in mice returned from the BION-M1 mission in space. *Immunobiology* (2015) 220(4):500–9. doi: 10.1016/j.imbio.2014.10.021
42. Schatten H, Lewis ML, Chakrabarti A. Spaceflight and clinorotation cause cytoskeleton and mitochondria changes and increases in apoptosis in cultured cells. *Acta Astronaut* (2001) 49(3-10):399–418. doi: 10.1016/S0094-5765(01)00116-3
43. Morey-Holton ER, Globus RK. Hindlimb unloading rodent model: technical aspects. *J Appl Physiol (1985)* (2002) 92(4):1367–77. doi: 10.1152/japplphysiol.00969.2001
44. Morey-Holton E, Globus RK, Kaplansky A, Durnova G. The hindlimb unloading rat model: literature overview, technique update and comparison with space flight data. *Adv Space Biol Med* (2005) 10:7–40. doi: 10.1016/S1569-2574(05)10002-1
45. Tahimic CGT, Paul AM, Schreurs AS, Torres SM, Rubinstein L, Steczina S, et al. Influence of Social Isolation During Prolonged Simulated Weightlessness by Hindlimb Unloading. *Front Physiol* (2019) 10:1147. doi: 10.3389/fphys.2019.01147
46. Mittal M, Siddiqui MR, Tran K, Reddy SP, Malik AB. Reactive oxygen species in inflammation and tissue injury. *Antioxid Redox Signal* (2014) 20(7):1126–67. doi: 10.1089/ars.2012.5149
47. Congdon CC, Allebban Z, Gibson LA, Kaplansky A, Strickland KM, Jago TL, et al. Lymphatic tissue changes in rats flown on Spacelab Life Sciences-2. *J Appl Physiol (1985)* (1996) 81(1):172–7. doi: 10.1152/jappl.1996.81.1.172
48. Huff W. Spacelab Life Sciences-2: early results are in. *Life Support Biosph Sci* (1994) 1(1):3–11.
49. Ritz BW, Lelkes PI, Gardner EM. Functional recovery of peripheral blood mononuclear cells in modeled microgravity. *FASEB J* (2006) 20(2):305–7. doi: 10.1096/fj.04-3122fje
50. Tackett N, Bradley JH, Moore EK, Baker SH, Minter SL, DiGiacinto B, et al. Prolonged exposure to simulated microgravity diminishes dendritic cell immunogenicity. *Sci Rep* (2019) 9(1):13825. doi: 10.1038/s41598-019-50311-z
51. Martinez EM, Yoshida MC, Candelario TL, Hughes-Fulford M. Spaceflight and simulated microgravity cause a significant reduction of key gene expression in early T-cell activation. *Am J Physiol Regul Integr Comp Physiol* (2015) 308(6):R480–8. doi: 10.1152/ajpregu.00449.2014
52. Wang Y, Wang W, Wang N, Tall AR, Tabas I. Mitochondrial Oxidative Stress Promotes Atherosclerosis and Neutrophil Extracellular Traps in Aged Mice. *Arterioscler Thromb Vasc Biol* (2017) 37(8):e99–e107. doi: 10.1161/ATVBAHA.117.309580
53. Wang Y, Wang GZ, Rabinovitch PS, Tabas I. Macrophage mitochondrial oxidative stress promotes atherosclerosis and nuclear factor-kappaB-mediated inflammation in macrophages. *Circ Res* (2014) 114(3):421–33. doi: 10.1161/CIRCRESAHA.114.302153
54. Schriner SE, Linford NJ, Martin GM, Treuting P, Ogburn CE, Emond M, et al. Extension of murine life span by overexpression of catalase targeted to mitochondria. *Science* (2005) 308(5730):1909–11. doi: 10.1126/science.1106653
55. Silvestre-Roig C, Hidalgo A, Soehnlein O. Neutrophil heterogeneity: implications for homeostasis and pathogenesis. *Blood* (2016) 127(18):2173–81. doi: 10.1182/blood-2016-01-688887
56. Wood B. Multicolor immunophenotyping: human immune system hematopoiesis. *Methods Cell Biol* (2004) 75:559–76. doi: 10.1016/S0091-679X(04)75023-2
57. Lakschevitz FS, Hassanpour S, Rubin A, Fine N, Sun C, Glogauer M. Identification of neutrophil surface marker changes in health and inflammation using high-throughput screening flow cytometry. *Exp Cell Res* (2016) 342(2):200–9. doi: 10.1016/j.yexcr.2016.03.007
58. Zhao L, Xu S, Fjaertoft G, Pauksen K, Hakansson L, Venge P. An enzyme-linked immunosorbent assay for human carcinoembryonic antigen-related cell adhesion molecule 8, a biological marker of granulocyte activities in vivo. *J Immunol Methods* (2004) 293(1-2):207–14. doi: 10.1016/j.jim.2004.08.009
59. Torsteinsdóttir I, Arvidson NG, Hällgren R, Håkansson L. Enhanced expression of integrins and CD66b on peripheral blood neutrophils and eosinophils in patients with rheumatoid arthritis, and the effect of glucocorticoids. *Scand J Immunol* (1999) 50(4):433–9. doi: 10.1046/j.1365-3083.1999.00602.x
60. Dale DC, Boxer L, Liles WC. The phagocytes: neutrophils and monocytes. *Blood* (2008) 112(4):935–45. doi: 10.1182/blood-2007-12-077917
61. Uhl B, Vadlau Y, Zuchtriegel G, Nekolla K, Sharaf K, Gaertner F, et al. Aged neutrophils contribute to the first line of defense in the acute inflammatory response. *Blood* (2016) 128(19):2327–37. doi: 10.1182/blood-2016-05-718999
62. Khan AA, Alsahli MA, Rahmani AH. Myeloperoxidase as an Active Disease Biomarker: Recent Biochemical and Pathological Perspectives. *Med Sci (Basel)* (2018) 6(2):33–54. doi: 10.3390/medsci6020033
63. Hosamani R, Leib R, Bhardwaj SR, Adams CM, Bhattacharya S. Elucidating the "Gravome": Quantitative Proteomic Profiling of the Response to Chronic Hypergravity in Drosophila. *J Proteome Res* (2016) 15(12):4165–75. doi: 10.1021/acs.jproteome.6b00030
64. Mokhtari V, Afsharian P, Shahhoseini M, Kalantar SM, Moini A. A Review on Various Uses of N-Acetyl Cysteine. *Cell J* (2017) 19(1):11–7. doi: 10.22074/cellj.2016.4872
65. Lee PY, Wang JX, Parisini E, Dascher CC, Nigrovic PA. Ly6 family proteins in neutrophil biology. *J Leukoc Biol* (2013) 94(4):585–94. doi: 10.1189/jlb.0113014
66. Mortaz E, Alipoor SD, Adcock IM, Mumby S, Koenderman L. Update on Neutrophil Function in Severe Inflammation. *Front Immunol* (2018) 9:2171. doi: 10.3389/fimmu.2018.02171
67. Odobasic D, Kitching AR, Holdsworth SR. Neutrophil-Mediated Regulation of Innate and Adaptive Immunity: The Role of Myeloperoxidase. *J Immunol Res* (2016) 2016:2349817. doi: 10.1155/2016/2349817
68. Lau D, Mollnau H, Eiserich JP, Freeman BA, Daiber A, Gehling UM, et al. Myeloperoxidase mediates neutrophil activation by association with CD11b/CD18 integrins. *Proc Natl Acad Sci USA* (2005) 102(2):431–6. doi: 10.1073/pnas.0405193102
69. Stendahl O, Coble BI, Dahlgren C, Hed J, Molin L. Myeloperoxidase modulates the phagocytic activity of polymorphonuclear neutrophil leukocytes. Studies with cells from a myeloperoxidase-deficient patient. *J Clin Invest* (1984) 73(2):366–73. doi: 10.1172/JCI111221

70. Leliefeld PH, Wessels CM, Leenen LP, Koenderman L, Pillay J. The role of neutrophils in immune dysfunction during severe inflammation. *Crit Care* (2016) 20:73. doi: 10.1186/s13054-016-1250-4
71. Biermann MH, Podolska MJ, Knopf J, Reinwald C, Weidner D, Maueroder C, et al. Oxidative Burst-Dependent NETosis Is Implicated in the Resolution of Necrosis-Associated Sterile Inflammation. *Front Immunol* (2016) 7:557. doi: 10.3389/fimmu.2016.00557
72. Prame Kumar K, Nicholls AJ, Wong CHY. Partners in crime: neutrophils and monocytes/macrophages in inflammation and disease. *Cell Tissue Res* (2018) 371(3):551–65. doi: 10.1007/s00441-017-2753-2
73. Kenne E, Erlandsson A, Lindbom L, Hillered L, Clausen F. Neutrophil depletion reduces edema formation and tissue loss following traumatic brain injury in mice. *J Neuroinflammation* (2012) 9:17. doi: 10.1186/1742-2094-9-17
74. Wright HL, Makki FA, Moots RJ, Edwards SW. Low-density granulocytes: functionally distinct, immature neutrophils in rheumatoid arthritis with altered properties and defective TNF signalling. *J Leukoc Biol* (2017) 101 (2):599–611. doi: 10.1189/jlb.5A0116-022R
75. Theilgaard-Mönch K, Jacobsen LC, Borup R, Rasmussen T, Bjerregaard MD, Nielsen FC, et al. The transcriptional program of terminal granulocytic differentiation. *Blood* (2005) 105(4):1785–96. doi: 10.1182/blood-2004-08-3346
76. Kaur I, Simons ER, Castro VA, Mark Ott C, Pierson DL. Changes in neutrophil functions in astronauts. *Brain Behav Immun* (2004) 18(5):443–50. doi: 10.1016/j.bbi.2003.10.005
77. Stowe RP, Sams CF, Mehta SK, Kaur I, Jones ML, Feeback DL, et al. Leukocyte subsets and neutrophil function after short-term spaceflight. *J Leukoc Biol* (1999) 65(2):179–86. doi: 10.1002/jlb.65.2.179
78. Grigorieva DV, Gorudko IV, Sokolov AV, Kostevich VA, Vasilyev VB, Cherenkevich SN, et al. Myeloperoxidase Stimulates Neutrophil Degranulation. *Bull Exp Biol Med* (2016) 161(4):495–500. doi: 10.1007/s10517-016-3446-7
79. Malle E, Waeg G, Schreiber R, Grone EF, Sattler W, Grone HJ. Immunohistochemical evidence for the myeloperoxidase/H2O2/halide system in human atherosclerotic lesions: colocalization of myeloperoxidase and hypochlorite-modified proteins. *Eur J Biochem* (2000) 267(14):4495–503. doi: 10.1046/j.1432-1327.2000.01498.x
80. Delp MD, Charvat JM, Limoli CL, Globus RK, Ghosh P. Apollo Lunar Astronauts Show Higher Cardiovascular Disease Mortality: Possible Deep Space Radiation Effects on the Vascular Endothelium. *Sci Rep* (2016) 6:29901. doi: 10.1038/srep29901
81. Angkananard T, Anothaisintawee T, McEvoy M, Attia J, Thakkinstian A. Neutrophil Lymphocyte Ratio and Cardiovascular Disease Risk: A Systematic Review and Meta-Analysis. *BioMed Res Int* (2018) 2018:2703518. doi: 10.1155/2018/2703518
82. Nathan C, Cunningham-Bussel A. Beyond oxidative stress: an immunologist's guide to reactive oxygen species. *Nat Rev Immunol* (2013) 13(5):349–61. doi: 10.1038/nri3423
83. Hildeman DA, Mitchell T, Kappler J, Marrack P. T cell apoptosis and reactive oxygen species. *J Clin Invest* (2003) 111(5):575–81. doi: 10.1172/JCI200318007
84. Schmielau J, Finn OJ. Activated granulocytes and granulocyte-derived hydrogen peroxide are the underlying mechanism of suppression of t-cell function in advanced cancer patients. *Cancer Res* (2001) 61(12):4756–60.
85. Bass DA, Parce JW, Dechatelet LR, Szejda P, Seeds MC, Thomas M. Flow cytometric studies of oxidative product formation by neutrophils: a graded response to membrane stimulation. *J Immunol* (1983) 130(4):1910–7.
86. Mao XW, Pecaut MJ, Stodieck LS, Ferguson VL, Bateman TA, Bouxsein M, et al. Spaceflight environment induces mitochondrial oxidative damage in ocular tissue. *Radiat Res* (2013) 180(4):340–50. doi: 10.1667/RR3309.1
87. Chatterjee S, Fisher AB. Mechanotransduction: forces, sensors, and redox signaling. *Antioxid Redox Signal* (2014) 20(6):868–71. doi: 10.1089/ars.2013.5753
88. Gollapudi S, Gupta S. Reversal of oxidative stress-induced apoptosis in T and B lymphocytes by Coenzyme Q10 (CoQ10). *Am J Clin Exp Immunol* (2016) 5 (2):41–7.
89. Tomasetti M, Littarru GP, Stocker R, Alleva R. Coenzyme Q10 enrichment decreases oxidative DNA damage in human lymphocytes. *Free Radic Biol Med* (1999) 27(9-10):1027–32. doi: 10.1016/S0891-5849(99)00132-X
90. Meehan RT, Neale LS, Kraus ET, Stuart CA, Smith ML, Cintron NM, et al. Alteration in human mononuclear leucocytes following space flight. *Immunology* (1992) 76(3):491–7.
91. Stowe RP, Sams CF, Pierson DL. Effects of mission duration on neuroimmune responses in astronauts. *Aviat Space Environ Med* (2003) 74(12):1281–4.
92. Kaur I, Simons ER, Castro VA, Ott CM, Pierson DL. Changes in monocyte functions of astronauts. *Brain Behav Immun* (2005) 19(6):547–54. doi: 10.1016/j.bbi.2004.12.006
93. Kaur I, Simons ER, Kapadia AS, Ott CM, Pierson DL. Effect of spaceflight on ability of monocytes to respond to endotoxins of gram-negative bacteria. *Clin Vaccine Immunol* (2008) 15(10):1523–8. doi: 10.1128/CVI.00065-08
94. Greenlee-Wacker MC. Clearance of apoptotic neutrophils and resolution of inflammation. *Immunol Rev* (2016) 273(1):357–70. doi: 10.1111/imr.12453
95. Zhou Z, Zhang S, Ding S, Abudupataer M, Zhang Z, Zhu X, et al. Excessive Neutrophil Extracellular Trap Formation Aggravates Acute Myocardial Infarction Injury in Apolipoprotein E Deficiency Mice via the ROS-Dependent Pathway. *Oxid Med Cell Longev* (2019) 2019:1209307. doi: 10.1155/2019/1209307
96. Uraz S, Tahan G, Aytekin H, Tahan V. N-acetylcysteine expresses powerful anti-inflammatory and antioxidant activities resulting in complete improvement of acetic acid-induced colitis in rats. *Scand J Clin Lab Invest* (2013) 73(1):61–6. doi: 10.3109/00365513.2012.734859
97. Wulaningsih W, Holmberg L, Abeler-Doner L, Ng T, Rohrmann S, Van Hemelrijck M. Associations of C-Reactive Protein, Granulocytes and Granulocyte-to-Lymphocyte Ratio with Mortality from Breast Cancer in Non-Institutionalized American Women. *PloS One* (2016) 11(6):e0157482. doi: 10.1371/journal.pone.0157482

Conflict of Interest: The authors declare that the research was conducted in the absence of any commercial or financial relationships that could be construed as a potential conflict of interest.

frontiers in Immunology

ORIGINAL RESEARCH
published: 08 December 2020
doi: 10.3389/fimmu.2020.586399

Deficiency of the Circadian Clock Gene *Bmal1* Reduces Microglial Immunometabolism

Xiao-Lan Wang[1,2,3*], *Samantha E. C. Wolff*[2,3], *Nikita Korpel*[2,3,4], *Irina Milanova*[2,3], *Cristina Sandu*[5], *Patrick C. N. Rensen*[6], *Sander Kooijman*[6], *Jean-Christophe Cassel*[1,7], *Andries Kalsbeek*[2,3,4], *Anne-Laurence Boutillier*[1,7] *and Chun-Xia Yi*[2,3,4]

[1] *Université de Strasbourg, Laboratoire de Neuroscience Cognitives et Adaptatives (LNCA), Strasbourg, France,* [2] *Department of Endocrinology and Metabolism, Amsterdam University Medical Center (UMC), University of Amsterdam, Amsterdam, Netherlands,* [3] *Laboratory of Endocrinology, Amsterdam University Medical Center (UMC), University of Amsterdam, Amsterdam Gastroenterology & Metabolism, Amsterdam, Netherlands,* [4] *Netherlands Institute for Neuroscience (NIN), Royal Dutch Academy of Arts and Sciences (KNAW), Amsterdam, Netherlands,* [5] *Centre National de la Recherche Scientifique, Université de Strasbourg, Institut des Neurosciences Cellulaires et Intégratives, Strasbourg, France,* [6] *Department of Medicine, Divison of Endocrinology, and Einthoven Laboratory for Experimental Vascular Medicine, Leiden University Medical Center, Leiden, Netherlands,* [7] *CNRS UMR 7364, LNCA, Strasbourg, France*

OPEN ACCESS

Edited by:
Pedro Manoel Mendes Moraes Vieira, Campinas State University, Brazil

Reviewed by:
Theresa Ramalho, University of São Paulo, Brazil
Erik Steven Musiek, Saint Louis University, United States

****Correspondence:***
Xiao-Lan Wang
xiao-lan.wang@etu.unistra.fr

Specialty section:
This article was submitted to Molecular Innate Immunity, a section of the journal Frontiers in Immunology

Received: *23 July 2020*
Accepted: *06 November 2020*
Published: *08 December 2020*

Citation:
Wang X-L, Wolff SEC, Korpel N, Milanova I, Sandu C, Rensen PCN, Kooijman S, Cassel J-C, Kalsbeek A, Boutillier A-L and Yi C-X (2020) Deficiency of the Circadian Clock Gene Bmal1 Reduces Microglial Immunometabolism. Front. Immunol. 11:586399. doi: 10.3389/fimmu.2020.586399

Microglia are brain immune cells responsible for immune surveillance. Microglial activation is, however, closely associated with neuroinflammation, neurodegeneration, and obesity. Therefore, it is critical that microglial immune response appropriately adapts to different stressors. The circadian clock controls the cellular process that involves the regulation of inflammation and energy hemostasis. Here, we observed a significant circadian variation in the expression of markers related to inflammation, nutrient utilization, and antioxidation in microglial cells isolated from mice. Furthermore, we found that the core clock gene-Brain and Muscle Arnt-like 1 (*Bmal1*) plays a role in regulating microglial immune function in mice and microglial BV-2 cells by using quantitative RT-PCR. *Bmal1* deficiency decreased gene expression of pro-inflammatory cytokines, increased gene expression of antioxidative and anti-inflammatory factors in microglia. These changes were also observed in *Bmal1* knock-down microglial BV-2 cells under lipopolysaccharide (LPS) and palmitic acid stimulations. Moreover, Bmal1 deficiency affected the expression of metabolic associated genes and metabolic processes, and increased phagocytic capacity in microglia. These findings suggest that *Bmal1* is a key regulator in microglial immune response and cellular metabolism.

Keywords: inflammation, palmitic acid, cellular metabolism, oxidative stress, microglia

INTRODUCTION

Microglia serve as the brain macrophages with immune-modulating and phagocytic capabilities. Microglial activation associated neuroinflammation has been firmly linked to the development and progression of neurodegenerative diseases, such as Alzheimer's disease, Parkinson's disease, and Huntington's disease (1). Severe systemic inflammation, such as sepsis, triggers microglial inflammatory activation which leads to neuronal injury and cognitive impairments in both

humans (2, 3) and rodents (4). High-fat diet-induced chronic microglial inflammation results in neuronal loss and obesity (5, 6). Our previous study shows that microglial activation follows a circadian rhythm in rodents (7).

Circadian rhythms are involved in the regulation and maintenance of various physiological processes, including immune responses, energy metabolism, and memory formation (8–10). A growing body of literature shows that endogenous circadian clock function plays a crucial role in the control of many cellular processes that affect overall physiology (11–17). For example, macrophages or microglial clock gene modulates the production of cytokines, following an immune challenge (18–20). Besides the involvement of clock genes, it has also been shown that the immune activity is highly dependent on cellular metabolic processes (21–23); reduced glucose or lipid utilization inhibits microglial activation and inflammation (22, 24). However, it is still unclear whether the intrinsic clock regulates microglial immune activity through modulation of cellular metabolism.

At the molecular level, the circadian clock machinery is based on transcriptional-translational feedback loops, which are present in almost every mammalian cell (25). The transcriptional factor Bmal1 (Brain and Muscle Arnt-like 1)/Clock complex activates the expression of the period genes (*Per1*, *Per2*) and cryptochrome genes (*Cry1*, *Cry2*). Per/Cry complex suppresses its own transcription by inhibiting the activity of the Bmal1/Clock complex (25, 26). Nuclear receptor subfamily 1, group D, member 1 (Nr1d1), and RAR-related orphan receptors (Rors) fine-tune the transcription of *Bmal1*. Apart from the autoregulation, clock transcription factors also control the expression of other genes, such as the gene-D site albumin promoter binding protein (*Dbp*), by binding to their promoter (27). In the current study, we focus on the core clock gene-*Bmal1*, which is highly expressed during the light phase in microglia in mice (28).

Bmal1 is closely linked with energy metabolism (29–32), redox hemostasis (13, 33), and immune responses (19). Cellular energy metabolism and redox hemostasis regulate immune cell function, including those of microglia (13, 24). This suggests a possible link between circadian clock-*Bmal1* and the microglial immune response, as well as cellular energy metabolism and redox hemostasis. Here, we used the global Bmal1 knockout mice which show a complete loss of their circadian rhythms (34). We found a significantly reduced inflammatory and metabolic associated gene expression in microglia isolated from Bmal1 knockout mice. The decrease of inflammatory markers was also observed in *Bmal1* knocked down microglial BV-2 cells under LPS and palmitic acid stimulations.

MATERIALS AND METHODS

Animals

Mice were housed in temperature (22 ± 1°C) and humidity (55 ± 5%) controlled room under a 12h/12h light/dark cycle {[lights on at 07:00 h, zeitgeber time 0 (ZT0)]}, with free access to food and water. B6.129-*Arntl*^{tm1Bra}/J mice (34) (Jax stock #009100) were obtained from the Jackson Laboratory. The helix-loop-helix domain within exon 4 and all of exon 5 were replaced to create the mutation. B6.129-*Arntl*^{tm1Bra}/J mice have a C57BL/6J background. The following primers were used for genotyping: common: 5'-GCC CAC AGT CAG ATT GAA AAG-3'; wild type reverse: 5'- CCC ACA TCA GCT CAT TAA CAA-3'; mutant reverse: 5'- GCC TGA AGA ACG AGA TCA GC-3'. Mutant band: 162 bp; wild type band: 329 bp; heterozygote band: 162 bp and 329 bp. The mice containing only a mutant band were regarded as Bmal1 knockout (*Bmal1* KO). C57BL/6J mice served as control (Ctrl) (**Supplementary Figure 1**). *Bmal1* KO male mice were killed at ZT6 at the age of 3 months. Experimental protocol (NIN18.30.02) and animal care complied with the institutional guidelines of the Netherlands (Amsterdam, the Netherlands).

C57BL/6J male mice used for microglial isolation were sacrificed at 8-time points from ZT0 at 10 weeks old. This study was approved by and performed according to the guidelines of the Institutional Animal Care and Use Committee of the Netherlands (Leiden, the Netherlands).

Two transgenic mice lines (*Cx3cr1*^{CreER} mice, Jax mice stock no: 021160; *Bmal1*$^{lox/lox}$ mice, Jax mice stock no: 007668) were used to generate microglia-specific Bmal1 KO mice (*Bmal1* lox-homozygous and Cre-positive) and Ctrl mice (Cre-positive, but with a *Bmal1* wild-type sequence). Experimental protocols and animal care were in compliance with institutional guidelines and international laws and policies. Our project has been reviewed and approved by the national and regional ethics committee in Strasbourg (France). Experimental protocols and animal care were in compliance with the institutional guidelines (council directive 87/848, October 19, 1987, Ministère de l'agriculture et de la Forêt, Service Vétérinaire de la Santé et de la Protection Animale) and international laws (directive 2010/63/UE, February 13, 2013, European Community) and policies. Our project has been reviewed and approved by the French national and regional ethics committee (APAFIS#6822-2016092118336690v3).

Acute Isolation of Microglia From Adult Mice Brain Tissue

Mice were decapitated, and brains were homogenized in RPMI medium (21875-034, Gibco) with a 15 ml Dounce homogenizer on ice until the sample is fully homogeneous, without any visible tissue fragments. The final homogenate was filtered through a 70 µm cell strainer (431751, Corning). Following 5 min centrifugation at 380 g at 4°C, cell pellets were resuspended with 7 ml RPMI medium (11875093, Gibco) and mixed with 3 ml stock isotonic Percoll (SIP) solution which was made by mixing one part 10x HBSS (14185052, Gibco) in nine parts of Percoll plus (GE17-5445-01, Sigma-Aldrich). The cell suspension was then layered slowly on top of 2 ml of 70% Percoll solution which was prepared by mixing three parts of HBSS (14170112, Gibco) with seven parts SIP in a new 15 ml falcon and centrifuged at 500 g speed for 30 min at 18°C, with minimal acceleration and break rate. After centrifugation, the

fuse interphases were transferred into a new 15 ml falcon with 8 ml HBSS and centrifuged at 500 g for 7 min again. The supernatant and cell debris were discarded and microglial cells were collected for RNA isolation.

RNA Isolation From Microglia and Quantitative PCR

Total RNA was isolated from acutely isolated microglia using RNeasy Micro Kit (74004, QIAGEN) following the manufacturer's recommendations. We used 180 ng RNA to make cDNA with a Transcriptor First Strand cDNA Synthesis Kit (04897030001, Roche) following the manufacturer's recommendations. 4.5 ng cDNA was used to perform qPCR with SensiFAST™ SYBR® No-ROX Kit (BIO-98020, Roche Bioline). The genes *Bmal1*, *Clock*, *Cry1*, *Cry2*, *Per1*, *Per2*, *Nr1d1*, *Dbp*, *Il1b*, *Tnfa*, *Il6*, *Il10*, *Nox2*, *Gsr*, *Hmox1*, *Glut5*, *Glut1*, *Lpl*, *Gls*, and *Pcx* were evaluated. Primer sequences are presented in **Supplementary Table 1**. Data were analyzed by LC480 Conversion and LinRegPCR software and normalized to the housekeeping gene hypoxanthine phosphoribosyltransferase 1 (*Hprt1*).

Microglial BV-2 Cell Culture and Transfection

Murine microglial BV-2 cells (35) were kindly provided by Noam Zelcer (36) and cultured in Dulbecco's Modified Eagle's medium (DMEM, 41965-039, Gibco) supplemented with 10% fetal bovine serum (FBS, Gibco) and 100 µg/ml penicillin-streptomycin at 37°C in a humidified atmosphere containing 5% CO_2. Microglial BV-2 cells were transfected with the *Bmal1* siRNA or scrambled siRNA (Dharmacon) by using Viromer (VB-01LB-01, lipocalyx, Germany) according to the manufacturer's protocol. The medium was replaced 6 h after transfection and cells were incubated as usual. 24 h after transfection, cells were synchronized with 100 nM of dexamethasone (Sigma-Aldrich) for 2 h, then washed with PBS, and followed by exposure to lipopolysaccharide (LPS, E. coli O111:B4, 100 ng/ml, L4391, Sigma-Aldrich), palmitic acid (P0500, Sigma-Aldrich) or vehicle, and finally harvested at the appropriate time points. The time at which cells were washed with PBS was defined as 0.

Palmitic Acid and Bovine Serum Albumin Conjugation Protocol

Palmitic acid was dissolved in 150 mM NaCl with robust shaking at 70°C. Fatty acid-free BSA (A8806, Sigma-Aldrich) was dissolved in 150 mM NaCl at 37°C to make a 3.2 mM BSA solution. Half of the BSA solution was mixed with the same volume of palmitic acid solution at 37°C while stirring overnight to make palmitic acid-BSA conjugated solution (5:1 molar ratio palmitic acid: BSA). Half of the BSA solution was added to the same volume of 150 mM NaCl at 37°C while stirring overnight to make a vehicle control solution. pH was adjusted to 7.4 and solutions were filtered using a 0.22 µm syringe filter.

RNA Isolation From BV-2 Cells

Total RNA was extracted using the High Pure RNA isolation kit (1182866500, Roche) following the manufacturer's instructions. Complementary DNA was obtained by reverse transcription of 400 ng of total mRNA using the Transcriptor First Strand cDNA Synthesis Kit (04897030001, Roche) following the manufacturer's recommendations.

Primary Microglial Culture

Microglial cultures were prepared as described previously (24). Briefly, brain tissues were harvested from microglia-specific Bmal1 KO and littermate Ctrl mice at postnatal days 1–4 (P1–P4), the meninges and blood vessels were removed, and the parenchyma minced and triturated in DMEM/F12 (10565018, Gibco), containing 10% FBS, 100 µg/ml penicillin-streptomycin. Suspended cells were filtered (70 µm) and seeded on poly-L-lysine-coated flasks. Six to 10 days later, the flasks were shaken (200 rpm) for 1 h to specifically detach microglia. Microglial cells were treated with 5 µM of 4-hydroxytamoxifen for 48 h to induce Cre-LoxP recombination and excise *Bmal1*. Cells isolated from microglia-specific Bmal1 KO and Ctrl mice served as Bmal1 KO and Ctrl, respectively. Next, microglia were synchronized with 100 nM dexamethasone for 2 h, washed with PBS, and then treated with 100 ng/ml LPS for 1 h or 100 µM palmitic acid for 4 h, for final analysis.

Western Blot Analyses

Primary microglial cells were homogenized in Laemmli buffer and sonicated for 10 s twice (ultrasonic processor, power 40%) followed by heating at 70°C for 10 min and then 100°C for 5 min. Lysates were centrifuged at 14,000 *g* for 5 min, and the supernatant was used for Western blot analyses. Proteins were loaded on Midi-PROTEAN TGX Stain-Free™ Precast Gels (4%–20%, Bio-Rad) and electrotransferred onto a nitrocellulose membrane. Primary antibodies used for Western blots were rabbit anti-Bmal1 (1:500, NB100-2288, Novus Biologicals) and rabbit anti-Actin (1:2000, A2066, Sigma-Aldrich), followed by horseradish peroxidase-conjugated secondary antibodies against rabbit (1:5000, Jackson ImmunoResearch). Immunoreactive bands were detected with ECL (Clarity, Bio-Rad) with a ChemiDoc Touch system (Bio-Rad).

2-NBDG Glucose Uptake Assay

Microglial cells were plated in 96-well black plates with 3.5 x 10^4 cells/well. After synchronization, cells were cultured in glucose-free medium with LPS or palmitic acid stimulation. At the end of treatment, 2-NBDG (ab235976, Abcam), a fluorescently-labeled deoxyglucose analog, was added to a final concentration of 200 µg/ml, and fluorescent signals were recorded at 2, 5, and 10 min by microplate reader at excitation/emission wavelengths = 480/530 nm.

Free Fatty Acid Uptake Assay

Microglial cells were seeded in 96-well black plates with 3.5 x 10^4 cells/well. After synchronization, cells were treated with LPS or palmitic acid in 100 µl FBS free culture medium. At the end of treatment, 100 µl fatty acid dye (TF2-C12)-loading solution (ab176768, Abcam) was incubated with microglia for 1 h at 37°C. Fluorescent signals were detected by microplate reader at 30, 45, and 60 min at excitation/emission wavelengths = 480/530 nm.

DCFDA-Cellular Reactive Oxygen Species Detection Assay

Microglial cells were plated in 96-well black plates with 3.5 x 10^4 cells/well. After synchronization, cells were stained by 25 μm DCFDA solution (ab113851, Abcam) for 25 min at 37°C. Fluorescent signals were detected immediately by microplate reader at excitation/emission wavelengths = 480/530 nm. Following the basal measurement, cells were challenged with 2% H_2O_2, and fluorescent signals were recorded up to 10 min.

Microsphere Uptake Assay

Microspheres (17154-10, polysciences) were coated with 10% FBS at 37°C for 1 h, followed by centrifugation (12,000 rpm, 2 min) and resuspended in PBS. Coated microspheres were added to the BV-2 cells (1000 microspheres per cell) at time 0, and 1 h later, cells were washed with PBS 3 times, then fixed by 4% paraformaldehyde for 5 min, followed by PBS washing. Mounting medium with DAPI was added for confocal imaging (Leica TCS SP5; Leica, Heidelberg, Germany). Five-μm z-stack confocal images were acquired at 0.3-μm intervals, with 40×/1.3 oil objective at 1× zoom. Images were analyzed by Imaris (Bitplane AG) to measure the total volume of microspheres in every view.

Statistical Analysis

Statistical analyses were performed using two-tailed unpaired *t*-test, one-way ANOVA, and two-way ANOVA with GraphPad Prism 8 (San Diego, California, USA). Daily variation in gene expression in microglia isolated from C57BL/6J mice was evaluated by one-way ANOVA (**Supplementary Table 2**). The daily rhythm of genes in microglia isolated from C57BL/6J mice and BV-2 cells was assessed by cosinor analysis with SigmaPlot 14.0 software (SPSS Inc, Chicago, IL, USA). Data were fitted to the following regression: $y = A + B \cdot \cos(2\pi(x-C)/24)$; A is the mean level; B is the amplitude and C is the acrophase of the fitted rhythm (37). An overall *p* value (main *p* value, *P*m) was considered to indicate the rhythmicity in **Supplementary Table 3**. All data are presented as mean ± s.e.m and significance was considered at $P < 0.05$.

RESULTS

Microglial Inflammatory Cytokine Genes Are Higher Expressed During the Light Phase

A previous rat study has demonstrated that microglial intrinsic clock genes and inflammatory cytokine genes show daily expression rhythms in the hippocampus and microglial inflammatory cytokine genes highly expressed during the light phase (38). It has also been shown that LPS treated rodents show increased sickness behavior or proinflammatory response during the light phase compared to the dark phase (38, 39). In the current mouse study, we found that in microglial cells, the gene expression of pro-inflammatory cytokines-interleukin 1 beta (*Il1b*) and interleukin 6 (*Il6*), but not tumor necrosis factor (*Tnfa*), followed a daily expression rhythm (**Figures 1A–C**, and **Supplementary Tables 2 and 3**). Both *Il1b* and *Il6* showed higher gene expression during the light phase than in the dark phase. The peak in *Tnfa* expression was also found during the light phase (**Figures 1A–C, I**). Moreover, the oxidation and inflammation-related gene NADPH oxidase 2 (*Nox2*) also showed rhythmic expression in microglia (**Figure 1D** and **Supplementary Table 3**). Together these findings suggest that microglia may have a higher innate immune activity during the light phase in mice.

Microglial Nutrient Utilization and the Antioxidation Transcripts Show Daily Rhythmicity

In physiological conditions, microglia are highly dynamic to clean the microenvironment and maintain neuronal survival and function (40). The previous study showed that microglial activity is higher during the dark phase when mice are more active as compared with the light phase when mice are mainly resting (7). Microglial activity is also highly dependent on cellular metabolism (24). Therefore, we evaluated gene expression of facilitated glucose transporter member 5 (*Glut5*), which is highly expressed by microglia, and lipoprotein lipase (*Lpl*), which mediates lipoprotein triglyceride-derived fatty acid uptake. Both *Glut5* and *Lpl* exhibited an increased expression during the dark phase (**Figures 1E, F, I**), which suggests an increased nutrient utilization when microglia are more active. Microglial activation leads to the production of more metabolites and ROS (41, 42) that need to be eliminated to maintain proper microglial function (43–45). Thus, we checked the gene expression of glutathione reductase (*Gsr*), a key enzyme for the production of sulfhydryl form glutathione (GSH). GSH acts as a scavenger and plays a critical role in preventing oxidative stress in cells. We also evaluated the rhythmic gene expression of heme oxygenase 1 (*Hmox1*), which has antioxidant anti-inflammation properties *via* the production of carbon monoxide (CO) (44). We observed an increased expression of *Gsr* and *Hmox1* during the dark phase (**Figures 1G–I**). The gene expression of *Glut5* and *Gsr* showed significant daily variation (**Supplementary Table 2**). These data indicate that the expression of nutrient utilization and the antioxidation associated genes in microglial cells follows a daily rhythm, which is in line with their activity.

Bmal1 Knockout Microglia Show Decreased Gene Expression of Inflammation and Nutrient Utilization

The circadian clock system is associated with the innate immune activity (16). Therefore, we were interested in whether the *Bmal1* regulates microglial immunometabolism and evaluated the related gene expression in microglia isolated from *Bmal1* KO mice and controls in the middle of the light phase (ZT6). Expression of clock genes in *Bmal1* KO microglia was disturbed, with a significant increase in *Cry1*, *Cry2*, and *Per2*, as well as a decrease in *Nr1d1*, and *Dbp* (**Figure 2A**). *Il1b* and

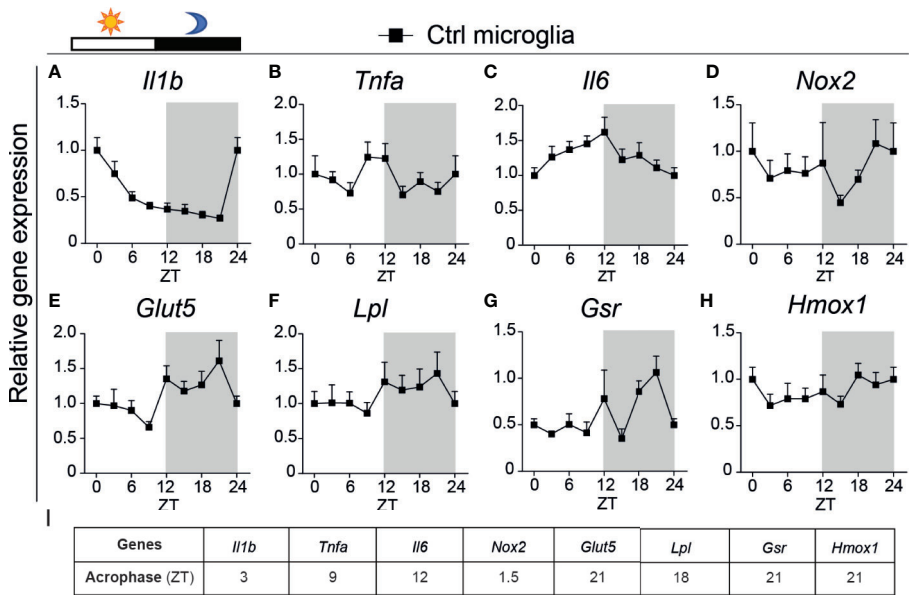

I

Genes	*Il1b*	*Tnfa*	*Il6*	*Nox2*	*Glut5*	*Lpl*	*Gsr*	*Hmox1*
Acrophase (ZT)	3	9	12	1.5	21	18	21	21

FIGURE 1 | Rhythmic gene expression of inflammatory cytokines, nutrient utilization, and antioxidant anti-inflammation in microglia. **(A–H)** Relative expression of inflammatory genes interleukin 1 beta (*Il1b*) **(A)**, tumor necrosis factor (*Tnfa*) **(B)**, interleukin 6 (*Il6*) **(C)**, and oxidation and inflammation-related gene NADPH oxidase 2 (*Nox2*) **(D)**, and nutrient utilization genes facilitated glucose transporter member 5 (*Glut5*) **(E)**, lipoprotein lipase (*Lpl*) **(F)**, as well as antioxidant anti-inflammation genes glutathione reductase (*Gsr*) **(G)**, heme oxygenase 1 (*Hmox1*) **(H)**, were evaluated in isolated microglia from C57BL/6J male mice brain every 3 h (n = 6–8 samples per group per time point). ZT0 = lights on; ZT12 = lights off. Data of ZT0 and ZT24 were from the same samples. **(I)** Acrophase determined for each of the genes. Statistical significance of rhythmic expression was determined by the Cosinor analysis and one-way ANOVA. Data are presented as means ± s.e.m.

Nox2 were significantly lower in *Bmal1* KO microglia, while *Tnfa* and *Il6* did not differ between both groups (**Figure 2B**). Moreover, *Gsr* and *Hmox1* expression were strikingly increased (**Figure 2C**). Taken together, these data suggest that *Bmal1* KO decreases inflammation and increases the anti-inflammation antioxidative effect in microglia. Furthermore, microglial *Glut5* and *Lpl* were significantly decreased in *Bmal1* KO mice (**Figure 2D**). While glutaminase (*Gls*), which is involved in glutamate utilization, and pyruvate carboxylase (*Pcx*), which participates in gluconeogenesis and lipogenesis, did not differ between the two groups (**Figure 2D**). These findings suggest reduced nutrient utilization in *Bmal1* KO microglia as compared to controls in physiological conditions.

Bmal1 Deletion Disturbs the Expression of Clock Genes in Microglial BV-2 Cells

To further study the relationships among the intrinsic clock, immune activity, cellular metabolism, and antioxidative effect, specifically in microglia, we performed experiments in microglial BV-2 cells. Rhythmic expression of clock genes can be achieved in microglial BV-2 cells after synchronization with 100 nM dexamethasone for 2 h (19). Using this cell model, we found that the inflammatory cytokines *Il1b*, *Tnfa*, interleukin 10 (*Il10*), and *Il6* showed a significant rhythmic expression after synchronization (**Supplementary Figure 2** and **Supplementary Table 3**). To evaluate whether the intrinsic clock regulates microglial function, we knocked down *Bmal1* in BV-2 cells. First, we checked the clock gene expression every 4 h for 28 h after synchronization. We observed that *Bmal1* gene expression was significantly decreased in the *Bmal1* knock-down group (*Bmal1* siRNA) compared with the control group (scrambled siRNA) (**Figure 3A**). *Bmal1* controlled genes, such as *Cry1*, *Cry2*, and *Per2*, and the *Bmal1* targeted gene *Dbp* showed a significant increase in the *Bmal1* knock-down group. While *Clock* was decreased 12 h after synchronization; *Per1* and *Nr1d1* expression did not change (**Figure 3A**). The rhythmic expression of *Bmal1* was disturbed in the *Bmal1* knock-down group, but *Clock*, *Cry1*, *Per1*, *Per2*, *Nr1d1*, and *Dbp* still showed rhythmic expression (**Supplementary Table 3**). These results indicate that *Bmal1* deletion disturbs the core clock machinery in BV-2 cells.

Bmal1 Deficiency Decreases the Expression of Inflammation and Nutrient Utilization Associated Genes in BV-2 Cells

To assess whether *Bmal1* deficiency also affects immune activity in microglial BV-2 cells, we evaluated the expression of inflammatory cytokine genes and related genes. As expected, expression of the pro-inflammatory cytokines *Il1b* and *Tnfa* was decreased and expression of the anti-inflammatory cytokine *Il10* was increased in the *Bmal1* knock-down group; *Il6* was not different between the two groups (**Figure 3B**). Gene expression of the glucose transporter

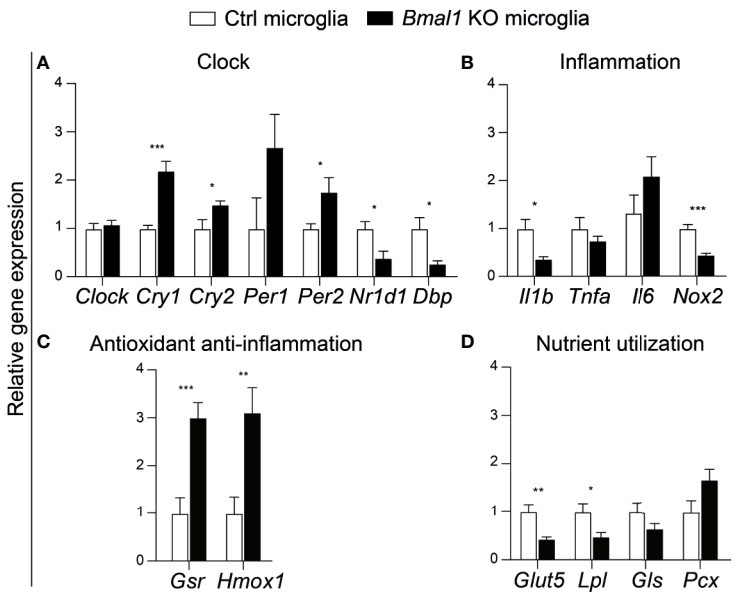

FIGURE 2 | *Bmal1* KO microglia show decreased inflammation and nutrient utilization in mice. **(A–D)** Relative expression of clock genes-*Clock*, cryptochrome (*Cry1*, *Cry2*), period (*Per1*, *Per2*), Nuclear receptor subfamily 1, group D, member 1 (Nr1d1), D site albumin promoter binding protein (*Dbp*) **(A)**, inflammation-related genes *Il1b*, *Tnfa*, *Il6*, *Nox2* **(B)**, and antioxidant anti-inflammation genes *Gsr*, *Hmox1* **(C)**, as well as cellular metabolic-related genes *Glut5*, *Lpl*, glutaminase (*Gls*), and pyruvate carboxylase (*Pcx*) **(D)**, were evaluated in isolated microglia from *Bmal1* KO mice and C57BL/6J mice brain at ZT6 (n = 8 samples per group). Data were analyzed with *t*-tests and are presented as means ± s.e.m. * $P < 0.05$, ** $P < 0.01$, and *** $P < 0.001$.

1 (*Glut1*), which is highly expressed in BV-2 cells, did not differ between the two groups (**Figure 3C**). While *Lpl* expression was significantly reduced and *Pcx*, which plays a crucial role in gluconeogenesis and lipogenesis, was increased in the *Bmal1* knock-down group (**Figure 3C**). These findings suggest reduced inflammation and nutrient utilization in the *Bmal1* knock-down group. Additionally, *Gsr* and *Hmox1* showed higher expression in the *Bmal1* knock-down group (**Figure 3D**). Inflammatory cytokines showed rhythmic expression in both groups (**Supplementary Table 3**). All of these data suggest that in basal conditions, *Bmal1* knock-down reduces the transcription of inflammation and nutrient utilization-related genes in BV-2 cells.

Bmal1 Deficient BV-2 Cells Show Less Inflammatory Gene Expression Under LPS Stimulation

To further verify the effect of *Bmal1* on the microglial immune response, we challenged the *Bmal1* knock-down and control BV-2 cells with LPS after synchronization. LPS treatment did not change the rhythmic expression of the clock genes-*Bmal1*, *Clock*, or *Per1* in either group (**Supplementary Figure 3** and **Supplementary Table 3**). The *Bmal1* knock-down group showed significantly less pro-inflammatory *Il1b*, *Tnfa*, and *Il6* expression at 4 h and 8 h after LPS treatment, and higher anti-inflammatory *Il10* expression at 4 h than the control group (**Figure 4A**). In addition to the production of inflammatory cytokines, LPS stimulation also upregulates Nox2 expression that contributes to oxidative stress (46). But there was no genotype difference in *Nox2* expression (**Figure 4B**). *Lpl*, which showed less expression in *Bmal1* deficient group in basal condition, was no difference between the *Bmal1* deficient group and controls after LPS treatment (**Figure 4C**). *Glut1*, *Gsr*, and *Hmox1* expression were similar between the two groups (**Figures 4C, D**). Taken together, these data indicate that *Bmal1* knock-down alters inflammation and nutrient utilization transcripts in BV-2 cells after LPS treatment.

Bmal1 Knock-Down Partially Alters the Expression of Inflammation-Related Genes in Palmitic Acid-Treated BV-2 Cells

It has been shown that consumption of a high-fat diet, especially of its main ingredient the saturated fatty acids, results in hypothalamic microglial activation and inflammation (24). It has also been demonstrated that the saturated fatty acid palmitic acid increases inflammation and oxidative stress in cultured microglial cells (47, 48). To test whether palmitic acid still induces inflammation after synchronization, cells were treated with two concentrations of palmitic acid (100 and 200 μM) for 12 h. We observed that both concentrations significantly increased *Il1b* and *Tnfa* expression; while only 100 μM palmitic acid stimulation increased *Il6* expression compared with vehicle (**Supplementary Figure 4**).

Since our previous study had shown that an HFD disturbs the expression of microglial clock genes and the daily rhythmicity in rats (49), we first studied clock genes expression in 100 μM palmitic acid-treated BV-2 cells under control and *Bmal1* knock-

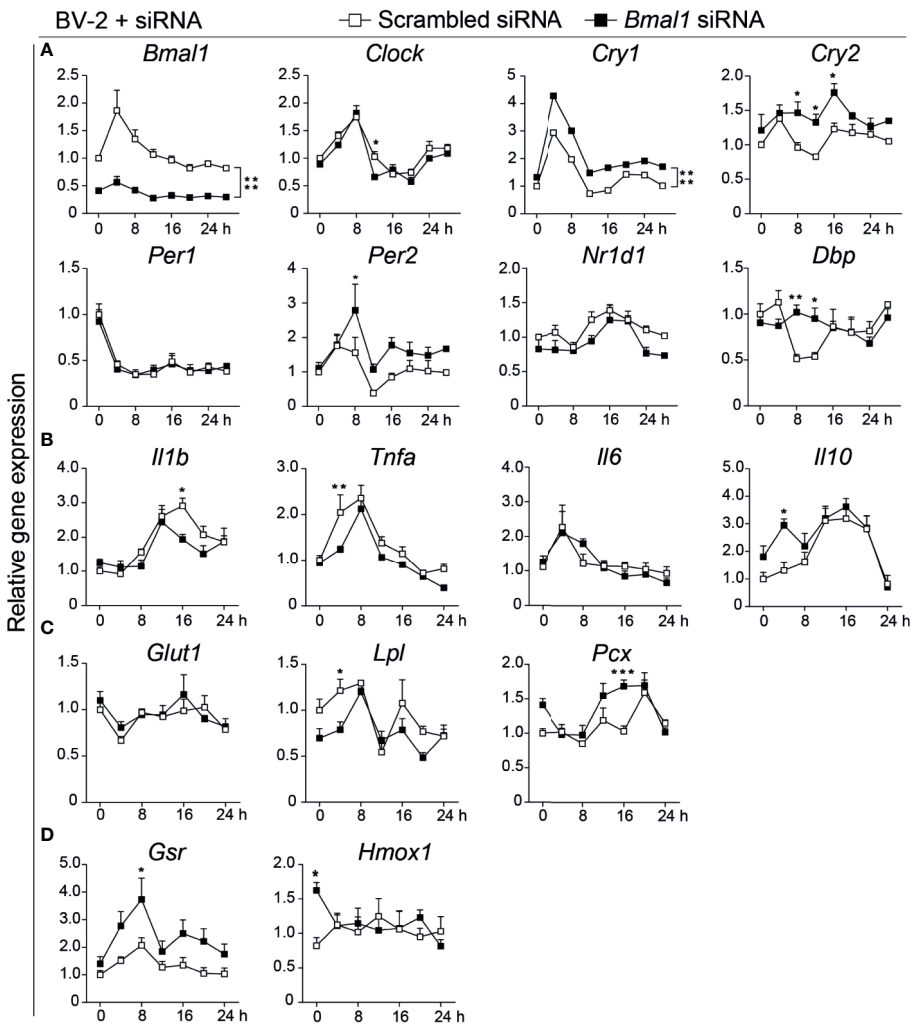

FIGURE 3 | *Bmal1* deficiency decreases inflammation and nutrient utilization of microglial BV-2 cells. **(A–D)** Relative gene expression in scrambled siRNA and *Bmal1* siRNA groups (n = 3–6 samples per group per time point). Clock genes *Bmal1*, *Clock*, *Cry1*, *Cry2*, *Per1*, *Per2*, *Nr1d1*, *Dbp* **(A)**, inflammatory cytokine genes *Il1b*, *Tnfa*, *Il6*, *Il10* **(B)**, glucose and fatty acid metabolism genes *Glut1*, *Lpl*, *Pcx* **(C)**, and antioxidant genes *Gsr*, *Hmox1* **(D)** were evaluated every 4 h for 28 h after BV-2 cells were exposed to Dex. Data were analyzed with two-way ANOVA. Statistical significance of rhythmic expression was determined by Cosinor analysis. Data are presented as means ± s.e.m. * $P < 0.05$, ** $P < 0.01$, and *** $P < 0.001$.

down conditions. Here, we observed that palmitic acid abolished the rhythmic expression of *Bmal1* and *Clock* in both groups and shifted the rhythmic expression of *Cry1*, *Cry2*, *Per2*, *Nr1d1*, and *Dbp* (**Supplementary Figure 5** and **Supplementary Table 3**). After palmitic acid treatment, clock genes showed a significant decrease at 4 h compared with 0 h. *Bmal1* expression was still lower in the *Bmal1* knock-down group than in controls from 8 h to 24 h. *Cry1*, *Cry2*, *Per2*, and *Dbp* kept an increased expression in the *Bmal1* knock-down group at some time points. While *Clock*, *Per1*, and *Nr1d1* did not differ between the two groups (**Supplementary Figure 5**).

Next, we evaluated whether *Bmal1* deficiency protects microglia from palmitic acid-induced inflammation. Surprisingly, *Il1b* was significantly increased at 16 h after palmitic acid treatment in the *Bmal1* knock-down group; *Il6* decreased at a later phase (20, 24 h) and *Il10* was increased at 20 h in the *Bmal1* knock-down group (**Figure 5A**). *Tnfa* expression did not differ between the control and *Bmal1* knock-down groups (**Figure 5A**). A previous study has shown that palmitic acid treatment induces oxidative stress through Nox2 upregulation, which also plays an important role in inflammation (50). Here the gene expression of *Nox2*, *Glut1*, *Lpl*, and *Gsr* showed no differences between the two groups (**Figures 5B–D**). But *Bmal1* deficiency increased *Hmox1* expression at 12 h after palmitic acid stimulation (**Figure 5D**). Together, these data suggest that *Bmal1* knock-down totally disturbs the rhythmic expression of clock genes, and only partially reduces the expression of palmitic acid-induced inflammation and oxidative stress associated genes in BV-2 cells.

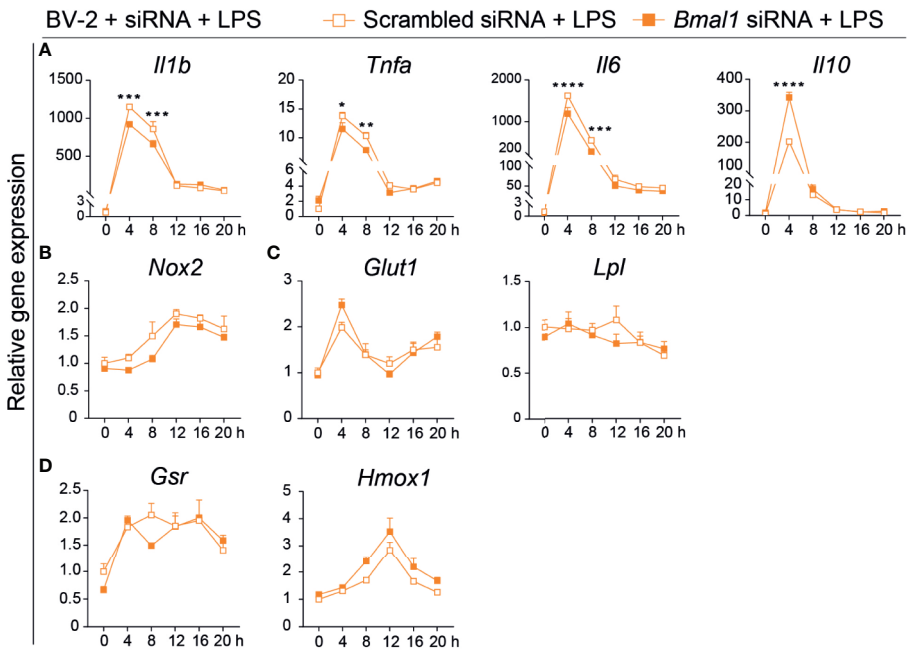

FIGURE 4 | *Bmal1* knock-down reduces the pro-inflammatory gene expression and increases the antioxidative anti-inflammatory gene expression of BV-2 cells after LPS stimulation. **(A–D)** Gene expression in scrambled siRNA and *Bmal1* siRNA groups every 4 h for 20 h in the presence of LPS (n = 3–6 samples per group per time point). Pro-inflammatory cytokine genes *Il1b*, *Tnfa*, *Il6* **(A)**, anti-inflammatory cytokine gene *Il10* **(A)**, oxidative stress gene *Nox2* **(B)**, glucose metabolism gene *Glut1*, and lipid metabolism gene *Lpl* **(C)**, and antioxidant anti-inflammation gene *Gsr*, *Hmox1* **(D)** were evaluated at 6-time points after LPS exposure. Statistical significance was determined using two-way ANOVA. Statistical significance of the rhythmic expression was determined by Cosinor analysis. Data are presented as means ± s.e.m. * $P < 0.05$, ** $P < 0.01$, and *** $P < 0.001$.

Bmal1 Deficiency Alters Metabolic Processes and Increases Phagocytosis of Microglia

To affirm the Bmal1 effects on nutrient utilization, we evaluated the dynamic process of glucose and free fatty acid uptake in primary microglial cells. Bmal1 was significantly decreased in Bmal1 KO microglia compared with Ctrls 48 h after the 4-hydroxytamoxifen treatment (**Figure 6A**). At 2 min after the treatment of 2-NBDG, we observed an increased glucose uptake in Bmal1 KO microglia compared to Ctrls in basal condition; LPS stimulation increased glucose uptake in Ctrls, however, which was not observed in Bmal1 KO microglia when compared with the basal conditions (**Figure 6B**). No differences were observed when extending the incubation of 2-NBDG to 5 and 10 min (**Figure 6B**). Interestingly, Bmal1 KO microglia treated with LPS showed less free fatty acid uptake compared with their basal condition at 45 and 60 min, respectively (**Figure 6C**). But there was no genotype difference in free fatty acid uptake at each time point (**Figure 6C**). Moreover, we saw less cellular ROS activity in Bmal1 KO microglia than Ctrl microglia under H2O2 stimulation, while no genotype difference in basal condition (**Figure 6D**). No differences were observed in glucose and free fatty acid uptake after palmitic acid stimulation (**Supplementary Figure 6**). Surprisingly, the phagocytic capacity was significantly increased in Bmal1 knock-down BV-2 cells (**Figures 6E, F**). These data indicate that Bmal1 KO microglia shift glucose and lipid utilization, and show an increase of phagocytosis.

DISCUSSION

Circadian rhythms are closely related to immunity and metabolism (10, 51, 52). However, it was still unclear whether and if so, how the endogenous circadian clock regulates microglial immune response and metabolism. Here, we observed a significant daily rhythmic expression of inflammation, nutrient utilization, and antioxidation related genes in microglia isolated from mice. We further found that deficiency of *Bmal1* affected inflammation and nutrient utilization associated gene expression in microglial cells (**Figure 7**).

We evaluated gene expression of inflammatory cytokines in *Bmal1* knock-down microglia in both *Bmal1* KO mice and BV-2 cells. Lacking *Bmal1* decreased pro-inflammatory gene expression and increased anti-inflammatory gene expression in microglial cells. It is known that *Bmal1* expression is higher during the light phase than the dark phase (28), which is

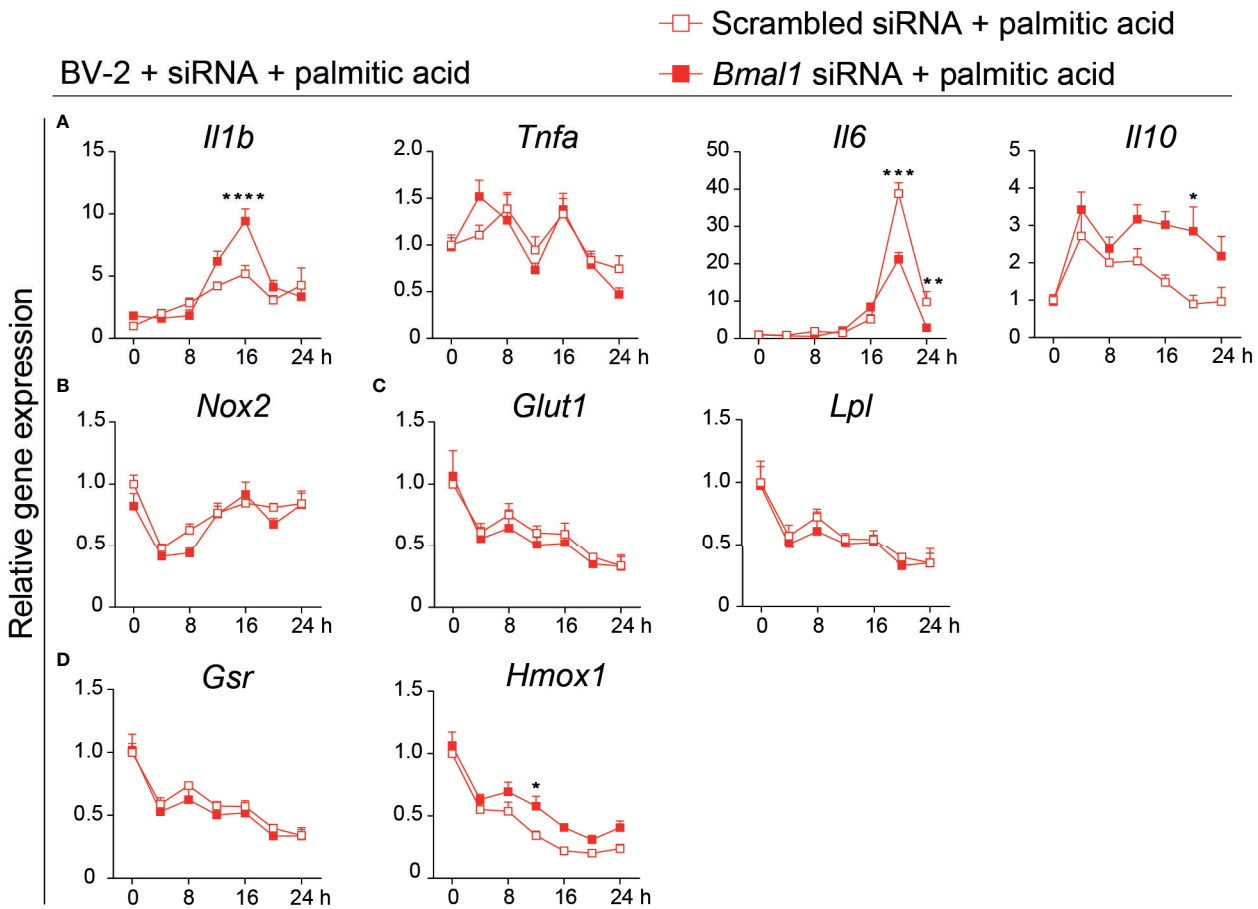

FIGURE 5 | *Bmal1* knock-down partially decreases the pro-inflammatory gene expression and increases the antioxidative anti-inflammatory gene expression in palmitic acid-treated BV-2 cells. **(A–D)** Gene expression in scrambled siRNA and *Bmal1* siRNA groups every 4 h for 24 h in the presence of palmitic acid (n = 3–6 samples per group per time point). Pro-inflammatory cytokine genes *Il1b*, *Tnfa*, *Il6* **(A)**, anti-inflammatory cytokine gene *Il10* **(A)**, oxidative stress gene *Nox2* **(B)**, glucose metabolism gene *Glut1*, and lipid metabolism gene *Lpl* **(C)**, and antioxidant anti-inflammation gene *Gsr*, *Hmox1* **(D)** were evaluated at 7-time points after palmitic acid treatment. Statistical significance was determined using two-way ANOVA. Statistical significance of rhythmic expression was determined by Cosinor analysis. Data are presented as means ± s.e.m. * $P < 0.05$, ** $P < 0.01$, and *** $P < 0.001$.

consistent with pro-inflammatory cytokine gene expression in microglia in mice under light/dark conditions. This may explain why *Bmal1* deficient microglia showed less inflammation. Moreover, Bmal1 as a transcription factor not only controls clock genes expression, but also regulates the expression of other genes *via* specific binding regulatory elements [E-box, D-box, and RORE (Ror/Rev-erb-binding element)] in their promoters (53–56). It has been shown that Bmal1 directly regulates *Il6* transactivation in microglia; conditional Bmal1 deficiency in microglial cells attenuates the ischemic neuronal damage in mice (19). In macrophages, Bmal1 regulates inflammation *via* controlling the gene expression of *Nrf2*, which plays a critical role in the innate immune system (13). Bmal1 deficiency in bone marrow-derived macrophages leads to increased IL-1β expression and increases polymicrobial infection in mice (13, 57). However, myeloid cell Bmal1 deletion protects against bacterial infection in the lung (58). We noticed that in peritoneal macrophages, *Bmal1* is highly expressed during the dark phase, which is different from the daily rhythm in microglia (57). In rat monocytes, *Bmal1* does not show a clear daily rhythm in gene expression, while *Tnfa* shows a high expression during the dark phase (49). These data suggest that Bmal1 regulates the innate immune system, but that the rhythmicity of clock genes and inflammatory cytokines is heterogeneous among innate immune cells and depends on the specific tissue.

Furthermore, we observed that *Bmal1* deletion affected the expression level of other clock genes, especially *Cry1*, *Cry2*, and *Per2* were significantly increased in *Bmal1* KO microglia. It has been shown that overexpression of Cry1 significantly decreases inflammation in atherosclerotic mice (59), whereas the absence of Cry1 and Cry2 leads to increased pro-inflammatory cytokine expression in macrophages (60). *Per2* negatively regulates the expression of pro-inflammatory

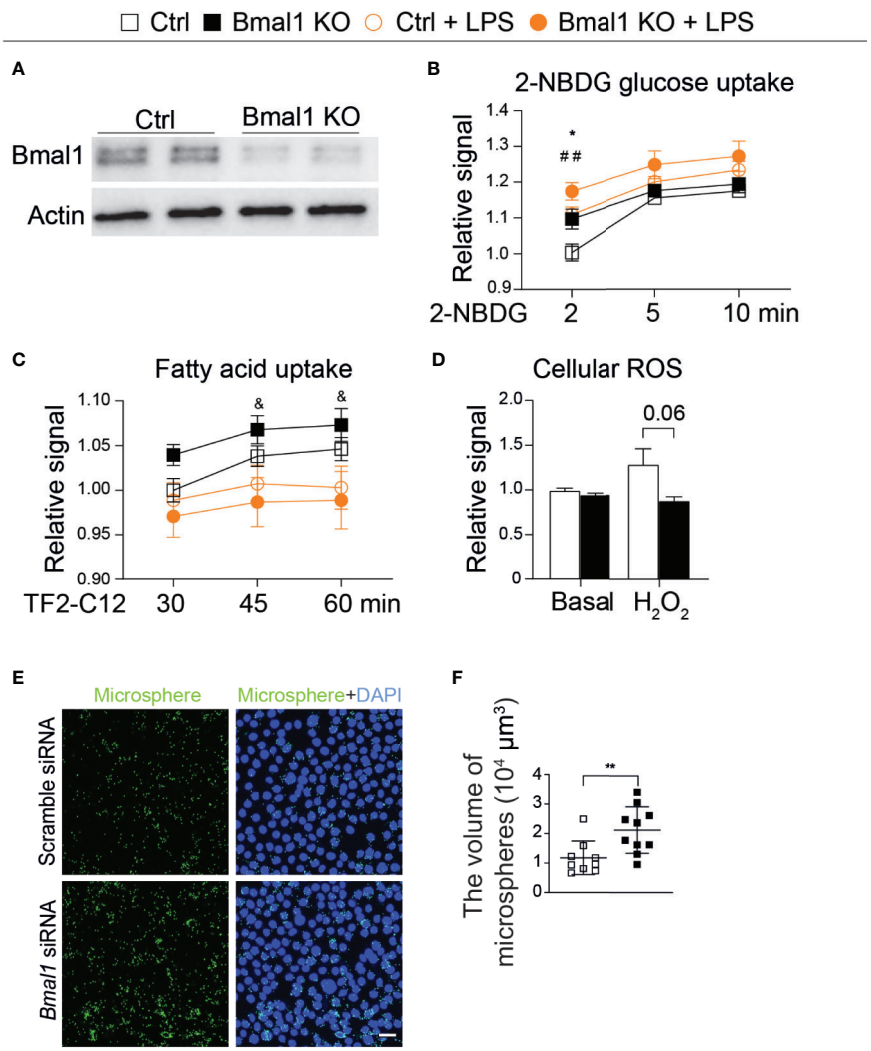

FIGURE 6 | Knockout of Bmal1 affects energy utilization of microglial cells. **(A)** Bmal1 KO efficiency in microglia (n = 4 samples per group). **(B, C)** 2-NBDG glucose uptake (B, n = 9–10 samples per group), and free fatty acid uptake (**C**, n = 5 samples per group) of Ctrl and Bmal1 KO microglia under basal and LPS conditions. *Bmal1 KO *vs.* Ctrl; ## Ctrl + LPS *vs* Ctrl; & Bmal1 KO + LPS *vs.* Bmal1 KO. **(D)** Cellular ROS level in Ctrl and Bmal1 KO microglia under basal and H_2O_2 stimulation (n = 5 samples per group). **(E)** Image of microspheres in BV-2 cells in scrambled siRNA and Bmal1 siRNA groups after 1 h incubation (n = 9-10 samples per group). Scale bar, 30 μm. **(F)** The uptake of microspheres. Statistical significance was determined using two-way ANOVA and unpaired *t*-test. Data are presented as means ± s.e.m. $^{*}P < 0.05$, $^{\&}P < 0.05$, and $^{\#\#}P < 0.01$.

cytokines in zebrafish (61). *Bmal1* deficiency-induced the increased gene expression of *Cry1*, *Cry2*, and *Per2* may also contribute to the reduced inflammation of *Bmal1* KO microglial cells.

Circadian clocks are fundamental physiological regulators in energy homeostasis and the immune system. Diurnal oscillations in glucose and lipid metabolism are due in part to daily changes in energy requirements (62). As the resident brain macrophages, microglia provide continually surveillant and scavenging functions in the brain (40). Here, we found that microglial glucose and lipid utilization transcripts show clear daily rhythmicity, and both are significantly higher during the regular activity period in mice (i.e. the dark period). *Bmal1* deficiency decreased the expression of nutrient utilization related genes in microglia under basal condition and shifted the metabolic processes under LPS stimulation. Reduced substrates utilization was observed in Bmal1 KO skeletal muscle (30, 63). A recent study showed that Bmal1 deletion also protects mice from insulin resistance induced by circadian disruption (64).

Prior work has demonstrated that ROS production and scavenging related genes exhibit a time-of-day specific expression under diurnal and circadian conditions (65). We found that *Bmal1* deficiency protected microglia from

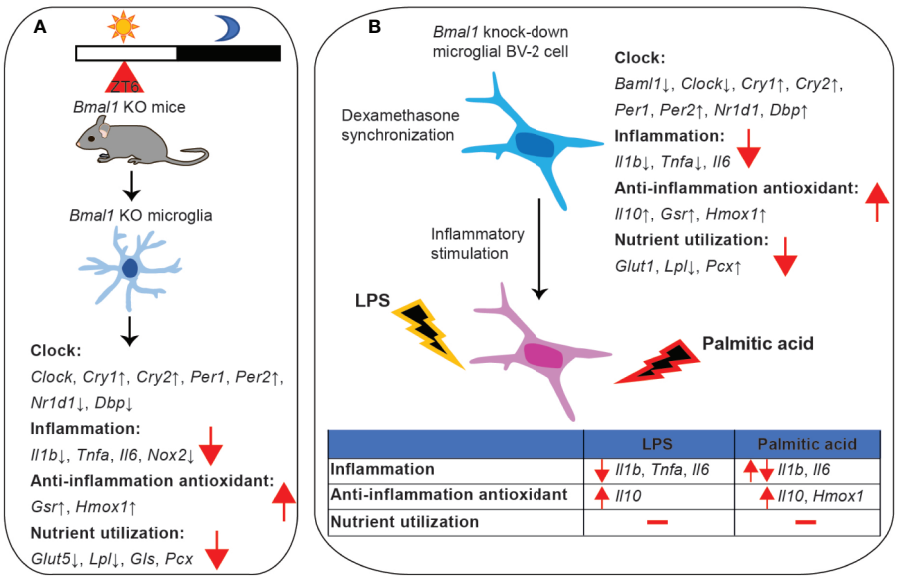

FIGURE 7 | Gene expression summary. **(A)** Summary of *Bmal1* KO effects in microglia isolated from mice. **(B)** Summary of *Bmal1* knock-down effects in microgial BV-2 cells.

oxidative damage and inflammation. On the other hand, neuronal Bmal1 deletion causes oxidative damage and impaired expression of the redox defense gene (33), which suggests that the effect of Bmal1 on oxidative stress is different depending on the cell type involved. Moreover, microglia can polarize into a pro-inflammatory or an anti-inflammatory phenotype (66, 67). *Bmal1* KO microglia may polarize into the anti-inflammatory state by increasing IL-10 gene expression to facilitate phagocytosis of cell debris and antagonizing the pro-inflammatory response.

Recently, it has been shown that the intrinsic circadian clocks, such as REV-ERBα, REV-ERBβ, and Bmal1, affect microglial amyloid-β clearance in the 5XFAD mouse model of Alzheimer's disease (68). Based on our findings, future work should measure inflammatory cytokine levels in combination with mitochondrial fuel utilization in microglia lacking Bmal1. Furthermore, the immune response in microglia-specific Bmal1 knockout mice still needs to be explored. Microglia are closely related to neuroinflammation, neurodegeneration, and obesity. Thus, future work should evaluate Bmal1 knockout microglial function and neuronal changes in mice under different stressful conditions, such as LPS and high-fat diet, or in combination with neurodegenerative diseases.

In conclusion, Bmal1 is a critical regulator in microglial function. Bmal1 deficiency alters microglial inflammatory profile, including inhibiting the gene expression of pro-inflammatory cytokines and elevating the expression of antioxidative anti-inflammatory factors, as well as affects microglial nutrient utilization and phagocytosis. Our work indicates that targeting the molecular biological clock-*Bmal1* in microglia might be a new approach to treat inflammation-related diseases in the brain.

DATA AVAILABILITY STATEMENT

The original contributions presented in the study are included in the article/**Supplementary Material**, further inquiries can be directed to the corresponding author/s.

ETHICS STATEMENT

The animal study was reviewed and approved by Netherlands Institute for Neuroscience, Royal Dutch Academy of Arts and Sciences, Amsterdam, the Netherlands; Department of Medicine, Division of Endocrinology, and Einthoven Laboratory for Experimental Vascular Medicine, Leiden University Medical Center, Leiden, the Netherlands; French national and regional ethics committee in Strasbourg.

AUTHOR CONTRIBUTIONS

X-LW, SW, NK, IM, and SK performed the experiments. X-LW analyzed the data and wrote the manuscript. X-LW, C-XY, and A-LB designed the study. AK and A-LB edited the manuscript. All authors contributed to the article and approved the submitted version

FUNDING

This work was supported by the "NeuroTime" Erasmus Mundus program, University of Strasbourg, CNRS and ANR-18-CE16-0008 (to A-LB).

ACKNOWLEDGMENTS

We would like to thank Marie-Paule Felder-Schmittbuhl (Institute of Cellular and Integrative Neurosciences, CNRS, Université de Strasbourg, Strasbourg, France) and people from Luc Dupuis laboratory (Université de Strasbourg, INSERM, UMR-S1118, Strasbourg, France) for helping with primary microglia cultures. This project has been funded with support from the NeuroTime Erasmus+ program of the European Commission, University of Strasbourg, CNRS. X-LW salary was supported by NeuroTime Erasmus+ program of the European Commission, as well as partly by ANR-18-CE16-0008 (to A-LB).

SUPPLEMENTARY MATERIAL

The Supplementary Material for this article can be found online at: https://www.frontiersin.org/articles/10.3389/fimmu.2020.586399/full#supplementary-material

REFERENCES

1. Hickman S, Izzy S, Sen P, Morsett L, El Khoury J. Microglia in neurodegeneration. *Nat Neurosci* (2018) 21:1359. doi: 10.1038/s41593-018-0242-x
2. Widmann CN, Heneka MT. Long-term cerebral consequences of sepsis. *Lancet Neurol* (2014) 13:630. doi: 10.1016/S1474-4422(14)70017-1
3. Semmler A, Widmann CN, Okulla T, Urbach H, Kaiser M, Widman G, et al. Persistent cognitive impairment, hippocampal atrophy and EEG changes in sepsis survivors. *J Neurol Neurosur Ps* (2013) 84:62. doi: 10.1136/jnnp-2012-302883
4. Semmler A, Frisch C, Debeir T, Ramanathan M, Okulla T, Klockgether T, et al. Long-term cognitive impairment, neuronal loss and reduced cortical cholinergic innervation after recovery from sepsis in a rodent model. *Exp Neurol* (2007) 204:733. doi: 10.1016/j.expneurol.2007.01.003
5. Thaler JP, Yi CX, Schur EA, Guyenet SJ, Hwang BH, Dietrich MO, et al. Obesity is associated with hypothalamic injury in rodents and humans (vol 1222012). *J Clin Invest* (2012) 122:pg 153778. doi: 10.1172/JCI62813
6. Valdearcos M, Douglass JD, Robblee MM, Dorfman MD, Stifler DR, Bennett ML, et al. Microglial Inflammatory Signaling Orchestrates the Hypothalamic Immune Response to Dietary Excess and Mediates Obesity Susceptibility. *Cell Metab* (2017) 26:185. doi: 10.1016/j.cmet.2017.05.015
7. Yi CX, Walter M, Gao YQ, Pitra S, Legutko B, Kalin S, et al. TNF alpha drives mitochondrial stress in POMC neurons in obesity. *Nat Commun* (2017) 8:15143. doi: 10.1038/Ncomms15143
8. Gerstner JR, Yin JC. Circadian rhythms and memory formation. *Nat Rev Neurosci* (2010) 11:577. doi: 10.1038/nrn2881
9. Curtis AM, Bellet MM, Sassone-Corsi P, O'Neill LA. Circadian clock proteins and immunity. *Immunity* (2014) 40:178. doi: 10.1016/j.immuni.2014.02.002
10. Man K, Loudon A, Chawla A. Immunity around the clock. *Science* (2016) 354:999. doi: 10.1126/science.aah4966
11. Barca-Mayo O, Pons-Espinal M, Follert P, Armirotti A, Berdondini L, De Pietri Tonelli D. Astrocyte deletion of Bmal1 alters daily locomotor activity and cognitive functions *via* GABA signalling. *Nat Commun* (2017) 8:14336. doi: 10.1038/ncomms14336
12. Barca-Mayo O, Boender AJ, Armirotti A, De Pietri Tonelli D. Deletion of astrocytic BMAL1 results in metabolic imbalance and shorter lifespan in mice. *Glia* (2019). doi: 10.1002/glia.23764
13. Early JO, Menon D, Wyse CA, Cervantes-Silva MP, Zaslona Z, Carroll RG, et al. Circadian clock protein BMAL1 regulates IL-1beta in macrophages *via* NRF2. *Proc Natl Acad Sci USA* (2018) 115:E8460. doi: 10.1073/pnas.1800431115 1800431115
14. Stenvers DJ, Scheer FAJL, Schrauwen P, la Fleur SE, Kalsbeek A. Circadian clocks and insulin resistance. *Nat Rev Endocrinol* (2019) 15:75. doi: 10.1038/s41574-018-0122-1
15. Bass J, Takahashi JS. Circadian integration of metabolism and energetics. *Science* (2010) 330:1349. doi: 10.1126/science.1195027
16. Rahman SA, Castanon-Cervantes O, Scheer FA, Shea SA, Czeisler CA, Davidson AJ, et al. Endogenous circadian regulation of pro-inflammatory cytokines and chemokines in the presence of bacterial lipopolysaccharide in humans. *Brain Behav Immun* (2015) 47:4. doi: 10.1016/j.bbi.2014.11.003
17. Gabriel BM, Zierath JR. Circadian rhythms and exercise - re-setting the clock in metabolic disease. *Nat Rev Endocrinol* (2019) 15:197. doi: 10.1038/s41574-018-0150-x
18. Griffin P, Dimitry JM, Sheehan PW, Lananna BV, Guo C, Robinette ML, et al. Circadian clock protein Rev-erba regulates neuroinflammation. *P Natl Acad Sci USA* (2019) 116:5102. doi: 10.1073/pnas.1812405116
19. Nakazato R, Hotta S, Yamada D, Kou M, Nakamura S, Takahata Y, et al. The intrinsic microglial clock system regulates interleukin-6 expression. *Glia* (2017) 65:198. doi: 10.1002/glia.23087
20. Sato S, Sakurai T, Ogasawara J, Takahashi M, Izawa T, Imaizumi K, et al. A circadian clock gene, Rev-erbalpha, modulates the inflammatory function of macrophages through the negative regulation of Ccl2 expression. *J Immunol* (2014) 192:407. doi: 10.4049/jimmunol.1301982
21. Vijayan V, Pradhan P, Braud L, Fuchs HR, Gueler F, Motterlini R, et al. Human and murine macrophages exhibit differential metabolic responses to lipopolysaccharide - A divergent role for glycolysis. *Redox Biol* (2019) 22:101147. doi: 10.1016/j.redox.2019.101147
22. Wang L, Pavlou S, Du X, Bhuckory M, Xu H, Chen M. Glucose transporter 1 critically controls microglial activation through facilitating glycolysis. *Mol Neurodegener* (2019) 14:2. doi: 10.1186/s13024-019-0305-9
23. Geltink RII, Kyle RL, Pearce EL. Unraveling the Complex Interplay Between T Cell Metabolism and Function. *Annu Rev Immunol* (2018) 36:461. doi: 10.1146/annurev-immunol-042617-053019
24. Gao YQ, Vidal-Itriago A, Kalsbeek MJ, Layritz C, Garcia-Caceres C, Tom RZ, et al. Lipoprotein Lipase Maintains Microglial Innate Immunity in Obesity. *Cell Rep* (2017) 20:3034. doi: 10.1016/j.celrep.2017.09.008
25. Dudek M, Meng QJ. Running on time: the role of circadian clocks in the musculoskeletal system. *Biochem J* (2014) 463:1. doi: 10.1042/BJ20140700
26. Gekakis N, Staknis D, Nguyen HB, Davis FC, Wilsbacher LD, King DP, et al. Role of the CLOCK protein in the mammalian circadian mechanism. *Science* (1998) 280:1564. doi: 10.1126/science.280.5369.1564
27. Ripperger JA, Schibler U. Rhythmic CLOCK-BMAL1 binding to multiple E-box motifs drives circadian Dbp transcription and chromatin transitions. *Nat Genet* (2006) 38:369. doi: 10.1038/ng1738
28. Hayashi Y, Koyanagi S, Kusunose N, Okada R, Wu Z, Tozaki-Saitoh H, et al. The intrinsic microglial molecular clock controls synaptic strength *via the* circadian expression of cathepsin S. *Sci Rep* (2013) 3:2744. doi: 10.1038/srep02744srep02744
29. Hatanaka F, Matsubara C, Myung J, Yoritaka T, Kamimura N, Tsutsumi S, et al. Genome-wide profiling of the core clock protein BMAL1 targets reveals a strict relationship with metabolism. *Mol Cell Biol* (2010) 30:5636. doi: 10.1128/MCB.00781-10
30. Schiaffino S, Blaauw B, Dyar KA. The functional significance of the skeletal muscle clock: lessons from Bmal1 knockout models. *Skelet Muscle* (2016) 6:33. doi: 10.1186/s13395-016-0107-5107
31. Rudic RD, McNamara P, Curtis AM, Boston RC, Panda S, Hogenesch JB, et al. BMAL1 and CLOCK, two essential components of the circadian clock, are involved in glucose homeostasis. *PloS Biol* (2004) 2:e377. doi: 10.1371/journal.pbio.0020377

32. Sussman W, Stevenson M, Mowdawalla C, Mota S, Ragolia L, Pan XY. BMAL1 controls glucose uptake through paired-homeodomain transcription factor 4 in differentiated Caco-2 cells. *Am J Physiol Cell Ph* (2019) 317:C492. doi: 10.1152/ajpcell.00058.2019
33. Musiek ES, Lim MM, Yang G, Bauer AQ, Qi L, Lee Y, et al. Circadian clock proteins regulate neuronal redox homeostasis and neurodegeneration. *J Clin Invest* (2013) 123:5389. doi: 10.1172/JCI7031770317
34. Bunger MK, Wilsbacher LD, Moran SM, Clendenin C, Radcliffe LA, Hogenesch JB, et al. Mop3 is an essential component of the master circadian pacemaker in mammals. *Cell* (2000) 103:1009. doi: 10.1016/S0092-8674(00)00205-1
35. Blasi E, Barluzzi R, Bocchini V, Mazzolla R, Bistoni F. Immortalization of murine microglial cells by a v-raf/v-myc carrying retrovirus. *J Neuroimmunol* (1990) 27:229. doi: 10.1016/0165-5728(90)90073-v
36. Zelcer N, Khanlou N, Clare R, Jiang Q, Reed-Geaghan EG, Landreth GE, et al. Attenuation of neuroinflammation and Alzheimer's disease pathology by liver x receptors. *Proc Natl Acad Sci U S A* (2007) 104:10601. doi: 10.1073/pnas.0701096104
37. Hogenboom R, Kalsbeek MJ, Korpel NL, de Goede P, Koenen M, Buijs RM, et al. Loss of arginine vasopressin- and vasoactive intestinal polypeptide-containing neurons and glial cells in the suprachiasmatic nucleus of individuals with type 2 diabetes. *Diabetologia* (2019). doi: 10.1007/s00125-019-4953-7
38. Fonken LK, Frank MG, Kitt MM, Barrientos RM, Watkins LR, Maier SF. Microglia inflammatory responses are controlled by an intrinsic circadian clock. *Brain Behav Immun* (2015) 45:171. doi: 10.1016/j.bbi.2014.11.009
39. Bellet MM, Deriu E, Liu JZ, Grimaldi B, Blaschitz C, Zeller M, et al. Circadian clock regulates the host response to Salmonella. *Proc Natl Acad Sci U S A* (2013) 110:9897. doi: 10.1073/pnas.1120636101120636110
40. Nimmerjahn A, Kirchhoff F, Helmchen F. Resting microglial cells are highly dynamic surveillants of brain parenchyma *in vivo*. *Science* (2005) 308:1314. doi: 10.1126/science.1110647
41. Ding XY, Zhang M, Gu RP, Xu GZ, Wu HX. Activated microglia induce the production of reactive oxygen species and promote apoptosis of co-cultured retinal microvascular pericytes. *Graef Arch Clin Exp* (2017) 255:777. doi: 10.1007/s00417-016-3578-5
42. Rojo AII, McBean G, Cindric M, Egea J, Lopez MG, Rada P, et al. Redox control of microglial function: molecular mechanisms and functional significance. *Antioxid Redox Signal* (2014) 21:1766. doi: 10.1089/ars.2013.5745
43. Poss KD, Tonegawa S. Reduced stress defense in heme oxygenase 1-deficient cells. *Proc Natl Acad Sci U S A* (1997) 94:10925. doi: 10.1073/pnas.94.20.10925
44. Piantadosi CA, Withers CM, Bartz RR, MacGarvey NC, Fu P, Sweeney TE, et al. Heme oxygenase-1 couples activation of mitochondrial biogenesis to anti-inflammatory cytokine expression. *J Biol Chem* (2011) 286:16374. doi: 10.1074/jbc.M110.207738
45. McLoughlin MR, Orlicky DJ, Prigge JR, Krishna P, Talago EA, Cavigli IR, et al. TrxR1, Gsr, and oxidative stress determine hepatocellular carcinoma malignancy. *Proc Natl Acad Sci U S A* (2019) 116:11408. doi: 10.1073/pnas.1903244116
46. Joseph LC, Kokkinaki D, Valenti MC, Kim GJ, Barca E, Tomar D, et al. Inhibition of NADPH oxidase 2 (NOX2) prevents sepsis-induced cardiomyopathy by improving calcium handling and mitochondrial function. *JCI Insight* (2017) 2:e94248. doi: 10.1172/jci.insight.94248
47. Yanguas-Casas N, Crespo-Castrillo A, de Ceballos ML, Chowen JA, Azcoitia I, Arevalo MA, et al. Sex differences in the phagocytic and migratory activity of microglia and their impairment by palmitic acid. *Glia* (2018) 66:522. doi: 10.1002/glia.23263
48. Hidalgo-Lanussa O, Avila-Rodriguez M, Baez-Jurado E, Zamudio J, Echeverria V, Garcia-Segura LM, et al. Tibolone Reduces Oxidative Damage and Inflammation in Microglia Stimulated with Palmitic Acid through Mechanisms Involving Estrogen Receptor Beta. *Mol Neurobiol* (2018) 55:5462. doi: 10.1007/s12035-017-0777-y
49. Milanova IV, Kalsbeek MJT, Wang XL, Korpel NL, Stenvers DJ, Wolff SEC, et al. Diet-Induced Obesity Disturbs Microglial Immunometabolism in a Time-of-Day Manner. *Front Endocrinol (Lausanne)* (2019) 10:424. doi: 10.3389/fendo.2019.00424
50. Ly LD, Xu S, Choi SK, Ha CM, Thoudam T, Cha SK, et al. Oxidative stress and calcium dysregulation by palmitate in type 2 diabetes. *Exp Mol Med* (2017) 49:e291. doi: 10.1038/emm.2016.157
51. Cedernaes J, Waldeck N, Bass J. Neurogenetic basis for circadian regulation of metabolism by the hypothalamus. *Genes Dev* (2019) 33:1136. doi: 10.1101/gad.328633.119
52. Scheiermann C, Kunisaki Y, Frenette PS. Circadian control of the immune system. *Nat Rev Immunol* (2013) 13:190. doi: 10.1038/nri3386
53. Reppert SM, Weaver DR. Coordination of circadian timing in mammals. *Nature* (2002) 418:935. doi: 10.1038/nature00965
54. Duffield GE. DNA microarray analyses of circadian timing: the genomic basis of biological time. *J Neuroendocrinol* (2003) 15:991. doi: 10.1046/j.1365-2826.2003.01082.x
55. Zhang R, Lahens NF, Ballance HII, Hughes ME, Hogenesch JB. A circadian gene expression atlas in mammals: implications for biology and medicine. *Proc Natl Acad Sci U S A* (2014) 111:16219. doi: 10.1073/pnas.1408886111408886111
56. Sato TK, Panda S, Miraglia LJ, Reyes TM, Rudic RD, McNamara P, et al. A functional genomics strategy reveals rora as a component of the mammalian circadian clock. *Neuron* (2004) 43:527. doi: 10.1016/j.neuron.2004.07.018
57. Deng W, Zhu S, Zeng L, Liu J, Kang R, Yang M, et al. The Circadian Clock Controls Immune Checkpoint Pathway in Sepsis. *Cell Rep* (2018) 24:366. doi: 10.1016/j.celrep.2018.06.026
58. Kitchen GB, Cunningham PS, Poolman TM, Iqbal M, Maidstone R, Baxter M, et al. The clock gene Bmal1 inhibits macrophage motility, phagocytosis, and impairs defense against pneumonia. *Proc Natl Acad Sci USA* (2020). doi: 10.1073/pnas.1915932117
59. Yang L, Chu Y, Wang L, Wang Y, Zhao X, He W, et al. Overexpression of CRY1 protects against the development of atherosclerosis *via the* TLR/NF-kappaB pathway. *Int Immunopharmacol* (2015) 28:525. doi: 10.1016/j.intimp.2015.07.001
60. Narasimamurthy R, Hatori M, Nayak SK, Liu F, Panda S, Verma IM. Circadian clock protein cryptochrome regulates the expression of proinflammatory cytokines. *Proc Natl Acad Sci U S A* (2012) 109:12662. doi: 10.1073/pnas.1209651091209965109
61. Ren DL, Zhang JL, Yang LQ, Wang XB, Wang ZY, Huang DF, et al. Circadian genes period1b and period2 differentially regulate inflammatory responses in zebrafish. *Fish Shellfish Immun* (2018) 77:139. doi: 10.1016/j.fsi.2018.03.048
62. Kumar Jha P, Challet E, Kalsbeek A. Circadian rhythms in glucose and lipid metabolism in nocturnal and diurnal mammals. *Mol Cell Endocrinol* (2015) 418:74. doi: 10.1016/j.mce.2015.01.024S0303-7207(15)00035-0
63. Dyar KA, Hubert MJ, Mir AA, Ciciliot S, Lutter D, Greulich F, et al. Transcriptional programming of lipid and amino acid metabolism by the skeletal muscle circadian clock. *PloS Biol* (2018) 16:e2005886. doi: 10.1371/journal.pbio.2005886
64. Yang G, Chen L, Zhang J, Ren B, FitzGerald GA. Bmal1 deletion in mice facilitates adaptation to disrupted light/dark conditions. *JCI Insight* (2019) 5:e125133. doi: 10.1172/jci.insight.125133
65. Lai AG, Doherty CJ, Mueller-Roeber B, Kay SA, Schippers JH, Dijkwel PP. CIRCADIAN CLOCK-ASSOCIATED 1 regulates ROS homeostasis and oxidative stress responses. *Proc Natl Acad Sci U S A* (2012) 109:17129. doi: 10.1073/pnas.1209148109
66. Orihuela R, McPherson CA, Harry GJ. Microglial M1/M2 polarization and metabolic states. *Br J Pharmacol* (2016) 173:649. doi: 10.1111/bph.13139
67. Olah M, Biber K, Vinet J, Boddeke HW. Microglia phenotype diversity. *CNS Neurol Disord Drug Targets* (2011) 10:108. doi: 10.2174/187152711794488575
68. Lee J, Kim DE, Griffin P, Sheehan PW, Kim DH, Musiek ES, et al. Inhibition of REV-ERBs stimulates microglial amyloid-beta clearance and reduces amyloid plaque deposition in the 5XFAD mouse model of Alzheimer's disease. *Aging Cell* (2020) 19:e13078. doi: 10.1111/acel.13078

Conflict of Interest: The authors declare that the research was conducted in the absence of any commercial or financial relationships that could be construed as a potential conflict of interest.

frontiers in Immunology

ORIGINAL RESEARCH
published: 19 January 2021
doi: 10.3389/fimmu.2020.595316

Activator-Mediated Pyruvate Kinase M2 Activation Contributes to Endotoxin Tolerance by Promoting Mitochondrial Biogenesis

Zhujun Yi[†], *Yilin Wu*[†], *Wenfeng Zhang*, *Tao Wang*, *Jianping Gong*, *Yao Cheng*[*] *and Chunmu Miao*[*]

Department of Hepatobiliary Surgery, The Second Affiliated Hospital of Chongqing Medical University, Chongqing, China

OPEN ACCESS

Edited by:
Edecio Cunha-Neto,
University of São Paulo, Brazil

Reviewed by:
Dong Li,
Jilin University, China
Itamar Goren,
University Hospital Frankfurt, Germany

***Correspondence:**
Yao Cheng
chengyao1986@hospital.cqmu.edu.cn
Chunmu Miao
luckmcm@163.com

[†]*These authors share first authorship*

Specialty section:
This article was submitted to Inflammation, a section of the journal Frontiers in Immunology

Received: *16 August 2020*
Accepted: *03 December 2020*
Published: *19 January 2021*

Citation:
Yi Z, Wu Y, Zhang W, Wang T, Gong J, Cheng Y and Miao C (2021) Activator-Mediated Pyruvate Kinase M2 Activation Contributes to Endotoxin Tolerance by Promoting Mitochondrial Biogenesis. Front. Immunol. 11:595316. doi: 10.3389/fimmu.2020.595316

Pyruvate kinase M2 (PKM2) is a key glycolysis enzyme, and its effect on macrophages has not been entirely elucidated. Here, we identified that the PKM2 small-molecule agonist TEPP-46 mediated PKM2 activation by inducing the formation of PKM2 tetramer and promoted macrophage endotoxin tolerance. Lipopolysaccharide (LPS)-tolerant mice had higher expression of the PKM2 tetramer, which was associated with a reduced *in vivo* immune response to LPS. Pretreatment of macrophages with TEPP-46 resulted in tolerance to LPS stimulation, as demonstrated by a significant reduction in the production of TNF-α and IL-6. We found that TEPP-46 induced mitochondrial biogenesis in macrophages. Inhibition of mitochondrial biogenesis by mtTFA knockdown effectively inhibited TEPP-46-mediated macrophage tolerance to endotoxins. We discovered that TEPP-46 promoted the expression of PGC-1α and that PGC-1α was the key regulator of mitochondrial biogenesis in macrophages induced by TEPP-46. PGC-1α was negatively regulated by the PI3K/Akt signaling pathway. Knockdown of PKM2 or PGC-1α uniformly inhibited TEPP-46-mediated endotoxin tolerance by inhibiting mitochondrial biogenesis. In addition, TEPP-46 protected mice from lethal endotoxemia and sepsis. Collectively, these findings reveal novel mechanisms for the metabolic control of inflammation and for the induction of endotoxin tolerance by promoting mitochondrial biogenesis. Targeting PKM2 appears to be a new therapeutic option for the treatment of sepsis and other inflammatory diseases.

Keywords: sepsis, mitochondrial biogenesis, endotoxin tolerance, pyruvate kinase M2, TEPP-46

INTRODUCTION

The systemic inflammatory response and multiple organ failure caused by severe sepsis and septic shock are important causes of high mortality in clinical patients (1, 2). The molecular mechanism is mainly related to the combination of endotoxin and Toll-like receptors (TLRs), which activates the inflammatory pathways of immune cells and then induces the release of a large number of pro-inflammatory factors, such as tumor necrosis factor-α (TNF-α), interleukin 6 (IL-6), and IL-1β (2–4).

The release of these proinflammatory cytokines not only induces inflammation but also modulates the immune response (5).

Macrophage endotoxin tolerance or lipopolysaccharide (LPS) tolerance is defined as a hyporesponsive state in response to a secondary lethal dose of LPS following primary low-dose LPS exposure (6, 7). Endotoxin tolerance provides a protective mechanism to reduce the proinflammatory cytokine levels in response to severe infection (8, 9). However, endotoxin tolerance is also a double-edged sword in regulating the immune response (10). For immunocompromised individuals, a prolonged endotoxin-tolerant state allows for the development of secondary infections, increasing mortality from sepsis (11–13). Therefore, understanding the mechanisms controlling endotoxin tolerance is important to design a good time frame for interventions to regulate the immune responses.

Growing evidence suggests that the development of sepsis is closely related to energy metabolism dysfunction in immune cells (14). Activated immune cells, such as macrophages and dendritic cells, also have the ability to switch their energy metabolism from oxidative phosphorylation to glycolysis, which is similar to the "Warburg effect" in tumor cells (15, 16). This switch in energy metabolism is directly involved in the regulation of the inflammatory response (17). Mitochondria are the main organelles of energy metabolism, and mitochondrial dysfunction is also closely related to the development of sepsis (18, 19). Normal mitochondrial function is the basic premise for immune cells to resist the inflammatory response (18). Mitophagy (selective degradation of dysfunctional mitochondria) and mitochondrial biogenesis (generation of new mitochondria) maintain the balance of mitochondrial mass, which plays an important role in maintaining the normal mitochondrial function (19–21). Mitochondrial biogenesis can be induced by cold exposure, oxidative stress, inflammatory cell stress, etc. Under these stimuli, expression of peroxisome proliferator-activated receptor gamma-1 coactivator family (PGC-1α), nuclear respiratory factor 1 (NRF1), NRF2 and mitochondrial transcription factor A (mtTFA/MTFA), which are closely related to mitochondrial biogenesis, was promoted (22, 23). In particular, PGC-1α has been confirmed as an important coordinator that regulates a wide variety of anti-inflammatory and metabolic nuclear genes (22, 24). The AMP-activated protein kinase (AMPK)/sirtuin 1 (SIRT1) pathway regulates mitochondrial biogenesis by inducing PGC-1α (25). However, in some inflammatory diseases, inhibiting the activation of the AMPK/SIRT1 pathway does not inhibit mitochondrial biogenesis, suggesting that there are other ways to regulate mitochondrial biogenesis (25, 26). Overall, inflammation can be modulated by regulating mitochondrial function, but the specific molecular mechanism remains to be further studied.

Pyruvate kinase M2 (PKM2) is a key glycolysis enzyme (27). The enzymatic activity of PKM2 is determined by the configuration of the enzyme into a tetramer, dimer, or monomer (27, 28). The PKM2 tetramer is located in the cytoplasm and is the active form of the enzyme; the PKM2 dimer and monomer are located in the nucleus and play an important role in regulating gene transcription (27, 28). Growing evidence suggests that the transition from a PKM2 tetramer to a PKM2 monomer/dimer (nuclear translocation) plays an important role in promoting the inflammatory response and tumor invasion and proliferation (29–31). LPS induces the formation of the PKM2 monomer/dimer, promotes the transcription of high mobility group box 1 (HMGB1) and NF-κB through interaction with hypoxia-inducible factor 1α (HIF-1α), and further promotes the release of the inflammatory factor IL-1β, which plays an important role in the development of sepsis (32). The small-molecule agonist DASA-58 or TEPP-46 can effectively inhibit the LPS-mediated macrophage inflammatory response by inhibiting the formation of the PKM2 monomer/dimer (33). In addition, TEPP-46 can improve glucose metabolism in podocytes, thus delaying the development of diabetic nephropathy (34). However, it is still unclear what role the PKM2 tetramer plays in inflammatory regulation and what its mechanism is. Overall, these studies have revealed a role for PKM2 in proinflammatory cytokine production and suggest that it is important to regulate PKM2 expression to modulate the inflammatory potential of macrophages.

We report here that the formation of the PKM2 tetramer, triggered by TEPP-46, is a novel mechanism for negatively regulating the inflammatory response and contributes to endotoxin tolerance. TEPP-46-induced activation of PKM2 promotes PGC-1α-mediated mitochondrial biogenesis by inhibiting the PI3K/Akt signaling pathway and promotes endotoxin tolerance by inhibiting the release of the proinflammatory factors TNF-α and IL-6 *in vitro* and *in vivo*. These results not only uncover a novel regulatory mechanism of the inflammatory response by PKM2 but also provide a new therapeutic target to prevent sepsis-mediated immunosuppression.

METHODS AND MATERIALS

Cell Isolation and Culture and Reagents

The isolation methods of peritoneal macrophages (PMs) and Kupffer cells (KCs) from C57BL/6 mice were carried out as previously Hu YC and Li PZ et al. described (35, 36). The RAW264.7 macrophage cell line was purchased from American Type Culture Collection (ATCC). These cell populations were cultured in DMEM (Gibco Life Technologies) with 10% FBS (PAN-Biotechnology) and 1% penicillin–streptomycin (Beyotime Biotechnology) at 37°C, 95% humidity, and 5% CO_2.

We used antibodies against PKM2 (Cell Signaling, #4053, 1:1,000), PKM1 (Cell Signaling, #7067, 1:1,000), PGC-1α (Cell Signaling, #2178, 1:1,000), PGC-1β (Abcam, ab176328, 1:1,000), p62 (Cell Signaling, #16177, 1:1,000), LC3 (Abcam, ab192890, 1:1,000), mtTFA (Abcam, ab252432, 1:1,000), NRF1 (Abcam, ab221792, 1:1,000), NRF2 (Abcam, ab137550, 1:1,000), p-AMPK (Cell Signaling, #4186, 1:500), AMPK (Cell Signaling, #4150, 1:1,000), SIRT1 (Abcam, ab189494, 1:1,000), p-Akt (Abcam, ab38449, 1:500), Akt (Abcam, ab8805, 1:500), p-PI3K (Cell Signaling, #17366, 1:1,000), PI3K (Cell Signaling, #4255, 1:1,000), and GAPDH (Santa Cruz, sc365062, 1:1,000). LPS

(L9641) was purchased from Sigma. The PKM2 activator TEPP-46, Akt activator SC79 and PI3K activator 740 Y-P were from MedChemExpress. Fluorescently labeled secondary antibodies were obtained from ZSGB-BIO. TNF-α and IL-6 enzyme-linked immunosorbent assay (ELISA) kits were from Boster Biological Technology.

siRNA and Lentivirus Transduction

Small interfering RNA (siRNA)-*PKM2* and control siRNA were prepared by GenePharma (Shanghai), and all short hairpin RNAs (shRNAs) (shRNA-*PGC-1α*, shRNA-*mtTFA* and control shRNAs) were prepared by GeneChem (Shanghai). siRNA and lentiviral transduction were performed according to the manufacturer's instructions. For siRNA transduction, 2×10^5 RAW264.7 cells (MOI=20) in 2 ml medium with 200 pmol siRNA and 5 μl Lipo8000 (Beyotime Biotechnology). Change the culture medium after 6 h. For lentivirus transduction, 1×10^5 RAW264.7 cells (MOI=20) in 1 ml medium with 10 μg/ml of polybrene (GeneChem) were incubated with 2 μl lentivirus. After 72 h of culture, western blot were used to analyze the transduction efficiency. The siRNA-*PKM2* sequences refer to Goldberg's work (siRNA 27 in Goldberg's work) (37). The sequences of siRNAs were as follows: mouse PKM2-siRNA (5'-AGGCAGAGGCUGCCAUCUA-3') and control siRNA (5'-UUCUCCGAACGUGUCACGU-3'). The target sequences of shRNAs were as follows: mouse PGC-1α-shRNA (5'-CCGGCCAGAACAAGAACAACGGTTTCTCGAGAAACCGTTGTTCTTGTTCTGGTTTTTG-3'), mouse mtTFA–shRNA (5'-CCGGCGGAGACATCTCTGAGCATTACTCGAGTAATGCTCAGAGATGTCTCCGTTTTTG-3') and control shRNA (5'-TTCTCCGAACGTGTCACGT-3').

Endotoxin Tolerance and Acute Endotoxemia and Sepsis Mouse Models

Male C57BL/6 mice (6–8 weeks old, 22–25 g) were purchased from the Experimental Animal Center of Chongqing Medical University and were maintained under the guidelines of the Animal Care and Use Committee of Chongqing Medical University. Animals were fed standard rodent chow in a temperature-controlled environment with 50% humidity and 12 h light/dark cycles in a cage of five mice. To develop the endotoxin tolerance mouse model, C57BL/6 mice were preinjected with a low dose of LPS (8 μg/kg body weight, peritoneally) for 16 h and then challenged with a lethal dose of LPS (8 mg/kg, peritoneally). Survival was monitored every hour for the next 10 h. An endotoxemia mouse model was induced in male C57BL/6 mice by LPS and a sepsis mouse model was induced by cecal ligation and puncture (CLP). For LPS-induced endotomexia, mice preinjected with saline solution or TEPP-46 (50 mg/kg, intraperitoneally) for 4 h were restimulated with LPS (5 mg/kg, intraperitoneally). Sepsis was induced in mice by CLP as previously Gong W et al. described (38). In brief, the mice were anesthetized with 2% isoflurane inhalation, and iodophor was used to disinfect the abdomen. Then, a 2 cm midline incision was made to expose the cecum and ligate the distal cecal tip with 4-0 silk. The cecum was punctured twice with a 22-gauge needle, and a small amount of feces was extruded. Then, the cecum was returned to the abdominal cavity, and the wound was closed. Sham mice underwent only laparotomy. Survival of these mice was monitored every day for the next week. The present study was approved by The Research Ethics Committee of Chongqing Medical University (No. 2017-36).

ELISA

The levels of TNF-α and IL-6 in mouse serum and cell supernatant were determined by using an ELISA kit from Boster Biological Technology according to the manufacturer's instructions.

Cell Viability of PMs and RAW264.7 Cells

Cell viability was used to evaluate the cytotoxicity of TEPP-46 to PMs and RAW264.7 cells. In brief, 5×10^3 cells were seeded in each well of a 96-well plate in 100 μl of medium and cultured for 24 h. Then, 10 μl of Cell Counting Kit-8 (CCK8, C0037, Beyotime Biotechnology) was added to each well, and the cells were incubated at 37°C for 1 h. The absorbance of each well was detected at 450 nm using a microplate reader.

Western Blot

Western blot analysis was carried out as previously Palsson-McDermott EM and Hu YC et al. described (33, 35). It is worth noting that the Western blot experiment performed for PKM2 was different from the Western blot experiment performed for other proteins. Due to the need to detect PKM2 protein expression with different configurations, the total protein extracted from the cells cannot be heat denatured. In addition, nondenatured gel sample loading buffer (Beyotime Biotechnology, P0016) replaced the SDS-PAGE sample loading buffer (Beyotime Biotechnology, P0015), and native PAGE electrophoresis buffer (Beyotime Biotechnology, P0014F) replaced the SDS-PAGE electrophoresis buffer (Beyotime Biotechnology, P0014A) in Western blot experiments of PKM2 but not in the Western blot experiments of other proteins. The other experimental steps were the same as a routine Western blot experiment. In brief, cells were harvested and lysed with a whole-protein extraction kit (KeyGen). Protein concentration was detected by a BCA protein assay kit (Beyotime Biotechnology). Except for the protein used to detect PKM2, the other proteins were mixed with loading buffer and boiled in water for 10 min. In total, 10~20 μg protein lysate was separated by SDS–PAGE with 8%~12% gels and transferred to PVDF membranes (Millipore), which were blocked with 5% BSA for 1 h at room temperature. The membranes were incubated with antibodies overnight at 4°C. The target bands were detected by using the corresponding secondary antibodies. Bands were analyzed using Quantity One software (Bio–Rad) after incubation with enhanced chemiluminescence reagent (MedChemExpress) at room temperature for 2~10 s.

Detection of PKM2 Nuclear Translocation by Immunofluorescence Staining

After KCs successfully established tolerant and nontolerant models, the cells were fixed with 4% paraformaldehyde for 10 min. After a brief wash with PBS, the cell membrane was lysed with 0.1% Triton for 10 min. Then, the membrane was

blocked with goat serum for 1 h. The cells were incubated with a rabbit mAb anti PKM2 (Cell Signaling, #4053, 1:100) overnight at 4°C. The next day, the cells were incubated with the corresponding fluorescent secondary antibody (ZSGB-BIO) for 1 h at room temperature. An appropriate amount of 4'-6-Diamidino-2-phenylindole (DAPI, MedChemExpress) was added to each plate for 3 min, and the protein expression of PKM2 was observed under an inverted microscope.

Real-Time Reverse Transcription-Polymerase Chain Reaction Analysis of Gene Expression

The RT-PCR experiment was used to detect the M2 polarization of RAW264.7 cells. The RT-PCR experimental procedure was performed as previously Hu YC et al. described (35). In brief, total RNA was extracted from RAW264.7 cells using TRIzol® reagent (Invitrogen), and then the RNA was reverse-transcribed to cDNA with the PrimeScript™ RT Reagent Kit (TaKaRa Biotechnology). Primers for RT-PCR were obtained from Sangon Biotech. The expression of the target gene was normalized to that of GAPDH. The primers used were as follows: Arg1, forward 5'-CACTACCCCACCCCACTC-3' and reverse 5'-AACGGAGCAAGACCCTGT-3'; CD206, forward 5'-GAAGCCAAGGTCCAGAAA-3' and reverse 5'-TGTTGA AAGCGTATGTCCA-3'; and GAPDH, forward 5'-CCTTCCG TGTCCCCACT-3' and reverse 5'-GCCTGCTTCACCACCTTC-3'. The relative gene expression was analyzed using the $2^{-\Delta\Delta Cq}$ method (39).

mtDNA Copy Number Detection

Total DNA was extracted from cells using the DNeasy Blood & Tissue Kit (Qiagen) and used for the detection of mtDNA copy number by RT-PCR using SYBR Green (TaKaRa Biotechnology) and an ABI PRISM 7900 Sequence Detection system (Thermo Fisher Scientific). The relative mtDNA copy number was determined by comparing the level of the mitochondrial NADH dehydrogenase subunit 1 (MTND1) gene (primers, forward 5'-GAGAACAAAGGTGAGAAGCAA-3' and reverse 5'-TCCACACAGATCCAGCATAA-3') to that of the nuclear reference gene B2M (primers, forward 5'-AGCAGAGAA TGGAAAGTCAAA-3' and reverse 5'-GATGGATGAAACCC AGACA-3'). The relative mtDNA copy number was defined as the total amount of mtDNA divided by the total amount of nuclear DNA.

Mitochondrial Mass Detection

The detection of mitochondrial mass was the same as that described in a previous study (40). In brief, the uptake of 2.5 μM nonyl acridine orange (NAO, a dye that localizes to cardiolipin on the inner mitochondrial membrane) by PMs/KCs/RAW264.7 cells over 30 min was determined by measuring fluorescence by using a flow cytometer.

Autophagy Detection

Western blot analysis of the LC3-II and p62 protein levels was used to assess the level of autophagy in RAW264.7 cells stimulated with TEPP-46 for 2 h.

Mitochondrial Respiration Detection

RAW264.7 cells with or without TEPP-46 treated in medium at pH 7.4 were transferred to the wells of an XF96 Seahorse assay plate to determine the mitochondrial oxygen consumption rate (OCR) during mitochondrial stress test by using the Seahorse XF96^{e} Extracellular Flux analyzer as previously John D et al. described (40). Before start the experiment, the cells were incubated at 37°C without CO_2 for 1 h. The OCR was measured at the baseline and following the sequential addition of 1 μM oligomycin to inhibit ATP synthase, and 0.5 μM carbonyl cyanide 4-(trifluoromethoxy) phenylhydrazone (FCCP) was added to yield maximal uncoupled respiration. Non-mitochondrial respiration was determined by adding 1 μM rotenone plus 1 μM antimycin A. Next, we quantitative analysis of mitochondrial basal respiration, ATP-linked respiration and maximal respiratory of the RAW264.7 cells with or without TEPP-46 treat.

Statistical Analysis

Statistical analyses were performed using SPSS 17.0 software (SPSS, Inc.). Data are presented as the mean ± SD of ≥3 independent biological replicates. Student's *t* test was performed for the comparison of parameters between two groups. One–way ANOVA and Tukey's test were performed to compare multiple groups. A *p*-value less than 0.05 was considered significant.

RESULTS

PKM2 Activation Promotes Macrophage Endotoxin Tolerance

The enzymatic activity of PKM2 is, in part, determined by the configuration of the enzyme into a tetramer, dimer, or monomer (27, 28). The PKM2 tetramer is located in the cytoplasm and is the active form of enzyme; the PKM2 dimer and monomer are located in the nucleus and play an important role in regulating gene transcription (27, 28). To determine whether PKM2 expression can be modulated by LPS exposure during the establishment of endotoxin tolerance, we intraperitoneally preinjected mice with saline (nontolerant) or a low dose of LPS (8 μg/kg body weight, tolerant) for 16 h, challenged all the mice with a lethal dose of LPS (8 mg/kg), and then monitored the survival of the mice. As predicted, exposure to a low dose of LPS prior to the lethal dose of LPS increased survival and decreased the serum levels of the inflammatory cytokines TNF-α and IL-6 in mice (**Figures 1A, B**). Then, we isolated PMs and liver macrophages (KCs) from tolerant and nontolerant mice (4 h after a lethal dose of LPS) and evaluated the protein expression of PKM2 in the cells. Interestingly, we found a higher protein level of the PKM2 tetramer and a lower protein level of the PKM2 dimer/monomer in both the PMs and KCs of tolerant mice compared to those of nontolerant mice, suggesting that endotoxin tolerance inhibits the nuclear translocation of PKM2 (**Figure 1C**). The protein level of PKM1, a member of the pyruvate kinase family, did not change significantly (**Figure 1C**).

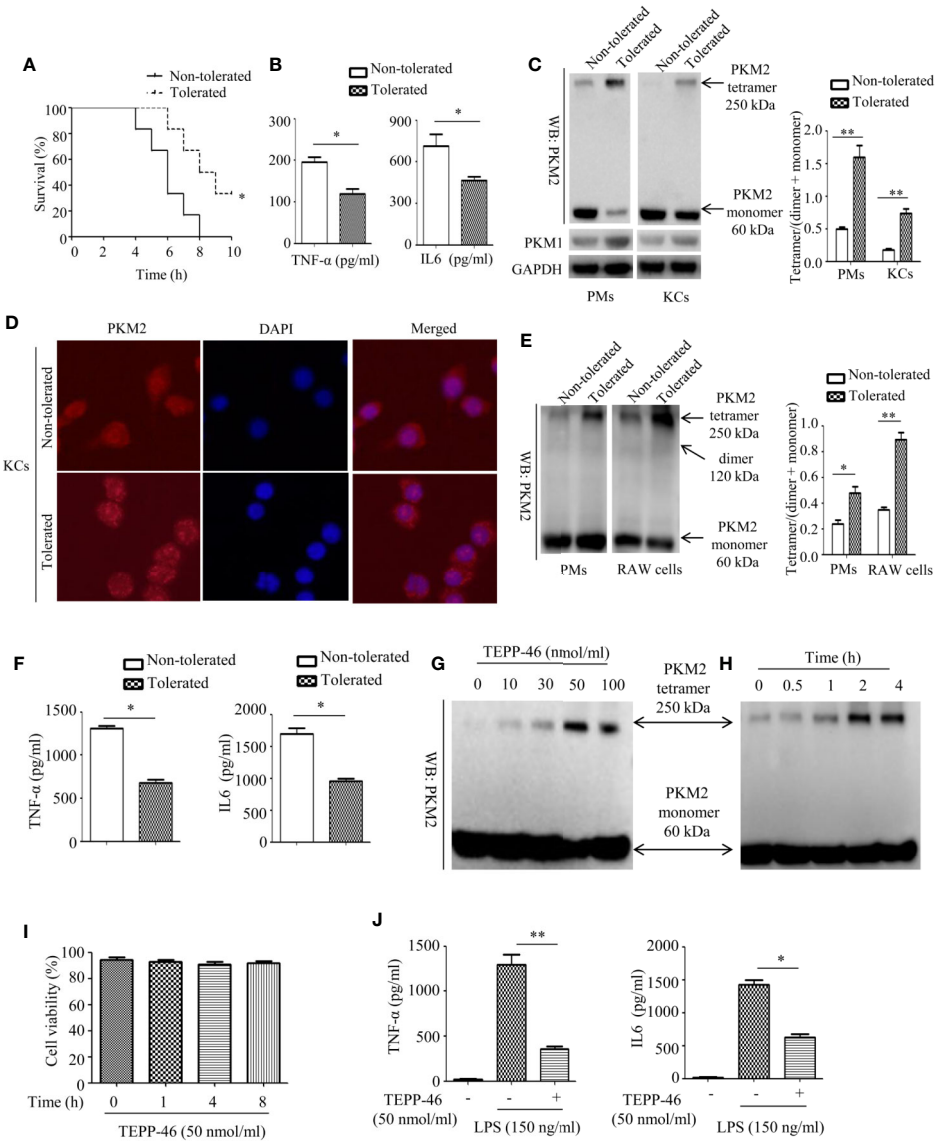

FIGURE 1 | Endotoxin tolerance promotes PKM2 tetramer formation of macrophages *in vivo* and *in vitro*. **(A)** Mouse survival was monitored every hour after constructing nontolerant and tolerant models (n=6 per group). **(B)** Serum TNF-α and IL-6 levels from tolerant and nontolerant mice were measured using ELISA (n=3). **(C)** The protein expression of PKM2 and PKM1 in PMs and KCs isolated from tolerant and nontolerant mice was measured using Western blot (n=3). **(D)** The protein expression of PKM2 (red) and DAPI staining for the nucleus (blue) in KCs isolated from tolerant and nontolerant mice were measured using immunofluorescence. **(E)** Protein expression of PKM2 in tolerant and nontolerant PMs and RAW264.7 cells *in vitro* (n=3). **(F)** Supernatant TNF-α and IL-6 levels in RAW264.7 cells were measured using ELISA (n=3). **(G, H)** Protein expression of PKM2 in RAW264.7 cells after stimulation with TEPP-46 at different concentrations and for different times (n=3). **(I)** Cell viability of RAW264.7 cells stimulated with 50 nmol/ml TEPP-46 for different times was measured using CCK8 (n=3). **(J)** Supernatant TNF-α and IL-6 levels in RAW264.7 cells after treatment with TEPP-46 for 2 h and LPS for 24 h (n=3). $^*p < 0.05$, $^{**}p < 0.01$.

Immunofluorescence further confirmed that exposure to a low dose of LPS prior to the lethal dose of LPS inhibited the nuclear translocation of PKM2 in PMs (data not shown) and in KCs (**Figure 1D**). Next, we performed an *in vitro* experiment by pre-stimulating PMs isolated from healthy mice or RAW264.7 macrophages with a low dose of LPS (10 ng/ml, tolerant) or PBS (nontolerant) for 24 h and then restimulating the cells with a high dose of LPS (150 ng/ml) for 24 h. Consistent with *in vivo* experiments, compared to nontolerant cells, tolerant cells had a significantly increased protein level of the PKM2 tetramer and significantly decreased expression of the PKM2 dimer/monomer (**Figure 1E**). The supernatant levels of TNF-α and IL-6 in also significantly decreased in tolerant cells (**Figure 1F**). These *in vivo* and *in vitro* studies confirmed that macrophage tolerance to endotoxins inhibits the nuclear translocation of PKM2 induced by LPS and promotes the formation of the PKM2 tetramer.

TEPP-46 is a small molecular agonist of PKM2 and can inhibit the nuclear translocation of PKM2 and promote the

formation of a PKM2 tetramer (41). As predicted, stimulation of RAW264.7 cells with different concentrations of TEPP-46 (0–100 nmol/ml) for 2 h or 50 nmol/ml TEPP-46 for different times (0–4 h) dose- and time-dependently promoted the protein level of the PKM2 tetramer (**Figures 1G, H**). We also assessed whether TEPP-46 has cytotoxic effects. We found that 50 nmol/ml TEPP-46 had no significant effect on cell viability under different stimulation times (0–8 h) (**Figure 1I**). To further investigate the role of the PKM2 tetramer (activated configuration of PKM2) in the establishment of endotoxin tolerance, we pretreated RAW264.7 cells with either PBS or TEPP-46 (50 nmol/ml) for 2 h and then restimulated these cells with LPS (150 ng/ml) for 24 h. We found that compared to cells treated with only LPS, RAW264.7 cells pretreated with TEPP-46 produced levels of TNF-α and IL-6 that were significantly decreased by 76% and 58%, respectively, in the culture supernatants (**Figure 1J**). Collectively, these results confirm the ability of TEPP-46 to induce endotoxin tolerance in macrophages by promoting the formation of the PKM2 tetramer.

Mitochondrial Biogenesis Is Induced in PKM2-Activated Macrophages

Mitophagy and mitochondrial biogenesis maintain the relative balance of mitochondrial mass, which plays an important role in maintaining the normal function of cells (19–21). A study showed that PKM2 activation may inhibit mitochondrial dysfunction of podocytes induced by high glucose (34). However, the effect of PKM2 activation on the mitochondrial function of macrophages is still unclear. Thus, we assessed the mitochondrial function of macrophages stimulated with TEPP-46. We observed a significantly increased level of the internal membrane marker cardiolipin in RAW264.7 cells stimulated with TEPP-46 (50 nmol/ml) for 0–24 h, which indicates an increase in mitochondrial mass under stimulation with TEPP-46 (**Figure 2A**). We next studied whether the increase in mitochondrial mass after treatment with TEPP-46 was caused by inhibiting the degradation of mitochondria (mitophagy). However, we did not observe changes in the protein levels of the autophagy markers LC3-II and p62 in RAW264.7 cells stimulated with TEPP-46 (50 nmol/ml) for 0–24 h (**Figure 2B**). In addition, there was no obvious change in mitochondrial morphology and no obvious decrease in the number of lysosomes stimulated with TEPP-46 (**Figure 2C**). The above results indicate that the overall autophagy level does not change under TEPP-46 stimulation. This means that the activation of PKM2 by TEPP-46 increased the level of mitochondrial mass but did not change the level of mitophagy in RAW264.7 cells. This reflects that mitochondrial mass may be increased by activation of mitochondrial biogenesis. As predicted, we observed a significant increase in mitochondrial DNA (mtDNA) copy number in RAW264.7 cells stimulated with TEPP-46 (50 ng/ml) for 0–24 h, and these results were consistent with the increased protein level of mitochondrial transcription factor A (mtTFA), a key regulator of mitochondrial biogenesis bound to mtDNA (**Figures 2D, E**). We repeated the above experiments after silencing the *PKM2* gene in RAW264.7 cells with siRNA-PKM2 (siPKM2). We found that TEPP-46 failed to increase the mtDNA copy number and the protein level of mtTFA in *PKM2*-knockdown RAW264.7 cells, suggesting that the effect of TEPP-46 is dependent on PKM2 (**Figures 2D, E**).

The effect of TEPP-46 on mitochondrial function was further assessed by measuring the mitochondrial oxygen consumption rate (OCR). We found that the basal respiration, ATP-linked respiration and maximal respiration were significantly increased in TEPP-46-treated RAW264.7 cells (**Figures 2F–I**). This effect of TEPP-46 was eliminated in *PKM2*-knockdown cells (**Figures 2F–I**). This indicates that the activation of PKM2 induced by TEPP-46 enhanced the mitochondrial respiratory capacity of macrophages. Collectively, we observed that PKM2 activation induced by TEPP-46 enhanced mitochondrial function by promoting mitochondrial biogenesis and increasing the mitochondrial mass but did not change the level of mitophagy.

Inhibiting Mitochondrial Biogenesis Reverses PKM2 Activation-Induced Macrophage Endotoxin Tolerance

Although we demonstrated that PKM2 activation by TEPP-46 contributes to endotoxin tolerance and that PKM2 activation also induces mitochondrial biogenesis in macrophages, we do not know whether PKM2 activation promotes endotoxin tolerance by inducing mitochondrial biogenesis. mtTFA is a key regulator of mitochondrial biogenesis bound to mtDNA (42). Several lines of evidence have suggested that inhibiting the expression of mtTFA could effectively inhibit mitochondrial biogenesis in various cells (42, 43). The mtTFA gene was knocked down in RAW264.7 cells by shRNA-mtTFA (shmtTFA) lentiviruses transduction. As predicted, the protein level of mtTFA decreased significantly after lentiviral transduction for 72 h (**Figure 3A**). Next, we observed a significant decrease in mitochondrial mass and mtDNA copy number in *mtTFA* knockdown RAW264.7 cells, suggesting that silencing *mtTFA* in RAW264.7 cells inhibits mitochondrial biogenesis (**Figures 3B, C**). We further assessed the effect of silencing *mtTFA* on endotoxin tolerance induced by PKM2 activation in macrophages. We found that silencing *mtTFA* inhibited the endotoxin tolerance of RAW264.7 cells induced by PKM2 activation, which was reflected in the levels of the inflammatory cytokines TNF-α and IL-6 in the supernatant of the *mtTFA* knockdown group (shmtTFA + TEPP-46 + LPS), which increased by 85% and 111%, respectively, compared to the levels in the endotoxin tolerance group (TEPP-46 + LPS) (**Figure 3D**). Endotoxin tolerance can inhibit LPS-mediated M1 type polarization of macrophages and promote the expression of M2 type markers, such as Arg1 and CD206 (44, 45). In this study, we found that LPS inhibited expression of Arg1 and CD206, and pretreatment with TEPP-46 promoted expression of Arg1 and CD206, suggesting that pretreatment with TEPP-46 promoted M2 polarization of macrophages (**Figure 3E**). Furthermore, TEPP-46 failed to promote the expression of Arg1 and CD206 after silencing of *mtTFA*, suggesting that the effect of TEPP-46 is dependent on mtTFA (mitochondrial biogenesis) (**Figure 3E**). Overall, these data indicate that inhibiting mitochondrial

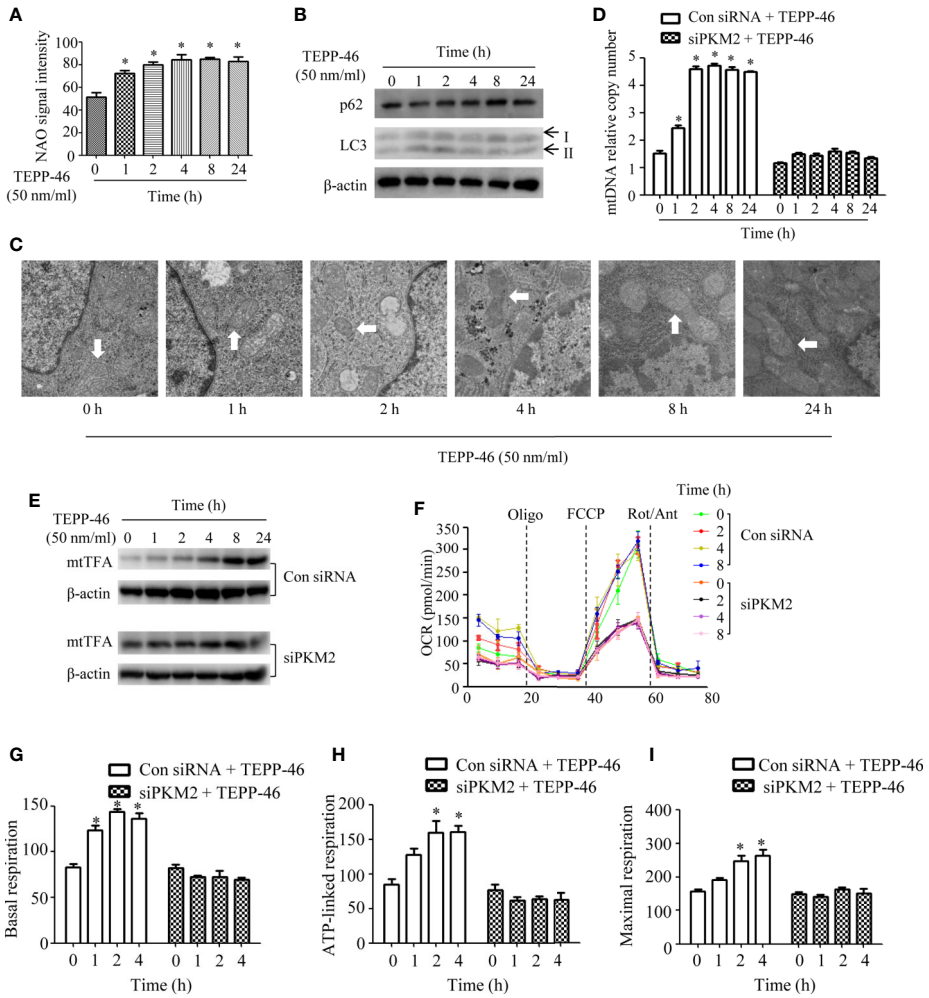

FIGURE 2 | Mitochondrial biogenesis is induced in PKM2-activated macrophages. **(A)** Mitochondrial mass was assessed by measuring the uptake of NAO by using flow cytometry (n=3). **(B)** The autophagy level of RAW264.7 cells after stimulation with TEPP-46 was assessed by measuring the protein expression of p62 and LC3 using Western blotting (n=3). **(C)** The microstructure of RAW264.7 cells stimulated with TEPP-46 was measured using transmission electron microscopy (TEM) (n=3). **(D)** mtDNA copy number was determined by measuring MTND1 relative to B2M using RT-PCR in RAW264.7 cells transducted with a control siRNA (con siRNA) or siPKM2 (n=4). **(E)** Western blot analysis of mtTFA in control or PKM2 knockdown RAW264.7 cells were stimulated with TEPP-46 for different times (n=3). **(F)** The mitochondrial OCR was measured in control or PKM2 knockdown RAW264.7 cells were stimulated with TEPP-46 by using a Seahorse XF96e Extracellular Flux analyzer. Dashed vertical lines indicate the addition of 1 μM oligomycin (Oligo), 0.5 μM carbonyl cyanide 4-(trifluoromethoxy) phenylhydrazone (FCCP), and 1 μM rotenone plus 1 μM antimycin A (Rot/Ant) (n=3). **(G–I)** Quantitative analysis of basal respiration, ATP-linked respiration and maximal respiration in control or PKM2 knockdown RAW264.7 cells were stimulated with TEPP-46 for different times (n=3). *$p < 0.05$.

biogenesis can effectively inhibit the macrophage tolerance to endotoxins induced by PKM2 activation.

PGC-1α Is the Key Regulator of PKM2 Tetramer-Induced Mitochondrial Biogenesis

PGC-1α, NRF1, NRF2, and mtTFA are the key regulatory factors that promote mitochondrial biogenesis (22, 23). The above results have shown that PKM2 activation induced by TEPP-46 could promote the expression of mtTFA (**Figure 2E**). Thus, we further assessed the effect of PKM2 activation on the expression of PGC-1α, NRF1 and NRF2. As predicted, the protein levels of PGC-1α, NRF1, and NRF2 increased in a time-dependent manner under stimulation with TEPP-46 (50 nmol/ml) (**Figure 4A**). The protein level of PGC-1β was not significantly changed (**Figure 4A**). Furthermore, we found that TEPP-46 failed to increase the protein levels of PGC-1α, NRF1 and NRF2 in *PKM2*-knockdown RAW264.7 cells, suggesting that the effect of TEPP-46 is dependent on PKM2 (**Figure 4B**). These results indicate that TEPP-46 promotes mitochondrial biogenesis by inducing PKM2 activation and by further promoting the expression of PGC-1α, NRF1, NRF2, and mtTFA. The AMP-activated protein kinase (AMPK)/sirtuin 1 (SIRT1)/PGC-1α pathway is a classical pathway that induces mitochondrial biogenesis (46). Therefore, we asked whether pretreatment with TEPP-46 could activate the AMPK/SIRT1/

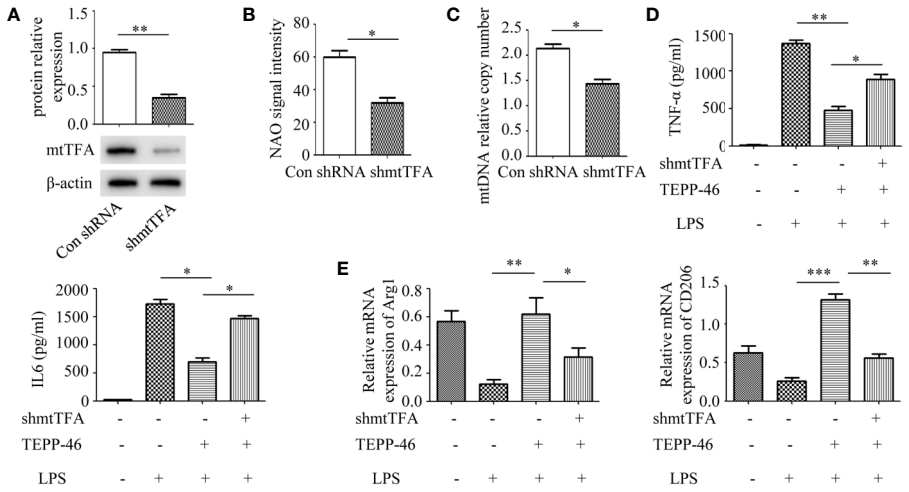

FIGURE 3 | Mitochondrial biogenesis is required for PKM2 activation-induced endotoxin tolerance. **(A)** RAW264.7 cells were treated with control shRNA or shmtTFA lentiviruses for 72 h. Protein expression of mtTFA was measured by Western blot (n=3). **(B)** NAO signal intensity was used to assess mitochondrial mass in control RAW264.7 cells (con shRNA) and in *mtTFA* knockdown RAW264.7 cells (shmtTFA) (n=4). **(C)** mtDNA copy number was determined by measuring MTND1 relative to B2M using RT-PCR (n=3). **(D)** Supernatant TNF-α and IL-6 levels in RAW264.7 cells stimulated with LPS and/or TEPP-46 were measured using ELISA (n=3). **(E)** RAW264.7 polarization level was assessed by measuring the relative mRNA expression of *Arg1* and *CD206* to that of GAPDH using RT-PCR (n=3). $^{*}p < 0.05$, $^{**}p < 0.01$, $^{***}p < 0.001$.

PGC-1α signaling pathway. However, we did not observe significant changes in the protein levels of p-AMPK, AMPK, and SIRT1, suggesting that TEPP-46-promoted expression of PGC-1α was not dependent on activation of the AMPK/SIRT1 pathway (**Figure 4C**). To further confirm that TEPP-46 induces mitochondrial biogenesis by activating PGC-1α, we silenced the *PGC-1α* gene in RAW264.7 cells by lentiviral transduction (**Figure 4D**). We found that silencing *PGC-1α* inhibited

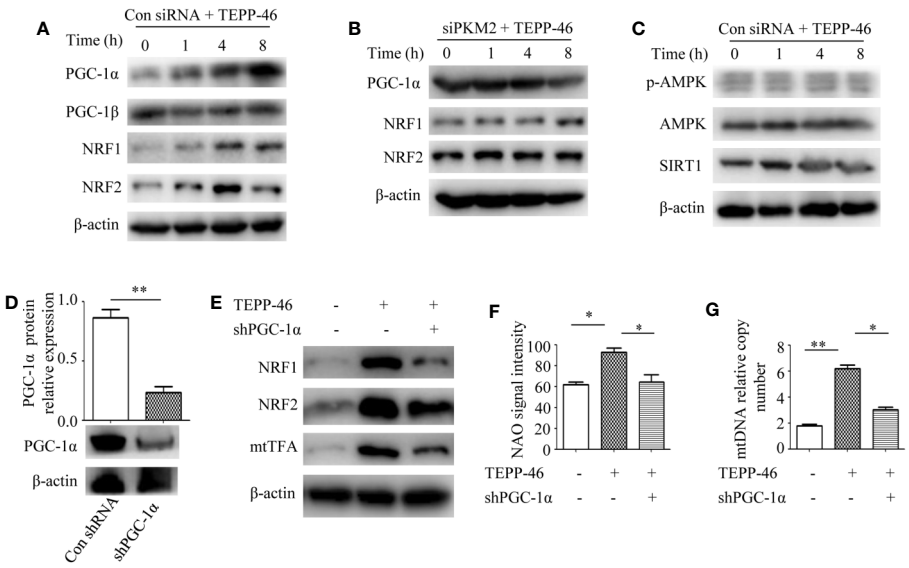

FIGURE 4 | PGC-1α is required for PKM2 activation-induced mitochondrial biogenesis. **(A)** Western blot analysis of PGC-1α, PGC-1β, NRF1, and NRF2 in RAW264.7 cells transduct with control siRNA after stimulation with TEPP-46 for 0–8 h (n=3). **(B)** Western blot analysis of PGC-1α, NRF1, and NRF2 in *PKM2*-knockdown RAW264.7 cells after stimulation with TEPP-46 for 0-8 h. (n=3). **(C)** Western blot analysis of p-AMPK, AMPK and SIRT1 in RAW264.7 cells transduct with control siRNA after stimulation with TEPP-46 for 0-8 h. (n=3). **(D)** RAW264.7 cells were treated with control shRNA or shPGC-1α lentiviruses for 72 h. Protein expression of PGC-1α was measured by Western blot (n=3). **(E)** Western blot analysis of NRF1, NRF2 and mtTFA in RAW264.7 cells. (n=3). **(F)** NAO signal intensity was used to assess mitochondrial mass in control RAW264.7 cells and in *PGC-1α* knockdown RAW264.7 cells (shPGC-1α) after stimulation with TEPP-46 (n=3). **(G)** mtDNA copy number was determined by measuring MTND1 relative to B2M using RT-PCR (n=3). $^{*}p < 0.05$, $^{**}p < 0.01$.

TEPP-46-induced expression of NRF1, NRF2 and mtTFA (**Figure 4E**). Furthermore, both the mitochondrial mass and mtDNA copy number were decreased in *PGC-1α*-knockdown cells compared to in TEPP-46-treated cells (**Figures 4F, G**). These data collectively suggest that PGC-1α is the key regulator of mitochondrial biogenesis induced by TEPP-46-mediated activation of PKM2.

PKM2 Tetramer Activates PGC-1α by Inhibiting the PI3K/Akt Signaling Pathway

We have confirmed that PKM2 activation induced by TEPP-46 promotes the activation of PGC-1α but not by activating the AMPK/SIRT1 signaling pathway. This means that activated PKM2 may promote PGC-1α by activating other pathways. Since Akt has been shown to be a negative regulator of PGC-1α (47), we then asked whether Akt participates in the TEPP-46-induced regulation of PGC-1α. We found that the protein level of phosphorylated Akt (p-Akt) was significantly decreased in RAW264.7 cells stimulated by TEPP-46 (50 nmol/ml) for 2 h (**Figure 5A**). SC79 is a small-molecule agonist of Akt, which promotes phosphorylation of Akt (**Figure 5B**) (48). RAW264.7 cells were pretreated with SC79 (4 μg/ml) for 30 min and then restimulated with TEPP-46 (50 nmol/ml) for 2 h. We found that pretreatment with SC79 effectively inhibited the protein level of PGC-1α induced by TEPP-46 (**Figure 5C**). These results indicate that TEPP-46-induced activation of PKM2 regulates PGC-1α by inhibiting Akt phosphorylation.

Phosphatidylinositol-3-kinase (PI3K) is an intracellular phosphatidylinositol kinase that promotes Akt activation (49). The PI3K/Akt signaling pathway plays an important role in the regulation of tumors and inflammation (50, 51). Since inducing the formation of the PKM2 monomer/dimer could promote the invasion and migration of tumor cells by activating the PI3K/Akt signaling pathway (52), we then asked whether the PKM2 tetramer induced by TEPP-46 could regulate Akt through PI3K in macrophages. We found that the expression of phosphorylated PI3K (p-PI3K) was significantly decreased in RAW264.7 cells stimulated by TEPP-46 (**Figure 5D**). 740 Y-P is a target agonist of PI3K, which promotes phosphorylation of PI3K (**Figure 5E**) (53). RAW264.7 cells were pretreated with 740 Y-P (50 μg/ml) for 24 h and then restimulated with TEPP-46 (50 nmol/ml) for 2 h. We found that the inhibitory effect of TEPP-46 on p-Akt was blocked by 740 Y-P (**Figure 5F**). Furthermore, pretreatment with 740 Y-P inhibited the mtDNA copy number and the protein levels of PGC-1α, NRF1, NRF2 and mtTFA induced by TEPP-46 (**Figures 5G, H**). Collectively, these data indicate that TEPP-46-induced activation of PKM2 promotes PGC-1α expression by inhibiting the PI3K/Akt signaling pathway.

Knockdown of PGC-1α Inhibits PKM2 Activation-Mediated Endotoxin Tolerance

We have confirmed that PGC-1α is a key regulator of mitochondrial biogenesis induced by activated PKM2. Next, we assessed the effect of PGC-1α on endotoxin tolerance mediated by PKM2 activation. TEPP-46-induced PKM2 activation promotes macrophage tolerance to endotoxins (**Figure 1J**). We found that knockdown of the *PGC-1α* gene inhibited TEPP-46-mediated endotoxin tolerance. This was evidenced by the levels of TNF-α and IL-6 in the supernatants of *PGC-1α*-knockdown cells (shPGC-1α + TEPP-46 + LPS) significantly increasing by 86% and 102%, respectively, compared to those of cells without *PGC-1α* gene knockdown (TEPP-46 + LPS) (**Figures 6A, B**). This indicates that knockdown of *PGC-1α* inhibits PKM2 activation-mediated endotoxin tolerance.

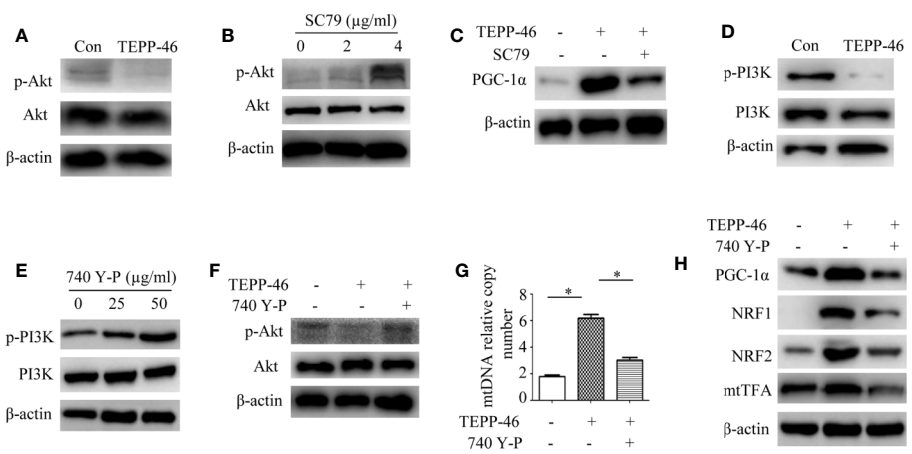

FIGURE 5 | The PI3K/Akt signaling pathway is required for PKM2 activation-induced PGC-1α expression. **(A)** Western blot analysis of p-Akt in normal RAW264.7 cells (Con) and TEPP-46-treated cells (TEPP-46) (*n*=3). **(B)** Western blot analysis of p-Akt in RAW264.7 cells after stimulation with different concentrations of SC79 for 30 min (*n*=3). **(C)** Western blot analysis of PGC-1α in RAW264.7 cells after stimulation with TEPP-46 and/or SC79 (*n*=3). **(D)** Western blot analysis of p-PI3K in RAW264.7 cells stimulated with TEPP-46 (*n*=3). **(E)** Western blot analysis of p-PI3K in RAW264.7 cells after stimulation with different concentrations of 740 Y-P for 24 h (*n*=3). **(F)** Western blot analysis of p-Akt in RAW264.7 cells after stimulation with TEPP-46 and/or 740 Y-P (*n*=3). **(G)** mtDNA copy number was determined by measuring MTND1 relative to B2M using RT-PCR (*n*=3). **(H)** Western blot analysis of PGC-1α, NRF1, NRF2 and mtTFA in RAW264.7 cells after stimulation with TEPP-46 and/or 740 Y-P (*n*=3). *$p < 0.05$.

TEPP-46 Protects Mice From Endotoxemia and Sepsis

We have confirmed that TEPP-46-mediated activation of PKM2 induces endotoxin tolerance by promoting mitochondrial biogenesis *in vitro*. We then asked whether TEPP-46 could protect mice from lethal endotoxemia by inhibiting cytokine release. To clarify this question, PMs and KCs were isolated from mice 4 h after the injection of TEPP-46 (50 mg/kg, intraperitoneally). We found that the protein level of the PKM2 tetramer was significantly increased under stimulation with TEPP-46, suggesting that TEPP-46 could effectively induce the activation of PKM2 in macrophages *in vivo*, similar to the *in vitro* results (**Figure 7A**). Furthermore, mitochondrial mass, mtDNA copy number and the protein levels of PGC-1α, NRF1, NRF2 and mtTFA were significantly increased in both PMs and KCs in TEPP-46-treated mice (**Figures 7B–G**). These results indicate that TEPP-46 also induced mitochondrial biogenesis in macrophages *in vivo*. To study the effect of TEPP-46 on endotoxemia in mice, mice were pretreated with TEPP-46 (50 mg/kg, intraperitoneally) or saline for 4 h and then restimulated with or without LPS (5 mg/kg, intraperitoneally). All of these mice were observed for 7 days, and we found that compared to endotoxemia mice (only LPS treated), mice pretreated with TEPP-46 (treated with TEPP-46 + LPS) had significantly improved survival (**Figure 7H**). No mice died during the observation period in the saline-treated group (control group), which was not reflected in the survival curve. In addition, the serum levels of TNF-α and IL-6 in TEPP-46-pretreated mice were significantly decreased compared to those in endotoxemia mice (**Figure 7I**). These findings suggest that TEPP-46 protects mice from LPS-induced endotoxemia by reducing the release of TNF-α and IL-6. Although LPS stimulation is a commonly used method to establish an endotoxemia model in mice, a more clinically relevant experimental model is sepsis model with a bacterial infection induced by CLP (38). To study the effect of TEPP-46 on sepsis in mice induced by CLP, the mice were divided into three groups: sham operation group, CLP group and TEPP-46 pretreatment group (TEPP-46 + CLP). All of these mice were observed for 7 days, and no mice died in the sham operation group (data not shown). The survival of mice significantly improved in TEPP-46-pretreated mice compared to in CLP mice (**Figure 7J**). As predicted, serum levels of TNF-α and IL-6 in the TEPP-46 pretreatment group were significantly decreased compared to those in the CLP group (**Figure 7K**). Collectively, these data suggest that the PKM2 tetramer agonist TEPP-46 protects mice from endotoxemia and sepsis induced by LPS or CLP by reducing the release of TNF-α and IL-6.

DISCUSSION

Macrophage endotoxin tolerance is defined as a hyporesponsive state in response to a secondary lethal dose of LPS following primary low-dose LPS exposure (6, 7). Studies have reported that endotoxin tolerance provides a protective mechanism to reduce the over-release of proinflammatory cytokines in response to severe infection (8, 9). In fact, endotoxin tolerance is a double-edged sword in regulating the immune response (10). In the acute inflammatory reaction stage, endotoxin tolerance serves as an important regulatory mechanism to prevent tissue damage from overactive inflammatory responses, which can cause sepsis syndrome (54). However, prolonged immune tolerance allows for the development of secondary infections, increasing mortality from sepsis, especially for immunocompromised individuals (12, 13). Therefore, further study on the mechanism of endotoxin tolerance is of great significance to better grasp the time frame of inducing immune tolerance and avoiding immunosuppression

Here, we present a novel function of the PKM2 small-molecule agonist TEPP-46 that contributes to macrophage tolerance to endotoxins by promoting mitochondrial biogenesis. As summarized in **Figure 8**, TEPP-46 induces the formation of PKM2 tetramer. Tetrameric PKM2 can promote the expression of PGC-1α by inhibiting the phosphorylation of PI3K and AKT, and promote mitochondrial biogenesis by further activating NRF1/2 and mtTFA, thus inhibiting the release of inflammatory factors mediated by LPS and promoting macrophage tolerance to endotoxins. PKM2 tetramer-induced expression of PGC-1α and PGC-1α-mediated mitochondrial biogenesis are two prerequisites for TEPP-46-mediated macrophage tolerance to endotoxins.

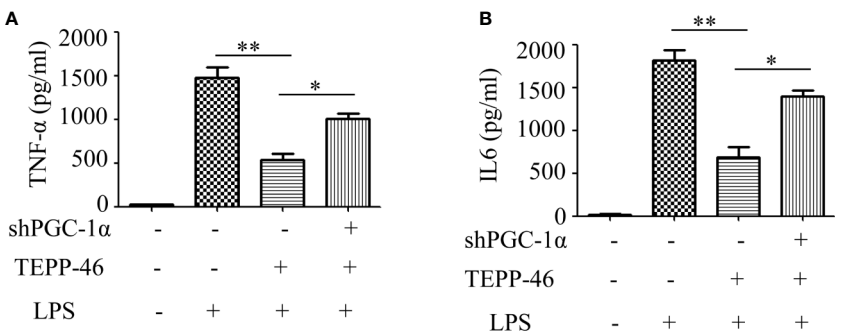

FIGURE 6 | PGC-1α is required for PKM2 activation-induced endotoxin tolerance. **(A, B)** Supernatant TNF-α and IL-6 levels in control RAW264.7 cells or *PGC-1α* knockdown RAW264.7 cells stimulated with LPS and/or TEPP-46 were measured using ELISA (n=3). $^{*}p < 0.05$, $^{**}p < 0.01$.

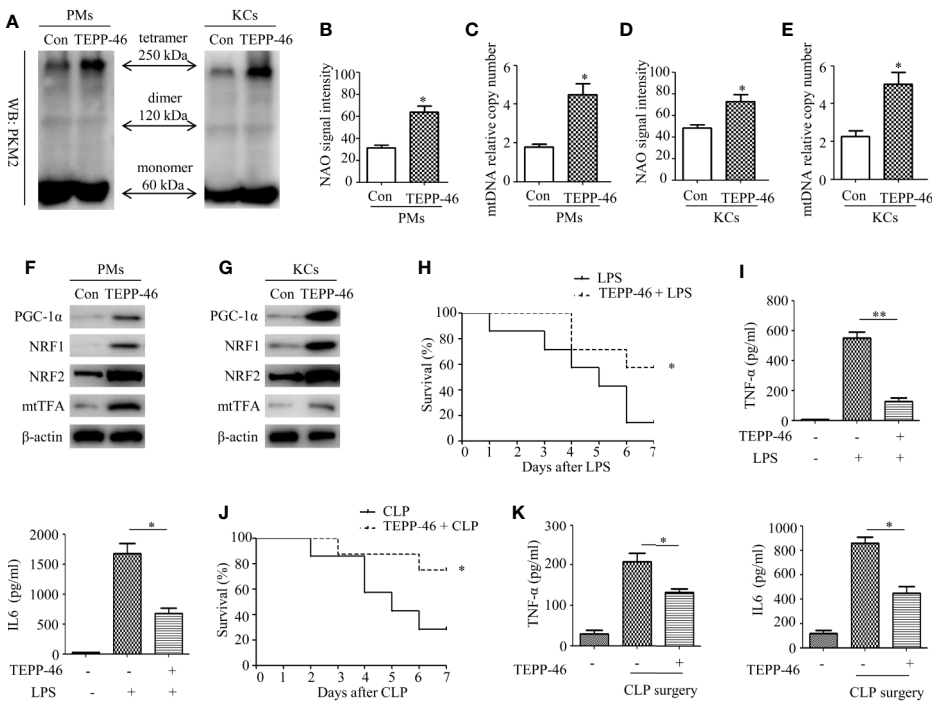

FIGURE 7 | TEPP-46-mediated formation of the PKM2 tetramer protects mice from endotoxemia and sepsis *in vivo*. **(A)** Western blot analysis of PKM2 in PMs and KCs isolated from mice with (TEPP-46)/without (Con) injections of TEPP-46 (n=4). **(B, D)** NAO signal intensity was used to assess the mitochondrial mass in PMs and KCs isolated from mice with (TEPP-46)/without (Con) injections of TEPP-46 (n=3). **(C, E)** mtDNA copy number in PMs and KCs was determined by measuring MTND1 relative to B2M using RT-PCR (n=3). **(F, G)** Western blot analysis of PGC-1α, NRF1, NRF2, and mtTFA in PMs and KCs isolated from mice with (TEPP-46)/without (Con) injections of TEPP-46 (n=3). **(H)** Mouse survival was monitored every day after constructing endotoxemia models with LPS (5 mg/kg, intraperitoneally), with or without pretreatment of TEPP-46 (n=7, per group). **(I)** Serum TNF-α and IL-6 levels in the mice of each group (n=3). **(J)** Mouse survival was monitored every day after constructing sepsis models with CLP, with or without pretreatment of TEPP-46 (n=7, per group). **(K)** Serum TNF-α and IL-6 levels in the mice of each group (n=3). $^{*}p < 0.05$, $^{**}p < 0.01$.

To our knowledge, this finding is the first example of negative regulation of an LPS-mediated inflammatory response through targeting PKM2-associated mitochondrial biogenesis. This study also reveals that PGC-1α is regulated by the PI3K/Akt signaling pathway, not by the AMPK/SIRT1 signaling pathway, and plays an important role in TEPP-46-mediated macrophage tolerance to endotoxins.

PKM2 is a key enzyme of glycolysis, and its function is mainly determined by its conformation, including monomer, dimer, and tetramer (27, 28). In tumor cells and inflammatory cells, there is the transformation from a PKM2 tetramer to a PKM2 monomer/dimer (27, 28). TEPP-46 and DASA-58 are two different small-molecule agonists of PKM2 and both can promote the formation of the PKM2 tetramer, which can not only inhibit the growth of tumor cells but also inhibit the inflammatory response of immune cells by promoting the formation of the PKM2 tetramer (29–31). In the latest research, Le et al. found that PKM2 activator TEPP-46 attenuates β-aminopropionitrile fumarate (BAPN)-induced mouse model of thoracic aortic aneurysm and dissection (TAAD) by inhibiting NLRP3 inflammasome-mediated IL-1β secretion. This provides a new treatment strategy for TAAD (55). In this study, we have shown direct evidence of PKM2 tetramer-mediated macrophage endotoxin tolerance in primary macrophages (PMs and KCs), as well as in the RAW264.7 cell line. We observed increased levels of PKM2 tetramers in PMs and KCs isolated from tolerant and nontolerant mice. These findings were consistent with the *in vitro* results. In addition, we observed decreased levels of TNF-α and IL-6 after treatment with LPS in RAW264.7 cells that had been pretreated with TEPP-46.

Our next focus was to identify a mechanism by which TEPP-46 induced endotoxin tolerance in macrophages. Previously, it has been shown that TEPP-46-mediated PKM2 activation may inhibit mitochondrial dysfunction of podocytes induced by high glucose (34). DASA-58-mediated PKM2 activation suppresses osteogenesis and facilitates adipogenesis of bone marrow mesenchymal stem cells (BMSCs) by regulating β-catenin signaling and mitochondrial fusion and fission (56). In addition, a recent study reported that PKM2 is a key regulator of mitochondrial fusion to promote mitochondrial fusion and oxidative phosphorylation (OXPHOS), further modulating cancer cell growth by attenuating glycolysis (57). Obviously, these data show that activation of PKM2 is closely related to the regulation of mitochondrial function. However, the effect of PKM2 activation on the macrophage mitochondrial function is still unclear. Mitophagy and mitochondrial biogenesis maintain the relative balance of mitochondrial mass, which plays an important role in maintaining the normal function of cells (19–21).

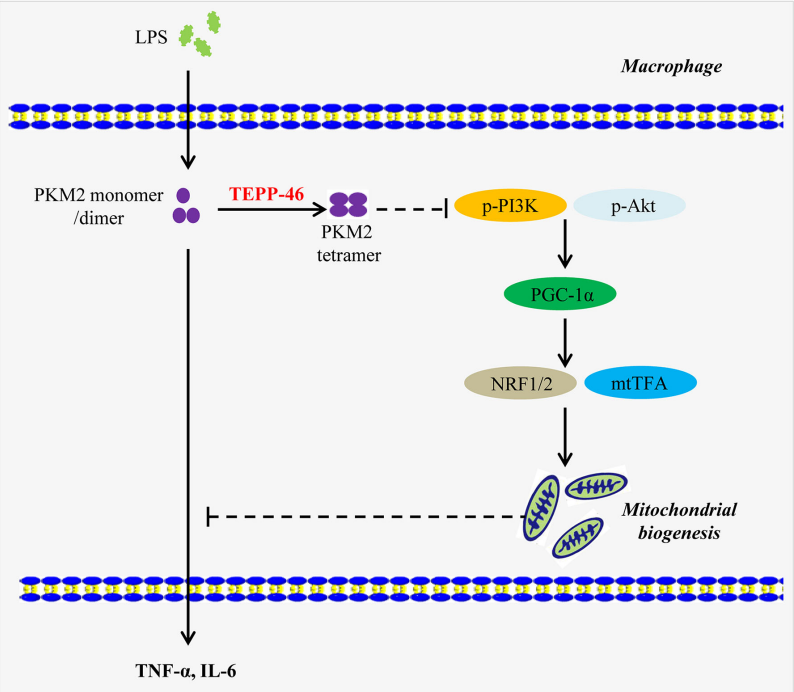

FIGURE 8 | A model depicting the mechanism of macrophage tolerance to endotoxin induced by TEPP-46. The solid arrow indicates a promoting effect. The dashed line without arrow indicates an inhibiting effect. Abbreviations: lipopolysaccharide (LPS); pyruvate kinase M2 (PKM2); phosphorylated Akt (p-Akt); phosphorylated phosphatidylinositol-3-kinase (p-PI3K); peroxisome proliferator-activated receptor gamma coactivator 1 alpha (PGC-1α); nuclear respiratory factor 1/2 (NRF1/2); mitochondrial transcription factor A (mtTFA); tumor necrosis factor-α (TNF-α); interleukin 6 (IL-6).

We observed a significantly increased level of mitochondrial mass in RAW264.7 cells after stimulation with TEPP-46. Decreased mitophagy or increased mitochondrial biogenesis can lead to an increase in the mitochondrial mass. Intriguingly, we did not observe changes in the protein levels of the autophagy markers LC3 and p62 in RAW264.7 cells stimulated with TEPP-46. However, we observed a significant increase in the mtDNA copy number in RAW264.7 cells stimulated with TEPP-46, which was significantly consistent with the increased protein level of mtTFA, a key regulator of mitochondrial biogenesis bound to mtDNA (22). This effect of TEPP-46 was eliminated in *PKM2*-knockdown cells, suggesting that the effect of TEPP-46 is dependent on PKM2. mtTFA is a key regulator of mitochondrial biogenesis (23). Several recent studies have reported that mtTFA upregulation augmented mitochondrial biogenesis and enhanced mitochondrial functions (22, 58). In our study, we knocked down mtTFA gene expression in RAW264.7 cells with shmtTFA lentiviruses, and this method effectively inhibited mitochondrial biogenesis. We found that silencing mtTFA inhibited RAW264.7 cell endotoxin tolerance induced by PKM2 activation, which was reflected in the levels of the inflammatory cytokines TNF-α and IL-6 in the supernatant of the mtTFA knockdown group (shmtTFA + TEPP-46 + LPS), which were increased by 85% and 111%, respectively, compared to those of the endotoxin tolerance group (TEPP-46 + LPS). In our previous study, we found that endotoxin tolerance can inhibit LPS-mediated M1-type polarization of macrophages and promote M2-type polarization (45). Our results further support the role of TEPP-46 in the negative regulation of the inflammatory response in macrophages. We found that pretreatment with TEPP-46 inhibited LPS-mediated M1-type polarization and promoted the expression of Arg1 and CD206 (M2 polarization markers). However, TEPP-46 failed to promote the expression of Arg1 and CD206 after silencing of mtTFA, suggesting that the effect of TEPP-46 is dependent on mtTFA (mitochondrial biogenesis).

PGC-1α, NRF1, NRF2, and mtTFA are the key regulatory factors that promote mitochondrial biogenesis, and the AMPK/SIRT1/PGC-1α signaling pathway is the classical pathway that induces mitochondrial biogenesis (25, 26). Therefore, we asked whether pretreatment with TEPP-46 could activate the AMPK/SIRT1/PGC-1α signaling pathway. However, we did not observe changes in the protein levels of SIRT1 and phosphorylated AMPK, suggesting that TEPP-46-promoted expression of PGC-1α was not dependent on activation of the AMPK/SIRT1 pathway. Inducing the formation of the PKM2 monomer/dimer could promote the invasion and migration of tumor cells by activating the PI3K/Akt signaling pathway (50). PI3K/Akt is the negative regulatory pathway of PGC-1α, which is involved in the regulation of various tumors and inflammatory diseases (50, 51). These results indicate that PKM2 may regulate the expression of PGC-1α by regulating the PI3K/Akt signaling pathway.

Interestingly, we found that the PI3K/Akt signaling pathway was significantly suppressed in RAW264.7 cells stimulated with TEPP-46. Furthermore, pretreatment with SC79 (agonist of Akt) or 740 Y-P (agonist of PI3K) inhibited the mtDNA copy number and the protein levels of PGC-1α, NRF1, NRF2 and mtTFA induced by TEPP-46. These data indicate that activation of PKM2 induced by TEPP-46 promotes PGC-1α expression by inhibiting the PI3K/Akt signaling pathway.

Although LPS-mediated endotoxemia is a useful model for investigating sepsis, a more clinically relevant experimental model for sepsis is a bacterial infection model induced by CLP (38). In this study, we established mouse endotoxemia models and sepsis models by intraperitoneal injections of LPS and CLP, respectively. We found that the PKM2 tetramer agonist TEPP-46 protects mice from endotoxemia and sepsis induced by LPS or CLP by reducing the release of TNF-α and IL-6. By isolating mouse PMs and KCs, we found that TEPP-46 also promotes the formation of the PKM2 tetramer and induces the expression of PGC-1α, NRF1, NRF2 and mtTFA in the cell populations *in vivo* as well as *in vitro*. Collectively, these data reveal a novel pathway of TEPP-46-mediated activation of PKM2 that contributes to endotoxin tolerance by promoting mitochondrial biogenesis *in vivo* and *in vitro*.

DATA AVAILABILITY STATEMENT

The datasets presented in this study can be found in online repositories. The names of the repository/repositories and accession number(s) can be found in the article/supplementary material.

ETHICS STATEMENT

The animal study was reviewed and approved by The Research Ethics Committee of Chongqing Medical University (No. 2017-36).

AUTHOR CONTRIBUTIONS

ZY and YW put forward the research hypothesis and designed the experiments. ZY, YW, WZ, and TW carried out the experimental procedures. JG carried out data analysis. YC and CM were presided the study and provided financial support. This manuscript was prepared by ZY, YW, YC, and MC. All authors contributed to the article and approved the submitted version.

FUNDING

This study was supported by the National Natural Science Foundation of China (No. 81701957 and No. 81701950), China Postdoctoral Science Foundation (2019M653352) and the Kuanren Talents Program of the second affiliated hospital of Chongqing Medical University.

REFERENCES

1. Gotts JE, Matthay MA. Sepsis: pathophysiology and clinical management. *BMJ (Clin Res Ed)* (2016) 353:i1585. doi: 10.1136/bmj.i1585
2. Bosmann M, Ward PA. The inflammatory response in sepsis. *Trends Immunol* (2013) 34(3):129–36. doi: 10.1016/j.it.2012.09.004
3. Rosadini CV, Kagan JC. Early innate immune responses to bacterial LPS. *Curr Opin Immunol* (2017) 44:14–9. doi: 10.1016/j.coi.2016.10.005
4. Kuzmich NN, Sivak KV, Chubarev VN, Porozov YB, Savateeva-Lyubimova TN, Peri F. TLR4 Signaling Pathway Modulators as Potential Therapeutics in Inflammation and Sepsis. *Vaccines* (2017) 5(4):34. doi: 10.3390/vaccines5040034
5. Cavaillon JM. Exotoxins and endotoxins: Inducers of inflammatory cytokines. *Toxicon* (2018) 149:45–53. doi: 10.1016/j.toxicon.2017.10.016
6. Biswas SK, Lopez-Collazo E. Endotoxin tolerance: new mechanisms, molecules and clinical significance. *Trends Immunol* (2009) 30(10):475–87. doi: 10.1016/j.it.2009.07.009
7. López-Collazo E, del Fresno C. Pathophysiology of endotoxin tolerance: mechanisms and clinical consequences. *Crit Care (London England)* (2013) 17(6):242. doi: 10.1186/cc13110
8. Cavaillon JM, Adib-Conquy M. Bench-to-bedside review: endotoxin tolerance as a model of leukocyte reprogramming in sepsis. *Crit Care (London England)* (2006) 10(5):233. doi: 10.1186/cc5055
9. Bessede A, Gargaro M, Pallotta MT, Matino D, Servillo G, Brunacci C, et al. Aryl hydrocarbon receptor control of a disease tolerance defence pathway. *Nature* (2014) 511(7508):184–90. doi: 10.1038/nature13323
10. Cavaillon JM, Adrie C, Fitting C, Adib-Conquy M. Endotoxin tolerance: is there a clinical relevance? *J Endotoxin Res* (2003) 9(2):101–7. doi: 10.1179/096805103125001487
11. Vergadi E, Vaporidi K, Tsatsanis C. Regulation of Endotoxin Tolerance and Compensatory Anti-inflammatory Response Syndrome by Non-coding RNAs. *Front Immunol* (2018) 9:2705:2705. doi: 10.3389/fimmu.2018.02705
12. Collins PE, Carmody RJ. The Regulation of Endotoxin Tolerance and its Impact on Macrophage Activation. *Crit Rev Immunol* (2015) 35(4):293–323. doi: 10.1615/critrevimmunol.2015015495
13. Seeley JJ, Baker RG, Mohamed G, Bruns T, Hayden MS, Deshmukh SD, et al. Induction of innate immune memory via microRNA targeting of chromatin remodelling factors. *Nature* (2018) 559(7712):114–9. doi: 10.1038/s41586-018-0253-5
14. Zheng Z, Ma H, Zhang X, Tu F, Wang X, Ha T, et al. Enhanced Glycolytic Metabolism Contributes to Cardiac Dysfunction in Polymicrobial Sepsis. *J Infect Dis* (2017) 215(9):1396–406. doi: 10.1093/infdis/jix138
15. Kelly B, O'Neill LA. Metabolic reprogramming in macrophages and dendritic cells in innate immunity. *Cell Res* (2015) 25(7):771–84. doi: 10.1038/cr.2015.68
16. Zhang D, Tang Z, Huang H, Zhou G, Cui C, Weng Y, et al. Metabolic regulation of gene expression by histone lactylation. *Nature* (2019) 574 (7779):575–80. doi: 10.1038/s41586-019-1678-1
17. Ip WKE, Hoshi N. Anti-inflammatory effect of IL-10 mediated by metabolic reprogramming of macrophages. *Science* (2017) 356(6337):513–9. doi: 10.1126/science.aal3535
18. Gkikas I, Palikaras K, Tavernarakis N. The Role of Mitophagy in Innate Immunity. *Front Immunol* (2018) 9:1283. doi: 10.3389/fimmu.2018.01283
19. Thornton C, Jones A, Nair S, Aabdien A, Mallard C, Hagberg H. Mitochondrial dynamics, mitophagy and biogenesis in neonatal hypoxic-ischaemic brain injury. *FEBS Lett* (2018) 592(5):812–30. doi: 10.1002/1873-3468.12943
20. Palikaras K, Lionaki E, Tavernarakis N. Coordination of mitophagy and mitochondrial biogenesis during ageing in C. elegans. *Nature* (2015) 521 (7553):525–8. doi: 10.1038/nature14300
21. Yau WW, Singh BK, Lesmana R, Zhou J, Sinha RA, Wong KA, et al. Thyroid hormone (T(3)) stimulates brown adipose tissue activation via mitochondrial biogenesis and MTOR-mediated mitophagy. *Autophagy* (2019) 15(1):131–50. doi: 10.1080/15548627.2018.1511263

22. Pfanner N, Warscheid B, Wiedemann N. Mitochondrial proteins: from biogenesis to functional networks. *Nat Rev Mol Cell Biol* (2019) 20(5):267–84. doi: 10.1038/s41580-018-0092-0
23. Ploumi C, Daskalaki I, Tavernarakis N. Mitochondrial biogenesis and clearance: a balancing act. *FEBS J* (2017) 284(2):183–95. doi: 10.1111/febs.13820
24. Fontecha-Barriuso M, Martín-Sánchez D, Martinez-Moreno JM, Carrasco S, Ruiz-Andrés O, Monsalve M, et al. PGC-1α deficiency causes spontaneous kidney inflammation and increases the severity of nephrotoxic AKI. *J Pathol* (2019) 249(1):65–78. doi: 10.1002/path.5282
25. Li L, Pan R, Li R, Niemann B, Aurich AC, Chen Y, et al. Mitochondrial biogenesis and peroxisome proliferator-activated receptor-γ coactivator-1α (PGC-1α) deacetylation by physical activity: intact adipocytokine signaling is required. *Diabetes* (2011) 60(1):157–67. doi: 10.2337/db10-0331
26. Thirupathi A, de Souza CT. Multi-regulatory network of ROS: the interconnection of ROS, PGC-1 alpha, and AMPK-SIRT1 during exercise. *J Physiol Biochem* (2017) 73(4):487–94. doi: 10.1007/s13105-017-0576-y
27. Zhang Z, Deng X, Liu Y, Liu Y. PKM2, function and expression and regulation. *Cell Biosci* (2019) 9:52. doi: 10.1186/s13578-019-0317-8
28. Israelsen WJ, Vander Heiden MG. Pyruvate kinase: Function, regulation and role in cancer. *Semin Cell Dev Biol* (2015) 43:43–51. doi: 10.1016/j.semcdb.2015.08.004
29. Xie M, Yu Y, Kang R, Zhu S, Yang L, Zeng L, et al. PKM2-dependent glycolysis promotes NLRP3 and AIM2 inflammasome activation. *Nat Commun* (2016) 7:13280. doi: 10.1038/ncomms13280
30. Singh JP, Qian K, Lee JS, Zhou J, Han X, Zhang B, et al. O-GlcNAcase targets pyruvate kinase M2 to regulate tumor growth. *Oncogene* (2020) 39(3):560–73. doi: 10.1038/s41388-019-0975-3
31. Rihan M, Nalla LV, Dharavath A, Shard A, Kalia K, Khairnar A. Pyruvate Kinase M2: a Metabolic Bug in Re-Wiring the Tumor Microenvironment. *Cancer Microenviron* (2019) 12(2-3):149–67. doi: 10.1007/s12307-019-00226-0
32. Yang L, Xie M, Yang M, Yu Y, Zhu S, Hou W, et al. PKM2 regulates the Warburg effect and promotes HMGB1 release in sepsis. *Nat Commun* (2014) 5:4436. doi: 10.1038/ncomms5436
33. Palsson-McDermott EM, Curtis AM, Goel G, Lauterbach MA, Sheedy FJ, Gleeson LE, et al. Pyruvate kinase M2 regulates Hif-1α activity and IL-1β induction and is a critical determinant of the warburg effect in LPS-activated macrophages. *Cell Metab* (2015) 21(1):65–80. doi: 10.1016/j.cmet.2014.12.005
34. Qi W, Keenan HA, Li Q, Ishikado A, Kannt A, Sadowski T, et al. Pyruvate kinase M2 activation may protect against the progression of diabetic glomerular pathology and mitochondrial dysfunction. *Nat Med* (2017) 23 (6):753–62. doi: 10.1038/nm.4328
35. Hu YC, Yi ZJ, Zhou Y, Li PZ, Liu ZJ, Duan SG, et al. Overexpression of RIP140 suppresses the malignant potential of hepatocellular carcinoma by inhibiting NF−κB−mediated alternative polarization of macrophages. *Oncol Rep* (2017) 37(5):2971–9. doi: 10.3892/or.2017.5551
36. Li PZ, Li JZ, Li M, Gong JP, He K. An efficient method to isolate and culture mouse Kupffer cells. *Immunol Lett* (2014) 158(1-2):52–6. doi: 10.1016/j.imlet.2013.12.002
37. Goldberg MS, Sharp PA. Pyruvate kinase M2-specific siRNA induces apoptosis and tumor regression. *J Exp Med* (2012) 209(2):217–24. doi: 10.1084/jem.20111487
38. Gong W, Wen H. Sepsis Induced by Cecal Ligation and Puncture. *Methods Mol Biol (Clifton NJ)* (2019) 1960:249–55. doi: 10.1007/978-1-4939-9167-9_22
39. Livak KJ, Schmittgen TD. Analysis of relative gene expression data using real-time quantitative PCR and the 2(-Delta C(T)) Method. *Methods (San Diego Calif)* (2001) 25(4):402–8. doi: 10.1006/meth.2001.1262
40. Widdrington JD, Gomez-Duran A, Pyle A, Ruchaud-Sparagano MH, Scott J, Baudouin SV, et al. Exposure of Monocytic Cells to Lipopolysaccharide Induces Coordinated Endotoxin Tolerance, Mitochondrial Biogenesis, Mitophagy, and Antioxidant Defenses. *Front Immunol* (2018) 9:2217:2217. doi: 10.3389/fimmu.2018.02217
41. Angiari S, Runtsch MC, Sutton CE, Palsson-McDermott EM, Kelly B, Rana N, et al. Pharmacological Activation of Pyruvate Kinase M2 Inhibits CD4(+) T Cell Pathogenicity and Suppresses Autoimmunity. *Cell Metab* (2020) 31 (2):391–405.e8. doi: 10.1016/j.cmet.2019.10.015
42. Kohno K, Wang KY, Takahashi M, Kurita T, Yoshida Y, Hirakawa M, et al. Mitochondrial Transcription Factor A and Mitochondrial Genome as Molecular Targets for Cisplatin-Based Cancer Chemotherapy. *Int J Mol Sci* (2015) 16(8):19836–50. doi: 10.3390/ijms160819836
43. Chandrasekaran K, Anjaneyulu M, Choi J, Kumar P, Salimian M, Ho CY, et al. Role of mitochondria in diabetic peripheral neuropathy: Influencing the NAD (+)-dependent SIRT1-PGC-1α-TFAM pathway. *Int Rev Neurobiol* (2019) 145:177–209. doi: 10.1016/bs.irn.2019.04.002
44. Arora H, Wilcox SM, Johnson LA, Munro L, Eyford BA, Pfeifer CG, et al. The ATP-Binding Cassette Gene ABCF1 Functions as an E2 Ubiquitin-Conjugating Enzyme Controlling Macrophage Polarization to Dampen Lethal Septic Shock. *Immunity* (2019) 50(2):418–31.e6. doi: 10.1016/j.immuni.2019.01.014
45. Li ZH, Wang LL, Liu H, Muyayalo KP, Huang XB, Mor G, et al. Galectin-9 Alleviates LPS-Induced Preeclampsia-Like Impairment in Rats via Switching Decidual Macrophage Polarization to M2 Subtype. *Front Immunol* (2018) 9:3142:3142. doi: 10.3389/fimmu.2018.03142
46. Bhargava P, Schnellmann RG. Mitochondrial energetics in the kidney. *Nat Rev Nephrol* (2017) 13(10):629–46. doi: 10.1038/nrneph.2017.107
47. Sajan MP, Lee MC, Foufelle F, Sajan J, Cleland C, Farese RV. Coordinated regulation of hepatic FoxO1, PGC-1α and SREBP-1c facilitates insulin action and resistance. *Cell Signal* (2018) 43:62–70. doi: 10.1016/j.cellsig.2017.12.005
48. Zhang D, Zhang H, Hao S, Yan H, Zhang Z, Hu Y, et al. Akt Specific Activator SC79 Protects against Early Brain Injury following Subarachnoid Hemorrhage. *ACS Chem Neurosci* (2016) 7(6):710–8. doi: 10.1021/acschemneuro.5b00306
49. Ghoneum A, Said N. PI3K-AKT-mTOR and NFκB Pathways in Ovarian Cancer: Implications for Targeted Therapeutics. *Cancers (Basel)* (2019) 11 (7):949. doi: 10.3390/cancers11070949
50. Murugan AK. Special issue: PI3K/Akt signaling in human cancer. *Semin Cancer Biol* (2019) 59:1–2. doi: 10.1016/j.semcancer.2019.10.022
51. Eräsalo H, Hämäläinen M, Leppänen T, Mäki-Opas I, Laavola M, Haavikko R, et al. Natural Stilbenoids Have Anti-Inflammatory Properties in Vivo and Down-Regulate the Production of Inflammatory Mediators NO, IL6, and MCP1 Possibly in a PI3K/Akt-Dependent Manner. *J Nat Prod* (2018) 81 (5):1131–42. doi: 10.1021/acs.jnatprod.7b00384
52. Wang C, Jiang J, Ji J, Cai Q, Chen X, Yu Y, et al. PKM2 promotes cell migration and inhibits autophagy by mediating PI3K/AKT activation and contributes to the malignant development of gastric cancer. *Sci Rep* (2017) 7 (1):2886. doi: 10.1038/s41598-017-03031-1
53. Liu JZ, Hu YL, Feng Y, Jiang Y, Guo YB, Liu YF, et al. BDH2 triggers ROS-induced cell death and autophagy by promoting Nrf2 ubiquitination in gastric cancer. *J Exp Clin Cancer Res CR* (2020) 39(1):123. doi: 10.1186/s13046-020-01620-z
54. Luan HH, Wang A, Hilliard BK, Carvalho F, Rosen CE, Ahasic AM, et al. GDF15 Is an Inflammation-Induced Central Mediator of Tissue Tolerance. *Cell* (2019) 178(5):1231–44.e11. doi: 10.1016/j.cell.2019.07.033
55. Le S, Zhang H, Huang X, Chen S, Wu J, Chen S, et al. PKM2 Activator TEPP-46 Attenuates Thoracic Aortic Aneurysm and Dissection by Inhibiting NLRP3 Inflammasome-Mediated IL-1β Secretion. *J Cardiovasc Pharmacol Ther* (2020) 25(4):364–76. doi: 10.1177/1074248420919966
56. Guo J, Ren R, Yao X, Ye Y, Sun K, Lin J, et al. PKM2 suppresses osteogenesis and facilitates adipogenesis by regulating β-catenin signaling and mitochondrial fusion and fission. *Aging* (2020) 12(4):3976–92. doi: 10.18632/aging.102866
57. Li T, Han J, Jia L, Hu X, Chen L, Wang Y. PKM2 coordinates glycolysis with mitochondrial fusion and oxidative phosphorylation. *Protein Cell* (2019) 10 (8):583–94. doi: 10.1007/s13238-019-0618-z
58. Fang Y, Akimoto M, Mayanagi K, Hatano A, Matsumoto M, Matsuda S, et al. Chemical acetylation of mitochondrial transcription factor A occurs on specific lysine residues and affects its ability to change global DNA topology. *Mitochondrion* (2020) 53:99–108. doi: 10.1016/j.mito.2020.05.003

Conflict of Interest: The authors declare that the research was conducted in the absence of any commercial or financial relationships that could be construed as a potential conflict of interest.

frontiers in Immunology

ORIGINAL RESEARCH
published: 02 February 2021
doi: 10.3389/fimmu.2020.589259

O-Linked N-Acetylglucosamine Modification of Mitochondrial Antiviral Signaling Protein Regulates Antiviral Signaling by Modulating Its Activity

*Junghwa Seo[1,2], Yun Soo Park[1,2], Tae Hyun Kweon[1,2], Jingu Kang[1,2], Seongjin Son[1,2], Han Byeol Kim[3], Yu Ri Seo[3], Min Jueng Kang[3], Eugene C. Yi[1,3], Yong-ho Lee[1,4], Jin-Hong Kim[1,5], Boyoun Park[1,6], Won Ho Yang[1,6] and Jin Won Cho[1,6]**

[1] Glycosylation Network Research Center, Yonsei University, Seoul, South Korea, [2] Interdisciplinary Program of Integrated OMICS for Biomedical Science, Graduate School, Yonsei University, Seoul, South Korea, [3] Department of Molecular Medicine and Biopharmaceutical Sciences, School of Convergence Science and Technology and College of Medicine or College of Pharmacy, Seoul National University, Seoul, South Korea, [4] Department of Internal Medicine, Yonsei University College of Medicine, Seoul, South Korea, [5] Department of Biological Sciences, College of Natural Sciences, Seoul National University, Seoul, South Korea, [6] Department of Systems Biology, College of Life Science and Biotechnology, Yonsei University, Seoul, South Korea

OPEN ACCESS

Edited by:
Edecio Cunha-Neto,
University of São Paulo, Brazil

Reviewed by:
Hao-Sen Chiang,
National Taiwan University, Taiwan
Gyorgy Fejer,
University of Plymouth,
United Kingdom

***Correspondence:**
Jin Won Cho
chojw311@yonsei.ac.kr

Specialty section:
This article was submitted to Molecular Innate Immunity, a section of the journal Frontiers in Immunology

Received: 30 July 2020
Accepted: 14 December 2020
Published: 02 February 2021

Citation:
Seo J, Park YS, Kweon TH, Kang J, Son S, Kim HB, Seo YR, Kang MJ, Yi EC, Lee Y-h, Kim J-H, Park B, Yang WH and Cho JW (2021) *O*-Linked N-Acetylglucosamine Modification of Mitochondrial Antiviral Signaling Protein Regulates Antiviral Signaling by Modulating Its Activity. Front. Immunol. 11:589259. doi: 10.3389/fimmu.2020.589259

Post-translational modifications, including *O*-GlcNAcylation, play fundamental roles in modulating cellular events, including transcription, signal transduction, and immune signaling. Several molecular targets of *O*-GlcNAcylation associated with pathogen-induced innate immune responses have been identified; however, the direct regulatory mechanisms linking *O*-GlcNAcylation with antiviral RIG-I-like receptor signaling are not fully understood. In this study, we found that cellular levels of *O*-GlcNAcylation decline in response to infection with Sendai virus. We identified a heavily *O*-GlcNAcylated serine-rich region between amino acids 249–257 of the mitochondrial antiviral signaling protein (MAVS); modification at this site disrupts MAVS aggregation and prevents MAVS-mediated activation and signaling. *O*-GlcNAcylation of the serine-rich region of MAVS also suppresses its interaction with TRAF3; this prevents IRF3 activation and production of interferon-β. Taken together, these results suggest that *O*-GlcNAcylation of MAVS may be a master regulatory event that promotes host defense against RNA viruses.

Keywords: host defense mechanism, innate immunity, mitochondrial antiviral signaling protein, *O*-linked N-Acetylglucosamine (*O*-GlcNAc), RIG-I-like receptors signaling

INTRODUCTION

Innate immune signaling in vertebrate species is orchestrated by three types of receptor families; toll-like-receptors (TLRs), NOD-like receptors, and RIG-I-like receptors (RLRs). Specifically, when an RNA virus enters a host cell, the viral double-stranded (ds)RNA exposed to the cytoplasm is detected by RLRs, as opposed to that recognized by TLRs on the cell surface. Upon detection of the

viral dsRNA, RIG-I undergoes various post-translational modifications, including acetylation and ubiquitination (1–3). This activated form of RIG-I then binds to mitochondrial antiviral signaling protein (MAVS), which is located in the mitochondrial outer membrane (4). The RIG-I-MAVS complex induces the formation of fully activated prion-like aggregates via caspase recruitment domain (CARD-CARD) interactions (5, 6). The resulting MAVS aggregates then recruit the E3 ligases, TRAF2, 3, and 6, to promote K63-linked ubiquitination to activate downstream kinases, including TBK1 and IKKε (3, 7). Interferon (IFN) regulatory factor-3 (IRF3) and NF-κB are then phosphorylated sequentially and translocated to the nucleus; these transcription factors (TFs) promote the production of type I IFNs, pro-inflammatory cytokines, and antiviral factors that are secreted and can modulate the responses of neighboring cells (5). This process ultimately contributes to host defense by promoting virus clearance.

Immune cells have well-established TLR systems that facilitate rapid and precise responses to pathogens. Macrophages play a significant role in governing optimal interactions between the TLRs and RLR. By contrast, expression of TLR genes in both epithelial cells and fibroblasts is remarkably low (8). As such, MAVS-mediated RLR signaling is a critical component of the immunological response to RNA virus infection of epithelial cells. Macrophages rely on important connections between glucose metabolism and antiviral host responses (9, 10). Specifically, increased glucose metabolism in macrophages at relatively early time points after virus infection can accelerate of the development of the innate immune response (9, 10). However, the relationship between glucose metabolism and RLR signaling in epithelial cells at later time point in infection, notably in cells that with ubiquitous expression of MAVS, should be further evaluated.

The processes leading to *O*-linked N-Acetylglucosamine (*O*-GlcNAc) are regulated by various cellular signals and external stress stimuli and is among the most sensitive and dynamic of the post-translational modifications (11, 12). Many proteins in the nucleus, cytoplasm, and mitochondria are targets of *O*-GlcNAc transferase (OGT) (13). OGT catalyzes the reversible attachment of a GlcNAc moiety to the hydroxyl groups of the serine or threonine residues using UDP-GlcNAc from the hexosamine biosynthetic pathway (HBP) as a substrate; *O*-GlcNAcase (OGA) catalyzes the removal of *O*-GlcNAc from the protein target (11–14). *O*-GlcNAc modifications serve to modulate mitochondrial motility through factors including Milton 1 (15) and mitochondrial trafficking via the actions of trafficking kinesin (TRAK) protein (16); likewise, *O*-GlcNAc modifications of proteins including Drp1 and OPA1 serve to regulate mitochondrial fission and fusion (17). *O*-GlcNAcylation has been identified at the C-terminus of MAVS, which is a key adapter protein in the RLR signaling pathway (9, 10); this modification has been shown to promote antiviral immunity. Interestingly, the serine/threonine content of MAVS is ~20% (i.e.,108 of 540 amino acids); as such, many sites are candidates for post-translational modification besides those previously identified.

Pathogen infection threatens host cell survival. Results from several reports have suggested a link between pathogen infection and levels of intracellular *O*-GlcNAcylation. For example, the DNA viruses herpes simplex virus (HSV) and the cytomegalovirus rely on OGT activity and *O*-GlcNAcylation to support their replication, proliferation, and propagation (18). Furthermore, high levels of OGT activity and *O*-GlcNAcylation were detected in human papillomavirus (HPV)-induced cervical neoplasms; increased levels of *O*-GlcNAcylation were observed in mouse embryonic fibroblasts in response to HPV E6 oncoprotein overexpression (19). Despite these findings, the way in which host cells defend themselves from virus infection and promote innate immune signaling via *O*-GlcNAcylation is still unclear.

Here, we report that transcription of OGT is dramatically decreased at early time points after infection with an RNA virus; this contributes to the depletion of the *O*-GlcNAcylation of MAVS at later time points after infection, which serves to promote an innate immune response. We also identified a heavily *O*-GlcNAcylated serine-rich region of MAVS that spans amino acids Serine 249 through Serine 257. *O*-GlcNAcylation was blocked via deletion of the MAVS serine-rich region (amino acids 249–257); this promoted the aggregation of MAVS, strengthened the interaction between MAVS and TRAF3, and ultimately resulted in an increase in the production of interferon-β (IFN-β). Collectively, these results provide new insights into the cross-talk between host defense mechanisms and *O*-GlcNAc metabolism and reveal both novel and distinctive antiviral functions mediated by *O*-GlcNAcylation.

MATERIALS AND METHODS

Cell Cultures

All epithelial cell lines used in this study were incubated at 37°C in 5% CO_2. HEK293 and MDA-MB-231 cells were cultured in Dulbecco's Modified Eagle's Medium (DMEM, Lonza, Basel, Switzerland) supplemented with 10% fetal bovine serum (HyClone, Logan, UT, USA). A549 was cultured in ATCC-formulated F-12K Medium (ATCC, USA, Catalog No. 30-2004) supplemented with 10% fetal bovine serum. HT-29, and U937 were cultured in Roswell Park Memorial Institute (RPMI) 1640 medium with HEPES and L-glutamine (HyClone, South Logan, Utah, USA, SH30255.01).

Sendai Virus Infection

SeV (Cantell strain; Charles River Laboratories) was used to infect cells at a concentration of 100 hemagglutination units (HAU)/ml. HEK293, A549, and other cells were plated 24 h before infection. Cells were infected with SeV in serum-free DMEM or RPMI-1640 for 1 h at 37°C, washed with 1× phosphate-buffered saline, and incubated in complete medium for various periods of time as indicated for each experiment.

Plasmids and Transfection

The plasmid pCS4-Myc-MAVS was kindly provided by Dr. Yukiko Gotoh (University of Tokyo, Tokyo, Japan). Myc-MAVS-1-265 and Myc-MAVS-266-540 were cloned into the pcDNA3.1-MycHisC

expression vector. Wild-type and mutant forms of human MAVS wild type were prepared by PCR and cloned into the pRK5-Flag expression vector (Genentech). The mutations were confirmed by DNA sequence analysis (Bionics, South Korea). The plasmid pEFBos-Flag-N-RIG was kindly provided by Dr. Michael Gale (University of Washington School of Medicine, Washington, USA), and the plasmid pKH3-3XHA-TRAF3 was kindly provided by Dr. Ying Zhu (Wuhan University, Wuhan, China). Human Flag-OGT, Flag-OGA, and Myc-OGT were cloned into the p3XFlag-CMV^{TM}-7.1 expression vector (Sigma-Aldrich) and into the pcDNA3.1-MycHisC vector. For transient overexpression, cells were transfected using Omicsfect (OmicsBio, Taipei, Taiwan) in serum-free medium according to the manufacturer's instructions for 24–48 h. In this paper, we transfected cells with DNA expression vectors or with the empty vector as control.

Reagent and RNAi Interference

Cells were treated with 1 μM Thiamet-G (Sigma-Aldrich) for 2 to 4 h before SeV infection or transfections. Cycloheximide (Sigma-Aldrich) treatment was performed for the times indicated. Cells were collected at each time point indicated. Transfection with poly (I:C) (Sigma-Aldrich) was performed using the TransIT-2020 Transfection Reagent (Mirus Bio, USA) according to the manufacturer's instructions. To establish knock-down of OGT or MAVS via siRNA interference, cells were transfected with siRNAs targeting OGT or MAVS with Lipofectamine RNAi MAX (Invitrogen, USA) according to the manufacturer's transfection protocol. The siRNA sequences targeting these proteins were as follows:

siCTL (control), #1, duplex, Cat.SN-1002, Bioneer, Korea siOGT, #1, sense, 5′- UAAUCAUUUCAAUAACUGCUU CUGC (dTdT) - 3′ siOGT, #1, antisense, 5′- GCAGAAGC AGUUAUUGAAAUGAUUA (dTdT) - 3′ siMAVS, #1, sense, 5′- GAGUCAGCCAUGAUUGCUU (dTdT) - 3′ siMAVS, #1, antisense, 5′- AAGCAAUCAUGGCUGACUC (dTdT) - 3′ siMAVS, #2, sense, 5′- GCUCACCAAUCCAGCACCA (dTdT) - 3′ siMAVS, #2, antisense, 5′- UGGUGCUGGAUUGGUGAGC (dTdT) - 3′.

Western Blotting, Succinylated-Wheat Germ Agglutinin Lectin Precipitation, and IP

For Western blotting assays, cells were lysed with buffer A (150 mM NaCl, 1 mM EDTA, 50 mM Tris-HCl (pH7.4), 1% NP-40) supplemented with a protease inhibitor cocktail (Roche, Mannheim, Germany) and a phosphatase inhibitor cocktail (Roche, Germany). Preparation of sWGA was as previously described (20). Briefly, 1.5 to 2 mg of total cell lysates were incubated with agarose-conjugated sWGA (Vector Laboratories, Burlingame, CA, USA) overnight at 4°C. For IP, 1.5 to 2 mg of total cell lysates were incubated with agarose-conjugated anti-FLAG antibody (MBL, Woburn, USA) or anti-Myc antibody (MBL, Woburn, USA) for 2 h at 4°C. For IP of endogenous MAVS, 3 mg of total cell lysates were incubated with anti-MAVS antibody (#166583, Santa Cruz, Dallas, TX, USA) overnight at 4°C followed by agarose-conjugated protein A/G (Santa Cruz, Dallas, TX, USA) for 2 h at room temperature. Purified proteins in sWGA/IP precipitates were washed four times with buffer B (150 mM NaCl, 2 mM EGTA, 2 mM $MgCl_2$, 20 mM HEPES (pH 7.4), and 0.1% NP-40) and were eluted with sodium-dodecyl sulfate (SDS) loading buffer at 95°C for 5 min. The eluents were analyzed via Western blots probed with specific antibodies described in the section to follow. For co-IP experiments, 1.5 to 2 mg of total cell lysates were lysed with buffer C (150 mM NaCl, 0.1 mM EDTA, 1 mM dithiothreitol, 50 mM Tris-HCl (pH 7.4), and 0.5% Triton-X100). For Western blotting, 20 to 30 μg of total cell lysate was loaded onto 8% to 10% SDS-PAGE gel. Exceptionally, 60 μg of total cell lysate was loaded on the SDS-PAGE gel to detect p-IRF3. The same amount of protein was loaded in each experiment. After separation onto SDS-PAGE gel, proteins are transferred to NC membrane to detect signals. EZ-Western kit (DoGenBio) or SuperSignal West Femto Chemiluminescent Substrate (Thermo Fisher Scientific, Inc.) and Amersham Imager 600 (GE Healthcare Life Sciences, Little Chalfont, UK) were used to signal detection. For quantifying signals, the immunoreactive protein band was detected and the integrated signal intensity was measured using AI600 imager system software. Thereafter, *O*-GlcNAcylation levels were normalized to integrated signal intensity of β-actin or GAPDH, the loading control of the same gel for each cell type. OGT protein levels were normalized to β-actin, a loading control of the same gel. To quantify proteins and *O*-GlcNAcylation levels, Loading control proteins including β-Actin and GAPDH, and target proteins to observe or *O*-GlcNAc levels were measured using AI600 imager system (GE Healthcare, Chicago, IL, USA) software.

Antibodies

The primary antibodies used for Western blotting included anti-*O*-GlcNAc (#MA1-072, Thermo Scientific), anti-OGT (DM17, #O6264, Sigma-Aldrich), anti-OGA (EPR7154(B) #ab124807, Abcam), anti-MAVS (#A300-782A, Bethyl Laboratories), anti-c-Myc (#sc-789, Santa Cruz), anti-GAPDH (#sc-32233, Santa Cruz), anti-IRF3 (#sc-8092, Santa Cruz), anti-SeV (#PD029, MBL), anti-FLAG (#PM020, MBL), anti-β-actin (#4970, CST), and anti-p-IRF3 (D601M, #29047, CST). NC membranes were probed with primary antibodies followed by secondary antibodies conjugated with HRP(horseradish peroxidase) in a ratio of 1:10000. Secondary antibodies included goat anti-rabbit IgG (#111-035-003, Jackson Immunoresearch), goat anti-mouse IgG (#115-035-003, Jackson Immunoresearch), and goat anti-mouse IgM (#115-005-020, Jackson Immunoresearch).

Semi-Denaturing Detergent-Polyacrylamide Gel Electrophoresis, Isolation of Mitochondria, and Semi-Denaturing Detergent-Agarose Gel Electrophoresis

SDD-PAGE was performed as previously described (21) to detect SDS-resistant high-molecular weight MAVS aggregates. Briefly, HEK293 cells were transfected with plasmids encoding Flag-MAVS or Myc-OGA or empty vector alone; after 24 h, cells were

harvested and lysed with Buffer A. The lysates were mixed with a 4× sample buffer both with and without β-mercaptoethanol followed by SDD-PAGE. To detect endogenous MAVS aggregates, mitochondria were isolated from cultured cells using a Mitochondria Isolation Kit (#89874, Thermo Scientific, Rockford, IL, USA) according to the manufacturer's instructions. Then, the mitochondrial fraction was re-suspended in 1% diaminodiphenylmethane-containing lysis buffer and analyzed by 2% agarose SDD-AGE.

Real-Time Quantitative RT-PCR

Total RNA was extracted from cultured cells using the TRIzol reagent (Invitrogen, USA). To obtain cDNA, RT was performed on 1 μg of the extracted total RNA using ReverTra Ace qPCR RT Master Mix (Toyobo, Japan) according to the manufacturer's instructions. The qPCR was conducted using SYBR Premix Ex Taq (Takara, Japan) using a CFX96™ real-time system (Bio-Rad). Relative mRNA levels of OGT and IFN-β were normalized to those of actin. The qPCR primer sequences were as follows:

IFN-β, Forward 5′-AAA CTC ATG AGC AGT CTG CA-3′
IFN-β, Reverse 5′-AGG AGA TCT TCA GTT TCG GAG G-3′
OGT, Forward 5′-CTT TAG CAC TCT GGC AAT TAA ACA G-3′
OGT, Reverse 5′-TCA AAT AAC ATG CCT TGG CTT C-3′
Actin, Forward 5′-AGA GCT ACG AGC TGC CTG AC-3′
Actin, Reverse 5′-AGC ACT GTG TTG GCG TAC AG-3′

Mapping O-GlcNAc Sites in Mitochondrial Antiviral Signaling Protein

The extracted peptides were dissolved in Solvent A (0.1% formic acid in H_2O). Peptides were separated using a PepMap™ RSLC C18 column (Thermo Fisher Scientific, San Jose, CA) with a linear gradient of 2% to 38% Solvent B (0.1% formic acid in acetonitrile) over 75 min at a flow rate of 300 ml/min. The sample was analyzed by Orbitrap Fusion Lumos Tribrid mass spectrometer (Thermo Fisher Scientific, San Jose, CA) that interfaced with an Easy nanoLC 1200 system (Thermo Fisher Scientific, San Jose, CA). The spray voltage was set to 1.9 kV and the temperature of the heated capillary was set to 275°C. The equipment was set in data-dependent mode with one survey MS scan followed by 10 MS/MS scans and a dynamic exclusion time of 30 s. Full scans were acquired at 350 to 1600 m/z. The resolution on mass spectrometry was 120,000 and the automatic gain control (AGC) target was set to $4e^5$. The MS/MS scans had a resolution of 30,000; the AGC target was set to $5e^4$ for high-energy collisional dissociation fragmentation. If oxonium product ions (m/z 204.0867, 138.0545) were observed in the higher-energy collisional dissociation (HCD) spectra, EThcD with user-defined charge dependent reaction time (45.20 ms for 3+ charged, 25.42 ms for 4+ charged) with 15% or 17% HCD supplemental activation was performed in a subsequent scan on the same precursor ion selected for HCD. The EThcD MS/MS scans had a resolution of 30,000 with the AGC target set to 1e5. The maximum injection time was 120 ms.

Collected MS/MS data were used in a search of the decoy UniProt human database (Release 2019_11, 186 532 entries) for the estimation of the false discovery rate (FDR) with the Sequest HT software in Proteome Discoverer 2.2 (Thermo Fisher Scientific). Precursor and fragment ion tolerance were set to 10 ppm and 0.02 Da, respectively. Trypsin was chosen as the enzyme with a maximum allowance of up to two missed cleavages. The following modifications were defined as static modification of carbamidomethyl (Cys), dynamic modification of HexNAc 203.079 Da (Ser and Thr), Phospho 79.966 Da (Ser and Thr), and Oxidation (Met). The data were also searched against the decoy database and the results were used to calculate q values of peptide–spectrum matches (PSMs) using the Fixed Value PSM Validator within the Proteome Discoverer. Peptide and protein results were filtered to a 1% FDR.

Statistical Analysis

Data are presented as mean ± SEM based on at least three independent experiments. Statistical analysis was performed using two-tailed Student t-tests to compare results from two groups and by One-way analysis of variance for multiple groups. A P values of <0.05 considered as significant.

RESULTS

Reduced *O*-GlcNAcylation in Response to Sendai Virus Infection Stimulates the Innate Immune Response

The glucose concentration in cells is closely associated with the production of UDP-GlcNAc via the HBP. Lactate, a glucose intermediate, was recently identified as a suppressor of MAVS-mediated RLR signaling (22). OGT, an enzyme that promotes *O*-GlcNAc cycling and that uses UDP-GlcNAc as a substrate, is expressed in most tissues, including epithelial cells (23). *O*-GlcNAcylation in cells functions as both a nutrient and stress sensor (12). In this study, we evaluated changes in *O*-GlcNAcylation in various types of cells over time in response to infection with SeV; this is a single-stranded RNA virus pathogen that presents dsRNA intermediates to pattern recognition receptors in the cytosol. Global levels of *O*-GlcNAcylation were drastically reduced at the later time points in response to SeV infection of HEK293 and A549 cells (**Figure 1A**). The primary cell, MEF (mouse embryonic fibroblast) cells, also showed a decrease in *O*-GlcNAcylation (**Figure 1A**). Furthermore, we also confirmed that SeV infection resulted in elevated levels of intracellular *O*-GlcNAcylation in monocyte-macrophage U937 cells in response to differentiation with phorbol 12-myristate 13-acetate; these findings are consistent with those reported previously in which infection of macrophages with an RNA virus resulted in a substantial increase in intracellular *O*-GlcNAcylation (**Figure 1A**) (9, 10). As shown in the present study, elevated levels of *O*-GlcNAcylation levels were detected only in U937 cells differentiated into macrophages (**Figure S1A**); by contrast, the global decline in *O*-GlcNAcylation levels was observed in both undifferentiated and differentiated U937 cells at the later time points after infection (**Figures 1A**, **S1A**). Furthermore, cells of the breast epithelial line MDA-MB-231 and the colon epithelial

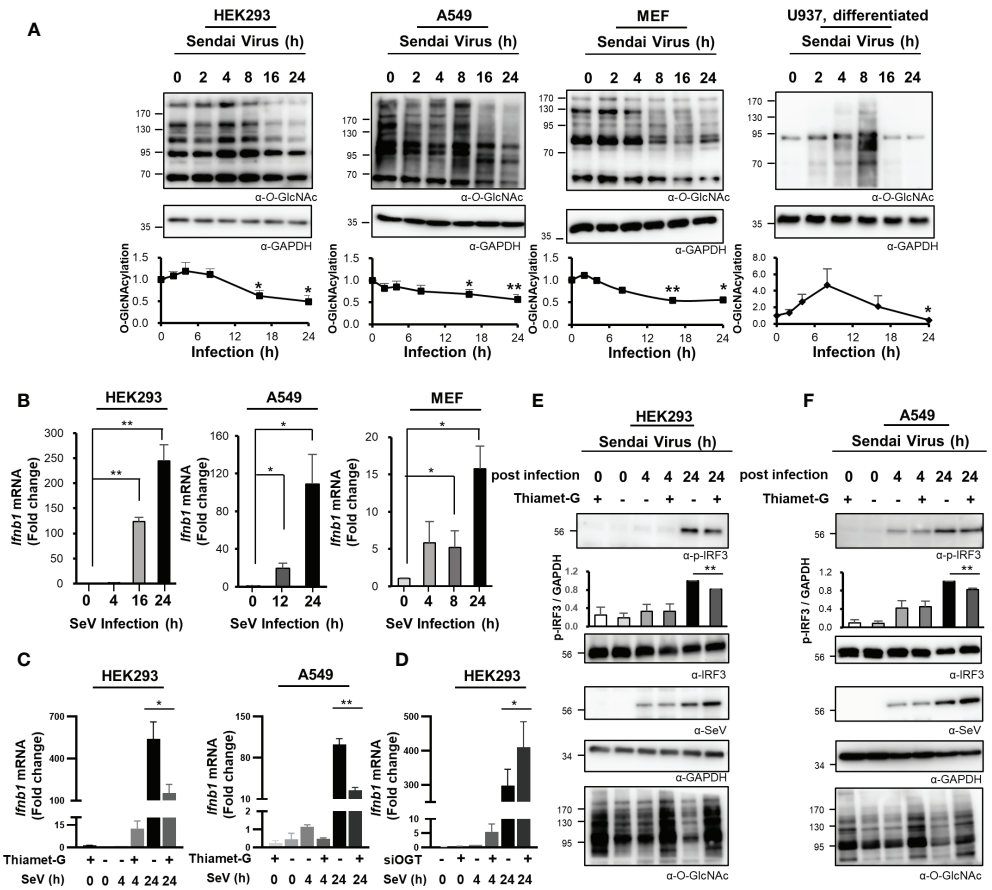

FIGURE 1 | Reduced *O*-GlcNAcylation in response to RNA virus infection activates the innate immune response. **(A)** *O*-GlcNAcylation over time after infection with Sendai virus (SeV; 100 HAU at t = 0) in HEK293, A549, MEF, and PMA-differentiated U937 cells as detected via Western blot analysis. In the graphs, cellular *O*-GlcNAcylation was normalized to GAPDH. **(B)** Expression of IFN-β mRNA over time as measured by real-time qRT-PCR after infection of HEK293 (left), A549 (middle) and MEF (right) cells with SeV (100 HAU). **(C)** HEK293 (left) and A549 (right) cells were treated with 1 μM of Thiamet-G(+) or PBS (–) for 4 h before infection with SeV (100 HAU). Cells were collected at 4 and 24 h post-infection. Expression of IFN-β was measured by real-time qPCR. Statistical significance was determined by two-tailed student t-test. **(D)** HEK293 cells were transiently transfected with siCTL or siOGT for 48 h before infection with SeV (100 HAU). Cells were collected at 4 and 24 h post-infection. Expression of IFN-β was measured by real-time qPCR. **(E, F)** Under the same conditions as in **(C)**, phosphorylation of IRF3 (Ser-396-p-IRF3) was evaluated via Western blot. Replication of SeV in HEK293 (left) and A549 (right) was also evaluated via Western blot. Statistical significance was determined by two-tailed student t-test. All experiments were repeated at least three times. Each figure was statistically analyzed with the indicated n number. **(A)** HEK293 (left, n = 4) A549 (middle to left, n = 3) MEF (middle to right, n = 3) U937(right, n = 4) **(B)** HEK293 (left, n = 3) A549 (middle, n = 4) MEF (right, n = 3) **(C)** HEK293(left, n = 5) A549(middle, n = 3) **(D)** HEK293(n = 4) **(E)** HEK293(n = 3) **(F)** A549(n = 3). Data are presented as mean ± standard error (SEM); $^{*}p < 0.05$, $^{**}p < 0.01$.

line HT-29 also responded to SeV infection with reduced levels of *O*-GlcNAcylation (**Figure S1A**). In order to confirm that reduced *O*-GlcNAcylation levels in the results presented above are due to host immune responses rather than direct effects of Sendai virus itself, we treated HEK293 and A549 with poly(I:C) and then observed the *O*-GlcNAcylation levels at later points; however there was no change (**Figure S1B**). Therefore, we hypothesized that a global decrease in cellular *O*-GlcNAcylation during the later phases of SeV infection is a phenomenon common to many cell targets. Remarkably, we also confirmed that IFN-β expression reached its peak in both HEK293 and A549 cells at 24 h of SeV infection (**Figure 1B**). In addition, MEF cells showed the highest IFN-β expression at 24 h, which is consistent with the expression in HEK293 and A549 (**Figure 1B**). IFN-β is a major type I interferon that is synthesized and secreted in response to infection that promotes viral clearance and host immunity. Therefore, we speculated that the decrease in cellular *O*-GlcNAcylation observed at 24 h of infection may have a direct impact on IFN-β expression. To examine this hypothesis, we measured IFN-β mRNA levels in SeV-infected HEK293 and A549 cells that were treated with the OGA inhibitor, Thiamet-G, using real-time reverse transcription–polymerase chain reaction (RT-PCR). The results revealed that transcription of IFN-β was inhibited in response to increased levels of cellular *O*-GlcNAcylation achieved by treatment with Thiamet-G (**Figure 1C**). We conversely inhibited OGT activity through siRNA to demonstrate the importance of OGT in the inhibition of IFN-β

expression. As a result, it was confirmed that the expression level of IFN-β increased in HEK293 when OGT was knocked down (**Figure 1D**). Under the same conditions as in **Figure 1C**, Thiamet-G introduced 24 h after SeV infection of HEK293 and A549 cells resulted in reduced phosphorylation of IRF3 by ~19% and ~17%, respectively, in association with amplified replication of SeV (**Figures 1E, F**). These results suggest that reduced levels of *O*-GlcNAcylation observed during the later stages of infection with an RNA virus serves to promote the innate immune response.

Host Cell-Mediated Downregulation of *O*-GlcNAc Transferase Transcription in Response to Sendai Virus Infection

Cellular levels of *O*-GlcNAcylation decreased at 24 h after SeV infection (**Figure 1A**). Therefore, we examined the expression of immunoreactive OGT protein at various times after infection as indicated. These observations revealed that the levels of OGT protein decreased drastically in response to the strong induction of the innate immune response (**Figures 2A, B**, **S2A**). To investigate this observation further, OGT mRNA levels were measured by real-time RT-PCR. Surprisingly, we found that transcription of OGT decreased dramatically at all time points examined, most notably at the earliest time point after infection (i.e., 4 h) (**Figures 2C**, **S2B**). Given that some viruses alter the host transcriptome to facilitate their own replication and proliferation, these results raised additional questions as to whether the decrease in OGT transcription was driven directly by the virus. To address this question, we transfected cells with poly(I:C), which is a ligand capable of activating RLR-mediated signaling in the absence of an overt virus infection. Similar to SeV infection, transfection with poly(I:C) also promoted a

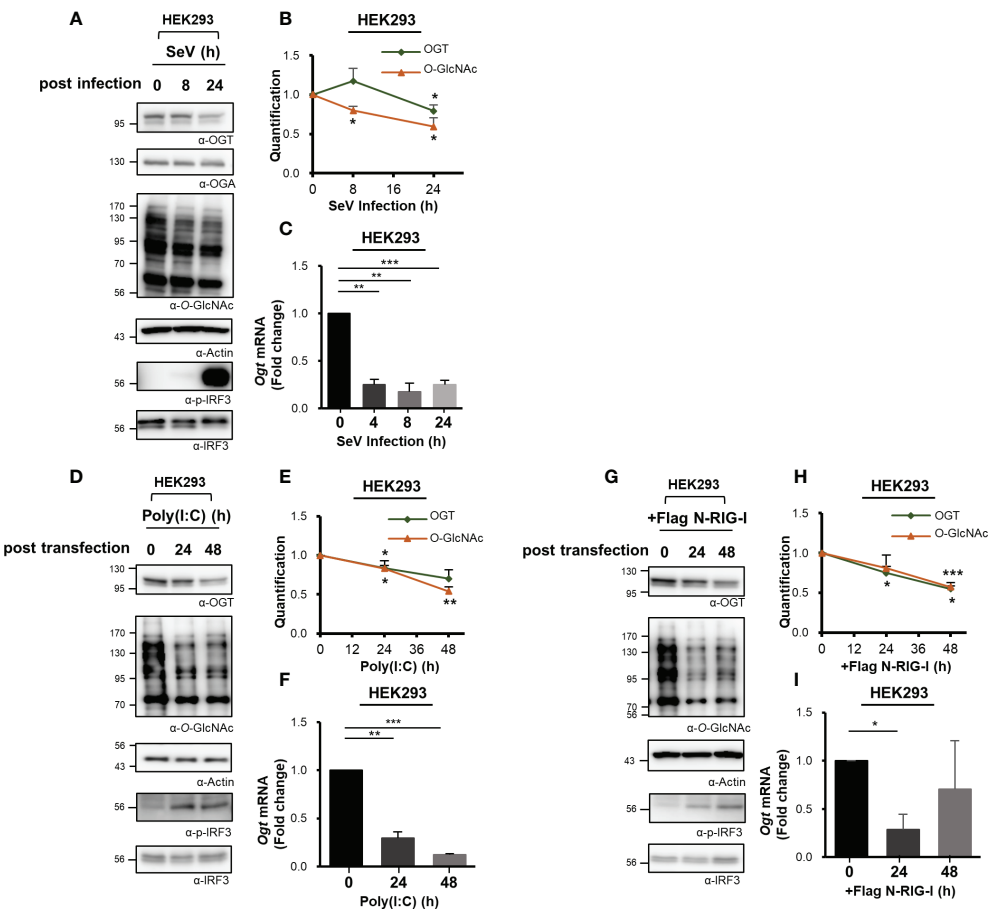

FIGURE 2 | Downregulated transcription of *O*-GlcNAc Transferase (OGT) in response to virus infection. **(A)** Immunoreactive OGT was evaluated via Western blot analysis in HEK293 cells infected with SeV (100 HAU) at the time points indicated. **(B)** Expression of OGT and *O*-GlcNAc as shown in **(A)** was normalized to actin or GAPDH. **(C)** Real-time qPCR was performed to measure OGT mRNA expression levels. **(D)** 10 μM Poly (I:C) was transfected into HEK293 cells which were evaluated at the times indicated. Western blot analysis was performed to detect immunoreactive OGT protein. **(E)** OGT and *O*-GlcNAc as shown in **(D)** were normalized to levels of actin or GAPDH. **(F)** Real-time qPCR was performed to measure OGT mRNA expression levels. **(G)** To activate RLR signaling, the N-RIG-I plasmid was used to transfect HEK293 cells; cells were collected at the times indicated to measure OGT protein and mRNA expression levels. **(H)** Expression levels of OGT and *O*-GlcNAc in **(G)** were normalized to actin or GAPDH. All experiments were repeated at least three times. **(I)** Real-time qPCR was performed to measure OGT mRNA expression levels. Each figure was statistically analyzed with the indicated n number. **(A)**, **(B)** n = 4, **(D, E, G, H)** n = 3 and **(C, F, I)** n = 3. Data are presented as mean ± SEM; $*p < 0.05$, $**p < 0.01$, $***p < 0.001$.

decrease in OGT protein levels (**Figures 2D, E**, **S2C**). In addition, in MEF primary cells and HDF (Human dermal fibroblast) primary cells, OGT protein levels decreased in response to poly(I:C) transfection (**Figure S2D**). Furthermore, levels of OGT mRNA were also significantly reduced in cells transfected with poly(I:C) (**Figures 2F**, **S2E**). As such, we inferred that the host response, rather than the virus per se, promoted the observed reductions in OGT gene transcription. This conclusion was supported by findings associated with the overexpression of activated (N-)RIG-I. Overexpression of N-RIG-I has been reported to promote MAVS activation (24); N-RIG-I DNA constructs were transfected into HEK293 cells, resulting in a decrease in OGT protein and mRNA levels; these findings are consistent with the results shown in **Figures 2D, F** (**Figures 2G, I**).

O-GlcNAcylation Directly Regulates Mitochondrial Antiviral Signaling Protein-Mediated Expression of Interferon-β

Given the decline in *O*-GlcNAcylation in various cell types and the resulting impact on RLR-mediated signaling and the downstream production of IFN-β, we then aimed to identify the specific mechanisms underlying this response. MAVS is a powerful immune sensor that promotes innate immune responses and stimulates the production of IFN-β (25, 26). We overexpressed MAVS in HEK293 cells to induce a condition that mimicked viral infection (5). Interestingly, the IFN-β mRNA expression induced in response to MAVS overexpression dropped significantly in cells treated with Thiamet-G (**Figure 3A**). Furthermore, the expression of IFN-β mRNA was inhibited when MAVS and OGT were both overexpressed. By contrast, expression of IFN-β mRNA induced by overexpression of MAVS overexpression increased even further when cellular *O*-GlcNAcylation was reduced by co-overexpression of OGA (**Figure 3B**). The same findings were observed in assays designed to detect IFN-β protein synthesis and secretion (**Figure 3C**). On the basis of these results, we hypothesized that cellular *O*-GlcNAcylation may have a direct role in the regulation of MAVS activity, notably upon activation of RLR signaling. To examine this hypothesis, MAVS knock-down was achieved using targeted siRNAs (**Figure S3A**). As shown in **Figure 3D**, Thiamet-G treatment inhibited the expression of IFN-β in response to SeV infection in the control group but in cells transfected with siMAVS. As such, we concluded that *O*-GlcNAcylation regulates RLR signaling in a MAVS-dependent manner.

Mitochondrial Antiviral Signaling Protein Is a Direct Target of *O*-GlcNAc Transferase

O-GlcNAc transferase (OGT) catalyzes the *O*-GlcNAcylation of numerous mitochondrial proteins (12). As such, we evaluated *O*-GlcNacylation of endogenously expressed MAVS via precipitation studies conducted with succinylated-wheat germ agglutinin (sWGA). Using this approach, we found that endogenous MAVS was *O*-GlcNAcylated (**Figure 3E**). Furthermore, recombinant (overexpressed) MAVS was also *O*-GlcNAcylated; *O*-GlcNAcylation of this target was increased in response to OGT overexpression (**Figures 3E**, **S3B**). We also evaluated *O*-GlcNAcylation of other intracellular proteins including STING, which is another immune sensor, as well as IKKϵ, a TBK1-associated factor involved in the innate immune response. Despite these efforts, our results indicated that MAVS alone was targeted for *O*-GlcNAcylation (**Figure 3F**). Even when IKKϵ or TBK1 was overexpressed with Flag tagged MAVS to activate MAVS signaling, we could not detect *O*-GlcNAcylation of IKKϵ or TBK1 (**Figure S3C**). We divided the 540-amino acid sequence of MAVS into N-terminal (1–265) and C-terminal (266–540) fragments to identify specific sites of *O*-GlcNAcylation. Full-length MAVS, the MAVS N-terminal fragment, and the MAVS C-terminal fragment were all overexpressed in HEK293 cells; *O*-GlcNAcylation of each polypeptide was investigated by sWGA-mediated precipitation. Significantly, we detected *O*-GlcNAcylation of both N- and C-terminal fragments of MAVS (**Figure 3G**). These results clearly indicate that there are potential *O*-GlcNAcylation sites in the N-terminal region of MAVS besides that previously identified (i.e., Serine 366) in its C-terminal region (9).

Mitochondrial Antiviral Signaling Protein Contains a Heavily *O*-GlcNAcylated Serine-Rich Region That Can Inhibit RIG-I-Like Receptors-Mediated Signaling

O-GlcNAcylation takes place at hydroxyl groups found on serine and threonine residues. Notably, serine and threonine represent 20% of the amino acids (108 of the total 540) in the MAVS polypeptide. *O*-GlcNAcylation sites within MAVS were identified by fusion mass spectrometry (Fusion M/S). A total of 20 *O*-GlcNAcylation sites were identified by this method (**Figures 4A–C**, **S4AF**). Remarkably, seven *O*-GlcNAcylation sites that were adjacent to one another were identified in a serine-rich region within the aforementioned N-terminal fragment of MAVS (**Figure 4C**). To evaluate the function of these *O*-GlcNAc modifications, we generated a MAVS mutant that deleted nine amino acids, including the seven potential *O*-GlcNAcylation sites (Δ249–257); *O*-GlcNAcylation levels were explored in HEK293 cells that overexpressed both the wild-type and the MAVS Δ249–257 deletion mutant. Consistent with the fusion M/S results, the *O*-GlcNAcylation levels of the MAVS Δ249–257 mutant were significantly lower than those detected in the MAVS wild-type polypeptide (**Figure 4D**). *O*-GlcNAcylation levels were also dramatically reduced in the 7S/T→7A substitution mutant in which all seven *O*-GlcNAcylation sites were substituted with alanine (**Figure 4E**). As such, we hypothesized that *O*-GlcNAcylation at the serine-rich region of MAVS would have an impact on IFN-β production in response to SeV infection. First, we examined phosphorylation of IRF3 to determine whether reduced *O*-GlcNAcylation in the MAVS Δ249–257 mutant had an impact on RLR-mediated signaling. We found that phosphorylation of IRF3 was increased in HEK293 cells transfected with MAVS Δ249–257 over that observed in response to MAVS wild-type when cells were infected with SeV (**Figure 4F**). Consistent with the results observed in HEK293 cells transfected with the MAVS Δ249–257 mutant, phosphorylation of IRF3 was further enhanced in cells transfected with the 7S/T→7A substitution mutant in

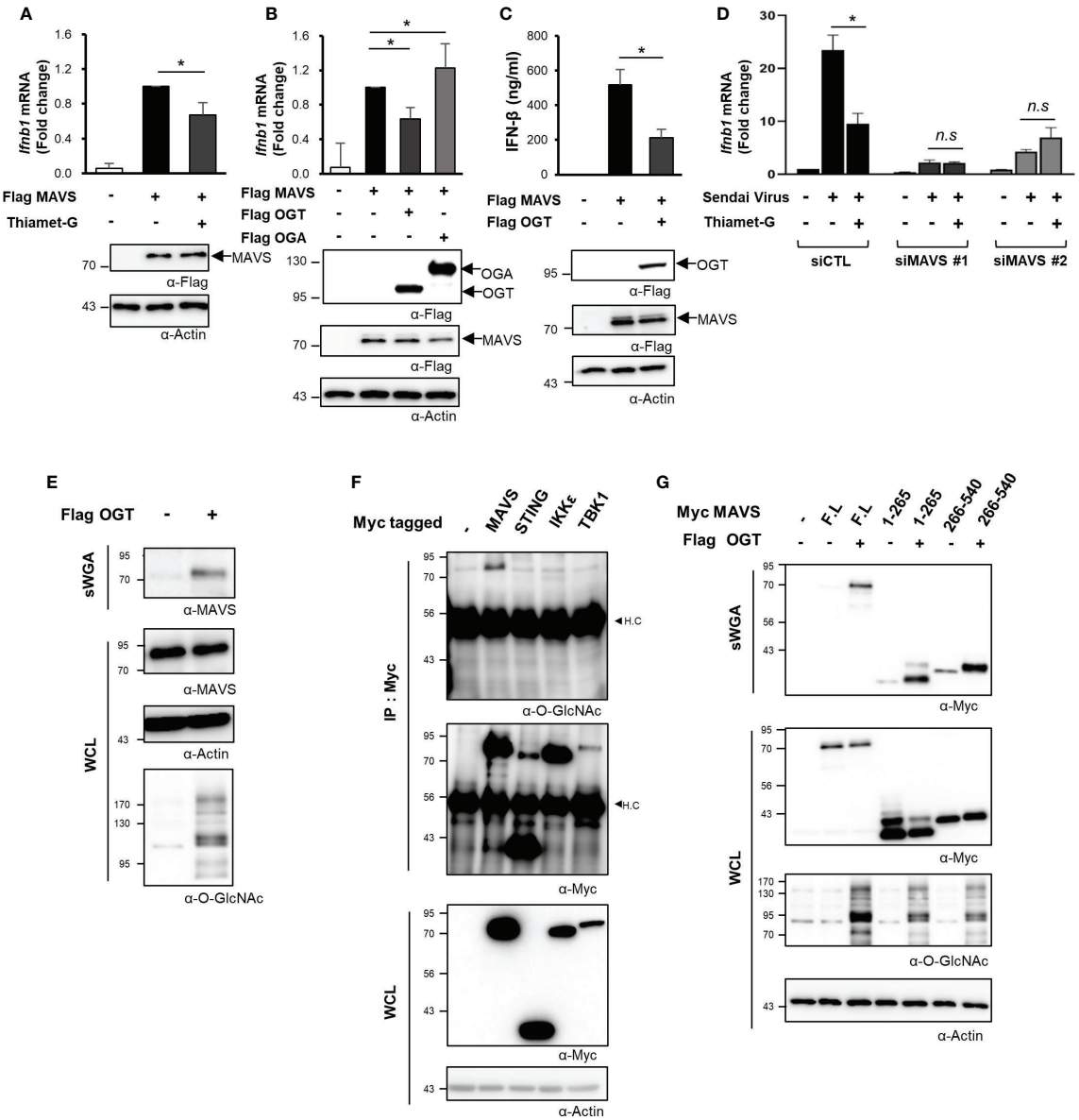

FIGURE 3 | *O*-GlcNAcylation directly regulates MAVS-mediated expression of IFN-β. **(A)** IFN-β mRNA was measured by real-time qPCR was conducted to measure mRNA expression levels under conditions that mimicked viral infections in HEK293 cells by treating with 1 μM Thiamet-G for 24 h before induction of MAVS overexpression via transfection of a Flag-MAVS expression plasmid. **(B)** IFN-β mRNA expression induced by MAVS overexpression under conditions mimicking virus infection was measured by real-time qPCR together with co-overexpression of OGT and OGA. **(C)** An ELISA assay was conducted to compare secretion of IFN-β in response to OGT overexpression with that observed in response to MAVS overexpression (control condition). **(D)** Knock-down of MAVS in HEK293 cells was performed via transfection with MAVS-targeting siRNAs and examined after 48 h. Inhibition of SeV-induced IFN-β production in response to treatment with Thiamet-G was not observed in cells with MAVS knock-down. *n.s* indicated not statistically significant. **(E)** Precipitation using the lectin, sWGA, was conducted to demonstrate *O*-GlcNAcylation of endogenous MAVS and to examine the increase in MAVS *O*-GlcNAcylation in response to OGT overexpression. 1.5—2 mg of whole cell lysates (WCLs) obtained from HEK293 were incubated with agarose-conjugated sWGA overnight at 4°C. Purified proteins in sWGA precipitates were eluted with 2× SDS loading buffer then analyzed via Western blotting. **(F)** IP and Western blots were performed to identify *O*-GlcNAcylated proteins associated with RLR signaling. 1.5—2 mg of WCLs obtained from HEK293 were incubated with agarose-conjugated anti-Myc antibodies for 2 h at 4°C. Purified proteins in IP precipitates were eluted with 2× SDS loading buffer and then analyzed via Western blotting. Of the major molecules involved in RLR signaling, only MAVS was subject to *O*-GlcNAc modification. H.C means heavy chain. **(G)** Precipitation with sWGA was to confirm the *O*-GlcNAcylation of the N- or C-termini of MAVS. Plasmids promoting overexpression of MAVS 1-265 and 266-540 were transfected and evaluated after 24 h with or without OGT. 1.5 to 2 mg of WCLs obtained from HEK293 were incubated with agarose-conjugated sWGA overnight at 4°C. Purified proteins in SWGA precipitates were eluted with 2× SDS loading buffer then analyzed via Western blotting. The 1–265 and 266–540 regions are both modified with *O*-GlcNAc. All experiments were repeated at least three times. **(A–G)** – indicated cells transfected with flag or myc empty vectors. Each figure was statistically analyzed with the indicated n number. **(A)** n = 6, **(B)** n = 5, **(C)** n = 3, **(D)** n=3. Statistical significance was determined by two tailed student t-test. Data are presented as mean ± SEM; $^{*}p < 0.05$, $^{**}p < 0.01$.

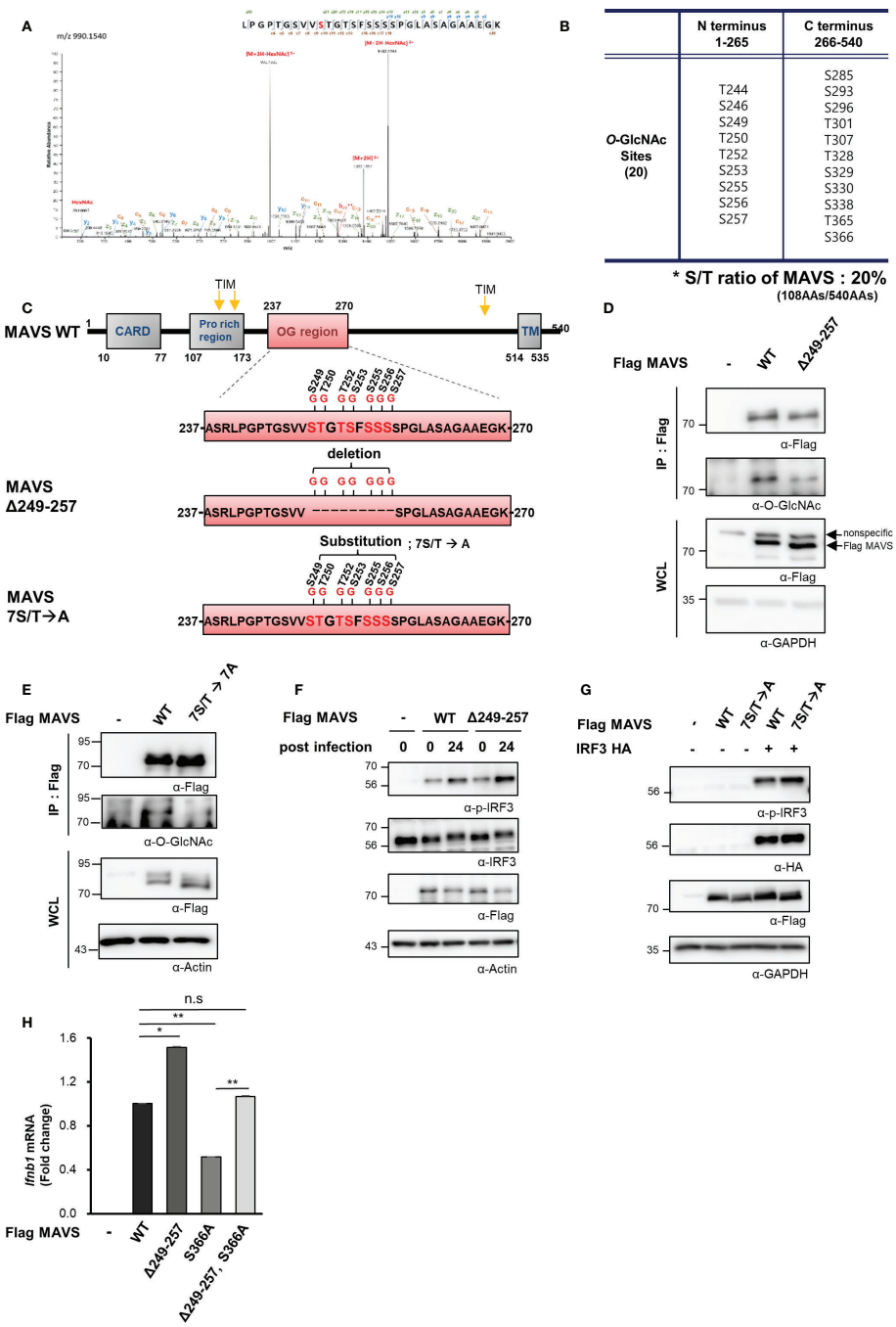

FIGURE 4 | MAVS contains a heavily O-GlcNAcylated serine-rich region that inhibits RLR signaling. **(A)** Fusion M/S analysis was conducted to identify sites of O-GlcNAcylation in MAVS. EThcD spectra of the O-glylcopeptide LPGPTGSVVSTGTSFSSSSPGLASAGAAEGK from human MAVS is as shown. The site of O-GlcNAc modification was identified as serine 249. The y, b, C, and z fragments detected are as indicated in the sequence. **(B, C)** MAVS O-GlcNAcylation sites and the protein structures of the wild-type and MAVS Δ249–257 mutant. **(D, E)** IP and Western blots were performed to compare the O-GlcNAcylation of wild-type MAVS with **(D)** the mutant in which the serine-rich region including the O-GlcNAcylation sites were detected and **(E)** the mutant with the 7S/T to alanine substitution. The pRK5-flag-tagged MAVS wild-type and mutant plasmids were transfected into HEK293 cells and evaluated 24 h later. WCLs were incubated with agarose-conjugated anti-FLAG antibody (M2) for 1–2 h at 4°C. **(F, G)** Western blot analysis of phospho-IRF3 (p-IRF3) in WCLs from HEK293 cells. The p-IRF3 levels were determined by transfection with pRK5-flag-tagged MAVS wild-type, **(F)** deletion mutant, or **(G)** substitution mutant plasmids followed by evaluation 24 h later; cells were infected with SeV (100 HAU) for 24 h followed by Western blotting. **(H)** Expression of IFN-β mRNA induced by overexpression of wild-type and mutant MAVS was measured by real-time qPCR. The decreased levels of IFN-β expression in response to the S366A mutant underwent full recovery in response to the Δ249–257 mutant containing S366A when compared to the wild type. n = 3. **(D–H)** Experiments were performed at least three times. **(D–H)** – indicated cells transfected with flag or myc empty vectors. Statistical significance of **(H)** was determined by one-way ANOVA. Results were presented as mean ± SEM; *p < 0.05, **p < 0.01.

response to SeV infection (**Figure 4G**). Furthermore, expression of IFN-β mRNA was also significantly elevated in cells transfected with the MAVS Δ249–257 mutant compared to the wild type (**Figure 4H**). Finally, and consistent with previous reports that describe *O*-GlcNAcylation at MAVS Serine 366 and its role in promoting RLR-mediated signaling, decreased expression of IFN-β was observed in cells transfected with a MAVS S366A mutant. Surprisingly, when compared to the results obtained from cells transfected with the MAVS S366A mutant, we observed full recovery of IFN-β expression upon deletion of the serine-rich 249–257 region from the S366A mutant. Collectively, these results suggest that *O*-GlcNAcylation at the serine-rich region of MAVS (amino acids 249–257) modulates MAVS-activated RLR-mediated signaling via a mechanism that is distinct and different from that associated with *O*-GlcNAcylation of S366.

Mitochondrial Antiviral Signaling Protein *O*-GlcNAcylation Interferes With the Formation of Its Aggregates

Thus far, we have demonstrated *O*-GlcNAcylation of the MAVS 249–257 serine-rich region results in down-regulated RLR signaling infection with SeV. We further examined the mechanism by which *O*-GlcNAcylation at this site suppresses the IFN-β response. Full activation of MAVS requires self-aggregation at the mitochondrial outer membrane. The aggregation and resolution responses of MAVS are strongly regulated by post-translational modifications, including ubiquitination (21, 27, 28). Results from earlier studies indicated that *O*-GlcNAcylation inhibited the formation of prion-like aggregates of proteins that include α-synuclein and tau (29, 30); as such, its role in preventing the formation of critical MAVS aggregates was explored. Intriguingly, upon co-overexpression of both MAVS and OGA, MAVS could form aggregates as revealed in a semi-denaturing detergent-polyacrylamide gel electrophoresis (SDD-PAGE) assay (**Figure 5A**). Furthermore, the degree of MAVS aggregation increased drastically in response to OGT knock-down (**Figures 5B**, **S5A**). Consistent with these results, endogenously generated MAVS aggregates were detected at higher levels in cells subjected to OGT knock-down during the later stages of SeV infection (at 16 h; **Figure 5C**). To exclude the possibility that the observed increase in MAVS aggregation was due to changes in MAVS protein stability that might result from reduced levels of *O*-GlcNAcylation, MAVS protein levels were evaluated in HEK293 and A549 cells treated with cycloheximide. Under these conditions, MAVS stability was not diminished in the presence or absence of Thiamet-G (**Figures S5B**, **S5C**). *O*-GlcNAcylation of endogenously expressed MAVS was found to have decreased at 24 h after SeV infection (**Figures 5D**, **S5D**). GlcNAc competition studies revealed that *O*-GlcNAcylation MAVS was significantly reduced under these conditions (**Figure 5D**). We then examined the degree of MAVS aggregation in cells overexpressing the MAVS Δ249–257 deletion mutant. As expected, the degree of aggregation was higher in cells overexpressing the MAVS Δ249–257 deletion mutant than that observed in cells overexpressing the MAVS wild type (**Figure 5E**); interestingly, we observed no increase in the degree of aggregation when comparing responses of the MAVS wild-type protein to that of the S366A mutant. Nevertheless, we were still able to observe the increased degree of aggregation in the deletion of the serine-rich 249–257 from the S366A mutant compared to the S366A mutant (**Figure 5E**). These results suggest that *O*-GlcNAcylation of MAVS specifically at the serine-rich region (249–257), restricts the formation of MAVS aggregates.

Mitochondrial Antiviral Signaling Protein *O*-GlcNAcylation Interferes With Its Interaction With TRAF3

The sequence of MAVS contains several TRAF-interacting motifs (TIMs) that facilitate its interactions with these signaling molecules. The interaction between MAVS and TRAFs is critical to activate MAVS-mediated downstream signaling. TRAF3 is recruited to aggregates of MAVS and thereby promotes the activation of IRF3 via the K63-ubiquitination of MAVS. The interaction between MAVS and TRAF3 was examined through co-immunoprecipitation (co-IP) studies designed to identify the mechanism by which *O*-GlcNAcylation of MAVS inhibits expression of IFN-β. The interaction between MAVS and TRAF3 was inhibited in cells overexpressing OGT (**Figure 5F**). Furthermore, we found that the interaction between TRAF3 and MAVS Δ249–257 was significantly enhanced compared with its interaction with wild-type MAVS (**Figure 5G**). Since there are previous reports that *O*-GlcNAcylation of MAVS regulates ubiquitination of MAVS, we needed to confirm whether *O*-GlcNAcylation at the serine-rich region (amino acids 249–257) also regulates ubiquitination of MAVS (9, 10). We confirmed that MAVS ubiquitination was slightly increased in MAVS Δ249–257 deletion mutant compared to wild type (**Figure S5E**). As such, we concluded that *O*-GlcNAcylation at the serine-rich region of MAVS specifically inhibits RLR signaling by interfering with the interaction between MAVS and TRAF3. Taken together, these findings suggest that *O*-GlcNAcylation is involved in modulating host defense mechanisms.

DISCUSSION

Dysregulated energy metabolism is directly linked to the pathogenesis of numerous diseases; an imbalance in energy metabolism has also been found to disrupt the host defense system (31, 32). In recent years, attempts have been made to identify a role for glucose metabolism, the central pathway associated with energy metabolism, in modulating one or more aspects of the innate immune response. As but one example, several groups have examined the relationship between glucose metabolism and RLR-mediated signaling. Among these findings, RLR-induced production of type-I IFNs was observed under conditions in which glucose metabolism was inhibited and that cells maintained in a low-glucose environment could produce higher levels of IFN than cells maintained in a high-glucose medium (22). By contrast, results from another study revealed that activation of RLR-mediated signaling resulted in an increase in glucose metabolism (9). These conflicting results will most certainly be important toward the effort to understand the full

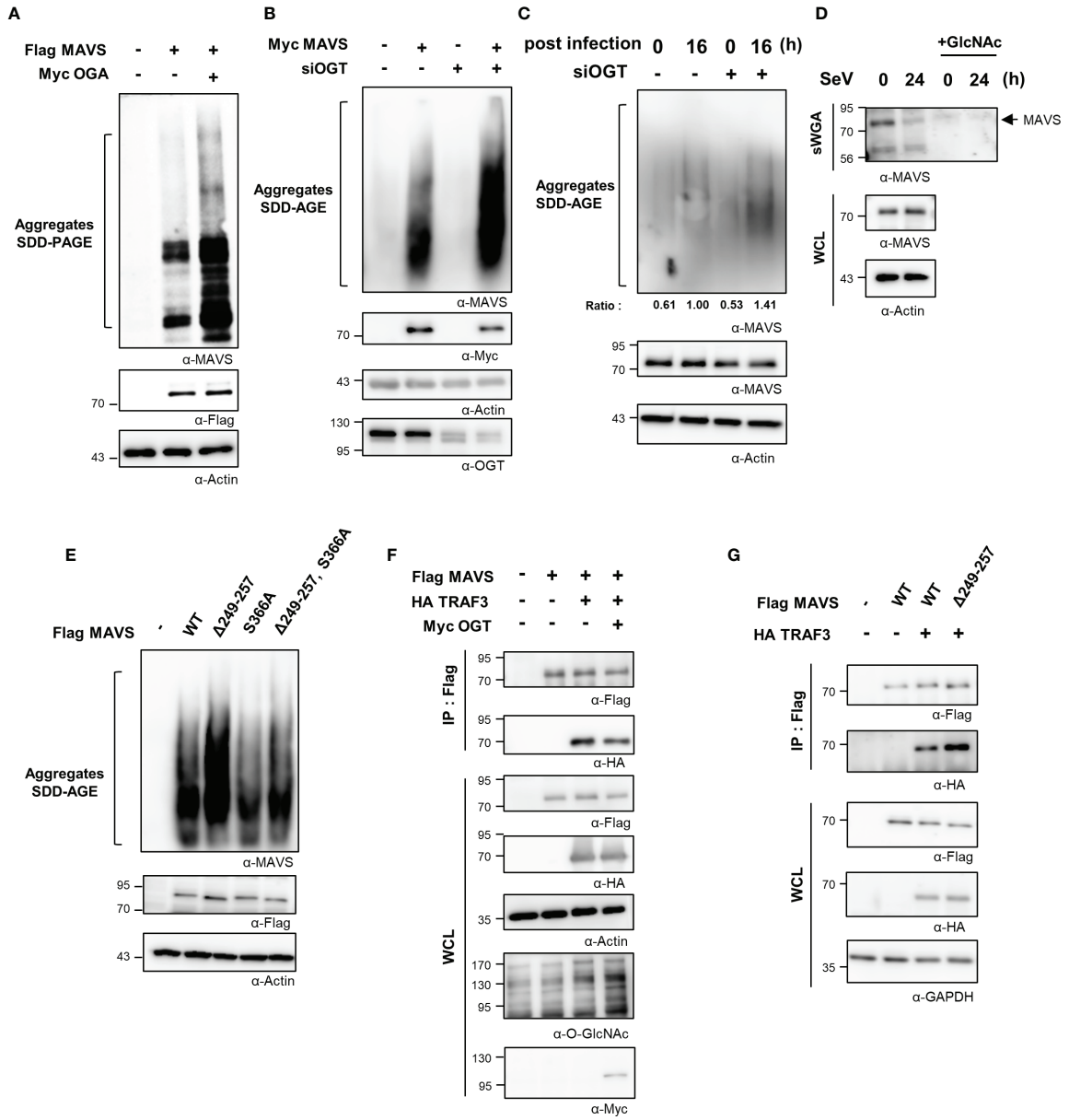

FIGURE 5 | O-GlcNAcylation of MAVS interferes with aggregate formation and interactions with TRAF3. **(A)** Non-reducing SDD-PAGE analysis was conducted to determine the level of MAVS aggregation. MAVS overexpression in HEK293 cells induced aggregate formation levels with or without overexpression of OGA. **(B)** Knock-down of OGT in HEK293 cells was detected at 48 h after transfection with specific siRNAs; this was performed before induction of MAVS overexpression for 24 h, after which SDD-AGE analysis was performed. **(C)** Endogenous MAVS aggregates were detected by SDD-AGE under conditions of OGT knock-down. HEK293 cells were transfected with siOGT; 48 h later, cells were infected with SeV (100 HAU) and evaluated at 16 h after infection. MAVS aggregates were normalized to the expression level of endogenous MAVS. **(D)** Precipitation was performed with sWGA followed by Western blot analysis to detect the O-GlcNAcylation levels of MAVS after a longer period of time after SeV infection (100 HAU). Cells were infected with SeV for 24 h before collection. WCLs were incubated with sWGA-conjugated beads overnight at 4°C and then were eluted for Western blot analysis. **(E)** An SDD-AGE assay was conducted to compare the levels of aggregation of wild-type MAVS and mutants with deleted O-GlcNAcylation sites. The pRK5-flag-tagged MAVS wild-type and mutant (Δ249–257, S366A, Δ249–257 containing S366A) plasmids were used to transfect HEK293 cells and were evaluated after 24 to 48 h. **(F)** A co-IP assay was performed to evaluate the interactions between MAVS and TRAF3. The pRK5-flag-tagged MAVS and HA-TRAF3 expression plasmids co-overexpressed in HEK293 cells both with and without Myc-OGT overexpression. **(G)** A co-IP assay was performed to evaluate the interactions between wild-type or the Δ249–257 mutant MAVS and HA-TRAF3 in HEK293 cells. Expression plasmids were used to transfect cells that were evaluated at 24 to 48 h. All experiments were repeated at least three times. **(A–G)** – means cells transfected with flag or Myc or HA empty vectors.

nature of the cross-talk between the innate immune response and glucose metabolism. In this study, we have demonstrated that levels of *O*-GlcNAcylation, which are known to respond rapidly to extracellular stimuli (33), decrease significantly in response to infection with an RNA virus; this ultimately leads to innate immune responses in target epithelial cells at later time points during infection that are associated with production of IFN-β. The functional mechanisms underlying cellular *O*-GlcNAcylation and their role in promoting RLR-mediated signaling are as shown in **Figure 6**. The host cell responds to virus infection by shutting down the expression of OGT. This response results in decreased levels of OGT and thus global depletion of cellular *O*-GlcNAcylation. This response has a specific impact on *O*-GlcNAcylation at the serine-rich region (amino acids 249–257) of MAVS; this promotes MAVS aggregation and enhances the interactions between MAVS and TRAF3. Because of these interactions, IRF3 is phosphorylated, undergoes dimerization, and is translocated into the nucleus where it promotes IFN-β transcription and thus activates IFN-β-mediated host defense responses. Taken together, the results presented in this study reveal that *O*-GlcNAcylation is a key link between glucose metabolism and the innate immune response.

Our study elucidated an important role for *O*-GlcNAcylation of MAVS; this post-translational modification resulted in suppression of RLR-mediated signaling in epithelial cells via a mechanism that was clearly different and distinct from those previously reported for MAVS Ser366 or for the seven associated sites at amino acids 322–347 within the MAVS polypeptide (9, 10). In these previous studies, O-GlcNAcylation of MAVS resulted in increased IFN-β production at relatively early time points after viral, similar to those identified for the IFN-β response of macrophages. However, in the case of epithelial cells, the time IFN-β production is typically observed at later time points when compared with those observed in infected macrophages (**Figure 1B**). We identified an unexpected decreased in the transcription of OGT in response to virus infection; this resulted in the global reduction of cellular O-GlcNAcylation and the specific reduction of the O-GlcNAcylation of MAVS. Our study revealed a mode of action that explains how *O*-GlcNAc modification modulates protein function in a site-specific manner. Furthermore, this mechanism suggests that *O*-GlcNAcylation, similar to phosphorylation, may serve as a central communicator promoting immune-mediated signal transduction.

The results of our study revealed drastic reductions in mRNA encoding OGT at early time points following SeV infection (**Figure 2**). This decline in OGT mRNA was not a response to specific viral proteins but appears to be modulated by host defense mechanisms. As such, we determined that the host response itself regulates transcription of OGT. Therefore, we proceeded to determine how the observed reduction of OGT mRNA was ultimately linked to the activation of RLR-mediated signaling. Given the recent reports indicating that OGT mRNA stability could be modulated by specific miRNAs (34, 35), we inferred that alterations of OGT might relate to specific post-transcriptional alterations that could promote mRNA decay. Further investigation will be needed to determine a role for virus-mediated activation of negative TFs and transcriptional co-repressors of OGT.

Some viruses are capable of sequential expression of immediate early (IE), early, and late viral genes that serve to support of their replication and propagation (36). *O*-GlcNAcylation of host transcriptional factors that promote viral gene expression, including HCF-1 and Sp1, have also been reported (37–39). However, we are not aware of any reports that describe host-mediated regulation of OGT

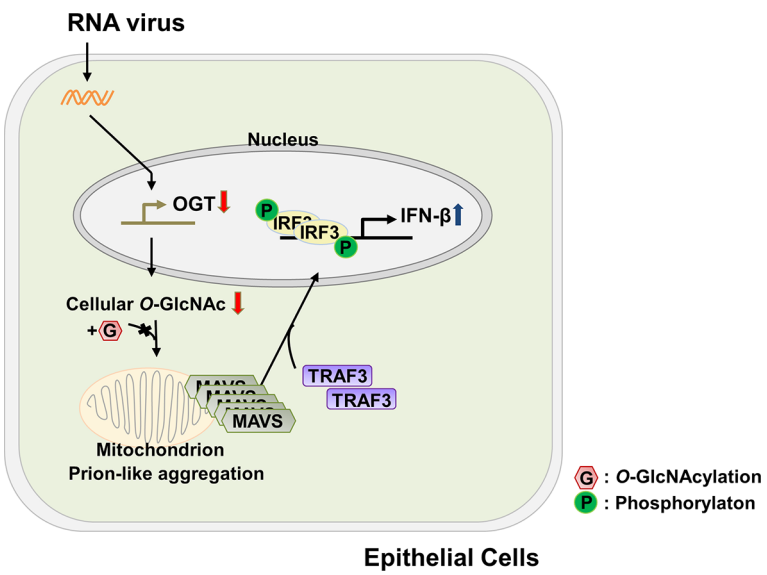

FIGURE 6 | Schematic of the proposed model depicting *O*-GlcNAcylation of MAVS at S249-S257 and its role in RLR-mediated signaling. The functional mechanism underlying cellular *O*-GlcNAcylation of MAVS and its role in promoting RLR-mediated signaling is described in **Figure 6**.

transcription in response to viral infection. As such, to the best of our knowledge, this is the first demonstration of transcriptional modulation of OGT mediated by virus-infected host cells that resulted in the reduction of *O*-GlcNAcylation and concomitant induction of an innate immune response. Moreover, it is important to discuss the role of *O*-GlcNAcylation of host TFs. For example, HCF1 is a host TF required for the transcriptional transactivation of the IE genes of HSV. *O*-GlcNAcylation of HCF1 promotes increased expression of HSV genes. When OGT activity is chemically inhibited by the OGT inhibitor, OSMI-1, late capsid formation of HSV and replication of both HSV and cytomegalovirus are inhibited (18). Furthermore, several of the TFs involved in the regulation of human immunodeficiency virus (HIV)-1 genes are modified by *O*-GlcNAcylation, including AP-1, yin-yang1 (YY1), NFATc1, NF-κB, and Sp1 (40–42). Among these findings, *O*-GlcNAcylation of Sp1 suppresses the long terminal repeat (LTR) region of HIV-1 and thereby inhibits HIV-1 replication (39). Besides the viral life cycle regulation via *O*-GlcNAcylation of host TFs, we have demonstrated that the virus infection results in alterations to the transcriptional patterns of the gene encoding the host OGT; we have shown that this is a host antiviral defense mechanism that ultimately leads to the continuous production of IFN-β.

In this study, we examined the functional significance of *O*-GlcNAcylation of the MAVS serine-rich region (249–257). However, the MAVS Δ249–257 deletion mutant still showed weak *O*-GlcNAcylation by OGT; this result suggested that there are likely to be additional *O*-GlcNAcylation sites on MAVS. Twenty potential MAVS *O*-GlcNAcylation sites were identified by Fusion M/S, including *O*-GlcNAcylation at Ser366 and a region including amino acids 324–347 on MAVS; these findings are consistent with those recently reported by Li et al (2018). and Song et al (2019).. The function of *O*-GlcNAcylation of Ser366 and the amino acids 324–347 region may be to promote RLR-mediate signaling in macrophages. However, we found that the aggregation and activity of MAVS were increased in epithelial cells with diminished levels of OGT and *O*-GlcNAcylation. Therefore, a more systematic approach will be needed to examine the nature of these differences and to identify their unique and important roles in promoting immune cell activation.

Additionally, our findings also confirmed that the viability of HEK293 and A549 cells was not significantly decreased within the 24 h after virus infection in as determined by MTT assays (**Figure S5F**). Ultimately, the absence of virus clearance mechanisms led to the death of host cells in response to the long-term infection. *O*-GlcNAcylation has protective effects concerning cell death; specifically, mechanisms that promote cell death also reduces the cellular levels of *O*-GlcNAcylation. However, cells that have been infected for a long period of time cannot activate IRF3 phosphorylation or produce IFN-β despite reductions in *O*-GlcNAcylation. As such, our study did present any reductions in *O*-GlcNAcylation associated with cell death and/or its impact on innate immune response.

MAVS activity is clearly regulated by the degree of *O*-GlcNAcylation as well as by processes including ubiquitination and phosphorylation (9, 21, 43–45). Furthermore, there is a yin–yang relationship between *O*-GlcNAcylation and phosphorylation. Interestingly, we also identified a phosphorylation site in MAVS (Serine 258). This phosphorylation site is very close to one of the *O*-GlcNAcylation sites identified in this study; as such, future studies will determine whether there are cooperative or competitive interactions between phosphorylation and *O*-GlcNAcylation at these sites. The results of this type of investigation will provide insight into how *O*-GlcNAcylation communicates with phosphorylation to modulate host defense mechanisms.

In summary, we demonstrated that MAVS-mediated RLR signaling, which is necessary for antiviral immune responses of epithelial cells, is inhibited by *O*-GlcNAcylation of MAVS, which restricts the formation of self-aggregates. *O*-GlcNAcylation of MAVS is also impaired via reduction of OGT mRNA expression, which is a newly discovered host defense mechanism that serve to accelerates innate immune responses. An improved understanding of *O*-GlcNAcylation and its role in RLR-mediated signaling in RNA virus-infected cells may present OGT as a potential therapeutic target for the treatment of patients with immune dysfunction.

DATA AVAILABILITY STATEMENT

The original contributions presented in the study are included in the article/**Supplementary Material**; further inquiries can be directed to the corresponding author/s.

AUTHOR CONTRIBUTIONS

JS and JC designed the study. JS and JC wrote the manuscript. JS performed most of the experiments. YP, TK, JK, and SS performed the experiments. YP assisted in editing the manuscript. HK, YS, MK, and EC identified the *O*-GlcNAcylation site of MAVS by using Fusion M/S. JC, WY, BP, JK, and YL supervised the study. All authors contributed to the article and approved the submitted version.

FUNDING

This research was supported by the National Research Foundation of Korea (NRF). Grants were given to JC from the Korean Government (NRF-2016R1A5A1010764 and NRF-2015M3A9B6073840).

SUPPLEMENTARY MATERIAL

The Supplementary Material for this article can be found online at: https://www.frontiersin.org/articles/10.3389/fimmu.2020.589259/full#supplementary-material

REFERENCES

1. Gack MU, Shin YC, Joo CH, Urano T, Liang C, Sun L, et al. TRIM25 RING-finger E3 ubiquitin ligase is essential for RIG-I-mediated antiviral activity. *Nature* (2007) 446:916–20. doi: 10.1038/nature05732
2. Choudhary C, Kumar C, Gnad F, Nielsen ML, Rehman M, Walther TC, et al. Lysine acetylation targets protein complexes and co-regulates major cellular functions. *Science* (2009) 325:834–40. doi: 10.1126/science.1175371
3. Okamoto M, Kouwaki T, Fukushima Y, Oshiumi H. Regulation of RIG-I Activation by K63-Linked Polyubiquitination. *Front Immunol* (2017) 8:1942. doi: 10.3389/fimmu.2017.01942
4. Gack MU. Mechanisms of RIG-I-like receptor activation and manipulation by viral pathogens. *J Virol* (2014) 88:5213–6. doi: 10.1128/JVI.03370-13
5. Seth RB, Sun L, Ea CK, Chen ZJ. Identification and characterization of MAVS, a mitochondrial antiviral signaling protein that activates NF-kappaB and IRF 3. *Cell* (2005) 122:669–82. doi: 10.1016/j.cell.2005.08.012
6. Hou F, Sun L, Zheng H, Skaug B, Jiang QX, Chen ZJ. MAVS forms functional prion-like aggregates to activate and propagate antiviral innate immune response. *Cell* (2011) 146:448–61. doi: 10.1016/j.cell.2011.06.041
7. Paz S, Vilasco M, Werden SJ, Arguello M, Joseph-Pillai D, Zhao T, et al. A functional C-terminal TRAF3-binding site in MAVS participates in positive and negative regulation of the IFN antiviral response. *Cell Res* (2011) 21:895–910. doi: 10.1038/cr.2011.2
8. Saha SK, Pietras EM, He JQ, Kang JR, Liu SY, Oganesyan G, et al. Regulation of antiviral responses by a direct and specific interaction between TRAF3 and Cardif. *EMBO J* (2006) 25:3257–63. doi: 10.1038/sj.emboj.7601220
9. Li T, Li X, Attri KS, Liu C, Li L, Herring LE, et al. O-GlcNAc Transferase Links Glucose Metabolism to MAVS-Mediated Antiviral Innate Immunity. *Cell Host Microbe* (2018) 24:791–803.e796. doi: 10.1016/j.chom.2018.11.001
10. Song N, Qi Q, Cao R, Qin B, Wang B, Wang Y, et al. MAVS O-GlcNAcylation Is Essential for Host Antiviral Immunity against Lethal RNA Viruses. *Cell Rep* (2019) 28:2386–96.e2385. doi: 10.1016/j.celrep.2019.07.085
11. Slawson C, Hart GW. O-GlcNAc signalling: implications for cancer cell biology. *Nat Rev Cancer* (2011) 11:678–84. doi: 10.1038/nrc3114
12. Ong Q, Han W, Yang X. O-GlcNAc as an Integrator of Signaling Pathways. *Front Endocrinol (Lausanne)* (2018) 9:599. doi: 10.3389/fendo.2018.00599
13. Yang X, Qian K. Protein O-GlcNAcylation: emerging mechanisms and functions. *Nat Rev Mol Cell Biol* (2017) 18:452–65. doi: 10.1038/nrm.2017.22
14. Banerjee PS, Hart GW, Cho JW. Chemical approaches to study O-GlcNAcylation. *Chem Soc Rev* (2013) 42:4345–57. doi: 10.1039/c2cs35412h
15. Pekkurnaz G, Trinidad JC, Wang X, Kong D, Schwarz TL. Glucose regulates mitochondrial motility via Milton modification by O-GlcNAc transferase. *Cell* (2014) 158:54–68. doi: 10.1016/j.cell.2014.06.007
16. Iyer SP, Akimoto Y, Hart GW. Identification and cloning of a novel family of coiled-coil domain proteins that interact with O-GlcNAc transferase. *J Biol Chem* (2003) 278:5399–409. doi: 10.1074/jbc.M209384200
17. Gawlowski T, Suarez J, Scott B, Torres-Gonzalez M, Wang H, Schwappacher R, et al. Modulation of dynamin-related protein 1 (DRP1) function by increased O-linked-beta-N-acetylglucosamine modification (O-GlcNAc) in cardiac myocytes. *J Biol Chem* (2012) 287:30024–34. doi: 10.1074/jbc.M112.390682
18. Angelova M, Ortiz-Meoz RF, Walker S, Knipe DM. Inhibition of O-Linked N-Acetylglucosamine Transferase Reduces Replication of Herpes Simplex Virus and Human Cytomegalovirus. *J Virol* (2015) 89:8474–83. doi: 10.1128/JVI.01002-15
19. Zeng Q, Zhao RX, Chen J, Li Y, Li XD, Liu XL, et al. O-linked GlcNAcylation elevated by HPV E6 mediates viral oncogenesis. *Proc Natl Acad Sci USA* (2016) 113:9333–8. doi: 10.1073/pnas.1606801113
20. Park SY, Kim HS, Kim NH, Ji S, Cha SY, Kang JG, et al. Snail1 is stabilized by O-GlcNAc modification in hyperglycaemic condition. *EMBO J* (2010) 29:3787–96. doi: 10.1038/emboj.2010.254
21. Yoo YS, Park YY, Kim JH, Cho H, Kim SH, Lee HS, et al. The mitochondrial ubiquitin ligase MARCH5 resolves MAVS aggregates during antiviral signalling. *Nat Commun* (2015) 6:7910. doi: 10.1038/ncomms8910
22. Zhang W, Wang G, Xu ZG, Tu H, Hu F, Dai J, et al. Lactate Is a Natural Suppressor of RLR Signaling by Targeting MAVS. *Cell* (2019) 178:176–89.e15. doi: 10.1016/j.cell.2019.05.003
23. Ryan P, Xu M, Davey AK, Danon JJ, Mellick GD, Kassiou M, et al. O-GlcNAc Modification Protects against Protein Misfolding and Aggregation in Neurodegenerative Disease. *ACS Chem Neurosci* (2019) 10:2209–21. doi: 10.1021/acschemneuro.9b00143
24. Jia Y, Song T, Wei C, Ni C, Zheng Z, Xu Q, et al. Negative regulation of MAVS-mediated innate immune response by PSMA7. *J Immunol* (2009) 183:4241–8. doi: 10.4049/jimmunol.0901646
25. Xu LG, Wang YY, Han KJ, Li LY, Zhai Z, Shu HB. VISA is an adapter protein required for virus-triggered IFN-beta signaling. *Mol Cell* (2005) 19:727–40. doi: 10.1016/j.molcel.2005.08.014
26. Kawai T, Takahashi K, Sato S, Coban C, Kumar H, Kato H, et al. IPS-1, an adaptor triggering RIG-I- and Mda5-mediated type I interferon induction. *Nat Immunol* (2005) 6:981–8. doi: 10.1038/ni1243
27. Shi Y, Yuan B, Zhu W, Zhang R, Li L, Hao X, et al. Ube2D3 and Ube2N are essential for RIG-I-mediated MAVS aggregation in antiviral innate immunity. *Nat Commun* (2017) 8:15138. doi: 10.1038/ncomms15138
28. Liu B, Zhang M, Chu H, Zhang H, Wu H, Song G, et al. The ubiquitin E3 ligase TRIM31 promotes aggregation and activation of the signaling adaptor MAVS through Lys63-linked polyubiquitination. *Nat Immunol* (2017) 18:214–24. doi: 10.1038/ni.3641
29. Marotta NP, Lin YH, Lewis YE, Ambroso MR, Zaro BW, Roth MT, et al. O-GlcNAc modification blocks the aggregation and toxicity of the protein alpha-synuclein associated with Parkinson's disease. *Nat Chem* (2015) 7:913–20. doi: 10.1038/nchem.2361
30. Yuzwa SA, Shan X, Macauley MS, Clark T, Skorobogatko Y, Vosseller K, et al. Increasing O-GlcNAc slows neurodegeneration and stabilizes tau against aggregation. *Nat Chem Biol* (2012) 8:393–9. doi: 10.1038/nchembio.797
31. Kapogiannis D, Mattson MP. Disrupted energy metabolism and neuronal circuit dysfunction in cognitive impairment and Alzheimer's disease. *Lancet Neurol* (2011) 10:187–98. doi: 10.1016/S1474-4422(10)70277-5
32. Zhang X, Zhang G, Zhang H, Karin M, Bai H, Cai D. Hypothalamic IKKbeta/NF-kappaB and ER stress link overnutrition to energy imbalance and obesity. *Cell* (2008) 135:61–73. doi: 10.1016/j.cell.2008.07.043
33. Zachara NE, Hart GW. O-GlcNAc a sensor of cellular state: the role of nucleocytoplasmic glycosylation in modulating cellular function in response to nutrition and stress. *Biochim Biophys Acta* (2004) 1673:13–28. doi: 10.1016/j.bbagen.2004.03.016
34. Herzog K, Bandiera S, Pernot S, Fauvelle C, Juhling F, Weiss A, et al. Functional microRNA screen uncovers O-linked N-acetylglucosamine transferase as a host factor modulating hepatitis C virus morphogenesis and infectivity. *Gut* (2019) 69:380–92. doi: 10.1136/gutjnl-2018-317423
35. Jiang M, Xu B, Li X, Shang Y, Chu Y, Wang W, et al. O-GlcNAcylation promotes colorectal cancer metastasis via the miR-101-O-GlcNAc/EZH2 regulatory feedback circuit. *Oncogene* (2019) 38:301–16. doi: 10.1038/s41388-018-0435-5
36. Gale MJr., Tan SL, Katze MG. Translational control of viral gene expression in eukaryotes. *Microbiol Mol Biol Rev* (2000) 64:239–80. doi: 10.1128/mmbr.64.2.239-280.2000
37. Capotosti F, Guernier S, Lammers F, Waridel P, Cai Y, Jin J, et al. O-GlcNAc transferase catalyzes site-specific proteolysis of HCF-1. *Cell* (2011) 144:376–88. doi: 10.1016/j.cell.2010.12.030
38. Zhu Y, Liu TW, Cecioni S, Eskandari R, Zandberg WF, Vocadlo DJ. O-GlcNAc occurs cotranslationally to stabilize nascent polypeptide chains. *Nat Chem Biol* (2015) 11:319–25. doi: 10.1038/nchembio.1774
39. Jochmann R, Thurau M, Jung S, Hofmann C, Naschberger E, Kremmer E, et al. O-linked N-acetylglucosaminylation of Sp1 inhibits the human immunodeficiency virus type 1 promoter. *J Virol* (2009) 83:3704–18. doi: 10.1128/JVI.01384-08
40. Ozcan S, Andrali SS, Cantrell JE. Modulation of transcription factor function by O-GlcNAc modification. *Biochim Biophys Acta* (2010) 1799:353–64. doi: 10.1016/j.bbagrm.2010.02.005
41. Golks A, Tran TT, Goetschy JF, Guerini D. Requirement for O-linked N-acetylglucosaminyltransferase in lymphocytes activation. *EMBO J* (2007) 26:4368–79. doi: 10.1038/sj.emboj.7601845
42. Yang WH, Park SY, Nam HW, Kim DH, Kang JG, Kang ES, et al. NFkappaB activation is associated with its O-GlcNAcylation state under hyperglycemic conditions. *Proc Natl Acad Sci USA* (2008) 105:17345–50. doi: 10.1073/pnas.0806198105
43. Vazquez C, Horner SM. MAVS Coordination of Antiviral Innate Immunity. *J Virol* (2015) 89:6974–7. doi: 10.1128/JVI.01918-14
44. Liu B, Gao C. Regulation of MAVS activation through post-translational modifications. *Curr Opin Immunol* (2018) 50:75–81. doi: 10.1016/j.coi.2017.12.002

45. Liu S, Cai X, Wu J, Cong Q, Chen X, Li T, et al. Phosphorylation of innate immune adaptor proteins MAVS, STING, and TRIF induces IRF3 activation. *Science* (2015) 347:aaa2630. doi: 10.1126/science.aaa2630

Conflict of Interest: The authors declare that the research was conducted in the absence of any commercial or financial relationships that could be construed as a potential conflict of interest.

frontiers in Immunology

REVIEW
published: 17 February 2021
doi: 10.3389/fimmu.2020.622602

Mitochondrial Regulation of Macrophage Response Against Pathogens

Subhadip Choudhuri[1], *Imran Hussain Chowdhury*[1] *and Nisha Jain Garg*[1,2*]

[1] Department of Microbiology and Immunology, University of Texas Medical Branch (UTMB), Galveston, TX, United States,
[2] Institute for Human Infections and Immunity, UTMB, Galveston, TX, United States

Innate immune cells play the first line of defense against pathogens. Phagocytosis or invasion by pathogens can affect mitochondrial metabolism in macrophages by diverse mechanisms and shape the macrophage response (proinflammatory *vs*. immunomodulatory) against pathogens. Besides β-nicotinamide adenine dinucleotide 2'-phosphate, reduced (NADPH) oxidase, mitochondrial electron transport chain complexes release superoxide for direct killing of the pathogen. Mitochondria that are injured are removed by mitophagy, and this process can be critical for regulating macrophage activation. For example, impaired mitophagy can result in cytosolic leakage of mitochondrial DNA (mtDNA) that can lead to activation of cGAS–STING signaling pathway of macrophage proinflammatory response. In this review, we will discuss how metabolism, mtDNA, mitophagy, and cGAS–STING pathway shape the macrophage response to infectious agents.

Keywords: mitochondria, metabolism, macrophage, innate immunity, cGAS-STING, mitophagy, noncoding RNA

OPEN ACCESS

Edited by:
Pedro Manoel Mendes Moraes Vieira, Campinas State University, Brazil

Reviewed by:
Albert Descoteaux, Université du Québec, Canada
Robert A. Harris, University of Kansas Medical Center, United States

***Correspondence:**
Nisha Jain Garg
nigarg@utmb.edu

Specialty section:
This article was submitted to Molecular Innate Immunity, a section of the journal Frontiers in Immunology

Received: *28 October 2020*
Accepted: *29 December 2020*
Published: *17 February 2021*

Citation:
Choudhuri S, Chowdhury IH and Garg NJ (2021) Mitochondrial Regulation of Macrophage Response Against Pathogens. Front. Immunol. 11:622602. doi: 10.3389/fimmu.2020.622602

INTRODUCTION

Macrophages (Mφ) are innate immune cells that reside in almost all of the tissues in the body. Two major lineages of Mφ include the blood-circulating monocytes originating from the myeloid progenitor cells in the bone marrow (BM) and those derived from the yolk sac (1). Mφ of both lineages are capable of responding to microbial invasion and other stimuli through production of proinflammatory molecules *e.g.* tumor necrosis factor (TNF)-α, interleukin (IL)-6, nitric oxide (NO), and reactive oxygen species (ROS), recruitment of immune cells, and antigen presentation to T cells for the initiation of adaptive immunity (2). Mφ may also play a role in resolution of inflammation and tissue injury by upregulating the anti-inflammatory mediators and scavenging receptors (*e.g.* mannose receptor), phagocytizing cellular debris, and secreting molecules [*e.g.*, metalloproteinase (MMP)-2, MMP-9, tumor growth factor (TGF)-β] to induce collagen production and scar formation associated with tissue repair and wound healing (3, 4). In recent studies, mitochondrial health and metabolic status have been recognized as drivers of Mφ response (5). For example, a switch in energy production from mitochondrial oxidative metabolism towards glycolysis elicits Mφ proinflammatory polarization (6). Bacterial lipopolysaccharide (LPS) elicits a large and transient increase in nicotinamide adenine dinucleotide (NAD^+) levels, which supports TNF-α production; and NAD^+ deficiency had an inhibitory effect on TNF-α release (7). Depletion

of cytoplasmic NAD^+ induces an impairment in adhesion and phagocytosis of zymosan particles (8).

A compromise in mitochondrial health in the presence of exogenous or endogenous stimuli may signal proinflammatory Mφ response through multiple routes, including release of mitochondrial ROS (mtROS) and mtDNA that interact with multiple receptors [*e.g.* cyclic GMP-AMP synthase (cGAS)/ stimulator of interferon genes (STING)] and transcription factors [*e.g.* nuclear factor kappa B (NF-κB)] (7). In this context, Mφ response may also be regulated by mitophagy involved in clearance of damaged and/or dysfunctional mitochondria (8). In this review, we will discuss how mitochondrial health *vs* mitochondrial dysfunction and compromised mitophagy shape the Mφ response. We will also discuss the signaling pathways (*i.e.*, cGAS/STING) that link mitochondrial control of Mφ response in health and disease.

DIVERSE FUNCTIONS OF MACROPHAGES

Macrophages exhibit remarkable flexibility in responding to pathogenic, environmental, and endogenous stimuli. Mφ utilize surface and cytosolic pattern recognition receptors (PRRs) to recognize pathogen associated molecular patterns (PAMPs) that are the molecules expressed by pathogens and the damage associated molecular patterns (DAMPs) which serve as immune activators when they are exposed under conditions of stress or injury. Major classes of PRR include C-type lectin receptors, NOD-like receptors, RIG-I-like receptors, and toll-like receptors (TLRs). PRR recognition of PAMPs and DAMPs initiates complex signaling cascade and interplay of cellular mediators and transcription factors that shape the Mφ defense against invading or intracellular pathogen or Mφ response for removal of cellular debris left after exposure to pathogenic and injurious stimuli. In-depth discussion of PRRs' function can be found in several recent articles (*e.g.* 9, 10).

Proinflammatory Response

Lipopolysaccarides (LPSs), components of the outer membrane of gram-negative bacteria, are perhaps the most studied PAMPs that are recognized by TLR4 and shown to elicit proinflammatory response in Mφ. TLRs, through a series of phosphorylation steps, signal the recruitment and degradation of proteins and kinases including TNF receptor associated factor 6 (TRAF6), myeloid differentiation primary response (MYD)88, and TGF-β activated kinase (TAK) that result in the induction of NF-κB transcription factor for the expression of proinflammatory molecules (11). Along with the PRRs, TNF-α and type II interferon (IFN)-γ are the most studied cytokines shown to enhance the proinflammatory activation of the Mφ *via* c-Jun N-terminal kinase (JNK)/signal transducers and activators of transcription (STAT)-1 signaling of NF-κB and hypoxia inducible factor (HIF)-1α transcription factors (12, 13). The classical model of Mφ activation by LPS/IFN-γ triggers an extensive profile of inflammatory cytokines (*e.g.* TNF-α, IL-6, IL-1β) and chemokines (such as CCL2/MCP-1, CCL3, CCL4, CCL5, CCL11, and CCL13) and are referred as proinflammatory or M1 phenotype (14). A feedback control of M1 Mφ activation is provided by a suppressor of cytokine signaling (SOCS) inhibition of STAT-3. The proinflammatory Mφ are also expected to generate high levels of reactive oxygen and nitrogen species which contribute to direct killing of the pathogen.

In Mφ, NADPH oxidase is considered to be the primary source of superoxide ($O_2\bullet^-$) that then is dismutated to peroxides, hydroxyl radical, and other forms of ROS (15). Recent studies have also addressed the role of mitochondrial respiration in contributing to ROS production in Mφ (16). Inducible nitric oxide synthase (iNOS) serves as the major source of nitric oxide (NO) utilizing oxygen and L-arginine in the process (17). The $O_2\bullet^-$ and NO radicals, together, produce peroxynitrite (ONOO) involved in microbicidal activity. Costimulatory molecules such as cluster of differentiation (CD)80, CD86, CD64, CD16, CD32, and iNOS are used as markers of M1 Mφ. Type I and type III interferons mediated antiviral responses that are central to host defense against viral infections are discussed in recent reviewes (18, 19).

Immunomodulatory Response

On the other end of the spectrum is the Mφ activation to M2 state that involves heterogenous functional profile depending upon the stimulating factors (20). For example, IL-4 produced by Mφ and T helper type 2 (Th2) cells and IL-13 produced by various T cell subsets and natural killer (NK) cells stimulate Mφ polarization towards immunomodulatory M2a state associated with anti-inflammatory role with production of IL-10, IL-1 receptor II (IL-1RII), and anti-helminth Th2 inflammation (21, 22). M2b regulatory Mφ are capable of possessing both protective and pathogenic roles and are activated in response to TLRs, IL-1R or immune complexes (23). The M2c Mφ respond to glucocorticoids, TGF-β, IL-10 *etc.*, and are involved in immune suppression, matrix deposition, tissue repair and tissue remodeling (24). The general mechanism underlying the M2 polarization includes the engagement of IL-4R, IL-10R, or IL-13R that signal through Janus kinase (JAK) and tyrosine kinase (TYK) to mediate an increase in STAT6 activity (25). STAT6 transcriptional activation is also enhanced by peroxisome proliferator activated receptor γ (PPAR-γ) and PPAR-γ coactivator 1 (PGC-1) that support the expression of genes involved in fatty acid (FA) oxidation and oxidative metabolism and have inhibitory effects on inflammatory gene transcription (26, 27). IL-4 and IL-13 also enhance the expression of the mannose receptor (CD206), dectin-1, and resistin-like molecule (RELM)-α, which play an important role in the recognition of fungal infections and activation of Th2 immunity (27). IL-10 activates STAT1 more than STAT3 and inhibits inflammatory cytokine (*e.g.*, TNF-α and IL-1β) production (28). Polarization of M2 Mφ towards M1 phenotype is prevented through SOCS-3 inhibition of STAT-3. Co-stimulatory molecules, including arginase 1 (supports cell proliferation), decoy receptor 3 (inhibits Fas ligand induced apoptosis), dectin 1 (a major β glucan receptor), CD206, and CD163 (scavenger receptor) are

used as markers of M2 Mφ. We note that this classification is not sufficient to cover the wide range of Mφ activation profile noted in various *in vivo* models of infection and other diseases.

Phagocytosis

Macrophages are classical phagocytes that uptake and degrade pathogens as well as cellular debris by an actin dependent and clathrin-independent mechanism. Phagocytosis in Mφ is activated by recognition through the complement-, Fcγ-, or mannose-receptors [reviewed in (29)]. The fusion of phagosome with lysosome filled with hydrolytic enzymes forms a phagolysosome where the engulfed material is digested and then disposed by exocytosis or the immunodominant peptides are loaded on to MHC. MHCII molecules translocate to cell surface for presentation of the antigen to $CD4^+$T cells (30). Macropinocytosis (non-specific uptake of soluble antigens) and receptor-mediated endocytosis of soluble antigens through clathrin-coated vesicles also deliver the antigenic peptides through endosome lysosome pathway for MHCII presentation (30). Some microbes that escape from phagolysosome into cell cytoplasm (*e.g. Trypanosoma cruzi*) and others that develop intracellularly (*e.g.* viruses) are degraded by proteasomes after which immunodominant peptides bind to MHCI molecules which are recognized by $CD8^+$T cells (31). Thus, as a professional antigen-presenting cell (APC), Mφ bridge the innate and adaptive immune systems.

Besides traditional phagocytosis that is mostly reserved for uptake of pathogens, Mφ are also involved in the uptake and clearance of apoptotic bodies. For this, Mφ respond to "eat-me" signals including nucleotides, chemokines, and lipid phosphatidylserine on the apoptotic cells by upregulation of the mannose receptors (CD163, CD206), cytokines (TGF-β and IL-10), arachidonic metabolites (*e.g.*, prostaglandin E2), and pro-resolving mediators that is then followed by anti-inflammatory and repair/healing responses (32). Further details on Mφ role in clearance of apoptotic cells can be found in a recent review (33).

METABOLIC SWITCH AND FUNCTIONAL PROFILE OF MACROPHAGES

Mitochondrial respiration and metabolism machinery, *i.e.*, tricarboxylic acid (TCA) cycle, electron transport chain (ETC), oxidative phosphorylation (OXPHOS), and fatty acid and amino acid metabolism provide the energy house status to mitochondria. Interestingly, these same metabolic pathways, along with glycolysis and pentose phosphate pathway (PPP), influence the functional polarization of Mφ and are discussed in brief here.

Metabolic Switch to Glycolysis in Proinflammatory Macrophages

Newsholme et al. (34) have noted a direct correlation between the increase in the rate of glycolysis and phagocytosis upon macrophage activation by inflammatory stimuli. Since then, the advent of new reagents and mass spectrometry approaches has facilitated large scale metabolome studies. Researchers have utilized these new approaches to address how metabolic profile impacts Mφ activation and the mechanisms employed by Mφ to switch metabolic program in response to various stimuli. Now, we know that proinflammatory Mφ induced by LPS/IFN-γ have impaired activities of the TCA, ETC, and OXPHOS pathways and rely on increased glucose uptake and glycolysis for energy needs and production of ROS/NO and proinflammatory cytokines (35). LPS-activated Mφ also utilize the glucose metabolic intermediates for triglycerides and FA synthesis and engulf free fatty acids for triglyceride accumulation (36), which are vital for their phagocytic function (37). Glycolysis in LPS-stimulated and M1-like Mφ is supported by upregulation of glucose transporter 1 (GLUT1), hexokinase 2 (catalyzes rate limiting first step of glycolysis) (38), ubiquitous 6-phosphofructo-2-kinase (uPFK2, produces higher concentrations of fructose 2,6-bisphosphate substrate than other isoforms), and pyruvate kinase M2 (PKM2, catalyzes final step of glycolysis) (39). Mφ switch to glycolysis is mediated by HIF-1α. In normal conditions, nuclear prolyl hydroxylase 1 (PHD1) produces 2S,4R-4-hydroxyproline from α-ketoglutarate for post-translational hydroxylation of HIF-1α that is then targeted for proteasomal degradation (40). Under hypoxic conditions, PHD1 inhibition allows stabilization and activation of HIF-1α (40). Nuclear localization of PKM2 enhances the STAT3 phosphorylation and HIF-1α transcriptional activity thereby facilitating increase in proinflammatory cytokines expression (41). HIF-1α also stimulates the expression of GLUT1, monocarboxylate transporter 4 (MCT4), and uPFK2 and induces lactate dehydrogenase (utilizes pyruvate to make lactate) and pyruvate dehydrogenase kinase (inhibits pyruvate entry into TCA cycle) that together promote glycolysis in Mφ (discussed in 6).

The ^{13}C metabolite labeling studies suggest that TCA cycle is disrupted at distinct points in M1 Mφ. Accumulation of succinate signals the stabilization of HIF-1α (42) and succinate-responsive succinate receptor 1 (SCNR1) and regulates ROS and IL-1β release in classically activated Mφ (43). Isocitrate dehydrogenase downregulation contributes to accumulation of citrate that is deemed important for the synthesis of the anti-bacterial itaconate compound (43). Further, excess citrate is transported from the mitochondria to cytosol where it is converted by citrate lyase to acetyl CoA and used for FA synthesis in proinflammatory Mφ (44). Other intermediates of TCA cycle, *e.g.* fumarate, succinate, and α-ketoglutarate are suggested to regulate the Mφ activation profile through influencing the epigenome (45).

Pentose phosphate pathway (PPP) branches off from glycolytic pathway with formation of 6-phosphate gluconate and NADPH from glucose-6-phosphate and serves an important role in nucleotide synthesis. Mφ utilize NADPH produced by PPP as electron carrier for ROS formation by NADPH oxidase (46) and as a co-substrate with L-arginine for the synthesis of L-citrulline and NO by inducible nitric oxide synthase (iNOS) (47). L-citrulline can also be involved

in L-arginine biosynthesis to feed the cyclic and continuous NO generation in proinflammatory Mφ (48). With regard to mitochondria, a decline in bioavailability of NAD^+ due to depletion of tryptophan (co-substrate for NAD^+ biosynthesis) or decreased influx from malate-aspartate and the glycerol-3-phosphate shuttles can disturb the NAD^+/NADH ratio. Alternatively, an accumulation of NADH in the mitochondria due to decreased OXPHOS requirement results in disturbances of the NAD^+/NADH ratio. Such flux in NAD^+/NADH can disturb mitochondrial membrane potential and ETC complexes and consequently causes increased leakage of electrons to O_2 favoring $O_2\bullet^-$ production in Mφ (49–52). Besides ETC, α-ketoglutarate dehydrogenase and pyruvate dehydrogenase complexes are also recognized as site of mtROS production (53, 54).

Oxidative Metabolism in Immunomodulatory Macrophages

Immunoregulatory (M2 type) Mφ rely on TCA cycle and OXPHOS sourced from FA uptake and lipids/FA oxidation to meet the energy demand (55). M2 Mφ depend on adenosine monophosphate-activated protein kinase (AMPK) and peroxisome proliferator activating receptors (PPARs) mediated activation of STAT6 transcription complex to promote the expression of genes for OXPHOS and FA oxidation pathways (56). Treatment with chemical inhibitors of OXPHOS pathway or of ATP synthase downregulated the M2-specific expression of genes (*e.g. Arg1, Mrc1*), surface markers (CD206), and arginase 1 activity in IL-4-stimulated Mφ (35). Conversely, LPS + IFN-γ-stimulated M1 Mφ lacked the competence to restore mitochondrial respiration and M2-specific receptor expression after IL-4 treatment (35). Collectively, current literature suggests that M2-like Mφ have an intact TCA cycle, FA oxidation, and aerobic glycolysis, while M1-like Mφ tend to depend on breakdown intermediates of glycolysis, PPP, and TCA cycle.

Metabolic Regulation of Macrophages in Infection

Very few studies have addressed the metabolic regulation of Mφ polarization in experimental models of health and disease, though metabolic perturbations elicited in Mφ by various infectious agents have been reported. For example, *Mycobacterium tuberculosis* invasion of Mφ was accompanied by increase in expression of glucose transporters and glucose uptake (57). Further, *M. tuberculosis* augmented the aerobic glycolysis that was associated with delayed apoptotic response of Mφ and increased replication and survival of the bacteria in Mφ (57). In contrast, HIV dampened the glucose uptake, glycolysis, and PPP intermediates to inhibit proinflammatory Mφ activation (58). Likewise, *Francisella tularensis* suppressed the lactate and HIF-1α stabilization and aerobic glycolysis in Mφ to ensure early replication of the bacteria (59). *Salmonella* infection activated M2 Mφ polarization despite the PPAR-δ mediated increase in glucose availability and favored the bacterial replication (60, 61). Pathogenic protozoans survive in Mφ and use Mφ as a vehicle for dissemination. For example, *Leishmania* sps. and *Toxoplasma gondii* utilized arginine metabolism for the synthesis of polyamines for their growth and replication in Mφ (62, 63). *Leishmania* also enhanced the AMPK/Sirtuin 1 (SIRT1) activity that supports mitochondrial metabolism (64) and levels of M2-associated intracellular metabolites (65), while glucose consumption was decreased in infected Mφ (65). *Trypanosoma cruzi* infection enhanced the expression of peroxisome proliferation activated receptor α (PPAR-α) in Mφ (66), and PPAR isoforms have been implicated in the gene transcription roles in M2 Mφ by several research groups (67). The cruciality of the PPP for providing substrates for ROS and NO production to control *T. cruzi* in Mφ was also noted (66). Others have indicated that PPP production of NADPH is utilized by *T. cruzi* to activate its antioxidant enzymes (*e.g.* trypanothione reductase) as defense against ROS/NO produced in Mφ (68). Together, these studies indicate that infectious agents employ various strategies to hijack the Mφ metabolism machinery for their own survival and replication; and microbe-specific studies identifying the steps in metabolic pathway(s) and/or metabolites that can be targeted to enhance the pathogen clearance by Mφ are required.

OTHER MITOCHONDRIAL PATHWAYS INTER-LINKED WITH MACROPHAGE RESPONSE TO PATHOGENS

Besides metabolic control, the mitochondria play several other key regulatory roles in shaping the Mφ response and reviewed in brief here.

Apoptosis

In conditions of stress, a feedback cycle of mitochondrial permeability transition (MPT), disturbance of electrochemical proton gradient across the respiratory chain complexes and mtROS production occurs. The mtROS and ROS-induced oxidants result in oxidation of glutathione and thiol (*e.g.* N-acetyl cysteine) pools that inhibit apoptosis (69) or through oxidation at mitochondrial membranes that generate MPT lead to cytochrome c (cyt c) release. Cytosolic cyt c interacts with apoptotic protease activating factor 1 (APAF-1) initiating recruitment and activation of caspase-9 and other effector caspases (caspase-3, -6, -7) leading to cell apoptosis (70, 71). Mitochondrial apoptosis-inducing factor and endonuclease G have also been identified as key signaling molecules of apoptosis (72) A wide range of pathogens, pathogen-shed vesicles, and bacterial toxins have been associated with mitochondrial disturbances, cyt c release and activation of apoptosis in Mφ. For example, *Shigella flexneri* invasion induced mitochondrial MPT and signaled cell death in Mφ (73). *M. tuberculosis* was shown to induce Bax translocation to the mitochondria, MPT, and cytosolic cyt c release in infected Mφ (73, 74). *Bacillus anthracis* lethal toxin and *Staphylococcus aureus* secreted pore-forming toxins signaled activation of NLRP1B (75, 76) and NLRP3 (77, 78) inflammasomes, respectively, which led to caspase-1 and IL-1β activation and Mφ pyroptosis (highly inflammatory form of programmed cell death), though mitochondrial involvement was not reported.

Mitochondrial Fusion and Fission

Mitochondrial dynamics (*i.e.*, repetitive cycles of fusion and fission) and mitophagy maintain mitochondrial homeostasis (79). For fusion, transmembrane dynamin related GTPase proteins named mitofusins (MFN1/MFN2) form dimers across the interface and tether mitochondria together. Mitofusins utilize GTP hydrolysis and redox signaling to induce conformation changes and enforce mitochondrial outer membrane fusion. Conversely, ubiquitination targets mitofusins for degradation that involves PTEN-induced kinase (PINK)1, Parkin, E3 ligase Huwe1, and Bcl-2 family members. Another dynamin related GTPase protein, optic atrophy protein 1 (OPA1) interacts with cardiolipin localized in cristae and intermembrane space to coordinate fusion of inner mitochondrial membranes. Mitochondrial fission involves dynamin related protein 1 (DRP1) and other adapter proteins that form a ring across the outer mitochondrial membrane. DRP1 is regulated by a variety of post-translational modifications, and organization of DRP1 ring offers conformational activation of GTPase activity leading to spiral constriction and separation of damaged and healthy mitochondrial portions (80). Fission 1 protein, regulated by ubiquitination by mitochondrial ubiquitin ligase, is involved in DRP1 binding, and it facilitates fragmentation of damaged portion of the mitochondria. Several other proteins, *e.g.*, mitochondrial fission factor (MFF), TNFR-associated protein 1 (TRAP1), and mitochondrial dynamics proteins (MID49, MId51) are also involved in the fission process, though their role is not fully explored (81).

Studies on the role of mitochondrial fission and fusion in pathogen control have yielded important results. An increase in mitochondrial fission and mtROS production that activated the NF-κB mediated expression of proinflammatory mediators was observed in LPS-stimulated microglial Mφ (82). *Streptococcus pneumoniae* infection triggered mitochondrial fission allowing energy switch and enhanced mtROS production in Mφ (83). *Helicobacter pylori* vacuolating toxin induced DRP1 activation, mitochondrial fragmentation, Bax translocation to mitochondria, and cyt c release, and it was suggested that *H. pylori* targets mitochondrial fragmentation and apoptosis to prevent proinflammatory Mφ response (84). Likewise, *Chlamydia trachomatis* maintained mitochondrial integrity and predominance of OXPHOS pathway through a miR-30c-5p-dependent inhibition of Drp1-mediated mitochondrial fission (85). *Vibrio cholerae* targeted mitochondrial Rho Miro GTPases to modulate mitochondrial dynamics and interfere with innate immunity (86). Overexpression of MFN2 increased the *M. tuberculosis* growth in Mφ (87). However, a recent study showed that LPS-induced MFN2 was required for the adaptation of mitochondrial respiration to stress conditions and increase in ROS production and phagocytosis activity in Mφ (88). Mφ treated with MFN2 inhibitor or knocked down in MFN2 encoding gene exhibited a significant decline in phagocytosis of apoptotic bodies, *Aeromonas hydrophila* and *E. coli* (88). Studies in mice with myeloid-specific MFN1 and MFN2 knockdown revealed that MFN2 (not MFN1) deficiency impaired the production of proinflammatory cytokines and nitric oxide. MFN2 deficiency was also associated with dysfunctional autophagy, apoptosis, and phagocytosis, and MFN2 depleted mice failed to control *Listeria* and *M. tuberculosis* infections (88). These observations support the notion that mitochondrial dynamics is closely linked to the phagocytic capacity and immune function of Mφ during infection.

Mitochondrial Biogenesis

Mitochondrial biogenesis refers to the process by which cells increase mitochondrial mass (89). Peroxisome proliferator-activated receptor gamma coactivator-1α (PGC1α) plays an important role in the activation of nuclear respiratory factors (NRF-1, NRF-2) and nuclear factor erythroid 2-related factor 2 (Nfe2l2) transcription factors that regulate the expression of nuclear DNA and mtDNA encoded genes for mitochondrial biogenesis (90, 91). Recent discoveries indicate that mitochondrial biogenesis is intricately engaged with inflammatory/immunomodulatory host response. For example, it is suggested that early-phase inflammatory mediator proteins interact with pathogen recognition receptors to activate NF-κB-, MAPK-, or protein kinase B/Akt-dependent pathways, resulting in increased expression and activity of cofactors and transcription factors involved in mitochondrial biogenesis [reviewed in (92)]. Nitric oxide and ROS generated by Mφ can stimulate PGC-1α/Nfe2l2 or redox-sensitive hemoxygenase systems, causing simultaneous induction of mitochondrial biogenesis and antioxidant gene expression and modulate inflammation (93, 94). Sirtuin 1 (SIRT1), a highly conserved member of the Sir2 histone deacetylases family, is also implicated in deacetylation of PGC1α at multiple lysine sites, consequently increasing PGC1α activity (95). Specifically, *Staphylococcus aureus* is shown to upregulate mitochondrial biogenesis through the upregulation of the PGC family (96, 97). The induction of mitochondrial biogenesis was dependent on TLR2 and TLR4, signifying that the innate immune function feeds into the regulation of mitochondrial health during bacterial infection (97). Plataki et al. (98) noted decreased ATP production, dysregulated mitochondrial gene expression, and decreased numbers of healthy mitochondria in aged adult Mφ and lungs in response to *S. pneumoniae* infection and showed that treatment with an anti-fibrotic drug improved the mitochondrial mass and health in aged Mφ and decreased the pulmonary edema in aged mouse lung during infection. Human cytomegalovirus also induced mitochondrial biogenesis accompanied with increased respiration, both of which were required for the viral replication (99). Summarizing, the complex network of pro- and anti-inflammatory pathways impact and, are impacted by, mitochondria. While some infectious agents exploit mitochondrial biogenesis to establish infection in the host, maintenance of mitochondrial biogenesis, health, and function, and cellular redox status is vital to host survival in unregulated acute inflammatory states such as sepsis.

Mitophagy

Mitophagy is a process used for the removal of fragmented mitochondria, and detailed mechanism of mitophagy is discussed in a recent review (79). Briefly, mitophagy is

triggered by outer membrane receptor proteins (*e.g.*, NIX/BNIP3L, BNIP3, and FUNDC) that have a classic motif to bind directly to microtubule associated light chain 3 (LC3) and initiate mitophagy (100). Mitophagy is also initiated by the PTEN-induced kinase 1 (PINK1)/Parkin. Loss of membrane potential in damaged mitochondria supports the accumulation of unprocessed PINK1 on the outer membrane surface where it recruits cytosolic Parkin to promote ubiquitin dependent mitophagy through interaction with LC3 protein (101).

In context to cell damage caused by invading and intracellular microbes, autophagy/mitophagy act as important defense systems to establish homeostasis in stressful cellular environment. Indeed, inhibition of mitophagy by 3-methyladenine resulted in Mφ polarization towards M1 phenotype (102), while rapamycin mediated induction of autophagy suppressed the mtROS and NLRP3 inflammasome activation and favored Mφ polarization towards M2 phenotype (102, 103). Further, PINK1 depletion enhanced the LPS/IFN-γ stimulated proinflammatory phenotype in microglial cells (104), and adoptive transfer of *Pink1*-deficient bone marrow promoted Mφ proinflammatory activation, which favored pathogen clearance and increased survival in a murine model of polymicrobial infection (8). However, PINK1 was required to trigger the RIG-I-mediated innate immune responses in Mφ infected with respiratory syncytial and herpes simplex viruses (105), and Parkin-deficiency increased the susceptibility of mice to intracellular pathogenic bacteria (*e.g.*, *M. tuberculosis, S. typhimurium, L. monocytogenes*, and *Pseudomonas aeruginosa (*106, 107*)*. Likewise, autophagy activation by isoniazid and bedaquiline treatment impaired the mycobacterial phagosome escape in Mφ, suggesting that drugs favoring autophagy would enhance bacterial clearance (108). These studies highlight that mitophagy has important and diverse roles in modulating the innate immunity against pathogens.

DNA SENSING BY cGAS–STING IN MACROPHAGE ACTIVATION

The cytosolic presence of mtDNA in Mφ can occur due to uptake of fragmented/damaged mitochondria released in the peripheral system by other cells or due to leakage of mtDNA from their own mitochondria. The mtDNA contains a significant number of unmethylated CpG DNA repeats, similar to those present in prokaryotic bacterial genome (109) and is recognized as a cellular DAMP. The role of mtDNA as a key inducer of inflammatory cytokines (IL-1β and IL-18) in Mφ through recognition by TLR9 and activation of NLRP3/ASC inflammasome has been recognized in previous studies (110, 111). The cytoplasmic mtDNA co-localizes with NLRP3 to induce IL-1β secretion and oxidized mtDNA is a potent inducer of IL-1β production in Mφ *(*112*)*. Further, NLRP3 activators trigger mtROS production, oxidized mtDNA release into cytosol and also mtDNA synthesis (without increase in mitochondrial mass) to fuel the proinflammatory activation in Mφ (113, 114). Detailed information on mtDNA signaling of inflammasomes can be found in recent reviews (115–117).

The pivotal role of double-stranded DNA sensor cGAS and STING in shaping the immune-surveillance by Mφ has been recognized recently (118). Briefly, STING was identified in 2008 (119) and cyclic guanosine monophosphate-adenosine monophosphate (cGAMP) was recognized as a novel secondary messenger serving as ligand of STING in 2013 (120). Subsequently, cGAS was noted to have cytosolic DNA-sensing ability, and the cGAS–STING pathway was identified to be indispensable for anti-viral host immunity (121). Later on, mtDNA and oxidized DNA were identified as key molecules to be recognized by cGAS–STING for the initiation of anti-viral type I interferon immunity (122). These authors showed that mtDNA stress elicited by a mitochondrial transcription factor A deficiency promoted mtDNA escape into cytosol where it engaged cGAS and signaled STING–IRF3-dependent increase in the expression of interferon stimulated genes (ISGs) in herpes viruses infection model (122). The findings that inhibition of DNA repair enzyme 8-oxoguanine DNA glycosylase 1, which removes 8-oxo-7,8-dihydroguanine lesions caused by ROS, enhanced the mtDNA-cGAS–STING–IRF3–IFN-β axis in favor of Mφ control of *P. aeruginosa (*123) showed that oxidized DNA is a more potent activator of cGAS–STING pathway. Indeed, impaired activity of DNA damage repair response mediators, such as ataxia telangiectasia mutated (ATM)-RAD3, poly ADP-ribose polymerase (PARP), and breast cancer1/2 (BRCA1/2) is associated with persisting double-stranded DNA breaks, accumulation of cytosolic DNA and activation of cGAS–STING pathway (124–126). The bone marrow derived dendritic cells and Mφ from cGAS$^{-/-}$, STING$^{-/-}$, or IRF-3$^{-/-}$ mice were deficient in anti-adenoviral responses (127, 128); however, cGAS$^{-/-}$ and STING$^{-/-}$ mice were not defective in the induction of adaptive immunity and achieved adenoviral clearance at a similar rate as was noted in WT mice (128).

Mechanistically, it was shown that activated STING binds to and be phosphorylated by TANK binding kinase 1 (TBK1) dimer or IκB kinase (IKK) (129, 130) and it was suggested that STING–TBK1/IKK signalosome produces a scaffold to phosphorylate IRF3 (activate-form) or inhibitor of NF-κBα (targeted for degradation) and consequently, signal IRF3-dependent type 1 ISGs and NF-κB activation, respectively. TBK1 is also suggested to control STING stimulation. The p62/SQSTM1, which is phosphorylated by TBK1, directs ubiquitinated STING to autophagosome for degradation (131). Others indicated that caspase-9 and caspase-3 can cleave cGAS and IRF3 to restrain deleterious inflammation.

The cGAS–STING has also been reported to interact with the autophagy machinery. The STING–TBK1 activation and ISG expression induced ER stress and mechanistic target of rapamycin complex 1 (mTORC1) dysfunction (132, 133). Both ER stress and mTORC1 disturbances can signal Unc-51-like autophagy activating kinase (ULK1) and Beclin-1-class III phosphatidylinositol 3-kinase (PI3KC3) complexes, which together promote initiation of the classical autophagy (132, 133). cGAS was also indicated to directly interact with beclin-1-PI3KC3 complex to trigger autophagy (134). Further, cGAS–STING-mediated inflammation was mitigated by PINK1 and Parkin,

which promote the clearance of damaged mitochondria (135). Some studies have also implicated the crosstalk between cGAS–STING and autophagy in pathogen clearance. For example, STING recognition of extracellular mycobacterial DNA enhanced the bacilli delivery to autophagosomes, and mice with monocytes incapable of delivering bacilli to the autophagy pathway were extremely susceptible to infection (136). Direct interaction between cGAS and beclin-1 not only halted the innate immune response against herpes simplex virus-1 infection but also enhanced the autophagy-mediated degradation of cytosolic pathogen DNA to prevent excessive cGAS activation and persistent immune stimulation (134). These findings suggest that autophagy/mitophagy provide a negative feedback control on over-activation of the cGAS–STING-mediated inflammation.

NON-CODING RNA REGULATION OF MITOCHONDRIAL HEALTH AND ITS POTENTIAL TO INFLUENCE INNATE IMMUNITY

A significant portion of the eukaryotes' genome encodes for non-coding RNAs (ncRNAs) of different sizes. The ncRNAs regulate diverse biological processes, and their significance in regulation of mitochondrial metabolic function has been recognized recently. In this section, we briefly discuss the influence of ncRNAs in shaping the mitochondrial health and interpolate its potential effects in shaping the host innate immunity.

Short, non-coding micro(mi)RNAs (~22 bp) regulate the gene expression by binding to the promoters, 5′ and 3′ untranslated regions (UTRs), or open reading frame (ORF) of the targeted mRNAs. For example, miR-23a/23b miRNAs participated in the regulation of mitochondrial TCA cycle *via* activation of glutaminase enzyme (137), and miR-30 family members inhibited mitochondrial fission and apoptosis through suppressing the *p53* and *Drp1* expression (138). These miRNAs, if present in Mφ, would potentially favor M2 phenotype. Conversely, several miRNAs suppress mitochondrial homeostasis and have a potential to favor M1 Mφ phenotype. Examples include miR-696 that inhibited FA oxidation and mitochondrial biogenesis by PGC-1α (139), miR-210 (upregulated in hypoxic conditions) that blocked mitochondrial respiration by inhibiting *Isc* gene homologs encoding for the iron sulfur clusters (140), and miR-195 that directly inhibits SIRT3 implicated in regulating mitochondrial metabolism (141). The miR-762 was recently shown to translocate to the mitochondria and inhibit translation of ND2 subunit of mitochondrial complex I, which enhanced mtROS generation (142).

Non-coding circular RNAs (circRNAs) form a covalent bond between their 5′ and 3′ ends and exhibit significant resistance to exonucleases. A mitochondrial fission and apoptosis-related circRNA (MFACR) was recently shown to enhance mitochondrial fission and apoptosis in cardiomyocytes, and MFACR knockdown attenuated mitochondrial fission and myocardial infarction in mice (143). Steatohepatitis-associated circRNA ATP5B Regulator (SCAR) is located in the mitochondria, where it binds to ATP5B and suppresses mtROS generation (144). Authors also showed that mitochondria-specific delivery of circRNA SCAR alleviated meta-inflammation *in vivo* (144). Mitochondrial genome-derived mc-COX2 circRNA was present in plasma of chronic lymphocytic leukemia (CLL); a decline in mc-COX2 affected mitochondrial functions and induced cell apoptosis and its upregulation was positively associated with worsening survival of CLL patients (145). How mitochondria targeted circRNAs influence inflammatory *vs*. immunomodulatory role of Mφ or other innate immune cells is not studied.

Long non-coding RNAs (lncRNAs; >200 nucleotides) bear many signatures of mRNAs, *e.g.*, 5′ capping and polyadenylation and can impact gene expression by interacting with DNA, RNA, or proteins (146). LncRNAs play a role in mitochondrial homeostasis by directly influencing the expression and/or stability of the mRNAs encoding for mitochondrial proteins or by indirectly affecting the miRNAs that may govern the half-life of mRNAs responsible for mitochondrial health. A few lncRNAs encoded by mtDNA include lncND5, lncND6, and lncCytb (147), though their role in mitochondrial function is not known. Recently, lncRNA Cerox1 (cytoplasmic endogenous regulator of oxidative phosphorylation 1) was identified to enhance the mitochondrial complex I activity by blocking regulatory effects of miR-488-3p on mRNAs for complex I subunits (148). Tug1 (taurine-upregulated gene 1) lncRNA regulates PGC-1α activity, and its overexpression enhanced the mitochondrial bioenergetics in the podocyte of diabetic nephropathy (149). Several lncRNAs have been identified to regulate apoptosis through their influence on mitochondrial health. For example, inhibition of AK055347 lncRNA was detrimental to cells' viability that was accompanied by downregulation of ETC, cyt P450, and ATP synthase (150). Cardiac apoptosis-related lncRNA (CARL) blocked mitochondrial fission and apoptosis by impairing miR-539-dependent PHB2 downregulation (151), while FAL1 lncRNA enhanced DRP1-mediated mitochondrial fission and apoptosis (152). GAS5 and SAMMSON lncRNAs are also shown to regulate apoptosis *via* diverse mechanisms.

Overall, it is becoming increasingly clear that ncRNAs, originated either from nuclear or mitochondrial genome, are involved in regulating the mitochondrial homeostasis and will have a role in shaping the innate immunity.

SUMMARY

In this review, we have summarized the current literature on various roles of mitochondria in influencing the Mφ response. It is well recognized that the mitochondria can satisfy cell energy requirements by maintaining their dynamicity, and alterations in mitochondrial structure and dynamics can modulate Mφ immune response. The various mechanisms applied by pathogens to perturb and reprogram Mφ metabolic health in

favor of their survival in the host are also appreciated in the current literature. We envision that novel therapeutic strategies targeting mitochondrial dynamics will be useful in controlling the pathogenic effects of the overly active immune system while achieving the beneficial effects against the intracellular pathogens.

AUTHOR CONTRIBUTIONS

SC wrote first draft, IC wrote the section on ncRNAs, and SC and NG contributed to editing and writing of the final version. All authors contributed to the article and approved the submitted version.

FUNDING

This work was supported by a grant from the National Institute of Allergy and Infectious Diseases (R01AI136031) of the National Institutes of Health to NG. The funders had no role in the study design, data collection and analysis, decision to publish, or preparation of the manuscript.

REFERENCES

1. Hume DA, Irvine KM, Pridans C. The Mononuclear Phagocyte System: The relationship between monocytes and macrophages. *Trends Immunol* (2019) 40:98–112. doi: 10.1016/j.it.2018.11.007
2. Haniffa M, Bigley V, Collin M. Human mononuclear phagocyte system reunited. *Semin Cell Dev Biol* (2015) 41:59–69. doi: 10.1016/j.semcdb.2015.05.004
3. Muraille E, Leo O, Moser M. TH1/TH2 paradigm extended: macrophage polarization as an unappreciated pathogen-driven escape mechanism? *Front Immunol* (2014) 5:603. doi: 10.3389/fimmu.2014.00603
4. Minutti CM, Knipper JA, Allen JE, Zaiss DM. Tissue-specific contribution of macrophages to wound healing. *Semin Cell Dev Biol* (2017) 61:3–11. doi: 10.1016/j.semcdb.2016.08.006
5. Tiku V, Tan MW, Dikic I. Mitochondrial functions in infection and immunity. *Trends Cell Biol* (2020) 30(4):263–75. doi: 10.1016/j.tcb.2020.01.006
6. Koo SJ, Garg NJ. Metabolic programming of macrophage functions and pathogens control. *Redox Biol* (2019) 24:101198. doi: 10.1016/j.redox.2019.101198
7. Chen Y, Zhou Z, Min W. Mitochondria, oxidative stress and innate immunity. *Front Physiol* (2018) 9:1487. doi: 10.3389/fphys.2018.01487
8. Patoli D, Mignotte F, Deckert V, Dusuel A, Dumont A, Rieu A, et al. Inhibition of mitophagy drives macrophage activation and antibacterial defense during sepsis. *J Clin Invest* (2020) 130(11):5858–74. doi: 10.1172/JCI130996
9. Olive C:. Pattern recognition receptors: sentinels in innate immunity and targets of new vaccine adjuvants. *Expert Rev Vaccines* (2012) 11:237–56. doi: 10.1586/erv.11.189
10. Mukhopadhyay S, Pluddemann A, Gordon S. Macrophage pattern recognition receptors in immunity, homeostasis and self tolerance. *Adv Exp Med Biol* (2009) 653:1–14. doi: 10.1007/978-1-4419-0901-5_1
11. Akira S, Takeda K. Toll-like receptor signalling. *Nat Rev Immunol* (2004) 4:499–511. doi: 10.1038/nri1391
12. Su X, Yu Y, Zhong Y, Giannopoulou EG, Hu X, Liu H, et al. Interferon-gamma regulates cellular metabolism and mRNA translation to potentiate macrophage activation. *Nat Immunol* (2015) 16:838–49. doi: 10.1038/ni.3205
13. Green DS, Young HA, Valencia JC. Current prospects of type II interferon gamma signaling and autoimmunity. *J Biol Chem* (2017) 292:13925–33. doi: 10.1074/jbc.R116.774745
14. Martinez FO, Gordon S. The M1 and M2 paradigm of macrophage activation: time for reassessment. *F1000Prime Rep* (2014) 6:13. doi: 10.12703/P6-13
15. Panday A, Sahoo MK, Osorio D, Batra S. NADPH oxidases: an overview from structure to innate immunity-associated pathologies. *Cell Mol Immunol* (2015) 12:5–23. doi: 10.1038/cmi.2014.89
16. Lopez M, Tanowitz HB, Garg NJ. Pathogenesis of chronic Chagas Disease: macrophages, Mitochondria, and oxidative stress. *Curr Clin Microbiol Rep* (2018) 5:45–54. doi: 10.1007/s40588-018-0081-2
17. Andrew PJ, Mayer B. Enzymatic function of nitric oxide synthases. *Cardiovasc Res* (1999) 43:521–31. doi: 10.1016/S0008-6363(99)00115-7
18. Mesev EV, LeDesma RA, Ploss A. Decoding type I and III interferon signalling during viral infection. *Nat Microbiol* (2019) 4:914–24. doi: 10.1038/s41564-019-0421-x
19. Tay MZ, Poh CM, Renia L, MacAry PA, Ng LFP. The trinity of COVID-19: immunity, inflammation and intervention. *Nat Rev Immunol* (2020) 20:363–74. doi: 10.1038/s41577-020-0311-8
20. Shapouri-Moghaddam A, Mohammadian S, Vazini H, Taghadosi M, Esmaeili SA, Mardani F, et al. Macrophage plasticity, polarization, and function in health and disease. *J Cell Physiol* (2018) 233(9):6425–40. doi: 10.1002/jcp.26429
21. Hoshino T, Winkler-Pickett RT, Mason AT, Ortaldo JR, Young HA. IL-13 production by NK cells: IL-13-producing NK and T cells are present in vivo in the absence of IFN-gamma. *J Immunol* (1999) 162:51–9.
22. Van Dyken SJ, Locksley RM. Interleukin-4- and interleukin-13-mediated alternatively activated macrophages: roles in homeostasis and disease. *Annu Rev Immunol* (2013) 31:317–43. doi: 10.1146/annurev-immunol-032712-095906
23. Wang LX, Zhang SX, Wu HJ, Rong XL, Guo J. M2b macrophage polarization and its roles in diseases. *J Leukoc Biol* (2019) 106:345–58. doi: 10.1002/JLB.3RU1018-378RR
24. Anders CB, Lawton TMW, Ammons MCB. Metabolic immunomodulation of macrophage functional plasticity in nonhealing wounds. *Curr Opin Infect Dis* (2019) 32:204–9. doi: 10.1097/QCO.0000000000000550
25. Jiang H, Harris MB, Rothman P. IL-4/IL-13 signaling beyond JAK/STAT. *J Allergy Clin Immunol* (2000) 105:1063–70. doi: 10.1067/mai.2000.107604
26. Wahli W, Michalik L. PPARs at the crossroads of lipid signaling and inflammation. *Trends Endocrinol Metab* (2012) 23:351–63. doi: 10.1016/j.tem.2012.05.001
27. Roszer T. Understanding the mysterious M2 macrophage through activation markers and effector mechanisms. *Mediators Inflamm* (2015) 2015:816460. doi: 10.1155/2015/816460
28. Couper KN, Blount DG, Riley EM. IL-10: the master regulator of immunity to infection. *J Immunol* (2008) 180:5771–7. doi: 10.4049/jimmunol.180.9.5771
29. Richards DM, Endres RG. The mechanism of phagocytosis: two stages of engulfment. *Biophys J* (2014) 107:1542–53. doi: 10.1016/j.bpj.2014.07.070
30. Mantegazza AR, Magalhaes JG, Amigorena S, Marks MS. Presentation of phagocytosed antigens by MHC class I and II. *Traffic* (2013) 14:135–52. doi: 10.1111/tra.12026
31. Jakubzick CV, Randolph GJ, Henson PM. Monocyte differentiation and antigen-presenting functions. *Nat Rev Immunol* (2017) 17:349–62. doi: 10.1038/nri.2017.28
32. Arandjelovic S, Ravichandran KS. Phagocytosis of apoptotic cells in homeostasis. *Nat Immunol* (2015) 16:907–17. doi: 10.1038/ni.3253
33. Gordon S, Pluddemann A. Macrophage clearance of apoptotic cells: a critical assessment. *Front Immunol* (2018) 9:127. doi: 10.3389/fimmu.2018.00127

34. Newsholme P, Gordon S, Newsholme EA. Rates of utilization and fates of glucose, glutamine, pyruvate, fatty acids and ketone bodies by mouse macrophages. *Biochem J* (1987) 242:631–6. doi: 10.1042/bj2420631
35. Van den Bossche J, Baardman J, Otto NA, van der Velden S, Neele AE, van den Berg SM, et al. Mitochondrial dysfunction prevents repolarization of inflammatory macrophages. *Cell Rep* (2016) 17:684–96. doi: 10.1016/j.celrep.2016.09.008
36. Feingold KR, Shigenaga JK, Kazemi MR, McDonald CM, Patzek SM, Cross AS, et al. Mechanisms of triglyceride accumulation in activated macrophages. *J Leukoc Biol* (2012) 92:829–39. doi: 10.1189/jlb.1111537
37. Ecker J, Liebisch G, Englmaier M, Grandl M, Robenek H, Schmitz G. Induction of fatty acid synthesis is a key requirement for phagocytic differentiation of human monocytes. *Proc Natl Acad Sci USA* (2010) 107:7817–22. doi: 10.1073/pnas.0912059107
38. Freemerman AJ, Johnson AR, Sacks GN, Milner JJ, Kirk EL, Troester MA, et al. Metabolic reprogramming of macrophages: glucose transporter 1 (GLUT1)-mediated glucose metabolism drives a proinflammatory phenotype. *J Biol Chem* (2014) 289:7884–96. doi: 10.1074/jbc.M113.522037
39. Rodriguez-Prados JC, Traves PG, Cuenca J, Rico D, Aragones J, Martin-Sanz P, et al. Substrate fate in activated macrophages: a comparison between innate, classic, and alternative activation. *J Immunol* (2010) 185:605–14. doi: 10.4049/jimmunol.0901698
40. Koivunen P, Hirsila M, Remes AM, Hassinen IE, Kivirikko KI, Myllyharju J. Inhibition of hypoxia-inducible factor (HIF) hydroxylases by citric acid cycle intermediates: possible links between cell metabolism and stabilization of HIF. *J Biol Chem* (2007) 282:4524–32. doi: 10.1074/jbc.M610415200
41. Demaria M, Poli V. PKM2, STAT3 and HIF-1alpha: The Warburg's vicious circle. *JAKSTAT* (2012) 1:194–6. doi: 10.4161/jkst.20662
42. Tannahill GM, Curtis AM, Adamik J, Palsson-McDermott EM, McGettrick AF, Goel G, et al. Succinate is an inflammatory signal that induces IL-1beta through HIF-1alpha. *Nature* (2013) 496:238–42. doi: 10.1038/nature11986
43. Mills EL, Kelly B, Logan A, Costa ASH, Varma M, Bryant CE, et al. Succinate dehydrogenase supports metabolic repurposing of mitochondria to drive inflammatory macrophages. *Cell* (2016) 167:457–70.e13. doi: 10.1016/j.cell.2016.08.064
44. Infantino V, Iacobazzi V, Palmieri F, Menga A. ATP-citrate lyase is essential for macrophage inflammatory response. *Biochem Biophys Res Commun* (2013) 440:105–11. doi: 10.1016/j.bbrc.2013.09.037
45. Ryan DG, Murphy MP, Frezza C, Prag HA, Chouchani ET, O'Neill LA, et al. Coupling Krebs cycle metabolites to signalling in immunity and cancer. *Nat Metab* (2019) 1:16–33. doi: 10.1038/s42255-018-0014-7
46. Ham M, Lee JW, Choi AH, Jang H, Choi G, Park J, et al. Macrophage glucose-6-phosphate dehydrogenase stimulates proinflammatory responses with oxidative stress. *Mol Cell Biol* (2013) 33:2425–35. doi: 10.1128/MCB.01260-12
47. Stuehr DJ. Enzymes of the L-arginine to nitric oxide pathway. *J Nutr* (2004) 134:2748S–51S. doi: 10.1093/jn/134.10.2748S
48. Wu GY, Brosnan JT. Macrophages can convert citrulline into arginine. *Biochem J* (1992) 281(Pt 1):45–8. doi: 10.1042/bj2810045
49. Jastroch M, Divakaruni AS, Mookerjee S, Treberg JR, Brand MD. Mitochondrial proton and electron leaks. *Essays Biochem* (2010) 47:53–67. doi: 10.1042/bse0470053
50. Al-Shabany AJ, Moody AJ, Foey AD, Billington RA. Intracellular NAD+ levels are associated with LPS-induced TNF-alpha release in pro-inflammatory macrophages. *Biosci Rep* (2016) 36:e00301. doi: 10.1042/BSR20150247
51. Petin K, Weiss R, Muller G, Garten A, Grahnert A, Sack U, et al. NAD metabolites interfere with proliferation and functional properties of THP-1 cells. *Innate Immun* (2019) 25:280–93. doi: 10.1177/1753425919844587
52. Minhas PS, Liu L, Moon PK, Joshi AU, Dove C, Mhatre S, et al. Macrophage de novo NAD(+) synthesis specifies immune function in aging and inflammation. *Nat Immunol* (2019) 20:50–63. doi: 10.1038/s41590-018-0255-3
53. Starkov AA. An update on the role of mitochondrial alpha-ketoglutarate dehydrogenase in oxidative stress. *Mol Cell Neurosci* (2013) 55:13–6. doi: 10.1016/j.mcn.2012.07.005
54. Mailloux RJ. An update on mitochondrial reactive oxygen species production. *Antioxidants (Basel)* (2020) 9(6):472. doi: 10.3390/antiox9060472
55. Huang SC, Everts B, Ivanova Y, O'Sullivan D, Nascimento M, Smith AM, et al. Cell-intrinsic lysosomal lipolysis is essential for alternative activation of macrophages. *Nat Immunol* (2014) 15:846–55. doi: 10.1038/ni.2956
56. Al-Khami AA, Rodriguez PC, Ochoa AC. Energy metabolic pathways control the fate and function of myeloid immune cells. *J Leukoc Biol* (2017) 102:369–80. doi: 10.1189/jlb.1VMR1216-535R
57. Mehrotra P, Jamwal SV, Saquib N, Sinha N, Siddiqui Z, Manivel V, et al. Pathogenicity of Mycobacterium tuberculosis is expressed by regulating metabolic thresholds of the host macrophage. *PLoS Pathog* (2014) 10:e1004265. doi: 10.1371/journal.ppat.1004265
58. Crowe SM, Westhorpe CL, Mukhamedova N, Jaworowski A, Sviridov D, Bukrinsky M. The macrophage: the intersection between HIV infection and atherosclerosis. *J Leukoc Biol* (2010) 87:589–98. doi: 10.1189/jlb.0809580
59. Wyatt EV, Diaz K, Griffin AJ, Rasmussen JA, Crane DD, Jones BD, et al. Metabolic reprogramming of host cells by virulent *Francisella tularensis* for optimal replication and modulation of inflammation. *J Immunol* (2016) 196:4227–36. doi: 10.4049/jimmunol.1502456
60. Bowden SD, Rowley G, Hinton JC, Thompson A. Glucose and glycolysis are required for the successful infection of macrophages and mice by *Salmonella enterica* serovar *typhimurium*. *Infect Immun* (2009) 77:3117–26. doi: 10.1128/IAI.00093-09
61. Eisele NA, Ruby T, Jacobson A, Manzanillo PS, Cox JS, Lam L, et al. *Salmonella* require the fatty acid regulator PPARδ for the establishment of a metabolic environment essential for long-term persistence. *Cell Host Microbe* (2013) 14:171–82. doi: 10.1016/j.chom.2013.07.010
62. Seabra SH, DaMatta RA, de Mello FG, de Souza W. Endogenous polyamine levels in macrophages is sufficient to support growth of *Toxoplasma gondii*. *J Parasitol* (2004) 90:455–60. doi: 10.1645/GE-179R
63. McConville MJ. Metabolic Crosstalk between *Leishmania* and the macrophage host. *Trends Parasitol* (2016) 32:666–8. doi: 10.1016/j.pt.2016.05.005
64. Moreira D, Rodrigues V, Abengozar M, Rivas L, Rial E, Laforge M, et al. *Leishmania infantum* modulates host macrophage mitochondrial metabolism by hijacking the SIRT1-AMPK axis. *PLoS Pathog* (2015) 11:e1004684. doi: 10.1371/journal.ppat.1004684
65. Lamour SD, Choi BS, Keun HC, Müller I, Saric J. Metabolic characterization of *Leishmania major* infection in activated and nonactivated macrophages. *J Proteome Res* (2012) 11:4211–22. doi: 10.1021/pr3003358
66. Koo SJ, Szczesny B, Wan X, Putluri N, Garg NJ. Pentose phosphate shunt modulates reactive oxygen species and nitric oxide production controlling *Trypanosoma cruzi* in macrophages. *Front Immunol* (2018) 9:202. doi: 10.3389/fimmu.2018.00202
67. Chawla A. Control of macrophage activation and function by PPARs. *Circ Res* (2010) 106:1559–69. doi: 10.1161/CIRCRESAHA.110.216523
68. Igoillo-Esteve M, Maugeri D, Stern AL, Beluardi P, Cazzulo JJ. The pentose phosphate pathway in *Trypanosoma cruzi: a* potential target for the chemotherapy of Chagas disease. *Acad Bras Cienc* (2007) 79:649–63. doi: 10.1590/S0001-37652007000400007
69. Redza-Dutordoir M, Averill-Bates DA. Activation of apoptosis signalling pathways by reactive oxygen species. *Biochim Biophys Acta* (2016) 1863:2977–92. doi: 10.1016/j.bbamcr.2016.09.012
70. Bao Q, Shi Y. Apoptosome: a platform for the activation of initiator caspases. *Cell Death Differ* (2007) 14:56–65. doi: 10.1038/sj.cdd.4402028
71. Dorstyn L, Akey CW, Kumar S. New insights into apoptosome structure and function. *Cell Death Differ* (2018) 25:1194–208. doi: 10.1038/s41418-017-0025-z
72. Hu WL, Dong HY, Li Y, Ojcius DM, Li SJ, Yan J. Bid-Induced Release of AIF/EndoG from mitochondria causes apoptosis of macrophages during infection with *Leptospira interrogans*. *Front Cell Infect Microbiol* (2017) 7:471. doi: 10.3389/fcimb.2017.00471
73. Koterski JF, Nahvi M, Venkatesan MM, Haimovich B. Virulent *Shigella flexneri* causes damage to mitochondria and triggers necrosis in infected human monocyte-derived macrophages. *Infect Immun* (2005) 73:504–13. doi: 10.1128/IAI.73.1.504-513.2005

74. Chen M, Gan H, Remold HG. A mechanism of virulence: virulent *Mycobacterium tuberculosis* strain H37Rv, but not attenuated H37Ra, causes significant mitochondrial inner membrane disruption in macrophages leading to necrosis. *J Immunol* (2006) 176:3707–16. doi: 10.4049/jimmunol.176.6.3707
75. Van Opdenbosch N, Gurung P, Vande Walle L, Fossoul A, Kanneganti TD, Lamkanfi M. Activation of the NLRP1b inflammasome independently of ASC-mediated caspase-1 autoproteolysis and speck formation. *Nat Commun* (2014) 5:3209. doi: 10.1038/ncomms4209
76. Levinsohn JL, Newman ZL, Hellmich KA, Fattah R, Getz MA, Liu S, et al. Anthrax lethal factor cleavage of Nlrp1 is required for activation of the inflammasome. *PLoS Pathog* (2012) 8:e1002638. doi: 10.1371/journal.ppat.1002638
77. Melehani JH, James DB, DuMont AL, Torres VJ, Duncan JA. *Staphylococcus aureus* Leukocidin a/b (lukab) kills human monocytes via host NLRP3 and ASC when extracellular, but not intracellular. *PLoS Pathog* (2015) 11: e1004970. doi: 10.1371/journal.ppat.1004970
78. Craven RR, Gao X, Allen IC, Gris D, Bubeck Wardenburg J, McElvania-Tekippe E, et al. *Staphylococcus aureus* alpha-hemolysin activates the NLRP3-inflammasome in human and mouse monocytic cells. *PLoS One* (2009) 4:e7446. doi: 10.1371/journal.pone.0007446
79. Pickles S, Vigie P, Youle RJ. Mitophagy and quality control mechanisms in mitochondrial maintenance. *Curr Biol* (2018) 28:R170–R85. doi: 10.1016/j.cub.2018.01.004
80. Adaniya SM, OU J, Cypress MW, Kusakari Y, Jhun BS. Posttranslational modifications of mitochondrial fission and fusion proteins in cardiac physiology and pathophysiology. *Am J Physiol Cell Physiol* (2019) 316: C583–604. doi: 10.1152/ajpcell.00523.2018
81. Cherok E, Xu S, Li S, Das S, Meltzer WA, Zalzman M, et al. Novel regulatory roles of Mff and Drp1 in E3 ubiquitin ligase MARCH5-dependent degradation of MiD49 and Mcl1 and control of mitochondrial dynamics. *Mol Biol Cell* (2017) 28:396–410. doi: 10.1091/mbc.e16-04-0208
82. Park J, Choi H, Min JS, Park SJ, Kim JH, Park HJ, et al. Mitochondrial dynamics modulate the expression of pro-inflammatory mediators in microglial cells. *J Neurochem* (2013) 127:221–32. doi: 10.1111/jnc.12361
83. Mohasin M, Balbirnie-Cumming K, Fisk E, Prestwich EC, Russell CD, Marshall J, et al. Macrophages utilize mitochondrial fission to enhance mROS production during responses to Streptococcus pneumoniae. *bioRxiv* (2019) 722603. doi: 10.1101/722603
84. Jain P, Luo ZQ, Blanke SR. *Helicobacter pylori* vacuolating cytotoxin A (VacA) engages the mitochondrial fission machinery to induce host cell death. *Proc Natl Acad Sci USA* (2011) 108:16032–7. doi: 10.1073/pnas.1105175108
85. Chowdhury SR, Reimer A, Sharan M, Kozjak-Pavlovic V, Eulalio A, Prusty BK, et al. *Chlamydia* preserves the mitochondrial network necessary for replication via microRNA-dependent inhibition of fission. *J Cell Biol* (2017) 216:1071–89. doi: 10.1083/jcb.201608063
86. Suzuki M, Danilchanka O, Mekalanos JJ. Vibrio cholerae T3SS effector VopE modulates mitochondrial dynamics and innate immune signaling by targeting Miro GTPases. *Cell Host Microbe* (2014) 16:581–91. doi: 10.1016/j.chom.2014.09.015
87. Lee J, Choi JA, Cho SN, Son SH, Song CH. Mitofusin 2-deficiency suppresses *Mycobacterium tuberculosis* survival in macrophages. *Cells* (2019) 8 (11):1355. doi: 10.3390/cells8111355
88. Tur J, Pereira-Lopes S, Vico T, Marin EA, Munoz JP, Hernandez-Alvarez M, et al. Mitofusin 2 in macrophages links mitochondrial ROS production, cytokine release, phagocytosis, autophagy, and bactericidal activity. *Cell Rep* (2020) 32:108079. doi: 10.1016/j.celrep.2020.108079
89. Ohira Y, Cartier LJ, Chen M, Holloszy JO. Induction of an increase in mitochondrial matrix enzymes in muscle of iron-deficient rats. *Am J Physiol* (1987) 253:C639–44. doi: 10.1152/ajpcell.1987.253.5.C639
90. Vats D, Mukundan L, Odegaard JI, Zhang L, Smith KL, Morel CR, et al. Oxidative metabolism and PGC-1beta attenuate macrophage-mediated inflammation. *Cell Metab* (2006) 4:13–24. doi: 10.1016/j.cmet.2006.05.011
91. Wan X, Wen JJ, Koo SJ, Liang LY, Garg NJ. SIRT1-PGC1alpha-NFkappaB pathway of oxidative and inflammatory stress during *Trypanosoma cruzi* infection: Benefits of SIRT1-targeted therapy in improving heart function in Chagas disease. *PLoS Pathog* (2016) 12:e1005954. doi: 10.1371/journal.ppat.1005954
92. Cherry AD, Piantadosi CA. Regulation of mitochondrial biogenesis and its intersection with inflammatory responses. *Antioxid Redox Signal* (2015) 22:965–76. doi: 10.1089/ars.2014.6200
93. Nisoli E, Clementi E, Paolucci C, Cozzi V, Tonello C, Sciorati C, et al. Mitochondrial biogenesis in mammals: the role of endogenous nitric oxide. *Science* (2003) 299:896–9. doi: 10.1126/science.1079368
94. MacGarvey NC, Suliman HB, Bartz RR, Fu P, Withers CM, Welty-Wolf KE, et al. Activation of mitochondrial biogenesis by heme oxygenase-1-mediated NF-E2-related factor-2 induction rescues mice from lethal Staphylococcus aureus sepsis. *Am J Respir Crit Care Med* (2012) 185:851–61. doi: 10.1164/rccm.201106-1152OC
95. Aquilano K, Vigilanza P, Baldelli S, Pagliei B, Rotilio G, Ciriolo MR. Peroxisome proliferator-activated receptor gamma co-activator 1alpha (PGC-1alpha) and sirtuin 1 (SIRT1) reside in mitochondria: possible direct function in mitochondrial biogenesis. *J Biol Chem* (2010) 285:21590–9. doi: 10.1074/jbc.M109.070169
96. Haden DW, Suliman HB, Carraway MS, Welty-Wolf KE, Ali AS, Shitara H, et al. Mitochondrial biogenesis restores oxidative metabolism during *Staphylococcus aureus* sepsis. *Am J Respir Crit Care Med* (2007) 176:768–77. doi: 10.1164/rccm.200701-161OC
97. Sweeney TE, Suliman HB, Hollingsworth JW, Piantadosi CA. Differential regulation of the PGC family of genes in a mouse model of *Staphylococcus aureus* sepsis. *PLoS One* (2010) 5:e11606. doi: 10.1371/journal.pone.0011606
98. Plataki M, Cho SJ, Harris RM, Huang HR, Yun HS, Schiffer KT, et al. Mitochondrial dysfunction in aged macrophages and lung during primary *Streptococcus pneumoniae* infection is improved with pirfenidone. *Sci Rep* (2019) 9:971. doi: 10.1038/s41598-018-37438-1
99. Kaarbo M, Ager-Wick E, Osenbroch PO, Kilander A, Skinnes R, Muller F, et al. Human cytomegalovirus infection increases mitochondrial biogenesis. *Mitochondrion* (2011) 11:935–45. doi: 10.1016/j.mito.2011.08.008
100. Wu X, Wu FH, Wu Q, Zhang S, Chen S, Sima M. Phylogenetic and molecular evolutionary analysis of mitophagy receptors under hypoxic conditions. *Front Physiol* (2017) 8:539. doi: 10.3389/fphys.2017.00539
101. Jin SM, Youle RJ. PINK1- and Parkin-mediated mitophagy at a glance. *J Cell Sci* (2012) 125:795–9. doi: 10.1242/jcs.093849
102. Zhou R, Yazdi AS, Menu P, Tschopp J. A role for mitochondria in NLRP3 inflammasome activation. *Nature* (2011) 469:221–5. doi: 10.1038/nature09663
103. Ko JH, Yoon SO, Lee HJ, Oh JY. Rapamycin regulates macrophage activation by inhibiting NLRP3 inflammasome-p38 MAPK-NFkappaB pathways in autophagy- and p62-dependent manners. *Oncotarget* (2017) 8:40817–31. doi: 10.18632/oncotarget.17256
104. Sun L, Shen R, Agnihotri SK, Chen Y, Huang Z, Bueler H. Lack of PINK1 alters glia innate immune responses and enhances inflammation-induced, nitric oxide-mediated neuron death. *Sci Rep* (2018) 8:383. doi: 10.1038/s41598-017-18786-w
105. Zhou J, Yang R, Zhang Z, Liu Q, Zhang Y, Wang Q, et al. Mitochondrial protein PINK1 Positively regulates rlr signaling. *Front Immunol* (2019) 10:1069. doi: 10.3389/fimmu.2019.01069
106. Manzanillo PS, Ayres JS, Watson RO, Collins AC, Souza G, Rae CS, et al. The ubiquitin ligase Parkin mediates resistance to intracellular pathogens. *Nature* (2013) 501:512–6. doi: 10.1038/nature12566
107. Kirienko NV, Ausubel FM, Ruvkun G. Mitophagy confers resistance to siderophore-mediated killing by *Pseudomonas aeruginosa*. *Proc Natl Acad Sci USA* (2015) 112:1821–6. doi: 10.1073/pnas.1424954112
108. Genestet C, Bernard-Barret F, Hodille E, Ginevra C, Ader F, Goutelle S, et al. Lyon TBsg: Antituberculous drugs modulate bacterial phagolysosome avoidance and autophagy in *Mycobacterium tuberculosis*-infected macrophages. *Tuberculosis (Edinb)* (2018) 111:67–70. doi: 10.1016/j.tube.2018.05.014
109. Sharma N, Pasala MS, Prakash A. Mitochondrial DNA: Epigenetics and environment. *Environ Mol Mutagen* (2019) 60:668–82. doi: 10.1002/em.22319
110. Ward GA, McGraw K, McLemore AF, Lam NB, Hou H-A, Meyer BS, et al. Oxidized mitochondrial DNA engages TLR9 to activate the NLRP3

inflammasome in myelodysplastic syndromes. *Blood* (2019) 134:774. doi: 10.1182/blood-2019-122358
111. Wu G, Zhu Q, Zeng J, Gu X, Miao Y, Xu W, et al. Extracellular mitochondrial DNA promote NLRP3 inflammasome activation and induce acute lung injury through TLR9 and NF-kappaB. *J Thorac Dis* (2019) 11:4816–28. doi: 10.21037/jtd.2019.10.26
112. Shimada K, Crother TR, Karlin J, Dagvadorj J, Chiba N, Chen S, et al. Oxidized mitochondrial DNA activates the NLRP3 inflammasome during apoptosis. *Immunity* (2012) 36:401–14. doi: 10.1016/j.immuni.2012.01.009
113. Coll RC, Holley CL, Schroder K. Mitochondrial DNA synthesis fuels NLRP3 activation. *Cell Res* (2018) 28:1046–7. doi: 10.1038/s41422-018-0093-8
114. Zhong Z, Liang S, Sanchez-Lopez E, He F, Shalapour S, Lin XJ, et al. New mitochondrial DNA synthesis enables NLRP3 inflammasome activation. *Nature* (2018) 560:198–203. doi: 10.1038/s41586-018-0372-z
115. He Y, Hara H, Nunez G. Mechanism and regulation of NLRP3 inflammasome activation. *Trends Biochem Sci* (2016) 41:1012–21. doi: 10.1016/j.tibs.2016.09.002
116. Piantadosi CA. Mitochondrial DNA, oxidants, and innate immunity. *Free Radic Biol Med* (2020) 152:455–61. doi: 10.1016/j.freeradbiomed.2020.01.013
117. Riley JS, Tait SW. Mitochondrial DNA in inflammation and immunity. *EMBO Rep* (2020) 21:e49799. doi: 10.15252/embr.201949799
118. Wan D, Jiang W, Hao J. Research advances in how the cGAS-STING pathway controls the cellular inflammatory response. *Front Immunol* (2020) 11:615. doi: 10.3389/fimmu.2020.00615
119. Ishikawa H, Barber GN. STING is an endoplasmic reticulum adaptor that facilitates innate immune signalling. *Nature* (2008) 455:674–8. doi: 10.1038/nature07317
120. Sun L, Wu J, Du F, Chen X, Chen ZJ. Cyclic GMP-AMP synthase is a cytosolic DNA sensor that activates the type I interferon pathway. *Science* (2013) 339:786–91. doi: 10.1126/science.1232458
121. Li XD, Wu J, Gao D, Wang H, Sun L, Chen ZJ. Pivotal roles of cGAS-cGAMP signaling in antiviral defense and immune adjuvant effects. *Science* (2013) 341:1390–4. doi: 10.1126/science.1244040
122. West AP, Khoury-Hanold W, Staron M, Tal MC, Pineda CM, Lang SM, et al. Mitochondrial DNA stress primes the antiviral innate immune response. *Nature* (2015) 520:553–7. doi: 10.1038/nature14156
123. Qin S, Lin P, Wu Q, Pu Q, Zhou C, Wang B, et al. Small-molecule inhibitor of 8-oxoguanine DNA glycosylase 1 regulates inflammatory responses during *Pseudomonas aeruginosa* infection. *J Immunol* (2020) 205:2231–42. doi: 10.4049/jimmunol.1901533
124. Heijink AM, Talens F, Jae LT, van Gijn SE, Fehrmann RSN, Brummelkamp TR, et al. BRCA2 deficiency instigates cGAS-mediated inflammatory signaling and confers sensitivity to tumor necrosis factor-alpha-mediated cytotoxicity. *Nat Commun* (2019) 10:100. doi: 10.1038/s41467-018-07927-y
125. Liu H, Zhang H, Wu X, Ma D, Wu J, Wang L, et al. Nuclear cGAS suppresses DNA repair and promotes tumorigenesis. *Nature* (2018) 563:131–6. doi: 10.1038/s41586-018-0629-6
126. Choudhuri S, Garg NJ. PARP1-cGAS-NFkB pathway of proinflammatory macrophage activation by extracellular vesicles released during *Trypanosoma cruzi* infection and Chagas disease. *PLoS Pathog* (2019) 16(4):e1008474. doi: 10.1371/journal.ppat.1008474
127. Di Paolo NC, Doronin K, Baldwin LK, Papayannopoulou T, Shayakhmetov DM. The transcription factor IRF3 triggers "defensive suicide" necrosis in response to viral and bacterial pathogens. *Cell Rep* (2013) 3:1840–6. doi: 10.1016/j.celrep.2013.05.025
128. Anghelina D, Lam E, Falck-Pedersen E. Diminished innate antiviral response to adenovirus vectors in cGAS/STING-deficient mice minimally impacts adaptive immunity. *J Virol* (2016) 90:5915–27. doi: 10.1128/JVI.00500-16
129. Liu S, Cai X, Wu J, Cong Q, Chen X, Li T, et al. Phosphorylation of innate immune adaptor proteins MAVS, STING, and TRIF induces IRF3 activation. *Science* (2015) 347:aaa2630. doi: 10.1126/science.aaa2630
130. Tanaka Y, Chen ZJ. STING specifies IRF3 phosphorylation by TBK1 in the cytosolic DNA signaling pathway. *Sci Signal* (2012) 5:ra20. doi: 10.1126/scisignal.2002521
131. Prabakaran T, Bodda C, Krapp C, Zhang BC, Christensen MH, Sun C, et al. Attenuation of cGAS-STING signaling is mediated by a p62/SQSTM1-dependent autophagy pathway activated by TBK1. *EMBO J* (2018) 37: e97858. doi: 10.15252/embj.201797858
132. Saxton RA, Sabatini DM. mTOR Signaling in growth, metabolism, and disease. *Cell* (2017) 168:960–76. doi: 10.1016/j.cell.2017.02.004
133. Hasan M, Gonugunta VK, Dobbs N, Ali A, Palchik G, Calvaruso MA, et al. Chronic innate immune activation of TBK1 suppresses mTORC1 activity and dysregulates cellular metabolism. *Proc Natl Acad Sci USA* (2017) 114:746–51. doi: 10.1073/pnas.1611113114
134. Liang Q, Seo GJ, Choi YJ, Kwak MJ, Ge J, Rodgers MA, et al. Crosstalk between the cGAS DNA sensor and Beclin-1 autophagy protein shapes innate antimicrobial immune responses. *Cell Host Microbe* (2014) 15:228–38. doi: 10.1016/j.chom.2014.01.009
135. Sliter DA, Martinez J, Hao L, Chen X, Sun N, Fischer TD, et al. Parkin and PINK1 mitigate STING-induced inflammation. *Nature* (2018) 561:258–62. doi: 10.1038/s41586-018-0448-9
136. Watson RO, Manzanillo PS, Cox JS. Extracellular M. tuberculosis DNA targets bacteria for autophagy by activating the host DNA-sensing pathway. *Cell* (2012) 150:803–15. doi: 10.1016/j.cell.2012.06.040
137. Gao P, Tchernyshyov I, Chang TC, Lee YS, Kita K, Ochi T, et al. c-Myc suppression of miR-23a/b enhances mitochondrial glutaminase expression and glutamine metabolism. *Nature* (2009) 458:762–5. doi: 10.1038/nature07823
138. Li J, Donath S, Li Y, Qin D, Prabhakar BS, Li P. miR-30 regulates mitochondrial fission through targeting p53 and the dynamin-related protein-1 pathway. *PLoS Genet* (2010) 6:e1000795. doi: 10.1371/journal.pgen.1000795
139. Aoi W, Naito Y, Mizushima K, Takanami Y, Kawai Y, Ichikawa H, et al. The microRNA miR-696 regulates PGC-1{alpha} in mouse skeletal muscle in response to physical activity. *Am J Physiol Endocrinol Metab* (2010) 298: E799–806. doi: 10.1152/ajpendo.00448.2009
140. Rouault TA, Tong WH. Iron-sulfur cluster biogenesis and human disease. *Trends Genet* (2008) 24:398–407. doi: 10.1016/j.tig.2008.05.008
141. Zhang X, Ji R, Liao X, Castillero E, Kennel PJ, Brunjes DL, et al. MicroRNA-195 regulates metabolism in failing myocardium via alterations in Sirtuin 3 expression and mitochondrial protein acetylation. *Circulation* (2018) 137:2052–67. doi: 10.1161/CIRCULATIONAHA.117.030486
142. Yan K, An T, Zhai M, Huang Y, Wang Q, Wang Y, et al. Mitochondrial miR-762 regulates apoptosis and myocardial infarction by impairing ND2. *Cell Death Dis* (2019) 10:500. doi: 10.1038/s41419-019-1734-7
143. Wang K, Gan TY, Li N, Liu CY, Zhou LY, Gao JN, et al. Circular RNA mediates cardiomyocyte death via miRNA-dependent upregulation of MTP18 expression. *Cell Death Diff* (2017) 24:1111–20. doi: 10.1038/cdd.2017.61
144. Zhao Q, Liu J, Deng H, Ma R, Liao JY, Liang H, et al. Targeting Mitochondria-located circRNA SCAR alleviates NASH via reducing mROS output. *Cell* (2020) 183:76–93.e22. doi: 10.1016/j.cell.2020.08.009
145. Wu Z, Sun H, Wang C, Liu W, Liu M, Zhu Y, et al. Mitochondrial genome-derived circRNA mc-COX2 functions as an oncogene in chronic lymphocytic leukemia. *Mol Ther Nucleic Acids* (2020) 20:801–11. doi: 10.1016/j.omtn.2020.04.017
146. Djebali S, Davis CA, Merkel A, Dobin A, Lassmann T, Mortazavi A, et al. Landscape of transcription in human cells. *Nature* (2012) 489:101–8. doi: 10.1038/nature11233
147. Rackham O, Shearwood AM, Mercer TR, Davies SM, Mattick JS, Filipovska A. Long noncoding RNAs are generated from the mitochondrial genome and regulated by nuclear-encoded proteins. *RNA* (2011) 17:2085–93. doi: 10.1261/rna.029405.111
148. Sirey TM, Roberts K, Haerty W, Bedoya-Reina O, Rogatti-Granados S, Tan JY, et al. The long non-coding RNA Cerox1 is a post transcriptional regulator of mitochondrial complex I catalytic activity. *Elife* (2019) 8:e45051. doi: 10.7554/eLife.50980
149. Long J, Badal SS, Ye Z, Wang Y, Ayanga BA, Galvan DL, et al. Long noncoding RNA Tug1 regulates mitochondrial bioenergetics in diabetic nephropathy. *J Clin Invest* (2016) 126:4205–18. doi: 10.1172/JCI87927
150. Chen G, Guo H, Song Y, Chang H, Wang S, Zhang M, et al. Long noncoding RNA AK055347 is upregulated in patients with atrial fibrillation and

regulates mitochondrial energy production in myocardiocytes. *Mol Med Rep* (2016) 14:5311–7. doi: 10.3892/mmr.2016.5893

151. Wang K, Long B, Zhou LY, Liu F, Zhou QY, Liu CY, et al. CARL lncRNA inhibits anoxia-induced mitochondrial fission and apoptosis in cardiomyocytes by impairing miR-539-dependent PHB2 downregulation. *Nat Commun* (2014) 5:3596. doi: 10.1038/ncomms4596
152. Liu T, Wang Z, Zhou R, Liang W. Focally amplified lncRNA on chromosome 1 regulates apoptosis of esophageal cancer cells via DRP1 and mitochondrial dynamics. *IUBMB Life* (2019) 71:254–60. doi: 10.1002/iub.1971

Conflict of Interest: The authors declare that the research was conducted in the absence of any commercial or financial relationships that could be construed as a potential conflict of interest.

frontiers in Immunology

ORIGINAL RESEARCH
published: 24 February 2021
doi: 10.3389/fimmu.2021.628168

NLRP3 Deficiency Protects Against Intermittent Hypoxia-Induced Neuroinflammation and Mitochondrial ROS by Promoting the PINK1-Parkin Pathway of Mitophagy in a Murine Model of Sleep Apnea

Xu Wu[1,2†], Linjing Gong[1†], Liang Xie[1,2], Wenyu Gu[3], Xinyuan Wang[4], Zilong Liu[1,2] and Shanqun Li[1,2*]*

[1] Department of Pulmonary Medicine, Zhongshan Hospital, Fudan University, Shanghai, China, [2] Clinical Centre for Sleep Breathing Disorder and Snoring, Zhongshan Hospital, Fudan University, Shanghai, China, [3] Department of Urology, Shanghai Tenth People's Hospital, Tongji University School of Medicine, Shanghai, China, [4] Department of Orthopaedics, Zhongshan Hospital, Fudan University, Shanghai, China

Obstructive sleep apnea (OSA) associated neurocognitive impairment is mainly caused by chronic intermittent hypoxia (CIH)-triggered neuroinflammation and oxidative stress. Previous study has demonstrated that mitochondrial reactive oxygen species (mtROS) was pivotal for hypoxia-related tissue injury. As a cytosolic multiprotein complex that participates in various inflammatory and neurodegenerative diseases, NLRP3 inflammasome could be activated by mtROS and thereby affected by the mitochondria-selective autophagy. However, the role of NLRP3 and possible mitophagy mechanism in CIH-elicited neuroinflammation remain to be elucidated. Compared with wild-type mice, NLRP3 deficiency protected them from CIH-induced neuronal damage, as indicated by the restoration of fear-conditioning test results and amelioration of neuron apoptosis. In addition, NLRP3 knockout mice displayed the mitigated microglia activation that elicited by CIH, concomitantly with elimination of damaged mitochondria and reduction of oxidative stress levels (malondialdehyde and superoxide dismutase). Elevated LC3 and beclin1 expressions were remarkably observed in CIH group. *In vitro* experiments, intermittent hypoxia (IH) significantly facilitated mitophagy induction and NLRP3 inflammasome activation in microglial (BV2) cells. Moreover, IH enhanced the accumulation of damaged mitochondria, increased mitochondrial depolarization and augmented mtROS release. Consistently, NLRP3 deletion elicited a protective phenotype against IH through enhancement of Parkin-mediated mitophagy. Furthermore, Parkin deletion or pretreated with 3MA (autophagy inhibitor) exacerbated these detrimental actions of IH, which was accompanied with NLRP3 inflammasome activation. These results revealed NLRP3 deficiency acted as a protective promotor through enhancing Parkin-depended mitophagy in CIH-induced neuroinflammation.

Edited by:
Pedro Manoel Mendes Moraes Vieira, Campinas State University, Brazil

Reviewed by:
Luz Pamela Blanco, National Institutes of Health (NIH), United States
Tarcio Teodoro Braga, Federal University of Paraná, Brazil

***Correspondence:**
Shanqun Li
lishanqun@163.com;
li.shanqun@zs-hospital.sh.cn
Zilong Liu
liu.zilong@zs-hospital.sh.cn

†These authors have contributed equally to this work

Specialty section:
This article was submitted to Inflammation, a section of the journal Frontiers in Immunology

Received: *11 November 2020*
Accepted: *12 January 2021*
Published: *24 February 2021*

Citation:
Wu X, Gong L, Xie L, Gu W, Wang X, Liu Z and Li S (2021) NLRP3 Deficiency Protects Against Intermittent Hypoxia-Induced Neuroinflammation and Mitochondrial ROS by Promoting the PINK1-Parkin Pathway of Mitophagy in a Murine Model of Sleep Apnea. Front. Immunol. 12:628168. doi: 10.3389/fimmu.2021.628168

Thus, NLRP3 gene knockout or pharmacological blockage could be as a potential therapeutic strategy for OSA-associated neurocognitive impairment.

Keywords: obstructive sleep apnea (OSA), neuroinflammation, nucleotide-binding domain like receptor protein 3 (NLRP3), reactive oxygen species (ROS), parkin-mediated mitophagy

INTRODUCTION

Obstructive sleep apnea (OSA) is characterized by the repetitive narrowed or collapsible upper airway, resulting in recurrent hypoxia during sleep (1). As the foremost pathophysiological process of OSA, nocturnal chronic intermittent hypoxia (CIH), causes structural neuron damage and dysfunction in the CNS that are most likely hippocampal-dependent and persistent (2). Clinically, it manifests as neurocognitive and behavioral deficits, or memory and learning impairments (3, 4). Emerging evidence showed that the deleterious effect eliciting by hypoxia in cognitive impairments may be related to ion-channel alterations, glutamate excitotoxicity release (5), oxidative stress overactivation (6), and upregulation of proinflammatory mediators (7). However, the precise mechanisms of neuroinflammation and oxidative stress in cognitive impairment induced by CIH exposure from OSA needs to be further explored.

Sustained hypoxia leads to the activation of microglia, thereby inducing a robust source of oxidative stress mainly through damaged mitochondria, NADPH oxidase and nitric oxide (NO) overproduction (6, 8). In response to cellular danger signals, the nucleotide-binding domain like receptor protein 3 (NLRP3) is recognized as a multiprotein complex sensor to interact with ASC (adapter apoptosis-associated speck-like protein containing a caspase recruitment domain) and procaspase-1, and then form the NLRP3 inflammasome, ultimately leading to the cleavage of caspase-1 and the release of pro-inflammatory interleukin (IL)-1β (9). Moreover, NLRP3 inflammasome has garnered much attention in a variety of neuroinflammatory and neurodegenerative diseases (10, 11). Given that microglia are dominant pro-inflammatory cells in CNS, caspase-1-processed cytokines IL-1β could be released by microglia in pathological conditions, thus aggravating the progression of neuroinflammation (11). And, inhibiting NLRP3 inflammasome activation attenuates neuroinflammation and improves neurological function in brain injury (12). In this regard, the inflammasome-mediated microglia activation may play an important role in the neuroinflammatory conditions.

Previously, we suggested that mitochondrial (mt) damage was a potential cause of NLRP3 inflammasome activation (13). Shimada et al. demonstrated that NLRP3 inflammation can be activated through mt damage-induced apoptotic cascade (14). Moreover, it has also been proven that the combined roles for caspase-8 and caspase-1/NLRP3 causing IL-1β maturation (15), indicating the crosstalk between apoptosis and pyroptosis (16). The mitochondria-selective autophagy, termed as mitophagy, is a conserved self-degradation process that can be negatively regulated by NLRP3 inflammasome (17, 18). To initiate mitophagy, the ubiquitin kinase PTEN-induced putative kinase1 (PINK1) is recruited to the mitochondrial outer membrane to further induce the ubiquitin phosphorylation (19). Subsequently, PINK1 recruits the E3 ubiquitin ligase Parkin from cytosol to damaged mitochondria to establish ubiquitin chains and assemble autophagy receptors (20). The process results in the commencement of mitophagy and then elimination of mitochondrial ROS that is required for NLRP3 inflammasomes induction. Most studies on Parkin-dependent mitophagy have been relevant to neurologic diseases (e.g., Parkinson's disease) (21, 22). However, the role of mitophagy in the setting of OSA is not clear yet.

In this study, we elucidated whether the mitophagy was linked to the protective effect of NLRP3 deficiency from CIH-induced neuroinflammation. Specifically, we focused our *in vitro* study on the Parkin-dependent mitophagy under CIH and determined the NLRP3-mediated mechanism controlling mitophagy. The present study reveals the relevance of Parkin-mediated mitophagy as the protective mechanism against neuroinflammation and presents NLRP3 as a potential therapeutic target.

MATERIAL AND METHODS

Animal and Experimental Model of CIH

$NLRP3^{-/-}$ mice and aged-matched controls on C57BL/6 background (Jackson Laboratory, Sacramento, CA) were housed under standard conditions with a 12-hr light/12-hr dark cycle at 22–24°C and allowed free access to water and food. The project was approved by the Medical Experimental Animal Administrative Committee of the Shanghai Medical College of the Fudan University, in accordance with the guidelines implemented by the National Institutes of Health Guide regarding the care and use of animals for experimental procedures. All effects were made to minimize animal suffering. WT or $NLRP3^{-/-}$ mice (male, 6–7 weeks old, 20–22 g) were randomly divided into four groups of six: the normal air (NA) plus WT mice group, the NA plus NLRP3-/- mice group, the CIH plus WT mice group, and the CIH plus NLRP3-/- mice group. The mice exposed to CIH were placed inside custom-made (28.5cm × 30.0cm × 51.5cm) chambers where flows of oxygen and nitrogen were controlled to obtain the desired profile of changes in oxygen level. CIH was administered for 10 h/day, from 7:00AM to 5:00PM, with the oxygen level oscillating between 24% and 7% with a period of 60s. The NA or CIH treatment was lasted for 7 d/week for 5 weeks. The oxygen concentration was measured automatically using an oxygen analyzer (Corporation, Shanghai, China).

Cell Culture and Treatment

Murine BV-2 microglial cell line was obtained from the Chinese Academyof Medical Sciences (Beijing, China). BV-2 cells were

maintained in DMEM medium supplemented with 10% fetal bovine serum, 100 U/ml penicillin and 100 mg/ml streptomycin (Sigma) in a humidified atmosphere incubator until 70–80% confluent. Microglial cells were maintained in a 37°C custom-made chamber with 5% CO_2. Consistent with animal experiments, the O_2 concentration of this chamber was alternated between 0 and 22% every 30 min *via* injecting oxygen or nitrogen. The dissolved O_2 inside the culture medium was monitored by a laser O_2 probe (Biospherix) and the IH reached to 5% O_2 and 21% O_2 as hypoxic and normoxic values sensed by the cells. After exposing to IH for 3, 6, 12, or 24 h, the microglial cells were collected for immunoblotting, flow cytometry analysis, or immunofluorescent staining. We constructed the NLRP3 knockout (KO) cell line *via* lentivirus transfection (LV) strategy (MOI 20). Cells were plated in 24-well (1×10^4) and cultured overnight before transfection. The cells were transfected with LV-NLRP3 or LV-NC, according to the manufacture's protocols (Obio Technology, Shanghai, China). After 72-h transfection, cells were selected with Puromycin (5 ug/ml) for 10 days to obtain stable strains. Parkin short hairpin RNA (shRNA) plasmids synthesized by GenePharma (Shanghai, China) were diluted in Opti-MEM® medium (Thermo Scientific). Transfection with shRNA was done by Lipofectamine 2000 (Invitrogen) according to the manufacturer's instructions. After 6 h of transfection, cells were cultured in 10%FBS DMEM medium for 48 h. The sequence of shRNA for Parkin was as follows: 5'-GCTTTGAACCTGATCACCAGC-3'. The BV2 cells incubated with 3-MA (5 mM) or the PBS vehicle for 6 h before exposure to IH.

Contextual Fear Conditioning Test

Based on a previously published model, contextual fear conditioning test (FCT) includes two parts: a training phase at 1 day before surgical operation and a test phase on postoperative 1 and 3 days. In training phase, mice receive fear conditioning to establish the long-term memory. Each animal was allowed to adapt to the conditioning chamber (context) for 120 s, followed by six cycles of conditional-unconditional stimuli. A cycle of conditional or unconditional stimuli was then applied as a 20 s, 80 dB tone (conditional stimuli)-30 s delay 5 s, 0.75 mA electrical foot shock (unconditional stimuli). The cycles of conditional/unconditional stimuli were separated by random intervals from 45 to 60 s. The context test, which represents hippocampal-dependent memory, is the major part of the test phase of the FCT. At post-operative 1 and 3 days, all mice were returned into the original conditioning chamber for 5 min, where no tone and no shock were released. The percentage of freezing time (not moving) was captured and collected by Any-Maze software (Xinruan, Shanghai, China).

Immunohistochemical Analysis

For histological analysis, mice were anesthetized and perfused transcardially with cold phosphate buffer solution (PBS). Then the fresh brain was fixed with 4% paraformaldehyde (PFA) and then were embedded in paraffin, and cut into 4-μm-thick sections that were deparaffinized with xylene and rehydrated in a graded series of alcohol. Antigen retrieval was carried out by microwaving in citric acid buffer. Sections were incubated with an antibody against ASC (1:100; Cell Signaling Technology, Danvers, MA, USA), washed, and then incubated with secondary antibody for 1 h at room temperature.

Immunofluorescence Analysis

Terminal deoxynucleotidyl transferase dUTP nick-end labeling (TUNEL) assay was to detect apoptotic cells with *in situ* cell death detection kit (Roche, Netley, NJ) according to the manufacturer's protocol. The final average percentage of apoptotic cells was calculated as TUNEL+/DAPI+ cells in six sections (observed at ×200 magnification). Immunofluorescent staining was also performed on brain slice. Sections were incubated overnight at 4°C with antibodies against LC3 (1:200, Abcam, Cambridge, UK), and Ionized Calcium Binding Adapter Molecule1 (Iba1) (1:100; Wako, Japan). After washing, the sections were incubated with secondary antibodies for 1 h at room temperature. Cell nuclei were counter-stained with 4',6-diamidino-2-phenylindole (DAPI).

BV2 cells were fixed with 4% paraformaldehyde at room temperature for 15–20 min and washed in PBS for three washes of 10 min each. The BV-2 cells were permeabilized for 10 min with 0.1% Triton X-100 in PBS, washed with PBS, and blocked in 1% bull serum albumin (BSA) for 30 min. The coverslips were incubated with mouse-anti-Parkin (1:100; Santacruz Biotechnologies), rabbit-anti-TOM20 (1:200; Beyotime Biotechnology), mouse-anti-LC3 (1:500; Cell Signal Technology), or rabbit-anti-LC3 (1:500; Cell Signal Technology) overnight at 4°C. After washing, the secondary antibody was added. The samples were incubated for 1 h at room temperature, and ultimately examined under a microscope (Olympus IX73, Japan) or a confocal microscope (Fluoview 1000, Olympus, Tokyo, Japan).

Determination of Oxidative Stress Production

The hippocampal and cortex tissues were homogenized in lysis buffer and centrifuged at 10,000 × g for 10 min at 4°C. The supernatants were collected to assess the malondialdehyde (MDA) content and activities of superoxide dismutase (SOD) (Beyotime, China). All results were normalized to the protein concentration and expressed as U/mg protein or nmol/mg protein as appropriate.

Mitochondrial ROS Measurement

The intact mitochondria of hippocampal region were isolated from brain using a commercial kit (Beyotime, China). The following experimental procedures were conducted according to the manufacturer's instructions. Briefly, the homogenate was centrifuged at 6,000 g at 4°C for 5 min. The collected supernatant was further centrifuged at 11,000 g at 4°C for 10 min to obtain a mitochondrial pellet. Then, the mitochondrial ROS was detected utilizing the ROS assay kit (Genmed Scientifics, Shanghai, China).

Cellular mitochondrial ROS activity was assessed with Mito SOX Red (Invitrogen) staining. BV2 cells were seeded onto six-well blank plates with a density of 1×10^5/ml with 3 parallel wells in each group. Cells were incubated with MitoSOX Red probe at a final concentration of 5 μM for 10 min at 37°C and washed twice with PBS. Quantification of mtROS release was conducted

by FACSCalibur (BD Biosciences). All data were analyzed on FlowJo software (Tree Star, San Carlos, CA).

Mitochondrial Membrane Potential

According to the manufacturer's instructions, changes in mitochondrial membrane potential (MMP) were determined using a JC-1 mitochondrial membrane potential assay kit (C2006, Beyotime, China). BV2 cells (1×10^5) were incubated with JC-1 (10 μg/ml) staining buffer for 20 min at 37°C. Then the cells were washed with PBS and observed under microscope or analyzed by FlowJo software. The ratio of aggregates (red fluorescence; good mitochondrial membrane potential) to monomers (green fluorescence; loss of mitochondrial membrane potential) was regarded as a marker of MMP loss.

Cell Apoptosis Detected by Flow Cytometry

As we previously described, BV-2 cells (1×10^5) were collected and then incubated with Annexin V-fluorescein isothiocyanate (FITC) and propidium iodide (PI) (Annexin V Apoptosis Detection Kit; BD Biosciences). The lower and upper right quadrants show the proportions of the early (Annexin V+/PI−) and the late (Annexin V+/PI+) apoptotic cells, respectively.

Western Blotting

Proteins from hippocampal tissues or cell lysates (20–40 μg of total protein) were separated by sodium dodecyl sulfate-polyacrylamide gel electrophoresis and transferred to a polyvinylidene difluoride membrane, and blocked with 5% BSA/Tris-buffered saline with Tween-20 (TBST) for 1 h at room temperature. Then, the membranes were incubated overnight at 4°C with primary antibodies at the following dilutions: NLRP3 (1:1000; abcam), caspase-1 (1:200; Santa cruz), ASC (1:1000; abcam), Bax (1:1000; CST), Bcl-2 (1:2000; CST), caspase-3 (1:1000; CST), Parkin (1:1000; CST), PINK1 (1:1000; abcam), LC3 (1:1000; CST), ATG5 (1:1000; CST), ATG7 (1:1000; CST), P62 (1:1000; CST), Beclin-1 (1:1000; CST), TOM20 (1:500; Beyotime), and GAPDH (1:500; Beyotime), followed by incubation with appropriate secondary antibodies after thoroughly washing three times with TBST. The bands were visualized using the chemiluminescence (ECL) detection system (Thermo Fisher Scientific) and quantified by Image J gel analysis software. Expression levels were normalized against GAPDH.

Quantitative Reverse Transcriptase-PCR (qRT-PCR)

Total RNA was extracted from hippocampal tissues of WT and NLRP3$^{-/-}$ mice from different groups using TRIzol reagent (Invitrogen, Carlsbad, CA) to detected relative IL-1β mRNA level. qRT-PCR was performed on a real-time PCR system (Applied Biosystems 7500HT; Applied Biosystems, Foster City, CA) using SYBR-Green Master Mix Plus (Toyobo, Osaka, Japan) according to the manufacturer's instructions. The expression of IL-1β mRNA was normalized to the mRNA level of GAPDH. The primers specific to IL-1β mRNA used were purchased from Sangon Biotech (Shanghai, China). And, the sequences were as followed: IL-1β-Forward: 5'-GGGCCTCAAAGGAAAGAATC-3', IL-1β-Reverse: 5'-TACCAGTTGGGGAACTCTGC-3'.

Transmission Electron Microscopy (TEM)

BV2 cells were fixed with 2% glutaraldehyde and 1% osmium tetroxide in 0.1 M phosphate buffer (PB) (pH 7.4) at 4°C. Then the cells were sliced into 70~80-nm-thick sections. After being dehydrated in ethanol with 3% uranyl acetate, embedded, and stained with lead citrate for contrast, the sections were examined under transmission electron microscope (JEM 1011, Japan). A blinded pathologist was invited to quantify each section independently.

Statistical Analysis

Data were analyzed with GraphPad Prism-7 statistic software (La Jolla, CA). All values were expressed as mean ± standard error of the mean (SEM). Qualitative data were analyzed by two-tailed t-test between two groups or one-way ANOVA, followed by post-hoc multiple comparisons among multiple groups. $P < 0.05$ was considered statistically significant. At least three independent experiments were performed in duplicate with all the results.

RESULTS

NLRP3 Deficiency Alleviates CIH-Induced Cognitive Dysfunction and Neuronal Apoptosis of Hippocampus

To investigate the potential mechanism regarding CIH-induced neurocognitive impairment, we first established a CIH mice model as described before (23). When the mice were performed the fear-conditioning test, we found the freezing times in the contextual and tone conditional tasks were significantly lower in the CIH group compared with the NA control group ($P < 0.01$, **Figure 1A**). Dramatically, NLRP3 deficiency tended to restore the decreased freezing time as compared to WT mice after CIH exposure ($P < 0.05$, **Figure 1A**). As illustrated in **Figure 1B**, ASC was highly expressed in hippocampus of WT mice exposed to CIH. In contrast, the immunohistochemical staining showed the ASC was faintly stained in the hippocampus of NLRP3$^{-/-}$ mice upon CIH treatment. Western blotting was applied to the cortex and hippocampus samples to detect NLRP3 and cleaved caspase-1. The levels of NLRP3 and activated caspase-1 in WT mice were shown to be upregulated in response to CIH stimulation, but lowly detectable in NLRP3$^{-/-}$ mice (**Figure 1C** and **Figure S1**). Besides, the expression level of IL-1β mRNA in the hippocampi of WT mice increased obviously after CIH treatment, which can be alleviated by the *NLRP3* gene knockout (**Figure 1D**). Neuronal apoptosis caused by neuroinflammation is one important mechanism of cognitive impairment induced by CIH (11). To ascertain it, the CIH group showed a significant increase in the number of TUNEL positive cells by immunofluorescence (33 ± 7.78%, $P < 0.01$). However, the absence of NLRP3 in mice underwent a 26% attenuation of the apoptotic cells compared with the WT mice following CIH exposure ($P < 0.01$, **Figures 1E, F**). It is worthy to note the enhanced neuronal apoptosis subjected

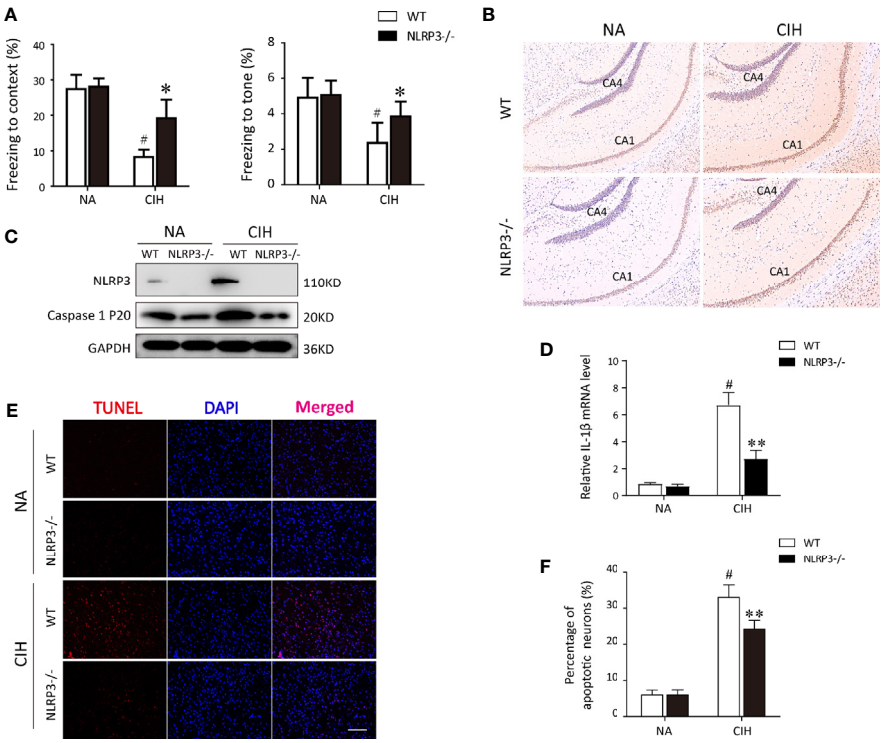

FIGURE 1 | Protective effect of NLRP3 deficiency on CIH-induced neuronal damage *in vivo*. **(A)** Effects of NLRP3 deficiency on fear-conditioning tests results. $^{\#}P < 0.01$ versus NA group; $^{*}P < 0.05$ versus CIH + WT group (n = 6 mice/group). **(B)** Representative photographs of immunostaining for ASC in hippocampus (×200 magnification). **(C)** Protein expressions of NLRP3 and cleaved caspase-1 in hippocampus tissues of NLRP3$^{-/-}$ mice and WT mice measured by western blot. **(D)** Expression levels of IL-1β mRNA in the hippocampi from WT or NLRP3$^{-/-}$ mice, exposing to NA or CIH. $^{\#}P < 0.01$ versus NA group; $^{**}P < 0.01$ versus CIH + WT group. **(E, F)** The neuronal apoptosis was assayed with TUNEL. Typical immunofluorescent micrographs for TUNEL (red) staining from hippocampus tissues of each group. Scale bar = 100 μm. Quantitative analyses of the number of TUNEL-positive cells. $^{\#}P < 0.01$ versus NA group; $^{**}P < 0.01$ versus CIH + WT group. All data are presented as means ± SEM. CIH, chronic intermittent hypoxia; NA, normal air; WT, wild type.

to CIH in the hippocampal region, thus selectively influencing contextual fear conditioning and hippocampal-dependent memory consolidation. Taken together, these results suggested the involvement of the NLRP3 inflammasome in the pathogenesis of CIH-induced cognitive dysfunction and neuronal damage.

NLRP3 Deficiency Attenuates CIH-Induced Microglia Activation and Oxidative Stress in Hippocampus

Since microglial cells were regarded as a predominant contributor to the pathogenesis of CIH-induced neuroinflammation (7, 24), we wonder whether NLRP3 inflammasome influences the behavioral changes of microglia during CIH exposure. As displayed in **Figure 2A**, CIH remarkably increased the numbers of activated microglia both in cortex and hippocampus compared with NA control group. However, in NLRP3$^{-/-}$ mice, the activated microglia were seldom observed in cortex and hippocampus section upon CIH treatment (**Figure 2B**). It is important to emphasize that the inflammasome activation to be associated with defective mitochondrial function and ROS accumulation (14). Hence, to examine the occurrence of mitochondrial dysfunction in microglia after CIH, the level of mitochondrial ROS (mtROS) production was measured. We found that exposed WT mice to CIH were shown to have the increased MDA levels and decreased SOD activities (**Figures 2C, D**), both of which were characterized as biomarkers of oxidative stress injury. Moreover, the hypoxic oxidative stress was accompanied with increased mtROS, as shown in **Figure 2E**. However, compared with the WT mice exposed to CIH, NLRP3 knockout eradicated the changes in MDA content and ameliorated the mitochondrial damage in hippocampus and cortex. According to the above results, our data demonstrated that activated microglial cells in a CIH model caused neuroinflammation and subsequently affected the behavior of the mice through producing a mass of mtROS.

NLRP3 Deficiency Enhances CIH-Induced Mitophagy and Increases Parkin Expression in Hippocampus

Next, the level of mitophagy was further detected in hippocampal tissues *via* immunoblotting and immunofluorescence staining. Western blot analysis showed obvious mitophagy induction in mice exposed to CIH, especially the NLRP3$^{-/-}$ mice, evidencing by decrease in TOM20 protein levels, and increase in LC3 II and

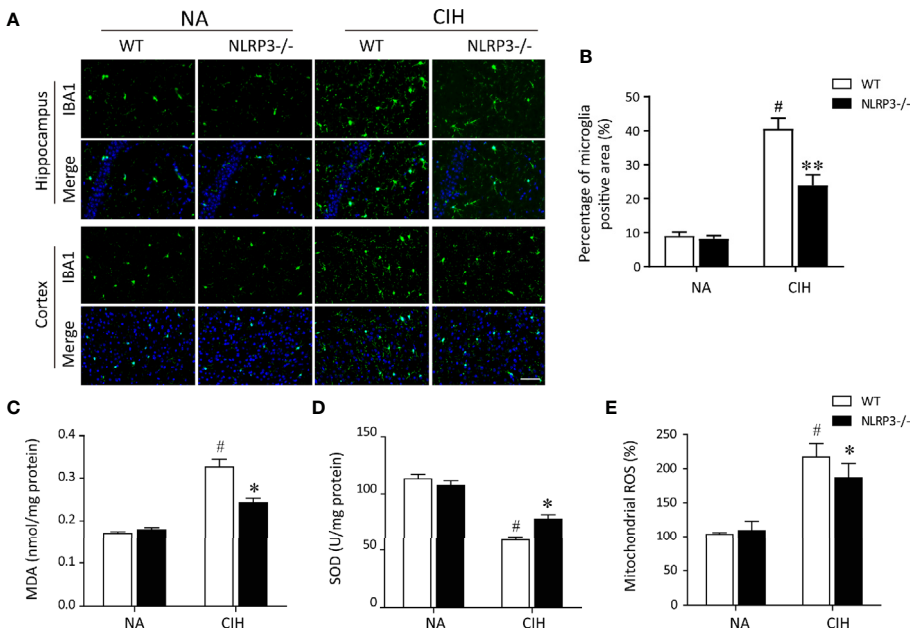

FIGURE 2 | NLRP3 deficiency prevents CIH-induced microglia activation and oxidative stress in hippocampus. **(A)** Microglia were detected with ionized calcium binding adapter molecule 1 (Iba1) antibody. Photomicrographs showed the Iba-1 (green) immunofluorescent staining from hippocampus and cortex tissues of each group. Note that Iba-1 was highly expressed in response to CIH. Scale bar = 50 μm. **(B)** Bar graphs displayed the percentage of Iba-1 positive cells per high-power field (n = 6). The hippocampal MDA content **(C)**, SOD activities **(D)**, and mitochondrial ROS levels **(E)** were measured in tissue homogenates (n = 6 per group). The data are presented as means ± SEM. $^{\#}P < 0.01$ versus NA group; $^{*}P < 0.05$ and $^{**}P < 0.01$ versus CIH + WT group. CIH, chronic intermittent hypoxia; NA, normal air; WT, wild type; MDA, malondialdehyde; SOD, superoxide dismutase.

Beclin-1 protein levels. In addition, CIH significantly increased the protein expression of Parkin in hippocampus compared with NA group, and NLRP3 knockout reinforced this trend (**Figure 3A**). To examine the formation of autophagosome in microglia of hippocampus, confocal microscopy showed that the expressions of autophagy markers LC3 were robustly stained in CIH group compared to NA control group. Further co-staining with IBA1 revealed that NLRP3 knockout remarkably enhanced the co-location of LC3 and IBA1 both in NA group and CIH group (**Figure 3B**). In this regard, mitophagy and autophagy could be up-regulated by CIH. NLRP3 deletion may further increase the formation of mitophagosome and autophagosome, which was also observed in microglia of hippocampus. Nevertheless, whether and how mtROS, NLRP3 inflammasome, and mitophagy interacted with each other in microglial cells needs to be further explored.

IH Facilitates NLRP3 Inflammasome Activation and Parkin-Mediated Mitophagy in BV2 Cells

To further study the regulatory relationship between mitophagy and NLRP3 inflammasome, we established an IH *in vitro* model as described previously (13, 23). As a selective form of specialized autophagy, mitophagy controls the turnover of dysfunctional, and damaged mitochondria, thus eliminating excessive mtROS as well as NLRP3-elicited inflammatory response (25, 26). Consistent with previous observations, NLRP3 inflammasome was activated in IH-induced microglial cells and all these results were in a time-dependent manner (**Figures 4A, B**). Meanwhile, immunoblot analysis showed that both autophagic and mitophagic activities (Atg7, p62, Atg5, LC3, Parkin, and PINK1) were augmented (**Figures 4C, D**). Considering that OSA is a kind of chronic disease, we finally chose IH exposure of 24 h as an *in vitro* model. Furthermore, as illustrated in **Figure 4E**, colocalization of Parkin (green) with mitochondrial related protein (TOM20, red) yielded that the bright green fluorescence of Parkin was largely enhanced following CIH exposure. Then, we further investigated the impact of IH on the changes to mitochondrial morphology in microglial cells by immunofluorescent staining. As illustrated in **Figure 4F**, exposure to IH can trigger the fragmentation of mitochondria in microglia cells, which was followed with the induction of mitophagy. In summary, these results suggested that the IH-related NLRP3 inflammasome activation was accompanied with Parkin-mediated mitophagy induction in microglia.

NLRP3 Deficiency Exerts Protective Effect Against IH *via* Parkin-Mediated Mitophagy *In Vitro*

To distinguish the deleterious contribution of NLRP3 inflammasome *in vitro*, we constructed the NLRP3 knockout cell line *via* lentivirus transfection strategy, and then verified the NLRP3- elicited inflammatory response by western blot.

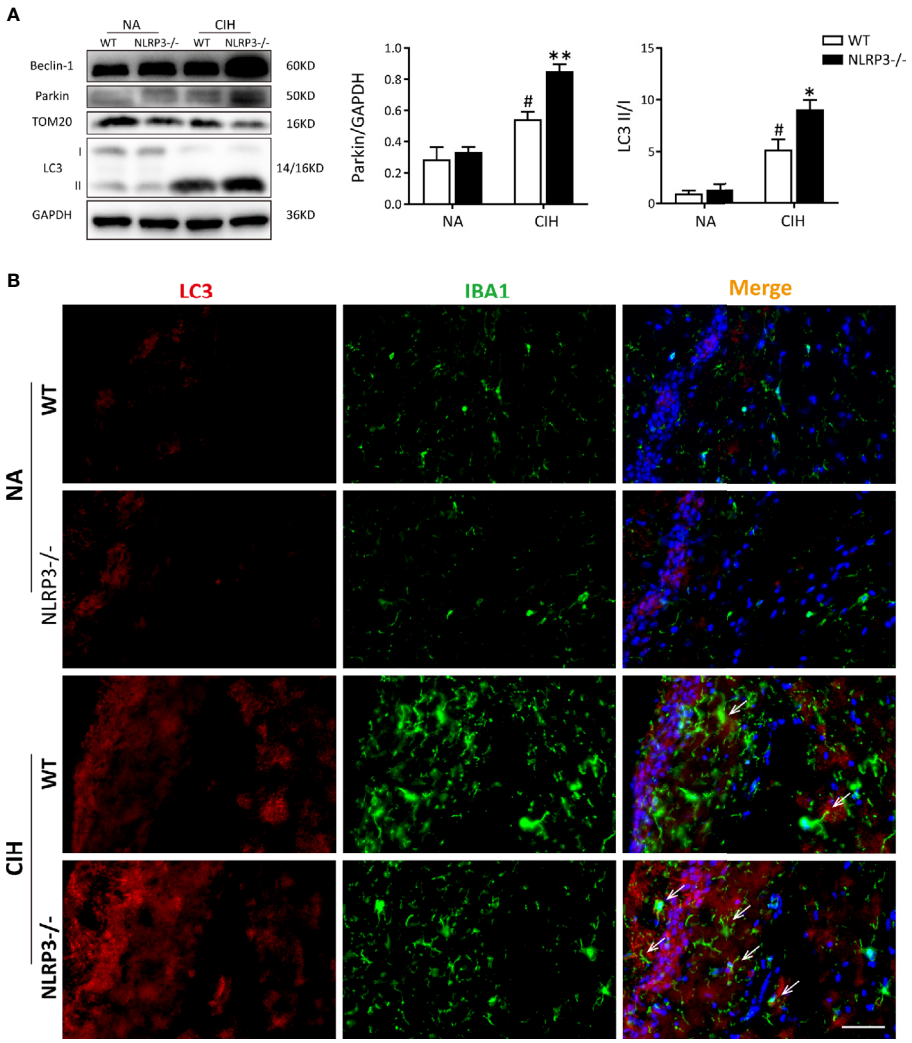

FIGURE 3 | NLRP3 deficiency enhances CIH-induced mitophagy and increases parkin expression *in vivo*. **(A)** Protein expressions of Beclin-1, Parkin, TOM20, and LC3 in hippocampal tissues of NLRP3$^{-/-}$ mice and WT mice measured by western blot. Values are expressed as means ± SEM. $^{\#}P < 0.05$ versus NA group; $^{*}P < 0.05$ and $^{**}P < 0.01$ versus CIH + WT group. **(B)** Representative images of double-labeled with LC3 and IBA1 (microglia, white arrow) in hippocampus revealed the increased autophagosome formation after 5 weeks of CIH exposure, especially the NLRP3-/- group. Scale bars = 50 μm. CIH, chronic intermittent hypoxia; NA, normal air; WT, wild type.

As expected, the immunoblot images of NLRP3, cleaved caspase-1 and ASC were not obviously detectable in NLRP3-deleted cells, confirming the knockout efficiency. Moreover, accumulation of ASC and cleaved caspase 1 induced by IH was substantially abolished by deletion of NLRP3 (**Figures 5A, B**). It is generally considered that mitochondria dysfunction is tightly associated with MMP loss and mtROS, subsequently affects apoptosis (14). Afterward, we monitored the MMP levels, mtROS production, and examined cell apoptosis. In line with the *in vivo* results, our *in vitro* data demonstrated that IH alone disrupted the MMP (red to green ratio, 1.09 ± 0.19%) and augmented mtROS release. NLRP3 deletion also blocked the MMP loss upon stimulation with IH (red to green ratio, 1.87 ± 0.21%, **Figures 5C, D**). Consistently, IH-triggered excessive mtROS generation (41.27 ± 2.27%) was significantly ameliorated by NLRP3 deficiency (32.13 ± 1.98%, **Figure 5E**). In addition, the expressions of cleaved caspase-3 p17 and pro-apoptotic protein Bax were both obviously upregulated in response to IH, whereas knockout of NLRP3 markedly attenuated their activations compared to the LV-NC group (**Figure 5F**). Notably, similar results were obtained in flow cytometric analysis, which showed the proportion of double-positive cells (Annexin V+/PI+) was the highest following IH exposure (13.39 ± 2.27%), while the percentage of apoptosis was significantly lower in NLRP3 knockout cells (8.65 ± 1.54%, $p < 0.05$, **Figure 5G**). These results suggested that deletion of NLRP3 can reduce CIH-triggered mitochondrial damage and alleviate microglial apoptosis.

To address how NLRP3 inflammasome modulates IH-induced mitophagy, we then verified the mitophagy and autophagy activities after NLRP3 deletion by western blot.

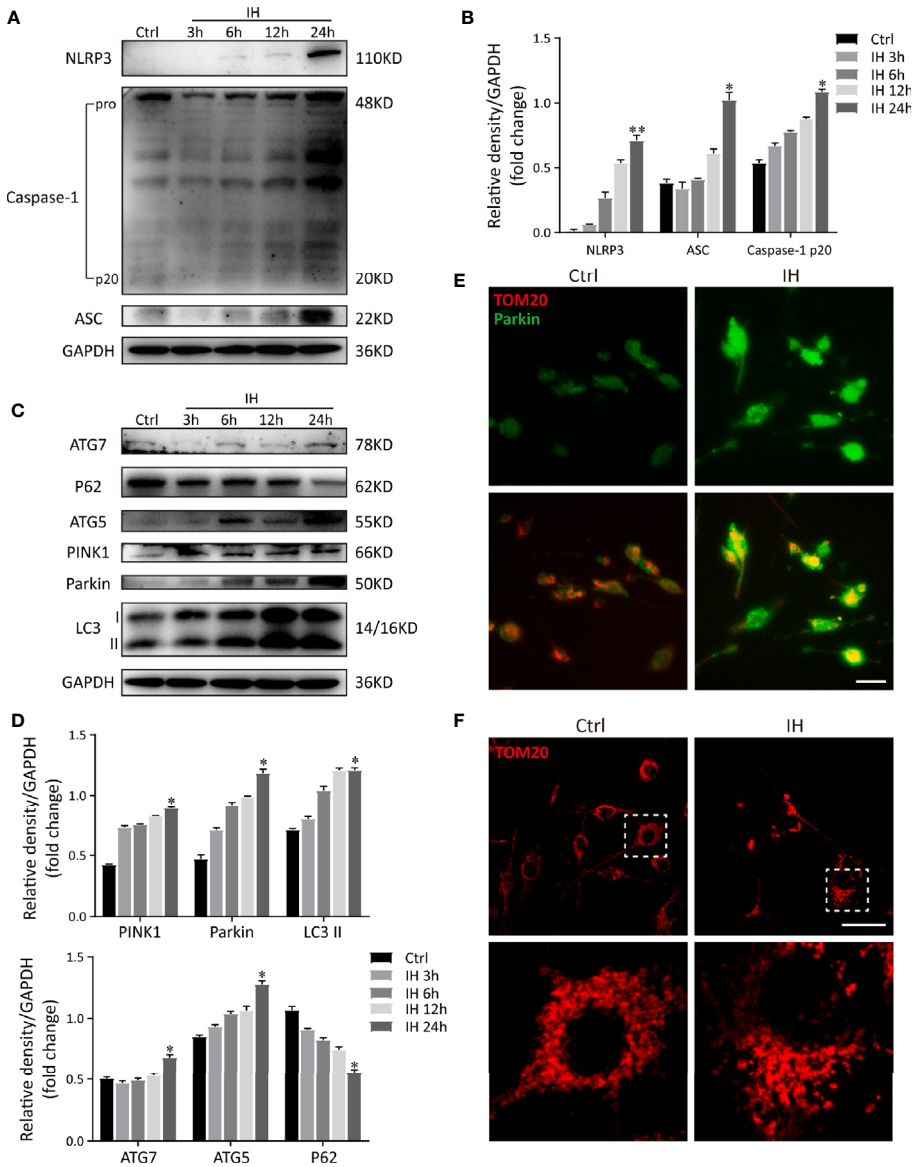

FIGURE 4 | IH induces NLRP3 inflammasome activation and Parkin-mediated mitophagy in BV2 cells. **(A)** Protein levels of NLRP3, cleaved caspase-1 and ASC increased significantly in BV2 cells subjected to 24h of IH, indicating activation of NLRP3 inflammasome. **(B)** Densitometric quantification of relative protein expression normalized to GAPDH was shown on the bar graphs. **(C)** Western blot revealed the significant increased levels of autophagic and mitophagic markers (ATG-5, ATG-7, PINK1, Parkin, and LC3-II), and decreased p62 expression in response to IH. **(D)** Quantification of relative protein expression assessed by densitometric analysis with GAPDH as an internal control. (n = 3 in each group). Values are expressed as means ± SEM. *P < 0.05 versus control group; **P < 0.01 versus control group. **(E)** Cells were double-labeled with parkin (green) and mitochondrial outer membrane protein TOM20 (red). Immunofluorescence images showed more parkin-positive cells colocalized with TOM20 following IH, suggesting the mitophagy induction. bar = 50 μm. **(F)** Confocal imaging presented the mitochondrial network stained for the MitoTracker (TOM20), in NA and IH microglial cells. bar = 50 μm. Similar results were obtained from three independent experiments. IH, intermittent hypoxia.

As compared to IH exposure alone, deletion of NLRP3 dramatically restored the levels of Parkin approximately 1.5-fold over basal levels. Conversely, silencing NLRP3 exerted an inhibitory effect on the P62 expression under normoxia, and further reduced P62 expression after exposure to IH (**Figures 6A, B**). Next, we performed immunofluorescence staining of Parkin (red) and TOM20 (green) to evaluate the degree of Parkin-mediated mitophagic activity. As the enhanced immunofluorescent co-staining shown in **Figure 6C**, Parkin was observed to be translocated on damaged mitochondria, thereby resulting in substantial mitophagy following IH exposure. In particular, abundant Parkin expression was prominently localized on the mitochondria in NLRP3-deficient cells after IH treatment, suggesting the accumulation of

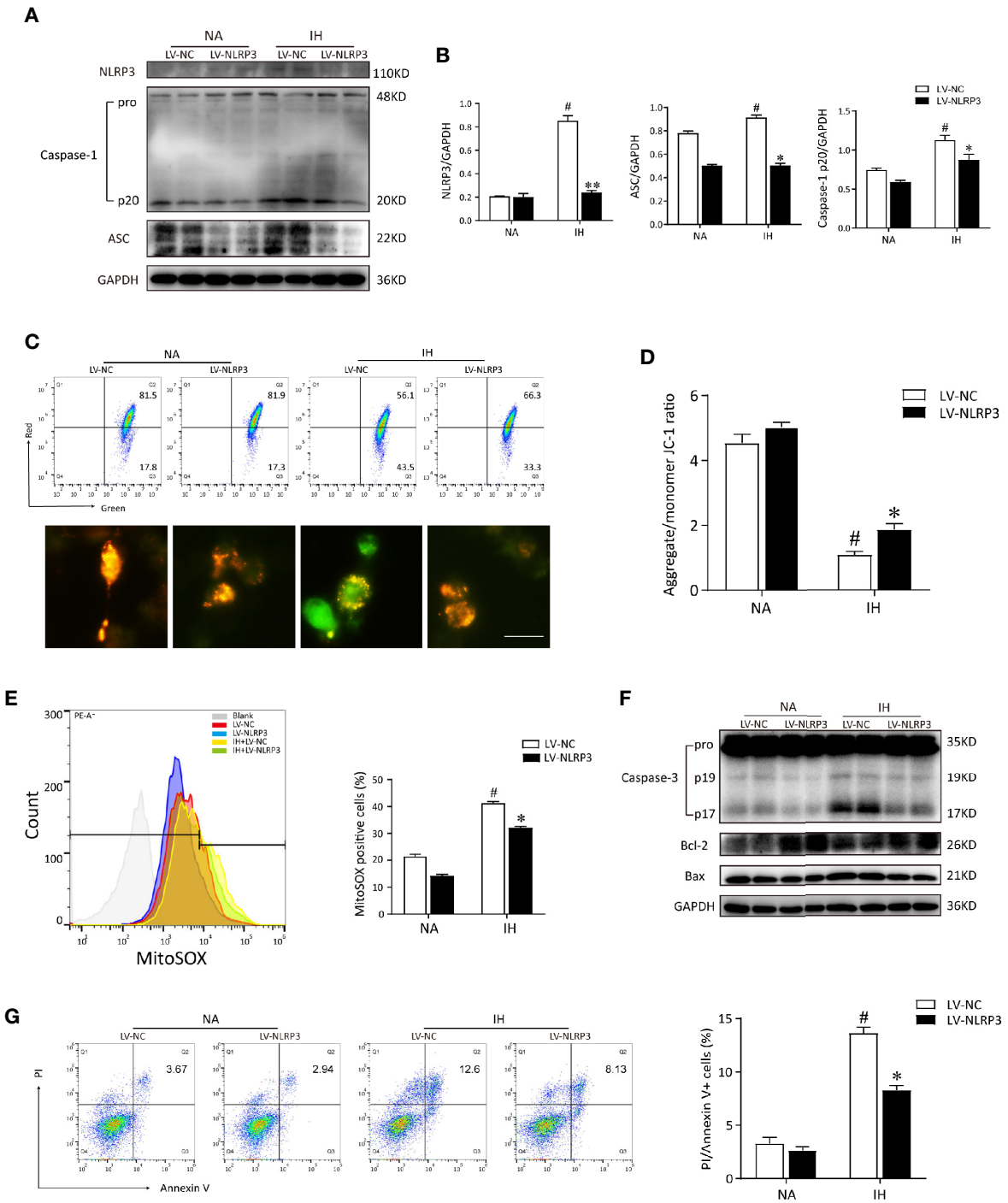

FIGURE 5 | NLRP3 knockout restores the IH from the mitochondrial dysfunction and reduces mtROS production *in vitro*. **(A)** Immunoblot protein expressions of NLRP3, ASC and caspase-1 in IH-treated BV2 cells transfected with LV-NLRP3 or LV-NC. **(B)** The amounts of each protein were quantified by densitometry and expressed relative to the amount of GAPDH in the same samples. **(C)** LV-NC or LV-NLRP3 transfected BV2 cells were stained with JC-1 and analyzed by flow cytometry (upper) and microscopy (below). Scale bar = 50 μm. **(D)** Quantification of MMP was represented as the ratio red to green fluorescence. **(E)** LV-NC or LV-NLRP3 transfected cells were stained with MitoSOX and analyzed by flow cytometry. IH-elicited mtROS generation was inhibited by NLRP3 deficiency. **(F)** Cell lysates were immunoblotted for apoptotic proteins in BV2 cells. **(G)** Apoptosis of cells transfected with LV-NLRP3 in the presence or absence of IH was assayed by Annexin-V/PI staining. The quantitative rate of apoptosis was presented on the right histogram. Values are expressed as means ± SEM of three independent experiments. $^{\#}P < 0.05$ versus LV-NC group; $^{*}P < 0.05$ versus IH + LV-NC group; $^{**}P < 0.01$ versus IH + LV-NC group. IH, intermittent hypoxia; NA, normal air; LV, lentivirus; mtROS, mitochondrial reactive oxygen species.

mitophagosomes. Moreover, the positive effect of NLRP3 deficiency on parkin-mediated mitophagy could also be counteracted by 3MA pre-treatment (5 mM). Then, we examine the effect of NLRP3 deletion on mitochondrial morphology under TEM. After IH exposure, mitochondria were observed to swell and loss of cristae in the matrix of microglial cells. Consistent with the results of immunofluorescence, more mitophagosome formations were noticed in NLRP3-deficient microglial cells after IH exposure compared to the IH exposure alone group (**Figure 6D**). Taken together, these results indicated that NLRP3 deficiency showed protective effect against IH *via* inducing Parkin-mediated mitophagy.

Parkin-Dependent Mitophagy Is Involved in the Protective Mechanism of NLRP3 Deficiency

To clarify whether Parkin is required in the positive effect of NLRP3 deletion on mitochondrial maintenance in microglia, we first deleted Parkin *via* shRNA. After Parkin knockdown, IH enhanced the accumulation of damaged mitochondria and neutralized the protective of NLRP3 deletion in microglia, evidencing by increasing mitochondrial depolarization (red to green ratio, 0.34 ± 0.11%) and augmenting mtROS release (79.47 ± 0.15%), as illustrated in **Figures 7A–D**. Thus, proper control of Parkin-dependent mitophagy is pivotal to restoration of mitochondrial integrity and function in microglial cells after NLRP3 knockout. To further discuss the role of Parkin-dependent mitophagy in NLRP3$^{-/-}$ microglia, we incubated BV2 cells with 3-MA (5 mM) or the PBS vehicle for 6h before exposure to IH. As shown in **Figure 7E**, both Parkin deletion or pretreated with 3MA exacerbated the cell apoptosis in NLRP3$^{-/-}$ microglial cells caused by IH. Furthermore, Parkin deletion or 3MA pretreatment upon IH exposure resulted in higher expression levels of caspase-3 p17 and Bax compared with IH control group. Moreover, inhibition of mitophagy by 3MA pretreatment had pronounced effect on NLRP3$^{-/-}$ microglial cells that further increased the protein expressions of NLRP3, ASC, pro-caspase-1 under IH condition compared to the IH control group ($p < 0.05$). The similar effect was observed in Parkin shRNA-transfected NLRP3$^{-/-}$ cells ($p < 0.05$, **Figures 7F, G**). These results collectively indicated that Parkin deficiency failed to elicit a protective phenotype in the context of IH after NLRP3 knockout.

Next, we detected the mitophagic activities in NLRP3$^{-/-}$ microglial cells after deletion of Parkin. Immunoblot analysis showed that silencing Parkin restrained the subsequent PINK1 mitophagy signaling under IH exposure and reversed the protective effect of NLRP3 deletion on IH-treated microglial cells, indicating the induction of mitophagy upon NLRP3 deficiency is Parkin-dependent (**Figures 8A, B**). Similarly, co-localization of LC3 (red) and TOM20 (green) demonstrated that Parkin ablation effectively prevented mitophagosomes formation upon IH challenge, evidenced by the weak red fluorescence of LC3 co-localized with TOM20. Moreover, after transfection with sh-Parkin, NLRP3 knockout no longer restored the impaired mitophagy after IH treatment. As expected, co-staining of LC3 and TOM20 showed faint double immunofluorescence in IH +LV-NLRP3+sh-Parkin group, as illustrated in **Figure 8C**. Taken together, our data showed that Parkin-dependent mitophagy plays a vital role in the NLRP3-deficient protective action under IH exposure, and inhibition of mitophagy *via* Parkin deletion abolished the positive effect of NLRP3 deficiency against IH (**Figure S2**).

DISCUSSION

At present, little is known about the mechanisms of structural neuron damage and the potential roles played by microglia during IH exposure from OSA. In our work, CIH elicited pathologies such as hippocampal apoptosis with learning deficits, while genetic deletion of NLRP3 displayed less neuronal damage or microglia activation after 5 weeks of CIH. In CNS, microglia are a robust source of oxidative stress, production of which are critical for self-activation of microglia and the overproduction of proinflammatory factors (6). As expected, we demonstrated that the microglia activation enhanced by CIH was accompanied by the elevated autophagy and mirophagy markers, LC3 and Parkin expressions *in vivo* experiments. In addition, we also indicated that NLRP3 deficiency can further enhanced Parkin-mediated mitophagy in hippocampus of IH mice, as well as autophagosomes formation in microglia of hippocampus. Of note, our data showed that CIH stimulated damaged mitochondria to release signals, such as mtROS and mtDNA, which further promoted the NLRP3 inflammasome complex assembly to activate the caspase-1 and the subsequent cytokines IL-1β release. The accumulation of proinflammatory cytokines as well as mitochondrial ROS was proposed to directly induce neuronal apoptosis, resulting in hippocampal-dependent impairment of learning and memory.

The major limitation of this article is that there is no clinically relevant data; however, some of researchers have provided clear evidences to show that neurocognitive deficit is identified as one of the main co-morbidities associated with OSA (4). Besides, previous studies also indicated the processes involved in the cognitive decline in patients with OSA were shown to overlap with those found in the pathogenesis of Alzheimer's disease (AD) (3). Continuous positive airway pressure (CPAP), the first-line treatment for OSA patients, can rapidly improve the oxyhemoglobin desaturation and cognitive function of them (27). After a short-term CPAP treatment, functional MRI was used to show that OSA patients revealed an improvement in memory and attention (28), which changes were associated with that in cerebellar cortices and bilateral hippocampi (29). Taken together, these data indicated that OSA patients were usually suffered from cognitive impairment, and improving oxygen saturation can alleviate the phenomenon through regulating hippocampal function.

In line with our findings, Racanelli et al. reported chronic hypoxia triggered autophagosome formation (30). Recently, receptor-mediated mitophagy was found to be activated in response to hypoxia or mitochondrial oxidative stress (31). A previous study has also documented that level of cleaved caspase-

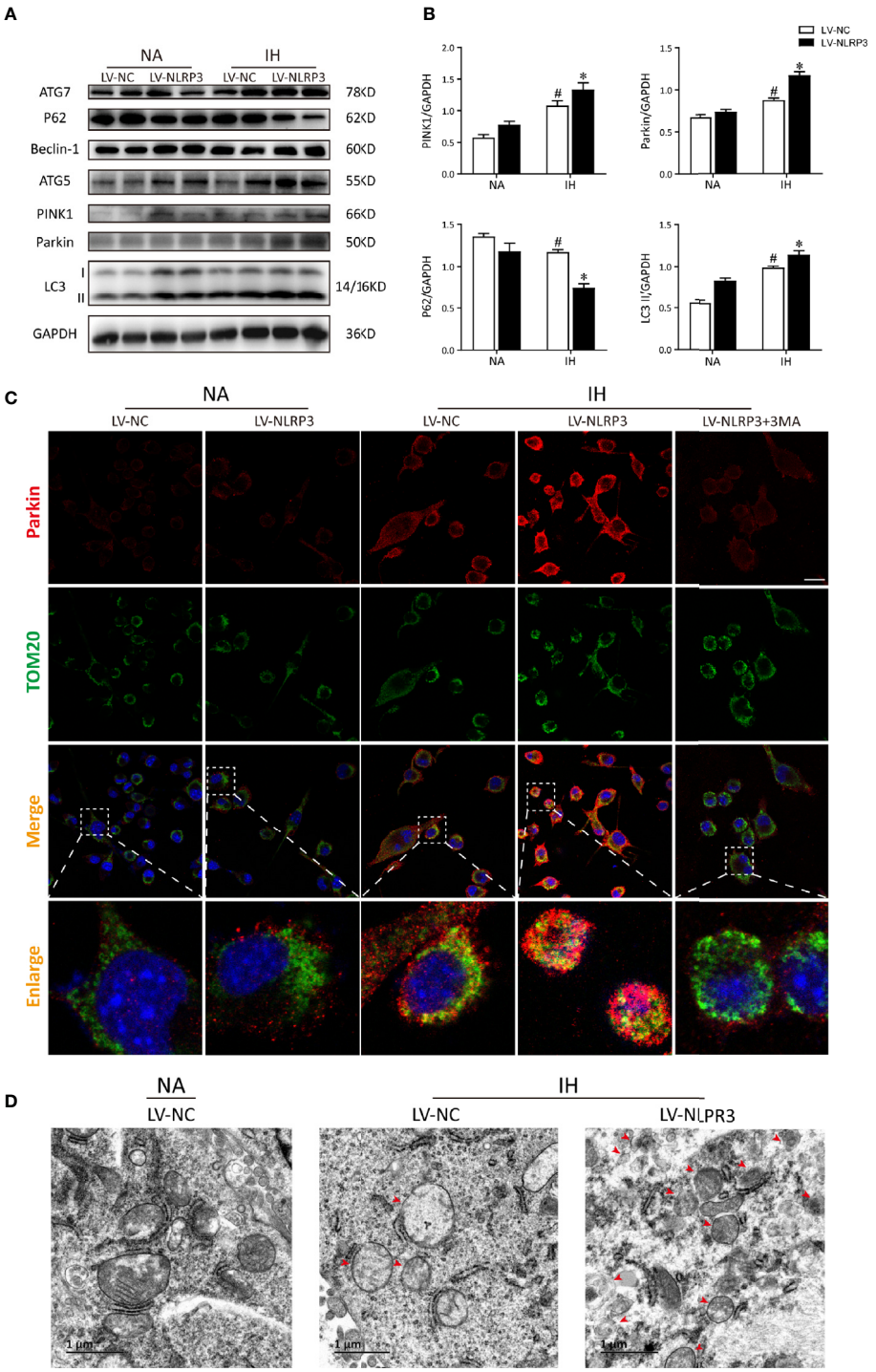

FIGURE 6 | NLRP3 knockout provides protective effect against IH *via* Parkin-dependent mitophagy *in vitro*. **(A)** Representative western blot bands from BV2 cells transfected with LV-NLRP3 or LV-NC showed autophagic and mitophagic protein expression in the presence or absence of IH. **(B)** Densitometric quantification of PINK1, Parkin, P62, and LC3-II levels in comparison with GAPDH as a loading control. The results of statistical analysis were shown three independent replicates. Values are expressed as means ± SEM. $^{\#}P < 0.01$ versus LV-NC group; $^{*}P < 0.05$ versus IH + LV-NC group. **(C)** Representative confocal microscopic images of gene-modified BV2 cells co-localization with Parkin (red) and TOM20 (green). Scale bar = 25 μm. **(D)** Representative TEM images of mitophagosomes (red arrow) in BV2 cells after IH exposure. Scale bar = 1 μm. IH, intermittent hypoxia; NA, normal air; LV, lentivirus; TEM, transmission electron microscopy.

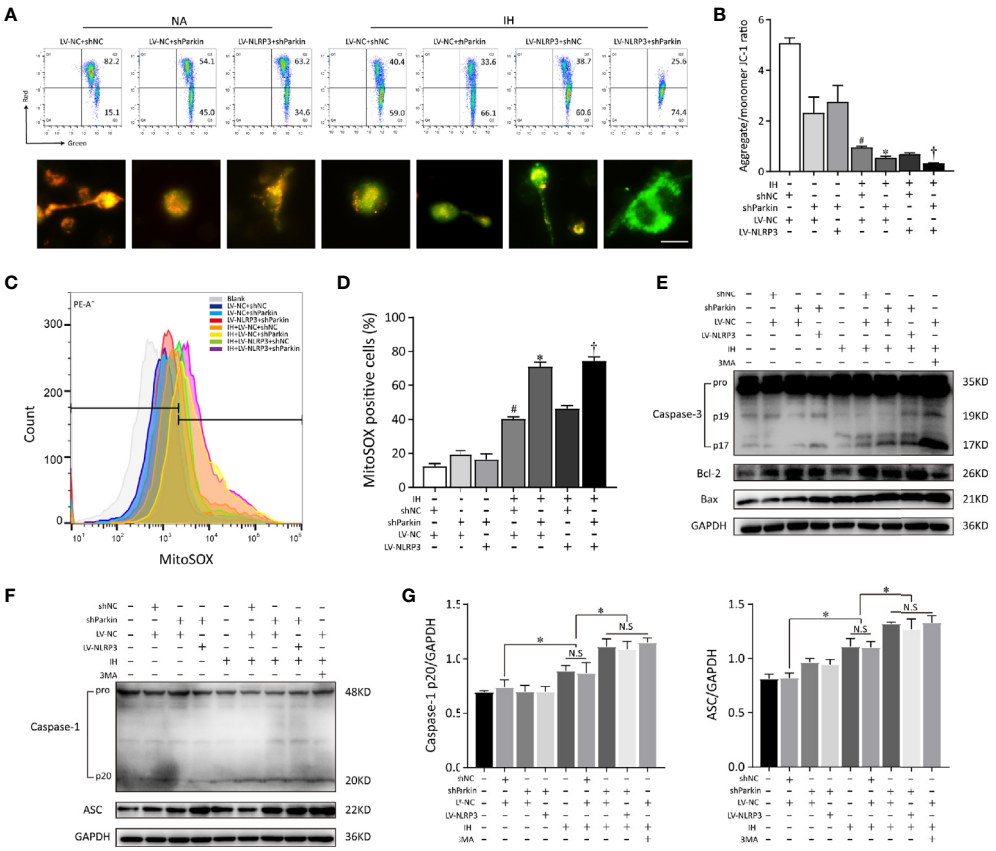

FIGURE 7 | Parkin knockdown reverses the positive effect of NLRP3 deletion on mitochondrial maintenance in microglia. Gene modified BV2 cells transfected with sh-Parkin or pretreated with 3MA (5 mM) for 6h before exposure to IH. **(A)** Flow cytometry and immunofluorescent staining reflected the MMP. Scale bar = 50 μm. **(B)** Quantification of MMP changes was represented as the ratio of red to green fluorescence. **(C)** Parkin sh-RNA transfected LV-NC or LV-NLRP3 cells were stained with MitoSOX. **(D)** The quantitative histograms from the obtained results. $^{\#}P < 0.05$ versus LV-NC + shNC group; $^{*}P < 0.05$ versus IH + LV-NC + shNC group; $^{\dagger}P < 0.05$ versus IH + LV-NC + shNC group. **(E)** Western blot analysis revealed that Parkin knockdown or pretreated with 3MA exacerbated the apoptosis that caused by IH, and neutralized the positive effect of NLRP3 knockout. **(F, G)** Effects of Parkin knockdown or 3MA pretreatment on cleaved caspase-1 and ASC protein expressions in gene modified BV2 cells exposed to IH. Representative histograms to quantify the relative levels and GADPH acted as an internal control. Similar results were obtained from three independent experiments. Data are presented as the mean ± SEM. $^{*}P < 0.05$. NC, negative control; NS, not significant; IH, intermittent hypoxia; NA, normal air.

3 and LC3 in hippocampal neurons were both upregulated by IH (32). Consistently, our results indicated that hypoxia initiated a time-dependent mitophagy activation whose ultimate goal was clearance of damaged mitochondria in BV2 cells. Meanwhile, IH-treated WT cells seemed more likely to apoptosis compared to NLRP3 knockout cells. In contrast, another study revealed that neuroinflammation activated the NLRP3-caspase-1 inflammasome in the hippocampus of mice and BV2 cells by triggering autophagy-lysosomal dysfunction, thus having specific relevance to neuronal cells damage (33). A possible mechanism has been proposed that a low ROS level specifically induces mitophagy without nonspecific autophagy, whereas excessive oxidative stress activates both autophagy and mitophagy as a negative-feedback to reduce mitochondria-derived ROS production (31). Actually, less severe protocols may elicit beneficial (compensatory) plasticity without morbidity (2). This diverse effect of IH on autophagy could in part be explained by the varying degrees of hypoxic paradigms: hypoxic events can be either neuroprotective or neurotoxic depending on the severity, frequency, and duration of the hypoxia.

Many researchers have attempted to link Parkin-PINK1 pathway to NLRP3 inflammasome. Several studies have reported that Parkin deficiency enhanced the production of inflammatory cytokines such as MCP-1, TNF-α and NF-kB (34). In addition, some investigators have found the enhanced NLRP3 signaling in Parkin-deficient cells (35). Sumpter et al. demonstrated the Parkin-dependent mitophagy limited NLRP3 activation in peripheral macrophages and primary fibroblasts (36). Intriguingly, Parkin can be cleaved by caspase-1, thus contributing to the resultant excessive inflammation cell death and pyroptosis. Herein, we revealed that NLRP3 deletion attenuated IH-induced injury through enhancement of Parkin-mediated mitophagy. In addition, inhibition of mitophagy *via* parkin deletion was shown to facilitate the cell apoptosis and abolish the protective effect of NLRP3 deficiency against IH.

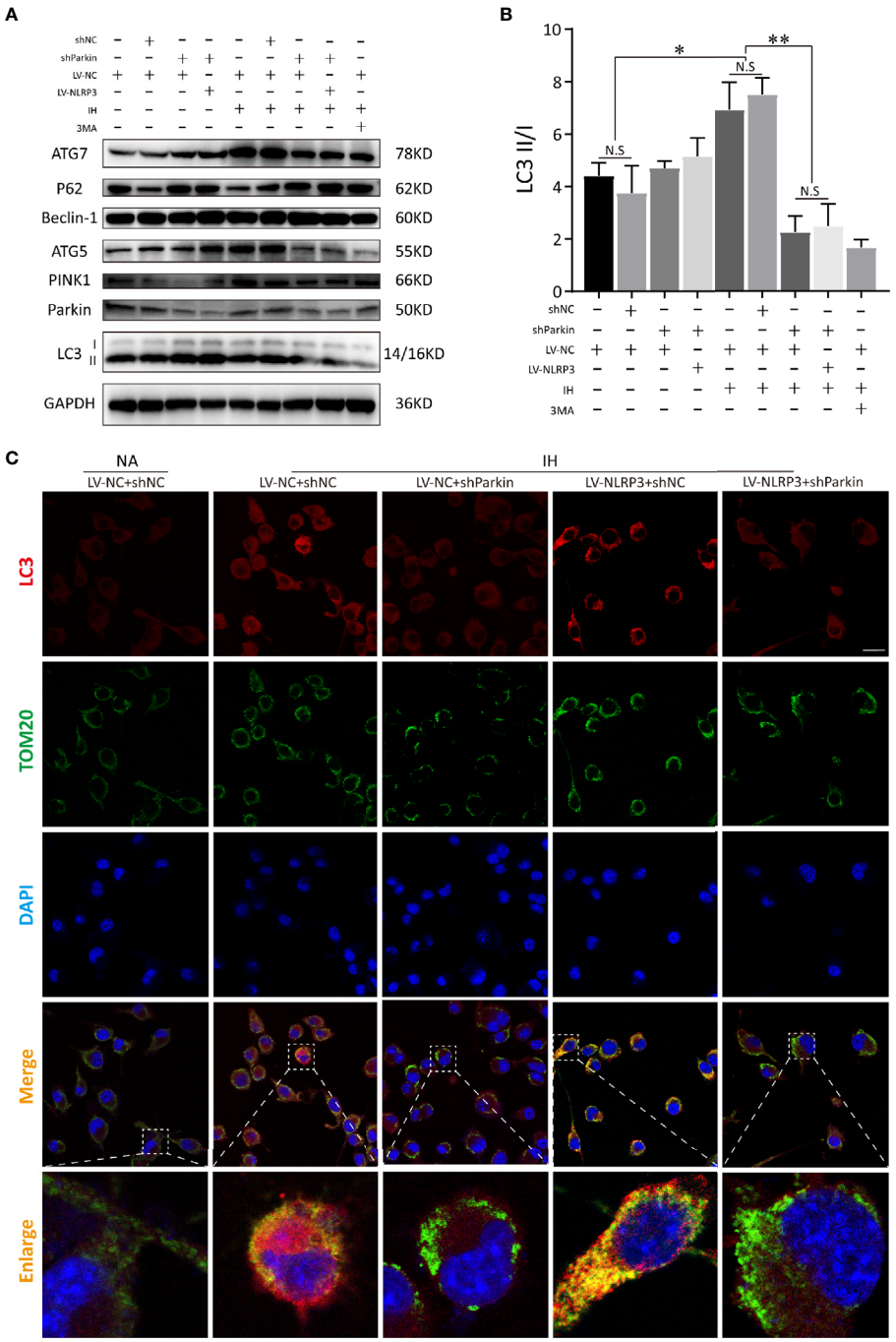

FIGURE 8 | Parkin knockdown blocks the activation of mitophagy inducing by NLRP3 deletion in IH-treated microglia. **(A)** Immunoblot showed that after NLRP3 deletion, Parkin knockdown or 3-MA (autophagy inhibitor) pretreatment restrained the autophagy and mitophagy expressions (LC3-II, Beclin-1, ATG-5, ATG-7, Parkin, and PINK1), but upregulated P62 under IH condition in BV2 cells. **(B)** Quantification of autophagic flux was represented as the ratio of LC3 II to LC3 I proteins levels. Data are indicated as the mean ± SEM (n = 3 in each group). *P < 0.05; **P < 0.01; N.S, not significant. **(C)** Transfection with sh-Parkin inhibited the co-localization with TOM20 (green) and LC3 (red) upon IH challenge in NLRP3$^{-/-}$ microglia. Scale bar = 25 μm. IH, intermittent hypoxia; NA, normal air; LV, lentivirus.

These data indicate that Parkin-mediated mitophagy is one of the self-limiting systems to protect cells from hyper-inflammation. Although hypoxia-induced mitophagy *via* receptors such as Parkin/PINK1, Bcl2/adenovirus E1B 19 kDa protein-interacting protein 3 (BNIP3)/NIX, and FUN14 domain containing 1 (FUNDC1) has been described (34, 35), the crucial molecular mechanisms for hypoxia-induced mitophagy appeared to be cell type-specific. Herein, we only presented *in*

vitro data that Parkin-dependent mitophagy controlled mitochondrial quality following hypoxia exposure. It would be interesting to further investigate the effect of NLRP3 deficiency on other mitophagy signaling.

Accumulation of misfolded proteins and damaged mitochondria has been documented to be hallmarks of neurologic disease (37). Coupled with lost membrane potential, most damaged mitochondria inhibit PINK1 imported to the inner mitochondrial membrane but stabilized on outer mitochondrial membrane (38). Then, the phosphorylated Parkin mediates mitochondrial ubiquitination, as an 'eat-me' signal that can be recognized by the adaptor p62 (21, 39). It is widely accepted that NLRP3 inflammasome stimuli could impair the mitochondria (26). By eliminating damaged mitochondria, mitophagy induction is dependent on recruitment of p62/SQSTM1 to limit inflammasome as a compensatory mechanism. Besides, damaged mitochondria further facilitate inflammasome inductive signals *via* mtDNA or mtROS, forming a vicious circle afterward (25). In the present study, protective effects of the NLRP3 deficiency on mitophagy and mitochondrial dysfunction have been undoubtedly identified. Furthermore, in IH-treated BV2 cells, we found p62 level to be dramatically suppressed compared to WT group, and further be restrained when NLRP3 deletion. This discrepancy is likely due to the excessive mtROS or NLRP3 inflammasome produced a large amount of autophagosome, caused overwork of lysosome, and subsequently resulted in failure of autophagy and mitophagy during CIH exposure. It accounts for the fact that decreased p62 levels represent the enhancement of autophagy flux, and the reason that NLRP3 deletion elicited more mitophagosomes formation attribute to the balance between the generation and elimination of harmful substances once again. Interestingly, some research found that p62 was dispensable for parkin-mediated mitophagy (39). Despite the controversial roles of P62, it is generally recognized that parkin recruits P62 to mediate mitophagy through selective cargo recognition. However, the inverse correlation between PINK1-Parkin pathway and P62 warranted to be explored in further study.

CONCLUSIONS

In summary, our study revealed that NLRP3 ablation or inhibition orchestrated a reparative inflammatory response, which was linked with enhanced Parkin-dependent mitophagy upon hypoxia. As a regulatory feedback loop that maintains homeostasis and favors intrinsic repair in response to mitochondrial oxidative stress, Parkin-dependent mitophagy is involved in the protective mechanism of NLRP3 deficiency. Although, the directly molecular mechanism between NLRP3 and Parkin is still unclear, our results highlight the significant implication of NLRP3-Parkin axis as an important signaling pathway that determines the fate of cells under hypoxia. The mechanism of how *NLRP3* gene knockdown leads to the elevated Parkin protein level will be further studied in our subsequent experiments. Overall, our observations suggest the imbalanced crosstalk of NLRP3-Parkin axis participates the pathogenesis of CIH-induced neuroinflammation. Gene knockout or pharmacological blockage of NLRP3 might serve as a potential therapeutic target for OSA associated neurocognitive impairment.

DATA AVAILABILITY STATEMENT

The raw data supporting the conclusions of this article will be made available by the authors, without undue reservation.

ETHICS STATEMENT

The animal study was reviewed and approved by the Medical Experimental Animal Administrative Committee of the Shanghai Medical College of the Fudan University.

AUTHOR CONTRIBUTIONS

XW and LG designed experiments and wrote the paper. XW, LG, LX, WG, and XYW performed experiments and acquired data. XW, LG, WG, XYW, ZL, and SL analyzed data and supervised the research. All authors contributed to the article and approved the submitted version.

FUNDING

The study was financially supported by grants from The National Key Research and Development Program of China (No. 2018YFC1313600), the National Natural Science Foundation of China, Grant/Award Number: (No. 82070094, 82000095, 81900086, 81800089, & 81873420), the Shanghai Top-Priority Clinical Key Disciplines Construction Project, Grant/Award Number: (No. 2017ZZ02013), and the fund for Fundamental Research Funds for the Central Universities (22120180576).

SUPPLEMENTARY MATERIAL

The Supplementary Material for this article can be found online at: https://www.frontiersin.org/articles/10.3389/fimmu.2021.628168/full#supplementary-material

Supplementary Figure 1 | Quantification of the relative protein (NLRP3, and Caspase-1 p20) levels in **Figure 1C**, and GADPH acted as an internal control. $^{\#}P < 0.01$ versus NA group; $^{**}P < 0.01$ versus CIH + WT group, $^{****}P < 0.001$ versus CIH + WT group.

Supplementary Figure 2 | Schematic diagram of the interaction between PINK1/Parkin-dependent mitophagy and NLRP3 inflammasome in OSA-associated neuroinflammation. CIH induced mitochondrial ROS production, and facilitated NLRP3 inflammasome assembly to subsequently activate the caspase-1 cleavage. NLRP3 deficiency by gene knockout or pharmacological blockage could restore the CIH-induced mitochondrial dysfunction, alleviate mtROS production, reduce cell apoptosis, and further enhance Parkin-mediated mitophagosome formation. Green lines: facilitation. Red lines: inhibition. CIH, intermittent hypoxia.

REFERENCES

1. Prabhakar NR, Peng YJ, Nanduri J. Hypoxia-inducible factors and obstructive sleep apnea. *J Clin Invest* (2020) 130:5042–51. doi: 10.1172/JCI137560
2. Wu X, Lu H, Hu L, Gong W, Wang J, Fu C, et al. Chronic intermittent hypoxia affects endogenous serotonergic inputs and expression of synaptic proteins in rat hypoglossal nucleus. *Am J Transl Res* (2017) 9:546–57.
3. Polsek D, Gildeh N, Cash D, Winsky-Sommerer R, Williams S, Turkheimer F, et al. Obstructive sleep apnoea and Alzheimer's disease: In search of shared pathomechanisms. *Neurosci Biobehav Rev* (2018) 86:142–9. doi: 10.1016/j.neubiorev.2017.12.004
4. Gildeh N, Drakatos P, Higgins S, Rosenzweig I, Kent BD. Emerging co-morbidities of obstructive sleep apnea: cognition, kidney disease, and cancer. *J Thorac Dis* (2016) 8:E901–17. doi: 10.21037/jtd.2016.09.23
5. Mkrtchyan GV, Graf A, Trofimova L, Ksenofontov A, Baratova L, Bunik V. Positive correlation between rat brain glutamate concentrations and mitochondrial 2-oxoglutarate dehydrogenase activity. *Anal Biochem* (2018) 552:100–9. doi: 10.1016/j.ab.2018.01.003
6. Lavie L. Oxidative stress in obstructive sleep apnea and intermittent hypoxia–revisited–the bad ugly and good: implications to the heart and brain. *Sleep Med Rev* (2015) 20:27–45. doi: 10.1016/j.smrv.2014.07.003
7. Liu X, Ma Y, Ouyang R, Zeng Z, Zhan Z, Lu H, et al. The relationship between inflammation and neurocognitive dysfunction in obstructive sleep apnea syndrome. *J Neuroinflamm* (2020) 17:229. doi: 10.1186/s12974-020-01905-2
8. Yang Q, Wang Y, Feng J, Cao J, Chen B. Intermittent hypoxia from obstructive sleep apnea may cause neuronal impairment and dysfunction in central nervous system: the potential roles played by microglia. *Neuropsych Dis Treat* (2013) 9:1077–86. doi: 10.2147/NDT.S49868
9. He Y, Hara H, Núñez G. Mechanism and Regulation of NLRP3 Inflammasome Activation. *Trends Biochem Sci* (2016) 41:1012–21. doi: 10.1016/j.tibs.2016.09.002
10. Freeman LC, Ting JP. The pathogenic role of the inflammasome in neurodegenerative diseases. *J Neurochem* (2016) 136(Suppl 1):29–38. doi: 10.1111/jnc.13217
11. Voet S, Srinivasan S, Lamkanfi M, Loo G. Inflammasomes in neuroinflammatory and neurodegenerative diseases. *EMBO Mol Med* (2019) 11:n/a–a. doi: 10.15252/emmm.201810248
12. Mao Z, Liu C, Ji S, Yang Q, Ye H, Han H, et al. The NLRP3 Inflammasome is Involved in the Pathogenesis of Parkinson's Disease in Rats. *Neurochem Res* (2017) 42:1104–15. doi: 10.1007/s11064-017-2185-0
13. Wu X, Chang SC, Jin J, Gu W, Li S. NLRP3 inflammasome mediates chronic intermittent hypoxia-induced renal injury implication of the microRNA-155/FOXO3a signaling pathway. *J Cell Physiol* (2018) 233:9404–15. doi: 10.1002/jcp.26784
14. Shimada K, Crother TR, Karlin J, Dagvadorj J, Chiba N, Chen S, et al. Oxidized Mitochondrial DNA Activates the NLRP3 Inflammasome during Apoptosis. *Immunity* (2012) 36:401–14. doi: 10.1016/j.immuni.2012.01.009
15. Gurung P, Burton A, Kanneganti T. NLRP3 inflammasome plays a redundant role with caspase 8 to promote IL-1β–mediated osteomyelitis. *Proc Natl Acad Sci* (2016) 113:4452–7. doi: 10.1073/pnas.1601636113
16. Zheng M, Kanneganti TD. The regulation of the ZBP1-NLRP3 inflammasome and its implications in pyroptosis, apoptosis, and necroptosis (PANoptosis). *Immunol Rev* (2020) 297:26–38. doi: 10.1111/imr.12909
17. Lazarou M. Keeping the immune system in check: a role for mitophagy. *Immunol Cell Biol* (2015) 93:3–10. doi: 10.1038/icb.2014.75
18. Kim M, Bae SH, Ryu J, Kwon Y, Oh J, Kwon J, et al. SESN2/sestrin2 suppresses sepsis by inducing mitophagy and inhibiting NLRP3 activation in macrophages. *Autophagy* (2016) 12:1272–91. doi: 10.1080/15548627.2016.1183081
19. McLelland GL, Soubannier V, Chen CX, McBride HM, Fon EA. Parkin and PINK1 function in a vesicular trafficking pathway regulating mitochondrial quality control. *EMBO J* (2014) 33:282–95. doi: 10.1002/embj.201385902
20. Johnson BN, Charan RA, LaVoie MJ. Recognizing the cooperative and independent mitochondrial functions of Parkin and PINK1. *Cell Cycle* (2012) 11:2775–6. doi: 10.4161/cc.21261
21. Barodia SK, Creed RB, Goldberg MS. Parkin and PINK1 functions in oxidative stress and neurodegeneration. *Brain Res Bull* (2017) 133:51–9. doi: 10.1016/j.brainresbull.2016.12.004
22. Cummins N, Götz J. Shedding light on mitophagy in neurons: what is the evidence for PINK1/Parkin mitophagy in vivo? *Cell Mol Life Sci* (2018) 75:1151–62. doi: 10.1007/s00018-017-2692-9
23. Fu C, Jiang L, Zhu F, Liu Z, Li W, Jiang H, et al. Chronic intermittent hypoxia leads to insulin resistance and impaired glucose tolerance through dysregulation of adipokines in non-obese rats. *Sleep Breath* (2015) 19:1467–73. doi: 10.1007/s11325-015-1144-8
24. Shi Y, Guo X, Zhang J, Zhou H, Sun B, Feng J. DNA binding protein HMGB1 secreted by activated microglia promotes the apoptosis of hippocampal neurons in diabetes complicated with OSA. *Brain Behav Immun* (2018) 73:482–92. doi: 10.1016/j.bbi.2018.06.012
25. Kim M, Yoon J, Ryu J. Mitophagy: a balance regulator of NLRP3 inflammasome activation. *BMB Rep* (2016) 49:529–35. doi: 10.5483/BMBRep.2016.49.10.115
26. Lin Q, Li S, Jiang N, Shao X, Zhang M, Jin H, et al. PINK1-parkin pathway of mitophagy protects against contrast-induced acute kidney injury via decreasing mitochondrial ROS and NLRP3 inflammasome activation. *Redox Biol* (2019) 26:101254. doi: 10.1016/j.redox.2019.101254
27. Gong LJ, Chang SC, Wu QH, Liu ZL, Wu X, Li SQ. Diagnostic accuracy of the Berlin questionnaire and therapeutic effect of nasal continuous positive airway pressure in OSAHS patients with glucose metabolic dysfunction. *Sleep Breath* (2020). doi: 10.1007/s11325-020-02198-8
28. Canessa N, Castronovo V, Cappa SF, Aloia MS, Marelli S, Falini A, et al. Obstructive sleep apnea: brain structural changes and neurocognitive function before and after treatment. *Am J Respir Crit Care Med* (2011) 183:1419–26. doi: 10.1164/rccm.201005-0693OC
29. Rosenzweig I, Glasser M, Crum WR, Kempton MJ, Milosevic M, McMillan A, et al. Changes in Neurocognitive Architecture in Patients with Obstructive Sleep Apnea Treated with Continuous Positive Airway Pressure. *EBIOMEDICINE* (2016) 7:221–9. doi: 10.1016/j.ebiom.2016.03.020
30. Racanelli AC, Kikkers SA, Choi AMK, Cloonan SM. Autophagy and inflammation in chronic respiratory disease. *Autophagy* (2018) 14:221–32. doi: 10.1080/15548627.2017.1389823
31. Frank M, Duvezin-Caubet S, Koob S, Occhipinti A, Jagasia R, Petcherski A, et al. Mitophagy is triggered by mild oxidative stress in a mitochondrial fission dependent manner. *Biochim Biophys Acta (BBA) - Mol Cell Res* (2012) 1823:2297–310. doi: 10.1016/j.bbamcr.2012.08.007
32. Song S, Tan J, Miao Y, Zhang Q. Effect of different levels of intermittent hypoxia on autophagy of hippocampal neurons. *Sleep Breath* (2017) 21:791–8. doi: 10.1007/s11325-017-1512-7
33. Wang D, Zhang J, Jiang W, Cao Z, Zhao F, Cai T, et al. The role of NLRP3-CASP1 in inflammasome-mediated neuroinflammation and autophagy dysfunction in manganese-induced, hippocampal-dependent impairment of learning and memory ability. *Autophagy* (2017) 13:914–27. doi: 10.1080/15548627.2017.1293766
34. Tran TA, Nguyen AD, Chang J, Goldberg MS, Lee JK, Tansey MG. Lipopolysaccharide and tumor necrosis factor regulate Parkin expression via nuclear factor-kappa B. *PLoS One* (2011) 6:e23660. doi: 10.1371/journal.pone.0023660
35. Mouton-Liger F, Rosazza T, Sepulveda-Diaz J, Ieang A, Hassoun S, Claire E, et al. Parkin deficiency modulates NLRP3 inflammasome activation by attenuating an A20-dependent negative feedback loop. *GLIA* (2018) 66:1736–51. doi: 10.1002/glia.23337
36. Sumpter R, Sirasanagandla S, Fernández ÁF, Wei Y, Dong X, Franco L, et al. Fanconi Anemia Proteins Function in Mitophagy and Immunity. *Cell* (2016) 165:867–81. doi: 10.1016/j.cell.2016.04.006
37. Dai C, Luo T, Luo S, Wang J, Wang S, Bai Y, et al. p53 and mitochondrial dysfunction: novel insight of neurodegenerative diseases. *J Bioenerg Biomembr* (2016) 48:337–47. doi: 10.1007/s10863-016-9669-5
38. Sowter HM, Ratcliffe PJ, Watson P, Greenberg AH, Harris AL. HIF-1-dependent regulation of hypoxic induction of the cell death factors BNIP3 and NIX in human tumors. *Cancer Res* (2001) 61:6669–73.

39. Lazarou M, Sliter DA, Kane LA, Sarraf SA, Wang C, Burman JL, et al. The ubiquitin kinase PINK1 recruits autophagy receptors to induce mitophagy. *Nature* (2015) 524:309–14. doi: 10.1038/nature14893

Conflict of Interest: The authors declare that the research was conducted in the absence of any commercial or financial relationships that could be construed as a potential conflict of interest.

frontiers in Immunology

REVIEW
published: 25 February 2021
doi: 10.3389/fimmu.2021.624538

Mitochondrial Regulation of Microglial Immunometabolism in Alzheimer's Disease

Lauren H. Fairley, Jia Hui Wong and Anna M. Barron *

Neurobiology of Aging and Disease Laboratory, Lee Kong Chian School of Medicine, Nanyang Technological University Singapore, Singapore, Singapore

Alzheimer's disease (AD) is an age-associated terminal neurodegenerative disease with no effective treatments. Dysfunction of innate immunity is implicated in the pathogenesis of AD, with genetic studies supporting a causative role in the disease. Microglia, the effector cells of innate immunity in the brain, are highly plastic and perform a diverse range of specialist functions in AD, including phagocytosing and removing toxic aggregates of beta amyloid and tau that drive neurodegeneration. These immune functions require high energy demand, which is regulated by mitochondria. Reflecting this, microglia have been shown to be highly metabolically flexible, reprogramming their mitochondrial function upon inflammatory activation to meet their energy demands. However, AD-associated genetic risk factors and pathology impair microglial metabolic programming, and metabolic derailment has been shown to cause innate immune dysfunction in AD. These findings suggest that immunity and metabolic function are intricately linked processes, and targeting microglial metabolism offers a window of opportunity for therapeutic treatment of AD. Here, we review evidence for the role of metabolic programming in inflammatory functions in AD, and discuss mitochondrial-targeted immunotherapeutics for treatment of the disease.

Keywords: beta amyloid (Aβ), neurodegeneration, metabolism, tau, microglia, mitochondria

OPEN ACCESS

Edited by:
Edecio Cunha-Neto, University of São Paulo, Brazil

Reviewed by:
Ravikanth Velagapudi, Duke University, United States
Maryna Skok, Palladin Institute of Biochemistry (NAS Ukraine), Ukraine

***Correspondence:**
Anna M. Barron
barron@ntu.edu.sg

Specialty section:
This article was submitted to Inflammation, a section of the journal Frontiers in Immunology

Received: *31 October 2020*
Accepted: *21 January 2021*
Published: *25 February 2021*

Citation:
Fairley LH, Wong JH and Barron AM (2021) Mitochondrial Regulation of Microglial Immunometabolism in Alzheimer's Disease. Front. Immunol. 12:624538. doi: 10.3389/fimmu.2021.624538

INTRODUCTION

Alzheimer's disease (AD) is an age-associated terminal neurodegenerative disease characterized by the presence of two hallmark proteinopathies: extracellular aggregates of toxic beta amyloid (Aβ) and intracellular neuronal accumulation of misfolded tau. Inflammation is also an early feature of the neurodegenerative cascade (1, 2), identified as a key driver in pathogenesis and a promising target for AD therapeutic development (3). Although once viewed as a downstream consequence of AD pathogenesis, genome-wide association studies have implicated innate immunity as causative in the disease process, with variants of microglial regulators identified as key AD risk factors such as triggering receptor myeloid 2 (TREM2) and its downstream signaling molecule, Src homology 2 (SH2) domain containing inositol polyphosphate 5-phosphatase 1 (SHIP1) (4–8). Whether microglial overactivation or insufficiency contributes to neurodegeneration in AD is still a matter

of controversy. However, in order to develop potential immunotherapeutics for AD, identification of mechanisms governing the switch between protective and dysfunctional microglial states is critical.

Emerging evidence indicates that metabolic function plays a critical role in the regulation of microglial immune function in AD, with several genetic risk factors for AD identified as important regulators of microglial metabolic fitness (3, 9, 10). Microglia are highly metabolically flexible and metabolic programming is a key regulator of functional plasticity, an emerging field known as immunometabolism (11, 12). Here we discuss the role of mitochondria as metabolic hubs and intracellular signaling platforms coordinating microglial immune functions in AD, and potential targets for the development of immunometabolic therapies for disease treatment.

INNATE IMMUNITY AND METABOLISM IN AD

Microglia perform a diverse range of specialist functions in the AD brain. They can mitigate neurodegeneration through phagocytic clearance of pathological Aβ (2, 13) and tau (14), by removing dying neurons thus preventing "bystander" neuronal death (15, 16) and releasing neurotrophic factors promoting neuronal support including nerve growth factor, brain-derived neurotrophic factor, and insulin-like growth factor-I (17–20). On the other hand, they can exacerbate neurodegeneration by mediating the spread of misfolded forms of tau, phagocytosing healthy or functional neurons, releasing neurotoxic cytokines and increasing oxidative stress through the generation of reactive oxygen species (ROS) (21–23).

Although activated microglia have previously been roughly divided into two categories—classically activated M1 host defence responses, with pro-inflammatory and cytotoxic properties, and alternatively activated M2 regeneration and repair responses—recent single cell transcriptomic analyses have revealed a high degree of heterogeneity and complexity within microglial states and populations that change with aging and disease (24–29). This microglial diversity is distinguished not only by unique immune signatures but also by altered metabolic phenotypes (3, 26, 29).

Diversity of mitochondrial structure, localization and function within and between cells has been identified as an important factor determining cell-to-cell heterogeneity, as well as contributing to heterogeneous outcomes in aging (30). In microglia, mitochondria coordinate energy supply, generation of ROS, and production of substrates for membrane biosynthesis, immune signaling molecules and growth factors (31). However, mitochondrial quality and activity declines in aging and age-related diseases, such as AD (32). Microglia have very low mitochondrial turnover (33) and are severely affected by mitochondrial impairment (34). Further, chronic exposure to pathogens such as Aβ and tau also induces mitochondrial toxicity and metabolic dysfunction in microglia (35). It is therefore important to understand the effect of aging and disease on microglial metabolic programming in AD.

MICROGLIAL METABOLISM IN AD

Microglial metabolism is tightly controlled in response to environmental cues, including nutrient availability, cytokines, and damage- or pathogen-associated molecular patterns (DAMPs and PAMPs), including Aβ and tauopathy. A recent large-scale proteomics analysis of AD brain demonstrated early metabolic changes associated with microglial activation (3). Similarly, proteomics analysis of microglia isolated from AD mice identified enrichment in proteins involved in energy metabolism and mitochondrial processes (36). Here we will examine how the AD microenvironment impacts microglial metabolism and mitochondrial function.

Nutrient Availability and Metabolic Stress

The AD brain is under metabolic stress, with impairments in nutrient availability including glucose occurring early in the disease due to impaired blood-brain glucose transfer (34, 37). Glucose is the primary substrate used by microglia for energy production and is taken into the cell *via* various glucose transporters (GLUTs) (38–40) where it can metabolise glucose *via* glycolysis in the cytoplasm, enzymatically converting glucose into pyruvate then lactate to generate energy in the form of adenosine triphosphate (ATP). Alternatively, pyruvate can be shuttled into the mitochondria where it is converted into acetyl coenzyme A (Acetyl CoA) and consumed by the tricarboxylic acid (TCA) cycle, generating substrates for oxidative phosphorylation (OXPHOS). Glycolysis is less efficient than OXPHOS, requiring nearly 20-fold more glucose to yield equivalent quantities of ATP, but much faster, making it ideal under conditions in which rapid energy production is required. Microglia express genes required for both glycolytic and oxidative metabolism (41, 42) and can switch between these metabolic programmes in response to inflammatory stimuli (35, 43–46).

Glucose can also be metabolized by microglia *via* the pentose phosphate pathway (PPP) to generate nicotinamide adenine dinucleotide phosphate (NADPH), which fuels NADPH oxidase to produce ROS as well as providing the building blocks for nucleotide synthesis (47). However, long-term reductions in glucose availability in aging and AD necessitate the use of alternative energy sources in microglia, or they risk metabolic derailment and dysfunction.

Microglia are also capable of using a range of non-glucose based energy sources, a potentially important adaptive function in the hypoglycemic AD brain. Fatty acids (FA), which are released following the degradation of lipid droplets, are transported into mitochondria and used to fuel mitochondrial OXPHOS, a process known as fatty acid β-oxidation (FAO). A number of genes involved in FAO are expressed in microglia (48), and FAs have been shown to fuel macrophage functions under glucose deprivation (49, 50). Microglia have also been shown to take up ketones and lactate, through the monocarboxylic transporters MCT1 and MCT2 (51). Glutamine is another alternative energy source consumed by microglia *via* glutaminolysis under hyperglycemic conditions, which feeds into the TCA cycle (52). Although the extent to which these non-glucose substrates fuel microglial function

in vivo is largely unknown, a recent study used fluorescence lifetime imaging (FLIM) to indirectly measure glycolysis and OXPHOS in the normal mouse brain under insulin-induced hypoglycaemia, demonstrating microglia shift to glutaminolysis in the absence of glucose (52). Positron emission tomography (PET) can also be used to visualize glycolysis and OXPHOS in both animals and the humans. Glycolysis can be measured using the glucose analogue, ^{18}F-fluoro-2-deoxy-D-glucose-PET (FDG-PET) (53, 54) in combination with cerebral oxygen consumption to measure glycolysis (55, 56), while OXPHOS can be measured using mitochondrial complex-I-PET (57). These metabolic imaging approaches will enable investigation of microglial metabolism in the living brain under both normal and AD conditions and may provide biomarkers of microglial metabolism.

Aβ and Tau Alter Microglial Metabolism

AD-associated proteinopathy, Aβ and tau, induce mitochondrial toxicity and metabolic dysfunction. Exposure to Aβ alone or in combination with other inflammatory stimuli has been shown to induce a shift in metabolic programming from OXPHOS to glycolysis, impairing ATP production, increasing the generation of ROS, and inducing mitochondrial fission, fragmentation and extracellular release (35, 45, 46, 58). Fragmented mitochondria released from microglia have been shown to impair not only microglia, but also nearby neurons and astrocytes (58). Likewise, microglia isolated from AD mice are characterized by dependence on glycolytic metabolism as well as impaired mitochondrial quality control due to inhibition of mitophagy (59). Consistent with this, PET studies have shown increased reliance on aerobic glycolysis in areas spatially correlated with Aβ deposition in the AD brain (55, 56). Similarly, pathological forms of tau can bind mitochondria and impair OXPHOS and ATP synthesis (60); and Aβ and tau act synergistically to induce defects in OXPHOS and ATP synthesis, while increasing ROS production in AD mice (61).

Aβ can influence mitochondrial metabolism through direct binding and accumulation within mitochondria (62–64), inducing toxicity (65–67) and mitochondrial bioenergetic impairments (68–70). Mechanistically, Aβ inhibits OXPHOS by targeting ATP synthase, the enzyme that catalyses ATP production in the final step of OXPHOS (71). Others have implicated the nutrient sensor, mammalian target of rapamycin (mTOR), in Aβ-induced microglial metabolic reprogramming. Exposure to Aβ increases phosphorylation of mTOR *via* serine/threonine protein kinase B (Akt), which increases the expression of HIF-1a, the master transcriptional regulator of glycolysis (35).

Additionally, Aβ and tau can indirectly affect metabolism through upregulation of cytokines classically associated with M1, proinflammatory responses, such as interleukin-1β (IL-1β) and interferon-γ (IFNγ). Inflammatory cytokines induce glycolytic programming accompanied by breaks in the TCA cycle and uncoupling of OXPHOS (43, 45, 46). OXPHOS uncoupling impairs ATP production from mitochondrial respiratory chain activity, causing an increase in ROS generation (72). To support glycolysis in response to pro-inflammatory cytokines, microglia upregulate expression of GLUTs to facilitate increased glucose (40). A metabolic break in citrate metabolism fragments the TCA cycle, increases citrate availability for FA synthesis (FAS) and lipogenesis (73). Further, Aβ has been implicated in the suppression of mitochondrial succinate dehydrogenase (74), which underlies a second TCA cycle break widely observed in pro-inflammatory microglia, leading to accumulation of succinate. These findings suggest that AD-associated stimuli directly alter metabolic processes in microglia in a variety of ways. However, the precise signaling mechanisms involved remain to be fully elucidated.

AD Genetic Risk Factors and Microglial Metabolism

A number of immune-related genetic risk factors for AD have been shown to modulate microglial metabolism. The most prevalent genetic risk factor for AD, apolipoprotein E4 (ApoE4), is primarily expressed by glia in the brain and has been shown to play a role in mitochondrial energy production (9). In human iPSC-derived microglia, the AD-associated E4 variant of ApoE severely impaired metabolism, inhibiting both glycolysis and OXPHOS (75). Further, cognitively normal ApoE4 carriers demonstrate abnormally low cerebral metabolic rates for glucose (76). Additionally, ApoE binds and transports lipoproteins, and ApoE knockdown has been shown to alter FA levels and lipid metabolism in the brain (77). Interestingly, ApoE is a ligand for TREM2, which is a microglial surface receptor required for diverse microglial responses in neurodegeneration, including proliferation, survival, clustering and phagocytosis (46, 78–80). Increased risk of developing AD is associated with loss-of-function variants of TREM2, and TREM2 has been shown to induce ApoE signaling in microglia (27, 81).

Recently, TREM2 has also been identified as a regulator of mitochondrial metabolic fitness in microglia and macrophages (10). TREM2-deficient microglia exhibit decreased expression of genes encoding glucose transporters, glycolytic enzymes, as well as decreased expression of the metabolic coordinator, mTOR (10). Combined transcriptomic and metabolic analysis of TREM2 deficient macrophages revealed reduced ATP production and defects in metabolites and enzymes involved in glycolysis, the TCA cycle and PPP (10). Furthermore, TREM2 knockout mice exhibit cerebral hypometabolism measured by FDG-PET (82, 83). TREM2 also plays an important role in lipid metabolism, with TREM2 deficiency causing pathogenic lipid accumulation in microglia (84).

The TREM2/ApoE axis has also been identified as a regulatory checkpoint in the differentiation of specialized microglial phenotypes associated with age and disease, coined disease-associated microglia (DAMs) (26). DAMs express high levels of lipid metabolism genes, including APOE, Cst7 and lipoprotein lipase (Lpl), which catalyse the release of FAs for FAO (50). Other studies have identified disease and injury associated microglial signatures that share overlap with some key DAM-associated genes, including APOE and Lpl (24, 25, 27). A recent study of microglial proteomic changes in AD mice demonstrated upregulation of the TREM2/ApoE axis and increased proteins involved in FA metabolism (85).

These findings indicate that AD-associated pathology and genetic risk factors are intricately associated with mitochondrial metabolic functions in microglia (summarized in **Figure 1**). However, further research is needed to elucidate the mechanistic pathways involved in metabolic regulation in microglia, which

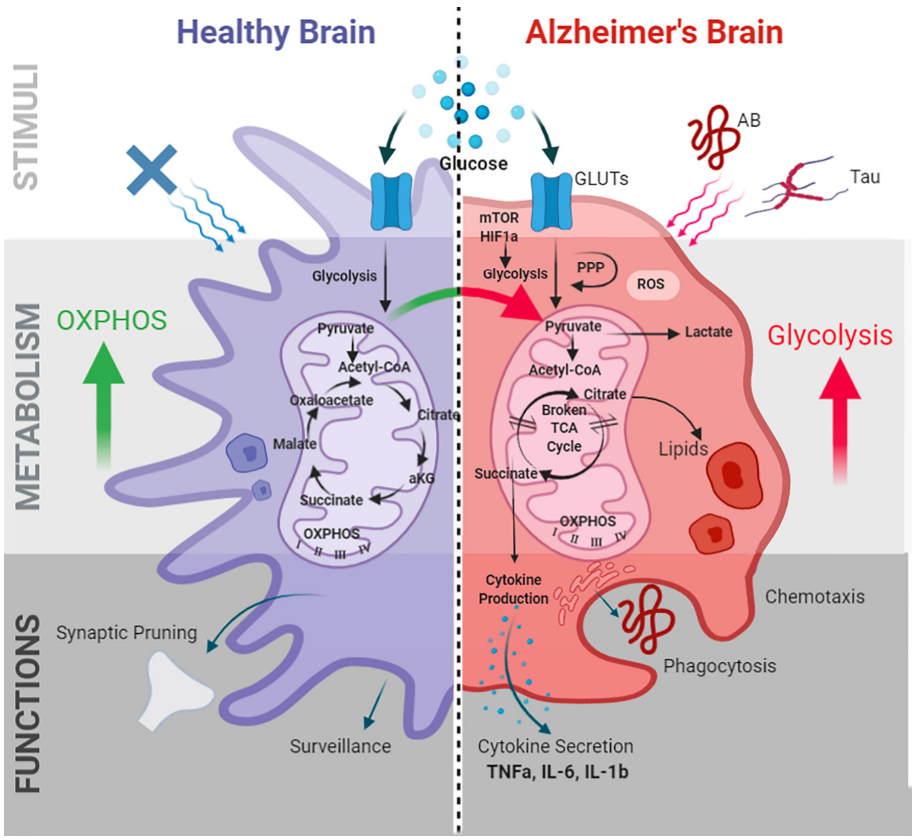

FIGURE 1 | Microglial metabolic programming and immune functions in AD. Alzheimer's pathogenic stimuli Aβ and tau induce microglial metabolic alterations. Metabolic alterations are mediated by the mTOR-HIF1a pathway and characterized by decreased OXPHOS, increased glycolysis, impaired ATP production, a "broken" TCA cycle, increased ROS, and lipid droplet accumulation. These alterations in turn effect microglial immune functions including phagocytosis, chemotaxis, cytokine production, membrane biogenesis, and antigen presentation. GLUTs, glucose transporters; PPP, pentose phosphate pathway; TCA, tricarboxylic acid; ROS, reactive oxygen species; OXPHOS, oxidative phosphorylation; TNF-α, tumor necrosis factor- α; IL-6, interleukin-6; IL-1β, interleukin-1β; HIF-1α, hypoxia inducible factor-1α; mTOR, mammalian target of rapamycin.

may in turn aid the identification of druggable targets to modulate immunometabolic impairment.

Aging and Microglial Metabolism

Aging is associated with a glycolytic metabolic shift in both human and mouse microglia, coupled with increased expression of markers of cellular senescence (86, 87). Aging also leads to accumulation of lipid droplets in microglia in the mouse and human brain, named lipid droplet accumulating microglia (LDAM) (29). LDAMs are characterized by upregulation of genes involved in lipogenesis, TCA cycle and FAO, and exhibit increased ROS production. Meanwhile, key enzymes involved in lipid degradation are downregulated. A recent study has demonstrated that physical coupling between the mitochondria and lipid droplets plays an important role in the regulation of glycolytic metabolic reprogramming in immune cells (88). Whether lipid droplet-mitochondrial interactions regulate metabolic programming in microglia remains to be addressed, but may provide important new insights into how microglial metabolism is coordinated in aging and AD.

MICROGLIAL METABOLISM AND THE INNATE IMMUNE RESPONSE IN AD

Microglial metabolism and immune function are reciprocally regulated. Microglia not only undergo adaptive metabolic reprogramming in response to inflammatory stimuli, but immune responses are dependent upon these metabolic shifts. Changes in cell morphology, chemotaxis, and phagocytosis all require reorganization of the actin cytoskeleton, which is dependent on the coordinated supply of ATP (89). Phagocytic degradation of engulfed materials, which plays an important role in the clearance of Aβ and tau, also relies upon the coordinated production and delivery of mitochondrial ROS to the phagolysosome (90). Similarly, the production of cytokines and growth factors requires resources such as amino acids, nucleotides, and fatty acids, which are supplied by metabolites generated during energy production. Mitochondrial metabolites are also utilized for lipogenesis to support membrane biogenesis for filopodia formation, antigen presentation and organelle biogenesis during proliferation and growth (73, 91). As such, changes in microglial

adaptive metabolic reprogramming underpins immune function. Here we will discuss how age and disease associated changes in microglial metabolic programming modulates critical microglial functions in AD.

In microglia, initiation of the classic pro-inflammatory response is dependent upon glycolytic metabolic reprogramming, with immune responses including phagocytosis and pro-inflammatory cytokine production blocked by inhibition of glycolysis (25, 40, 92–94). In addition to rapidly generating ATP for energetically demanding chemotaxis and phagocytosis, upregulation of glycolysis and its branched pathway, the PPP, has been shown to be essential for the production of ROS-dependent phagosome degradation (95). In the AD brain, proteomics analysis has demonstrated a strong association between microglia and glycolytic metabolism (3). Upregulation of markers enriched in the AD brain was observed in microglia undergoing active Aβ phagocytosis in AD mouse brain, suggesting a protective function of hyperglycolytic microglia in AD (3). Markers identified in this study overlapped with markers of the TREM2-dependent, protective, phagocytic microglial subpopulation, DAMs (26). Knockout studies have shown that TREM2 promotes a metabolic programme fuelled by glycolysis, PPP and the TCA cycle to support phagocytosis (10). TREM2 deletion impairs microglial chemotaxis and phagocytosis in AD mice, resulting in inability of microglia to cluster around and clear aggregates of Aβ (10). These microglial deficits were mitigated with dietary cyclocreatine, a creatine analog that can supply ATP, indicating metabolic impairments caused the immune function impairments following TREM2 deletion (10).

Microglial hyperglycolysis is also observed in the aging brain but, in contrast is associated with compromised chemotaxis, phagocytosis and Aβ engulfment, and elevated secretion of pro-inflammatory cytokines (86, 87). Likewise, Aβ-induced glycolysis is associated with impaired chemotaxis and phagocytosis of Aβ in cultured microglia, a phenomena also observed in microglia isolated from AD mice (59). Further, multiple studies have shown that microglial Aβ phagocytosis is enhanced by promoting OXPHOS, rather than glycolysis (96, 97). One potential explanation for these differences may come from the chronic versus acute effects of Aβ on microglial function. Because glycolysis is metabolically inefficient, persistent reliance on glycolysis in microglia may lead to impaired immune function and reduced capacity to perform immune functions over time (97). In line with this, acute exposure to Aβ increased glycolysis and enhanced immune functions in microglia, whereas chronic exposure induced metabolic dysregulation and diminished immune functions, including phagocytosis and cytokine secretion (35). Further, Aβ-induced mitochondrial toxicity may disrupt coordinated immunometabolic programming. Consistent with this, in AD mice pharmacological induction of mitophagy to restore mitochondrial quality control enhanced microglial phagocytosis of Aβ and decreased the production of pro-inflammatory cytokines TNF-α and IL-6 (98).

Lipid metabolism has also been identified as important in microglial phagocytic functions in aging and AD. Lpl, the major enzyme responsible for liberating FAs from lipid droplets, is upregulated by Aβ in microglia, and silencing Lpl has been shown to impair Aβ phagocytosis (99). In macrophages, phagocytosis has been shown to be dependent on the availability of FAs following the degradation of lipid droplets, linking effective lysis of lipid droplets with successful phagocytosis (49). Supporting this, Lpl has been identified as a key marker of DAMs. In contrast, LDAMs, which are characterized by lipid droplet accumulation, lipogenesis and reduced FAO, also exhibit impaired phagocytosis (29). Lipid accumulation is a key feature observed in immune dysfunction, for example foamy macrophages observed in atherosclerotic lesions and lipid droplets have been identified as potential structural markers of inflammation (100). Interestingly, inhibition of FA synthesis restored phagocytic function in these microglia, again highlighting the potential to restore microglial immune function by restoring metabolic function in aging and AD.

MICROGLIAL METABOLIC REPROGRAMMING FOR THE TREATMENT OF AD

AD is one of the leading causes of death worldwide with no effective treatments available, leading to urgent calls for the development of disease modifying-agents (101). Given the pivotal role of inflammation in AD pathophysiology, here we discuss potential therapeutic strategies that improve microglial function through regulation of metabolism.

Ketone Body Therapeutics

Microglia can utilize ketone bodies as an alternative energy substrate to glucose, and ketosis has been shown to modulate a range of microglial inflammatory processes and reduce Aβ and tau accumulation in AD mice (101–106). Ketosis can be induced through several methods, including dietary modification, ketone body supplements, and pharmacological inhibitors of glycolysis. High-fat, low-carbohydrate ketogenic diets are thought to trigger a shift from glucose metabolism towards fatty acid metabolism, which in turn yields increased ketone body concentrations. Ketogenic diet decreased microglia activation and pro-inflammatory cytokine IL-6, IL-1β and TNF-α levels (107). Similarly, oral administration of ketone body metabolites such as β-hydroxybutyrate (β-OHB) have been shown to reduce microglial inflammation (108), reduce expression of pro-inflammatory cytokines IL-1b, IL-6, CCL2/MCP-1 (109), and inhibit NLRP3 inflammasome activation (110). Competitive inhibitors of glycolysis, such as 2-deoxy-D-glucose (2-DG) have been shown to induce compensatory metabolic processes and promote ketosis. Transgenic AD mice fed a diet supplemented with 2-DG exhibited increased serum ketone body levels and brain expression of enzymes required for ketone body metabolism, as well as decreased oxidative stress and reduced levels of Aβ oligomers (111). Further, pharmacological treatment with 2-DG has been shown to reduce markers of microglial activation following LPS treatment (41), reduce expression of inducible nitric oxide synthase (iNOS) (112), and decrease IL-6, IL-1β levels (113) in BV2 and primary microglia. These findings suggest that treatments targeted towards increasing microglial ketosis in AD may have therapeutic

benefits, however ketogenic diet, β-OHB, and 2-DG are all known to exert non-microglial specific effects in a range of cell types in the brain. Further research aimed at identifying microglia-specific promoters of ketosis may be of benefit in the treatment of neuroinflammatory diseases such as AD.

Exercise

Exercise is consistently associated with improvement in cognitive and neuronal function in aged animals (114, 115) and reductions in Aβ and tau pathology in AD mice (116–118). The mechanism underlying exercise-related benefits in the brain is not well understood, however decreased pro-inflammatory cytokine expression has been proposed as one potential mechanism (119, 120). Recently, metabolic reprogramming has been identified as a mediator of exercise-relate changes in cognition and immune functions, as exercise attenuated age-dependent inflammatory cytokine expression and cognitive decline in mice, while decreasing glycolytic enzymes and increasing phagocytosis in isolated microglia (86). However, whether exercise exerts beneficial effects by promoting OXPHOS or FAO, or alternative substrate use, remains to be elucidated. Although no study to date has investigated whether metabolic reprogramming underlies exercise-related changes in inflammation and pathology in an AD-specific context, these findings suggest that exercise is a promising avenue for therapeutic investigation.

mTOR Targeted Therapeutics

The mTOR-HIF-1α pathway is a central mediator of inflammation in the brain and has been implicated in the regulation of microglial metabolic reprogramming in AD (10, 35). Two compounds that target the mTOR pathway and are currently being trialled for clinical efficacy in AD are rapamycin and metformin. Rapamycin directly inhibits mTOR *via* binding of mTOR Complex 1 (mTORC1), whereas metformin acts upstream of mTOR by targeting the glycolytic inhibitor AMP-activated protein kinase (AMPK). Both compounds have been shown to reduce glycolytic metabolism in favor of increased OXPHOS in immune cells (121, 122) and decrease the production of proinflammatory cytokines by microglia and macrophages (123, 124). As the mTOR pathway is found ubiquitously in all cell types, targeting microglial-specific mTOR signaling is challenging and both rapamycin and metformin are known to exert non-immune related effects in neurons and astrocytes. TREM2 has recently been identified as a microglial-specific target that regulates mTOR in AD (10), however there is currently a paucity of druggable targets identified in the TREM2-mTOR signaling pathway. SHIP1, which is primarily expressed in microglia, is one of the only therapeutic targets in the TREM2-specific mTOR signaling pathway that is under investigation for the treatment of AD. SHIP1 is known to inhibit TREM2 signaling (125) and pan-SHIP1/2 inhibitors have been shown to increase microglial phagocytosis of Aβ1-42 *in vitro via* mTOR regulation (126). These findings suggest that modulating TREM2-dependent mTOR signaling could provide neuroprotective effects in AD, however further research is needed to identify additional targets for therapeutic modulation in this pathway.

TSPO Targeted Therapeutics

The translocator protein (TSPO) is an outer mitochondrial membrane protein that is predominantly expressed in microglia in the brain and is upregulated in AD (127, 128). Consequently, TSPO is widely regarded as a biomarker of neuroinflammation, and TSPO ligands have been shown to exert a range of protective effects in mouse models of neurodegeneration (129, 130). In particular, ligands targeting TSPO have been shown to decrease Aβ deposition and reduce markers of inflammation in mouse models of AD (131). TSPO has also been implicated in microglial metabolic programming, as TSPO deficiency suppressed both OXPHOS and glycolysis, resulting in overall metabolic deficits in primary microglia (132) and increased fatty acid oxidation in steroidogenic cells (133). In contrast, treatment with TSPO ligands improved mitochondrial respiration, decreased oxidative stress-induced cell death by reducing ROS, and lowered Aβ levels in H1299 cells (134). These findings suggest that TSPO may be a marker of beneficial microglial phenotypes, and treatments aimed at increasing TSPO expression may confer neuroprotective effects in AD. However, further research investigating the metabolic modulatory effects of TSPO ligands in microglia specifically is required.

DISCUSSION

Innate immunity plays a causative role in the pathogenesis of AD, and coordinated microglial immune responses have the potential to either ameliorate or exacerbate AD pathology, depending on microglial phenotypes. However, efforts to elucidate the cellular mechanisms and molecular signals mediating neuroinflammatory responses in AD have been hampered by the large heterogeneity in immune cell types and responses within the brain. Emerging evidence indicates that metabolic function plays a critical role in the regulation of microglial function in AD, with metabolic programming underlying diverse microglial immune functions and phenotypes. Further, therapeutic strategies modulating microglial metabolic programming have shown neuroprotective effects, by reducing amyloid and tau load, and improving cognitive deficits. These findings suggest that microglial function and metabolism are intricately associated processes in AD, however, further research is needed to elucidate the mechanistic pathways involved in metabolic regulation in microglia, which may in turn aid in the identification of druggable targets to modulate immunometabolic impairment.

AUTHOR CONTRIBUTIONS

LF, JW, and AB wrote and reviewed the manuscript. LF: prepared the figure. All authors contributed to the article and approved the submitted version.

FUNDING

AB acknowledges funding support from the Singapore Ministry of Education under its Singapore Ministry of Education

Academic Research Fund Tier 1 (RG42/18), Nanyang Assistant Professorship from Nanyang Technological University Singapore, and the Alzheimer's Association (AARG-18-566427).

ACKNOWLEDGMENTS

Figure created with BioRender.com.

REFERENCES

1. Frenkel D, Wilkinson K, Zhao L, Hickman SE, Means TK, Puckett L, et al. Scara1 deficiency impairs clearance of soluble amyloid-beta by mononuclear phagocytes and accelerates Alzheimer's-like disease progression. *Nat Commun* (2013) 4:2030. doi: 10.1038/ncomms3030
2. Hickman SE, Allison EK, El Khoury J. Microglial dysfunction and defective beta-amyloid clearance pathways in aging Alzheimer's disease mice. *J Neurosci* (2008) 28(33):8354–60. doi: 10.1523/JNEUROSCI.0616-08.2008
3. Johnson ECB, Dammer EB, Duong DM, Ping L, Zhou M, Yin L, et al. Large-scale proteomic analysis of Alzheimer's disease brain and cerebrospinal fluid reveals early changes in energy metabolism associated with microglia and astrocyte activation. *Nat Med* (2020) 26(5):769–80. doi: 10.1038/s41591-020-0815-6
4. Gratuze M, Leyns CEG, Holtzman DM. New insights into the role of TREM2 in Alzheimer's disease. *Mol Neurodegener* (2018) 13(1):66. doi: 10.1186/s13024-018-0298-9
5. Guerreiro R, Hardy J. Genetics of Alzheimer's disease. *Neurotherapeutics* (2014) 11(4):732–7. doi: 10.1007/s13311-014-0295-9
6. Jonsson T, Stefansson H, Steinberg S, Jonsdottir I, Jonsson PV, Snaedal J, et al. Variant of TREM2 associated with the risk of Alzheimer's disease. *N Engl J Med* (2013) 368(2):107–16. doi: 10.1056/NEJMoa1211103
7. Malik M, Parikh I, Vasquez JB, Smith C, Tai L, Bu G, et al. Genetics ignite focus on microglial inflammation in Alzheimer's disease. *Mol Neurodegener* (2015) 10(1):52. doi: 10.1186/s13024-015-0048-1
8. Tanzi RE. The genetics of Alzheimer disease. *Cold Spring Harb Perspect Med* (2012) 2(10):1–10. doi: 10.1101/cshperspect.a006296
9. Liao F, Yoon H, Kim J. Apolipoprotein E metabolism and functions in brain and its role in Alzheimer's disease. *Curr Opin Lipidol* (2017) 28(1):60. doi: 10.1097/MOL.0000000000000383
10. Ulland TK, Song WM, Huang SC, Ulrich JD, Sergushichev A, Beatty WL, et al. TREM2 Maintains Microglial Metabolic Fitness in Alzheimer's Disease. *Cell* (2017) 170(4):649–63.e13. doi: 10.1016/j.cell.2017.07.023
11. Angajala A, Lim S, Phillips JB, Kim J-H, Yates C, You Z, et al. Diverse Roles of Mitochondria in Immune Responses: Novel Insights Into Immuno-Metabolism. *Front Immunol* (2018) 9:1605. doi: 10.3389/fimmu.2018.01605
12. Lauro C, Limatola C. Metabolic Reprograming of Microglia in the Regulation of the Innate Inflammatory Response. *Front Immunol* (2020) 11(493):1–8. doi: 10.3389/fimmu.2020.00493
13. Lee CD, Landreth GE. The role of microglia in amyloid clearance from the AD brain. *J Neural Transm* (2010) 117(8):949–60. doi: 10.1007/s00702-010-0433-4
14. Luo W, Liu W, Hu X, Hanna M, Caravaca A, Paul SM. Microglial internalization and degradation of pathological tau is enhanced by an anti-tau monoclonal antibody. *Sci Rep* (2015) 5(1):11161. doi: 10.1038/srep11161
15. Hsieh CL, Koike M, Spusta SC, Niemi EC, Yenari M, Nakamura MC, et al. A role for TREM2 ligands in the phagocytosis of apoptotic neuronal cells by microglia. *J Neurochem* (2009) 109(4):1144–56. doi: 10.1111/j.1471-4159.2009.06042.x
16. Takahashi K, Rochford CD, Neumann H. Clearance of apoptotic neurons without inflammation by microglial triggering receptor expressed on myeloid cells-2. *J Exp Med* (2005) 201(4):647–57. doi: 10.1084/jem.20041611
17. Sampaio TB, Savall AS, Gutierrez MEZ, Pinton S. Neurotrophic factors in Alzheimer's and Parkinson's diseases: implications for pathogenesis and therapy. *Neural Regen Res* (2017) 12(4):549. doi: 10.4103/1673-5374.205084
18. Parkhurst CN, Yang G, Ninan I, Savas JN, Yates JRII, Lafaille JJ, et al. Microglia promote learning-dependent synapse formation through brain-derived neurotrophic factor. *Cell* (2013) 155(7):1596–609. doi: 10.1016/j.cell.2013.11.030
19. Rajendran L, Paolicelli RC. Microglia-mediated synapse loss in Alzheimer's disease. *J Neurosci* (2018) 38(12):2911–9. doi: 10.1523/JNEUROSCI.1136-17.2017
20. Suh H-S, Zhao M-L, Derico L, Choi N, Lee SC. Insulin-like growth factor 1 and 2 (IGF1, IGF2) expression in human microglia: differential regulation by inflammatory mediators. *J Neuroinflamm* (2013) 10(1):805. doi: 10.1186/1742-2094-10-37
21. Asai H, Ikezu S, Tsunoda S, Medalla M, Luebke J, Haydar T, et al. Depletion of microglia and inhibition of exosome synthesis halt tau propagation. *Nat Neurosci* (2015) 18(11):1584. doi: 10.1038/nn.413
22. Bhaskar K, Maphis N, Xu G, Varvel NH, Kokiko-Cochran ON, Weick JP, et al. Microglial derived tumor necrosis factor-alpha drives Alzheimer's disease-related neuronal cell cycle events. *Neurobiol Dis* (2014) 62:273–85. doi: 10.1016/j.nbd.2013.10.007
23. Wilkinson BL, Landreth GE. The microglial NADPH oxidase complex as a source of oxidative stress in Alzheimer's disease. *J Neuroinflamm* (2006) 3:30. doi: 10.1186/1742-2094-3-30
24. Frigerio CS, Wolfs L, Fattorelli N, Thrupp N, Voytyuk I, Schmidt I, et al. The major risk factors for Alzheimer's disease: age, sex, and genes modulate the microglia response to Aβ plaques. *Cell Rep* (2019) 27(4):1293–306. e6. doi: 10.1016/j.celrep.2019.03.099
25. Hammond TR, Dufort C, Dissing-Olesen L, Giera S, Young A, Wysoker A, et al. Single-cell RNA sequencing of microglia throughout the mouse lifespan and in the injured brain reveals complex cell-state changes. *Immunity* (2019) 50(1):253–71.e6. doi: 10.1016/j.immuni.2018.11.004
26. Keren-Shaul H, Spinrad A, Weiner A, Matcovitch-Natan O, Dvir-Szternfeld R, Ulland TK, et al. A Unique Microglia Type Associated with Restricting Development of Alzheimer's Disease. *Cell* (2017) 169(7):1276–90.e17. doi: 10.1016/j.cell.2017.05.018
27. Krasemann S, Madore C, Cialic R, Baufeld C, Calcagno N, El Fatimy R, et al. The TREM2-APOE pathway drives the transcriptional phenotype of dysfunctional microglia in neurodegenerative diseases. *Immunity* (2017) 47(3):566–81.e9. doi: 10.1016/j.immuni.2017.08.008
28. Li Q, Barres BA. Microglia and macrophages in brain homeostasis and disease. *Nat Rev Immunol* (2018) 18(4):225–42. doi: 10.1038/nri.2017.125
29. Marschallinger J, Iram T, Zardeneta M, Lee SE, Lehallier B, Haney MS, et al. Lipid-droplet-accumulating microglia represent a dysfunctional and proinflammatory state in the aging brain. *Nat Neurosci* (2020) 23(2):194–208. doi: 10.1038/s41593-019-0566-1
30. Aryaman J, Johnston IG, Jones NS. Mitochondrial Heterogeneity. *Front Genet* (2019) 9:718. doi: 10.3389/fgene.2018.00718
31. West AP, Shadel GS, Ghosh S. Mitochondria in innate immune responses. *Nat Rev Immunol* (2011) 11(6):389–402. doi: 10.1038/nri2975
32. Sun N, Youle RJ, Finkel T. The Mitochondrial Basis of Aging. *Mol Cell* (2016) 61(5):654–66. doi: 10.1016/j.molcel.2016.01.028
33. Hayashi Y, Yoshida M, Yamato M, Ide T, Wu Z, Ochi-Shindou M, et al. Reverse of age-dependent memory impairment and mitochondrial DNA damage in microglia by an overexpression of human mitochondrial transcription factor a in mice. *J Neurosci* (2008) 28(34):8624–34. doi: 10.1523/jneurosci.1957-08.2008
34. Ryu JK, Nagai A, Kim J, Lee MC, McLarnon JG, Kim SU. Microglial activation and cell death induced by the mitochondrial toxin 3-nitropropionic acid: in vitro and in vivo studies. *Neurobiol Dis* (2003) 12(2):121–32. doi: 10.1016/s0969-9961(03)00002-0
35. Baik SH, Kang S, Lee W, Choi H, Chung S, Kim J, et al. A breakdown in metabolic reprogramming causes microglia dysfunction in Alzheimer's disease. *Cell Metab* (2019) 30(3):493–507.e6. doi: 10.1016/j.cmet.2019.06.005
36. Rangaraju S, Dammer EB, Raza SA, Gao T, Xiao H, Betarbet R, et al. Quantitative proteomics of acutely-isolated mouse microglia identifies novel immune Alzheimer's disease-related proteins. *Mol Neurodegener* (2018) 13(1):34. doi: 10.1186/s13024-018-0266-4

37. Backes H, Walberer M, Ladwig A, Rueger MA, Neumaier B, Endepols H, et al. Glucose consumption of inflammatory cells masks metabolic deficits in the brain. *NeuroImage* (2016) 128:54–62. doi: 10.1016/j.neuroimage.2015.12.044
38. Kalsbeek MJ, Mulder L, Yi C-X. Microglia energy metabolism in metabolic disorder. *Mol Cell Endocrinol* (2016) 438:27–35. doi: 10.1016/j.mce.2016.09.028
39. Sasaki A, Yamaguchi H, Horikoshi Y, Tanaka G, Nakazato Y. Expression of glucose transporter 5 by microglia in human gliomas. *Neuropathol Appl Neurobiol* (2004) 30(5):447–55. doi: 10.1111/j.1365-2990.2004.00556.x
40. Wang L, Pavlou S, Du X, Bhuckory M, Xu H, Chen M. Glucose transporter 1 critically controls microglial activation through facilitating glycolysis. *Mol Neurodegener* (2019) 14(1):2. doi: 10.1186/s13024-019-0305-9
41. Ghosh S, Castillo E, Frias ES, Swanson RA. Bioenergetic regulation of microglia. *Glia* (2018) 66(6):1200–12. doi: 10.1002/glia.23271
42. Zhang Y, Chen K, Sloan SA, Bennett ML, Scholze AR, O'Keeffe S, et al. An RNA-sequencing transcriptome and splicing database of glia, neurons, and vascular cells of the cerebral cortex. *J Neurosci* (2014) 34(36):11929–47. doi: 10.1523/jneurosci.1860-14.2014
43. Holland R, McIntosh AL, Finucane OM, Mela V, Rubio-Araiz A, Timmons G, et al. Inflammatory microglia are glycolytic and iron retentive and typify the microglia in APP/PS1 mice. *Brain Behav Immun* (2018) 68:183–96. doi: 10.1016/j.bbi.2017.10.017
44. Nair S, Sobotka KS, Joshi P, Gressens P, Fleiss B, Thornton C, et al. Lipopolysaccharide-induced alteration of mitochondrial morphology induces a metabolic shift in microglia modulating the inflammatory response in vitro and in vivo. *Glia* (2019) 67(6):1047–61. doi: 10.1002/glia.23587
45. Volobouéva LA, Emery JF, Sun X, Giffard RG. Inflammatory response of microglial BV-2 cells includes a glycolytic shift and is modulated by mitochondrial glucose-regulated protein 75/mortalin. *FEBS Lett* (2013) 587(6):756–62. doi: 10.1016/j.febslet.2013.01.067
46. Wang Y, Ulland TK, Ulrich JD, Song W, Tzaferis JA, Hole JT, et al. TREM2-mediated early microglial response limits diffusion and toxicity of amyloid plaques. *J Exp Med* (2016) 213(5):667–75. doi: 10.1084/jem.20151948
47. Gimeno-Bayón J, López-López A, Rodríguez M, Mahy N. Glucose pathways adaptation supports acquisition of activated microglia phenotype. *J Neurosci Res* (2014) 92(6):723–31. doi: 10.1002/jnr.23356
48. Mauerer R, Ebert S, Langmann T. High glucose, unsaturated and saturated fatty acids differentially regulate expression of ATP-binding cassette transporters ABCA1 and ABCG1 in human macrophages. *Exp Mol Med* (2009) 41(2):126–32. doi: 10.3858/emm.2009.41.2.015
49. Chandak PG, Radovic B, Aflaki E, Kolb D, Buchebner M, Frohlich E, et al. Efficient phagocytosis requires triacylglycerol hydrolysis by adipose triglyceride lipase. *J Biol Chem* (2010) 285(26):20192–201. doi: 10.1074/jbc.M110.107854
50. Yin B, Loike JD, Kako Y, Weinstock PH, Breslow JL, Silverstein SC, et al. Lipoprotein lipase regulates Fc receptor-mediated phagocytosis by macrophages maintained in glucose-deficient medium. *J Clin Invest* (1997) 100(3):649–57. doi: 10.1172/JCI119576
51. Moreira TJ, Pierre K, Maekawa F, Repond C, Cebere A, Liljequist S, et al. Enhanced cerebral expression of MCT1 and MCT2 in a rat ischemia model occurs in activated microglial cells. *J Cereb Blood Flow Metab* (2009) 29(7):1273–83. doi: 10.1038/jcbfm.2009.50
52. Bernier L-P, York EM, Kamyabi A, Choi HB, Weilinger NL, MacVicar BA. Microglial metabolic flexibility supports immune surveillance of the brain parenchyma. *Nat Commun* (2020) 11(1):1–17. doi: 10.1038/s41467-020-15267-z
53. Barron AM, Tokunaga M, Zhang MR, Ji B, Suhara T, Higuchi M. Assessment of neuroinflammation in a mouse model of obesity and beta-amyloidosis using PET. *J Neuroinflamm* (2016) 13(1):221. doi: 10.1186/s12974-016-0700-x
54. Tsukada H, Nishiyama S, Fukumoto D, Kanazawa M, Harada N. Novel PET probes 18F-BCPP-EF and 18F-BCPP-BF for mitochondrial complex I: a PET study in comparison with 18F-BMS-747158-02 in rat brain. *J Nucl Med* (2014) 55(3):473–80. doi: 10.2967/jnumed.113.125328
55. Vaishnavi SN, Vlassenko AG, Rundle MM, Snyder AZ, Mintun MA, Raichle ME. Regional aerobic glycolysis in the human brain. *Proc Natl Acad Sci U S A* (2010) 107(41):17757–62. doi: 10.1073/pnas.1010459107
56. Vlassenko AG, Vaishnavi SN, Couture L, Sacco D, Shannon BJ, Mach RH, et al. Spatial correlation between brain aerobic glycolysis and amyloid-beta (Abeta) deposition. *Proc Natl Acad Sci U S A* (2010) 107(41):17763–7. doi: 10.1073/pnas.1010461107
57. Barron AM, Ji B, Fujinaga M, Zhang M-R, Suhara T, Sahara N, et al. In vivo positron emission tomography imaging of mitochondrial abnormalities in a mouse model of tauopathy. *Neurobiol Aging* (2020) 94:140–8. doi: 10.1016/j.neurobiolaging.2020.05.003
58. Joshi AU, Minhas PS, Liddelow SA, Haileselassie B, Andreasson KI, Dorn G2nd, et al. Fragmented mitochondria released from microglia trigger A1 astrocytic response and propagate inflammatory neurodegeneration. *Nat Neurosci* (2019) 22(10):1635–48. doi: 10.1038/s41593-019-0486-0
59. McIntosh A, Mela V, Harty C, Minogue AM, Costello DA, Kerskens C, et al. Iron accumulation in microglia triggers a cascade of events that leads to altered metabolism and compromised function in APP/PS1 mice. *Brain Pathol* (2019) 29(5):606–21. doi: 10.1111/bpa.12704
60. Atlante A, Amadoro G, Bobba A, de Bari L, Corsetti V, Pappalardo G, et al. A peptide containing residues 26-44 of tau protein impairs mitochondrial oxidative phosphorylation acting at the level of the adenine nucleotide translocator. *Biochim Biophys Acta* (2008) 1777(10):1289–300. doi: 10.1016/j.bbabio.2008.07.004
61. Rhein V, Song X, Wiesner A, Ittner LM, Baysang G, Meier F, et al. Amyloid-beta and tau synergistically impair the oxidative phosphorylation system in triple transgenic Alzheimer's disease mice. *Proc Natl Acad Sci U S A* (2009) 106(47):20057–62. doi: 10.1073/pnas.0905529106
62. Cenini G, Rüb C, Bruderek M, Voos W. Amyloid β-peptides interfere with mitochondrial preprotein import competence by a coaggregation process. *Mol Biol Cell* (2016) 27(21):3257–72. doi: 10.1091/mbc.E16-05-0313
63. Mamada N, Tanokashira D, Ishii K, Tamaoka A, Araki W. Mitochondria are devoid of amyloid β-protein (Aβ)-producing secretases: Evidence for unlikely occurrence within mitochondria of Aβ generation from amyloid precursor protein. *Biochem Biophys Res Commun* (2017) 486(2):321–8. doi: 10.1016/j.bbrc.2017.03.035
64. Schaefer PM, von Einem B, Walther P, Calzia E, von Arnim CA. Metabolic Characterization of Intact Cells Reveals Intracellular Amyloid Beta but Not Its Precursor Protein to Reduce Mitochondrial Respiration. *PLoS One* (2016) 11(12):e0168157. doi: 10.1371/journal.pone.0168157
65. Aleardi A, Benard G, Augereau O, Malgat M, Talbot J, Mazat J, et al. Gradual alteration of mitochondrial structure and function by β-amyloids: importance of membrane viscosity changes, energy deprivation, reactive oxygen species production, and cytochrome c release. *J Bioenerg Biomembr* (2005) 37(4):207–25. doi: 10.1007/s10863-005-6631-3
66. Manczak M, Anekonda TS, Henson E, Park BS, Quinn J, Reddy PH. Mitochondria are a direct site of A beta accumulation in Alzheimer's disease neurons: implications for free radical generation and oxidative damage in disease progression. *Hum Mol Genet* (2006) 15(9):1437–49. doi: 10.1093/hmg/ddl066
67. Petersen CAH, Alikhani N, Behbahani H, Wiehager B, Pavlov PF, Alafuzoff I, et al. The amyloid β-peptide is imported into mitochondria via the TOM import machinery and localized to mitochondrial cristae. *Proc Natl Acad Sci* (2008) 105(35):13145–50. doi: 10.1073/pnas.0806192105
68. Du H, Guo L, Fang F, Chen D, Sosunov AA, McKhann GM, et al. Cyclophilin D deficiency attenuates mitochondrial and neuronal perturbation and ameliorates learning and memory in Alzheimer's disease. *Nat Med* (2008) 14(10):1097–105. doi: 10.1038/nm.1868
69. Lustbader JW, Cirilli M, Lin C, Xu HW, Takuma K, Wang N, et al. ABAD directly links Abeta to mitochondrial toxicity in Alzheimer's disease. *Science* (2004) 304(5669):448–52. doi: 10.1126/science.1091230
70. Manczak M, Calkins MJ, Reddy PH. Impaired mitochondrial dynamics and abnormal interaction of amyloid beta with mitochondrial protein Drp1 in neurons from patients with Alzheimer's disease: implications for neuronal damage. *Hum Mol Genet* (2011) 20(13):2495–509. doi: 10.1093/hmg/ddr139
71. Chiozzi P, Sarti AC, Sanz JM, Giuliani AL, Adinolfi E, Vultaggio-Poma V, et al. Amyloid beta-dependent mitochondrial toxicity in mouse microglia requires P2X7 receptor expression and is prevented by nimodipine. *Sci Rep* (2019) 9(1):6475. doi: 10.1038/s41598-019-42931-2
72. Zuo H, Wan Y. Metabolic Reprogramming in Mitochondria of Myeloid Cells. *Cells* (2019) 9(1):1–17. doi: 10.3390/cells9010005

73. Jha AK, Huang SC, Sergushichev A, Lampropoulou V, Ivanova Y, Loginicheva E, et al. Network integration of parallel metabolic and transcriptional data reveals metabolic modules that regulate macrophage polarization. *Immunity* (2015) 42(3):419–30. doi: 10.1016/j.immuni.2015.02.005
74. Kaneko I, Yamada N, Sakuraba Y, Kamenosono M, Tutumi S. Suppression of Mitochondrial Succinate Dehydrogenase, a Primary Target of β-Amyloid, and Its Derivative Racemized at Ser Residue. *J Neurochem* (1995) 65 (6):2585–93. doi: 10.1046/j.1471-4159.1995.65062585.x
75. Konttinen H, Ohtonen S, Wojciechowski S, Shakirzyanova A, Caligola S, Giugno R, et al. PSEN1ΔE9, APPswe, and APOE4 confer disparate phenotypes in human iPSC-derived microglia. *Stem Cell Rep* (2019) 13 (4):669–83. doi: 10.1016/j.stemcr.2019.08.004
76. Reiman EM, Caselli RJ, Chen K, Alexander GE, Bandy D, Frost J. Declining brain activity in cognitively normal apolipoprotein E epsilon 4 heterozygotes: A foundation for using positron emission tomography to efficiently test treatments to prevent Alzheimer's disease. *Proc Natl Acad Sci U S A* (2001) 98(6):3334–9. doi: 10.1073/pnas.061509598
77. Lee J, Choi J, Wong GW, Wolfgang MJ. Neurometabolic roles of ApoE and Ldl-R in mouse brain. *J Bioenerg Biomembr* (2016) 48(1):13–21. doi: 10.1007/s10863-015-9636-6
78. Ulrich JD, Finn MB, Wang Y, Shen A, Mahan TE, Jiang H, et al. Altered microglial response to Abeta plaques in APPPS1-21 mice heterozygous for TREM2. *Mol Neurodegener* (2014) 9:20. doi: 10.1186/1750-1326-9-20
79. Yeh FL, Wang Y, Tom I, Gonzalez LC, Sheng M. TREM2 Binds to Apolipoproteins, Including APOE and CLU/APOJ, and Thereby Facilitates Uptake of Amyloid-Beta by Microglia. *Neuron* (2016) 91 (2):328–40. doi: 10.1016/j.neuron.2016.06.015
80. Yuan P, Condello C, Keene CD, Wang Y, Bird TD, Paul SM, et al. TREM2 Haplodeficiency in Mice and Humans Impairs the Microglia Barrier Function Leading to Decreased Amyloid Compaction and Severe Axonal Dystrophy. *Neuron* (2016) 90(4):724–39. doi: 10.1016/j.neuron.2016.05.003
81. Atagi Y, Liu C-C, Painter MM, Chen X-F, Verbeeck C, Zheng H, et al. Apolipoprotein E is a ligand for triggering receptor expressed on myeloid cells 2 (TREM2). *J Biol Chem* (2015) 290(43):26043–50. doi: 10.1074/jbc.M115.679043
82. Götzl JK, Brendel M, Werner G, Parhizkar S, Sebastian Monasor L, Kleinberger G, et al. Opposite microglial activation stages upon loss of PGRN or TREM 2 result in reduced cerebral glucose metabolism. *EMBO Mol Med* (2019) 11(6):e9711. doi: 10.1523/JNEUROSCI.2070-18.2019
83. Kleinberger G, Brendel M, Mracsko E, Wefers B, Groeneweg L, Xiang X, et al. The FTD-like syndrome causing TREM 2 T66M mutation impairs microglia function, brain perfusion, and glucose metabolism. *EMBO J* (2017) 36(13):1837–53. doi: 10.15252/embj.201796516
84. Nugent AA, Lin K, Van Lengerich B, Lianoglou S, Przybyla L, Davis SS, et al. TREM2 regulates microglial cholesterol metabolism upon chronic phagocytic challenge. *Neuron* (2020) 105(5):837–54.e9. doi: 10.1016/j.neuron.2019.12.007
85. Monasor LS, Müller SA, Colombo AV, Tanrioever G, König J, Roth S, et al. Fibrillar Aβ triggers microglial proteome alterations and dysfunction in Alzheimer mouse models. *Elife* (2020) 9:e54083. doi: 10.7554/eLife.54083
86. Mela V, Mota BC, Milner M, McGinley A, Mills KH, Kelly ÁM, et al. Exercise-induced re-programming of age-related metabolic changes in microglia is accompanied by a reduction in senescent cells. *Brain Behav Immun* (2020) 87:413–28. doi: 10.1016/j.bbi.2020.01.012
87. Olah M, Patrick E, Villani AC, Xu J, White CC, Ryan KJ, et al. A transcriptomic atlas of aged human microglia. *Nat Commun* (2018) 9 (1):539. doi: 10.1038/s41467-018-02926-5
88. Bosch M, Sánchez-Álvarez M, Fajardo A, Kapetanovic R, Steiner B, Dutra F, et al. Mammalian lipid droplets are innate immune hubs integrating cell metabolism and host defense. *Science* (2020) 370(6514):1–12. doi: 10.1126/science.aay8085
89. Brusco J, Haas K. Interactions between mitochondria and the transcription factor myocyte enhancer factor 2 (MEF2) regulate neuronal structural and functional plasticity and metaplasticity. *J Physiol* (2015) 593(16):3471–81. doi: 10.1113/jphysiol.2014.282459
90. Geng J, Sun X, Wang P, Zhang S, Wang X, Wu H, et al. Kinases Mst1 and Mst2 positively regulate phagocytic induction of reactive oxygen species and bactericidal activity. *Nat Immunol* (2015) 16(11):1142–52. doi: 10.1038/ni.3268
91. Feingold KR, Shigenaga JK, Kazemi MR, McDonald CM, Patzek SM, Cross AS, et al. Mechanisms of triglyceride accumulation in activated macrophages. *J Leukoc Biol* (2012) 92(4):829–39. doi: 10.1189/jlb.1111537
92. Freemerman AJ, Johnson AR, Sacks GN, Milner JJ, Kirk EL, Troester MA, et al. Metabolic reprogramming of macrophages: glucose transporter 1 (GLUT1)-mediated glucose metabolism drives a proinflammatory phenotype. *J Biol Chem* (2014) 289(11):7884–96. doi: 10.1074/jbc.M113.522037
93. Michl J, Ohlbaum DJ, Silverstein SC. 2-Deoxyglucose selectively inhibits Fc and complement receptor-mediated phagocytosis in mouse peritoneal macrophages II. Dissociation of the inhibitory effects of 2-deoxyglucose on phagocytosis and ATP generation. *J Exp Med* (1976) 144(6):1484–93. doi: 10.1084/jem.144.6.1484
94. Pavlou S, Wang L, Xu H, Chen M. Higher phagocytic activity of thioglycollate-elicited peritoneal macrophages is related to metabolic status of the cells. *J Inflamm* (2017) 14(1):4. doi: 10.1186/s12950-017-0151-x
95. Koo SJ, Szczesny B, Wan X, Putluri N, Garg NJ. Pentose Phosphate Shunt Modulates Reactive Oxygen Species and Nitric Oxide Production Controlling Trypanosoma cruzi in Macrophages. *Front Immunol* (2018) 9:202. doi: 10.3389/fimmu.2018.00202
96. Pan RY, Ma J, Kong XX, Wang XF, Li SS, Qi XL, et al. Sodium rutin ameliorates Alzheimer's disease-like pathology by enhancing microglial amyloid-beta clearance. *Sci Adv* (2019) 5(2):eaau6328. doi: 10.1126/sciadv.aau6328
97. Rubio-Araiz A, Finucane OM, Keogh S, Lynch MA. Anti-TLR2 antibody triggers oxidative phosphorylation in microglia and increases phagocytosis of beta-amyloid. *J Neuroinflamm* (2018) 15(1):247. doi: 10.1186/s12974-018-1281-7
98. Fang EF, Hou Y, Palikaras K, Adriaanse BA, Kerr JS, Yang B, et al. Mitophagy inhibits amyloid-beta and tau pathology and reverses cognitive deficits in models of Alzheimer's disease. *Nat Neurosci* (2019) 22(3):401–12. doi: 10.1038/s41593-018-0332-9
99. Ma Y, Bao J, Zhao X, Shen H, Lv J, Ma S, et al. Activated cyclin-dependent kinase 5 promotes microglial phagocytosis of fibrillar beta-amyloid by up-regulating lipoprotein lipase expression. *Mol Cell Proteomics* (2013) 12 (10):2833–44. doi: 10.1074/mcp.M112.026864
100. Gibson MS, Domingues N, Vieira OV. Lipid and Non-lipid Factors Affecting Macrophage Dysfunction and Inflammation in Atherosclerosis. *Front Physiol* (2018) 9:654. doi: 10.3389/fphys.2018.00654
101. Prince M, Wimo AGM, Ali GC, Wu YT, Prina M. World Alzheimer Report 2015: the global impact of dementia: an analysis of prevalence, incidence, cost and trends. London: Alzheimer's Disease International (2015). p. 1–87. https://www.alzint.org/u/WorldAlzheimerReport2015.pdf.
102. Broom GM, Shaw IC, Rucklidge JJ. The ketogenic diet as a potential treatment and prevention strategy for Alzheimer's disease. *Nutrition* (2019) 60:118–21. doi: 10.1016/j.nut.2018.10.003
103. Henderson ST, Vogel JL, Barr LJ, Garvin F, Jones JJ, Costantini LC. Study of the ketogenic agent AC-1202 in mild to moderate Alzheimer's disease: a randomized, double-blind, placebo-controlled, multicenter trial. *Nutr Metab (Lond)* (2009) 6:31. doi: 10.1186/1743-7075-6-31
104. Kashiwaya Y, Bergman C, Lee JH, Wan R, King MT, Mughal MR, et al. A ketone ester diet exhibits anxiolytic and cognition-sparing properties, and lessens amyloid and tau pathologies in a mouse model of Alzheimer's disease. *Neurobiol Aging* (2013) 34(6):1530–9. doi: 10.1016/j.neurobiolaging.2012.11.023
105. Ota M, Matsuo J, Ishida I, Takano H, Yokoi Y, Hori H, et al. Effects of a medium-chain triglyceride-based ketogenic formula on cognitive function in patients with mild-to-moderate Alzheimer's disease. *Neurosci Lett* (2019) 690:232–6. doi: 10.1016/j.neulet.2018.10.048
106. Taylor MK, Sullivan DK, Mahnken JD, Burns JM, Swerdlow RH. Feasibility and efficacy data from a ketogenic diet intervention in Alzheimer's disease. *Alzheimers Dement (N Y)* (2018) 4:28–36. doi: 10.1016/j.trci.2017.11.002
107. Yang X, Cheng B. Neuroprotective and anti-inflammatory activities of ketogenic diet on MPTP-induced neurotoxicity. *J Mol Neurosci* (2010) 42 (2):145–53. doi: 10.1007/s12031-010-9336-y
108. Huang C, Wang P, Xu X, Zhang Y, Gong Y, Hu W, et al. The ketone body metabolite beta-hydroxybutyrate induces an antidepression-associated

ramification of microglia via HDACs inhibition-triggered Akt-small RhoGTPase activation. *Glia* (2018) 66(2):256–78. doi: 10.1002/glia.23241
109. Dupuis N, Curatolo N, Benoist JF, Auvin S. Ketogenic diet exhibits anti-inflammatory properties. *Epilepsia* (2015) 56(7):e95–8. doi: 10.1111/epi.13038
110. Youm YH, Nguyen KY, Grant RW, Goldberg EL, Bodogai M, Kim D, et al. The ketone metabolite beta-hydroxybutyrate blocks NLRP3 inflammasome-mediated inflammatory disease. *Nat Med* (2015) 21(3):263–9. doi: 10.1038/nm.3804
111. Yao J, Chen S, Mao Z, Cadenas E, Brinton RD. 2-Deoxy-D-glucose treatment induces ketogenesis, sustains mitochondrial function, and reduces pathology in female mouse model of Alzheimer's disease. *PLoS One* (2011) 6(7):e21788. doi: 10.1371/journal.pone.0021788
112. Forstermann U, Kleinert H. Nitric oxide synthase: expression and expressional control of the three isoforms. *Naunyn Schmiedebergs Arch Pharmacol* (1995) 352(4):351–64. doi: 10.1007/BF00172772
113. Fodelianaki G, Lansing F, Bhattarai P, Troullinaki M, Zeballos MA, Charalampopoulos I, et al. Nerve Growth Factor modulates LPS - induced microglial glycolysis and inflammatory responses. *Exp Cell Res* (2019) 377(1-2):10–6. doi: 10.1016/j.yexcr.2019.02.023
114. Birch AM, Kelly ÁM. Lifelong environmental enrichment in the absence of exercise protects the brain from age-related cognitive decline. *Neuropharmacology* (2019) 145:59–74. doi: 10.1016/j.neuropharm.2018.03.042
115. Svensson M, Andersson E, Manouchehrian O, Yang Y, Deierborg T. Voluntary running does not reduce neuroinflammation or improve non-cognitive behavior in the 5xFAD mouse model of Alzheimer's disease. *Sci Rep* (2020) 10(1):1–10. doi: 10.1038/s41598-020-58309-8
116. Tapia-Rojas C, Aranguiz F, Varela-Nallar L, Inestrosa NC. Voluntary Running Attenuates Memory Loss, Decreases Neuropathological Changes and Induces Neurogenesis in a Mouse Model of A lzheimer's Disease. *Brain Pathol* (2016) 26(1):62–74. doi: 10.1111/bpa.12255
117. Xu ZQ, Zhang LQ, Wang Q, Marshall C, Xiao N, Gao JY, et al. Aerobic Exercise Combined with Antioxidative Treatment does not Counteract Moderate-or Mid-Stage A lzheimer-Like Pathophysiology of APP/PS 1 Mice. *CNS Neurosci Ther* (2013) 19(10):795–803. doi: 10.1111/cns.12139
118. Zhang J, Guo Y, Wang Y, Song L, Zhang R, Du Y. Long-term treadmill exercise attenuates Aβ burdens and astrocyte activation in APP/PS1 mouse model of Alzheimer's disease. *Neurosci Lett* (2018) 666:70–7. doi: 10.1016/j.neulet.2017.12.025
119. Gibbons T. *Enhancing learning and memory in the aged: Interactions between dietary supplementation and exercise*. Urbana: University of Illinois (2014). http://hdl.handle.net/2142/49842Ñ20.
120. Speisman RB. *Identifying inflammatory biomarkers of cognitive aging through relationships between measures of inflammation, neurogenesis and cognition in aged rats*. Florida: University of Florida (2013). https://ufdc.ufl.edu/UFE0045275/00001
121. Caslin HL, Taruselli MT, Haque T, Pondicherry N, Baldwin EA, Barnstein BO, et al. Inhibiting Glycolysis and ATP Production Attenuates IL-33-Mediated Mast Cell Function and Peritonitis. *Front Immunol* (2018) 9:3026. doi: 10.3389/fimmu.2018.03026
122. Poulain L, Sujobert P, Zylbersztejn F, Barreau S, Stuani L, Lambert M, et al. High mTORC1 activity drives glycolysis addiction and sensitivity to G6PD inhibition in acute myeloid leukemia cells. *Leukemia* (2017) 31(11):2326–35. doi: 10.1038/leu.2017.81
123. Kelly B, Tannahill GM, Murphy MP, O'Neill LA. Metformin Inhibits the Production of Reactive Oxygen Species from NADH:Ubiquinone Oxidoreductase to Limit Induction of Interleukin-1beta (IL-1beta) and Boosts Interleukin-10 (IL-10) in Lipopolysaccharide (LPS)-activated Macrophages. *J Biol Chem* (2015) 290(33):20348–59. doi: 10.1074/jbc.M115.662114
124. Ou Z, Kong X, Sun X, He X, Zhang L, Gong Z, et al. Metformin treatment prevents amyloid plaque deposition and memory impairment in APP/PS1 mice. *Brain Behav Immun* (2018) 69:351–63. doi: 10.1016/j.bbi.2017.12.009
125. Peng Q, Malhotra S, Torchia JA, Kerr WG, Coggeshall KM, Humphrey MB. TREM2- and DAP12-dependent activation of PI3K requires DAP10 and is inhibited by SHIP1. *Sci Signal* (2010) 3(122):ra38. doi: 10.1126/scisignal.2000500
126. Pedicone C, Fernandes S, Dungan OM, Dormann SM, Viernes DR, Adhikari AA, et al. Pan-SHIP1/2 inhibitors promote microglia effector functions essential for CNS homeostasis. *J Cell Sci* (2020) 133(5):1–12. doi: 10.1242/jcs.238030
127. Cosenza-Nashat M, Zhao ML, Suh HS, Morgan J, Natividad R, Morgello S, et al. Expression of the translocator protein of 18 kDa by microglia, macrophages and astrocytes based on immunohistochemical localization in abnormal human brain. *Neuropathol Appl Neurobiol* (2009) 35(3):306–28. doi: 10.1111/j.1365-2990.2008.01006.x
128. Gulyás B, Makkai B, Nagy K, Vas Á, Kása P, Andersson J, et al. In vitro evidence for competitive tspo binding of the imaging biomarker candidates vinpocetine and two iodinated daa1106 analogues in post mortem autoradiography experiments on whole hemisphere human brain slices. *Curr Radiopharm* (2009) 2(1):42–8. doi: 10.2174/1874471010902010042
129. Gong J, Szego ÉM, Leonov A, Benito E, Becker S, Fischer A, et al. Translocator protein ligand protects against neurodegeneration in the MPTP mouse model of Parkinsonism. *J Neurosci* (2019) 39(19):3752–69. doi: 10.1523/JNEUROSCI.2070-18.2019
130. Leva G, Klein C, Benyounes J, Hallé F, Bihel F, Collongues N, et al. The translocator protein ligand XBD173 improves clinical symptoms and neuropathological markers in the SJL/J mouse model of multiple sclerosis. *Biochim Biophys Acta (BBA)-Mol Basis Dis* (2017) 1863(12):3016–27. doi: 10.1016/j.bbadis.2017.09.007
131. Barron AM, Garcia-Segura LM, Caruso D, Jayaraman A, Lee JW, Melcangi RC, et al. Ligand for translocator protein reverses pathology in a mouse model of Alzheimer's disease. *J Neurosci* (2013) 33(20):8891–7. doi: 10.1523/JNEUROSCI.1350-13.2013
132. Yao R, Pan R, Shang C, Li X, Cheng J, Xu J, et al. Translocator Protein 18 kDa (TSPO) Deficiency Inhibits Microglial Activation and Impairs Mitochondrial Function. *Front Pharmacol* (2020) 11:986. doi: 10.3389/fphar.2020.00986
133. Tu LN, Zhao AH, Hussein M, Stocco DM, Selvaraj V. Translocator Protein (TSPO) Affects Mitochondrial Fatty Acid Oxidation in Steroidogenic Cells. *Endocrinology* (2016) 157(3):1110–21. doi: 10.1210/en.2015-1795
134. Zeineh N, Denora N, Laquintana V, Franco M, Weizman A, Gavish M. Efficaciousness of Low Affinity Compared to High Affinity TSPO Ligands in the Inhibition of Hypoxic Mitochondrial Cellular Damage Induced by Cobalt Chloride in Human Lung H1299 Cells. *Biomedicines* (2020) 8(5):1–18. doi: 10.3390/biomedicines8050106

Conflict of Interest: The authors declare that the research was conducted in the absence of any commercial or financial relationships that could be construed as a potential conflict of interest.

frontiers in Immunology

REVIEW
published: 16 March 2021
doi: 10.3389/fimmu.2021.624919

Unraveling the Link Between Mitochondrial Dynamics and Neuroinflammation

Lilian Gomes de Oliveira[1,2†], *Yan de Souza Angelo*[1,2†], *Antonio H. Iglesias*[3] *and Jean Pierre Schatzmann Peron*[1,2,3*]

[1] Neuroimmune Interactions Laboratory, Immunology Department – Institute of Biomedical Sciences (ICB) IV, University of São Paulo (USP), São Paulo, Brazil, [2] Neuroimmunology of Arboviruses Laboratory, Scientific Platform Pasteur-USP, University of São Paulo (USP), São Paulo, Brazil, [3] Loyola University Medical Center, Stritch School of Medicine, Loyola University Chicago, Chicago, IL, United States

OPEN ACCESS

Edited by:
Christophe Chevillard, INSERM U1090 Technologies Avancées pour le Génome et la Clinique, France

Reviewed by:
Paola Italiani, National Research Council (CNR), Italy
Eva Bartok, University Hospital Bonn, Germany

***Correspondence:**
Jean Pierre Schatzmann Peron
jeanpierre@usp.br

[†]These authors have contributed equally to this work

Specialty section:
This article was submitted to Molecular Innate Immunity, a section of the journal Frontiers in Immunology

Received: 01 November 2020
Accepted: 25 February 2021
Published: 16 March 2021

Citation:
de Oliveira LG, Angelo YdS, Iglesias AH and Peron JPS (2021) Unraveling the Link Between Mitochondrial Dynamics and Neuroinflammation. Front. Immunol. 12:624919. doi: 10.3389/fimmu.2021.624919

Neuroinflammatory and neurodegenerative diseases are a major public health problem worldwide, especially with the increase of life-expectancy observed during the last decades. For many of these diseases, we still lack a full understanding of their etiology and pathophysiology. Nonetheless their association with mitochondrial dysfunction highlights this organelle as an important player during CNS homeostasis and disease. Markers of Parkinson (PD) and Alzheimer (AD) diseases are able to induce innate immune pathways induced by alterations in mitochondrial Ca^{2+} homeostasis leading to neuroinflammation. Additionally, exacerbated type I IFN responses triggered by mitochondrial DNA (mtDNA), failures in mitophagy, ER-mitochondria communication and mtROS production promote neurodegeneration. On the other hand, regulation of mitochondrial dynamics is essential for CNS health maintenance and leading to the induction of IL-10 and reduction of TNF-α secretion, increased cell viability and diminished cell injury in addition to reduced oxidative stress. Thus, although previously solely seen as power suppliers to organelles and molecular processes, it is now well established that mitochondria have many other important roles, including during immune responses. Here, we discuss the importance of these mitochondrial dynamics during neuroinflammation, and how they correlate either with the amelioration or worsening of CNS disease.

Keywords: mitochondria, neuroinflammation, neurodegenerative diseases, Alzheimer disease, Parkinson disease, multiple sclerosis

INTRODUCTION

The central nervous system (CNS) depends on a complex and intricate network of molecular and cellular interactions to maintain appropriate function and homeostasis. This well-organized network when disturbed, leads to resident cells activation, inflammatory leukocyte infiltration, and further tissue damage. During recovery, counterregulatory mechanisms take place, and the activated cells return to the homeostatic state. However, in the absence of these finely tuned

regulatory loops, the coordination is broken and chronic neurodegenerative and neuroinflammatory diseases may occur.

Neurodegenerative diseases represent a heterogeneous group of diseases of major public health concern. The World Health Organization (WHO) have estimated that until 2030, deaths attributed to neurological diseases will increased up to 12.22% (1). Due to their overly complex pathophysiology, interdisciplinary approaches and breakthrough science are highly needed to unravel disease mechanisms, and thus developing effective new therapies. In fact, with the extension of our life expectancy and the dramatic change in the age pyramid during the last decades, these studies are mandatory either to avoid or delay their impact on society and economy.

A common feature of neurodegenerative and neuroinflammatory diseases is the activation of CNS resident cells (2–4). Microglia and astrocytes may actively start, promote, or dampen neuroinflammation (5–8). The reason is because many immune-related receptors and molecules are extensively produced by these cells, not only during disease but also during physiological processes (3, 9). Conversely, these mechanisms demand high energy consumption, promoting important metabolic changes in the cell. In this context, the importance of mitochondria and mitochondria-related pathways is unquestionable.

More than just *power houses* of the cells (10), the role of mitochondria have been remarkably appreciated and revisited. Recent research has revealed important correlation of mitochondrial dynamics and the pathophysiology of brain diseases, as Alzheimer's. Disease (AD), Parkinson's Disease (PD) and Multiple Sclerosis (MS) (11–13). Disturbances in mitochondrial dynamics may influence many cellular and molecular pathways, as calcium-dependent immune activation, transcription factors phosphorylation, cytokine secretion, organelle transference and even cell death. Moreover, dysfunctional dynamics may also affect the release of mitochondrial damage-associated molecular patterns (mDAMPs), triggering innate immune responses in both resident and infiltrating cells (14). The release of mDAMPs leads to NOD-like receptors (NLRs), Toll-like receptors (TLRs) and cGAS-STING activation, promoting inflammatory cytokine, chemokines, and reactive oxygen species production, impacting disease outcome. However, although much has been learned regarding mitochondrial function during health and disease, mitochondrial dynamics during neuroinflammation and neurodegenerative disorders remains to be fully elucidated. Here, we aimed to summarize recent knowledge in the field, correlating dysfunctional mitochondrial dynamics with the worsening of CNS diseases.

MITOCHONDRIAL DYNAMICS AND NEUROINFLAMMATION

Mitochondrial dynamics is a process by which this organelle changes size, location, shape, and function inside the cell (15). Mitochondrial fusion and fission greatly correlate with metabolic changes, depending on the stimuli and energy demand, as it regulates cellular functions during health as well as during disease. There is now a better understanding of the changes that occur during mitochondrial dynamics changes and its relationship with CNS resident cells.

Mitochondrial Location and Mitochondria-ER Communication

Mitochondria location within the cell is mostly regulated by the outer mitochondrial membrane (OMM), anchoring it to the cytoskeleton's microtubules motor proteins, kinesin and dynein (16). For instance, mitochondria's position in astrocytes influences Ca^{2+} levels, directly affecting astrocyte survival and communication with nearby neurons (17). Intracellular calcium level is dictated by the transferring between mitochondrial reticulum (mitRet) and endoplasmic reticulum (ER). Remarkably, several neurodegenerative diseases correlate with detrimental calcium homeostasis, evidenced by the disruption of mitRet and ER communication, as observed in Amyotrophic Lateral Sclerosis (ALS), a severe condition characterized by progressive weakness, muscle wasting and paralysis. Impaired electron transportation chain (ETC) and reduced glutamate uptake were already described in ALS. This greatly increases Ca^{2+} permeable activation of AMPA receptors, leading to excitotoxicity (16).

Mitochondria-ER associated membranes (MAMs) consist of around 1500 active proteins. Regardless of their fundamental importance for cellular metabolism and Ca^{2+} homeostasis, the molecular mechanisms that underly the recruitment and tethering of ER-mitochondria are not fully understood, and extensively debated. It has been proposed that MAMs tethering is dependent on the interaction between mitofusin 2 (MFN2) in the ER, and MFN1 and MFN2 in the OMM (16). Supporting this, ablation of MFN2 loosens ER–mitochondria interaction strongly impairing mitochondrial Ca^{2+} uptake (18). However, the role of MFN2 is not a consensus in the literature and some studies consider MFN2 a tethering antagonist that suppresses the excessive binding between the organelles, preventing toxic Ca^{2+} transfer within mit-Ret and ER (19, 20).

Tyrosine phosphatase-interacting protein 51 (PTPIP51), and the integral ER protein vesicle-associated membrane protein-associated protein B (VAPB) are also listed as tethering molecules for MAMs formation. Interestingly, during ALS, fronto-temporal dementia (FTD) and PD, disruption in the PTPIP51-VAPB interaction also induces dysregulated Ca^{2+} homeostasis and decreased ATP production (21, 22). Strikingly, it was orchestrated by fused in sarcoma (FUS) protein, and not by directly altering PTPIP51- VAPB expression, but by activating glycogen synthase kinase 3-beta (GSK-3b), evidencing a correlation between this molecule and ALS.

Additionally, the communication between mitochondrial voltage-dependent anion channel (VDAC) and inositol 1,4,5-trisphosphate receptor (IP3R) within the ER membrane *via* GRP75 was suggested as a bond of MAMs (23, 24). Curiously, the PD associated protein, DJ1, is necessary for mitochondrial Ca^{2+} uptake and was related with VDAC-IP3R-GRP75 complex

in the maintenance of MAMS (25). Noteworthy the fact that mitochondrial Ca^{2+} uptake occurs in response to ER IP3R activation (19) and that fluctuations in channel activity does not affect the binding of MAM (26). Moreover, it is important to mention that IP3R activation is an important signaling pathway for immune response (27), as observed for nuclear factor of activated T cells (NFAT) (28).

NFAT activation typically leads to the transcription of inflammatory mediators that are upregulated during some neurodegenerative diseases. For instance, amyloid beta (Aβ) protein uptake by microglia induces dysregulated NFAT expression, increasing TNF-α secretion and neuronal death *in vitro* (29). Interestingly, Aβ and α-synuclein deposition, hallmarks of AD and PD, can both trigger inflammatory responses *via* TLR-2 and TLR-4, respectively (30–32). Conversely, Ma et al. (33) demonstrated that the crosstalk between TLR-4 and NFAT1 signaling into the mitochondria is a TRIF-dependent phenomenon, culminating in pro-inflammatory cytokine and ROS production, mitochondrial morphological changes and finally, prolonged microglia activation (33).

Corroborating the proinflammatory statement, it was demonstrated that cytokine activation of primary astrocytes and microglia upregulate intracellular Ca^{2+} mobilization and NFAT activation. NFAT upregulated genes are associated with a neurotoxic phenotype of astrocytes, known as A1 astrocytes. In A1 astrocytes ($C3^{+}GBP2^{+}$), NFAT is positively regulated by IL-1β and, in a positive feedback loop, IL-1β expression is NFAT and L-type Ca^{2+} channel dependent (34). Thus, bidirectional interactions between ER and mitochondrial Ca^{2+} levels, NFAT activation and upregulated inflammatory mediators, sustain a positive feedback loop that correlate with the chronicity of the neuroinflammatory microenvironment.

Mitochondrial Dynamics and Programmed Cell Death

Besides location and interaction with other organelles within the cell, mitochondrial fusion and fission is a crucial process for regulating cell death. Fusion is coordinated by a family of GTPase proteins with tethering activity. This family of proteins is localized on the outer mitochondria membrane (OMM), highlighting MFN1 and MFN2, and in the inner mitochondria membrane (IMM), optic atrophy 1 (OPA1) (35). The steps that orchestrate mitochondrial elongation are not fully understood, but a model suggests that the interaction of MFNs from two opposing mitochondrion is stabilized by coil-coil heptad repeat-2 (HR2) (36), increasing the surface of contact (37). Following this, at the interaction site, guanosine triphosphate (GTP) is hydrolyzed culminating in conformational changes in the MFNs and thus, OMMs fusion. Different isoforms of OPA-1 such as long membrane-bound OPA1 (L-OPA1) and short soluble OPA-1(S-OPA1), generated by proteolytic cleavage of L-OPA1, are associated with fusion and fission balance (38). Complete fusion occurs when cardiolipin (CL) interacts with L-OPA1 resulting in IMM unification following OPA1-dependent GTP hydrolysis (39). Mitochondria elongation is associated with efficient metabolism and maintenance of ATP production even during nutrient deprivation, thus increasing cellular viability (40).

On the opposite, mitochondrial fission is initiated following the assembly of a pre-constriction site, directing the dynamin related protein 1 (DRP1) binding site of the OMM. One of the proteins that compose the pre-constriction site is fission protein 1 (FIS1), that also inhibits fusion by preventing GTP hydrolysis of OPA1 and MFN1/2 (41). The constriction site is not randomly located, instead is pinpointed on ER-mitochondria interaction site (42). ER tubules induce actin polymerization at the narrowing site, whereas myosin mediates actin contraction and mechanical pressure to ensure pre-constriction. Then, DRP1 is recruited forming a ring-like oligomer which following the GTP hydrolysis squeezes the pre-existing constriction site. Lastly, dynamin 2 is recruited to DRP1-compression site for mitochondrial fragmentation (43). The processes that coordinate the OMM fission are better known that the ones related to IMM. So far, it was shown that prior to DRP1 recruitment, Ca^{2+} promotes constriction in the IMM by favoring proteolytic cleavage of OPA-1 (44). Strikingly, the pre-constriction site is also spatially linked and critical to maintain mtDNA replication in the matrix (42). Fragmented mitochondria tend to present increased stress oxidation, membrane depolarization and impaired ATP production (45).

OPA1 and MFN2 genes are essentially related to the formation of healthy mitochondrial networks. Mechanistically, total or partial loss of function of OPA1 results in fragmented mitochondria, leading to a loss of mitochondria membrane potential ($\Delta\Psi m$) and thus initiating autophagic and apoptotic pathways (46, 47). Importantly, in the CNS, these alterations may lead to massive neuronal and glial cell death, as seen in optic atrophy-1 and Charcot-Marie-Tooth disease and hereditary peripheral neuropathy (46, 47). Only recently, studies have described the role of mitochondrial fusion and fission in programmed cell death due to DRP1 and MFN2 interaction with BAX and BAK, respectively. As a result of exposure to toxic levels of nitric oxide (NO), BAX interacts with DRP1 in neurons inducing mitochondria fragmentation. In this context, inhibition of DRP1 impairs BAX deposition and pore formation, improving neuronal survival (48, 49).

The degradation of damaged organelles and cytosolic components usually results in autophagy, leading to the delivery of damaged cellular components to autophagosomes for degradation (50, 51). Mitochondria specialized autophagy, named mitophagy, is triggered by OPA-1, DRP1 and MFN2. These proteins, besides their regulatory role in mitochondria dynamics, are also responsible for autophagosome formation (50, 51). Mitophagy initiation is also dependent on PTEN–induced putative kinase 1 (PINK1) and E3-ubiquitin ligase protein (Parkin). These proteins accumulate in the OMM and ubiquitinate mitochondria target proteins (52, 53). As OMM has plenty of PINK1 and MFN2, Parkin is recruited from the cytoplasm and phosphorylated, hence exerting its ubiquitin activity (54). Consequently, DRP1, NF-κB essential modulator (NEMO) and mitochondrial Rho GTPase protein 1 (MIRO1) are targeted for proteasomal degradation (55, 56). Mitophagy is consolidated when MIRO1 is degraded by the proteasome and

mitochondria is detached from its anchoring microtubules (57). Lastly, mitochondria is sequestrated in a double membrane vesicle that fuses with autolysosomes that further "digests" the organelle (58). Importantly, the correlation between Parkin and PINK1 mutations to autosomal-recessive cases of PD is widely known (59). In this context, the unbalance between damaged mitochondria and its removal, importantly contributes for PD progress. This unbalanced mitochondrial dynamic correlates with impaired clearance of dysfunctional organelles through Parkin and PINK1 pathway, resulting in deleterious accumulation. The benefits of mitophagy, however, goes beyond the removal of damaged mitochondria (59). Ip et al. (60) demonstrated that PINK1 is essential for microglial secretion of IL-10 and reduction of TNF-α secretion. Remarkably, elevated IL-10 secretion correlated with mitophagy induction in macrophages *via* mTORC1 inhibition and consequently decreasing inflammation (60). Using a mouse microglial cell line, it was shown that mitophagy increases ΔΨm and diminishes TNF-α induced apoptosis by hampering the increase in pro-apoptotic proteins (61). Furthermore, the role of mitophagy during neurodegenerative diseases overcome the regulation of immune responses. In a mouse model of AD, microglial cells under mitophagy have elevated levels of intracellular Aβ aggregates, suggesting increased phagocytic activity, and thus clearing the harmful Aβ deposits (62).

Autophagy may be beneficial to rebuild healthy mitochondrial dynamics after pro-inflammatory responses. Following mitochondrial fragmentation, autophagy is triggered due to dysregulated respiratory chain and ROS production. Such mitochondria alterations are promoted by IFN-γ and LPS upregulation of DRP1 and LC3, an autophagy-related protein. For instance, this mechanism is essential to restore tubular mitochondrial networks after inflammatory stimulation in astrocytes, as shown in a mouse model of cortical lesion. Interestingly, astrocytes located in the core or penumbra exhibited different mitochondrial patterns, with core mitochondria prominently fragmented, as opposed to those in the penumbra (63). This evidences the importance of the neuroinflammatory microenvironment in orchestrating mitochondrial shape and size.

Astrocyte-to-Neurons Mitochondria Exchange

Many factors released from astrocytes provide neurotrophic and metabolic support for nearby neurons. These range from DNA, microRNAs, glucose-related molecules, cytokines and even organelles, such as the mitochondria (64, 65). Despite not completely understood, several reports have already demonstrated the importance of damaged and healthy mitochondria transference in between cells for neuronal metabolism and survival. During brain injury, astrocytes may release damaged mitochondria to minimize the amount of detrimental ROS and dysregulated Ca^{2+} balance (66). Conversely, healthy mitochondria may also be donated from astrocytes to damaged neighboring neurons, increasing its viability (67). Moreover, Davis et al. (68), firstly demonstrated that the exchange of mitochondria among neurons and astrocytes seem to work in a bidirectional way (68).

The release of mitochondria by astrocytes is a CD38/Ca^{2+} dependent phenomenon (69). It upregulates survival pathways in neurons after stroke, indicating a neuroprotective role for the glia-to-neuron mitochondria communication. Also, mitochondria acquired from astrocytes have a crucial role in maintaining neuronal energy production under glucose-oxygen starvation.

Joshi et al. (70) showed that previous mitochondria fragmentation is an essential step for organelle release to the extracellular space (70). They observed that inhibition of DRP1 diminishes astrocytic and microglial activation and ameliorates pro-inflammatory phenotype in mice models of AD, ALS and Huntington's disease (HD). Interestingly, this phenotype was dependent on the release of damaged mitochondria by microglia cells, triggering neuronal death in consequence of A1-inflammatory-astrocyte activation (70).

MITOCHONDRIAL DAMPS AND NEURODEGENERATION

Since Polly Matzinger's "danger theory" (71), the introduction of damage-associated molecular patterns (DAMPs) has greatly broadened our understanding of how the immune system works during tissue damage and repair (71). The idea of recognizing "danger" and "alarm" signals produced by cells, as DNA, ATP and HSPs (heat-shock proteins) (72), during inflammatory events, completely changed the view of inflammatory processes. Naturally, many advances in the biology of danger signals, along with the discovery of stress-associated molecules acting as DAMPs were achieved (71, 73). Accordingly, one important source of DAMPs that has gained increased attention is the *mitochondria*.

Examples of mDAMPs receptors are the classical PRRs (pattern recognition receptors), such as the TLRs, NLR (NOD-like receptors), as well as STING (stimulator of interferon-genes) and RAGE (receptor for advanced glycation products) (74). It is important to note that the signaling of these receptors, ultimately lead to inflammatory responses that may promote an auspicious environment for neurodegeneration. Moreover, the activation of TLR-7/9 and STING induces a IFN-I response (75) which has been recently demonstrated by microglial single-cell analysis in mice that, during aging, three clusters of interferon-responsive microglia appear, and that they correlate with subsequent CNS disease (76). Although the role for mitochondrial dynamics in this phenomenon is still to be addressed, the existence of mDAMP-IFN pathways denotes a possible correlation, as reviewed (74).

Cardiolipin is a phospholipid located at the IMM providing the structure for the electron transportation chain (ETC), binding to Complex IV and maintaining other ETC complexes and mitochondrial content in place and sharply functional (77). Cardiolipin molecules are particularly sensitive to oxidative damage created by unbalanced mitochondrial functioning and/

or ROS produced by activated microglia. Interestingly, a highly oxidative environment causes loss of Δψm and promotes the repositioning of cardiolipin molecules to the OMM (77). Then, it can be sensed by cytosolic immune receptors, as NLRP3, initiating inflammasome activation, inflammatory cytokine secretion and dysregulation of mitochondrial dynamics (78). Other effects include loss of functional ETC and release of intrinsic apoptotic molecules located between the IMM and OMM, such as cytochrome C and SMAC/Diablo (79, 80). The release of Mitochondrial Transcription Factor A (MTFA) can also initiate inflammatory processes when released extracellularly. This is because MTFA shares high homology with High Mobility Group Box (HMGB), an important DAMP, and thus proinflammatory (65). Interestingly, a subset of Gamma-delta T cells (Tγδ) increased in Multiple Sclerosis (MS) patients has been shown to be activated by cardiolipin. Although their exact role is still not clear, it suggests an important role for cardiolipin also activating adaptive immune responses during CNS disease progression (81).

Mitochondrial DNA is the most studied mDAMP, and it has a high correlation with many pathological processes. Among their distinct characteristics, mtDNA codes only 13 proteins, including mitochondrial ribosomal subunits and ETC components, essential for proper mitochondrial function (82, 83). Failures in mitochondrial dynamics often result in the accumulation of mutated mtDNA, as they lack a robust repair mechanism (83, 84). This affects the cellular capacity in producing energy and also set in motion inflammatory processes (83, 84). mtDNA is not packed and has motifs usually perceived as harmful by innate immunity receptors. During mild stressful situations when apoptotic caspases are not mobilized, loss of mitochondrial membrane action potential (Δψm) for example, facilitates both OMM and IMM permeabilization and the induction of BAX/BAK pores, enabling mtDNA release to the cytosol. Then, it can be sensed by the cyclic GMP-AMP synthase (cGAS) receptor, activating its adaptor protein STING (stimulator of interferon genes) (85). Interestingly, this mtDNA-dependent Type I interferon (IFN-I) induction is beneficial in the context of viral infection because it primes the cell into an antiviral state (86). Still, the same issue occurs when mtDNA is present extracellularly, as internalized mtDNA signals through endosomal TLR-9, resulting in NF-κB and IRFs activation, and further interferon transcription (87, 88).

Another important mDAMP are mtROS produced at high levels by the mitochondria (89). Mitochondrial ROS (mtROS) are mainly byproducts of the mitochondrial ETC. During respiration, O_2 that does not get reduced into H_2O forms the O_2^- radical specially by the activity of ETC complexes I and III, which can be later converted in H_2O_2 mainly by enzymes that are present in the organelle (90, 91). Other mitochondrial and cellular events can also enhance the production of mtROS, such as a decreased ΔΨm, inhibition of the ETC, mitochondrial Ca^{2+} influx, oxygen concentration and even mitochondrial morphology (90, 92). These molecules can act both as signaling (93) or as damaging molecules, causing mtDNA mutations, oxidation in fatty acids and amino acid residues, leading to deleterious disruption of the cellular redox signaling (94–96). Specially in the brain, the damage caused by ROS are linked to protein aggregation (93, 97).

In summary, although the mitochondria represent a vital organelle, providing energy and regulating metabolic processes of the cell, it also represents a "time-bomb" capable of inflicting and propagating devastating damage to the organism. This characteristic is especially significant on the CNS, where most resident cells are extremely susceptible to mitochondrial dysfunctions, as evidenced by the metabolic linked pathogeny of the neurodegenerative diseases, that will be further described in this review.

UnDAMPening Mitochondria in Neurodegenerative Diseases

Mitochondria and Type I Interferon Responses

As mentioned, mDAMPs may signal through PRRs resulting in type I interferon responses (75, 98). Although their importance is mostly known during viral infections (99, 100), IFN-I responses in the CNS have a dual effect. In fact, there are evidences showing that IFN-I responses linked to mDAMPs in neurodegenerative diseases may also have a neuroprotective role (101, 102). Type IFN-I responses in the CNS have already been greatly reviewed by Deczkowska and colleagues (103), in which they discuss this complex signaling network duality. As an example, studies demonstrating that T cells derived IFN-I and IFN-γ are crucial to the blood brain barrier (BBB) permeability, as well as to the production of neurotrophic factors that aid the maintenance of cognitive functions. Corroborating this, the lack of IFN-β in the brain of knockout mice promotes progressive cognitive loss and impaired motor function (104).

Recognized mainly by TLR-9 and STING (75, 105), mtDNA has already been shown to be elevated in the serum of patients with ischemic brain injury (106, 107). Type I IFNs signaling rely on the interaction with Type I Interferon Receptors (IFNAR) and subsequent intracellular cascades that culminates in the phosphorylation of Jak-STATS and IRFs, and the transcription of Interferon Stimulated Genes (ISGs) (100). IFNAR are present in many cell types and, recently, transcriptome analysis in the brain showed the expression of IFNAR1 and IFNAR2 in almost every brain cell subset, including glial cells and neurons (108). In the CNS, the major IFN-αβ secreting sources are astrocytes and microglia. However, during neuroinflammation, disruption of BBB integrity facilitates the infiltration of IFN-I secreting cells, as monocytes and neutrophils (103, 108–111). Moreover, it is important to mention that the concept of CNS immune privilege is being extensively revisited, as many cell types are being described in the brain-circulation interfaces, as the choroid plexus and the meninges (112, 113), as well as within a complex network of lymphatic vessels (114).

It is also known that autocrine action of IFN-I induces significant shifts of the cellular metabolism, as augmented fatty acid oxidation and OXPHOS (65, 115, 116). These shifts are particularly important to astrocytes, as they rely on a tight controlled metabolite production to energetically supply nearby

neurons, mainly by the lactate shuttle. For example, unbalanced glycolysis lowers the expression of glutathione, facilitating oxidative damage (65). Zhang et. al. 2019 recently reported that lactate, a key metabolite of the glycolytic pathway, interacts with the Mitochondrial Antiviral-Signaling protein (MAVS), preventing its oligomerization and maintaining Hexokinase 2 activity (HK2) (117). Although this was described using a model of viral infection, MAVS is increasingly showing to interact with many important enzymes beyond its role as an adaptor for cytosolic PRRs RIG-I and MDA-5. Importantly, the signaling trough MDA-5/MAVS has shown to be one of the main recognition pathways of cytosolic mtDNA, as evidenced during BAK/BAX mitochondrial disruption and failures of mtDNA turnover, being responsible for the major mtDNA induced IFN-I response (118, 119). Also, recent reports evidenced that phospholipase A2 binds to MAVS causing a disruption in the HK2 activity and increasing NF-κB phosphorylation, a novel pathway described in the experimental autoimmune encephalomyelitis (EAE) model (120). This not only give us important cues on how mtDAMPs and dysregulated type I IFN responses could accentuate neurodegenerative diseases, but also brings us new therapeutic avenues.

Mitochondria as Borrowers: Sphingolipid Metabolism and Demyelination Processes

As discussed earlier, the metabolism of sphingolipids is an important player in neuroinflammation, as they critically participate in myelin maintenance (121, 122). For example, the compromised action potential of neurons, that is caused by intracellular changes or by the progressive loss of myelin due to metabolic failure of oligodendrocytes (123), clearly evidences the importance of a proper mitochondrial functioning (124).

The myelination process is tightly regulated both during neurodevelopment and tissue repair, when oligodendrocytes keep contributing for myelin remodeling (125–127) and remyelination (128). It requires great amount of energy, leading to high oxygen and ATP consumption, evidenced by high mitochondrial content within oligodendrocyte's interface with myelin sheets (129). Thus, oligodendrocytes support the long-term myelination by maintaining high glycolytic rates. Conversely, mtDNA mutations in mitochondrial complex IV (mCOX-IV) subunits correlate with more extensive demyelination (129, 130). This phenomenon, along with increased iron deposits in oligodendrocytes, lowers the expression of anti-oxidative enzymes, rendering this cell population exceptionally susceptible to oxidative damage (125, 131), facilitating disease progression.

These characteristics are most evident in diseases as MS and AD, where the inflammatory milieu may drastically affect oligodendrocytes. Cytokines as IL-1, TNF-α and IFN-γ, may cause important mitochondrial distress. In fact, IFN-I impair glycolysis in oligodendrocytes, which is crucial for maintaining axonal integrity through myelin remodeling (132–134).

Furthermore, myelin production itself can be targeted during CNS pathologies. The sphingomyelinase/ceramide pathways play important roles in oligodendrocyte death by promoting the release of ceramide. Ceramide is the precursor of sphingomyelin lipids, the main component of myelin (135). This molecule, like other sphingolipids, has important bioactive functions, as promoting apoptosis and cell cycle arrest (11, 135). Increasing evidences has shown that ceramide can act directly on mitochondria (122) and also activate the NLRP3 inflammasome (136). In rat liver, it has been demonstrated that ceramide can be found in intimate contact with the IMM and OMM, thus leading to loss of Δψm and activating intrinsic apoptotic pathways and mitochondrial dynamics disbalance (137). This has also been discussed during CNS inflammation, as inflammasome activation by ceramide leads to hyperphosphorylation of leptin receptor (Obr) and thus abrogating signaling pathway, as observed during obesity and metabolic syndrome (135, 138).

A STING in the Brain

Although the loss of Δψm is mostly studied during mitochondrial distress, novel data evidence that this event is also crucial for activating cytokine signaling cascades. For instance, the consequent Δψm mediated release of mtDNA can trigger cGAS activation (102, 139–141). Recent structural analysis revealed insights on how cGAS senses different dsDNA residues and, interestingly, it has a higher preference for mtDNA (142).

Discovered in the last decade (143), the cGAS-STING pathway has an important role during intracellular infections, being only recently valued under different contexts. CGAS catalyzes the production of cGAMP (cyclic GTP-AMP) in the presence of cytosolic dsDNA, serving as a second messenger for the activation of the STING adaptor protein. This promotes the phosphorylation of the Tank Binding Kinase 1 (TBK1) protein and further IRF3 nuclear translocation and IFN I transcription (144). Of note, the STING induction of type I IFN responses is a process that occurs only when the cell are not mobilizing apoptotic caspases (85). Thus, it evidences the importance of the cGAS-STING-IRF3 axis during neuropathology, as traumatic brain injury and hypoxia (145–147).

cGAS/STING also initiates NLRP3 responses by the elevation of K^+ influx post lysosomal rupture (148). The NLRP3 induced IL-1β is an important acute phase cytokine that is critical to the pathophysiology of CNS diseases, as AD, PD, MS and even seizure disorders (72, 149–151). Recent research have shown that altered Δψm is dependent on IL-1R activation for further NF-κB, IRF3 and IFN-I expression (150). This novel pathway induces the release of mtDNA and further cytosolic detection by cGAS, but it is important to note that this discovery was made in monocytes and transformed lung cells (150). However, evidences indicate the presence of this axis in the CNS, as STING also modulates microglial reactivity during EAE (98, 152, 153). Moreover, the antiviral drug Ganciclovir promotes beneficial STING dependent type I IFN response in EAE model, dampening the harmful activity of activated microglia (154). Interestingly, mice knocked-out for mitophagy genes, as Parkin and PINK, that leads to inflammation and neuronal death in PD, had more prominent loss of dopaminergic neurons, which was reverted in the absence of STING. This provides an important

link between STING and PD pathogenesis, evidencing the need for more studies on the biology cGAS-STING during neurodegenerative and neuroinflammatory diseases (155).

Greasing Brain Engines: Cardiolipin

Damage to the mitochondrial membrane accounts for the release of mDAMPs. Accordingly, cardiolipin holds great responsibility for the structural stability of the ETC and the functional mitochondrial shape (156, 157). Cardiolipin is mostly associated with heart diseases, mainly due to its high content and impact in this organ (130). On the other hand, its impact over the CNS is an issue that has recently gained attention. Mutations in genes involved in cardiolipin biogenesis, *e.g.* the trans-acylase tafazzin (TAZ), have shown to affect cognitive functions in TAZ knock-out mice, expanding their classical role in X-linked myopathies (12, 158). This lipid is found in the body in different isoforms and, despite the dominance of the tetra linoleoyl cardiolipin isoform in the periphery, studies showed that in the CNS, there is a huge number of cardiolipin isoforms, distributed among different brain regions and cellular subtypes (159). Differences in cardiolipin composition and isoforms correlate to mitochondrial position inside the cell. For instance, as total cardiolipin increases, the closer they are to the synapses (160), which seem to correlate with the capacity of cardiolipin to influence ATP production (161).

Unsaturated lipids as cardiolipin are affected by mtROS and have their function compromised during oxidative stress (162). Proportional to the extension of cardiolipin peroxidation, there is a massive reduction of mitochondrial production of ATP due to $\Delta\psi m$ loss and impairment of ETC complexes I, III, IV and V. Conversely, impaired ATP production by CNS cells is a common factor in aging and degenerative diseases (84). Studies in PD evidenced that cardiolipin interacts with α-synuclein by modifying its structure and exerting a protective role, by preventing its aggregation. Regarding this issue, divergent results demonstrated that this interaction can also affect cardiolipin functioning, resulting in increased pathology (163, 164). Moreover, α-synuclein binding to cardiolipin impairs the detection of cytosolic cytochrome c and thus inhibiting apoptotic cell death by dampening cellular oxidative stress (165).

The presence of cardiolipin in the OMM induces the recognition and further engulfment of dysfunctional mitochondria by LC3 mediated autophagy. Under conditions when the number of dysfunctional mitochondria exceeds the autophagy capacity, cardiolipin recruits BAX to form pores that release cytochrome c to the cytoplasm and triggering apoptosis. Thus, apart from the ETC complexes, cardiolipin also anchors important kinases that participate in the translocation of lipidic content through the mitochondrial membrane. When this mechanisms are impaired, it leads to a deleterious accumulation of dysfunctional mitochondria (156, 166).

Give Me Fuel, Give Me Fire: Inflammasome Activation and Neuroinflammation

In addition to the induction of type I IFN response, mDAMPs also modulate the activation of inflammasomes. Canonical inflammasome activation leads to the proteolytic cleavage of pro-caspase-1 to caspase-1 and the subsequent pro-IL-1β/IL-18 and gasdermin 1 for further extracellular release (167). Both cytokines strongly activate pro-inflammatory responses, and they have an unquestionable importance during neuroinflammation, for instance, promoting the disruption of the blood-brain-barrier (BBB) and ROS production.

NLRP3 inflammasome is activated by a wide range of molecules, including mtROS, cardiolipin and mtDNA (148, 167). Importantly, for NLRP3 complete activation, an initial priming step is required to increase the expression of inflammasome effector molecules, as the NLRP3 itself, caspase-1 and pro-IL-1β. This is mediated by the activation of TLR-4, NOD receptor 2 (NOD2) and cytokines as TNF-α and IL-1β itself. This leads to NF-κB phosphorylation and nuclear translocation to promote NLRP3-related gene transcription (167–169). However, how inflammasome senses and interacts with stressors and the details of its activation remains not fully understood.

Interestingly, inflammasome activation is closely related to ER and mitochondria communication in many ways, and mitochondrial Ca^{2+} imbalance may also result in inflammasome activation (170). This may occur either by directly promoting NLRP3 complex formation or by mitochondrial Ca^{2+} overload and further mitochondrial dysfunction. Corroborating this, blocking ER IP3R, a major regulator of ER-to-cytoplasm Ca^{2+}exchange, effectively attenuates NLRP3 activation (171, 172). Accordingly, mitochondria calcium homeostasis is closely related to ER Ca^{2+} metabolism since the MAMs plays a key role in material transfer and signaling between both organelles (16).

Inactivated forms of NLRP3 are localized in the ER membrane, although under certain stimuli, NLRP3 is redistributed across the MAMs (173). Under stress conditions, cardiolipin is exposed on the OMM and serves as a bridge between NLRP3 and MAMs (78). The localization of NLRP3 over the MAMs induces clusters of mitochondria around the Golgi apparatus and the release of NLRP3 to the cytosol for inflammasome mature form assembling (173). The mitochondrial location of NLRP3 is also affected by the interaction between MFN2 and MAVS during viral infections, which recruits the inflammasome to the MAMs. However, MAVS are not essential for NLRP3 activation under other stimuli (16). Mitophagy is also an important player during inflammasome activation since the removal of impaired mitochondria reduces ROS production. The continuous production of ROS occurs during oxidative phosphorylation and several studies have demonstrated that inhibitors of complex I, II and III develop an important role in mtROS production reflecting in decreased inflammasome activation (174, 175).

Interestingly, mtROS and Ca^{2+} have a synergic role for pore formation within mitochondria membranes. Mitochondrial permeability transition (MPT) pores allow the release of mtDNA. Interestingly, oxidized mtDNA in the cytoplasm triggers IL-1β secretion by preferentially activating NLRP3 but not AIM-2 (176). Additionally, IL-1β production was

significantly enhanced with oxidized versus normal DNA (176). Importantly, the induction of NLRP3 also induces mtDNA release in the cytosol, thus creating a positive loop in the induction of inflammasome pathway (14, 176).

CNS disorders may occur due to NLRP3 dysfunctions and its close link with mitochondrial health (177). In EAE for example, increased levels of IL-1β and NLRP3 were related to disease progression. Additionally, microglia deletion of A20, an immune suppressive protein correlated with increased NLRP3 activation and IL-1β/IL18 secretion (178). Conversely, the role of IFN-β, a well-established treatment for MS, was demonstrated to be dependent on NLRP3 activation during EAE (179).

The correlation of inflammasomes and AD pathophysiology is also debated, since increased levels of IL-1β were reported in the Aβ neighboring microglia cells. Halle et al. (180) observed that Aβ phagocytosed by microglia triggers caspase-1 and subsequent release of IL-1β, *in vitro*. Corroborating this, *in vivo* studies shown that loss of NLRP3 is associated with reduced Aβ deposition, cytokine production and lead to ameliorated spatial memory deficits in AD mouse model. As Aβ, α-synuclein also induces NLRP3 activation in mouse microglial cell line. *In vivo*, the administration of caspase-1 inhibitor decreases the activation of NLRP3 and induces an increase in the number of dopaminergic neurons, consequently relating a better PD prognosis (177). Interestingly, caspase-1 is also able to cleave α-synuclein, and NLRP3 inhibition abrogates synuclein aggregation, ameliorating cell damage in murine PD model (181).

Penghu and collaborators showed that mtROS induced NLRP3 activation in hippocampal microglia (182). Sarkar et al. (182) evidenced that the inhibition of mitochondrial complex I by rotenone increased ROS production, leading to augmented

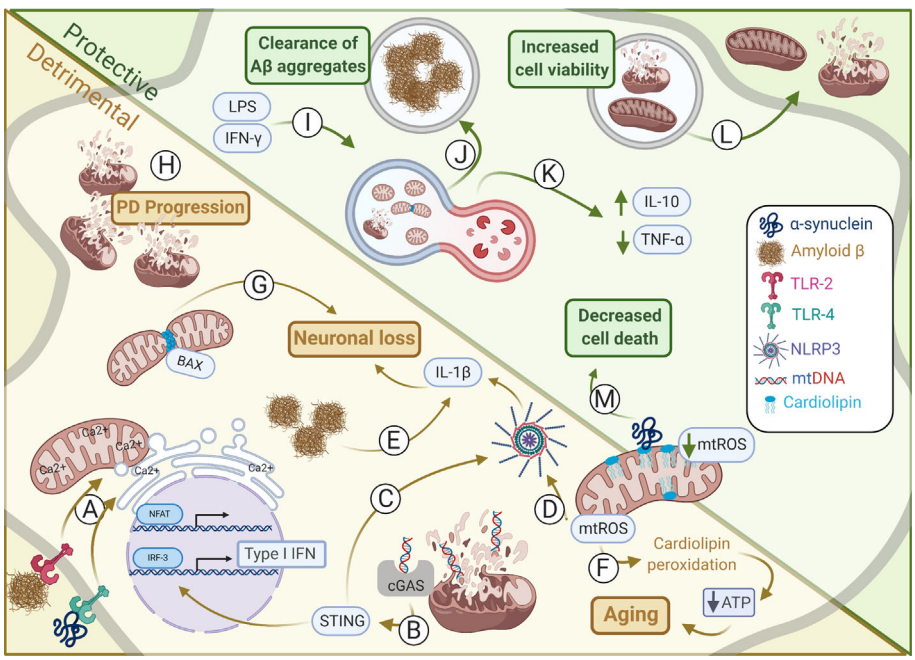

FIGURE 1 | Mitochondrial alterations in protective and detrimental processes within CNS. Alterations in mitochondrial dynamics may induce either harmful or helpful immune responses affecting in CNS homeostasis. **(A)** Amyloid-β and α-synuclein induces TLR-2 and TLR-4 activation, respectively, promoting the interaction between outer mitochondria membrane (OMM) and endoplasmic reticulum (ER) membrane to synergically increase Ca^{2+} uptake and NFAT activation. **(B)** Type I IFN production is induced by mtDNA activation of cGAS-STING during sustained mitochondrial damage promoting neurodegeneration. **(C)** STING may also induce activation of NLRP3. **(D)** The NLRP3 may also be induced by mtROS thus coordinating IL-1β secretion by microglia and astrocytes promoting neuronal loss. **(E)** Amyloid-β aggregates induce NLRP3 inflammasome activation and IL-1β secretion by microglia. **(F)** mtROS induces cardiolipin peroxidation that deregulates ATP production, as observed during aging. **(G)** In neurons, BAX interacts with DRP1 inducing mitochondrial fragmentation. This is critical for BAX-dependent pore formation and neuronal survival. **(H)** Failure in mitophagy culminates in damaged mitochondria accumulation which contributes for Parkinson's disease (PD) progress. **(I)** Mitophagy may be induced by IFN-γ and LPS upregulation of DRP1 and LC3, an autophagy-related protein. This is essential to restore tubular mitochondrial networks after inflammatory stimulation in astrocytes. **(J)** Microglial cells under mitophagy have elevated levels of intracellular Aβ aggregates, suggesting increased phagocytic activity, and thus clearing the harmful Aβ deposits. **(K)** PINK1 regulation of mitophagy is essential for CNS homeostasis establishment and induction of IL-10 and reduction of TNF-α secretion. **(L)** Instead of mitophagy the release of damage mitochondria may also minimize overall cell injury. Conversely, healthy mitochondria may also be donated from astrocytes to damaged neighboring neurons increasing its viability and maintaining its metabolism. **(M)** Cardiolipin can interact with α-synuclein preventing its aggregation by modifying its structure and impairing the release of cytosolic cytochrome c and thus inhibiting apoptosis and dampening cellular oxidative stress. Illustration prepared by the authors using www.biorender.com.

cleavage of caspase-1 and NLRP3 expression in microglia cells. Conversely, they also evidenced that this pathway culminates in a more prominent dopaminergic neuronal loss (183).

CONCLUDING REMARKS

Although first believed to be solely the power houses of the cell, it is now accepted that mitochondria have an active role in many cellular processes, especially during inflammation. In **Figure 1** we summarize some of these relevant aspects concerning the correlation between mitochondria and brain disease. Although many of these diseases have their pathology linked to either mild or robust inflammatory responses, recent findings have unraveled that many of these mechanisms correlate with mitochondrial unbalanced function. Either because neuroinflammation can drastically impact cellular metabolism and further mitochondrial biology, for instance promoting mROS secretion or impairing ETC function, or because mitochondrial disfunction leads to the release of pro-inflammatory factors, as mtDNA. In this sense, innate immunity receptors as NLRP3 and MAVS greatly evidences the role of mitochondria as both effectors and sensors of neuroinflammation, respectively. Interestingly, structural changes in mitochondrial shape, size and turnover inside the cell, has also shown great relevance. For instance, OPA and MFN proteins defects, responsible for mitochondrial fusion are observed in Charcot-Marie-Tooth disease and optic atrophy. Mitochondria may also correlate with homeostasis and resolution of neuroinflammation. During mitophagy, for instance, there is the induction of IL-10 secretion and inflammation control, as observed in PD models. More interesting, inflammation activated astrocytes may actively transfer mitochondria to nearby neurons as an effort to avoid or reduce tissue damage, whereas damaged mitochondria are also released in order to avoid excessive ROS production, as described during stroke. In summary, the role of mitochondria during neuroinflammation and neurodegeneration has started to be better understood, not only unraveling important biological processes but also indicating that mitochondria-related immunometabolic pathways may serve as promising therapeutic targets for CNS diseases. This is corroborated by the fact that are currently 160 studies registered in www.clinicaltrials.gov found for the terms mitochondria and brain.

AUTHOR CONTRIBUTIONS

LGO and YSA wrote the manuscript and designed the figure; AHI wrote and edited the manuscript; JPSP wrote, elaborated the topics, edited and reviewed the manuscript. All authors contributed to the article and approved the submitted version.

FUNDING

Neuroimmune interactions laboratory is supported by FAPESP (#2017/26170; #2017/22504-1), CAPES and CNPq.

REFERENCES

1. World Health Organization. *Neurological Disorders: Public health challenges* (2021). Available at: https://www.who.int/mental_health/neurology/neurodiso/en/ (Accessed February 12, 2021).
2. Mayo L, Trauger SA, Blain M, Nadeau M, Patel B, Alvarez JI, et al. Regulation of astrocyte activation by glycolipids drives chronic CNS inflammation. *Nat Med* (2014) 20:1147–56. doi: 10.1038/nm.3681
3. Peron JPS, Oliveira D, Brandão WN, Fickinger A, De Oliveira APL, Rizzo LV, et al. *Central Nervous System Resident Cells in Neuroinflammation: A Brave New World*. James Chan, ed. London, UK: IntechOpen (2012). 1536–77 p.
4. Chakraborty S, Kaushik DK, Gupta M, Basu A. Inflammasome signaling at the heart of central nervous system pathology. *J Neurosci Res* (2010) 88:1615–31. doi: 10.1002/jnr.22343
5. Shao W, Zhang S, Tang M, Zhang X, Zhou Z, Yin Y, et al. Suppression of neuroinflammation by astrocytic dopamine D2 receptors via αB-crystallin. *Nature* (2013) 494:90–4. doi: 10.1038/nature11748
6. Barbierato M, Facci L, Argentini C, Marinelli C, Skaper SD, Giusti P. Astrocyte-microglia cooperation in the expression of a pro-inflammatory phenotype. *CNS Neurol Disord Drug Targets* (2013) 12:608–18.
7. Luheshi NM, Kovács KJ, Lopez-Castejon G, Brough D, Denes A. Interleukin-1α expression precedes IL-1β after ischemic brain injury and is localised to areas of focal neuronal loss and penumbral tissues. *J Neuroinflamm* (2011) 8:186. doi: 10.1186/1742-2094-8-186
8. Farez MF, Quintana FJ, Gandhi R, Izquierdo G, Lucas M, Weiner HL. Toll-like receptor 2 and poly(ADP-ribose) polymerase 1 promote central nervous system neuroinflammation in progressive EAE. *Nat Immunol* (2009) 10:958–64. doi: 10.1038/ni.1775
9. Hasegawa-Ishii S, Takei S, Inaba M, Umegaki H, Chiba Y, Furukawa A, et al. Defects in cytokine-mediated neuroprotective glial responses to excitotoxic hippocampal injury in senescence-accelerated mouse. *Brain Behav Immun* (2011) 25:83–100. doi: 10.1016/j.bbi.2010.08.006
10. Mills EL, Kelly B, O'Neill LAJ. Mitochondria are the powerhouses of immunity. *Nat Immunol* (2017) 18:488–98. doi: 10.1038/ni.3704
11. Wentling M, Lopez-Gomez C, Park HJ, Amatruda M, Ntranos A, Aramini J, et al. A metabolic perspective on CSF-mediated neurodegeneration in multiple sclerosis. *Brain* (2019) 142:2756–74. doi: 10.1093/brain/awz201
12. Cole LK, Kim JH, Amoscato AA, Tyurina YY, Bayır H, Karimi B, et al. Aberrant cardiolipin metabolism is associated with cognitive deficiency and hippocampal alteration in tafazzin knockdown mice. *Biochim Biophys Acta - Mol Basis Dis* (2018) 1864:3353–67. doi: 10.1016/j.bbadis.2018.07.022
13. Morató L, Bertini E, Verrigni D, Ardissone A, Ruiz M, Ferrer I, et al. Mitochondrial dysfunction in central nervous system white matter disorders. *Glia* (2014) 1–17. doi: 10.1002/glia.22670
14. Zhong Z, Liang S, Sanchez-Lopez E, He F, Shalapour S, Lin Xj, et al. New mitochondrial DNA synthesis enables NLRP3 inflammasome activation. *Nature* (2018) 560:198–203. doi: 10.1038/s41586-018-0372-z
15. Tilokani L, Nagashima S, Paupe V, Prudent J. Mitochondrial dynamics: overview of molecular mechanisms. *Essays Biochem* (2018) 62:341–60. doi: 10.1042/EBC20170104
16. Missiroli S, Patergnani S, Caroccia N, Pedriali G, Perrone M, Previati M, et al. Mitochondria-associated membranes (MAMs) and inflammation. *Cell Death Dis* (2018) 9. doi: 10.1038/s41419-017-0027-2

17. Jackson JG, Robinson MB. Reciprocal regulation of mitochondrial dynamics and calcium signaling in astrocyte processes. *J Neurosci* (2015) 35:15199–213. doi: 10.1523/JNEUROSCI.2049-15.2015
18. De Brito OM, Scorrano L. Mitofusin 2 tethers endoplasmic reticulum to mitochondria. *Nature* (2008) 456:605–10. doi: 10.1038/nature07534
19. Boitier E, Rea R, Duchen MR. Mitochondria exert a negative feedback on the propagation of intracellular Ca2+ waves in rat cortical astrocytes. *J Cell Biol* (1999) 145:795–808. doi: 10.1083/jcb.145.4.795
20. Filadi R, Greotti E, Turacchio G, Luini A, Pozzan T, Pizzo P. Mitofusin 2 ablation increases endoplasmic reticulum-mitochondria coupling. *Proc Natl Acad Sci U S A* (2015) 112:E2174–81. doi: 10.1073/pnas.1504880112
21. Stoica R, Paillusson S, Gomez-Suaga P, Mitchell JC, Lau DH, Gray EH, et al. ALS/FTD-associated FUS activates GSK-3β to disrupt the VAPB–PTPIP51 interaction and ER–mitochondria associations. *EMBO Rep* (2016) 17:1326–42. doi: 10.15252/embr.201541726
22. Paillusson S, Gomez-Suaga P, Stoica R, Little D, Gissen P, Devine MJ, et al. α-Synuclein binds to the ER–mitochondria tethering protein VAPB to disrupt Ca2+ homeostasis and mitochondrial ATP production. *Acta Neuropathol* (2017) 134:129–49. doi: 10.1007/s00401-017-1704-z
23. Rapizzi E, Pinton P, Szabadkai G, Wieckowski MR, Vandecasteele G, Baird G, et al. Recombinant expression of the voltage-dependent anion channel enhances the transfer of Ca 2 microdomains to mitochondria. *J Cell Biol* (2002) 159:613–24. doi: 10.1083/jcb.200205091
24. Szabadkai G, Bianchi K, Várnai P, De Stefani D, Wieckowski MR, Cavagna D, et al. Chaperone-mediated coupling of endoplasmic reticulum and mitochondrial Ca2+ channels. *J Cell Biol* (2006) 175:901–11. doi: 10.1083/jcb.200608073
25. Ottolini D, Calì T, Negro A, Brini M. The Parkinson disease-related protein DJ-1 counteracts mitochondrial impairment induced by the tumour suppressor protein p53 by enhancing endoplasmic reticulum-mitochondria tethering. *Hum Mol Genet* (2013) 22:2152–68. doi: 10.1093/hmg/ddt068
26. Bartok A, Weaver D, Golenár T, Nichtova Z, Katona M, Bánsághi S, et al. IP3 receptor isoforms differently regulate ER-mitochondrial contacts and local calcium transfer. *Nat Commun* (2019) 10:1–14. doi: 10.1038/s41467-019-11646-3
27. Akimzhanov AM, Boehning D. IP3R function in cells of the immune system. *Wiley Interdiscip Rev Membr Transp Signal* (2012) 1:329–39. doi: 10.1002/wmts.27
28. Kim MS, Usachev YM. Mitochondrial Ca2+ cycling facilitates activation of the transcription factor NFAT in sensory neurons. *J Neurosci* (2009) 29:12101–14. doi: 10.1523/JNEUROSCI.3384-09.2009
29. Agostinho P, Lopes JP, Velez Z, Oliveira CR. Overactivation of calcineurin induced by amyloid-beta and prion proteins. *Neurochem Int* (2008) 52:1226–33. doi: 10.1016/j.neuint.2008.01.005
30. Liu S, Liu Y, Hao W, Wolf L, Kiliaan AJ, Penke B, et al. TLR2 Is a Primary Receptor for Alzheimer's Amyloid β Peptide To Trigger Neuroinflammatory Activation. *J Immunol* (2012) 188:1098–107. doi: 10.4049/jimmunol.1101121
31. Salminen A, Ojala J, Kauppinen A, Kaarniranta K, Suuronen T. Inflammation in Alzheimer's disease: Amyloid-β oligomers trigger innate immunity defence via pattern recognition receptors. *Prog Neurobiol* (2009) 87:181–94. doi: 10.1016/j.pneurobio.2009.01.001
32. Rannikko EH, Weber SS, Kahle PJ. Exogenous α-synuclein induces toll-like receptor 4 dependent inflammatory responses in astrocytes. *BMC Neurosci* (2015) 16:57. doi: 10.1186/s12868-015-0192-0
33. Ma B, Yu J, Xie C, Sun L, Lin S, Ding J, et al. Toll-like receptors promote mitochondrial translocation of nuclear transcription factor nuclear factor of activated T-cells in prolonged microglial activation. *J Neurosci* (2015) 35:10799–814. doi: 10.1523/JNEUROSCI.2455-14.2015
34. Sama MA, Mathis DM, Furman JL, Abdul HM, Artiushin IA, Kraner SD, et al. Interleukin-1β-dependent signaling between astrocytes and neurons depends critically on astrocytic calcineurin/NFAT activity. *J Biol Chem* (2008) 283:21953–64. doi: 10.1074/jbc.M800148200
35. Brandt T, Cavellini L, Kühlbrandt W, Cohen MM. A mitofusin-dependent docking ring complex triggers mitochondrial fusion in vitro. *Elife* (2016) 5:1–23. doi: 10.7554/eLife.14618
36. Huang X, Zhou X, Hu X, Joshi AS, Guo X, Zhu Y, et al. Sequences flanking the transmembrane segments facilitate mitochondrial localization and membrane fusion by mitofusin. *Proc Natl Acad Sci U S A* (2017) 114:E9863–72. doi: 10.1073/pnas.1708782114
37. Eura Y, Ishihara N, Yokota S, Mihara K. Two Mitofusin Proteins, Mammalian Homologues of FZO, with Distinct Functions Are Both Required for Mitochondrial Fusion. *J Biochem* (2003) 134:333–44. doi: 10.1093/jb/mvg150
38. Liu YJ, McIntyre RL, Janssens GE, Houtkooper RH. Mitochondrial fission and fusion: A dynamic role in aging and potential target for age-related disease. *Mech Ageing Dev* (2020) 186:111212. doi: 10.1016/j.mad.2020.111212
39. DeVay RM, Dominguez-Ramirez L, Lackner LL, Hoppins S, Stahlberg H, Nunnari J. Coassembly of Mgm1 isoforms requires cardiolipin and mediates mitochondrial inner membrane fusion. *J Cell Biol* (2009) 186:793–803. doi: 10.1083/jcb.200906098
40. Rambold AS, Kostelecky B, Elia N, Lippincott-Schwartz J. Tubular network formation protects mitochondria from autophagosomal degradation during nutrient starvation. *Proc Natl Acad Sci U S A* (2011) 108:10190–5. doi: 10.1073/pnas.1107402108
41. Liesa M, Van Der Bliek A, Shirihai OS. To Fis or not to Fuse? This is the question!. *EMBO J* (2019) 38(8):1–3. doi: 10.15252/embj.2019101839
42. Lewis SC, Uchiyama LF, Nunnari J. ER-mitochondria contacts couple mtDNA synthesis with Mitochondrial division in human cells. *Sci (80-)* (2016) 353(6296):aaf5549. doi: 10.1126/science.aaf5549
43. Friedman JR, Lackner LL, West M, DiBenedetto JR, Nunnari J, Voeltz GK. ER tubules mark sites of mitochondrial division. *Sci (80-)* (2011) 334:358–62. doi: 10.1126/science.1207385
44. Cho B, Cho HM, Jo Y, Kim HD, Song M, Moon C, et al. Constriction of the mitochondrial inner compartment is a priming event for mitochondrial division. *Nat Commun* (2017) 8:1–17. doi: 10.1038/ncomms15754
45. Liesa M, Shirihai OS. Mitochondrial dynamics in the regulation of nutrient utilization and energy expenditure. *Cell Metab* (2013) 17:491–506. doi: 10.1016/j.cmet.2013.03.002
46. Delettre C, Lenaers G, Griffoin JM, Gigarel N, Lorenzo C, Belenguer P, et al. Nuclear gene OPA1, encoding a mitochondrial dynamin-related protein, is mutated in dominant optic atrophy. *Nat Genet* (2000) 26:207–10. doi: 10.1038/79936
47. Züchner S, Noureddine M, Kennerson M, Verhoeven K, Claeys K, De Jonghe P, et al. Mutations in the pleckstrin homology domain of dynamin 2 cause dominant intermediate Charcot-Marie-Tooth disease. *Nat Genet* (2005) 37:289–94. doi: 10.1038/ng1514
48. Maes ME, Grosser JA, Fehrman RL, Schlamp CL, Nickells RW. Completion of BAX recruitment correlates with mitochondrial fission during apoptosis. *Sci Rep* (2019) 9:16565. doi: 10.1038/s41598-019-53049-w
49. Duan C, Kuang L, Xiang X, Zhang J, Zhu Y, Wu Y, et al. Drp1 regulates mitochondrial dysfunction and dysregulated metabolism in ischemic injury via Clec16a-, BAX-, and GSH- pathways. *Cell Death Dis* (2020) 11:251. doi: 10.1038/s41419-020-2461-9
50. Kanki T, Wang K, Klionsky DJ. A genomic screen for yeast mutants defective in mitophagy. *Autophagy* (2010) 6:278–80. doi: 10.4161/auto.6.2.10901
51. Yamashita SI, Jin X, Furukawa K, Hamasaki M, Nezu A, Otera H, et al. Mitochondrial division occurs concurrently with autophagosome formation but independently of Drp1 during mitophagy. *J Cell Biol* (2016) 215:649–65. doi: 10.1083/jcb.201605093
52. Wang L, Chen R-F, Liu J-W, Lee I-K, Lee C-P, Kuo H-C, et al. DC-SIGN (CD209) Promoter –336 A/G Polymorphism Is Associated with Dengue Hemorrhagic Fever and Correlated to DC-SIGN Expression and Immune Augmentation. *PloS Negl Trop Dis* (2011) 5:e934. doi: 10.1371/journal.pntd.0000934
53. Lazarou M, Narendra DP, Jin SM, Tekle E, Banerjee S, Youle RJ. PINK1 drives parkin self-association and HECT-like E3 activity upstream of mitochondrial binding. *J Cell Biol* (2013) 200:163–72. doi: 10.1083/jcb.201210111
54. Tang MY, Vranas M, Krahn AI, Pundlik S, Trempe JF, Fon EA. Structure-guided mutagenesis reveals a hierarchical mechanism of Parkin activation. *Nat Commun* (2017) 8:1–14. doi: 10.1038/ncomms14697

55. Wang H, Song P, Du L, Tian W, Yue W, Liu M, et al. Parkin ubiquitinates Drp1 for proteasome-dependent degradation: Implication of dysregulated mitochondrial dynamics in Parkinson disease. *J Biol Chem* (2011) 286:11649–58. doi: 10.1074/jbc.M110.144238
56. Henn IH, Bouman L, Schlehe JS, Schlierf A, Schramm JE, Wegener E, et al. Parkin mediates neuroprotection through activation of IκB kinase/nuclear factor-κB signaling. *J Neurosci* (2007) 27:1868–78. doi: 10.1523/JNEUROSCI.5537-06.2007
57. Wang X, Winter D, Ashrafi G, Schlehe J, Wong YL, Selkoe D, et al. PINK1 and Parkin target miro for phosphorylation and degradation to arrest mitochondrial motility. *Cell* (2011) 147:893–906. doi: 10.1016/j.cell.2011.10.018
58. Sato M, Sato K. Degradation of paternal mitochondria by fertilization-triggered autophagy in C. elegans embryos. *Sci (80-)* (2011) 334:1141–4. doi: 10.1126/science.1210333
59. Arpd-associated M, Pink P. Parkin function in Parkinson's disease. *Science* (2018) 267–8.
60. Ip WKE, Hoshi N, Shouval DS, Snapper S, Medzhitov R. Anti-inflammatory effect of IL-10 mediated by metabolic reprogramming of macrophages. *Sci (80-)* (2017) 356:513–9. doi: 10.1126/science.aal3535
61. Lei Q, Tan J, Yi S, Wu N, Wang Y, Wu H. Mitochonic acid 5 activates the MAPK–ERK–yap signaling pathways to protect mouse microglial BV-2 cells against TNFα-induced apoptosis via increased Bnip3-related mitophagy. *Cell Mol Biol Lett* (2018) 23:14. doi: 10.1186/s11658-018-0081-5
62. Fang EF, Hou Y, Palikaras K, Adriaanse BA, Kerr JS, Yang B, et al. Mitophagy inhibits amyloid-β and tau pathology and reverses cognitive deficits in models of Alzheimer's disease. *Nat Neurosci* (2019) 22:401–12. doi: 10.1038/s41593-018-0332-9
63. Motori E, Puyal J, Toni N, Ghanem A, Angeloni C, Malaguti M, et al. Inflammation-induced alteration of astrocyte mitochondrial dynamics requires autophagy for mitochondrial network maintenance. *Cell Metab* (2013) 18:844–59. doi: 10.1016/j.cmet.2013.11.005
64. Sriram S. Role of glial cells in innate immunity and their role in CNS demyelination. *J Neuroimmunol* (2011) 239:13–20. doi: 10.1016/j.jneuroim.2011.08.012
65. Fiebig C, Keiner S, Ebert B, Schäffner I, Jagasia R, Lie DC, et al. Mitochondrial dysfunction in astrocytes impairs the generation of reactive astrocytes and enhances neuronal cell death in the cortex upon photothrombotic lesion. *Front Mol Neurosci* (2019) 12:40. doi: 10.3389/fnmol.2019.00040
66. Verkhratsky A, Matteoli M, Parpura V, Mothet J, Zorec R. Astrocytes as secretory cells of the central nervous system: idiosyncrasies of vesicular secretion. *EMBO J* (2016) 35:239–57. doi: 10.15252/embj.201592705
67. Quintana DD, Garcia JA, Sarkar SN, Jun S, Engler-Chiurazzi EB, Russell AE, et al. Hypoxia-reoxygenation of primary astrocytes results in a redistribution of mitochondrial size and mitophagy. *Mitochondrion* (2019) 47:244–55. doi: 10.1016/j.mito.2018.12.004
68. Davis CHO, Kim KY, Bushong EA, Mills EA, Boassa D, Shih T, et al. Transcellular degradation of axonal mitochondria. *Proc Natl Acad Sci U S A* (2014) 111:9633–8. doi: 10.1073/pnas.1404651111
69. Hayakawa K, Esposito E, Wang X, Terasaki Y, Liu Y, Xing C, et al. Transfer of mitochondria from astrocytes to neurons after stroke. *Nature* (2016) 535:551–5. doi: 10.1038/nature18928
70. Joshi AU, Minhas PS, Liddelow SA, Haileselassie B, Andreasson KI, Dorn GW, et al. Fragmented mitochondria released from microglia trigger A1 astrocytic response and propagate inflammatory neurodegeneration. *Nat Neurosci* (2019) 22:1635–48. doi: 10.1038/s41593-019-0486-0
71. Pradeu T, Cooper EL. The danger theory: 20 years later. *Front Immunol* (2012) 3:287. doi: 10.3389/fimmu.2012.00287
72. Roh JS, Sohn DH. Damage-associated molecular patterns in inflammatory diseases. *Immune Netw* (2018) 18:1635–48. doi: 10.4110/in.2018.18.e27
73. Harris HE, Raucci A. Alarmin(g) news about danger: Workshop on Innate Danger Signals and HMGB1. *EMBO Rep (European Mol Biol Organization)* (2006) 774–8. doi: 10.1038/sj.embor.7400759
74. Grazioli S, Pugin J. Mitochondrial damage-associated molecular patterns: From inflammatory signaling to human diseases. *Front Immunol* (2018) 9:832. doi: 10.3389/fimmu.2018.00832
75. Maekawa H, Inoue T, Ouchi H, Jao TM, Inoue R, Nishi H, et al. Mitochondrial Damage Causes Inflammation via cGAS-STING Signaling in Acute Kidney Injury. *Cell Rep* (2019) 29:1261–73.e6. doi: 10.1016/j.celrep.2019.09.050
76. Hammond TR, Dufort C, Dissing-Olesen L, Giera S, Young A, Wysoker A, et al. Single-Cell RNA Sequencing of Microglia throughout the Mouse Lifespan and in the Injured Brain Reveals Complex Cell-State Changes. *Immunity* (2019) 50:253–71.e6. doi: 10.1016/j.immuni.2018.11.004
77. Nguyen HM, Mejia EM, Chang W, Wang Y, Watson E, On N, et al. Reduction in cardiolipin decreases mitochondrial spare respiratory capacity and increases glucose transport into and across human brain cerebral microvascular endothelial cells. *J Neurochem* (2016) 139:68–80. doi: 10.1111/jnc.13753
78. Iyer SS, He Q, Janczy JR, Elliott EI, Zhong Z, Olivier AK, et al. Mitochondrial cardiolipin is required for Nlrp3 inflammasome activation. *Immunity* (2013) 39:311–23. doi: 10.1016/j.immuni.2013.08.001
79. Wang C, Youle RJ. The Role of Mitochondria. *Annu Rev Genet* (2009) 43:95–118. doi: 10.1146/annurev-genet-102108-134850
80. Elmore S. Apoptosis: A Review of Programmed Cell Death. *Toxicol Pathol* (2007) 35:495–516. doi: 10.1080/01926230701320337
81. Migalovich Sheikhet H, Villacorta Hidalgo J, Fisch P, Balbir-Gurman A, Braun-Moscovici Y, Bank I. Dysregulated CD25 and Cytokine Expression by γδ T Cells of Systemic Sclerosis Patients Stimulated With Cardiolipin and Zoledronate. *Front Immunol* (2018) 9:753. doi: 10.3389/fimmu.2018.00753
82. Madsen PM, Pinto M, Patel S, Mccarthy S, Gao H, Taherian M, et al. Neurobiology of Disease Mitochondrial DNA Double-Strand Breaks in Oligodendrocytes Cause Demyelination, Axonal Injury, and CNS Inflammation. *J Neurosci* (2017) 10185–99. doi: 10.1523/JNEUROSCI.1378-17.2017
83. Chinnery PF, Hudson G. Mitochondrial genetics. *Br Med Bull* (2013) 106:135–59. doi: 10.1093/bmb/ldt017
84. Cabral-Costa JV, Kowaltowski AJ. Neurological disorders and mitochondria. *Mol Aspects Med* (2020) 71:100826. doi: 10.1016/j.mam.2019.10.003
85. Rongvaux A, Jackson R, Harman CCD, Li T, West AP, De Zoete MR, et al. Apoptotic caspases prevent the induction of type i interferons by mitochondrial DNA. *Cell* (2014) 159:1563–77. doi: 10.1016/j.cell.2014.11.037
86. West AP, Khoury-Hanold W, Staron M, Tal MC, Pineda CM, Lang SM, et al. Mitochondrial DNA stress primes the antiviral innate immune response. *Nature* (2015) 520:553–7. doi: 10.1038/nature14156
87. Iwasaki A, Medzhitov R. Toll-like receptor control of the adaptive immune responses. *Nat Immunol* (2004) 5:987–95. doi: 10.1038/ni1112
88. Schumacker PT, Gillespie MN, Nakahira K, Choi AMK, Crouser ED, Piantadosi CA, et al. Mitochondria in lung biology and pathology: More than just a powerhouse. *Am J Physiol - Lung Cell Mol Physiol* (2014) 306:L962. doi: 10.1152/ajplung.00073.2014
89. Andreyev AY, Kushnareva YE, Starkov AA. Mitochondrial metabolism of reactive oxygen species. *Biochem* (2005) 70:200–14. doi: 10.1007/s10541-005-0102-7
90. Kowaltowski AJ, de Souza-Pinto NC, Castilho RF, Vercesi AE. Mitochondria and reactive oxygen species. *Free Radic Biol Med* (2009) 47:333–43. doi: 10.1016/j.freeradbiomed.2009.05.004
91. Fridavich I. Superoxide radical and superoxide dismutases. *Annu Rev Biochem* (1995) 64:97–112. doi: 10.1146/annurev.bi.64.070195.000525
92. Angelova PR, Abramov AY. Role of mitochondrial ROS in the brain: from physiology to neurodegeneration. *FEBS Lett* (2018) 592:692–702. doi: 10.1002/1873-3468.12964
93. Lee YM, He W, Liou Y-C. The redox language in neurodegenerative diseases: oxidative post-translational modifications by hydrogen peroxide. *Cell Death Dis* (2021) 12:58. doi: 10.1038/s41419-020-03355-3
94. Zorov DB, Juhaszova M, Sollott SJ. Mitochondrial reactive oxygen species (ROS) and ROS-induced ROS release. *Physiol Rev* (2014) 94:909–50. doi: 10.1152/physrev.00026.2013
95. Murphy MP. How mitochondria produce reactive oxygen species. *Biochem J* (2009) 417:1–13. doi: 10.1042/BJ20081386
96. Nissanka N, Moraes CT. Mitochondrial DNA damage and reactive oxygen species in neurodegenerative disease. *FEBS Lett* (2018) 592:728–42. doi: 10.1002/1873-3468.12956

97. Lévy E, El Banna N, Baïlle D, Heneman-Masurel A, Truchet S, Rezaei H, et al. Causative links between protein aggregation and oxidative stress: A review. *Int J Mol Sci* (2019) 20. doi: 10.3390/ijms20163896
98. Yang K, Huang R, Fujihira H, Suzuki T, Yan N. N-glycanase NGLY1 regulates mitochondrial homeostasis and inflammation through NRF1. *J Exp Med* (2018) 215:2600–16. doi: 10.1084/jem.20180783
99. Giovannoni F, Bosch I, Polonio CM, Torti MF, Wheeler MA, Li Z, et al. AHR is a Zika virus host factor and a candidate target for antiviral therapy. *Nat Neurosci* (2020) 23:939–51. doi: 10.1038/s41593-020-0664-0
100. McNab F, Mayer-Barber K, Sher A, Wack A, O'Garra A. Type I interferons in infectious disease. *Nat Rev Immunol* (2015) 15:87–103. doi: 10.1038/nri3787
101. Main BS, Zhang M, Brody KM, Kirby FJ, Crack PJ, Taylor JM. Type-I interferons mediate the neuroinflammatory response and neurotoxicity induced by rotenone. *J Neurochem* (2017) 141:75–85. doi: 10.1111/jnc.13940
102. Nazmi A, Field RH, Griffin EW, Haugh O, Hennessy E, Cox D, et al. Chronic neurodegeneration induces type I interferon synthesis via STING, shaping microglial phenotype and accelerating disease progression. *Glia* (2019) 67:1254–76. doi: 10.1002/glia.23592
103. Deczkowska A, Baruch K, Schwartz M. Type I/II Interferon Balance in the Regulation of Brain Physiology and Pathology. *Trends Immunol* (2016) 37:181–92. doi: 10.1016/j.it.2016.01.006
104. Hosseini S, Michaelsen-Preusse K, Grigoryan G, Chhatbar C, Kalinke U, Korte M. Type I Interferon Receptor Signaling in Astrocytes Regulates Hippocampal Synaptic Plasticity and Cognitive Function of the Healthy CNS. *Cell Rep* (2020) 31:107666. doi: 10.1016/j.celrep.2020.107666
105. Ward GA, McGraw K, McLemore AF, Lam NB, Hou H-A, Meyer BS, et al. Oxidized Mitochondrial DNA Engages TLR9 to Activate the NLRP3 Inflammasome in Myelodysplastic Syndromes. *Blood* (2019) 134:774–4. doi: 10.1182/blood-2019-122358
106. Bruno DCF, Donatti A, Martin M, Almeida VS, Geraldis JC, Oliveira FS, et al. Circulating nucleic acids in the plasma and serum as potential biomarkers in neurological disorders. *Braz J Med Biol Res = Rev Bras Pesqui medicas e Biol* (2020) 53:e9881. doi: 10.1590/1414-431x20209881
107. Otandault A, Abraham JD, Al Amir Dache Z, Khalyfa A, Jariel-Encontre I, Forné T, et al. Hypoxia differently modulates the release of mitochondrial and nuclear DNA. *Br J Cancer* (2020) 122:715–25. doi: 10.1038/s41416-019-0716-y
108. Baruch K, Deczkowska A, David E, Castellano JM, Miller O, Kertser A, et al. Aging-induced type I interferon response at the choroid plexus negatively affects brain function. *Sci (80-)* (2014) 346:89–93. doi: 10.1126/science.1252945
109. Klein RS, Garber C, Funk KE, Salimi H, Soung A, Kanmogne M, et al. Neuroinflammation During RNA Viral Infections. *Annu Rev Immunol* (2019) 37:73–95. doi: 10.1146/annurev-immunol-042718-041417
110. Pestka S, Krause CD, Walter MR. Interferons, interferon-like cytokines, and their receptors. *Immunol Rev* (2004) 202:8–32. doi: 10.1111/j.0105-2896.2004.00204.x
111. Vainchtein ID, Molofsky AV. Astrocytes and Microglia: In Sickness and in Health. *Trends Neurosci* (2020) 43:144–54. doi: 10.1016/j.tins.2020.01.003
112. Niederkorn JY. See no evil, hear no evil, do no evil: The lessons of immune privilege. *Nat Immunol* (2006) 7:354–9. doi: 10.1038/ni1328
113. Forrester JV, McMenamin PG, Dando SJ. CNS infection and immune privilege. *Nat Rev Neurosci* (2018) 19:655–71. doi: 10.1038/s41583-018-0070-8
114. Louveau A, Smirnov I, Keyes TJ, Eccles JD, Rouhani SJ, Peske JD, et al. Structural and functional features of central nervous system lymphatic vessels. *Nature* (2015) 523:337–41. doi: 10.1038/nature14432
115. Wu D, Sanin DE, Everts B, Chen Q, Qiu J, Buck MD, et al. Type 1 Interferons Induce Changes in Core Metabolism that Are Critical for Immune Function. *Immunity* (2016) 44:1325–36. doi: 10.1016/j.immuni.2016.06.006
116. Buck MDD, O'Sullivan D, Klein Geltink RII, Curtis JDD, Chang CH, Sanin DEE, et al. Mitochondrial Dynamics Controls T Cell Fate through Metabolic Programming. *Cell* (2016) 166:63–76. doi: 10.1016/j.cell.2016.05.035
117. Zhang W, Wang G, Xu Z-G, Zhang X, Li H, Lin H-K. Lactate Is a Natural Suppressor of RLR Signaling by Targeting MAVS. *Cell* (2019) 178:176–89. doi: 10.1016/j.cell.2019.05.003
118. Reikine S, Nguyen JB, Modis Y. Pattern recognition and signaling mechanisms of RIG-I and MDA5. *Front Immunol* (2014) 5:342. doi: 10.3389/fimmu.2014.00342
119. Ren Z, Ding T, Zuo Z, Xu Z, Deng J, Wei Z. Regulation of MAVS Expression and Signaling Function in the Antiviral Innate Immune Response. *Front Immunol* (2020) 11:1030. doi: 10.3389/fimmu.2020.01030
120. Chao CC, Gutiérrez-Vázquez C, Rothhammer V, Mayo L, Wheeler MA, Tjon EC, et al. Metabolic Control of Astrocyte Pathogenic Activity via cPLA2-MAVS. *Cell* (2019) 179:1483–98.e22. doi: 10.1016/j.cell.2019.11.016
121. Fecher C, Trovò L, Müller SA, Snaidero N, Wettmarshausen J, Heink S, et al. Cell-type-specific profiling of brain mitochondria reveals functional and molecular diversity. *Nat Neurosci* (2019) 22:1731–42. doi: 10.1038/s41593-019-0479-z
122. Hernández-Corbacho MJ, Salama MF, Canals D, Senkal CE, Obeid LM. Sphingolipids in mitochondria. *Biochim Biophys Acta - Mol Cell Biol Lipids* (2017) 1862:56–68. doi: 10.1016/j.bbalip.2016.09.019
123. Bradl M, Lassmann H. Oligodendrocytes: Biology and pathology. *Acta Neuropathol* (2010) 119:37–53. doi: 10.1007/s00401-009-0601-5
124. Peterson LK, Fujinami RS. Inflammation, demyelination, neurodegeneration and neuroprotection in the pathogenesis of multiple sclerosis. *J Neuroimmunol* (2007) 184:37–44. doi: 10.1016/j.jneuroim.2006.11.015
125. Rose J, Brian C, Woods J, Pappa A, Panayiotidis MI, Powers R, et al. Mitochondrial dysfunction in glial cells: Implications for neuronal homeostasis and survival. *Toxicology* (2017) 391:109–15. doi: 10.1016/j.tox.2017.06.011
126. Pelvig DP, Pakkenberg H, Stark AK, Pakkenberg B. Neocortical glial cell numbers in human brains. *Neurobiol Aging* (2008) 29:1754–62. doi: 10.1016/j.neurobiolaging.2007.04.013
127. Jellinger KA. Basic mechanisms of neurodegeneration: A critical update. *J Cell Mol Med* (2010) 14:457–87. doi: 10.1111/j.1582-4934.2010.01010.x
128. Jarjour A a, Zhang H, Bauer N, Ffrench-Constant C, Williams A. In vitro modeling of central nervous system myelination and remyelination. *Glia* (2012) 60:1–12. doi: 10.1002/glia.21231
129. Rinholm JE, Vervaeke K, Tadross MR, Tkachuk AN, Kopek BG, Brown TA, et al. Movement and structure of mitochondria in oligodendrocytes and their myelin sheaths. *Glia* (2016) 64:810–25. doi: 10.1002/glia.22965
130. Pope S, Land JM, Heales SJR. Oxidative stress and mitochondrial dysfunction in neurodegeneration; cardiolipin a critical target? *Biochim Biophys Acta - Bioenerg* (2008) 1777:794–9. doi: 10.1016/j.bbabio.2008.03.011
131. Philips T, Rothstein JD. Oligodendroglia: Metabolic supporters of neurons. *J Clin Invest* (2017) 127:3271–80. doi: 10.1172/JCI90610
132. Minchenberg SB, Massa PT. The control of oligodendrocyte bioenergetics by interferon-gamma (IFN-γ) and Src homology region 2 domain-containing phosphatase-1 (SHP-1). *J Neuroimmunol* (2019) 331:46–57. doi: 10.1016/j.jneuroim.2017.10.015
133. Luo F, Herrup K, Qi X, Yang Y, Yang Y. Inhibition of Drp1 hyper-activation is protective in animal models of experimental multiple sclerosis Correspondence to HHS Public Access. *Exp Neurol* (2017) 292:21–34. doi: 10.1016/j.expneurol.2017.02.015
134. Balabanov R, Strand K, Goswami R, McMahon E, Begolka W, Miller SD, et al. Interferon-γ-oligodendrocyte interactions in the regulation of experimental autoimmune encephalomyelitis. *J Neurosci* (2007) 27:2013–24. doi: 10.1523/JNEUROSCI.4689-06.2007
135. Jana A, Hogan EL, Pahan K. Ceramide and neurodegeneration: Susceptibility of neurons and oligodendrocytes to cell damage and death. *J Neurol Sci* (2009) 278:5–15. doi: 10.1016/j.jns.2008.12.010
136. Vandanmagsar B, Youm Y-H, Ravussin A, Galgani JE, Stadler K, Mynatt RL, et al. The NLRP3 inflammasome instigates obesity-induced inflammation and insulin resistance. *Nat Med* (2011) 17:179–88. doi: 10.1038/nm.2279
137. Novgorodov SA, Wu BX, Gudz TI, Bielawski J, Ovchinnikova TV, Hannun YA, et al. Novel pathway of ceramide production in mitochondria: Thioesterase and neutral ceramidase produce ceramide from sphingosine and acyl-CoA. *J Biol Chem* (2011) 286:25352–62. doi: 10.1074/jbc.M110.214866
138. Singh I, Pahan K, Khan M, Singh AK. Cytokine-mediated induction of ceramide production is redox-sensitive: Implications to proinflammatory

cytokine-mediated apoptosis in demyelinating diseases. *J Biol Chem* (1998) 273:20354–62. doi: 10.1074/jbc.273.32.20354
139. Pal S, Rao GN, Pal A. High glucose-induced ROS accumulation is a critical regulator of ERK1/2-Akt-tuberin-mTOR signalling in RGC-5 cells. *Life Sci* (2020) 256:117914. doi: 10.1016/j.lfs.2020.117914
140. Harris J, Deen N, Zamani S, Hasnat MA. Mitophagy and the release of inflammatory cytokines. *Mitochondrion* (2018) 41:2–8. doi: 10.1016/j.mito.2017.10.009
141. Bader V, Winklhofer KF. Mitochondria at the interface between neurodegeneration and neuroinflammation. *Semin Cell Dev Biol* (2019) 99:163–71. doi: 10.1016/j.semcdb.2019.05.028
142. Gao P, Ascano M, Zillinger T, Wang W, Dai P, Serganov AA, et al. Structure-function analysis of STING activation by c[G(2′,5′) pA(3′,5′)p] and targeting by antiviral DMXAA. *Cell* (2013) 154:748–62. doi: 10.1016/j.cell.2013.07.023
143. Ishikawa H, Barber GN. STING is an endoplasmic reticulum adaptor that facilitates innate immune signalling. *Nature* (2008) 455:674–8. doi: 10.1038/nature07317
144. Motwani M, Pesiridis S, Fitzgerald KA. DNA sensing by the cGAS–STING pathway in health and disease. *Nat Rev Genet* (2019) 20:657–74. doi: 10.1038/s41576-019-0151-1
145. Reshi L, Wang H-V, Hong J-R. Modulation of Mitochondria During Viral Infections. In: *Mitochondrial Diseases*. London, UK: InTech. doi: 10.5772/intechopen.73036
146. Chin AC. PERK-STING signaling drives neuroinflammation in traumatic brain injury. *J Neurosci* (2020) 40:2384–6. doi: 10.1523/JNEUROSCI.2881-19.2020
147. Chen Q, Sun L, Chen ZJ. Regulation and function of the cGAS-STING pathway of cytosolic DNA sensing. *Nat Immunol* (2016) 17:1142–9. doi: 10.1038/ni.3558
148. Gaidt MM, Ebert TS, Chauhan D, Ramshorn K, Pinci F, Zuber S, et al. The DNA Inflammasome in Human Myeloid Cells Is Initiated by a STING-Cell Death Program Upstream of NLRP3. *Cell* (2017) 171:1110–24.e18. doi: 10.1016/j.cell.2017.09.039
149. Banerjee I, Behl B, Mendonca M, Sarkar SN, Fitzgerald KA, Rathinam Correspondence VAK. Gasdermin D Restrains Type I Interferon Response to Cytosolic DNA by Disrupting Ionic Homeostasis. *Immunity* (2018) 49:413–26.e5. doi: 10.1016/j.immuni.2018.07.006
150. Aarreberg LD, Esser-Nobis K, Driscoll C, Shuvarikov A, Roby JA, Gale M. Interleukin-1β Induces mtDNA Release to Activate Innate Immune Signaling via cGAS-STING. *Mol Cell* (2019) 74:801–15.e6. doi: 10.1016/j.molcel.2019.02.038
151. Hewett SJ, Jackman NA, Claycomb RJ. Interleukin-1β in Central Nervous System Injury and Repair. *Eur J Neurodegener Dis* (2012) 1:195–211.
152. Xu Q, Xu W, Cheng H, Yuan H, Tan X. Efficacy and mechanism of cGAMP to suppress Alzheimer's disease by elevating TREM2. *Brain Behav Immun* (2019) 81:495–508. doi: 10.1016/j.bbi.2019.07.004
153. Wuertz KMG, Treuting PM, Hemann EA, Esser-Nobis K, Snyder AG, Graham JB, et al. STING is required for host defense against neuropathological West Nile virus infection. *PloS Pathog* (2019) 15. doi: 10.1371/journal.ppat.1007899
154. Mathur V, Burai R, Vest RT, Bonanno LN, Lehallier B, Zardeneta ME, et al. Activation of the STING-Dependent Type I Interferon Response Reduces Microglial Reactivity and Neuroinflammation. *Neuron* (2017) 96:1290–302.e6. doi: 10.1016/j.neuron.2017.11.032
155. Sliter DA, Martinez J, Hao L, Chen X, Sun N, Fischer TD, et al. Parkin and PINK1 mitigate STING-induced inflammation HHS Public Access. *Nature* (2018) 561:258–62. doi: 10.1038/s41586-018-0448-9
156. Li XX, Tsoi B, Li YF, Kurihara H, He RR. Cardiolipin and Its Different Properties in Mitophagy and Apoptosis. *J Histochem Cytochem* (2015) 63:301–11. doi: 10.1369/0022155415574818
157. Nagashima S, Takeda K, Ohno N, Ishido S, Aoki M, Saitoh Y, et al. MITOL deletion in the brain impairs mitochondrial structure and ER tethering leading to oxidative stress. *Life Sci Alliance* (2019) 2. doi: 10.26508/lsa.201900308
158. Chao H, Anthonymuthu TS, Kenny EM, Amoscato AA, Cole LK, Hatch GM, et al. Disentangling oxidation/hydrolysis reactions of brain mitochondrial cardiolipins in pathogenesis of traumatic injury. *JCI Insight* (2018) 3. doi: 10.1172/jci.insight.97677
159. Pointer CB, Wenzel TJ, Klegeris A. Extracellular cardiolipin regulates select immune functions of microglia and microglia-like cells. *Brain Res Bull* (2019) 146:153–63. doi: 10.1016/j.brainresbull.2019.01.002
160. Pointer CB, Klegeris A. Cardiolipin in Central Nervous System Physiology and Pathology. *Cell Mol Neurobiol* (2017) 37:1161–72. doi: 10.1007/s10571-016-0458-9
161. Paradies G, Paradies V, De Benedictis V, Ruggiero FM, Petrosillo G. Functional role of cardiolipin in mitochondrial bioenergetics. *Biochim Biophys Acta - Bioenerg* (2014) 1837:408–17. doi: 10.1016/j.bbabio.2013.10.006
162. Aitken RJ, Wingate JK, De Iuliis GN, Koppers AJ, McLaughlin EA. Cis-unsaturated fatty acids stimulate reactive oxygen species generation and lipid peroxidation in human spermatozoa. *J Clin Endocrinol Metab* (2006) 91:4154–63. doi: 10.1210/jc.2006-1309
163. Ghio S, Camilleri A, Caruana M, Ruf VC, Schmidt F, Leonov A, et al. Cardiolipin Promotes Pore-Forming Activity of Alpha-Synuclein Oligomers in Mitochondrial Membranes. *ACS Chem Neurosci* (2019) 10:3815–29. doi: 10.1021/acschemneuro.9b00320
164. Ryan T, Bamm VV, Stykel MG, Coackley CL, Humphries KM, Jamieson-Williams R, et al. Cardiolipin exposure on the outer mitochondrial membrane modulates α-synuclein. *Nat Commun* (2018) 9:1–17. doi: 10.1038/s41467-018-03241-9
165. Díaz-Quintana A, Pérez-Mejías G, Guerra-Castellano A, De La Rosa MA, Díaz-Moreno I. Wheel and Deal in the Mitochondrial Inner Membranes: The Tale of Cytochrome c and Cardiolipin. *Oxid Med Cell Longev* (2020) 2020:1–20. doi: 10.1155/2020/6813405
166. Chu CT, Bayir H, Kagan VE. LC3 binds externalized cardiolipin on injured mitochondria to signal mitophagy in neurons: Implications for Parkinson disease. *Autophagy* (2014) 10:376–8. doi: 10.4161/auto.27191
167. Lamkanfi M, Dixit VM. Mechanisms and functions of inflammasomes. *Cell* (2014) 157:1013–22. doi: 10.1016/j.cell.2014.04.007
168. He Y, Hara H, Núñez G. Mechanism and Regulation of NLRP3 Inflammasome Activation. *Trends Biochem Sci* (2016) 41:1012–21. doi: 10.1016/j.tibs.2016.09.002
169. Swanson KV, Deng M, Ting JPY. The NLRP3 inflammasome: molecular activation and regulation to therapeutics. *Nat Rev Immunol* (2019) 19:477–89. doi: 10.1038/s41577-019-0165-0
170. Murakami T, Ockinger J, Yu J, Byles V, McColl A, Hofer AM, et al. Critical role for calcium mobilization in activation of the NLRP3 inflammasome. *Proc Natl Acad Sci U S A* (2012) 109:11282–7. doi: 10.1073/pnas.1117765109
171. Rossol M, Pierer M, Raulien N, Quandt D, Meusch U, Rothe K, et al. Extracellular Ca2+ is a danger signal activating the NLRP3 inflammasome through G protein-coupled calcium sensing receptors. *Nat Commun* (2012) 3:1–9. doi: 10.1038/ncomms2339
172. Lee GS, Subramanian N, Kim AI, Aksentijevich I, Goldbach-Mansky R, Sacks DB, et al. The calcium-sensing receptor regulates the NLRP3 inflammasome through Ca2+ and cAMP. *Nature* (2012) 492:123–7. doi: 10.1038/nature11588
173. Zhang Z, Meszaros G, He WT, Xu Y, Magliarelli H de F, Mailly L, et al. Protein kinase D at the Golgi controls NLRP3 inflammasome activation. *J Exp Med* (2017) 214:2671–93. doi: 10.1084/jem.20162040
174. Heid ME, Keyel PA, Kamga C, Shiva S, Watkins SC, Salter RD. Mitochondrial Reactive Oxygen Species Induces NLRP3-Dependent Lysosomal Damage and Inflammasome Activation. *J Immunol* (2013) 191:5230–8. doi: 10.4049/jimmunol.1301490
175. Won JH, Park S, Hong S, Son S, Yu JW. Rotenone-induced Impairment of Mitochondrial Electron Transport Chain Confers a Selective Priming Signal for NLRP3 Inflammasome Activation. *J Biol Chem* (2015) 290:27425–37. doi: 10.1074/jbc.M115.667063
176. Shimada K, Crother TR, Karlin J, Dagvadorj J, Chiba N, Chen S, et al. Oxidized Mitochondrial DNA Activates the NLRP3 Inflammasome during Apoptosis. *Immunity* (2012) 36:401–14. doi: 10.1016/j.immuni.2012.01.009
177. Voet S, Srinivasan S, Lamkanfi M, Van Loo G. Inflammasomes in neuroinflammatory and neurodegenerative diseases. *EMBO Mol Med* (2019) 11:10248. doi: 10.15252/emmm.201810248
178. Voet S, Mc Guire C, Hagemeyer N, Martens A, Schroeder A, Wieghofer P, et al. A20 critically controls microglia activation and inhibits inflammasome-

dependent neuroinflammation. *Nat Commun* (2018) 9:1–15. doi: 10.1038/s41467-018-04376-5

179. Inoue M, Shinohara ML. The role of interferon-β in the treatment of multiple sclerosis and experimental autoimmune encephalomyelitis - in the perspective of inflammasomes. *Immunology* (2013) 139:11–8. doi: 10.1111/imm.12081
180. Halle A, Hornung V, Petzold GC, Stewart CR, Monks BG, Reinheckel T, et al. The NALP3 inflammasome is involved in the innate immune response to amyloid-beta. *Nat Immunol* (2008) 9(8):857–65. doi: 10.1038/ni.1636
181. Gordon R, Albornoz EA, Christie DC, Langley MR, Kumar V, Mantovani S, et al. Inflammasome inhibition prevents -synuclein pathology and dopaminergic neurodegeneration in mice. *Sci Transl Med* (2018) 10. doi: 10.1126/scitranslmed.aah4066
182. Wei P, Yang F, Zheng Q, Tang W, Li J. The potential role of the NLRP3 inflammasome activation as a link between mitochondria ROS generation and neuroinflammation in postoperative cognitive dysfunction. *Front Cell Neurosci* (2019) 13:73. doi: 10.3389/fncel.2019.00073
183. Sarkar S, Malovic E, Harishchandra DS, Ghaisas S, Panicker N, Charli A, et al. Mitochondrial impairment in microglia amplifies NLRP3 inflammasome proinflammatory signaling in cell culture and animal models of Parkinson's disease. *NPJ Park Dis* (2017) 3:1–15. doi: 10.1038/s41531-017-0032-2

Conflict of Interest: The authors declare that the research was conducted in the absence of any commercial or financial relationships that could be construed as a potential conflict of interest.

frontiers in Immunology

REVIEW
published: 03 September 2021
doi: 10.3389/fimmu.2021.695257

Mitochondria in Injury, Inflammation and Disease of Articular Skeletal Joints

James Orman Early[1†], *Lauren E. Fagan*[1,2*†], *Annie M. Curtis*[2] *and Oran D. Kennedy*[1,3*]

[1] Department of Anatomy and Regenerative Medicine and Tissue Engineering Research Group, Royal College of Surgeons in Ireland, Dublin, Ireland, [2] School of Pharmacy and Biomolecular Sciences and Tissue Engineering Research Group, Royal College of Surgeons in Ireland, Dublin, Ireland, [3] Department of Mechanical and Manufacturing Engineering, Trinity College Dublin, Dublin, Ireland

Inflammation is an important biological response to tissue damage caused by injury, with a crucial role in initiating and controlling the healing process. However, dysregulation of the process can also be a major contributor to tissue damage. Related to this, although mitochondria are typically thought of in terms of energy production, it has recently become clear that these important organelles also orchestrate the inflammatory response *via* multiple mechanisms. Dysregulated inflammation is a well-recognised problem in skeletal joint diseases, such as rheumatoid arthritis. Interestingly osteoarthritis (OA), despite traditionally being known as a 'non-inflammatory arthritis', now appears to involve an element of chronic inflammation. OA is considered an umbrella term for a family of diseases stemming from a range of aetiologies (age, obesity etc.), but all with a common presentation. One particular OA sub-set called Post-Traumatic OA (PTOA) results from acute mechanical injury to the joint. Whether the initial mechanical tissue damage, or the subsequent inflammatory response drives disease, is currently unclear. In the former case; mechanobiological properties of cells/tissues in the joint are a crucial consideration. Many such cell-types have been shown to be exquisitely sensitive to their mechanical environment, which can alter their mitochondrial and cellular function. For example, in bone and cartilage cells fluid-flow induced shear stresses can modulate cytoskeletal dynamics and gene expression profiles. More recently, immune cells were shown to be highly sensitive to hydrostatic pressure. In each of these cases mitochondria were central to these responses. In terms of acute inflammation, mitochondria may have a pivotal role in linking joint tissue injury with chronic disease. These processes could involve the immune cells recruited to the joint, native/resident joint cells that have been damaged, or both. Taken together, these observations suggest that mitochondria are likely to play an important role in linking acute joint tissue injury, inflammation, and long-term chronic joint degeneration - and that the process involves mechanobiological factors. In this review, we will explore the links between mechanobiology, mitochondrial function, inflammation/tissue-damage in joint injury and disease. We will also explore some emerging mitochondrial therapeutics and their potential for application in PTOA.

Keywords: mitochondria, cartilage, osteoarthritis, inflammation, mechanobiology

OPEN ACCESS

Edited by:
Pedro Manoel Mendes Moraes Vieira, State University of Campinas, Brazil

Reviewed by:
Rubina Shaikh, University of Eastern Finland, Finland
Angela Castoldi, Federal University of Pernambuco, Brazil

***Correspondence:**
Oran D. Kennedy
orankennedy@rcsi.ie
Lauren E. Fagan
laurenfagan@rcsi.ie

[†]*These authors have contributed equally to this work*

Specialty section:
This article was submitted to Molecular Innate Immunity, a section of the journal Frontiers in Immunology

Received: *14 April 2021*
Accepted: *30 July 2021*
Published: *03 September 2021*

Citation:
Early JO, Fagan LE, Curtis AM and Kennedy OD (2021) Mitochondria in Injury, Inflammation and Disease of Articular Skeletal Joints. Front. Immunol. 12:695257. doi: 10.3389/fimmu.2021.695257

INTRODUCTION

Osteoarthritis (OA) is the most commonly occurring form of joint disease worldwide, affecting approximately 3% of the global population (1). The primary hallmark of OA is the degeneration of articular cartilage, but dysregulation in other joint tissues such as subchondral bone and synovium are also significant factors (2). Joint degeneration results in debilitating stiffness and pain, with major societal and economic implications. Despite the widespread prevalence of OA, and its significant consequences, disease modifying treatments are lacking. Current treatment options are confined to either conservative (physical therapy, exercise, or pain management) or surgical (joint replacement) approaches (3). OA is often associated with aging, but other risk factors such as age, obesity and steroid use exist (4). In addition, acute injury that involves damage of the primary joint tissues (such as the anterior cruciate ligament rupture in the knee), is also a well-established risk factor for joint degeneration – even in relatively young cohorts. The version of disease which develops in this scenario is called Post-traumatic OA (PTOA). PTOA makes up approximately 12% of the overall disease burden of OA and this proportion is set to increase due to increased intensity of exercise/activity being taken up by ever younger age-groups (5). The initial inflammatory response to the injury, driven by a host of molecular and cellular mechanisms, are likely to "set the course" of subsequent disease progression (6). However precisely how the inflammatory response drive resident joint cells into a state of chronic dysfunction is unknown. Interestingly, recent advances in the field suggest a role for altered mitochondrial function as part of the inflammatory response to injury (7), which may be linked to subsequent chronic degeneration. In this review, we will specifically address the links between mitochondrial function, inflammation, and joint disease (**Figure 1**). We will also explore recent advances in mechanobiology and how this may relate to PTOA.

JOINT CELLS AND IMMUNE CELLS ARE INVOLVED IN PTOA DEVELOPMENT

Although many cell types and tissues exist within the joint, it is cartilage and its degeneration which is the central focus of OA (2). Chondrocytes which are the primary resident cells in articular cartilage, are unique in that they exist in an aneural, alymphatic and avascular microenvironment (8). The cartilage extracellular matrix (ECM) is mostly comprised of collagen and proteoglycans (as well as water) (9) all of which are produced by chondrocytes under normal healthy circumstances,. However post-injury, chondrocytes begin to produce enzymes (such as metalloproteases (MMP) and aggrecanases) which are harmful to the ECM (10). This process occurs *via* activation of various pathways such as NF-kB and MAP kinases and is also linked to

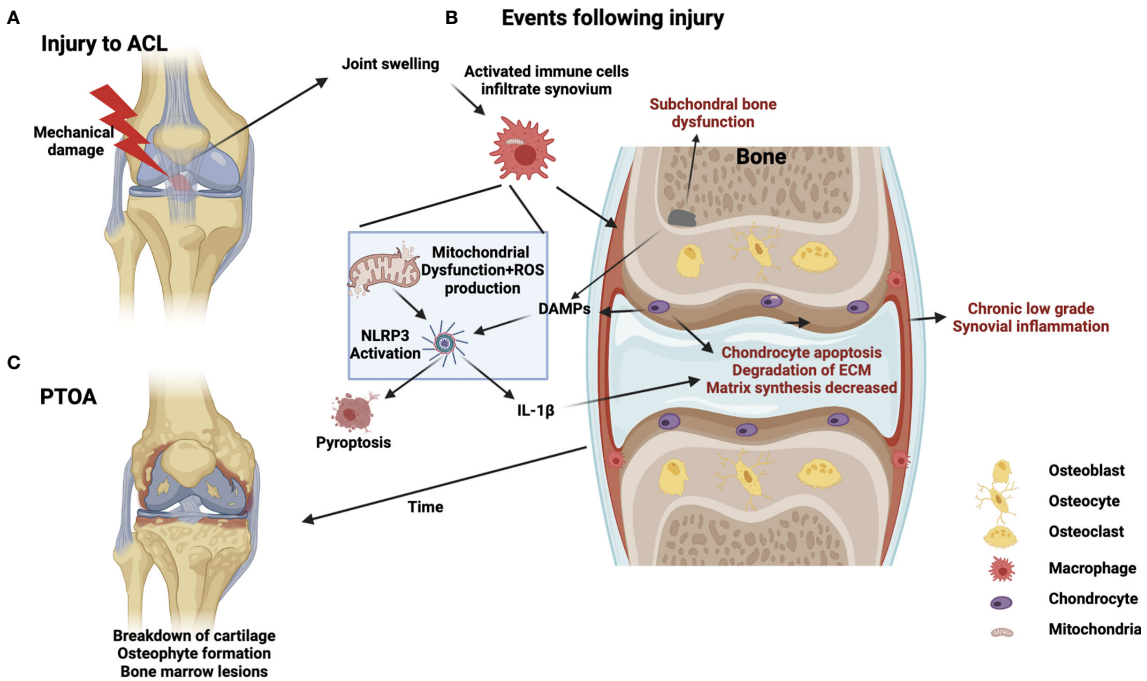

FIGURE 1 | Schematic of PTOA progression illustrating potential mitochondrial involvement in injury, inflammation, and disease. **(A)** Acute injury, such as ACL rupture, results in joint swelling and infiltration of immune cells. **(B)** Crosstalk between immune cells, chondrocytes and subchondral bone cells occurs involving DAMPS, PRRs, mechanotransduction, NLRP3 activation, cell-death/pyroptosis, mitochondrial dysfunction, cytokine release and ROS production from immune cells generating a feed-forward loop to drive chronic inflammation, matrix degradation and subchondral bone dysfunction **(C)** Chronic development of PTOA, long-term low-grade inflammation, bone marrow lesions and cartilage degeneration.

increased production of Reactive Oxygen Species (ROS), originating from mitochondria (11, 12). These degradative proteases gradually disrupt the collagen network, promoting a loss of proteoglycans and drive degradative changes in the matrix which in turn feeds back to affect chondrocyte health and function (13). Alongside these disruptive changes, the production of collagens and aggrecans, which are required for health homeostasis, are dramatically reduced (14, 15). This switch, whereby chondrocytes reduce production of beneficial ECM proteins, and increase production of harmful enzymes, is thought to involve altered mitochondrial function (16). Injury also has the effect of increasing crosstalk between cartilage and surrounding joint tissues such as subchondral bone and the synovial membrane (17). The latter of which is the central source of acute inflammatory factors as it becomes quickly infiltrated by activated immune cells in response to joint injury (18). Whether immune cells are the initiator of the degenerative switch within the damaged joint or an additional contributor to disease, is not entirely known. Nonetheless it is becoming increasingly clear that immune cells are central to PTOA development. At the cellular level, within the damaged joint, synovial macrophages, fibroblasts and infiltrating monocytes, and T-cells, B-cells, natural killer cells and dendritic cells are all involved in responding to injury and driving local inflammation (19, 20). It now appears likely that crosstalk also occurs between these immune cells and chondrocytes/subchondral bone populations. While the nature of this relationship is unclear it is well established that mitochondrial function governs many aspects of immune function and may play a role in this situation (21, 22). This is especially well documented in macrophages, in which mitochondrial dynamics and function regulate cellular trafficking, cytokine production, phagocytosis and wound repair. While these processes have been well documented in multiple macrophage subtypes, it is yet unclear if they hold true in every population of macrophage that may be involved in PTOA development, such as bone marrow macrophages, osteal macrophages and macrophage like synoviocytes. However, it is conceivable that the mitochondrial changes produce similar effects in these cells and that changes in mitochondrial function influence and drive the development of PTOA after injury. Thus, understanding the details of events that occurs between immune and joint cell-types, in the aftermath of injury, and in particular the role of mitochondria will be crucial in developing new treatments to prevent disease progression.

JOINT INJURY, INFLAMMATION AND MECHANOBIOLOGY HAVE A ROLE IN DEVELOPMENT OF PTOA

Originally, the process of inflammation was not deemed to be a central factor in the aetiology of OA. Indeed historically it has been known as 'non-inflammatory OA', especially when compared to highly inflammatory versions of arthritis such as rheumatoid, psoriatic, and juvenile arthritis. However, it is now established that the persistence of a dysregulated inflammatory response does impact on PTOA (18). Intriguingly, mitochondrial activities have also recently been shown to be significantly modulated by these inflammatory stimuli (23), as well as by other factors such as mechanical stimulus. Therefore, understanding mitochondrial function (including morphology/metabolism) within joint cells in response to injury, may provide new insights in terms of the pathology of PTOA and therapeutic development.

Despite lacking an underlying mechanism to describe the link between mechanical injury and inflammation, it is clear that mechanical joint damage causes migration of immune cells from the circulation through the synovial membrane and into the synovial fluid (19, 20). Injury also causes a certain proportion of cell death in the region. This cell death results in the production of damage associated molecular patterns (DAMPs), which are then detected by Toll-Like Receptor (TLR) proteins on cell surfaces (24). These further promote inflammatory cascades and cell and fluid infiltration and thus a damaging feed-back loop is established. One central mechanism by which DAMPs have been shown to promote inflammation in the joint is *via* activation of the NLRP3 inflammasome in macrophages and subsequent production of IL-1β (25). This mechanism will be discussed in detail below, specifically in the context of joint injury.

IL-1B IS CENTRAL TO TISSUE DAMAGE, INFLAMMATION AND MITOCHONDRIAL RESPONSES TO INJURY

IL-1β is a highly pro-inflammatory cytokine that is involved in a wide variety of disease states and is also increased in cases of OA (26). Specifically, in this scenario, IL-1β is capable of shifting chondrocytes to a catabolic state (27) thus providing a direct link between joint injury, immune cell mitochondria and cartilage degeneration. The specific details of how chondrocytes respond to IL-1β have been studied extensively *in vitro* (27, 28), but importantly it has also been shown to be present in significant quantities in synovial fluid immediately after injury (6) (along with some of its important precursors, such as NLRP3 (29) and other DAMPs [Basic Calcium Phosphate (BSU) (30), monosodium urate (MSU) (31) and ATP (32)]. Intriguingly, IL-1β levels remain elevated for months post-injury (18, 33). Thus, this is likely to be a primary mediator in the pathological process that begins with joint injury and leads to disease. An interesting supporting example of this stems from the large Canakinumab Anti-Inflammatory Thrombosis Outcomes Study (CANTOS), which involved >10,000 patients. CANTOS was a randomized, double-blinded, placebo-controlled trial that investigated the use of canakinumab, a monoclonal antibody targeting IL-1β, on high-risk patients with established atherosclerotic disease who had survived a myocardial infarction (MI) (34). Post-hoc retrospective analyses of this cohort, found that canakinumab treatment was associated with reduced rates of joint replacement as well as OA symptoms. Regulation of IL-1β occurs at both the transcriptional and post-translational levels – and both of these

processes have been shown to be mediated by mitochondria which we will detail further below.

Since this cytokine plays such a central role in the response to injury, it seems reasonable to consider it as a potential target for direct OA prevention – following the encouraging data that emerged from the CANTOS trial (34). In fact, treatment strategies that directly target IL-1β and/or its cognate receptor (IL-1R) have been tested (26). However, somewhat surprisingly, these efforts have achieved only limited success. One potential reason for this is that targeting any aspect of the IL-1β pathway, once it has been activated, may be a case of 'too little, too late'. In order for IL-1β to be released from cells like macrophages it must first be cleaved by an intracellular complex called the inflammasome (25). The inflammasome is a multi-protein complex that responds to both pathogenic micro-organisms and, of direct relevance here, DAMPs which are released within the joint after injury (25). The inflammasome is thus an obligate precursor step to IL-1β activation and most importantly to its release. Targeting inflammasome activation and thus the release of IL-1β may prove to be a more promising therapeutic strategy than targeting released IL-1β in the joint which may already have exerted its catabolic effect on chondrocytes. There are multiple inflammasomes that respond to a host of different signals. However, one in particular called NLRP3 is the most likely candidate for involvement in joint inflammation and responses to DAMP signalling. The NLPR3 inflammasome is composed of (1) a receptor protein called NLRP3, (2) an adaptor molecule called ASC, and (3) Caspase 1 (25). Once NLRP3 senses an activating signal, it oligomerises with ASC and Caspase-1. This activates Caspase-1 allowing it to cleave IL-1β into its active form. This entire process has been shown to be under mitochondrial control. Specifically, high mitochondrial membrane potential (35), mitochondrial ROS (36) and mtDNA (37) are all involved in regulating inflammasome activation. Of equal importance, is the fact that inflammasome activation is also closely linked to the process of pyroptosis, a specific form of inflammatory cell-death - also regulated by mitochondria (38). Pyroptosis also ultimately results in IL-1β release, as well as other inflammatory factors and DAMPs that could potentiate the inflammatory response and drive cartilage degeneration further.

MULTIPLE JOINT TISSUES ARE INVOLVED IN INFLAMMATION AFTER INJURY

The source(s) of NLRP3 in the injured joint have not been explicitly identified; however the synovial tissues are an extremely promising candidate - since they have a central role in other examples of joint inflammation. Synoviocytes are the resident cell types of this tissue, (with two sub-types: fibroblasts and 'Macrophage Like Synoviocytes [MLS]') and both have been shown to produce high levels of NLRP3 in culture conditions (29, 39). Interestingly, a very recent study has shown that chondrocytes *in vitro* are also capable of expressing inflammasome components and can undergo NLRP3 activation, pyroptosis and IL-1β release when stimulated with LPS and ATP *in vitro* (40). While TLRs are known to be present in chondrocytes, and their expression to be altered in OA (41), the presence of chondrocyte specific inflammasomes is a recent and novel development. These interesting findings must still be balanced against other inflammatory pathways, activated by TNFα for example, which do not act through TLRs, but still increase MMP activity, suggesting that IL-1β may not be the only driver of OA progression. It has also been proposed that even in the presence of NLRP3, ASC and Caspase 1 in chondrocytes, OA cartilage is unable to produce active IL-1β (42). However, these studies used isolated cartilage explant models which lack externally infiltrating immune cells, which are likely to be central to IL-1β release and, thus NLRP3 activity.

Subchondral bone is also known to be involved in the early post-injury phase, evident by the presence of Bone Marrow Lesions (BMLs) in most cases of acute joint injury (17). However, NLRP3 activity has yet to be identified in native bone cells in the osteoblast lineage. Intriguingly however, hydroxyapatite, which is the primary inorganic component of bone tissue, is the predominant form of BCP crystal found in OA joints (43, 44). It is possible that following injury, hydroxyapatite is indirectly released into the joint, following increased subchondral remodelling, (which has been also shown to occur early after injury) or in relation to osteophytes which form later in the disease process. Hydroxyapatite drives NLRP3 activation in macrophages *in vitro* and *in vivo* through potassium efflux and ROS dependant mechanisms (45). Direct delivery of BCP crystals to mouse knees was shown to cause synovial macrophage infiltration, chondrocyte death, synovitis, and cartilage degeneration (46, 47). However, this study concluded that this mechanism was NLRP3 and IL-1 independent. A similar study showed that BCP crystals also impact on macrophage metabolism, creating a shift from oxidative phosphorylation to a glycolytic phenotype, and promoting the expression of the highly pro-inflammatory transcription factor HIF-1α48). Thus subchondral bone and its release of hydroxyapatite may be a novel target tissue for indirect modulation of NLRP3 function and macrophage metabolism.

Taken together, these findings suggest that NLRP3 activation, which is tightly regulated by mitochondrial activities, may have an important role in damage responses of multiple joint tissues. Whether there is one critical cellular source leading to NLRP3 activation, or an aggregated combination of many, has yet to be determined. Nonetheless NLRP3, as an obligate gate-keeper of IL-1β activation, potentially in multiple joint tissues, is a prime target in the search for novel therapeutics to limit PTOA.

MODULATING MITOCHONDRIAL RESPONSES TO INJURY AS A NEW AVENUE FOR PTOA PREVENTION

While the specific aspects of mitochondrial function that relate to NLRP3 and IL-1β production in the joint remain poorly

understood, there are some clear contenders for central involvement. For example, mitochondria-derived ROS, which is the predominant source of ROS in cells, is involved in multiple pathologies as well as in the process of ageing (49, 50). A strategy of targeting ROS activity in infiltrating immune, and/or joint, cells could lead to alternative ways to limit catabolic events in the joint post-injury. For example promotion of natural ROS inhibitors *via* antioxidants, falls into this category. Immediately following joint injury and/or cartilage damage, alterations in mitochondrial activity, swelling, polarisation and ROS production occur in chondrocytes (51). The normally hypoxic cartilage microenvironment is quickly altered and chondrocytes become exposed to increased levels of oxygen as well as a variety of other chemical species *via* neovascularisation of subchondral bone and altered synovial activities (52). NRF2 is a master antioxidant factor, which plays an important role in oxidative stress regulation. NRF2 can limit NLRP3 inflammasome activity in macrophages (53) and chondrocytes (40) and thus ultimately inhibit IL-1β activity. NRF2 has also been found to be upregulated in OA patient samples and surgical OA rodent models, suggesting it may have a role in the natural protective response to injury (29).

In addition to the local inflammatory state within the joint, an interesting study showed that the overall inflammatory state of an organism can also affect PTOA development. Priming of mice with lipopolysaccharide (LPS), a major component of bacteria, 5 days prior to joint injury was found to exacerbate the severity of PTOA resulting from injury (53). Subsequent RNA-seq analyses highlighted the same set of genes, that was previously found to be elevated in synovial macrophages from rheumatoid arthritis patients. This suggests the existence of a compounding effect of synovitis along with LPS administration. Furthermore, significantly increased numbers of activated macrophages were found in the injured joint, while cartilage loss and subchondral bone changes were also seen following LPS administration prior to injury (53). These findings have added further support to the concept that overall inflammatory status at the time of injury could also influence eventual disease severity. Viewed from a different perspective, this also suggests that mechanobiological responses may vary depending on overall inflammatory state of a given tissue, at the time of injury. This once again highlights the intersections of immune function and status with mechanobiology in this scenario.

MECHANOBIOLOGICAL RESPONSES ARE LINKED TO INFLAMMATION AND MITOCHONDRIAL DYNAMICS

Independent of the inflammatory responses to injury, although possibly involved in their initiation, the mechanobiological properties of joint tissues are likely to be involved in linking injury with subsequent disease. Furthermore, as with inflammatory stimulus, mechanical forces have been shown to be capable of modulating mitochondrial function (54, 55). It is clear that mechanical forces are inherent in joint function, and that joint (and general) health can benefit greatly from moderate mechanical loading (i.e. exercise, which is viewed, in many quarters, as being a highly effective tool/treatment to combat OA) (56). Mechanical stresses that exercise generates are manifested at the cellular level in a variety of ways. For example shear stress (which can be defined as a force that causes deformation in the plane of the surface) is generated within the joint by the flow of synovial/interstitial fluid across, and through, cartilage tissue (57). Also hydrostatic pressures can be generated in the joint from the compression and expansion of the ECM (58). However, when mechanical forces exceed a certain threshold (i.e. injury) joint damage, can occur which is in turn linked to consequent chronic diseases like PTOA (56). Surprisingly, precisely which cell type in the joint predominates in the mechanobiological response is not currently clear. Cells in synovial, bone and cartilage tissue itself have all been found to be highly mechanosensitive (i.e. show altered biochemical activities solely due to changes in their physical/mechanical environment). Mechanotransduction in human primary synovial fibroblasts was demonstrated experimentally by application of uniaxial cyclical stretch tests (using a membrane deformation assay), resulting in cell orientation, and cytoskeletal alignment, changes perpendicular to the applied stress. Those studies used the same system to show that stretch testing also resulted in significant increases in intracellular calcium [Ca^{2+}]. This response was then blocked using nonspecific calcium channel blockers [Ruthenium Red (RR)] (59). While this method did not directly assess the level of mitochondrial involvement, it is interesting to note that RR has also been shown to block mitochondrial Ca^{2+} uptake in other scenarios (60), which points to a potential link between these processes. In a similar study, synovial fibroblasts were exposed to shear stresses by application controlled fluid flow in a specialized bioreactor culture system, and again were found to be highly sensitive to changes in shear stress. This study also demonstrated a robust calcium signalling response involving both external and internal calcium sources (61), again highlighting the importance of mechanobiology and mitochondrial dynamics in joint tissue responses to injury.

As described above, in addition to synovial fibroblasts the intimal synovial membrane also contains resident macrophage like synoviocytes (MLS), under normal healthy conditions. The total number of these cells present in the synovium increases dramatically after injury, when circulating monocytes are recruited from the vasculature to the subintimal layer (62, 63). As with synovial fibroblasts, macrophages have also been found to be responsive to mechanical stimulus. A recent study reported that macrophages express high levels of Piezo1, a mechanically activated calcium channel (64). This study was focused on lung inflammation, where hydrostatic pressures predominate in the cellular microenvironment. Thus, by applying hydrostatic pressure to macrophages, Piezo1 was shown to facilitate calcium influx, driving activation of AP-1, which in turn causes release of Endothelin 1 and stabilization of HIF-1α. This upregulates a spectrum of pro-inflammatory genes, including IL-1β. While this paper focused on hydrostatic pressure within the respiratory

system, it nonetheless suggests that this mechanistic response may be preserved in macrophages at other sites, and in other tissues. Also, while the role of mitochondria in the response was not addressed these studies, it is well documented that mitochondria can stabilise HIF-1α *via* the production of mitochondrial ROS pointing to a potential mitochondrial connection (65). TRPV4 is another calcium influx channel which has been shown to be involved in mechanotransduction and oxidative stresses responses in macrophages. This channel becomes activated in macrophages following a range of stimuli including mechanical stretch (66). Stimulating this channel results in an increase in mitochondrial membrane potential, *via* as yet unknown mechanisms, as well as greater ROS and nitric oxide production. While this was shown to be relevant to the pro-inflammatory response induced by hydrostatic pressure, it is likely that a similar mechanism may occur in the mechanical environment of the joint.

Cartilage cells themselves have also been shown to be highly sensitive to mechanical stimulus and damage. Intriguingly, Piezo channels 1 and 2 (and TRPV4) were again found to be central and were identified in human chondrocytes where they were shown to be intimately involved in mechanotransduction and injury responses (67, 68). Their expression was also significantly increased in human osteoarthritic cartilage. Increased Piezo1 expression in chondrocytes resulted in a feed-forward mechanism whereby it induced excess intracellular Ca^{2+}, at baseline and in response to mechanical deformation (69) Using a bioreactor system with human chondrocytes isolated from end stage OA cartilage Delco et al. (51) also demonstrated acute cartilage responses to mechanical loading. Within 2 hours of stimulus/injury the endogenous mitochondrial respiratory function was impaired and membrane depolarisation had occurred. Targeting of mitochondrial potential, capacity, and membrane polarisation early in the post-injury period may lead to discovery of factors that drive cartilage degradation after injury. It may become possible to intervene, early after injury, using targeted mitochondrial therapeutics to rescue the joint from significant long-term damage. The extent/severity of mechanical force/impact which the cartilage undergoes is also important in determining the eventual outcome of disease - adding yet further complexity to understanding this injury/disease system. Bonnevie et al. (70) reported that mechanically impacting cartilage tissue, in the stress range of 15-20 MPa, results in significant chondrocyte death. It has also been shown that impact forces below this range can induce matrix breaches (6), depolarisation of mitochondrial membranes (71), and catabolic cellular responses (72) and upregulation of matrix degradation enzymes including MMP and ADAMTS.

Mechanical loading of cartilage, above a certain threshold level has also been shown to create an imbalance in mitochondrial superoxide levels (9). For example, delivery of a permeable antioxidant ascorbyl 6-palmitate 2-phosphate (APPS), a derivative of vitamin C, to the site of injury was shown to effectively suppress the response and reduce cartilage degeneration in mice (9). Elsewhere, repeated mechanical overloading of cartilage was shown to produce an oxidant-dependant state of mitochondrial dysfunction in chondrocytes (73). Furthermore it was shown that this damaging outcome could be rescued *via* introduction of free radical scavengers or disruptors of the electron transport chain (ETC), such as rotenone (inhibitor of complex 1 of the ETC) (74). In a related, and very relevant, study using a porcine model of PTOA, targeting mitochondrial responses following mechanical injury had favourable outcomes in terms of reducing disease severity at six months post-injury (75). Injury-induced changes to the ETC in chondrocytes has been linked with greater oxidative damage and ultimately cell death (12). This study used amobarbital to inhibit chondrocyte electron transport or N-acetylcysteine (NAC) to inhibit oxidative stress further downstream (75). Both treatments resulted in maintenance of proteoglycan content, decreased histological severity, and more normalised chondrocyte metabolic function 6 months post injury. These studies once again show that mitochondrial function is critical for maintenance of cellular energy production *via* the gradient created in the ETC in joint tissues. Pathogenic unfolding of membrane cristae and loss of membrane polarisation are characteristic of diseases in many tissues, but it is interesting to note that the same has recently been shown to be true in OA (76). These studies also support the potential application of antioxidants and targeting chondrocyte mitochondrial metabolism after injury to mediate PTOA and promote healthy cartilage (75). Ultimately, while this work is still at a relatively early stage, and biological means of repairing damage to cartilage after injury remains elusive; determining the role of mechanotransduction in damaged joint tissues, and the intersection this has with mitochondrial function, inflammation and PTOA, may reveal exciting possibilities for new therapies and targets in the joint.

THERAPEUTIC POTENTIAL

Taking these findings together, the emerging theme is that mitochondria, through a number of mechanisms, are extremely important for joint injury and disease. Therefore the next question is whether we can target this organelle and its function for therapeutic gain in the treatment of joint disease. It has been demonstrated that therapies aimed at mitochondrial repair, for example Szeto-Schiller (SS) peptides developed by Szeto et al. (77–79) – in particular SS-31, are protective to mitochondria after impact and subsequent degeneration. This effect is achieved *via* targeting the permeability of the mitochondrial membrane and production of ROS (77). Specifically, SS peptides work by interacting with cardiolipin and cytochrome c (78) thus producing an antioxidant effect on the inner mitochondrial membrane (80). These peptides have also been shown to protect chondrocyte viability by prevention of cytochrome c release and induction of apoptotic cascade (80). Moreover, they have the ability to preserve cartilage integrity and chondrocyte cell viability after impact in an *ex vivo* model (81). Investigation of mitochondrial therapy at this level suggests that compounds which target these pathways may have great utility in prevention of the onset of PTOA, even in cases where administration occurs up to 12 hours post-injury (81).

Another potential strategy involves targeting mitochondrial ROS production directly. A recent study used the antioxidant, Licochalcone A (Lico A), to limit NLRP3 inflammasome induced

damage to chondrocytes *in vitro* and in a surgical model of OA (40). Those studies showed that Lico A can ameliorate chondrocyte damage and death by promoting the NRF2/HO-1 axis to limit NF-kB activation during injury. Further studies have identified the therapeutic potential of nanoparticles to successfully deliver and retain anti-oxidant agents to chondrocytes, and cartilage protection. While promoting the use of antioxidants, these studies also highlighted the viability of NLRP3 inhibitors in OA. A potent inhibitor of NLRP3, MCC950, has also come to prominence in the wider field of immunology, and has been shown to be both safe and effective in limiting NLRP3 activity in human models of disease (82). While joint diseases such as gout, which involves direct activation of NLRP3 within the joint may be the first targets of such drugs, there is also great potential for them to provide benefits as a first line, early intervention, strategy in PTOA prevention.

CONCLUSION

In conclusion strong links have recently emerged between mechanobiology, mitochondrial function, inflammation/tissue-damage in skeletal joint pathologies. As or understanding of these links are further developed, they combine to form new paradigms for therapeutic intervention, particularly at early stages post-injury, to prevent the subsequent development of chronic PTOA.

AUTHOR CONTRIBUTIONS

LF and JE contributed equally to writing and reviewing the manuscript. OK and AC developed the initial idea for the topic and critically evaluated the manuscript through each of the writing stages. All authors contributed to the article and approved the submitted version.

FUNDING

This work was funded by the following awards: a Science Foundation Ireland [Career Development Award (17/CDA/4699)] to OK, a Science Foundation Ireland [Career Development Award (17/CDA/4688)] and an Irish Research Council Laureate Award (IRCLA/2017/110) to AC, and LF was funded by an Irish Research Council Government of Ireland Postgraduate Scholarship GOIPG/2018/2752.

REFERENCES

1. Shane Anderson A, Loeser RF. Why is Osteoarthritis an Age-Related Disease? *Best Pract Res Clin Rheumatol* (2010) 24(1):15–26. doi: 10.1016/j.berh.2009.08.006
2. Castañeda S, Vicente EF. Osteoarthritis: More Than Cartilage Degeneration. *Clin Rev Bone Mineral Metab* (2017) 15(2):69–81. doi: 10.1007/s12018-017-9228-6
3. Katz JN, Arant KR, Loeser RF. Diagnosis and Treatment of Hip and Knee Osteoarthritis: A Review. *JAMA* (2021) 325(6):568–78. doi: 10.1001/jama.2020.22171
4. Palazzo C, Nguyen C, Lefevre-Colau MM, Rannou F, Poiraudeau S. Risk Factors and Burden of Osteoarthritis. *Ann Phys Rehabil Med* (2016) 59 (3):134–8. doi: 10.1016/j.rehab.2016.01.006
5. Ramme AJ, Lendhey M, Raya JG, Kirsch T, Kennedy OD. A Novel Rat Model for Subchondral Microdamage in Acute Knee Injury: A Potential Mechanism in Post-Traumatic Osteoarthritis. *Osteoarthritis Cartilage* (2016) 24:1776–85. doi: 10.1016/j.joca.2016.05.017
6. Furman BD, Mangiapani DS, Zeitler E, Bailey KN, Horne PH, Huebner JL, et al. Targeting Pro-Inflammatory Cytokines Following Joint Injury: Acute Intra-Articular Inhibition of Interleukin-1 Following Knee Injury Prevents Post-Traumatic Arthritis. *Arthritis Res Ther* (2014) 16(3):R134–4. doi: 10.1186/ar4591
7. Mao X, Fu P, Wang L, Xiang C. Mitochondria: Potential Targets for Osteoarthritis. *Front Med (Lausanne)* (2020) 7:581402. doi: 10.3389/fmed.2020.581402
8. Kazemnejad S, Khanmohammadi M, Baheiraei N, Arasteh S. Current State of Cartilage Tissue Engineering Using Nanofibrous Scaffolds and Stem Cells. *Avicenna J Med Biotechnol* (2017) 9(2):50–65.
9. Yue B. Biology of the Extracellular Matrix: An Overview. *J Glaucoma* (2014) 23(8 Suppl 1):S20–3. doi: 10.1097/IJG.0000000000000108
10. Murphy G, Lee MH. What are the Roles of Metalloproteinases in Cartilage and Bone Damage? *Ann Rheumatic Dis* (2005) 64(suppl 4):iv44. doi: 10.1136/ard.2005.042465
11. Choi M-C, Jo J, Park J, Kang HK, Park Y. NF-κb Signaling Pathways in Osteoarthritic Cartilage Destruction. *Cells* (2019) 8(7):734. doi: 10.3390/cells8070734
12. Zahan OM, Serban O, Gherman C, Fodor D. The Evaluation of Oxidative Stress in Osteoarthritis. *Med Pharm Rep* (2020) 93(1):12–22. doi: 10.15386/mpr-1422
13. Troeberg L, Nagase H. Proteases Involved in Cartilage Matrix Degradation in Osteoarthritis. *Biochim Biophys Acta* (2012) 1824(1):133–45. doi: 10.1016/j.bbapap.2011.06.020
14. Huang K, Wu LD. Aggrecanase and Aggrecan Degradation in Osteoarthritis: A Review. *J Int Med Res* (2008) 36(6):1149–60. doi: 10.1177/147323000803600601
15. Poole AR, Kobayashi M, Yasuda T, Laverty S, Mwale F, Kojima T, et al. Type II Collagen Degradation and its Regulation in Articular Cartilage in Osteoarthritis. *Ann Rheumatic Dis* (2002) 61(suppl 2):ii78. doi: 10.1136/ard.61.suppl_2.ii78
16. Liu H, Li Z, Cao Y, Cui Y, Yang X, Meng Z, et al. Effect of Chondrocyte Mitochondrial Dysfunction on Cartilage Degeneration: A Possible Pathway for Osteoarthritis Pathology at the Subcellular Level. *Mol Med Rep* (2019) 20 (4):3308–16. doi: 10.3892/mmr.2019.10559
17. Coughlin TR, Kennedy OD. The Role of Subchondral Bone Damage in Post Traumatic Osteoarthritis. *Anna N Y Acad Sci* (2016) 1383(1):58–66. doi: 10.1111/nyas.13261
18. Lieberthal J, Sambamurthy N, Scanzello CR. Inflammation in Joint Injury and Post-Traumatic Osteoarthritis. *Osteoarthritis Cartilage* (2015) 23(11):1825–34. doi: 10.1016/j.joca.2015.08.015
19. Woodell-May JE, Sommerfeld SD. Role of Inflammation and the Immune System in the Progression of Osteoarthritis. *J Orthopaedic Res* (2020) 38 (2):253–7. doi: 10.1002/jor.24457
20. Furman BD, Zeitlin JH, Buchanan MW, Huebner JL, Kraus VB, Yi JS, et al. Immune Cell Profiling in the Joint Following Human and Murine Articular Fracture. *Osteoarthritis Cartilage* (2021) 29(6):915–23. doi: 10.1016/j.joca.2021.02.565
21. Angajala A, Lim S, Phillips JB, Kim JH, Yates C, You Z, et al. Diverse Roles of Mitochondria in Immune Responses: Novel Insights Into Immuno-Metabolism. *Front Immunol* (2018) 9:1605. doi: 10.3389/fimmu.2018.01605
22. Early JO, Curtis AM. Immunometabolism: Is It Under the Eye of the Clock? *Semin Immunol* (2016) 28(5):478–90. doi: 10.1016/j.smim.2016.10.006
23. Weinberg SE, Sena LA, Chandel NS. Mitochondria in the Regulation of Innate and Adaptive Immunity. *Immunity* (2015) 42(3):406–17. doi: 10.1016/j.immuni.2015.02.002

24. Roh JS, Sohn DH. Damage-Associated Molecular Patterns in Inflammatory Diseases. *Immune Netw* (2018) 18(4):e27. doi: 10.4110/in.2018.18.e27
25. Jo EK, Kim JK, Shin DM, Sasakawa C. Molecular Mechanisms Regulating NLRP3 Inflammasome Activation. *Cell Mol Immunol* (2016) 13(2):148–59. doi: 10.1038/cmi.2015.95
26. Kimmerling KA, Furman BD, Mangiapani DS, Moverman MA, Sinclair SM, Huebner JL, et al. Sustained Intra-Articular Delivery of IL-1RA From a Thermally-Responsive Elastin-Like Polypeptide as a Therapy for Post-Traumatic Arthritis. *Eur Cells materials* (2015) 29:124–40. doi: 10.22203/eCM.v029a10
27. Lawyer T, Wingerter S, Tucci M, Benghuzzi H. Cellular Effects of Catabolic Inflammatory Cytokines on Chondrocytes - Biomed 2011. *BioMed Sci Instrum* (2011) 47:252–7.
28. Lv M, Zhou Y, Polson SW, Wan LQ, Wang M, Han ML, et al. Identification of Chondrocyte Genes and Signaling Pathways in Response to Acute Joint Inflammation. *Sci Rep* (2019) 9(1):93. doi: 10.1038/s41598-018-36500-2
29. Chen Z, Zhong H, Wei J, Lin S, Zong Z, Gong F, et al. Inhibition of Nrf2/HO-1 Signaling Leads to Increased Activation of the NLRP3 Inflammasome in Osteoarthritis. *Arthritis Res Ther* (2019) 21(1):300. doi: 10.1186/s13075-019-2085-6
30. MacMullan P, McMahon G, McCarthy G. Detection of Basic Calcium Phosphate Crystals in Osteoarthritis. *Joint Bone Spine* (2011) 78(4):358–63. doi: 10.1016/j.jbspin.2010.10.008
31. Denoble AE, Huffman MK, Stabler TV, Kelly SJ, Hershfield MS, McDaniel GE, et al. Uric Acid is a Danger Signal of Increasing Risk for Osteoarthritis Through Inflammasome Activation. *Proc Natl Acad Sci* (2011) 108(5):2088. doi: 10.1073/pnas.1012743108
32. Okamoto M, Atsuta Y. Cartilage Degeneration is Associated With Augmented Chemically-Induced Joint Pain in Rats: A Pilot Study. *Clin Orthop Relat Res* (2010) 468(5):1423–7. doi: 10.1007/s11999-009-1193-z
33. Marks PH, Donaldson ML. Inflammatory Cytokine Profiles Associated With Chondral Damage in the Anterior Cruciate Ligament-Deficient Knee. *Arthroscopy* (2005) 21(11):1342–7. doi: 10.1016/j.arthro.2005.08.034
34. Ridker PM, Everett BM, Thuren T, MacFadyen JG, Chang WH, Ballantyne C, et al. Antiinflammatory Therapy With Canakinumab for Atherosclerotic Disease. *N Engl J Med* (2017) 377(12):1119–31. doi: 10.1056/NEJMoa1707914
35. Ichinohe T, Yamazaki T, Koshiba T, Yanagi Y. Mitochondrial Protein Mitofusin 2 is Required for NLRP3 Inflammasome Activation After RNA Virus Infection. *Proc Natl Acad Sci* (2013) 110(44):17963. doi: 10.1073/pnas.1312571110
36. Heid ME, Keyel PA, Kamga C, Shiva S, Watkins SC, Salter RD, et al. Mitochondrial Reactive Oxygen Species Induces NLRP3-Dependent Lysosomal Damage and Inflammasome Activation. *J Immunol (Baltimore Md.: 1950)* (2013) 191(10):5230–8. doi: 10.4049/jimmunol.1301490
37. Carlos D, Costa FRC, Pereira CA, Rocha FA, Yaochite JNU, Oliveira GG, et al. Mitochondrial DNA Activates the NLRP3 Inflammasome and Predisposes to Type 1 Diabetes in Murine Model. *Front Immunol* (2017) 8:164. doi: 10.3389/fimmu.2017.00164
38. Li Q, Shi N, Cai C, Zhang M, He J, Tan Y, et al. The Role of Mitochondria in Pyroptosis. *Front Cell Dev Biol* (2021) 8:630771–1. doi: 10.3389/fcell.2020.630771
39. Zheng S-C, Zhu X-X, Xue Y, Zhang L-H, Zou H-J, Qiu J-H, et al. Role of the NLRP3 Inflammasome in the Transient Release of IL-1β Induced by Monosodium Urate Crystals in Human Fibroblast-Like Synoviocytes. *J Inflammation* (2015) 12(1):30. doi: 10.1186/s12950-015-0070-7
40. Yan Z, Qi W, Zhan J, Lin Z, Lin J, Xue X, et al. Activating Nrf2 Signalling Alleviates Osteoarthritis Development by Inhibiting Inflammasome Activation. *J Cell Mol Med* (2020) 24(22):13046–57. doi: 10.1111/jcmm.15905
41. Sillat T, Barreto G, Clarijs P, Soininen A, Ainola M, Pajarinen J, et al. Toll-Like Receptors in Human Chondrocytes and Osteoarthritic Cartilage. *Acta orthopaedica* (2013) 84(6):585–92. doi: 10.3109/17453674.2013.854666
42. Bougault C, Gosset X, Houard C, Salvat L, Godmann T, Pap C, et al. Stress-Induced Cartilage Degradation Does Not Depend on the NLRP3 Inflammasome in Human Osteoarthritis and Mouse Models. *Arthritis Rheum* (2012) 64(12):3972–81. doi: 10.1002/art.34678
43. Stack J, McCarthy G. Basic Calcium Phosphate Crystals and Osteoarthritis Pathogenesis: Novel Pathways and Potential Targets. *Curr Opin Rheumatol* (2016) 28(2):122–6. doi: 10.1097/BOR.0000000000000245
44. Mahon OR, Dunne A. Disease-Associated Particulates and Joint Inflammation; Mechanistic Insights and Potential Therapeutic Targets. *Front Immunol* (2018) 9:1145. doi: 10.3389/fimmu.2018.01145
45. Jin C, Frayssinet P, Pelker R, Cwirka D, Hu B, Vignery A, et al. NLRP3 Inflammasome Plays a Critical Role in the Pathogenesis of Hydroxyapatite-Associated Arthropathy. *Proc Natl Acad Sci USA* (2011) 108(36):14867–72. doi: 10.1073/pnas.1111101108
46. McCarthy GM, Dunne A. Calcium Crystal Deposition Diseases — Beyond Gout. *Nat Rev Rheumatol* (2018) 14(10):592–602. doi: 10.1038/s41584-018-0078-5
47. Ea H-K, Chobaz V, Nguyen C, Nasi S, van Lent P, Daudon M, et al. Pathogenic Role of Basic Calcium Phosphate Crystals in Destructive Arthropathies. *PloS One* (2013) 8(2):e57352–2. doi: 10.1371/journal.pone.0057352
48. Mahon OR, Kelly DJ, McCarthy GM, Dunne A. Osteoarthritis-Associated Basic Calcium Phosphate Crystals Alter Immune Cell Metabolism and Promote M1 Macrophage Polarization. *Osteoarthritis Cartilage* (2020) 28(5):603–12. doi: 10.1016/j.joca.2019.10.010
49. Rimessi A, Previati M, Nigro F, Wieckowski MR, Pinton P. Mitochondrial Reactive Oxygen Species and Inflammation: Molecular Mechanisms, Diseases and Promising Therapies. *Int J Biochem Cell Biol* (2016) 81:281–93. doi: 10.1016/j.biocel.2016.06.015
50. Sanz A. OP-20 - Mitochondrial ROS and Ageing. *Free Radical Biol Med* (2017) 108:S9. doi: 10.1016/j.freeradbiomed.2017.04.059
51. Delco ML, Bonnevie ED, Bonassar LJ, Fortier LA. Mitochondrial Dysfunction is an Acute Response of Articular Chondrocytes to Mechanical Injury. *J Orthopaedic Res* (2018) 36(2):739–50. doi: 10.1002/jor.23651
52. Henrotin Y, Kurz B, Aigner T. Oxygen and Reactive Oxygen Species in Cartilage Degradation: Friends or Foes? *Osteoarthritis Cartilage* (2005) 13(8):643–54. doi: 10.1016/j.joca.2005.04.002
53. Liu X, Zhang X, Ding Y, Zhou W, Tao L, Lu P, et al. Nuclear Factor E2-Related Factor-2 Negatively Regulates NLRP3 Inflammasome Activity by Inhibiting Reactive Oxygen Species-Induced NLRP3 Priming. *Antioxidants Redox Signaling* (2017) 26(1):28–43. doi: 10.1089/ars.2015.6615
54. Helle SCJ, Feng Q, Aebersold MJ, Hirt L, Grüter RR, Vahid A, et al. Mechanical Force Induces Mitochondrial Fission. *eLife* (2017) 6:e30292. doi: 10.7554/eLife.30292
55. Liao H, Qi Y, Ye Y, Yue P, Zhang D, Li Y. Mechanotranduction Pathways in the Regulation of Mitochondrial Homeostasis in Cardiomyocytes. *Front Cell Dev Biol* (2021) 8:1–17. doi: 10.3389/fcell.2020.625089
56. Sun HB. Mechanical Loading, Cartilage Degradation, and Arthritis. *Ann N Y Acad Sci* (2010) 1211:37–50. doi: 10.1111/j.1749-6632.2010.05808.x
57. Wang P, Guan P-P, Guo C, Zhu F, Konstantopoulos K, Wang Z-Y. Fluid Shear Stress-Induced Osteoarthritis: Roles of Cyclooxygenase-2 and its Metabolic Products in Inducing the Expression of Proinflammatory Cytokines and Matrix Metalloproteinases. *FASEB J* (2013) 27(12):4664–77. doi: 10.1096/fj.13-234542
58. Cambre I, Gaublomme D, Burssens A, Jacques P, Schryvers N, De Muynck A, et al. Mechanical Strain Determines the Site-Specific Localization of Inflammation and Tissue Damage in Arthritis. *Nat Commun* (2018) 9(1):4613. doi: 10.1038/s41467-018-06933-4
59. Sakamoto Y, Ishijima M, Kaneko H, Kurebayashi N, Ichikawa N, Futami I, et al. Distinct Mechanosensitive Ca2+ Influx Mechanisms in Human Primary Synovial Fibroblasts. *J Orthop Res* (2010) 28(7):859–64. doi: 10.1002/jor.21080
60. Rigoni F, Deana R. Ruthenium Red Inhibits the Mitochondrial Ca2+ Uptake in Intact Bovine Spermatozoa and Increases the Cytosolic Ca2+ Concentration. *FEBS Lett* (1986) 198(1):103–8. doi: 10.1016/0014-5793(86)81193-0
61. Estell EG, Murphy la, Silverstein AM, Tan AR, Shah RP, Ateshian GA, et al. Fibroblast-Like Synoviocyte Mechanosensitivity to Fluid Shear is Modulated by Interleukin-1α. *J biomechanics* (2017) 60:91–9. doi: 10.1016/j.jbiomech.2017.06.011
62. Utomo L, Fahy N, Kops N, van Tiel ST, Waarsing J, Verhaar JAN, et al. Macrophage Phenotypes and Monocyte Subsets After Destabilization of the Medial Meniscus in Mice. *J Orthopaedic Res* (2020) 2020:1–11. doi: 10.1002/jor.24958
63. Uchida K, Satoh M, Inoue G, Onuma K, Miyagi M, Iwabuchi K, et al. CD11c (+) Macrophages and Levels of TNF-α and MMP-3 are Increased in Synovial and Adipose Tissues of Osteoarthritic Mice With Hyperlipidaemia. *Clin Exp Immunol* (2015) 180(3):551–9. doi: 10.1111/cei.12607

64. Solis AG, Bielecki P, Steach HR, Sharma L, Harman CC, Yun D, et al. Mechanosensation of Cyclical Force by PIEZO1 is Essential for Innate Immunity. *Nature* (2019) 573(7772):69–74. doi: 10.1038/s41586-019-1485-8
65. Mills EL, Kelly B, Logan A, Costa ASH, Varma M, Bryant CE, et al. Succinate Dehydrogenase Supports Metabolic Repurposing of Mitochondria to Drive Inflammatory Macrophages. *Cell* (2016) 167(2):457–70.e13. doi: 10.1016/j.cell.2016.08.064
66. Hamanaka K, Jian MY, Townsley MI, King JA, Liedtke W, Weber DS, et al. TRPV4 Channels Augment Macrophage Activation and Ventilator-Induced Lung Injury. *Am J Physiol Lung Cell Mol Physiol* (2010) 299(3):L353–62. doi: 10.1152/ajplung.00315.2009
67. Du G, Li L, Zhang X, Liu J, Hao J, Zhu J, et al. Roles of TRPV4 and Piezo Channels in Stretch-Evoked Ca(2+) Response in Chondrocytes. *Exp Biol Med (Maywood)* (2020) 245(3):180–9. doi: 10.1177/1535370219892601
68. O'Conor CJ, Ramalingam S, Zelenski NA, Benefield HC, Rigo I, Little D, et al. Cartilage-Specific Knockout of the Mechanosensory Ion Channel TRPV4 Decreases Age-Related Osteoarthritis. *Sci Rep* (2016) 6:29053. doi: 10.1038/srep29053
69. Nims RJ, Savadipour A, Leddy H, Liu F, McNulty A, et al. A Inflammatory Signaling Sensitizes Piezo1 Mechanotransduction in Articular Chondrocytes as a Pathogenic Feed-Forward Mechanism in Osteoarthritis. *Proc Natl Acad Sci USA* (2021) 118(13):1–10. doi: 10.1073/pnas.2001611118
70. Bonnevie ED, Delco ML, Galesso D, Secchieri C, Fortier L, Bonassar A, et al. Sub-Critical Impact Inhibits the Lubricating Mechanisms of Articular Cartilage. *J Biomech* (2017) 53:64–70. doi: 10.1016/j.jbiomech.2016.12.034
71. Huser CA, Davies ME. Calcium Signaling Leads to Mitochondrial Depolarization in Impact-Induced Chondrocyte Death in Equine Articular Cartilage Explants. *Arthritis Rheum* (2007) 56(7):2322–34. doi: 10.1002/art.22717
72. Natoli RM, Scott CC, Athanasiou KA. Temporal Effects of Impact on Articular Cartilage Cell Death, Gene Expression, Matrix Biochemistry, and Biomechanics. *Ann BioMed Eng* (2008) 36(5):780–92. doi: 10.1007/s10439-008-9472-5
73. Coleman MC, Ramakrishnan PS, Brouillette MJ, Martin JA. Injurious Loading of Articular Cartilage Compromises Chondrocyte Respiratory Function. *Arthritis Rheumatol* (2016) 68(3):662–71. doi: 10.1002/art.39460
74. Goodwin W, McCabe D, Sauter E, Reese E, Walter M, Buckwalter J, et al. Rotenone Prevents Impact-Induced Chondrocyte Death. *J Orthop Res* (2010) 28(8):1057–63. doi: 10.1002/jor.21091
75. Coleman MC, Goetz JE, Brouillette MJ, Seol D, Willey M, Petersen C, et al. Targeting Mitochondrial Responses to Intra-Articular Fracture to Prevent Posttraumatic Osteoarthritis. *Sci Transl Med* (2018) 10(427):eaan5372. doi: 10.1126/scitranslmed.aan5372
76. Bartell LR, Fortier LA, Bonassar LJ, Szeto HH, Cohen I, Delco ML, et al. Mitoprotective Therapy Prevents Rapid, Strain-Dependent Mitochondrial Dysfunction After Articular Cartilage Injury. *J Orthop Res* (2020) 38(6):1257–67. doi: 10.1002/jor.24567
77. Zhao K, Zhao GM, Wu D, Soong Y, Birk AV, Schiller PW, et al. Cell-Permeable Peptide Antioxidants Targeted to Inner Mitochondrial Membrane Inhibit Mitochondrial Swelling, Oxidative Cell Death, and Reperfusion Injury. *J Biol Chem* (2004) 279(33):34682–90. doi: 10.1074/jbc.M402999200
78. Szeto HH. First-in-Class Cardiolipin-Protective Compound as a Therapeutic Agent to Restore Mitochondrial Bioenergetics. *Br J Pharmacol* (2014) 171(8):2029–50. doi: 10.1111/bph.12461
79. Szeto HH. Cell-Permeable, Mitochondrial-Targeted, Peptide Antioxidants. *AAPS J* (2006) 8(2):E277–83. doi: 10.1007/BF02854898
80. Rocha M, Hernandez-Mijares A, Garcia-Malpartida K, Banuls C, Bellod L, Victor VM, et al. Mitochondria-Targeted Antioxidant Peptides. *Curr Pharm Des* (2010) 16(28):3124–31. doi: 10.2174/138161210793292519
81. Delco ML, et al. Mitoprotective Therapy Preserves Chondrocyte Viability and Prevents Cartilage Degeneration in an *Ex Vivo* Model of Posttraumatic Osteoarthritis. *J Orthop Res* (2018) 36(2):739–50. doi: 10.1002/jor.23882
82. Coll RC, Robertson AA, Chae JJ, Higgins SC, Munoz-Planillo R, Inserra MC, et al. A Small-Molecule Inhibitor of the NLRP3 Inflammasome for the Treatment of Inflammatory Diseases. *Nat Med* (2015) 21(3):248–55. doi: 10.1038/nm.3806

Conflict of Interest: The authors declare that the research was conducted in the absence of any commercial or financial relationships that could be construed as a potential conflict of interest.

Publisher's Note: All claims expressed in this article are solely those of the authors and do not necessarily represent those of their affiliated organizations, or those of the publisher, the editors and the reviewers. Any product that may be evaluated in this article, or claim that may be made by its manufacturer, is not guaranteed or endorsed by the publisher.

frontiers in Immunology

ORIGINAL RESEARCH
published: 11 November 2021
doi: 10.3389/fimmu.2021.755862

Co-Exposure of Cardiomyocytes to IFN-γ and TNF-α Induces Mitochondrial Dysfunction and Nitro-Oxidative Stress: Implications for the Pathogenesis of Chronic Chagas Disease Cardiomyopathy

João Paulo Silva Nunes[1,2,3,4†], Pauline Andrieux[4†], Pauline Brochet[4], Rafael Ribeiro Almeida[1,3], Eduardo Kitano[1], André Kenji Honda[1], Leo Kei Iwai[5], Débora Andrade-Silva[5], David Goudenège[6], Karla Deysiree Alcântara Silva[1,2], Raquel de Souza Vieira[1], Débora Levy[1], Sergio Paulo Bydlowski[1], Frédéric Gallardo[4], Magali Torres[4], Edimar Alcides Bocchi[7], Miguel Mano[8], Ronaldo Honorato Barros Santos[9], Fernando Bacal[9], Pablo Pomerantzeff[9], Francisco Rafael Martins Laurindo[10], Priscila Camillo Teixeira[11], Helder I. Nakaya[12], Jorge Kalil[1,2,3], Vincent Procaccio[13], Christophe Chevillard[4‡] and Edecio Cunha-Neto[1,2,3*‡]*

[1] Laboratory of Immunology, Heart Institute (Incor), Hospital das Clínicas da Faculdade de Medicina da Universidade de São Paulo, São Paulo, Brazil, [2] Division of Clinical Immunology and Allergy, Faculdade de Medicina da Universidade de São Paulo, São Paulo, Brazil, [3] iii-Institute for Investigation in Immunology, Instituto Nacional de Ciência e Tecnologia (INCT), São Paulo, Brazil, [4] INSERM, UMR_1090, Aix Marseille Université, TAGC Theories and Approaches of Genomic Complexity, Institut MarMaRa, Marseille, France, [5] Laboratório Especial de Toxinologia Aplicada, Center of Toxins, Immune-Response and Cell Signaling (CeTICS), Instituto Butantan, São Paulo, Brazil, [6] Department of Biochemistry and Genetics, University Hospital of Angers, Angers, France, [7] Heart Failure Team, Heart Institute (Incor) Hospital das Clínicas da Faculdade de Medicina da Universidade de São Paulo, São Paulo, Brazil, [8] Functional Genomics and RNA-based Therapeutics Laboratory, Center for Neuroscience and Cell Biology (CNC), University of Coimbra, Coimbra, Portugal, [9] Division of Surgery, Heart Institute, School of Medicine, University of São Paulo, São Paulo, Brazil, [10] Laboratory of Vascular Biology, Heart Institute of the School of Medicine, University of São Paulo, São Paulo, Brazil, [11] Translational Research Sciences, Pharma Research and Early Development F. Hoffmann-La Roche, Basel, Switzerland, [12] Hospital Israelita Albert Einstein, São Paulo, Brazil, [13] MitoLab, UMR CNRS 6015-INSERM U1083, Université d'Angers, Angers, France

Infection by the protozoan *Trypanosoma cruzi* causes Chagas disease cardiomyopathy (CCC) and can lead to arrhythmia, heart failure and death. Chagas disease affects 8 million people worldwide, and chronic production of the cytokines IFN-γ and TNF-α by T cells together with mitochondrial dysfunction are important players for the poor prognosis of the disease. Mitochondria occupy 40% of the cardiomyocytes volume and produce 95% of cellular ATP that sustain the life-long cycles of heart contraction. As IFN-γ and TNF-α have been described to affect mitochondrial function, we hypothesized that IFN-γ and TNF-α are involved in the myocardial mitochondrial dysfunction observed in CCC patients. In this study, we quantified markers of mitochondrial dysfunction and nitro-oxidative stress in CCC heart tissue and in IFN-γ/TNF-α-stimulated AC-16 human cardiomyocytes. We found that CCC myocardium displayed increased levels of nitro-oxidative stress and reduced mitochondrial DNA as compared with myocardial tissue from patients with dilated cardiomyopathy (DCM). IFN-γ/TNF-α treatment of AC-16 cardiomyocytes induced increased nitro-oxidative stress and decreased the mitochondrial membrane potential

OPEN ACCESS

Edited by:
Clarissa M. Maya-Monteiro, Oswaldo Cruz Foundation (Fiocruz), Brazil

Reviewed by:
Emiliano Medei, Federal University of Rio de Janeiro, Brazil
Joseli Lannes-Vieira, Oswaldo Cruz Foundation (Fiocruz), Brazil
Claudia Paiva, Federal University of Rio de Janeiro, Brazil

***Correspondence:**
Edecio Cunha-Neto
edecunha@gmail.com
Christophe Chevillard
christophe.chevillard@univ-amu.fr

†These authors have contributed equally to this work

‡These authors have contributed equally to this work

Specialty section:
This article was submitted to Inflammation, a section of the journal Frontiers in Immunology

Received: *09 August 2021*
Accepted: *11 October 2021*
Published: *11 November 2021*

Citation:
Nunes JPS, Andrieux P, Brochet P, Almeida RR, Kitano E, Honda AK, Iwai LK, Andrade-Silva D, Goudenège D, Alcântara Silva KD, Vieira RdS, Levy D, Bydlowski SP, Gallardo F, Torres M, Bocchi EA, Mano M, Santos RHB, Bacal F, Pomerantzeff P, Laurindo FRM, Teixeira PC, Nakaya HI, Kalil J, Procaccio V, Chevillard C and Cunha-Neto E (2021) Co-Exposure of Cardiomyocytes to IFN-γ and TNF-α Induces Mitochondrial Dysfunction and Nitro-Oxidative Stress: Implications for the Pathogenesis of Chronic Chagas Disease Cardiomyopathy. Front. Immunol. 12:755862. doi: 10.3389/fimmu.2021.755862

(ΔΨm). We found that the STAT1/NF-κB/NOS2 axis is involved in the IFN-γ/TNF-α-induced decrease of ΔΨm in AC-16 cardiomyocytes. Furthermore, treatment with mitochondria-sparing agonists of AMPK, NRF2 and SIRT1 rescues ΔΨm in IFN-γ/TNF-α-stimulated cells. Proteomic and gene expression analyses revealed that IFN-γ/TNF-α-treated cells corroborate mitochondrial dysfunction, transmembrane potential of mitochondria, altered fatty acid metabolism and cardiac necrosis/cell death. Functional assays conducted on Seahorse respirometer showed that cytokine-stimulated cells display decreased glycolytic and mitochondrial ATP production, dependency of fatty acid oxidation as well as increased proton leak and non-mitochondrial oxygen consumption. Together, our results suggest that IFN-γ and TNF-α cause direct damage to cardiomyocytes' mitochondria by promoting oxidative and nitrosative stress and impairing energy production pathways. We hypothesize that treatment with agonists of AMPK, NRF2 and SIRT1 might be an approach to ameliorate the progression of Chagas disease cardiomyopathy.

Keywords: mitochondrial dysfunction, chronic Chagas disease cardiomyopathy, interferon gamma, energy metabolism, mitochondria

INTRODUCTION

Heart failure (HF) is an important worldwide public health problem. Available therapies are insufficient and do not fully address molecular abnormalities that occur in cardiomyocytes (1). Chagas disease cardiomyopathy (CCC) accounts for 25% of HF cases and is a major cause of death in Latin America (2, 3). CCC is a severe inflammatory dilated cardiomyopathy caused by persistent infection by the protozoan *Trypanosoma cruzi*. While 60% of Chagas Disease (CD) patients are mostly asymptomatic in the so-called "indeterminate" form (IF) and do not develop heart disease, CCC patients (30%, roughly 8 million people) display HF, arrhythmia, and disability (4, 5). CCC patients have 50% shorter survival rate and worse prognosis compared to patients with cardiomyopathies of non-inflammatory etiologies, such as ischemic, idiopathic and hypertensive cardiomyopathies (2).

The pathogenesis of CCC is still to be completely understood (6). Low-grade chronic *T. cruzi* persistence, which drives continued production of IFN-γ and TNF-α by Th1 T cells immune cells, plays a central pathogenic role in CCC (2, 4, 5). Indeed, omics and immunohistochemistry studies revealed higher levels of IFN-γ and TNF-α in heart tissue from CCC patients compared to other cardiomyopathies (7–11). Activation of the NF-κB/NOS2 axis by the continued production of IFN-γ/TNF-α can promote increased levels of intracellular reactive nitrogen species (RNS) which are important for parasite control (12, 13). However, long-term sustained activation of this axis may promote damaging accumulation of reactive oxygen species (ROS) through induction of NADP oxidases and overproduction of mitochondrial reactive oxygen species (ROS), such as hydrogen peroxide (H_2O_2) and superoxide anion (O_2^-) and RNS, molecules widely known to induce mitochondrial dysfunction and disturbances of heart function (14, 15).

The heart is the most metabolically active organ in the body and has the highest content of mitochondria of any tissue (16). This is needed to meet the ever-demanding energy requirement for contraction and relaxation and about 95% of cellular ATP is utilized to support the contraction–relaxation cycle within the myocardium (16). Indeed, mitochondria contribute to the proper function of cardiomyocytes by multiple mechanisms (17). Beyond contraction, mitochondria also fine-tune cellular calcium homeostasis, apoptosis and oxidative stress and it has become increasingly clear that mitochondrial dysfunction is the source of heart energy deprivation in cardiomyopathies and heart failure of diverse etiologies (16).

Several myocardial mitochondrial enzymes were found to be selectively depressed in CCC as compared to other cardiomyopathies, including ATP synthase α, multiple fatty acid β-oxidation enzymes and creatine kinase activity [(18–20) and our unpublished observations] additionally, *in vivo* myocardial ATP production was shown to be reduced in CCC as determined by ^{31}P-NMR spectroscopy (21). Taken together, results suggest that mitochondrial dysfunction may contribute to the worse prognosis of CCC. Since inflammatory cytokines IFN-γ and TNF-α are abundantly produced and are top upstream regulators of gene expression changes in in CCC myocardium (9), and the sustained ROS and RNS production are known inducers of cardiomyocyte damage and mitochondrial dysfunction (22, 23), we hypothesized that such cytokines contribute to mitochondrial dysfunction observed in CCC (5).

Thus, this study aimed to investigate 1) whether CCC myocardial tissue display increased levels of mitochondrial dysfunction and oxidative/nitrosative stress markers compared to non-chagasic dilated cardiomyopathy biopsies (DCM); 2) whether IFN-γ and TNF-α promote mitochondrial dysfunction and nitro-oxidative stress in the human cardiomyocyte cell line AC-16; 3) whether the mitochondrial dysfunction in cardiomyocytes is

triggered by the cytokines through the STAT1/NF-κB/NOS2 signaling pathway; 4) whether agonists of mitochondrial protection pathways, such as AMPK, NRF2 and SIRT1 ameliorate mitochondrial dysfunction driven by the IFN-γ and TNF-α.

METHODS

Ethics Statement

Tissue collection was approved by the Institutional Review Board of the University of São Paulo, School of Medicine (CAPPesq approval number 852/05) and written informed consent was obtained from the patients. All experimental methods comply with the Helsinki declaration.

Patients and Sample Collection

Human left ventricular free wall heart tissue was collected from end-stage heart failure CCC patients (n=40) and non-chagasic dilated cardiomyopathy (DCM, n=31) patients (NYHA class 3 and 4) at the moment of heart transplantation. CCC patients presented positive *T. cruzi* serology and typical heart conduction abnormalities (right bundle branch block and/or left anterior division hemiblock) and had a histopathological diagnosis of myocarditis, fibrosis and hypertrophy. All heart tissue samples were cleared from pericardium and fat and quickly frozen in liquid nitrogen and stored at -80°C. The list of patients is described in **Table 1**.

Reagents

Interferon-gamma (IFN-γ, 300-02) and tumor necrosis factor alpha (TNF-α, 300-01A) were purchased from Peprotech. AMPK agonists Metformin hydrochloride (PHR1084), AICAR (A9978), Resveratrol (R5010); SIRT1 agonist SRT1720 (SRT1720) and NRF-2/HO-1 agonist Protoporphyrin IX cobalt chloride (C1900) were purchased from Sigma-Aldrich. Inhibitors of NF-κB Emodin (E7881) and JSH23 (J4455); IKKβ inhibitor IKK16 (SML1138); STAT1 inhibitor Fludarabine (F2773) and NOS2 inhibitor 1400W (W4262) were purchased from Sigma-Aldrich. Inhibitors of MEK1 and MEK2 PD98059 (ab120234), JNK SP600125 (ab120065) and MAPK SB202190 (ab120638) were purchased from Abcam. Reagents were dissolved in DMSO or water (Metformin and AICAR) at 100x stock concentrations and maximum DMSO concentration used in cells was 1%. Monoclonal antibody against 3-nitrotyrosine (ab61392) was purchased from Abcam. Monoclonal antibody against NF-κB p65 (sc-8008) was purchased from Santa Cruz Biotechnology.

Cell Culture

Human adult ventricular cardiomyocytes cell line AC-16 was kindly provided by Dr. Mercy Davidson (Columbia University, USA) (24). The cell line was propagated using Dulbecco's modified Eagle's medium/F-12 medium with 12.5% fetal bovine serum (FBS) without antibiotics for no longer than 8 passages. AC-16 cells were screened monthly for mycoplasma contamination (MycoAlert Mycoplasma Detection Kit, Lonza)

TABLE 1 | List of the patients included in this study.

Code	Etiology	Sex	Age	EF (%)
CCC-S01	Severe CCC	F	61	27
CCC-S02	Severe CCC	M	60	35
CCC-S03	Severe CCC	F	64	30
CCC-S04	Severe CCC	M	61	21
CCC-S05	Severe CCC	F	60	20
CCC-S06	Severe CCC	M	41	19
CCC-S07	Severe CCC	M	15	17
CCC-S08	Severe CCC	M	28	29
CCC-S09	Severe CCC	M	32	12
CCC-S10	Severe CCC	F	32	19
CCC-S11	Severe CCC	M	41	23
CCC-S12	Severe CCC	M	58	20
CCC-S13	Severe CCC	M	36	25
CCC-S14	Severe CCC	F	47	27
CCC-S15	Severe CCC	F	63	37
CCC-S16	Severe CCC	F	44	25
CCC-S17	Severe CCC	M	39	20
CCC-S18	Severe CCC	M	58	25
CCC-S19	Severe CCC	M	66	21
CCC-S20	Severe CCC	M	50	25
CCC-S21	Severe CCC	M	51	23
CCC-S22	Severe CCC	M	58	29
CCC-S23	Severe CCC	M	58	28
CCC-S24	Severe CCC	F	66	25
CCC-S25	Severe CCC	F	45	20
CCC-S26	Severe CCC	F	60	24
CCC-S27	Severe CCC	F	39	20
CCC-S28	Severe CCC	M	51	35
CCC-S29	Severe CCC	F	61	15
CCC-S30	Severe CCC	F	47	35
CCC-S31	Severe CCC	F	46	20
CCC-S32	Severe CCC	F	61	27
CCC-S33	Severe CCC	F	58	30
CCC-S34	Severe CCC	F	49	15
CCC-S35	Severe CCC	M	49	21
CCC-S36	Severe CCC	M	62	21
CCC-S37	Severe CCC	M	57	29
CCC-S38	Severe CCC	M	59	17
CCC-S39	Severe CCC	M	48	19
CCC-S40	Severe CCC	F	54	36
DCM-01	DCM	M	52	30
DCM-02	DCM	F	32	20
DCM-03	DCM	F	24	29
DCM-04	DCM	M	46	25
DCM-05	DCM	M	15	29
DCM-06	DCM	M	55	25
DCM-07	DCM	F	29	25
DCM-08	DCM	M	36	14
DCM-09	DCM	M	26	25
DCM-10	DCM	M	42	9
DCM-11	DCM			
DCM-12	DCM	F	57	27
DCM-13	DCM	M	48	39
DCM-14	DCM	F	66	20
DCM-15	DCM	M	43	26
DCM-16	DCM	M	53	19
DCM-17	DCM	M	39	28
DCM-18	DCM	M	58	21
DCM-19	DCM	F	12	22
DCM-20	DCM	F	56	18
DCM-21	DCM	M	29	26
DCM-22	DCM	M	61	27
DCM-23	DCM	M	15	20

(Continued)

TABLE 1 | Continued

Code	Etiology	Sex	Age	EF (%)
DCM-24	DCM	F	58	17
DCM-25	DCM	M	28	16
DCM-26	DCM	M	56	16
DCM-27	DCM	M	27	25
DCM-28	DCM	F	53	27
DCM-29	DCM	M	51	15
DCM-30	DCM	M	56	35
DCM-31	DCM	M	37	16

and were authenticated by PCR-based DNA Profiling (Eurofins Genomics, France).

Cell Stimuli and Investigation of Molecular Pathways

AC-16 cells were seeded (10^3 cells per 0.34 cm^2) for 24 hours (h) prior to stimulation with 10 ng/ml IFN-γ, or with 5 ng/ml TNF-α or with IFN-γ plus TNF-α for 48h. In certain experiments, cells were treated with serially diluted, by a factor of two, with agonists of AMPK (metformin, AICAR and resveratrol), NRF2 (Protoporphyrin IX cobalt chloride), SIRT1 (SRT1720) or inhibitors of NF-κB (Emodin, JSH23), IKKβ (IKK16), STAT1 (Fludarabine), NOS2 (1400W), MEK1 and MEK2 (PD98059), JNK (SP600125) and MAPK (SB202190) in combination or not with IFN-γ, TNF-α or both. Compound doses that provided the highest effect on mitochondrial ΔΨm and less than 10% loss on cell number were selected for further analysis.

LDH Release Assay

The release of lactate dehydrogenase (LDH) in the conditioned media is an indicator of cell cytotoxicity. AC-16 cardiomyocytes were stimulated with the cytokines for 48h and the LDH content was quantified using a LDH-Cytotoxicity Assay Kit II (Abcam) using SpectraMax® Paradigm®.

Mitochondrial Membrane Potential and Cellular ROS

AC-16 cardiomyocytes were seeded in 96 well black plate (Corning 3603) at a density of 10^3 cells per 0.34 cm^2 and incubated in a humidified incubator at 37°C and 5% CO_2 for 24h. Then, cells were stimulated with the cytokines with or without the agonists/inhibitors for 48h. For mitochondrial membrane potential, cells were multi-labeled with 1.0 μM of tetramethylrhodamine, methyl ester, perchlorate (TMRM, ThermoFisher Scientific), 400 nM of MitoTracker DeepRed (ThermoFisher Scientific), NucGreen dead (ReadyProbes) and 1.0 μM of Hoechst 33342 (ThermoFisher Scientific) at 37°C 5% CO_2 for 30 min. Cells were washed once with Hanks' Balanced Salt solution containing calcium and magnesium (HBSS++). Micrographs were captured using ImageXpress Micro XLS Widefield High-Content Analysis system (Molecular Devices) at 100x magnification and the mitochondrial membrane potential was evaluated in live cells (NucGreen negative) using the web-based software Columbus 2.7.1.133403 (PerkinElmer Inc.). Overlapped TMRM and Mitotracker DeepRed fluorescence were considered for the measurement of mitochondrial ΔΨm. For cellular ROS, stimulated cells were washed once with HBSS++ and then labeled in the dark with 10 μM of H_2DCFDA (Abcam) and 1.0 μM of Hoechst 33342 (ThermoFisher Scientific) at 37°C 5% CO_2 for 30 min and fluorescence were measured at Ex/Em 485/535 nm and 360/461 nm respectively using SpectraMax® Paradigm®.

NF-κB Translocation

Stimulated AC-16 cells were fixed with 4% paraformaldehyde, pH=7.4 for 15 min at room temperature (RT), then incubated with ice-cold 0.5% Triton-X for 15 min and blocked with 3% BSA in PBS for 1h RT. Cells were incubated with 1:50 monoclonal mouse anti-NF-κB p65 (SC-8008, Santa Cruz Biotechnology) in PBS + 1% BSA overnight at 4°C, then washed and kept in the dark with goat anti-mouse IgG1 Cross-Adsorbed Secondary Antibody (P-21129, ThermoFisher Scientific) 1:1000 in PBS + 1% BSA for 1h RT. Nuclei were stained with 2.5 μg/ml of DAPI (ThermoFisher Scientific) for 1h RT and images were acquired using ImageXpress Micro XLS Widefield High-Content Analysis system (Molecular Devices) at 40x magnification. Nuclear NF-κB translocation was measured using the software Columbus 2.7.1.133403 (PerkinElmer Inc.).

Assessment of 3-Nitrotyrosine

Relative quantification of nitrated protein was performed by assessing 3-nitrotyrosine (3-NT) as a mean to detect nitrosative stress. Cardiac fragments and stimulated AC-16 cells were lysed in aqueous lysis solution containing 10 mM HEPES, 0.32 M sucrose, 0.1 mM Na_2EDTA, 1.0 mM dithiothreitol, 125 μg/ml PMSF and 1.0 μl/ml of proteinase inhibitor cocktail (Sigma), pH=7.4. Cardiac fragments were lysed in a tissue homogenizer (Precellys 24) pre-chilled 4°C using 2.8 mm ceramic beads for 3 cycles of 10s (seconds) with 15s intervals at 5500 rpm. Cells were lysed with 1.4 mm ceramic beads for 2 cycles of 30s with 10s intervals at 5000 rpm. Cardiac and cell lysates were clarified by centrifugation at 10,000 rcf for 30 min at 4°C. A total of 5 μg of proteins was added to a nitrocellulose membrane, dried at 60°C for 15 min and then blocked with 3% Blotting Grade Blocker (BioRad) + TBS-T, for 1h at RT, under stirring. Membrane was washed with TBS-T and incubated with 1:1000 primary monoclonal antibody 3-nitrotyrosine (Abcam) in 3% BSA + TBS-T overnight 4°C. Then, membrane was washed twice and incubated with 1:1000 secondary antibody for 2h at RT, under agitation and protected from light. Fluorescence was captured using a scanner (LI-COR, Odyssey) or ECL revelation. Ponceau S images were captured using ImageQuant LAS-400 (GE Healthcare) and used for protein normalization.

ATP and Nitrite Production

Nitrite (NO_2^-) was measured in the conditioned media (phenol-free) of stimulated AC-16 cells using Griess Reagent Kit for Nitrite Determination (Molecular Probes) according to manufacturer's instructions. The cells were collected and lysed with TE buffer (100 mM Tris, 4 mM EDTA, pH=7.5) and ATP measured with a luciferase-based assay kit (ATP Determination Kit, ThermoFisher Scientific) according to manufacturer's instructions.

Nitrite absorbance and ATP-derived luminescence were measured in AC-16 cardiomyocytes using SpectraMax® Paradigm® (Molecular Devices). Measurement of nitrite in myocardial homogenates was performed by chemiluminescence with Nitric Oxide Analyzer (NOA 280, Zysense, United Kingdom).

Bioenergetic Function Analysis

A Seahorse XFe24 Analyzer (Agilent, Les Ulis, France) was used to survey bioenergetic function by measuring the oxygen consumption rate (OCR) and extracellular acidification rate (ECAR) of live cells. A quantity of 3,500 cells/0.32cm^2 were seeded in 150 µl of specific media, incubated for 1h at room temperature for adhesion and stimulated with 350 µl of specific media containing IFN-γ (10 ng/ml final) and TNF-α (5 ng/ml final) for 48h. OCR and ECAR were obtained from 90% confluent monolayer culture. All the experiments were done according to the protocol provided by the manufacturer. Briefly, the Agilent Seahorse Cell Mito Stress Test kit assesses mitochondrial function. Multiple parameters are obtained such as, basal respiration, ATP-linked respiration, maximal and reserve capacities, and non-mitochondrial respiration. The ATP Real-Time rate kit is the only assay that quantifies the ATP production from glycolysis and mitochondria simultaneously. The Agilent Seahorse Mito Fuel Flex Test kit measures the basal state of mitochondrial fuel oxidation in live cells by providing information on the relative contributions of glucose, glutamine and long-chain fatty acid oxidation to basal respiration. All analyses were performed using the software Wave 2.6.1 (Agilent, Les Ulis, France).

mtDNA Quantification

Total DNA from cardiac fragments and AC-16 cells was extracted using the DNA extraction kit FlexiGene DNA kit (QIAgen) according to the manufacturer's instructions. PCR reaction was conducted using MAXIMA SYBR Green/ROX qPCR Master Mix (2x) (Thermo Scientific), 1 ng of template DNA and primers for mitochondrial encoded genes NADH: ubiquinone oxidoreductase subunit 1 (MT-ND1, 5 pmol/µl), cytochrome b (MT-CYTB, 5 pmol/µl), cytochrome c oxidase subunit 3 (MT-COXIII, 5 pmol/µl). Nuclear gene Telomerase (TERT, 15 pmol/µl) was used as the endogenous control. The PCR reactions were done in QuantStudio 12K (Applied Biosystem) with the following cycling program, 1 cycle of 50°C for 2 min, 95°C for 10 min, and 40 cycles of 50°C for 2 min, 95°C for 15s, and 60°C for 1 min. The ratio of mtDNA/nuDNA was calculated using the formula $2x2^{\Delta CT}$ (25).

RNA Extraction and Sequencing

AC-16 cells were crushed with ceramic beads (VK05, diameter 1.4 mm) in 350 µl of RLT lysis buffer supplemented with 3.5 µl of β-mercapto-ethanol. Total RNA was extracted by using the RNeasy Mini Kit adapted with Trizol. RNA quantity was measured with a 2100 Bioanalyzer. Total RNA Sequencing was provided by Genewiz. Ribosomal RNAs have been depleted, and samples were prepared for sequencing according to the Illumina TruSeq RNA Preparation Kit and subjected to pairwise sequencing (2x150 bp) with the Illumina Novaseq sequencer. After sequencing, the raw data files (fastq) were generated.

Differential Expression Analysis

Raw data quality has been verified with FastQC (v0.11.5). Low-quality reads, Illumina adapters and reads smaller than 20 nucleotides were removed with Trimmomatic (v0.39) (26), using default values for other options. Reads were aligned on GRCh37 (hg19) human reference genome from Ensembl using STAR (v2.5.4b) (27), specifying that the reads are 2x150 nucleotides (paired-end). Alignment quality has been checked by BAMQC (qualimap v2.2.1) (28). Gene quantification was done with featureCounts (v2.0.0) (29), using the exons as features and the genes as attributes. The DESeq2 package (v1.26.0) has been used to normalize data and to perform the differential expression test (30). To improve log2 fold change accuracy, DESeq2 shrinkage function has been applied to the test results, and p-value was corrected with Benjamini-Hochberg method. Genes having an adjusted p-value ≤ 0.05 and a $|\log2(FC)| \geq 1.5$ were considered to be differentially expressed genes (DEG). Then, results were analyzed by graphical methods with EnhancedVolcano (v1.4.0) and ggplot2 packages. Moreover, hierarchical clustering (HCA) based on spearman correlation was computed using gplots (v3.0.4) package, and principal component analysis (PCA) with factoextra (v1.0.7) and FactoMineR (v2.3) packages. We compared the AC-16 gene expression profile with the CCC gene expression profile (GSE84796) (31).

Proteomic Analysis of AC-16 Cardiomyocytes

The proteomic analysis of AC-16 cells under IFN-γ (10 ng/ml) and TNF-α (5 ng/ml) treatment was assessed by high-resolution mass spectrometric analysis. After 48h incubation with the combination of IFN-γ and TNF-α, proteins from AC-16 were extracted using lysis buffer (12 mM sodium deoxycholate, 12 mM *N*-lauroylsarcosine sodium salt, 100 mM Tris-HCl, pH=9.0) supplemented with protease inhibitor cocktail (Sigma-Aldrich). Total cell lysates from control and IFN-γ+TNF-α-treated cells were subject to in-solution trypsin digestion according to Phase Transfer Surfactant (PTS)-aided trypsin digestion protocol (32). Digested proteins were desalted using StageTip protocol (33) and dried by centrifugation under vacuum. Peptide samples were analyzed by RP-LC-MS/MS. For MS analysis, peptide mixtures were dissolved in 0.1% formic acid (solution A). Aliquots of 3 µl were automatically injected by a nano chromatography EASY-nLCII system (Thermo Scientific) on a 40 mm x 100 µm ID C-18 pre-column packed with Jupiter 10 µm resin (Phenomenex) and submitted to a chromatographic separation in a 100 mm x 75 µm ID C-18 column packed with Reprosil-Pur 3 µm C-18 beads (Dr. Maisch) coupled to an LTQ Orbitrap Velos (Thermo Scientific). Peptides were eluted with a linear gradient of 5-30% solution B (0.1% formic acid in acetonitrile) at 200 nl/min for 55 min. Spray voltage was set at 2.5kV and the mass spectrometer was operated in data dependent mode, in which one full MS scan was acquired in the m/z range of 400-1,800 at 60,000 resolution (at 400m/z)

followed by collisional induced fragmentation (CID) and MS/MS acquisition of the ten most intense ions from MS scan. Unassigned and +1 charge states were not subjected to fragmentation. The maximum injection time and AGC target were set to 100ms (milliseconds) and 1E6 for full MS, and 10ms and 1E4 for MS/MS. The minimum signal threshold to trigger fragmentation event, isolation window and normalized collision energy (NCE) were set to, respectively, 1000 cps, 2m/z and 35%. Dynamic peak exclusion (list size of 500) was applied to avoid the same m/z of being selected for the next 30s. Mass spectrometric raw data were processed using the software MaxQuant [version 1.6.2.10 (34)] and searched against a target human protein database (*Homo sapiens*, UniprotKB reviewed, 26,526 sequences) for protein identification and quantification. A False Discovery Rate (FDR) of 1% was required for both protein and peptide identifications. Label Free Quantification [MaxLFQ (35)] method was enabled. T-test was used for relative protein quantification and p-values were adjusted with the Benjamini-Hochberg method. Proteins with adjusted p-values ≤ 0.05 were considered to be differentially expressed.

Statistical Analysis

Cell data are reported as the ratio to non-treated cells. Cell viability was calculated as the ratio of the number of live cells (NucGreen-negative) and total cells (NucGreen-negative plus NucGreen-positive cells) x100. The results were expressed as mean ± standard deviation (SD) or standard error of the mean (SEM) when noted. Statistical analysis was performed using the GraphPad Prism 9.2.0 software (GraphPad Software, Inc., CA). Data were tested for normality using the Shapiro-Wilk test before statistical tests. A nonparametric Mann-Whitney test was applied if data were not normally distributed. In all other cases, one-way ANOVA followed by Dunn's *post hoc* test was applied for multiple comparisons. A p-value < 0.05 was considered statistically significant.

RESULTS

Increased RNS and Decreased mtDNA Content in CCC Myocardial Tissue

We compared the nitro-oxidative profile of CCC and DCM myocardium. We first measured nitrite, a reactive nitrogen species (RNS) marker, by chemiluminescence with a NO Analyzer. We observed that CCC biopsies possess higher content of nitrite (132%; $p < 0.001$) in comparison to DCM lysates (**Figure 1A**). Detection of nitrotyrosine, an additional nitro-oxidative stress marker, was performed by dot-blot. We observed a significantly higher nitrotyrosine immunoreactivity in CCC (27%; $p < 0.01$) than DCM myocardial lysates (**Figure 1B**), indicating previous exposure to peroxynitrite. Also, mitochondrial DNA (MT-ND1) was lower in CCC (44%; $p < 0.001$) than DCM myocardial samples (**Figure 1C**) indicating a reduction of mitochondrial mass.

IFN-γ and TNF-α Impair AC-16 Cardiomyocyte Mitochondrial Membrane Potential (ΔΨm)

To investigate the role of IFN-γ and TNF-α on AC-16 cardiomyocytes, we stimulated the cells with several concentrations of IFN-γ and TNF-α and we measured the mitochondrial ΔΨm in a high content screening platform. This was performed to stablish the concentrations of the cytokines for subsequent analyses. We observed that IFN-γ impaired the ΔΨm of AC-16 48h after stimulation and this impairment was enhanced when IFN-γ was combined with TNF-α; TNF-α alone failed to cause statistically significant reductions in ΔΨm (**Figures 2A, B**). We then selected the concentrations of 10 ng/ml of IFN-γ and 5 ng/ml of TNF-α and we detected that IFN-γ and TNF-α decrease ΔΨm of mitochondria larger than 10 μm^2 (**Figures 2C, D**) and the impact is higher on larger mitochondria (**Supplementary Figure 1**). We performed the LDH assay of the selected doses of IFN-γ (10 ng/ml) and TNF-α (5 ng/ml) and we observed no cytotoxicity (**Figure 2E**).

Cytokine-Stimulated AC-16 Cells Display Increased RNS and Decreased ATP and mtDNA

We investigated whether IFN-γ and TNF-α prompt nitrosative and oxidative stress in AC-16 cardiomyocytes. We used the Griess reaction to measure nitrite in the supernatant of 48h IFN-γ and TNF-α-stimulated AC-16 cells. Nitrite accumulation in the supernatant of AC-16 was increased by TNF-α alone and not by IFN-γ or their combination after 48h of incubation (**Figure 3A**). Detection of 3-NT was performed by dot-blot. We observed that although IFN-γ or the cytokine combination induced a median increase of 25-72% in protein nitration, this was not statistically significant, most likely due to the high dispersion (**Figure 3B**). Cytokine treatment of AC-16 cardiomyocytes with IFN-γ, TNF-α and combined for 48h reduced the amount of MT-ND1 as compared to non-stimulated cells (**Figure 3C**). We also measured reactive oxygen species (ROS) production in AC-16 stimulated cells stained with the fluorogenic dye H_2DCFDA and we found a 43% increase in ROS after stimulation with IFN-γ and TNF-α and 23% with TNF-α (**Figure 3D**). In addition, luminescence assay also showed that the TNF-α alone or combined with IFN-γ decreased 50% and 58%, respectively, the ATP content in AC-16 cardiomyocytes (**Figure 3E**).

Molecular Pathways Analysis of Cytokine-Induced Δψm Reduction

In order to better understand the mechanisms by which IFN-γ and TNF-α diminish AC-16 ΔΨm, cells were treated with several compounds that activate or inhibit specific pathways. Each drug was titrated and the concentration of each compound was selected based on the highest restorative effect on ΔΨm and no more than 10% loss on cell number (**Supplementary Figures 2**, **3**). Concurrent treatment showed that agonists of signaling pathways related to response to stress and mitochondrial protection, such as AMPK (metformin, AICAR, resveratrol),

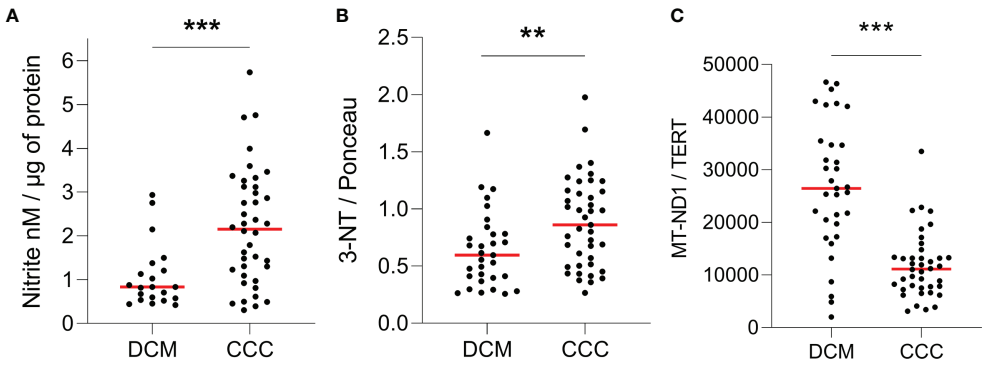

FIGURE 1 | Quantification of ROS, RNS and mitochondrial DNA in heart tissue. Lysates of left ventricular heart tissue were obtained from CCC (n = 40) and DCM (n = 31) patients and used for the quantification of **(A)** nitrite (nM) by chemiluminescence assay; **(B)** 3-nitrotyrosine by dot-blot and **(C)** copy number of the mitochondrial gene MT-ND1 by real time PCR. Red line: median; **p < 0.01; ***p < 0.001; Mann-Whitney test.

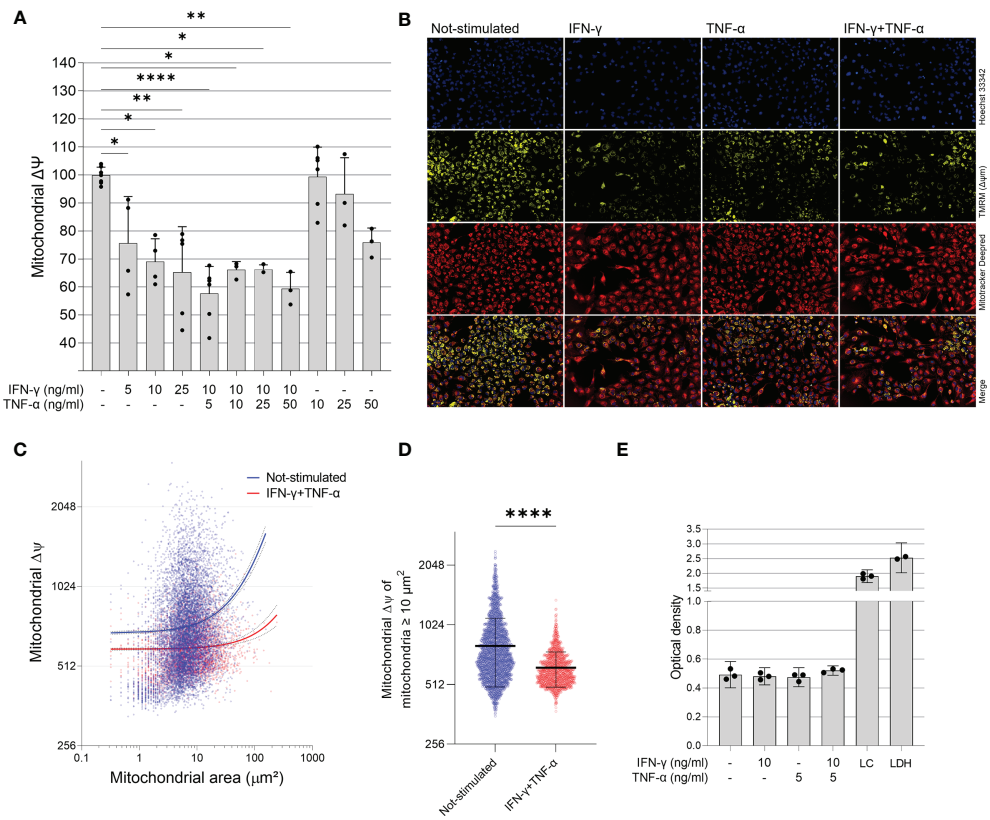

FIGURE 2 | Effect of IFN-γ and TNF-α on mitochondrial membrane potential in human cardiomyocytes AC-16 cells. Stimulated cells were multi-labelled with TMRM, Mitotracker DeepRed, NucGreen and DAPI. TMRM fluorescence was measured when colocalized with the fluorescence of Mitotracker Deep Red in live cells (NucGreen-negative). **(A)** IFN-γ and IFN-γ plus TNF-α downmodulate ΔΨm 48h after stimulation. Data shown as percentage to not-stimulated cells. *p < 0.05; **p < 0.01; ****p < 0.0001; One-way Anova, Dunn's post test. **(B)** Representative micrographs of the effect of IFN-γ (10 ng/ml), TNF-α (5 ng/ml) and both on the fluorescence of TMRM. Magnification 100x. **(C)** Correlation between size (µm^2) and TMRM fluorescence intensity of segmented mitochondria of cells stimulated with 10 ng/ml of IFN-γ and 5 ng/ml of TNF-α. **(D)** ΔΨm of mitochondria larger ≥ 10 µm^2 of cells stimulated with 10 ng/ml of IFN-γ and 5 ng/ml of TNF-α. ****p < 0.0001 Mann-Whitney test. **(E)** Supernatant quantification of lactate dehydrogenase (LDH assay) on stimulated cells. Each dot in bar graphs represents an independent experimental replicate n≥3. LC: lysed AC-16 cells; LDH: lactate dehydrogenase positive control.

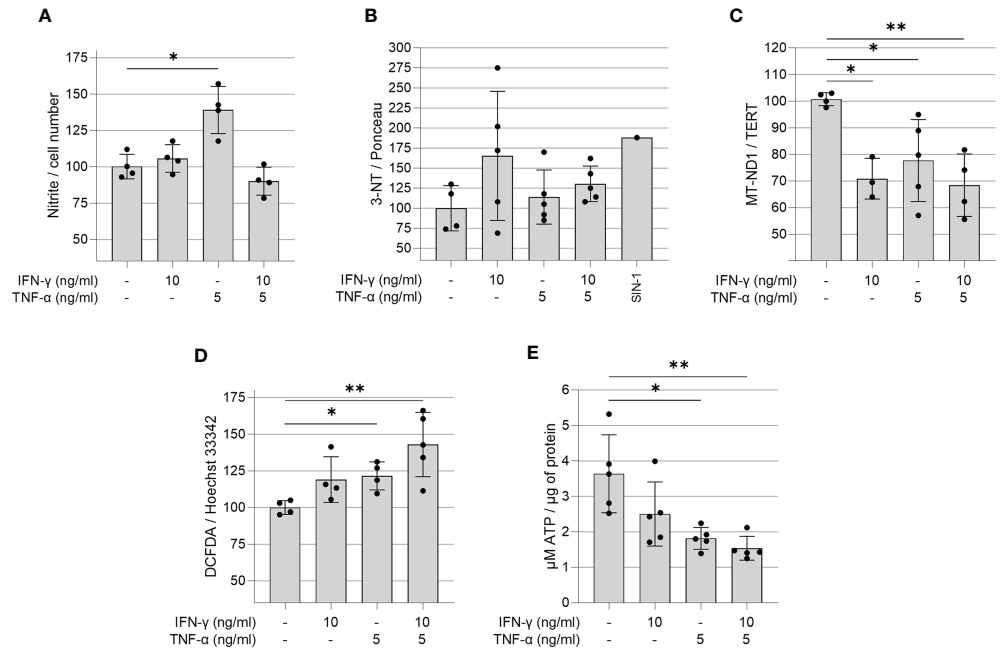

FIGURE 3 | Quantification of ROS, RNS, ATP and mitochondrial DNA in IFN-γ and TNF-α stimulated AC-16 cells. Human cardiomyocytes AC-16 cells were stimulated with 10 ng/ml of IFN-γ, 5 ng/ml of TNF-α or both for 48h. Then, cell lysates were used for the quantification of **(A)** nitrite (µM) by Griess Reaction; **(B)** 3-nitrotyrosine by dot blot; **(C)** copy number of the mitochondrial gene MT-ND1 by real time PCR; **(D)** cellular reactive oxygen species (ROS) by fluorescence assay using the probe DCFDA and **(E)** ATP by luciferase-based assay. Data are shown as percentage to not-stimulated cells in **(A–D)** *p < 0.05; **p < 0.01; one-way Anova Dunn's post test. Each dot represents an independent experiment n≥3.

NRF2 (Resveratrol and Protoporphyrin XI) and SIRT1 (SRT1720) restore ΔΨm (**Figures 4A–C**). Additionally, inhibition of IFN-γ downstream molecules with selected antagonists such as fludarabine (STAT1 inhibitor), emodin (NF-κB activation) JSH23 (NF-κB nuclear translocation), IKK16 (IκB kinase) and NOS2 (1400W) also restores AC-16 ΔΨm (**Figures 4D–G**). Finally, inhibition of TNF-α-downstream molecules such as MEK (PD98059), JNK (SP600125) and MAPK (SB202190) also restores AC-16 ΔΨm (**Figures 4H–J** respectively). The effect of NF-κB inhibitors on NF-κB nuclear translocation was validated by additional experiments. Immunocytochemistry shows that IFN-γ and TNF-α promote NF-κB nuclear translocation (**Figure 4K**), which was antagonized with emodin and JSH23 and simultaneously restored ΔΨm in AC-16 cardiomyocytes (**Figures 4L–M**). In addition, **Figure 4N** shows that NOS inhibitor 1400W significantly decreased nitrite accumulation caused by TNF-α ($p < 0.001$). A schematic representation of the signaling pathways and the targets of the compounds are detailed in **Supplementary Figure 4**.

IFN-γ+TNF-α Costimulation on the AC-16 Cell Line Induces a Significant Decrease of Total, Glycolysis and Mitochondrial ATP Production

The effect of IFN-γ+TNF-α stimulation on AC-16 was investigated by measuring the two major production pathways in mammalian cells (glycolysis and oxidative phosphorylation). Twenty-two independent measurements were done on non-stimulated AC-16 cells and 16 independent measurements were done on IFN-γ+TNF-α stimulated AC-16 cells. The OCR, ECAR and PER values were used to calculate glycolytic and mitochondrial ATP (**Figures 5A–D**). IFN-γ+TNF-α induced a significant decrease of total ATP production (33%; p=0.0001) (**Figure 5E**), glycolysis ATP production (30%; p<0.0001) (**Figure 5F**), and the mitochondrial ATP production (41%; p=0.02) (**Figure 5G**) was in line with the previous finding (**Figure 3E**). The percentage of oxidative phosphorylation was unchanged (**Figure 5H**).

IFN-γ+TNF-α Costimulation on the AC-16 Cell Line Induces an Increase of the Basal Respiration, Maximal Respiration, and Spare Respiratory Capacity

Metabolic flux analyses were performed on AC-16 cells with or without cytokine stimulation during 48h (n=21) (**Figure 5I**). **Figure 5J** illustrates the parameters analyzed. Cytokine-stimulated AC-16 cardiomyocytes increased basal respiration (53%; p=0.0007) compared to unstimulated cells (n=20) (**Figure 5K**). Also, the cytokines increased 54% (p=0.0009) the basal respiration used to drive ATP production (**Figure 5L**). Cytokine stimulation for 48h induces a proton leak (51%) indicating alteration of the mitochondria integrity (p=0.021) (**Figure 5M**). We also identified that cytokine stimulation

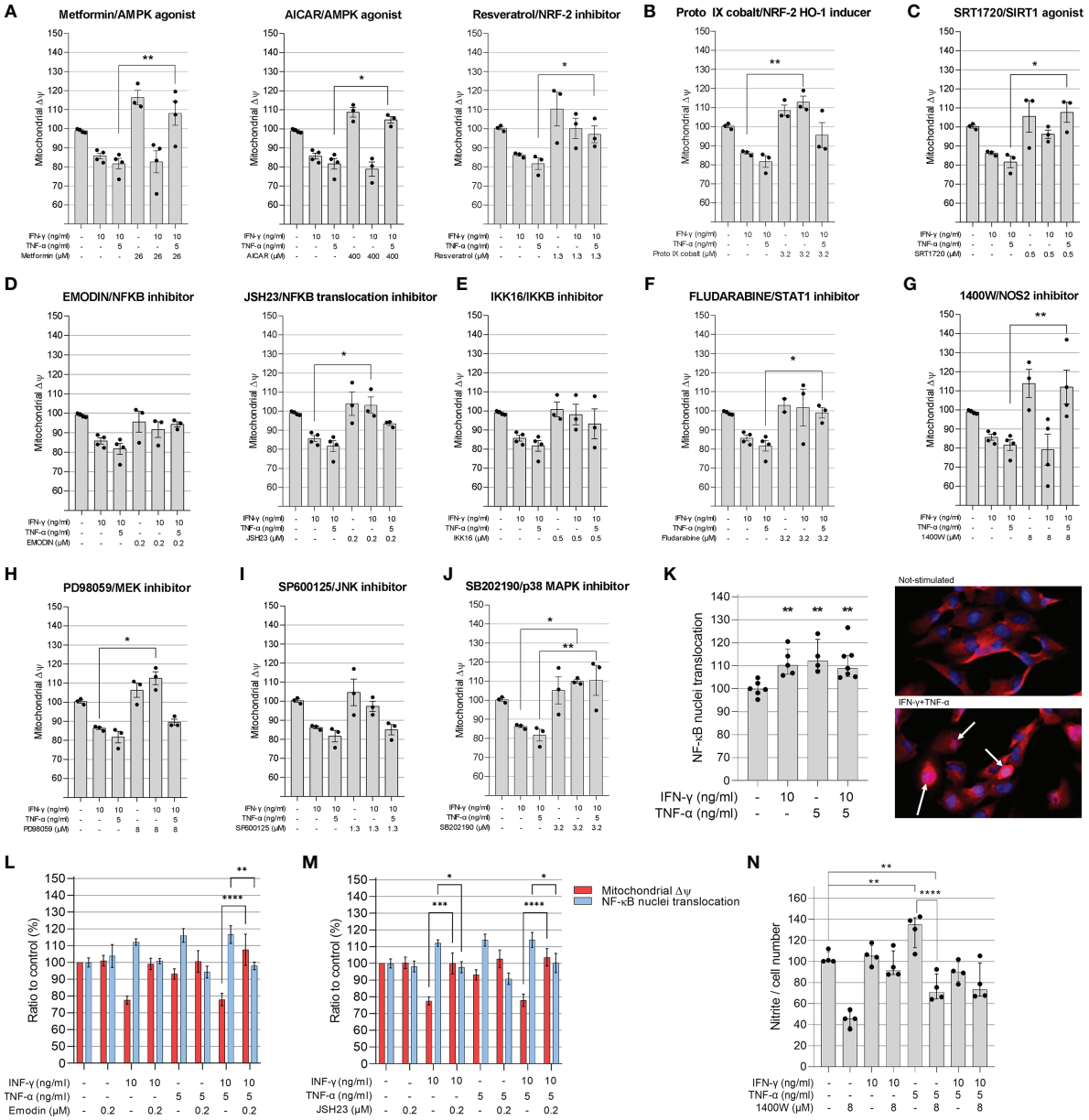

FIGURE 4 | Evaluation of compounds in the mitochondrial membrane potential of AC-16 cells. Selected doses of agonists of AMPK **(A)**, NRF2 **(B)**, SIRT1 **(C)** or inhibitors of NF-κB **(D)**, IKKβ **(E)**, STAT1 **(F)**, NOS2 **(G)**, MEK1 and MEK2 **(H)**, JNK **(I)** and MAPK **(J)** were used alone or in combination with 10 ng/ml of IFN-γ or IFN-γ plus 5 ng/ml of TNF-α. Specific doses were selected based on the highest effect on mitochondrial ΔΨm and less than 10% loss on cell number. **(K)** The nuclear translocation of NF-κB in AC-16 cells was quantified by immunocytochemistry. Simultaneous measurement of ΔΨm and NF-κB translocation of cells stimulated with 10 ng/ml of IFN-γ or IFN-γ plus 5 ng/ml of TNF-α in combination with the NF-κB inhibitors **(L)** emodin and **(M)** JSH23. Statistics shown only when both ΔΨm and NF-κB translocation were significant. **(N)** the amount of nitrite (μM) in conditioned medium was measured by Griess reaction of cells stimulated with 10 ng/ml of IFN-γ or IFN-γ plus 5 ng/ml of TNF-α in combination with NOS2 inhibitor 1400W. Micrographs of NF-κB stains in the nucleus (white arrow). All data are shown as percentage to not-stimulated cells. Standard deviation is from ≥3 independent experiments. *p < 0.05; **p < 0.01; ****p < 0.0001 one-way Anova Dunn's post test.

increases the maximal respiration (44% higher) compared with unstimulated cells (p=0.0005) (**Figure 5N**). Similar results are obtained for the spare respiratory capacity, which is the difference between maximal respiration and basal respiration (p=0.005) (**Figure 5O**). Cytokine stimulation also induced an increase in non-mitochondrial respiration (74%) compared to the non-mitochondrial respiration detected on unstimulated cells (p=0.014) (**Figure 5P**).

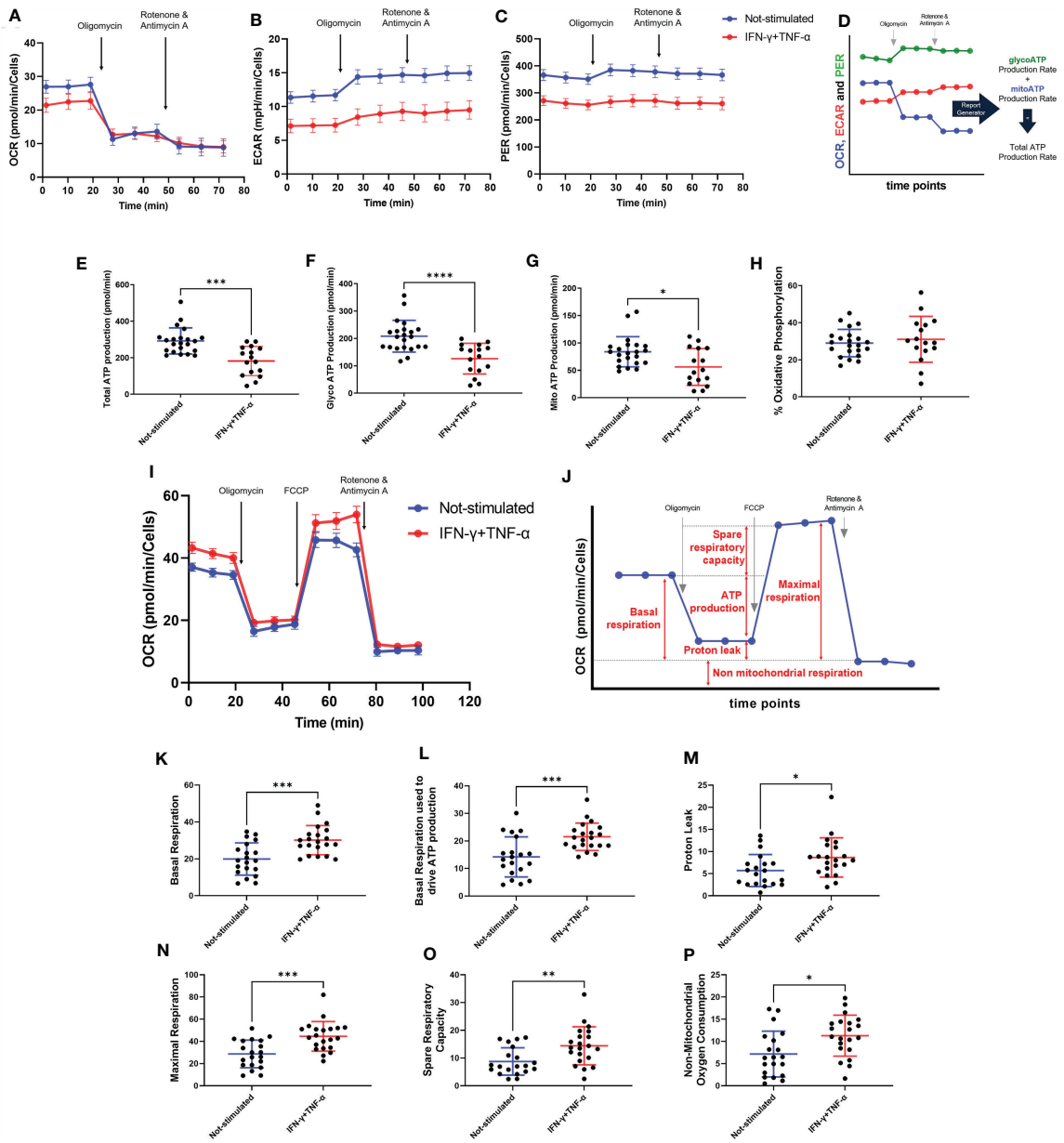

FIGURE 5 | Assessment of AC-16 respiration and ATP production in response to IFN-γ and TNF-α stimulation. Oxygen consumption rate (OCR), extracellular acidification rate (ECAR) and proton Efflux Rate (PER) of 48h IFN-γ (10 ng/ml) and TNF-α (5 ng/ml) -stimulated AC-16 cells were obtained in Seahorse XFe24 Analyzer. Arrows show injection of inhibitors of ATP synthase (oligomycin), mitochondrial oxidative phosphorylation uncoupler (FCCP) and OXPHOS complex I and III inhibitors (Rotenone and Antimycin A). **(A–C)** OCR, ECAR and PER measurement respectively obtained from ATP rate assay. **(D)** Calculation of mitochondrial and glycolytic ATP. **(E–G)** Quantification of total, glycolytic and mitochondrial ATP. **(H)** Percentage of oxidative phosphorylation. **(I)** OCR measurement of not-stimulated and cytokines-stimulated cells in the Mitostress test. **(J)** Representative graph showing the different parameters evaluated, such as **(K)** basal respiration, **(L)** basal respiration used to drive ATP production, **(M)** proton leak, **(N)** maximal respiration, **(O)** spare respiratory capacity and **(P)** non-mitochondrial oxygen consumption. Standard error of the mean in line graphs. Standard deviation is from ≥16 independent measurements. *p < 0.05; **p < 0.01; ***p < 0.001; ****p < 0.0001 Mann-Whitney test.

IFN-γ+TNF-α Costimulation Decreases AC-16 Cells' Dependency of Fatty Acid and Glutamine Oxidation

We investigated the effect of IFN-γ+TNF-α on AC-16 cell's dependency and capacity of fuel oxidation using Seahorse. We measured oxygen consumption after injection of different inhibitors (combined or not), such as: UK5099, inhibitor of the mitochondrial pyruvate carrier (MPC, glucose oxidation), BPTES, inhibitor of glutaminase GLS1 (KGA, glutamine oxidation) and etomoxir, an inhibitor of carnitine

palmitoyltransferase-1 (CPT-1, fatty acid oxidation). We then calculated the dependency, which is the cell's reliance on a particular fuel pathway to maintain basal respiration, and capacity, i.e. the ability of mitochondria to oxidize a fuel when other fuel pathways are inhibited.

We found that 48h stimulation with IFN-γ+TNF-α decreased 62% (p=0.0104 n=9) the reliance of AC-16 cells on glutamine (**Figures 6A, D**) and 87% dependency of fatty acid oxidation (p=0.0411 n≥9) (**Figures 6B, E**), with no effect on glucose dependency (**Figures 6C, F**). In addition, cells' capacity to oxidize fatty acid and glucose increased 46% (p=0.0037 n≥10 **Figures 6H, K**) and 105% (p<0.0001 n≥11 **Figures 6I, L**) respectively after stimulation with the cytokines. No changes were detected in glutamine capacity (**Figures 6G, J**). A summary of the global fuel oxidation of not-stimulated and cytokine-stimulated cells is shown in **Figure 6M**.

Mitochondrial Proteins Are Differentially Expressed Both in CCC and Cytokine-Treated AC-16 Cardiomyocytes

Extracted proteins from AC-16 were submitted to LC-MS/MS and comparative quantitative analysis of 1,211 identified proteins resulted in 275 differentially expressed proteins (DEP) between IFN-γ+TNF-α-treated AC-16 and non-treated AC-16; 37 DEPs were mitochondrial proteins, 25 being down-modulated and 12 up-regulated (**Supplementary Table 1**). Among downregulated proteins, 6 belonged to the TCA cycle and OXPHOS (ACO2, DLAT, FH, CS, NDUFV2, NDUFS8). We found reduced expression of two mitochondrial protein import enzymes (TIMM23, TOMM22) two linked to protein synthesis (RARS, GRSF1) and 2 to maintenance of mitochondrial membrane function and polarization (TRAP1, IMMT) and reduced levels of the ion carriers SLC25A40, SLC25A11, SLC25A3. We found downregulated proteins belonging to the lipid beta oxidation (ACOT13, HADH, FASN, ACAT1) and involved in ATP metabolism, ATP synthase regulation and ATP transport to the cytoplasm (ATPIF1, USMG5, PPIF and SLC25A6). PRDX3 and PRDX5 were downregulated and SOD2 was upregulated, consistent with oxidative stress. Reactome analysis of differentially expressed mitochondrial proteins disclosed repressed mitochondrial beta-oxidation and TCA cycle, increased glycolysis, increased mitochondrial protein import, ketone body metabolism and detoxification of reactive oxygen species. IPA canonical pathways analysis indicated mitochondrial dysfunction, reduced sirtuin-1 signaling, reduced TCA cycle, downregulated ketolysis, upregulation of superoxide radical degradation. A comparison of DEPs both in the cytokine-stimulated AC-16 cardiomyocytes and CCC myocardium (data not shown; submitted for publication) identified 19 matching proteins. Twelve out of the 19 were mitochondrial or related to energy metabolism, and 8 of them were similarly modulated in both proteome datasets. Among matching and differentially expressed mitochondrial proteins, we observed reduced expression of proteins including HADH and ACAT1 (fatty acid beta-oxidation), NDUFV2 (OXPHOS), and FH (TCA), with increased expression of PKM (glycolysis) and LAP3 (apoptosis).

Mitochondrial Genes Are Differentially Expressed in Cytokine-Treated AC-16 Cardiomyocytes

The AC-16 cell line was stimulated with IFN-γ and TNF-α during 1h to 48h. Gene expression analysis was performed in the various time points taking as reference the T=0h time point. We considered differentially expressed genes, genes characterized by a corrected p-value<0.05 (Benjamini Hochberg) and absolute log2 Fold Change>1.5. A total of 1443 DEGs were detected in all these comparisons (**Supplementary Table 2**). These DEGs include mainly protein coding genes (n=1149, 79.6%), as well as pseudogenes (n=68, 4.7%), antisense (n=89, 6.2%) and lnRNAs (n=94, 6.5%). The largest number of DEGs were detected at 6h or 12h (T=1h: n=214; T=6h: n=858; T=12h: n=847; T=24h: n=588; T=48h: n=234). Volcano plots and heatmaps are described in **Supplementary Figure 5** and **Supplementary Table 3**. The main pathways are linked to the immune response, to inflammation, to intracellular defense mechanisms, to fibrosis and cardiac diseases. Just after 1h of cytokine stimulation AC-16 cells increased the expression of cytokines and chemokines such as CXCL1, CCL2, CXCL2 and IL8, IRF1 and IRF9, indicating an interferon and pro-inflammatory signaling cascade with an overexpression of TNFAIP3 and NFKBIA which act as NFKB inhibitors. After 6h of stimulation, a large number of cytokine and chemokine genes and their receptors was upregulated, including CCL2, CCL7, CCL8, CCL13, CX3CL1, CXCL1, CXCL2, CXCL3, CXCL5, CXCL9, CXCL10, CXCL11, IFNAR2, IFNGR2, STAT1, TNF, IL1A, IL1B, IL4R, IL6, IL7, IL7R, IL12A, IL15, IL15RA, IL20RB, IL21R, IL32, IL33 genes). We also performed the same experiments with IFN-γ or TNF-α alone (**Figure 7** and **Supplementary Table 4**). Overall, we found 67 mitochondrial genes to be differentially expressed across at least one of the time points in response to combined cytokine stimulation. Differentially expressed mitochondrial genes peaked at 12h (46 genes) of which 25 were upregulated and 21 down-regulated (**Supplementary Table 5**). Among the top 10 canonical pathways of mitochondrial DEGs at 12h stimulus, we observed inhibition of the sirtuin signaling pathway, activation of aryl hydrocarbon receptor signaling, interferon signaling, and mitochondrial dysfunction. Toxicity-function pathways analysis at 12h indicated decreased transmembrane potential of mitochondria, fatty acid metabolism, mitochondrial dysfunction, pro-apoptosis, cardiac necrosis/cell death, cardiac hypertrophy among others (**Supplementary Table 6**). Mitochondrial dysfunction and decreased transmembrane potential were enriched toxicity functions in all time points starting at 6h (data not shown).

DISCUSSION

In this study, we investigated the mitochondrial function, nitro-oxidative profile, and gene and protein expression of myocardial samples from CCC patients. We also surveyed the effect of IFN-γ and TNF-α in AC-16 cardiomyocytes' mitochondria. These

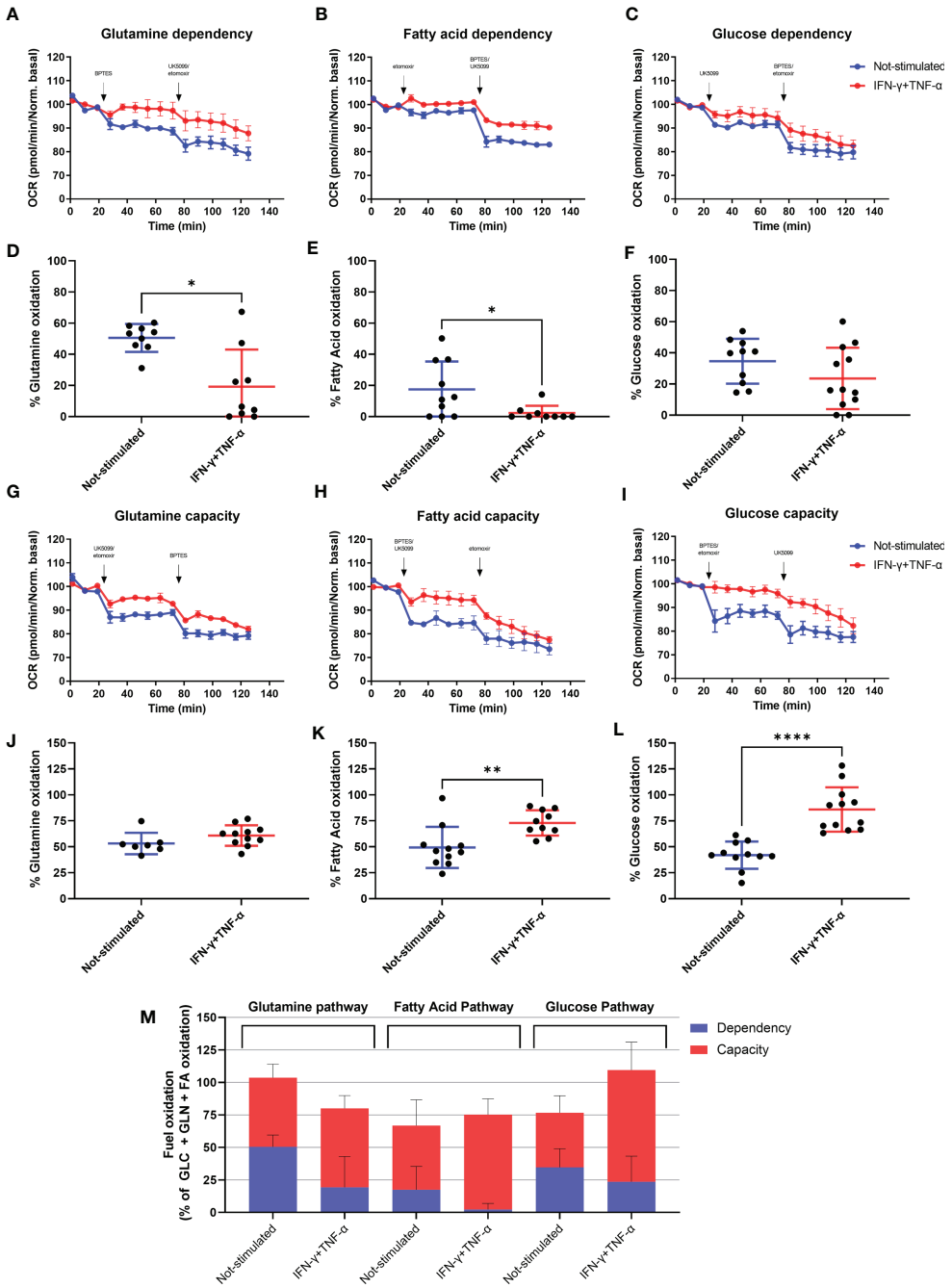

FIGURE 6 | Assessment of AC-16 fuel oxidation in response to IFN-γ and TNF-α stimulation. Oxygen consumption rate of 48h IFN-γ (10 ng/ml) and TNF-α (5 ng/ml)-stimulated AC-16 cells was obtained in Seahorse XFe24 Analyzer. Arrows show injection of inhibitors (combined or not) of molecules specific to different fuel oxidation pathways, such as; BPTES, inhibitor of glutaminase GLS1 (KGA, glutamine pathway), etomoxir, inhibitor of carnitine palmitoyltransferase-1 (CPT-1, fatty acid pathway) and UK5099, inhibitor of the mitochondrial pyruvate carrier (MPC, glucose pathway). **(A–F)** OCR dependency of glutamine, fatty acid oxidation and glucose. **(G–L)** OCR capacity of glutamine, fatty acid oxidation and glucose. **(M)** Global fuel oxidation. Standard error of the mean in line graphs. Standard deviation is from ≥9 independent measurements. *p < 0.05; **p < 0.01; ****p < 0.0001 Mann-Whitney test.

cytokines are known to be selectively produced by the myocardium of CCC patients and not DCM (7–11, 36, 37). We have identified that CCC myocardium displays an increased nitro-oxidative stress profile, as well as reduced mtDNA content in comparison to DCM samples and that these phenomena were also observed by IFN-γ/TNF-α treatment of AC-16 cardiomyocyte cell line. We performed mechanistic studies to better understand the role of the multiple signaling pathways in

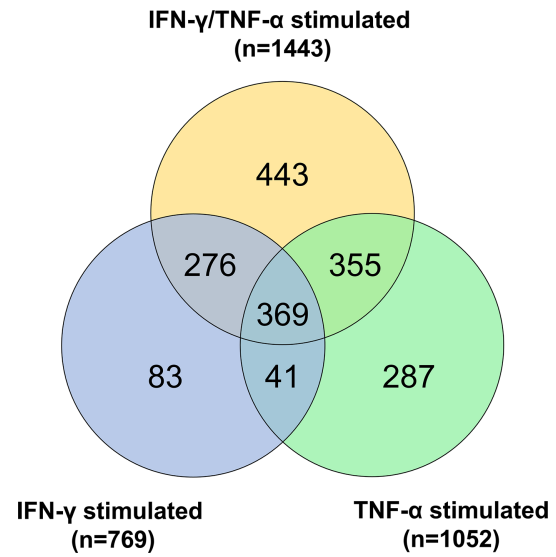

FIGURE 7 | Gene expression analysis on AC-16 cardiomyocytes. Cells were stimulated with IFN-γ (10 ng/ml) or TNF-α (5 ng/ml) or IFN-γ + TNF-α during 1 or 6 or 12 or 24 or 48h. On cardiomyocytes stimulated with TNF-α 1052 DEGs were detected whereas on cardiomyocytes stimulated with IFN-γ 769 DEGs were detected. Finally, on cardiomyocytes stimulated 48h with IFN-γ + TNF-α 1443 DEGs were detected. Venn diagram describes the DEGs shared by the various stimulations. Each stimulation was performed 4 times (4n).

the mitochondrial function of IFN-γ/TNF-α-treated AC-16 cardiomyocytes. We have found that the inhibition of STAT1/NF-κB/NOS2 axis and activation of AMPK, NRF2 and SIRT1 signaling pathways promoted protective effects in the IFN-γ/TNF-α-induced impairment of mitochondrial ΔΨ. Pathways analysis of gene and protein expression involved mitochondrial dysfunction and decreased ΔΨm were found in cytokine-treated AC-16 cells. In addition, we observed a cytokine-induced reduction in ATP production at the expense of mitochondrial energy metabolism in AC-16 cardiomyocytes that paralleled that observed in CCC myocardial tissue.

IFN-γ, but not TNF-α alone, was shown to impair the mitochondrial ΔΨm of AC-16 cells. We also observed that concurrent treatment with IFN-γ and TNF-α results in a further decrease in ΔΨm, and this reduction is higher in larger mitochondria. This finding is especially crucial since the mitochondrial ΔΨm is the OXPHOS proton motive force that drives ATP production through the ATP synthesis complex and thus it is an essential mechanism for contraction and survival of cardiac cells (38). Several *in vitro* studies have found the suppressing effect of TNF-α (39–42) and IFN-γ plus TNF-α (43) in mitochondrial ΔΨm in different cell types.

IFN-γ exerts its deleterious effects in the mitochondria at least partially by potentiating TNF-α-mediated NF-κB signaling (44). Activation of NF-κB triggers transcriptional activity of NOS2, which in turn produces nitric oxide (NO) and in the presence of reactive oxygen species (ROS) produces peroxynitrite ($ONOO^-$) one on the most toxic and highly oxidative reactive species with substantial effects in mitochondria (45, 46). In our observations, IFN-γ and/or TNF-α can increase NF-κB nuclear translocation, nitrite and ROS production, and 3-nitrotyrosine accumulation in AC-16 cardiomyocytes. Peroxynitrite and protein nitration cause inactivation of enzymes, poly(ADP-ribosylation), mitochondrial dysfunction, impaired stress signaling and also potently inhibits myofibrillar creatine kinase (MM-CK), an important controller of heart contractility (47, 48) whose activity has been shown to be decreased in CCC (18). Increases in ROS by IFN-γ and/or TNF-α was also reported in several cell lines (39, 41, 49, 50), including cardiomyocytes (42, 51–53). Enhanced ROS production is associated with increased levels of lipid peroxidation, decreased mtDNA copy number and impaired OXPHOS capacity, affecting cardiomyocyte structure and function which triggers signaling pathways involved in myocardial remodeling and failure (54, 55). Enhanced oxidative stress has been observed in CCC heart tissue as measured by the accumulation of malondialdehyde (submitted for publication). We here reported reduction of mtDNA content in CCC myocardium and IFN-γ/TNF-α-stimulated cardiomyocytes. The mtDNA is a circular double stranded DNA located in the mitochondrial matrix and codes for 37 genes (56) and the 13 polypeptides are the essential subunits of the OXPHOS complexes I, III, IV, and V (56, 57). Deficiency in mtDNA replication was shown to cause ROS accumulation and oxidative stress in murine cardiomyocytes (58, 59), which is also indicative of a reduced mitochondrial mass. Thus, our data suggest that mtDNA reduction observed in the CCC myocardium might be linked to the oxidative stress observed in IFN-γ and TNF-α-treated human cardiomyocytes. This is corroborated by the gene and protein expression analysis in cytokine-treated AC-16 cardiomyocytes, where decreased levels of proteins involved in ATP generation mitochondrial protein

and ion import and mitochondrial structural maintenance proteins and upregulated expression of proteins involved in ATP catabolism and mitochondrial transition pore. In addition, we observed pathways analysis of CCC heart tissue indicative of mitochondrial dysfunction, increased oxidative stress, and cardiac necrosis, all pointing towards mitochondrial stress and reduced functional capacity. In line with these, stimulation with IFN-γ and TNF-α depleted ATP production in AC-16 cells. Previous studies described the dampening of energy metabolism enzymes in CCC heart tissue, such as ATP synthase α and creatine kinase activity in patients (18–20, 60) and studies with animal models correlated with this outcome (61). Decreased *in vivo* ATP production was also observed in the CCC myocardium (21). In addition, our group identified an accumulation of heterozygous pathogenic variations including loss-of-function and stopgain/truncation of key mitochondrial genes in CCC patients (62). The loss of function mutation in one of the studied families was dihydroorotate dehydrogenase (DHODH) R135C. DHODH is involved in the oxidative phosphorylation by donating electrons to complex III and treatment with DHODH inhibitor Brequinar in IFN-γ+TNF-α-treated AC-16 cardiomyocytes caused additive damage to mitochondrial ΔΨm (62).

The inhibition of IFN-γ and TNF-α downstream molecules and pathways - STAT1/NF-κB, NOS2 - was important for the restoration of AC-16 ΔΨm and reduction of nitrite levels in AC-16 cardiomyocytes. The inflammatory milieu (IFN-γ, TNF-α, and IL-1b) enhanced ROS production in *T. cruzi* infected cardiomyocytes (51). Also, ROS production directly signaled the nuclear translocation of RelA (p65), NF-κB activation in AC-16 cells (63), indicating a positive feedback loop of stimulation between oxidative stress and NF-κB signaling. Studies reported that long-term sustained increase in ROS and RNS promotes cardiomyocyte dysfunction and apoptosis (64) resulting in reduction of mitochondrial ΔΨm, lipid beta-oxidation (65) and ATP generation (66, 67).

We found that the treatment of AC-16 cells with agonists of AMPK (resveratrol, AICAR and metformin) and NRF2 (protoporphyrin IX cobalt and resveratrol) rescued ΔΨm. AMPK and NRF2 are involved in the cellular response to oxidative stress by countering the damaging effects of NF-κB and by promoting ATP production and regulation of important physiological processes to restore heart function, such as autophagy (68–72). Our data showed that these agonists ameliorate IFN-γ/TNF-α-damaging effect to cardiomyocytes ΔΨm. Similarly, activation of AMPK (metformin) was shown to inhibit the enhancing effect of IFN-γ on the DOX-induced cardiotoxicity and prolonged the survival time in DOX-treated mice (65). Indeed, a recent study showed that antioxidants such as resveratrol and mitochondria-targeted antioxidants have potential benefits for the control of oxidative stress in the myocardium of mice with experimental Chagas disease cardiomyopathy (73). Our work potentially found the mechanistic link for the findings that treatment of chronically *T. cruzi*-infected mice with SIRT1 and/or AMPK agonists SRT1720, resveratrol and metformin or antioxidants reduced myocardial NF-κB transcriptional activity, inflammation and oxidative stress, resulting in beneficial results for restoration of cardiac function (73, 74).

Our transcriptomic profiling on cytokine-stimulated AC-16 cardiomyocytes over time (0 to 48h) showed that a cardiomyocyte can respond to inflammatory stimuli by producing inflammatory cell-attracting chemokines and inflammatory cytokines on its own as early as 1h after stimulus, perpetuating inflammation. Previous studies by our group in a subset of 10 out of the 30 CCC samples studied here observed increased mRNA expression of multiple chemokines and cytokines (9, 36, 75) in CCC heart tissue. At each time point, several genes associated with the mitogen-activated protein kinase (MAPK) signaling pathway were differentially expressed. This pathway is also one of the main inducers of the NF-κB pathway that is activated after inflammatory stimulus, ischemia/reperfusion, in congestive heart failure, dilated cardiomyopathy, after ischemic and pharmacological preconditioning, and in hypertrophy of isolated cardiomyocytes (76). Pathway analyses of gene and protein expression in the IFN-γ and TNF-α stimulated AC-16 cardiomyocytes profile were consistent with disturbances of ATP production and increased levels of reactive oxygen species. These metabolic changes affect cardiac ion channel gating, electrical conduction, intracellular calcium handling, and fibrosis formation.

As shown in the functional energy metabolism experiments, the integrity of the mitochondria is affected (proton leak). Therefore, cytokine-treated cardiomyocytes significantly increased their respiration (basal respiration, maximal respiration, spare respiratory capacity, as well as the percentage of basal respiration used to produce ATP. However, as mitochondria are less numerous (as seen with the reduced mitochondrial DNA) and their integrity is affected, the production of mitochondrial and glycolytic ATP is decreased in association with a significant decrease of the glutamine and fatty acid oxidation dependency – a reduction in metabolic flexibility that is found in failing hearts (77). This is in line with the IFN-γ and TNF-α induced NF-κB activation and activation of expression of NADP oxidases, and inducible nitric oxide synthase (NOS2), leading to the production of large amounts of NO and reactive nitrogen species (12, 78, 79) leading to synthesis of the peroxynitrite anion ($ONOO^-$) production, a strong oxidant arising from the reaction of NO with superoxide radical (O_2^-) (46).

This study has limitations, since we studied frozen human heart tissue samples and cytokine-treated human cardiomyocytes *in vitro*. Although some of the changes observed in IFN-γ and TNF-α-treated AC-16 cardiomyocytes closely parallel those observed in CCC heart tissue, this convergence is not proof that the findings in tissue are induced by the same cytokines, since several other mechanisms can induce nitro-oxidative stress and mitochondrial damage in CCC myocardium and as a consequence of heart failure. Conversely, our results with cytokine-treated cardiomyocytes can bring insight not only about Chagas disease, but also in other cardiac disorders where IFN-γ and TNF-α play a role, such as inflammatory cardiomyopathies of other etiology.

This study demonstrated that stimulation with IFN-γ and TNF-α in human cardiomyocytes causes mitochondrial damage, oxidative and nitrosative stress, paralleling events observed in the cytokine-rich CCC heart tissue. It is important to notice that the part of the CCC samples analyzed here have been previously assessed for cytokine expression and IFN-γ was among the most highly expressed cytokine, while IFN-γ and TNF-α were the top upstream regulators (9, 36). Both CCC myocardium and stimulated cells exhibited damaging profiles in markers of cellular stress and increased ROS and RNS, and decreased ATP. Several mitochondrial-related pathways important for mitochondrial integrity, function and ATP production were dysregulated in cytokine-stimulated cells. Also, cytokine-stimulated cells exhibited impaired ΔΨm and increased ROS and RNS and higher amounts of ROS. It is important to point out the direct involvement of the STAT1/NF-κB/NOS2 signaling pathway in the damaging effects of IFN-γ and TNF-α in cardiomyocytes' ΔΨm, as well as the restorative effects of stimulating the AMPK, NRF2 and SIRT1 pathways (**Figure 8**). Our results suggest that cytokine-induced disturbances in mitochondrial function and energy metabolism might play a role in the worse prognosis of Chagas disease cardiomyopathy. Therapy targeting mitochondrial function and energy imbalance should thus in principle be beneficial to restore cardiac function in CCC and other IFN-γ-dependent inflammatory heart diseases, like viral myocarditis and inflammatory cardiomyopathy of other etiologies, age-related myocardial inflammation and functional decline (80), myocardial infarction (81), and anthracycline antitumoral agent cardiotoxicity (65).

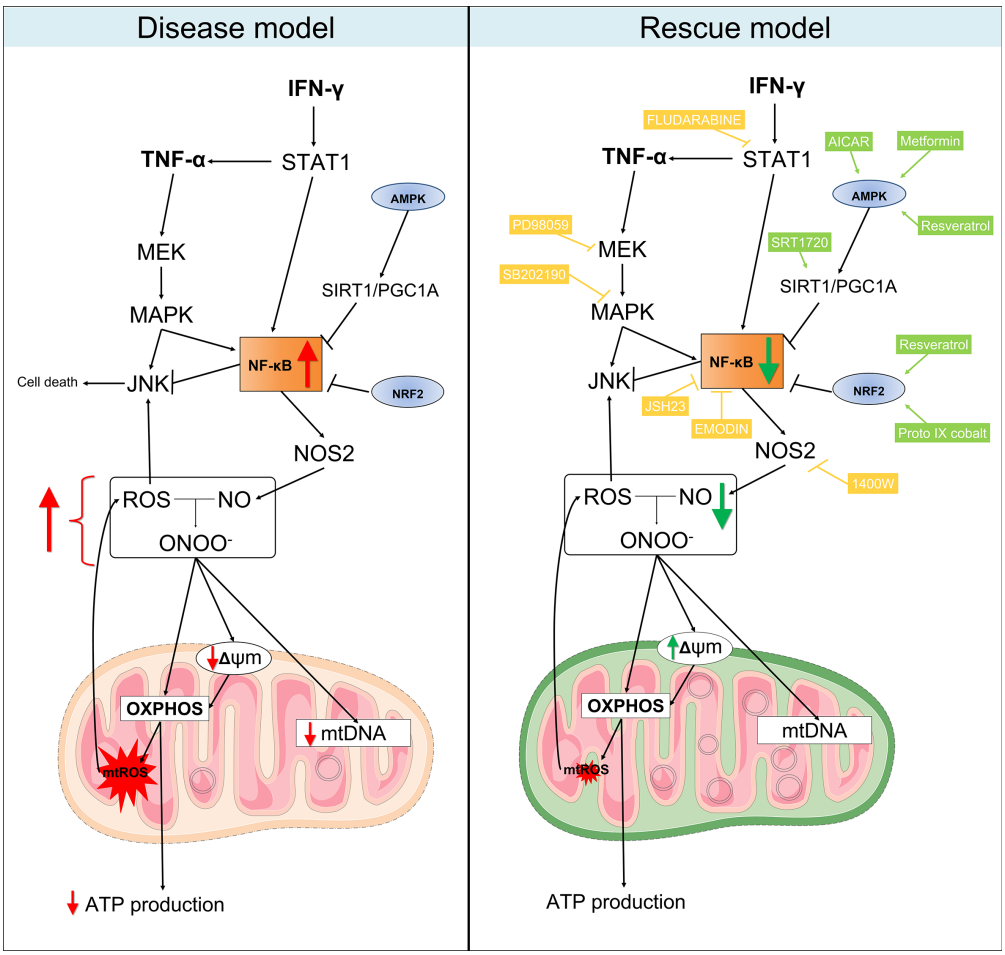

FIGURE 8 | Proposed model for the mitochondrial dysfunction in Chagas disease cardiomyopathy. Left panel: in summary, our results showed that heart tissues from CCC patients have increased production of RNS and reduced content of mitochondrial DNA in comparison with patients with DCM. Similarly, stimulation of AC-16 cardiomyocytes with IFN-γ/TNF-α increased ROS, RNS and proton leak, impaired ΔΨm, depleted ATP production and changed the metabolic profile of the cells. Right panel: in our rescue model, we showed that pharmacological inhibition of molecules involved in the IFN-γ/TNF-α/NF-κB/NOS2 pathway ameliorated the ΔΨm and NO production. Additionally, activation of AMPK/SIRT1 and NRF2 had beneficial impact on the ΔΨm. Thus, we hypothesize that mitochondrial dysfunction is driven by the excessive production of IFN-γ/TNF-α in CCC myocardium and is an essential component for the poor prognosis of Chagas disease cardiomyopathy. Mitochondria-targeted therapies might improve CCC disease progression. Compounds in yellow are inhibitors; Compounds in light green are agonists. Connecting arrows indicate activation and flat line means inhibitory interaction. Red and green arrows indicate the changes observed before and after treatment with the compounds.

Further studies with induced pluripotent stem cells derived cardiomyocytes (iPS-CM) can be employed to investigate, in a personalized, patient-specific manner, the effect of the cytokines in mitochondrial function.

DATA AVAILABILITY STATEMENT

The original contributions presented in the study are included in the article/**Supplementary Material**. Further inquiries can be directed to the corresponding authors.

ETHICS STATEMENT

The protocol was also approved by the INSERM Internal Review Board and the Brazilian National Ethics in Research Commission (CONEP). The patients/participants provided their written informed consent to participate in this study.

AUTHOR CONTRIBUTIONS

Study design: EC-N, CC, JN, FL, and JK. Phenotype characterization: EB, RS, FB, and PP. Experimental analysis: JN, PA, RA, EK, AH, LI, DA-S, KS, RV, DL, SB, FG, MT, and PT. Statistical analysis: HN, JN, PB, DG, and MM. Manuscript preparation: EC-N, CC, JN, and VP. All authors contributed to the article and approved the submitted version.

FUNDING

This work was supported by the Institut National de la Santé et de la Recherche Médicale (INSERM); the Aix-Marseille University (grant number: AMIDEX "International_2018" MITOMUTCHAGAS); the French Agency for Research (Agence Nationale de la Recherche-ANR (grant numbers: "Br-Fr-Chagas", "landscardio"); the CNPq (Brazilian Council for Scientific and Technological Development); and the FAPESP (São Paulo State Research Funding Agency Brazil (grant numbers: 2013/50302-3, 2014/50890-5); the National Institutes of Health/USA (grant numbers: 2P50AI098461-02 and 2U19AI098461-06). This work was founded by the Inserm Cross-Cutting Project GOLD. This project has received funding from the Excellence Initiative of Aix-Marseille University - A*Midex a French "Investissements d'Avenir programme"- Institute MarMaRa AMX-19-IET-007. JN was a recipient of a MarMaRa fellowship. ECN and JK are recipients of productivity awards by CNPq. The funders did not play any role in the study design, data collection and analysis, decision to publish, or preparation of the manuscript.

ACKNOWLEDGMENTS

We thank Andréia Kuramoto Takara (Laboratory of Immunology, InCor) and Victor Debbas (Laboratory of Vascular Biology, InCor) for their always helpful technical assistance.

SUPPLEMENTARY MATERIAL

The Supplementary Material for this article can be found online at: https://www.frontiersin.org/articles/10.3389/fimmu.2021.755862/full#supplementary-material

Supplementary Figure 1 | Stratification of mitochondria area and membrane potential after stimulation with IFN-γ and TNF-α in human cardiomyocytes AC-16 cells. Cells were stimulated with 10 ng/ml of IFN-γ + 5 ng/ml of TNF-α for 48 hours and then multi-labelled with TMRM, Mitotracker DeepRed, NucGreen and DAPI. TMRM fluorescence was measured when colocalized with the fluorescence of Mitotracker Deep Red in live cells (NucGreen-negative). Mitochondria were stratified based on their area in: lower than 5 **(A)**, between 5-10 **(B)**, between 10-25 **(C)**, between 25-50 **(D)** and **(E)** higher than 50 μm^2. **(F)** average (± SEM) value obtained from the mitochondrial membrane potential of each stratification of mitochondrial size. ****$p < 0.0001$; Mann Whitney test.

Supplementary Figure 2 | Compound screening in AC-16 mitochondrial membrane potential. AC-16 cells were treated with serially diluted agonists of AMPK **(A)**, NRF2 **(B)**, SIRT1 **(C)** or inhibitors of NF-κB **(D)**, IKKβ **(E)**, STAT1 **(F)**, NOS2 **(G)**, MEK1 and MEK2 **(H)**, JNK **(I)** and MAPK **(J)** alone (blue line) or in combination with 10 ng/ml IFN-γ (red line) or 10 ng/ml of IFN-γ plus 5 ng/ml TNF-α (green line) for 48 hours. Specific doses were selected based on the highest effect on mitochondrial $\Delta\Psi m$ and less than 10% loss on cell number. The first dot of the titration (to the left) is without compounds. Grey arrows indicate concentrations selected for . All data are shown as percentage to not-stimulated cells. Standard error of the mean is from 3 independent experiments.

Supplementary Figure 3 | Compound screening in the cell number of AC-16. AC-16 cells were treated with serially diluted agonists of AMPK **(A)**, NRF2 **(B)**, SIRT1 **(C)** or inhibitors of NF-κB **(D)**, IKKβ **(E)**, STAT1 **(F)**, NOS2 **(G)**, MEK1 and MEK2 **(H)**, JNK **(I)**, MAPK **(J)** and DMSO **(K)** alone (blue line) or in combination with 10 ng/ml of IFN-γ (red line) or 10 ng/ml of IFN-γ plus 5 ng/ml of TNF-α (green line) for 48 hours. The first dot of each titration (to the left) is without compounds. Grey arrows indicate concentrations selected for. Standard error of the mean is from 3 independent experiments.

Supplementary Figure 4 | Schematic representation of the inhibitors and agonists and their targets in the IFN-γ and TNF-α signaling pathways. The pro-inflammatory cytokine IFN-γ interacts with its transmembrane receptor IFNGR1 and signals mainly through the signal transducer and activator of transcription 1 (STAT1) and Interferon Regulatory Factor 1 (IRF1) intracellular transduction pathway to achieve transcriptional activation of IFN-γ-inducible genes, such as TNF-α and Nuclear Factor Kappa B (NF-κB). Activation of NF-κB leads to an upregulation of Nitric oxide synthase 2 (NOS2) gene, which in turn increases the amount of intracellular nitric oxide (NO), reacting to reactive oxygen species (ROS) to generate peroxynitrite ($ONOO^-$). Arrows indicate activation and flat line means inhibitory interaction. While $ONOO^-$ is important for pathogenic response, it causes damages to mitochondria, leading to reduction of mitochondria membrane potential and fragmentation. Proteins such AMPK and NRF2 are involved in the cellular response to oxidative stress countering the damaging effects of NF-κB. Compounds highlighted in yellow are inhibitors and green are agonists.

Supplementary Figure 5 | Transcriptomic analysis on AC-16 cardiomyocyte cell line stimulated with IFN-γ and TNF-α. AC-16 cells were stimulated with IFN-γ and TNF-α during 1h to 48h. Gene expression analysis was done between the various time points taking as reference the T=0h time point. At each time is provided the volcano plot and the heatmap. Each stimulation was performed 4 times.

REFERENCES

1. Savarese G, Lund LH. Global Public Health Burden of Heart Failure. *Card Fail Rev* (2017) 3(1):7–11. doi: 10.15420/cfr.2016:25:2
2. Bocchi EA, Bestetti RB, Scanavacca MI, Cunha Neto E, Issa VS. Chronic Chagas Heart Disease Management: From Etiology to Cardiomyopathy Treatment. *J Am Coll Cardiol* (2017) 70(12):1510–24. doi: 10.1016/j.jacc.2017.08.004
3. Issa VS, Ayub-Ferreira SM, Schroyens M, Chizzola PR, Soares PR, Lage SHG, et al. The Course of Patients With Chagas Heart Disease During Episodes of Decompensated Heart Failure. *ESC Heart Fail* (2021) p. 1460–71. doi: 10.1002/ehf2.13232
4. Cunha-Neto E, Chevillard C. Chagas Disease Cardiomyopathy: Immunopathology and Genetics. *Mediators Inflamm* (2014) 2014:683230. doi: 10.1155/2014/683230
5. Chevillard C, Nunes JPS, Frade AF, Almeida RR, Pandey RP, Nascimento MS, et al. Disease Tolerance and Pathogen Resistance Genes May Underlie. *Front Immunol* (2018) 9:2791. doi: 10.3389/fimmu.2018.02791
6. Frade-Barros AF, Ianni BM, Cabantous S, Pissetti CW, Saba B, Lin-Wang HT, et al. Polymorphisms in Genes Affecting Interferon-γ Production and Th1 T Cell Differentiation Are Associated With Progression to Chagas Disease Cardiomyopathy. *Front Immunol* (2020) 11:1386. doi: 10.3389/fimmu.2020.01386
7. Reis MM, Higuchi MEL, Benvenuti LA, Aiello VD, Gutierrez PS, Bellotti G, et al. An *in Situ* Quantitative Immunohistochemical Study of Cytokines and IL-2R+ in Chronic Human Chagasic Myocarditis: Correlation With the Presence of Myocardial Trypanosoma Cruzi Antigens. *Clin Immunol Immunopathol* (1997) 83(2):165–72. doi: 10.1006/clin.1997.4335
8. Abel LC, Rizzo LV, Ianni B, Albuquerque F, Bacal F, Carrara D, et al. Chronic Chagas' Disease Cardiomyopathy Patients Display an Increased IFN-Gamma Response to Trypanosoma Cruzi Infection. *J Autoimmun* (2001) 17(1):99–107. doi: 10.1006/jaut.2001.0523
9. Laugier L, Ferreira LRP, Ferreira FM, Cabantous S, Frade AF, Nunes JP, et al. miRNAs may Play a Major Role in the Control of Gene Expression in Key Pathobiological Processes in Chagas Disease Cardiomyopathy. *PLoS Negl Trop Dis* (2020) 14(12):e0008889. doi: 10.1371/journal.pntd.0008889
10. Reis DD, Jones EM, Tostes S, Lopes ER, Gazzinelli G, Colley DG, et al. Characterization of Inflammatory Infiltrates in Chronic Chagasic Myocardial Lesions: Presence of Tumor Necrosis Factor-Alpha+ Cells and Dominance of Granzyme A+, CD8+ Lymphocytes. *Am J Trop Med Hyg* (1993) 48(5):637–44. doi: 10.4269/ajtmh.1993.48.637
11. Rocha Rodrigues DB, dos Reis MA, Romano A, Pereira SA, Teixeira VEP, Tostes S, et al. *In Situ* Expression of Regulatory Cytokines by Heart Inflammatory Cells in Chagas' Disease Patients With Heart Failure. *Clin Dev Immunol* (2012) 2012:361730. doi: 10.1155/2012/361730
12. Hölscher C, Köhler G, Müller U, Mossmann H, Schaub GA, Brombacher F. Defective Nitric Oxide Effector Functions Lead to Extreme Susceptibility of Trypanosoma Cruzi-Infected Mice Deficient in Gamma Interferon Receptor or Inducible Nitric Oxide Synthase. *Infect Immun* (1998) 66(3):1208–15. doi: 10.1128/IAI.66.3.1208-1215.1998
13. Wu Y, Antony S, Juhasz A, Lu J, Ge Y, Jiang G, et al. Up-Regulation and Sustained Activation of Stat1 Are Essential for Interferon-Gamma (IFN-Gamma)-Induced Dual Oxidase 2 (Duox2) and Dual Oxidase A2 (DuoxA2) Expression in Human Pancreatic Cancer Cell Lines. *J Biol Chem* (2011) 286 (14):12245–56. doi: 10.1074/jbc.M110.191031
14. Kuroda J, Sadoshima J. NADPH Oxidase and Cardiac Failure. *J Cardiovasc Transl Res* (2010) 3(4):314–20. doi: 10.1007/s12265-010-9184-8
15. Sirker A, Zhang M, Murdoch C, Shah AM. Involvement of NADPH Oxidases in Cardiac Remodelling and Heart Failure. *Am J Nephrol* (2007) 27(6):649–60. doi: 10.1159/000109148
16. Brown DA, Perry JB, Allen ME, Sabbah HN, Stauffer BL, Shaikh SR, et al. Expert Consensus Document: Mitochondrial Function as a Therapeutic Target in Heart Failure. *Nat Rev Cardiol* (2017) 14(4):238–50. doi: 10.1038/nrcardio.2016.203
17. Chen L, Knowlton AA. Mitochondria and Heart Failure: New Insights Into an Energetic Problem. *Minerva Cardioangiol* (2010) 58(2):213–29.
18. Teixeira PC, Santos RH, Fiorelli AI, Bilate AM, Benvenuti LA, Stolf NA, et al. Selective Decrease of Components of the Creatine Kinase System and ATP Synthase Complex in Chronic Chagas Disease Cardiomyopathy. *PLoS Negl Trop Dis* (2011) 5(6):e1205. doi: 10.1371/journal.pntd.0001205
19. Wen JJ, Dhiman M, Whorton EB, Garg NJ. Tissue-Specific Oxidative Imbalance and Mitochondrial Dysfunction During Trypanosoma Cruzi Infection in Mice. *Microbes Infect* (2008) 10(10-11):1201–9. doi: 10.1016/j.micinf.2008.06.013
20. Wan X, Gupta S, Zago MP, Davidson MM, Dousset P, Amoroso A, et al. Defects of mtDNA Replication Impaired Mitochondrial Biogenesis During Trypanosoma Cruzi Infection in Human Cardiomyocytes and Chagasic Patients: The Role of Nrf1/2 and Antioxidant Response. *J Am Heart Assoc* (2012) 1(6):e003855. doi: 10.1161/JAHA.112.003855
21. Leme AM, Salemi VM, Parga JR, Ianni BM, Mady C, Weiss RG, et al. Evaluation of the Metabolism of High Energy Phosphates in Patients With Chagas' Disease. *Arq Bras Cardiol* (2010) 95(2):264–70. doi: 10.1590/S0066-782X2010005000099
22. Lee HJ, Oh YK, Rhee M, Lim JY, Hwang JY, Park YS, et al. The Role of STAT1/IRF-1 on Synergistic ROS Production and Loss of Mitochondrial Transmembrane Potential During Hepatic Cell Death Induced by LPS/d-GalN. *J Mol Biol* (2007) 369(4):967–84. doi: 10.1016/j.jmb.2007.03.072
23. Meyer A, Laverny G, Allenbach Y, Grelet E, Ueberschlag V, Echaniz-Laguna A, et al. IFN-β-Induced Reactive Oxygen Species and Mitochondrial Damage Contribute to Muscle Impairment and Inflammation Maintenance in Dermatomyositis. *Acta Neuropathol* (2017) 134(4):655–66. doi: 10.1007/s00401-017-1731-9
24. Davidson MM, Nesti C, Palenzuela L, Walker WF, Hernandez E, Protas L, et al. Novel Cell Lines Derived From Adult Human Ventricular Cardiomyocytes. *J Mol Cell Cardiol* (2005) 39(1):133–47. doi: 10.1016/j.yjmcc.2005.03.003
25. Quiros PM, Goyal A, Jha P, Auwerx J. Analysis of mtDNA/nDNA Ratio in Mice. *Curr Protoc Mouse Biol* (2017) 7(1):47–54. doi: 10.1002/cpmo.21
26. Bolger AM, Lohse M, Usadel B. Trimmomatic: A Flexible Trimmer for Illumina Sequence Data. *Bioinformatics* (2014) 30(15):2114–20. doi: 10.1093/bioinformatics/btu170
27. Dobin A, Davis CA, Schlesinger F, Drenkow J, Zaleski C, Jha S, et al. STAR: Ultrafast Universal RNA-Seq Aligner. *Bioinformatics* (2013) 29(1):15–21. doi: 10.1093/bioinformatics/bts635
28. Okonechnikov K, Conesa A, García-Alcalde F. Qualimap 2: Advanced Multi-Sample Quality Control for High-Throughput Sequencing Data. *Bioinformatics* (2016) 32(2):292–4. doi: 10.1093/bioinformatics/btv566
29. Liao Y, Smyth GK, Shi W. Featurecounts: An Efficient General Purpose Program for Assigning Sequence Reads to Genomic Features. *Bioinformatics* (2014) 30(7):923–30. doi: 10.1093/bioinformatics/btt656
30. Love MI, Huber W, Anders S. Moderated Estimation of Fold Change and Dispersion for RNA-Seq Data With Deseq2. *Genome Biol* (2014) 15(12):550. doi: 10.1186/s13059-014-0550-8
31. Laugier L, Frade AF, Ferreira FM, Baron MA, Teixeira PC, Cabantous S, et al. Whole Genome Cardiac DNA Methylation Fingerprint and Gene Expression Analysis Provide New Insights in the Pathogenesis of Chronic Chagas Disease Cardiomyopathy. *Clin Infect Dis* (2017) p. 1103–11. doi: 10.1093/cid/cix506
32. Masuda T, Tomita M, Ishihama Y. Phase Transfer Surfactant-Aided Trypsin Digestion for Membrane Proteome Analysis. *J Proteome Res* (2008) 7(2):731–40. doi: 10.1021/pr700658q
33. Rappsilber J, Mann M, Ishihama Y. Protocol for Micro-Purification, Enrichment, Pre-Fractionation and Storage of Peptides for Proteomics Using StageTips. *Nat Protoc* (2007) 2(8):1896–906. doi: 10.1038/nprot.2007.261
34. Cox J, Mann M. MaxQuant Enables High Peptide Identification Rates, Individualized P.P.B.-Range Mass Accuracies and Proteome-Wide Protein Quantification. *Nat Biotechnol* (2008) 26(12):1367–72. doi: 10.1038/nbt.1511
35. Cox J, Hein MY, Luber CA, Paron I, Nagaraj N, Mann M. Accurate Proteome-Wide Label-Free Quantification by Delayed Normalization and Maximal Peptide Ratio Extraction, Termed MaxLFQ. *Mol Cell Proteomics* (2014) 13 (9):2513–26. doi: 10.1074/mcp.M113.031591
36. Nogueira LG, Santos RH, Fiorelli AI, Mairena EC, Benvenuti LA, Bocchi EA, et al. Myocardial Gene Expression of T-Bet, GATA-3, Ror-γt, FoxP3, and Hallmark Cytokines in Chronic Chagas Disease Cardiomyopathy: An Essentially Unopposed TH1-Type Response. *Mediators Inflamm* (2014) 2014:914326. doi: 10.1155/2014/914326

37. Cunha-Neto E, Rizzo LV, Albuquerque F, Abel L, Guilherme L, Bocchi E, et al. Cytokine Production Profile of Heart-Infiltrating T Cells in Chagas' Disease Cardiomyopathy. *Braz J Med Biol Res* (1998) 31(1):133–7. doi: 10.1590/S0100-879X1998000100018
38. Kolwicz SC, Purohit S, Tian R. Cardiac Metabolism and Its Interactions With Contraction, Growth, and Survival of Cardiomyocytes. *Circ Res* (2013) 113 (5):603–16. doi: 10.1161/CIRCRESAHA.113.302095
39. Kastl L, Sauer S, Beissbarth T, Becker M, Krammer P, Gülow K. TNF-A Stimulation Enhances ROS-Dependent Cell Migration *via* NF-?B Activation in Liver Cells. *Free Radic Biol Med* (2014) 75(Suppl 1):S32. doi: 10.1016/j.freeradbiomed.2014.10.765
40. Doll DN, Rellick SL, Barr TL, Ren X, Simpkins JW. Rapid Mitochondrial Dysfunction Mediates TNF-Alpha-Induced Neurotoxicity. *J Neurochem* (2015) 132(4):443–51. doi: 10.1111/jnc.13008
41. Gottlieb E, Vander Heiden MG, Thompson CB. Bcl-X(L) Prevents the Initial Decrease in Mitochondrial Membrane Potential and Subsequent Reactive Oxygen Species Production During Tumor Necrosis Factor Alpha-Induced Apoptosis. *Mol Cell Biol* (2000) 20(15):5680–9. doi: 10.1128/MCB.20.15.5680-5689.2000
42. Cao YY, Chen ZW, Gao YH, Wang XX, Ma JY, Chang SF, et al. Exenatide Reduces Tumor Necrosis Factor-α-Induced Apoptosis in Cardiomyocytes by Alleviating Mitochondrial Dysfunction. *Chin Med J (Engl)* (2015) 128 (23):3211–8. doi: 10.4103/0366-6999.170259
43. Maiti AK, Sharba S, Navabi N, Forsman H, Fernandez HR, Lindén SK. IL-4 Protects the Mitochondria Against Tnfα and Ifnγ Induced Insult During Clearance of Infection With Citrobacter Rodentium and Escherichia Coli. *Sci Rep* (2015) 5:15434. doi: 10.1038/srep15434
44. Cheshire JL, Baldwin AS. Synergistic Activation of NF-kappaB by Tumor Necrosis Factor Alpha and Gamma Interferon *via* Enhanced I kappaB Alpha Degradation and *De Novo* I Kappabbeta Degradation. *Mol Cell Biol* (1997) 17 (11):6746–54. doi: 10.1128/MCB.17.11.6746
45. Kauppinen A, Suuronen T, Ojala J, Kaarniranta K, Salminen A. Antagonistic Crosstalk Between NF-κb and SIRT1 in the Regulation of Inflammation and Metabolic Disorders. *Cell Signal* (2013) 25(10):1939–48. doi: 10.1016/j.cellsig.2013.06.007
46. Rakshit S, Chandrasekar BS, Saha B, Victor ES, Majumdar S, Nandi D. Interferon-Gamma Induced Cell Death: Regulation and Contributions of Nitric Oxide, Cjun N-Terminal Kinase, Reactive Oxygen Species and Peroxynitrite. *Biochim Biophys Acta* (2014) 1843(11):2645–61. doi: 10.1016/j.bbamcr.2014.06.014
47. Mihm MJ, Coyle CM, Schanbacher BL, Weinstein DM, Bauer JA. Peroxynitrite Induced Nitration and Inactivation of Myofibrillar Creatine Kinase in Experimental Heart Failure. *Cardiovasc Res* (2001) 49(4):798–807. doi: 10.1016/S0008-6363(00)00307-2
48. Stavniichuk R, Shevalye H, Lupachyk S, Obrosov A, Groves JT, Obrosova IG, et al. Peroxynitrite and Protein Nitration in the Pathogenesis of Diabetic Peripheral Neuropathy. *Diabetes Metab Res Rev* (2014) 30(8):669–78. doi: 10.1002/dmrr.2549
49. Wang F, Zhang S, Jeon R, Vuckovic I, Jiang X, Lerman A, et al. Interferon Gamma Induces Reversible Metabolic Reprogramming of M1 Macrophages to Sustain Cell Viability and Pro-Inflammatory Activity. *EBioMedicine* (2018) 30:303–16. doi: 10.1016/j.ebiom.2018.02.009
50. Koo SJ, Chowdhury IH, Szczesny B, Wan X, Garg NJ. Macrophages Promote Oxidative Metabolism To Drive Nitric Oxide Generation in Response to Trypanosoma Cruzi. *Infect Immun* (2016) 84(12):3527–41. doi: 10.1128/IAI.00809-16
51. Gupta S, Bhatia V, Wen JJ, Wu Y, Huang MH, Garg NJ. Trypanosoma Cruzi Infection Disturbs Mitochondrial Membrane Potential and ROS Production Rate in Cardiomyocytes. *Free Radic Biol Med* (2009) 47(10):1414–21. doi: 10.1016/j.freeradbiomed.2009.08.008
52. Estrada D, Specker G, Martínez A, Dias PP, Hissa B, Andrade LO, et al. Cardiomyocyte Diffusible Redox Mediators Control. *Biochem J* (2018) 475 (7):1235–51. doi: 10.1042/BCJ20170698
53. Roberge S, Roussel J, Andersson DC, Meli AC, Vidal B, Blandel F, et al. TNF-α-Mediated Caspase-8 Activation Induces ROS Production and TRPM2 Activation in Adult Ventricular Myocytes. *Cardiovasc Res* (2014) 103(1):90–9. doi: 10.1093/cvr/cvu112
54. Ide T, Tsutsui H, Kinugawa S, Utsumi H, Kang D, Hattori N, et al. Mitochondrial Electron Transport Complex I Is a Potential Source of Oxygen Free Radicals in the Failing Myocardium. *Circ Res* (1999) 85 (4):357–63. doi: 10.1161/01.RES.85.4.357
55. Dutta D, Calvani R, Bernabei R, Leeuwenburgh C, Marzetti E. Contribution of Impaired Mitochondrial Autophagy to Cardiac Aging: Mechanisms and Therapeutic Opportunities. *Circ Res* (2012) 110(8):1125–38. doi: 10.1161/CIRCRESAHA.111.246108
56. Elorza AA, Soffia JP. mtDNA Heteroplasmy at the Core of Aging-Associated Heart Failure. An Integrative View of OXPHOS and Mitochondrial Life Cycle in Cardiac Mitochondrial Physiology. *Front Cell Dev Biol* (2021) 9:625020. doi: 10.3389/fcell.2021.625020
57. Yan C, Duanmu X, Zeng L, Liu B, Song Z. Mitochondrial DNA: Distribution, Mutations, and Elimination. *Cells* (2019) 8(4):1–15. doi: 10.3390/cells8040379
58. Lewis W, Day BJ, Kohler JJ, Hosseini SH, Chan SS, Green EC, et al. Decreased mtDNA, Oxidative Stress, Cardiomyopathy, and Death From Transgenic Cardiac Targeted Human Mutant Polymerase Gamma. *Lab Invest* (2007) 87 (4):326–35. doi: 10.1038/labinvest.3700523
59. Blasco N, Cámara Y, Núñez E, Beà A, Barés G, Forné C, et al. Cardiomyocyte Hypertrophy Induced by Endonuclease G Deficiency Requires Reactive Oxygen Radicals Accumulation and Is Inhibitable by the Micropeptide Humanin. *Redox Biol* (2018) 16:146–56. doi: 10.1016/j.redox.2018.02.021
60. Cunha-Neto E, Teixeira PC, Fonseca SG, Bilate AM, Kalil J. Myocardial Gene and Protein Expression Profiles After Autoimmune Injury in Chagas' Disease Cardiomyopathy. *Autoimmun Rev* (2011) 10(3):163–5. doi: 10.1016/j.autrev.2010.09.019
61. Garg N, Gerstner A, Bhatia V, DeFord J, Papaconstantinou J. Gene Expression Analysis in Mitochondria From Chagasic Mice: Alterations in Specific Metabolic Pathways. *Biochem J* (2004) 381(Pt 3):743–52. doi: 10.1042/BJ20040356
62. Ouarhache M, Marquet S, Frade AF, Ferreira AM, Ianni B, Almeida RR, et al. Rare Pathogenic Variants in Mitochondrial and Inflammation-Associated Genes May Lead to Inflammatory Cardiomyopathy in Chagas Disease. *J Clin Immunol* (2021) 41(July 2021):1048–63. doi: 10.1007/s10875-021-01000-y
63. Ba X, Gupta S, Davidson M, Garg NJ. Trypanosoma Cruzi Induces the Reactive Oxygen Species-PARP-1-RelA Pathway for Up-Regulation of Cytokine Expression in Cardiomyocytes. *J Biol Chem* (2010) 285 (15):11596–606. doi: 10.1074/jbc.M109.076984
64. Levick SP, Goldspink PH. Could Interferon-Gamma be a Therapeutic Target for Treating Heart Failure? *Heart Fail Rev* (2014) 19(2):227–36. doi: 10.1007/s10741-013-9393-8
65. Ni C, Ma P, Wang R, Lou X, Liu X, Qin Y, et al. Doxorubicin-Induced Cardiotoxicity Involves Ifnγ-Mediated Metabolic Reprogramming in Cardiomyocytes. *J Pathol* (2019) 247(3):320–32. doi: 10.1002/path.5192
66. Buoncervello M, Maccari S, Ascione B, Gambardella L, Marconi M, Spada M, et al. Inflammatory Cytokines Associated With Cancer Growth Induce Mitochondria and Cytoskeleton Alterations in Cardiomyocytes. *J Cell Physiol* (2019) 234(11):20453–68. doi: 10.1002/jcp.28647
67. Gupta S, Dhiman M, Wen JJ, Garg NJ. ROS Signalling of Inflammatory Cytokines During Trypanosoma Cruzi Infection. *Adv Parasitol* (2011) 76:153–70. doi: 10.1016/B978-0-12-385895-5.00007-4
68. Cuadrado A, Manda G, Hassan A, Alcaraz MJ, Barbas C, Daiber A, et al. Transcription Factor NRF2 as a Therapeutic Target for Chronic Diseases: A Systems Medicine Approach. *Pharmacol Rev* (2018) 70(2):348–83. doi: 10.1124/pr.117.014753
69. Sivandzade F, Prasad S, Bhalerao A, Cucullo L. NRF2 and NF-Ƙb Interplay in Cerebrovascular and Neurodegenerative Disorders: Molecular Mechanisms and Possible Therapeutic Approaches. *Redox Biol* (2019) 21:101059. doi: 10.1016/j.redox.2018.11.017
70. Saha S, Buttari B, Panieri E, Profumo E, Saso L. An Overview of Nrf2 Signaling Pathway and Its Role in Inflammation. *Molecules* (2020) 25(22):1–31. doi: 10.3390/molecules25225474
71. Li X, Liu J, Lu Q, Ren D, Sun X, Rousselle T, et al. AMPK: A Therapeutic Target of Heart Failure-Not Only Metabolism Regulation. *Biosci Rep* (2019) 39(1):1–13. doi: 10.1042/BSR20181767
72. Salminen A, Hyttinen JM, Kaarniranta K. AMP-Activated Protein Kinase Inhibits NF-κb Signaling and Inflammation: Impact on Healthspan and Lifespan. *J Mol Med (Berl)* (2011) 89(7):667–76. doi: 10.1007/s00109-011-0748-0

73. Sánchez-Villamil JP, Bautista-Niño PK, Serrano NC, Rincon MY, Garg NJ. Potential Role of Antioxidants as Adjunctive Therapy in Chagas Disease. *Oxid Med Cell Longev* (2020) 2020:9081813. doi: 10.1155/2020/9081813
74. Wan X, Wen JJ, Koo SJ, Liang LY, Garg NJ. SIRT1-Pgc1α-Nfκb Pathway of Oxidative and Inflammatory Stress During Trypanosoma Cruzi Infection: Benefits of SIRT1-Targeted Therapy in Improving Heart Function in Chagas Disease. *PLoS Pathog* (2016) 12(10):e1005954. doi: 10.1371/journal.ppat.1005954
75. Nogueira LG, Santos RH, Ianni BM, Fiorelli AI, Mairena EC, Benvenuti LA, et al. Myocardial Chemokine Expression and Intensity of Myocarditis in Chagas Cardiomyopathy Are Controlled by Polymorphisms in CXCL9 and CXCL10. *PLoS Negl Trop Dis* (2012) 6(10):e1867. doi: 10.1371/journal.pntd.0001867
76. Jones WK, Brown M, Ren X, He S, McGuinness M. NF-kappaB as an Integrator of Diverse Signaling Pathways: The Heart of Myocardial Signaling? *Cardiovasc Toxicol* (2003) 3(3):229–54. doi: 10.1385/CT:3:3:229
77. Karwi QG, Uddin GM, Ho KL, Lopaschuk GD. Loss of Metabolic Flexibility in the Failing Heart. *Front Cardiovasc Med* (2018) 5:68. doi: 10.3389/fcvm.2018.00068
78. Silva JS, Vespa GN, Cardoso MA, Aliberti JC, Cunha FQ. Tumor Necrosis Factor Alpha Mediates Resistance to Trypanosoma Cruzi Infection in Mice by Inducing Nitric Oxide Production in Infected Gamma Interferon-Activated Macrophages. *Infect Immun* (1995) 63(12):4862–7. doi: 10.1128/iai.63.12.4862-4867.1995
79. Vila-del Sol V, Punzón C, Fresno M. IFN-Gamma-Induced TNF-Alpha Expression Is Regulated by Interferon Regulatory Factors 1 and 8 in Mouse Macrophages. *J Immunol* (2008) 181(7):4461–70. doi: 10.4049/jimmunol.181.7.4461
80. Ramos GC, van den Berg A, Nunes-Silva V, Weirather J, Peters L, Burkard M, et al. Myocardial Aging as a T-Cell-Mediated Phenomenon. *Proc Natl Acad Sci USA* (2017) 114(12):E2420–9. doi: 10.1073/pnas.1621047114
81. Houssari M, Dumesnil A, Tardif V, Kivelä R, Pizzinat N, Boukhalfa I, et al. Lymphatic and Immune Cell Cross-Talk Regulates Cardiac Recovery After Experimental Myocardial Infarction. *Arterioscler Thromb Vasc Biol* (2020) 40(7):1722–37. doi: 10.1161/ATVBAHA.120.314370

Conflict of Interest: The authors declare that the research was conducted in the absence of any commercial or financial relationships that could be construed as a potential conflict of interest.

Publisher's Note: All claims expressed in this article are solely those of the authors and do not necessarily represent those of their affiliated organizations, or those of the publisher, the editors and the reviewers. Any product that may be evaluated in this article, or claim that may be made by its manufacturer, is not guaranteed or endorsed by the publisher.

frontiers in Immunology

ORIGINAL RESEARCH
published: 12 November 2021
doi: 10.3389/fimmu.2021.755782

Impairment of Multiple Mitochondrial Energy Metabolism Pathways in the Heart of Chagas Disease Cardiomyopathy Patients

*Priscila Camillo Teixeira[1,2], Axel Ducret[2], Hanno Langen[2], Everson Nogoceke[2], Ronaldo Honorato Barros Santos[3], João Paulo Silva Nunes[1,4,5,6], Luiz Benvenuti[7], Debora Levy[1], Sergio Paulo Bydlowski[1], Edimar Alcides Bocchi[8], Andréia Kuramoto Takara[1], Alfredo Inácio Fiorelli[3], Noedir Antonio Stolf[3], Pablo Pomeranzeff[3], Christophe Chevillard[4], Jorge Kalil[1,5,6] and Edecio Cunha-Neto[1,5,6]**

[1] Laboratory of Immunology, Heart Institute (Incor) Hospital das Clínicas da Faculdade de Medicina da Universidade de São Paulo, São Paulo, Brazil, [2] Roche Pharma Research and Early Development, Roche Innovation Center Basel, F. Hoffmann-La Roche, Basel, Switzerland, [3] Division of Surgery, Heart Institute, School of Medicine, University of São Paulo, São Paulo, Brazil, [4] INSERM, UMR_1090, Aix Marseille Université, TAGC Theories and Approaches of Genomic Complexity, Institut MarMaRa, Marseille, France, [5] Division of Clinical Immunology and Allergy, Faculdade de Medicina da Universidade de São Paulo, São Paulo, Brazil, [6] Instituto Nacional de Ciência e Tecnologia, INCT, iii- Institute for Investigation in Immunology, São Paulo, Brazil, [7] Anatomical Pathology Division, Heart Institute (Incor) Hospital das Clínicas da Faculdade de Medicina da Universidade de São Paulo, São Paulo, Brazil, [8] Heart Failure Team, Heart Institute (Incor) Hospital das Clínicas da Faculdade de Medicina da Universidade de São Paulo, São Paulo, Brazil

OPEN ACCESS

Edited by:
Clarissa M Maya-Monteiro, Oswaldo Cruz Foundation (Fiocruz), Brazil

Reviewed by:
Erika M Palmieri, National Cancer Institute at Frederick, United States
Qun Zang, Loyola University Chicago, United States

***Correspondence:**
Edecio Cunha-Neto
edecunha@gmail.com

Specialty section:
This article was submitted to Inflammation, a section of the journal Frontiers in Immunology

Received: *09 August 2021*
Accepted: *26 October 2021*
Published: *12 November 2021*

Citation:
Teixeira PC, Ducret A, Langen H, Nogoceke E, Santos RHB, Silva Nunes JP, Benvenuti L, Levy D, Bydlowski SP, Bocchi EA, Kuramoto Takara A, Fiorelli AI, Stolf NA, Pomeranzeff P, Chevillard C, Kalil J and Cunha-Neto E (2021) Impairment of Multiple Mitochondrial Energy Metabolism Pathways in the Heart of Chagas Disease Cardiomyopathy Patients. Front. Immunol. 12:755782. doi: 10.3389/fimmu.2021.755782

Chagas disease cardiomyopathy (CCC) is an inflammatory dilated cardiomyopathy occurring in 30% of the 6 million infected with the protozoan *Trypanosoma cruzi* in Latin America. Survival is significantly lower in CCC than ischemic (IC) and idiopathic dilated cardiomyopathy (DCM). Previous studies disclosed a selective decrease in mitochondrial ATP synthase alpha expression and creatine kinase activity in CCC myocardium as compared to IDC and IC, as well as decreased *in vivo* myocardial ATP production. Aiming to identify additional constraints in energy metabolism specific to CCC, we performed a proteomic study in myocardial tissue samples from CCC, IC and DCM obtained at transplantation, in comparison with control myocardial tissue samples from organ donors. Left ventricle free wall myocardial samples were subject to two-dimensional electrophoresis with fluorescent labeling (2D-DIGE) and protein identification by mass spectrometry. We found altered expression of proteins related to mitochondrial energy metabolism, cardiac remodeling, and oxidative stress in the 3 patient groups. Pathways analysis of proteins differentially expressed in CCC disclosed mitochondrial dysfunction, fatty acid metabolism and transmembrane potential of mitochondria. CCC patients' myocardium displayed reduced expression of 22 mitochondrial proteins belonging to energy metabolism pathways, as compared to 17 in DCM and 3 in IC. Significantly, 6 beta-oxidation enzymes were reduced in CCC, while only 2 of them were down-regulated in DCM and 1 in IC. We also observed that the cytokine IFN-gamma, previously described with increased levels in CCC, reduces mitochondrial membrane potential in cardiomyocytes. Results suggest a major reduction of mitochondrial energy

metabolism and mitochondrial dysfunction in CCC myocardium which may be in part linked to IFN-gamma. This may partially explain the worse prognosis of CCC as compared to DCM or IC.

Keywords: chronic Chagas disease cardiomyopathy, ischemic cardiomyopathy, idiopathic dilated cardiomyopathy, proteomics, two-dimensional electrophoresis with fluorescent labeling, mitochondria, energy metabolism, interferon-gamma

INTRODUCTION

Heart failure can be seen as a progressive disorder resulting from loss of cardiomyocyte function and contractility decline in the ability of the heart, due to molecular and structural modifications, collectively called cardiac remodeling (1). Chagas' disease is a neglected disease and a significant cause of morbidity and mortality in Central and South America, affecting about 6 million people (2). The disease is caused by infection with the intracellular protozoan parasite *Trypanosoma cruzi (T. cruzi)*. About 30% of infected patients develop chronic Chagas' disease cardiomyopathy (CCC), an inflammatory dilated cardiomyopathy that occurs decades after the initial infection, while 60% remain asymptomatic (ASY) and 10% develop gastrointestinal motility disorders. Chagas disease is the most common cause of non-ischemic cardiomyopathy in Latin America, where 6 million people are infected, causing approximately 10,000 deaths/year, mainly due cardiac compromise (2). Clinical progression, length of survival and overall prognosis are significantly worse in CCC patients compared with patients with dilated cardiomyopathy of non-inflammatory etiology (3–6). Due to migration to non-endemic countries, Chagas disease cardiomyopathy is now a global health problem (7). Refractory heart failure due to CCC is one of the main indications for heart transplantation in endemic countries. A recent report disclosed 25 cases of heart transplantation due to CCC in the USA, indicating the presence of patients with severe complications from Chagas disease (8). As the currently licensed anti-*T. cruzi* drugs are not effective in preventing the progression of heart lesions of CCC (9), treatment is only supportive. The absence of alternative specific treatment for CCC is a consequence of limited knowledge about the pathogenesis.

The pathogenesis of CCC is incompletely understood, and multiple mechanisms have been proposed, but myocarditis seems to play an important role [Reviewed in (2, 10)]. After acute infection by *T. cruzi*, parasitism is partially controlled by the immune response. Low-grade parasite persistence fuels the systemic production of inflammatory cytokines like IFN-gamma and TNF-alpha by T cells, which is more intense in CCC than ASY patients along the chronic phase of infection (11–13). CCC is characterized by a myocarditis rich in monocytes and IFN-gamma-producing T cells attracted to the heart by locally produced chemokines such as CCL5 and CXCL9 (14), with cardiomyocyte damage, fibrosis and hypertrophy; *T. cruzi* parasites are very scarce. Indeed, IFN-gamma is the most highly expressed cytokine in CCC myocardium (11, 12, 14–19) and a significant number of genes expressed in CCC myocardium is modulated by IFN-gamma (15, 20). T cells infiltrating the heart of CCC patients recognize both *T. cruzi* (21, 22) and pathogen-cross reactive autoimmune targets in the heart, like cardiac myosin and *T cruzi* antigen B13 (21). This aggressive myocarditis is without parallel in other etiologies of dilated cardiomyopathy, which may suggest the pathogenesis of cardiomyopathy due to Chagas disease may be distinct from non-inflammatory cardiomyopathy. In addition, the myocardium from CCC patients with ventricular dysfunction displays selectively decreased levels and activity of several mitochondrial energy metabolism enzymes, including mitochondrial ATP synthase alpha expression and creatine kinase activity, as compared with idiopathic dilated or ischemic cardiomyopathy (DCM and IC respectively) (23). Patients with CCC also displayed decreased *in vivo* myocardial ATP flux as determined by ^{31}P-NMR spectroscopy (24). These mitochondrial changes are thought to contribute to the worse prognosis of CCC as compared to other cardiomyopathies (25).

Systems biology approaches have been used to understand the pathogenesis of CCC, including gene expression and miRNA expression profiling (15, 20) and DNA methylation studies (26). Collectively, omics studies in Chagas disease indicate induction of genes related to cardiac hypertrophy, fibrosis, mitochondria/oxidative stress and arrhythmia, in common with other cardiomyopathies, but with a prominent set of differentially expressed inflammatory and IFN-gamma-dependent genes. Proteomic analysis has been widely applied to study cardiovascular disease also pointing toward the embryonic/hypertrophic phenotype and fibrosis (27–30). Studies are also needed to map the main proteins involved in the development of cardiovascular diseases. Given the striking inflammatory pattern and increased number of IFN-gamma-inducible gene among differentially expressed genes in CCC myocardium, we could hypothesize that proteomic analysis may shed light on the mechanisms of pathogenesis in CCC and its worse prognosis as compared to other cardiomyopathies. Given the ability of IFN-gamma to directly induce genes expression on cardiomyocytes (15) we assessed its ability to cause functional impairment in cardiomyocytes.

MATERIAL AND METHODS

Patients and Samples of Human Myocardium

Myocardial samples were obtained from left ventricular-free wall heart tissue from end-stage heart failure patients at the moment of

heart transplantation. Samples from 4 CCC (serological diagnosis, positive epidemiology for Chagas disease), 4 idiopathic dilated cardiomyopathy (DCM; dilated cardiomyopathy in the absence of ischemic disease, negative epidemiology and serology for Chagas disease) and 4 coronary angiography-proven dilated cardiomyopathy (IC) patients were collected for proteomic analysis (**Table 1**). Left ventricular free wall samples were also obtained from healthy hearts from organ donors, which were not designated for transplantation for technical reasons (control group). Additional myocardium samples from patients with CCC, DCM and IC and organ donors were used for confirmatory experiments (real-time PCR and immunoblotting) (**Supplemental Table S1**). Samples were cleared from pericardium and fat tissue, quickly frozen in liquid nitrogen and stored at -70° C. Protein homogenates were obtained using lysing solution (1:10w/v) containing 7mol/L urea, 10mmol/L Tris, 5mmol/L magnesium acetate and 4% CHAPS, pH 8.0, with mechanical homogenization (PowerGen, Fisher Scientific). The homogenate was then sonicated for three cycles of 10 seconds each to 10 Watts (60 Dismembrator Sonic, Fisher Scientific), centrifuged at 12,000g for 30 minutes. Supernatants were collected and stored at -70°C. Protein quantification was performed with the Bradford method (BioRad).

Two-Dimensional Electrophoresis (2D-DIGE)

For the separation of the myocardium proteins we used two-dimensional electrophoresis with a multiplexing fluorescent labeling approach (**Supplemental Figure S1**), that enables detection of small differences in protein levels as well as inclusion of an internal standard. The standard is a pool of all the samples within the experiment and therefore contains all proteins relevant for the experiment. By using an internal standard, gel-to-gel variation can be eliminated, quantification is accurate and system variation can be separated from biological variation. The first step was the individual labelling of each sample; 50ug protein of each sample (concentration 5μg/μL and pH 8.5) were labeled with 400pmol of one of the fluorophores (CY2, 3, or 5 - GE Healthcare) reconstituted with dimethylformamide. The reaction occurred on ice for 30 minutes, and stopped by adding 1μL of lysine 10mM. The individual samples were labeled with Cy3 or Cy5 fluorophores, and the standard sample ("pool") was labeled with the fluorophore Cy2. For each gel, two individual samples, one labeled with Cy3 and one labeled with Cy5, plus the internal standard ("pool") labeled with Cy2 were combined and applied to the two-dimensional electrophoresis. This procedure was performed for the preparation of the analytical gels. For the identification of proteins by mass spectrometry, a "preparative gel" was performed using the pool sample (500μg total protein: 450μg of unlabeled protein and 50μg of labeled protein with Cy2, the internal standard). The first dimension was performed in isoelectric focusing system "Ettan IPGphor" (GE Healthcare). The strips of immobilized pH gradient at pH 3 to 11 nonlinear gradient of 24cm (IPG strip) were rehydrated for at least 12 hours, with rehydration solution "DeStreak Rehydratation Solution" containing 0.5% "IPG buffer 3-11NL" (GE Healthcare). The electrodes were placed at the ends of the strips, and were then taken to the platform of "Ettan IPGphor (GE Healthcare) for isoelectric focusing so that the end of the focus was accumulated 64kV. After isoelectrofocusing, the strips were subjected to two rounds of equilibrium for the preparation of proteins for the second dimension. The first step, the reduction of proteins, was performed with the equilibrium solution (50mM tris-HCl, 6M urea, 30% glycerol, 2% SDS and 0.002% bromophenol blue, pH = 8.8) plus 10mg/mL of DTT (dithiothreitol) for 15 minutes. Second, alkylation of proteins was performed with the equilibrium solution plus 25 mg/ml iodoacetamide for 15 minutes. The second dimension was performed in the electrophoresis vertical "Ettan Daltsix" (6 gels of 25.5 x 20.5cm) (GE Healthcare). For gels with samples labeled

TABLE 1 | Baseline characteristics of patients included in the differential proteomic analysis.

Etiol*	Patient	Gender	Age	EF (%)†	RVDD (cm)‡	Fibrosis§	Myocarditis‖
CCC	#1	M	50	11	82	2+	2/3+
CCC	#2	M	57	29	71	1+	2/3+
CCC	#3	M	58	29	64	2+	2+
CCC	#4	M	59	17	64	2+	3+
IC	#1	M	49	25	76	1+	0
IC	#2	M	61	33	79	3+	0
IC	#3	M	52	20	62	3+	0
IC	#4	M	55	16	83	2+	0
DCM	#1	M	53	19	77	1/2+	0
DCM	#2	M	55	25	51	3+	0
DCM	#3	M	56	16	99	2+	0
DCM	#4	M	61	27	76	3+	0
N	#1	M	17	na	na	na	na
N	#2	M	22	na	na	na	na
N	#3	M	28	na	na	na	na
N	#4	M	40	na	na	na	na

**Etiol., Etiology; †EF, Ejection Fraction (reference value, ≥55%); ‡ LVDD, Left Ventricular Diastolic Diameter (reference value, 39-53mm); § and ‖ as rated by histopatology (0, absent; 1 +, mild; 2 +, moderate; 3 +, intense); N, individuals without cardiomyopathies; CCC, chronic Chagas disease cardiomyopathy; DCM, idiopathic dilated cardiomyopathy; IC, ischemic cardiomyopathy; M, Male; na, not applicable or not available.*

with the fluorophore, we used glass plates with low fluorescence. The polyacrylamide gels were 12.5%, over which the strips were placed. The set was sealed with 0.5% agarose in electrophoresis buffer. The electrophoresis was performed in buffer containing 25mM Tris-HCl, 192mM glycine, and 0.1% SDS, pH 8.3 with a power of 2.5W/gel for 30 minutes and 100W total by the end of the race. To maintain the temperature to 20°C in the tank "DaltSix" was used a cooler "MultiTemp III (GE Healthcare) at 10°C. After the second dimension, gels were fixed in a solution containing 40% methanol and 10% acetic acid. Only the "preparative gel" was stained in a solution containing 8% ammonium sulfate, 0.8% phosphoric acid, 0.08% Coomassie Blue G-250 and 20% methanol, and then bleached in water. The gels were kept in a solution containing 15% ethanol. The "preparative gel" stained with Colloidal Coomassie Blue were scanned by the device "ImageScanner" (GE Healthcare) using green filter, transparent and 300dpi resolution. The "analytical gels" containing samples labeled with fluorophores were scanned by the device "Typhoon 9410 Variable Mode Imager" (GE Healthcare), using the following parameters: Cy2, 488nm excitation and 520 nm-BP 40nm emission filter; Cy3, 532nm excitation and 580nm - BP 40nm emission filter; Cy5, 633nm excitation and 670nm - BP 40nm emission; with resolution 100micra and the sensitivity ranged from 450 to 550PTM.

Statistical Analysis of Differential Protein Expression Using the DIGE

The analysis of differential protein expression using the DIGE technique was performed using the DeCyder Differential Analysis version 6.5 software (GE Healthcare). The volume of each spot was normalized in relation to the total volume of spots selected, and the gels were normalized together using the image of the pool of samples labeled with Cy2. The proteomic profiles of each disease group were compared with healthy donor subjects (control group). For each experimental group, spots present in at least 80% of samples were considered. One of the gels was chosen as a reference ("master" gel, Cy2 labeling in the preparative gel) for the spots matching between the gels. Statistically significant differences of 2D-DIGE data were computed by analysis of variance (ANOVA) and Student t-tests. False discovery rate was applied as a multiple test correction in order to keep the overall error rate as low as possible, according to software manual and literature (31). Power analysis was conducted on statistically changed spots, and only spots that reached a sensitivity threshold > 0.8 were considered as differentially expressed. We considered a protein to be differentially expressed if one or more of the associated spots was differentially expressed ($p<0.01$). The Ingenuity Pathways Analysis (IPA©, Qiagen, Redwood City, USA) software was used to analyze the differentially expressed protein profile. Qiagen Ingenuity Pathway analysis software provides a P value representing Fisher's exact test representation of proteins in each pathway that are present or not in each pathway. The more proteins in the pathway, the lower the P value. No FDR calculation was applied in this analysis.

Automatic in Gel Protein Digestion

After detection of spots, these were picked from the "preparative gel" (previously stained with Colloidal Coomassie Blue) and processed by automated system "Ettan Spot Handling Workstation" (GE Healthcare). In this system the spots were removed from the gel and submitted to tryptic "in gel" digestion. The tryptic peptide fragments were extracted from the gel spots for further analysis by mass spectrometry. In summary, gel spots were treated with solutions containing ammonium bicarbonate and acetonitrile. Each spot gel was dried and trypsin (1.6mg/ml in 20mM ammonium bicarbonate) was added. Digestion was performed at 37°C for 6 hours. The product of tryptic digestion was extracted from the spot gel with a solution containing 50% acetonitrile and 0.45% trifluoroacetic acid (TFA). The product was then dried and resuspended in 5μL of 50% acetonitrile and 0.5% TFA prior to mass spectrometry analysis.

Analysis by Mass Spectrometry and Protein Identification

An aliquot (1μL) of the tryptic digest was placed onto a MALDI target slide and 1.5μL matrix solution with standards [5 mg/ml α-Cyano-4-hydroxycinnamic acid in 50% Acetonitrile and 0.1% TFA, containing the peptides bradykinin (Brad, 10fmol/μL, MW = 904.46 kDa) and adrenocorticotropic hormone (ACTH, 40fmol/μL, MW = 2465.19 kDa)]. The standard peptides were used for calibration during the mass determination. The samples were analyzed on a MALDI-TOF/TOF mass spectrometer (MS), "Matrix assisted laser desorption/ionization - Time-of-Flight, Ultraflex III (Bruker). The analysis was performed in the "Reflectron" positive node. The detection mass range was between 880 – 3480, and the number of shots ca. 200-300. The spectrum calibration was done by quadratic fit using the internal calibrating peptides: ACTH (18–39), mass selected 2465.20 and des-Arg_Brad_MH+_mono, mass selected 904.47. The result was a list of values that correspond to the ratio mass/charge (m/z) of each peptide present in the tryptic digested sample. Peptide matching and protein searches were performed automatically with the use of in-house developed software "Poseidon" (32) or using the tool Mascot (www.matrixscience.com). The peptide masses (Peptide Mass Fingerprinting, PMF) were compared with the theoretical peptide masses of all available proteins from *Homo sapiens* specie in the database "SwissProt". Monoisotopic masses were used and a mass tolerance of 0.0025% was allowed. The probability of a false positive match with a given MS-spectrum was determined for each analysis (Score). Unmatched peptides or miscleavage sites were not considered. Analysis in the MS/MS mode was performed using the instrument's software. The significance threshold was set at P-value < 0.05. No mass and pI constraints were applied, and trypsin was set as enzyme. One missed cleavage per peptide was allowed, and carbamidomethylation was set as fixed modification while methionine oxidation as variable modification. Mass tolerance was set at 30ppm for MS spectra.

Functional analysis of proteins expressed in the myocardium was performed using the bioinformatics tools as the "Locus Link" (www.ncbi.nlm.nih.gov/locuslink) and based on the classification "Gene Ontology". The names and acronyms, as

well as the access number of proteins, were obtained by the tool UniProt (http://www.uniprot.org).

Analysis of Protein Levels by Immunoblotting

Extracts of myocardial samples containing 30μg of protein were heated for 5 minutes at 95°C and subjected to one-dimensional electrophoresis (SDS-PAGE) using 12.5% polyacrylamide gel and the vertical electrophoresis system Ruby SE600 (GE Healthcare). After electrophoresis, proteins were transferred from the gel to a nitrocellulose membrane using the TE Semi-Dry Transfer Unit (GE Healthcare). The nitrocellulose membranes were incubated with monoclonal antibodies to specific proteins found with altered levels in the proteomic analysis: anti-CATA (catalase, mouse monoclonal antibody, 1 μg/mL, Sigma), anti-ACADVL (Very long-chain specific acyl-CoA dehydrogenase, mouse monoclonal antibody, 1 μg/mL, Abcam) and anti-DECR1 (2,4-dienoyl-CoA reductase 1, mouse monoclonal antibody, 1 μg/mL, Abcam). Each membrane was subjected to incubation with compatible secondary antibodies conjugated with peroxidase, developed using ECL Plus Western Blotting Detection Reagents (GE Healthcare) and detection using X-ray equipment. Analysis of densitometry was performed using the program ImageQuant TL (GE Healthcare). The relative abundance of a specific protein across the lanes of the blot was given by the normalization to the total amount of protein in each lane. Statistical analysis was performed with the Graphpad Prism software (Graphpad Software Inc, San Diego, USA). One-way ANOVA was used to compare the different unmatched groups, followed by the Tukey-Kramer test, which compares every mean with every other group mean and allows for the possibility of unequal sample sizes.

Analysis of mRNA Expression by Real-Time Reverse Transcriptase (RT)-PCR

Total RNA from left ventricle samples was isolated using the RNeasy Fibrous tissue kit (Qiagen). Contaminating DNA was removed by treatment with RNase-free DNase I. cDNA was obtained from 5μg total RNA using Super-script II™ reverse transcriptase (Invitrogen). mRNA expression was analyzed by real-time quantitative reverse transcriptase (RT)-PCR with SYBR Green I PCR Master Mix (Applied Biosystems) and 250nM of sense and anti-sense primers using the ABI Prism 7500 Real Time PCR System (Applied Biosystems). The following primers were designed using Primer Express software version 3.0 (Applied Biosystems): HPRT1 (hypoxanthine phosphoribosyltransferase 1); (F) 5' ATTAAAGCACTGAAT AGAAAT 3', (R) 3' TAAAGATAAGTCACGAAATTA 5', amplicon 108bp; ACADVL: (F) 5'-CCATACCCGTCCGTGCT-3'; (R) 5'-GAGCGTCATTCTTGGCGG-3', amplicon 109bp; DERC1: (F) 5' AAGCACAGAAAGGAGCAGCA 3', (R) 5' TCATGGCTTCCACACCTGC 3', amplicon 108bp. After every PCR, an amplicon melting point curve was obtained. This yielded a single peak with the expected temperature provided by Primer Express software, confirming the specificity of the PCR. HPRT mRNA expression was used for normalization. The amount of mRNA in the left ventricle samples was calculated using the $2^{-\delta Ct}$ method (33). Statistical analysis was also performed with the Graphpad Prism software (Graphpad Software Inc, San Diego, USA). One-way ANOVA was used to compare the different unmatched groups, followed by the Tukey-Kramer test, which compares every mean with every other group mean and allows for the possibility of unequal sample sizes.

Lipid Peroxidation Evaluation

Lipid peroxidation levels were evaluated by the TBARS (thiobarbituric acid reactive substance) method based on the reaction of malonaldehyde (MDA), the major lipid oxidation product, with thiobarbituric acid (TBA), which leads to the formation of the TBA-MDA adduct (TBARS). The adduct has fluorescence property and was isolated and detected by high performance liquid chromatography (HPLC) with a fluorescence detector (34). Briefly, 50mg tissue was processed in 500μL TKM solution (Tris-HCl 50mM, KCl 25mM; $MgCl_2$ 5mM; pH 7.5). For a 200μL aliquot of the tissue homogenate, further 200μL of TKM solution was added and subsequently 500μL of a 0.4%(w/v) solution of TBA in HCl 0.2N/H_2O (2:1), 75μL of 0.2% (w/v) solution of BHT in 95% ethanol and 50μL of 10% (w/v) SDS. The mixture was heated to 90°C for 45 min, cooled on ice, and extracted with an equal volume of isobutanol. The isobutanolic phase was injected through a Shimadzu auto injector model SIL-10AD/VP (Shimadzu, Kyoto, Japan) in a Shimadzu HPLC system, consisting of two pumps LC-6AD connected to a Lichrosorb 10 RP-18 (Phenomenex, Torrance, CA) reversed-phase column. The flow rate was 0.8mL/min (5–25% acetonitrile in H_2O deionized). The MDA-TBA adduct was detected with a RF-10A/XL fluorescence detector set at an excitation wavelength of 515nm and an emission wavelength of 550nm, and data were processed using Shimadzu ClassVP 5.03 software. Malonaldehyde-bisdiethylacetal was used as a standard. Statistical analysis was performed with the Graphpad Prism software (Graphpad Software Inc, San Diego, USA). One-way ANOVA was used to compare the different unmatched groups, followed by the Tukey-Kramer test, which compares every mean with every other group mean and allows for the possibility of unequal sample sizes.

Effect of IFN-Gamma on Cardiomyocyte Mitochondrial Membrane Potential

Human adult ventricular cardiomyocyte cell line AC16 was propagated using DMEM:F12 supplemented with 12.5% inactivated fetal bovine serum (FBS) without antibiotics and used during 8 passages. A quantity of 0.10x10e4 cells were seeded per 0.34cm² and incubated in a humidified incubator at 37°C and 5% CO_2 for 24 hours. Then, cells were treated with 5, 10 or 25ng/ml of IFN-gamma for 48 hours. At the end of treatment, cells were stained using 1μM of tetramethylrhodamine, methyl ester, perchlorate (TMRM, ThermoFisher Scientific), 400nM of mitotracker DeepRed (ThermoFisher Scientific), 500ng/ml of propidium iodide (PI, Sigma) and 1μM of Hoechst 33342 (ThermoFisher Scientific) at 37°C and 5% CO_2 for 30 minutes and cells were washed once with Hanks' Balanced Salt solution (HBSS) containing calcium and magnesium. Micrographs were captured using ImageXpress Micro XLS Widefield High-Content

Analysis system at 100x magnification and the mitochondrial membrane potential was evaluated in live cells (PI negative) using and the web-based software Columbus 2.7.1.133403 (PerkinElmer Inc.). Mitochondrial $\Delta\Psi$ was measured only in regions of co-localization of TMRE and mitotracker deepred fluorescences and data are reported as the ratio to not-treated cells. Cell viability was calculated as the ratio of the number of live cells (PI-negative) and total cells (PI-negative plus PI-positive cells) x 100; n=3.

RESULTS

We performed a differential proteomic analysis in the left ventricular free wall myocardial samples from patients with CCC, DCM and IC in comparison to subjects without cardiomyopathy (control group N), using a multiplexing methodology of 2-Dimentional Fluorescence Difference Gel Electrophoresis (2D-DIGE) (**Supplemental Figure S2**). Patients from the three cardiomyopathy groups included in the analysis displayed cardiomyocyte hypertrophy and fibrosis upon histopathological analysis, but lymphocytic myocarditis was only observed in myocardial samples from CCC patients (**Table 1**). No significant differences were found in age, ejection fraction (EF) or left ventricular diastolic diameter (LVDD) among the three cardiomyopathy groups. However, the control group – organ donors whose heart was not designated for transplantation – was inherently younger than the patient groups, since usually the preferential donors for organ transplantation are among younger individuals.

The proteomic analysis covered a total of 683 spots present in at least 80% of each of the fluorescent analytical gels. **Supplemental Figures S2A, B** display the Coomassie stained gel (preparative gel), and a representative 2D-DIGE stained gel (analytical gel), respectively. A total of 565 spots could be matched in the Coomassie colloidal blue stain-preparative gel and submitted to mass spectrometry identification; from which we were able to identify 439 proteins; and among those, 230 were distinct proteins (**Supplemental Table S2**). The majority of proteins (63%) were identified in a single spot. The remaining 37% of proteins have been identified in more than one spot. For some of these "multispot" proteins, only some of the spots were differentially expressed, while other spots corresponding to the same protein showed no difference in expression. This can be explained by the fact that some proteins could have different isoforms or post-translational modification that change their charge and consequently their isoelectric point. In this study, the deeper analysis of post-translational modification was not performed due to the complexity of such analysis and limitations of the method. **Supplemental Figures S3A–C** show Volcano plots displaying fold change and P values of the spots in the myocardial samples from CCC, DCM and IC patients as compared to the control group.

Figure 1 and **Supplemental Figure S4** show Venn diagrams indicating the number of differentially expressed identified proteins and spots, that were shared or unique in any of the disease groups as compared to the control group. When compared with the control group, myocardial samples from patients with CCC and DCM showed a higher number of differentially expressed proteins than the IC group. Approximately 77% of differentially expressed proteins in CCC myocardium were shared with the DCM group, 29% were shared with the IC group, and 26% of differentially expressed proteins were shared between the 3 groups.

Pathways analysis of differentially expressed proteins (**Figure 2**) disclosed enrichment in cardiac hypertrophy and cardiac fibrosis for all 3 diseases, while oxidative stress was enriched for both CCC and DCM. We observed a higher enrichment in CCC and DCM in the mitochondrial dysfunction pathway, and much higher enrichment in CCC in the fatty acid metabolism (beta-oxidation), transmembrane potential of mitochondria, and cardiac necrosis pathways. The compilation of the data from all analyzed spots and proteins can be found in **Supplemental Table S2**. **Table 2** and **Supplemental Figure S5A** shows the cellular component classification of the total identified proteins. Most of the identified proteins were

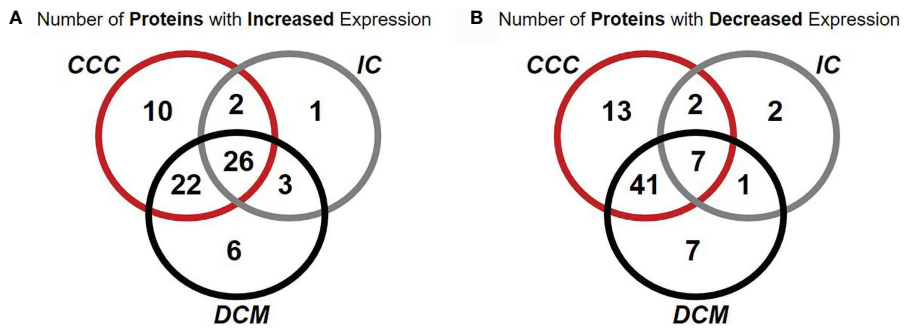

FIGURE 1 | Venn diagrams representing the occurrence of proteins differentially expressed in common or unique relationships between groups of patients with cardiomyopathy group compared with individuals without cardiomyopathies. Number of proteins with increased **(A)** or decreased **(B)** expression of at least one spot in samples from patients when compared with samples from subjects without cardiomyopathy. Over 67% of proteins differentially expressed in CCC were contained in a single spot.

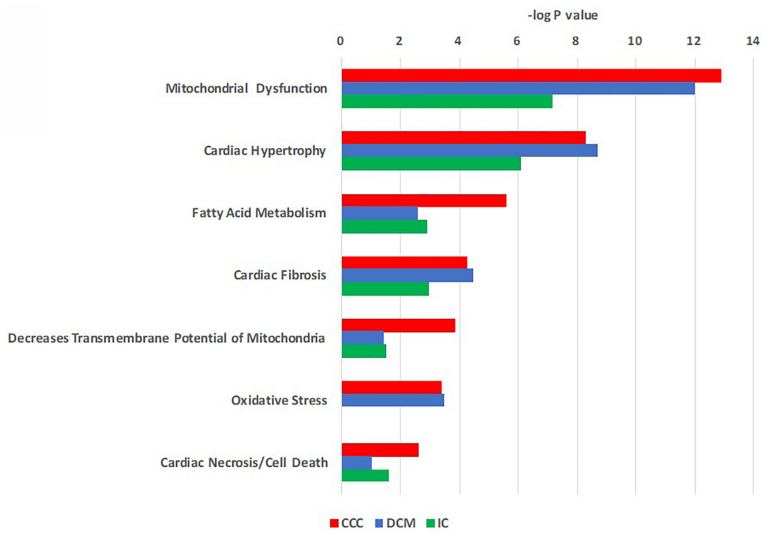

FIGURE 2 | Toxicity function pathways analysis of differentially expressed proteins in CCC, DCM and IC myocardium. Proteins differentially expressed in heart tissue were analyzed using Ingenuity Pathways Analysis® (Qiagen) using the tox-list function, which classifies gene or protein sets into pathological/toxicological pathways. Bars indicate the –log p value for a given pathway or process.

classified as cytoplasmic (35%), mitochondrial (28%), or cytoskeletal (13%). **Table 3** and **Supplemental Figure S5B** shows the functional classification of the total identified proteins. Through this classification, most of the proteins were classified as proteins related to metabolism (37%), structural and contractile proteins (14%) and proteins involved in the stress response and apoptosis (12%). Analysis of differentially expressed proteins in samples from each clinical group disclosed a similar distribution, as can also be observed in the **Tables 2** and **3**.

Table 4 displays the differentially expressed proteins in the different clinical groups (CCC, DCM or IC) as compared with individuals without cardiomyopathy (control group N), classified by biological process, and shows which of these proteins were shared among the groups. We found 128 differentially expressed proteins in myocardial samples from patients with CCC when compared to the control group (**Table 4**, section a). Among these, 25 proteins (ca. 20%) were found exclusively modulated in CCC samples. Among the 25, 12 were upregulated; between those, 3 belonged to the stress response/apoptosis process and 2 to metabolism (glycolysis). Thirteen proteins were down-modulated exclusively in CCC myocardium. Five belonged to the mitochondrial energy metabolism (oxidation, tricarboxylic acid cycle and oxidative phosphorylation), 4 were structural/contractile proteins, and one belonged to the stress response and apoptosis process. Regarding IC (**Table 4**, section b) and DCM (**Table 4**, section c), we identified 113 and 44 differentially expressed proteins as compared to the control group. The

TABLE 2 | Cellular component classification of the proteins differentially expressed in the myocardium from patients with CCC, IC and DCM.

Cellular Component	Total prot.*	T. diff. prot.†	CCC/N		IC/N		DCM/N	
			↑	↓	↑	↓	↑	↓
Cytoplasm	81	54	25	22	9	3	21	25
Cytoskeleton	30	22	6	11	3	5	7	9
Endoplasmic reticulum	8	5	5	0	0	0	5	0
Membrane	13	8	3	4	2	0	2	3
Mitochondria	64	41	13	22	13	3	14	17
Nucleus	20	8	3	4	0	0	3	3
Secreted	10	8	6	0	5	0	7	0
Other	4	3	2	0	1	1	1	0
Total	**230**	**149**	**63**	**63**	**33**	**12**	**60**	**57**

**Total prot., Total number of proteins identified in each cellular component; †T. diff. prot., Total number of proteins in each cellular component that were found to be differentially expressed in the myocardium from patients with CCC, IC and DCM as compared to individuals without cardiomyopathies (N).*

Bold means the total number of protein in each column.

↑ means upregulated expression ↓ means downregulated expression.

Bold means the total number of protein in each column.

TABLE 3 | Functional classification of the proteins differentially expressed in the myocardium from patients with CCC, IC and DCM.

Function	Total prot.*	T. diff. prot.†	CCC/N		IC/N		DCM/N	
			↑	↓	↑	↓	↑	↓
1. Structural and Contractile Proteins	32	25	7	13	4	5	8	10
2. Metabolism	86	60	19	32	16	6	19	29
2.1. Glycolysis	15	11	5	5	3	0	3	6
2.2. Lipid Metabolism/ß-Oxidation	11	7	0	6	1	1	1	2
2.3. Tricarboxylic Acid Cycle	8	7	1	4	1	0	2	3
2.4. Oxidative Phosphorylation and Electron Transport	18	14	5	8	5	2	4	8
2.5. Creatine Kinase System (Energy Transduction)	3	2	0	2	0	1	0	2
2.6. Other Metabolic Processes	31	19	8	7	6	2	9	8
3. Stress Response and Apoptosis	27	22	13	6	2	0	12	6
4. Immune Response	3	3	3	0	2	0	2	0
5. Cell Signaling	13	4	2	1	0	0	1	2
6. Transcription and Translation Processes	18	6	2	2	0	0	3	3
7. Transport	8	3	2	1	2	0	2	1
8. Proteasome-Ubiquitin Process	6	3	3	0	0	0	2	0
9. Other Functions	37	23	12	8	7	1	11	6
Total	**230**	**149**	**63**	**63**	**33**	**12**	**60**	**57**

**Total prot., Total number of proteins identified in each functional classification; †T. diff. prot., Total number of proteins in each functional classification that were found to be differentially expressed in the myocardium from patients with CCC, IC and DCM as compared to individuals without cardiomyopathies (N).*
↑ means upregulated expression ↓ means downregulated expression.
Bold means the total number of protein in each column

TABLE 4 | List of the differentially expressed proteins identified in the myocardium from patients with CCC, IC and DCM when compared to individuals without cardiomyopathies.

a) Differentially Expressed Proteins Only in CCC patients			Total Spots‡	CCC/N		IC/N		DCM/N	
Entry name*	Protein names†	Function		↑↓	S§	↑↓	S§	↑↓	S§
ARP3	Actin-like protein 3	1. Structural and Contractile Proteins	1	↑	1				
ENOA	Alpha-enolase (Non- neural enolase)	2.1. Glycolysis	6	↑	1				
G3P	Glyceraldehyde-3-phosphate dehydrogenase (GAPDH)	2.1. Glycolysis	7	↑	2				
MCCB	Methylcrotonoyl-CoA carboxylase beta chain, mitochondrial	2.6. Other Metabolic Processes	1	↑	1				
CATA	Catalase	3. Stress Response and Apoptosis	2	↑	2				
HSPB7	Heat shock protein beta-7	3. Stress Response and Apoptosis	1	↑	1				
TR10B	Tumor necrosis factor receptor superfamily member 10B	3. Stress Response and Apoptosis	1	↑	1				
LEG3	Galectin-3	4. Immune Response	1	↑	1				
BLK	Tyrosine-protein kinase BLK	5. Cell Signaling	1	↑	1				
PSME1	Proteasome activator complex subunit 1 (Interferon gamma up-regulated I-5111 protein)	8. Proteasome-Ubiquitin Process/Immune response	1	↑	1				
APOA1	Apolipoprotein A-I precursor	9. Other Functions	2	↑	1				
F90AM	Putative protein FAM90A22	9. Other Functions	1	↑	1				
ACTA	Actin, aortic smooth muscle (Alpha-actin-2)	1. Structural and Contractile Proteins	1	↓	1				
MYL4	Myosin light polypeptide 4 (Myosin light chain 1, embryonic muscle/ atrial isoform)	1. Structural and Contractile Proteins	1	↓	1				
STML2	Stomatin-like protein 2	1. Structural and Contractile Proteins	1	↓	1				
TPM1	Tropomyosin-1 alpha chain	1. Structural and Contractile Proteins	1	↓	1				
ACADVL	Very long-chain specific acyl-CoA dehydrogenase, mitochondrial	2.2. Lipid Metabolism/ß-Oxidation	5	↓	3				
HCDH	Hydroxyacyl-coenzyme A dehydrogenase, mitochondrial	2.2. Lipid Metabolism/ß-Oxidation	4	↓	4				
THIM	3-ketoacyl-CoA thiolase, mitochondrial	2.2. Lipid Metabolism/ß-Oxidation	2	↓	1				
MDHM	Malate dehydrogenase, mitochondrial	2.3. Tricarboxylic Acid Cycle	4	↓	3				
NDUS1	NADH-ubiquinone oxidoreductase 75 kDa subunit, mitochondrial	2.4. Oxidative Phosphorylation and Electron Transport	3	↓	2				
ROA2	Heterogeneous nuclear ribonucleoproteins A2/B1	2.6. Other Metabolic Processes	2	↓	1				
HSPB1	Heat-shock protein beta-1 (Heat shock 27 kDa protein)	3. Stress Response and Apoptosis	3	↓	1				
KELL	Kell blood group glycoprotein	9. Other Functions	1	↓	1				
SKT	Sickle tail protein homolog	9. Other Functions	1	↓	1				

(Continued)

TABLE 4 | Continued

b) Differentially Expressed Proteins Only in IC patients			Total Spots‡	CCC/N		IC/N		DCM/N	
Entry name*	**Protein names†**	**Function**		↑↓	**S§**	↑↓	**S§**	↑↓	**S§**
ACON	Aconitate hydratase, mitochondrial (Aconitase)	2.3. Tricarboxylic Acid Cycle	8			↑	3		
KI26A	Kinesin-like protein KIF26A	1. Structural and Contractile Proteins	1			↓	1		
W19L5	Putative WBSCR19-like protein 5	9. Other Functions	1			↓	1		

c) Differentially Expressed Proteins Only in DCM patients			Total Spots‡	CCC/N		IC/N		DCM/N	
Entry name*	**Protein names†**	**Function**		↑↓	**S§**	↑↓	**S§**	↑↓	**S§**
PDLI1	PDZ and LIM domain protein 1	1. Structural and Contractile Proteins	1					↑	1
VINC	Vinculin (Metavinculin)	1. Structural and Contractile Proteins	2					↑	2
ODO2	2-oxoglutarate dehydrogenase E2 component, mitochondrial	2.3. Tricarboxylic Acid Cycle	2					↑	1
COQ9	Ubiquinone biosynthesis protein COQ9, mitochondrial	2.6. Other Metabolic Processes	1					↑	1
HSP7C	Heat shock cognate 71 kDa protein (Heat shock 70 kDa protein 8).	3. Stress Response and Apoptosis	2					↑	2
SAMP	Serum amyloid P-component precursor	3. Stress Response and Apoptosis	1					↑	1
ZN799	Zinc finger protein 799	6. Transcription and Translation Processes	1					↑	1
IFIT5	Interferon-induced protein with tetratricopeptide repeats 5	9. Other Functions	1					↑	1
CAZA2	F-actin capping protein subunit alpha-2 (CapZ alpha-2)	1. Structural and Contractile Proteins	1					↓	1
MYOZ2	Myozenin-2	1. Structural and Contractile Proteins	3					↓	1
TPIS	Triosephosphate isomerase	2.1. Glycolysis	3					↓	1
NDUAD	NADH dehydrogenase [ubiquinone] 1 alpha subcomplex subunit 13	2.4. Oxidative Phosphorylation and Electron Transport	1					↓	1
GSTM2	Glutathione S-transferase Mu 2	2.6. Other Metabolic Processes	1					↓	1
CRYAB	Alpha crystallin B chain	3. Stress Response and Apoptosis	3					↓	1
GBG5	Guanine nucleotide-binding protein G(I)/G(S)/G(O) subunit gamma-5	5. Cell Signaling	2					↓	1
EDC4	Enhancer of mRNA-decapping protein 4	6. Transcription and Translation Processes	1					↓	1

d) Differentially Expressed Proteins Shared by CCC and IC patients			Total Spots‡	CCC/N		IC/N		DCM/N	
Entry name*	**Protein names†**	**Function**		↑↓	**S§**	↑↓	**S§**	↑↓	**S§**
NDUS3	NADH dehydrogenase [ubiquinone] iron-sulfur protein 3, mitochondrial	2.4. Oxidative Phosphorylation and Electron Transport	2	↑	1	↑	1		
CHCH3	Coiled-coil-helix-coiled-coil-helix domain-containing protein 3, mitochondrial	9. Other Functions	2	↑	1	↑	1		
ACTN2	Alpha-actinin-2 (Alpha actinin skeletal muscle isoform 2)	1. Structural and Contractile Proteins	4	↓	1	↓	1		
D3D2	3,2-trans-enoyl-CoA isomerase, mitochondrial	2.2. Lipid Metabolism/ß-Oxidation	1	↓	1	↓	1		

e) Differentially Expressed Proteins Shared by CCC and DCM patients			Total Spots‡	CCC/N		IC/N		DCM/N	
Entry name*	**Protein names†**	**Function**		↑↓	**S§**	↑↓	**S§**	↑↓	**S§**
TBA1C	Tubulin alpha-1C chain	1. Structural and Contractile Proteins	1	↑	1			↑	1
TBB5	Tubulin beta-5 chain	1. Structural and Contractile Proteins	3	↑	2			↑	2
IDH3A	Isocitrate dehydrogenase [NAD] subunit alpha, mitochondrial	2.3. Tricarboxylic Acid Cycle	2	↑	2			↑	1
DPYL2	Dihydropyrimidinase-related protein 2	2.6. Other Metabolic Processes	1	↑	1			↑	1
SCOT1	Succinyl-CoA:3-ketoacid-coenzyme A transferase 1, mitochondrial	2.6. Other Metabolic Processes	2	↑	1			↑	2
ENPL	Endoplasmin precursor (Heat shock protein 90 kDa beta member 1)	3. Stress Response and Apoptosis	2	↑	1			↑	1
GRP78	78 kDa glucose-regulated protein (Heat shock 70 kDa protein 5)	3. Stress Response and Apoptosis	3	↑	3			↑	3
HS90A	Heat shock protein HSP 90-alpha	3. Stress Response and Apoptosis	1	↑	1			↑	1
HSP71	Heat shock 70 kDa protein 1	3. Stress Response and Apoptosis	2	↑	1			↑	2
PDIA1	Protein disulfide-isomerase precursor	3. Stress Response and Apoptosis	1	↑	1			↑	1
PDIA3	Protein disulfide-isomerase A3 precursor	3. Stress Response and Apoptosis	2	↑	2			↑	2
ANXA1	Annexin A1 (Annexin I)	3. Stress Response and Apoptosis	1	↑	1			↑	1
ANXA5	Annexin A5 (Annexin V)	3. Stress Response and Apoptosis	2	↑	2			↑	2
1433Z	14-3-3 protein zeta/delta	5. Cell Signaling	1	↑	1			↑	1

(Continued)

TABLE 4 | Continued

e) Differentially Expressed Proteins Shared by CCC and DCM patients			Total Spots‡	CCC/N		IC/N		DCM/N	
Entry name*	Protein names†	Function		↑↓	S§	↑↓	S§	↑↓	S§
SYAC	Alanyl-tRNA synthetase, cytoplasmic	6. Transcription and Translation Processes	3	↑	2			↑	1
ZN658	Zinc finger protein 658	6. Transcription and Translation Processes	1	↑	1			↑	1
MIB2	E3 ubiquitin-protein ligase MIB2	8. Proteasome-Ubiquitin Process	1	↑	1			↑	1
RNF25	E3 ubiquitin-protein ligase	8. Proteasome-Ubiquitin Process	1	↑	1			↑	1
ANXA2	Annexin A2 (Annexin II)	9. Other Functions	3	↑	3			↑	2
F13A	Coagulation factor XIII A chain	9. Other Functions	1	↑	1			↑	1
AMPL	Cytosol aminopeptidase	9. Other Functions	2	↑	2			↑	1
PDZD4	PDZ domain-containing protein 4	9. Other Functions	1	↑	1			↑	1
AINX	Alpha-internexin	1. Structural and Contractile Proteins	1	↓	1			↓	1
MLRV	Myosin regulatory light chain 2, ventricular/cardiac muscle isoform	1. Structural and Contractile Proteins	4	↓	1			↓	3
MYL3	Myosin light polypeptide 3 (Myosin light chain 1, slow-twitch muscle B/ventricular isoform)	1. Structural and Contractile Proteins	4	↓	2			↓	2
TNNT2	Troponin T, cardiac muscle	1. Structural and Contractile Proteins	7	↓	1			↓	1
VIME	Vimentin	1. Structural and Contractile Proteins	1	↓	1			↓	1
ALDOA	Fructose-bisphosphate aldolase A (Muscle-type aldolase)	2.1. Glycolysis	6	↓	1			↓	2
ALDOC	Fructose-bisphosphate aldolase C (Brain-type aldolase)	2.1. Glycolysis	2	↓	2			↓	2
ENOB	Beta-enolase (Skeletal muscle enolase)	2.1. Glycolysis	1	↓	1			↓	1
K6PF	6-phosphofructokinase, muscle type	2.1. Glycolysis	2	↓	1			↓	1
PGAM2	Phosphoglycerate mutase 2	2.1. Glycolysis	2	↓	2			↓	2
ACADM	Medium-chain specific acyl-CoA dehydrogenase, mitochondrial	2.2. Lipid Metabolism/ß-Oxidation	1	↓	1			↓	1
DECR	2,4-dienoyl-CoA reductase, mitochondrial	2.2. Lipid Metabolism/ß-Oxidation	3	↓	1			↓	2
DHSB	Succinate dehydrogenase [ubiquinone] iron-sulfur subunit, mitochondrial	2.3. Tricarboxylic Acid Cycle	1	↓	1			↓	1
FUMH	Fumarate hydratase, mitochondrial	2.3. Tricarboxylic Acid Cycle	3	↓	1			↓	1
IDHP	Isocitrate dehydrogenase [NADP], mitochondrial	2.3. Tricarboxylic Acid Cycle	3	↓	3			↓	3
ATP5H	ATP synthase D chain, mitochondrial	2.4. Oxidative Phosphorylation and Electron Transport	1	↓	1			↓	1
NDUAA	NADH dehydrogenase [ubiquinone] 1 alpha subcomplex subunit 10	2.4. Oxidative Phosphorylation and Electron Transport	1	↓	1			↓	1
NDUV1	NADH dehydrogenase [ubiquinone] flavoprotein 1, mitochondrial	2.4. Oxidative Phosphorylation and Electron Transport	4	↓	2			↓	1
QCR1	Cytochrome b-c1 complex subunit 1, mitochondrial	2.4. Oxidative Phosphorylation and Electron Transport	3	↓	2			↓	1
QCR2	Cytochrome b-c1 complex subunit 2, mitochondrial	2.4. Oxidative Phosphorylation and Electron Transport	1	↓	1			↓	1
KCRS	Creatine kinase, sarcomeric mitochondrial	2.5. Creatine Kinase System (Energy Transduction)	5	↓	1			↓	1
KU86	ATP-dependent DNA helicase 2 subunit 2	2.6. Other Metabolic Processes	1	↓	1			↓	1
BLVRB	Flavin reductase	2.6. Other Metabolic Processes	1	↓	1			↓	1
KAD1	Adenylate kinase isoenzyme 1	2.6. Other Metabolic Processes	2	↓	1			↓	1
MDHC	Malate dehydrogenase, cytoplasmic	2.6. Other Metabolic Processes	3	↓	1			↓	1
THIL	Acetyl-CoA acetyltransferase, mitochondrial	2.6. Other Metabolic Processes	1	↓	1			↓	1
AKT2	RAC-beta serine/threonine-protein kinase	3. Stress Response and Apoptosis	1	↓	1			↓	1
NEIL1	Endonuclease VIII-like 1	3. Stress Response and Apoptosis	1	↓	1			↓	1
PRDX2	Peroxiredoxin-2	3. Stress Response and Apoptosis	1	↓	1			↓	1
PRDX3	Peroxiredoxin-3	3. Stress Response and Apoptosis	1	↓	1			↓	1
PRDX6	Peroxiredoxin-6	3. Stress Response and Apoptosis	3	↓	1			↓	3
KC1E	Casein kinase I isoform epsilon	5. Cell Signaling	1	↓	1			↓	1
EIF3J	Eukaryotic translation initiation factor 3 subunit	6. Transcription and Translation Processes	1	↓	1			↓	1
IF4H	Eukaryotic translation initiation factor 4H	6. Transcription and Translation Processes	1	↓	1			↓	1
UCP2	Mitochondrial uncoupling protein 2	7. Transport	1	↓	1			↓	1
EHD4	EH domain-containing protein 4	9. Other Functions	1	↓	1			↓	1
GAB3	GRB2-associated-binding protein 3	9. Other Functions	1	↓	1			↓	1
JKIP1	Janus kinase and microtubule-interacting protein 1	9. Other Functions	1	↓	1			↓	1
MYG	Myoglobin	9. Other Functions	8	↓	2			↓	3
PEBP1	Phosphatidylethanolamine-binding protein 1	9. Other Functions	1	↓	1			↓	1
WDFY2	WD repeat and FYVE domain-containing protein 2	9. Other Functions	1	↓	1			↓	1

(Continued)

TABLE 4 | Continued

f) Differentially Expressed Proteins Shared by IC and DCM patients			Total Spots‡	CCC/N		IC/N		DCM/N	
Entry name*	Protein names†	Function		↑↓	S§	↑↓	S§	↑↓	S§
ECHM	Enoyl-CoA hydratase, mitochondrial	2.2. Lipid Metabolism/ß-Oxidation	1			↑	1	↑	1
AOFB	Amine oxidase [flavin-containing] B	2.6. Other Metabolic Processes	1			↑	1	↑	1
BPIL3	Bactericidal/permeability-increasing protein-like 3	9. Other Functions	1			↑	1	↑	1
GSTP1	Glutathione S-transferase P	2.6. Other Metabolic Processes	1			↓	1	↓	1

g) Differentially Expressed Proteins Shared by CCC, IC and DCM patients			Total Spots‡	CCC/N		IC/N		DCM/N	
Entry name*	Protein names†	Function		↑↓	S§	↑↓	S§	↑↓	S§
DESM	Desmin	1. Structural and Contractile Proteins	9	↑	4	↑	2	↑	8
GELS	Gelsolin precursor (Actin-depolymerizing factor)	1. Structural and Contractile Proteins	6	↑	5	↑	1	↑	5
LUM	Lumican precursor	1. Structural and Contractile Proteins	1	↑	1	↑	1	↑	1
TNNI3	Troponin I, cardiac muscle	1. Structural and Contractile Proteins	1	↑	1	↑	1	↑	1
G6PI	Glucose-6-phosphate isomerase	2.1. Glycolysis	1	↑	1	↑	1	↑	1
KPYM	Pyruvate kinase isozymes M1/M2	2.1. Glycolysis	4	↑	1	↑	1	↑	3
PGAM1	Phosphoglycerate mutase 1	2.1. Glycolysis	2	↑	2	↑	2	↑	2
AL4A1	Delta-1-pyrroline-5-carboxylate dehydrogenase, mitochondrial	2.4. Oxidative Phosphorylation and Electron Transport	1	↑	1	↑	1	↑	1
ATPA	ATP synthase subunit alpha, mitochondrial	2.4. Oxidative Phosphorylation and Electron Transport	8	↑	4	↑	3	↑	3
DHSA	Succinate dehydrogenase [ubiquinone] flavoprotein subunit, mitochondrial	2.4. Oxidative Phosphorylation and Electron Transport	4	↑	2	↑	2	↑	2
DLDH	Dihydrolipoyl dehydrogenase, mitochondrial precursor	2.4. Oxidative Phosphorylation and Electron Transport	4	↑	3	↑	1	↑	3
CATD	Cathepsin D	2.6. Other Metabolic Processes	2	↑	1	↑	1	↑	1
DHE3	Glutamate dehydrogenase 1, mitochondrial	2.6. Other Metabolic Processes	1	↑	1	↑	1	↑	1
MMSA	Methylmalonate-semialdehyde dehydrogenase [acylating], mitochondrial	2.6. Other Metabolic Processes	1	↑	1	↑	1	↑	1
TGM2	Protein-glutamine gamma-glutamyltransferase 2	2.6. Other Metabolic Processes	3	↑	3	↑	1	↑	3
UGPA	UTP–glucose-1-phosphate uridylyltransferase	2.6. Other Metabolic Processes	1	↑	1	↑	1	↑	1
GRP75	Stress-70 protein, mitochondrial	3. Stress Response and Apoptosis	2	↑	2	↑	2	↑	2
TRAF3	TNF receptor-associated factor 3	3. Stress Response and Apoptosis	2	↑	1	↑	1	↑	2
CO3	Complement C3 precursor	4. Immune Response	2	↑	1	↑	1	↑	2
IGHG1	Ig gamma-1 chain C region.	4. Immune Response	3	↑	3	↑	3	↑	3
FRRS1	Ferric-chelate reductase 1	7. Transport	1	↑	1	↑	1	↑	1
SNAB	Beta-soluble NSF attachment protein	7. Transport	1	↑	1	↑	1	↑	1
ALBU	Serum albumin precursor	9. Other Functions	4	↑	4	↑	2	↑	4
CSRP3	Cysteine and glycine-rich protein 3	9. Other Functions	1	↑	1	↑	1	↑	1
IMMT	Mitochondrial inner Membrane protein (Mitofilin)	9. Other Functions	4	↑	3	↑	2	↑	3
TRFE	Serotransferrin precursor (Transferrin)	9. Other Functions	4	↑	3	↑	3	↑	3
YP016	Uncharacterized protein MGC16385	9. Other Functions	1	↑	1	↑	1	↑	1
ACTC	Actin, alpha cardiac muscle 1 (Alpha-cardiac actin)	1. Structural and Contractile Proteins	15	↓	8	↓	1	↓	5
LDB3	LIM domain-binding protein 3	1. Structural and Contractile Proteins	5	↓	5	↓	5	↓	5
MYH7	Myosin-7 (Myosin heavy chain, cardiac muscle beta isoform)	1. Structural and Contractile Proteins	2	↓	1	↓	1	↓	1
AT5F1	ATP synthase subunit b, mitochondrial	2.4. Oxidative Phosphorylation and Electron Transport	3	↓	2	↓	1	↓	2
NDUV2	NADH dehydrogenase [ubiquinone] flavoprotein 2, mitochondrial	2.4. Oxidative Phosphorylation and Electron Transport	1	↓	1	↓	1	↓	1
KCRM	Creatine kinase M-type	2.5. Creatine Kinase System (Energy Transduction)	5	↓	5	↓	2	↓	5
AATC	Aspartate aminotransferase, cytoplasmic	2.6. Other Metabolic Processes	3	↓	2	↓	2	↓	2

Entry name: Mnemonic identifier for a UniProtKB entry, all the entry names are followed by "_HUMAN"; †Protein names: Name of the protein according to UniProtKB; ‡Total spots: Number of spots identified as such protein; §S: Number of differentially expressed spots identified as such protein for each comparison. Other annotations and comments, fold change and statistical values, as well as protein identification score values of all identified spots are included in the* ***Supplemental Table 2* *from Online* ***Supplemental Data****.*
↑ means upregulated expression ↓ means downregulated expression.

Table 4 also includes the list of the protein that were differentially expressed in more than one specific disease group as compared to control group.

We then focused the analysis on metabolism-related proteins because they were the most frequently modulated in our study. Among the energy metabolism proteins with reduced expression only in CCC samples, we found several enzymes from the beta-oxidation process, as depicted in **Figure 3**. Very long-chain specific acyl-CoA dehydrogenase (ACADVL) was found in decreased levels in 3 out of 5 spots only in CCC samples. Moreover, the total level of ACADVL was also found differentially expressed when evaluated by immunoblotting (**Figure 4A** and **Supplemental Figure S9**). CCC patients show reduced total levels of ACADVL as compared to samples from the control group and from patients with IC. mRNA levels of the ACADVL gene (**Figure 4B**) were also reduced in CCC samples as compared to the control group, suggesting transcriptional regulation. Moreover, all spots identified as hydroxyacyl-coenzyme A dehydrogenase (HCDH) and one out of two spots identified as the protein 3-ketoacyl-CoA thiolase (THIM) were found to be decreased only in CCC samples as compared to samples from individuals without cardiomyopathies. Medium-chain specific acyl-CoA dehydrogenase (ACADM) showed decreased levels in CCC and also DCM samples. The enzymes 2,4-dienoyl-CoA reductase (DECR) (**Supplemental Figure S9**) and 3,2-trans-enoyl-CoA isomerase (D3D2), which participate in the metabolism of unsaturated fatty enoyl-CoA esters, also showed reduced expression in samples of patients with CCC and DCM, and in samples of patients with CCC and IC, respectively, when compared to control samples. Enoyl-CoA hydratase (ECHM), which participates in the second reaction of beta-oxidation, shows increased expression in patients with IC and DCM, but not in patients with CCC. We further evaluate by immunoblotting the protein levels of the protein DECR, that presented decreased levels in CCC samples as compared to IC samples and samples from the control group. This reduction was also observed in the DECR mRNA level evaluated by RT-qPCR (**Figure S6**). Taken together, the number of beta-oxidation enzymes with reduced expression in CCC is considerable higher than DCM and IC samples (6, 2 and 1, respectively) (**Table 3**), which may indicate that fatty acid beta-oxidation is more impaired in CCC than DCM or IC.

Evaluating further other pathways from the energetic metabolism, nine proteins involved in glycolysis were differentially expressed in the cardiomyopathy groups (**Supplemental Figure S7A**). Three were upregulated in all patient samples, while ENOA and G3PDH were exclusively upregulated in CCC. Five enzymes showed reduced expression in both CCC and DCM (**Table 4**).

Regarding the tricarboxylic acid cycle (**Supplemental Figure S7B**), six enzymes were differentially expressed in the cardiomyopathies; three of them with reduced expression in CCC and DCM samples as compared to control group: Fumarate hydratase (FUMH); Succinate dehydrogenase [ubiquinone] iron-sulfur subunit (DHSB) and Isocitrate dehydrogenase [NADP] (IDHP). IDHP participates in the tricarboxilic acid cycle, but is

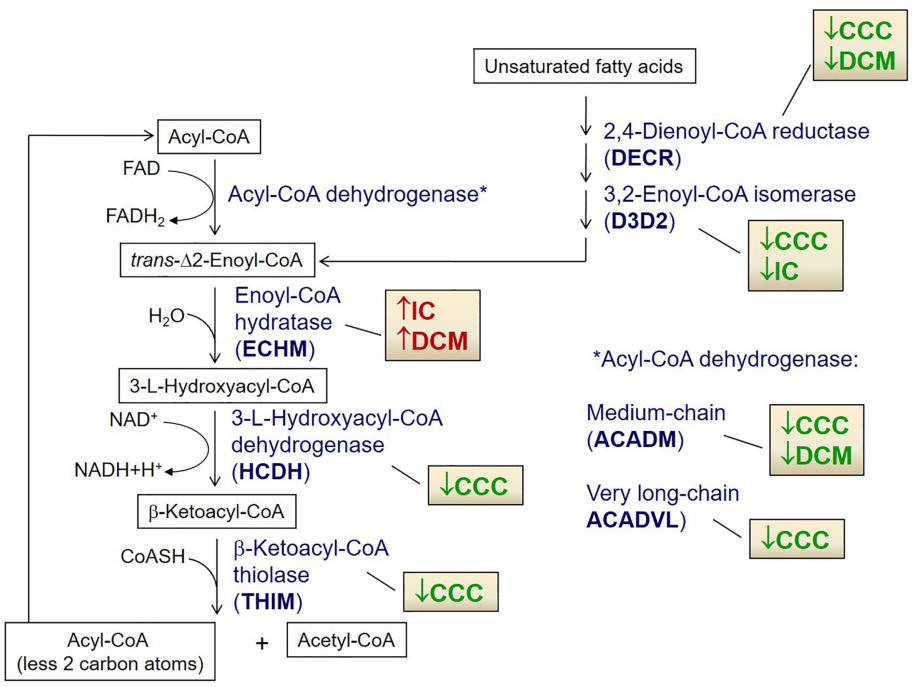

FIGURE 3 | Cartoon depicting fatty acid β-oxidation enzymes differentially expressed in CCC, DCM and IC myocardium. Arrows indicate up-regulated (red) or down-regulated (green) expression as compared to control myocardial samples in the proteomic analysis. *Indicates the right place for in the metabolic pathway for Acyl coA dehydrogenases ACADVL and ACADM.

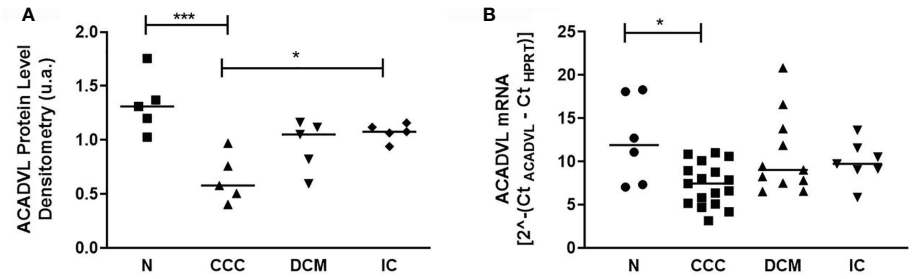

FIGURE 4 | Protein and mRNA levels of ACADVL (Very long-chain specific acyl-CoA dehydrogenase) in myocardial tissue of CCC, DCM, IC and controls. **(A)** Densitometry measurement of ACADVL protein levels using immunoblot (One-Way ANOVA p = 0.0011). **(B)**. ACADVL mRNA levels assessed using real time RT-qPCR (One-Way ANOVA p = 0.0154). The horizontal lines show statistically significant changes between groups by the Tukey-Kramer test: *p < 0.05; ***p < 0.001.

also involved in antioxidant mechanisms. Moreover, we observed reduced levels of the protein Malate dehydrogenase (MDHM) exclusively in the CCC group. On the other hand, we found increased protein levels of Isocitrate dehydrogenase [NAD] subunit alpha (IDH3A) in CCC and DCM samples. Aconitate hydratase, mitochondrial (Aconitase, ACON) had increased levels in the IC samples only.

Moving to the energy production by the respiratory chain pathway, we identified 13 differentially expressed proteins belonging to complexes I, II, III and V of the oxidative phosphorylation process (**Table 4** and **Supplemental Figure S7C**). Ten of them, including uncoupling protein 2 (UCP2), were reduced in CCC and DCM. Complex I NADH-ubiquinone oxidoreductase 75 kDa subunit (NDUS1) was reduced only in samples from patients with CCC. Creatine kinase M (KCRM) and mitochondrial sarcomeric creatine kinase (KCRS), involved in the translocation of the ATP from the mitochondria to myofibrils, were found to be decreased in samples from patients with CCC and the other cardiomyopathies (**Table 4** and **Supplemental Figure S7D**).

Regarding the stress response related proteins, we found 14 differentially expressed proteins in at least one of the patient groups, including chaperone, redox homeostasis and apoptosis-related proteins. The antioxidant peroxiredoxins (PRDX2, PRDX3 and PRDX6) displayed reduced expression in CCC and DCM. Catalase (CATA) was upregulated only in CCC patients; immunoblotting analysis showed that the total catalase protein level was increased as compared to the other IC samples and the control group (**Figure 5A**); protein disulfide-isomerases PDIA1 and PDIA3 were upregulated in CCC and DCM. Multiple chaperones were upregulated in CCC and DCM. Other proteins involved in apoptosis, such as TRAF3, which mediates pathological hypertrophy and apoptosis, was upregulated in the three cardiomyopathies. Tumor necrosis factor receptor superfamily member 10B (TR10B) - a receptor for the cytotoxic ligand TRAIL, and the antiapoptotic protein annexin A5 (ANXA5) showed increased expression CCC and DCM, while antiapoptotic heat shock 27 kDa protein (HSPB1), displayed decreased expression only in CCC.

Based on proteomic, immunoblotting and real time PCR data, the fatty acid beta-oxidation pathway seems to be significantly impaired in CCC, which could result in fatty acid accumulation. The reduction of peroxiredoxins - shared with DCM - and the increase in catalase - exclusively in CCC - is consistent with increased oxidative stress in CCC myocardium (**Supplemental Figure S9**). The increased levels of malonaldehyde (MDA), the major lipid oxidation product, were observed only in CCC, which indicates lipid peroxidation suggestive of lipotoxicity (**Figure 5B**).

We identified 20 differentially expressed proteins belonging to the structural and contractile protein group (**Table 4** and **Supplemental Figure S8**). From these, 5 proteins are exclusively modulated in CCC samples (e.g. actin-like protein 3 – ARP3 - and tropomyosin-1 alpha chain – TPM1, with increased and decreased levels, respectively). CCC and DCM samples shared 7 differentially expressed proteins, while CCC and IC shared only one differentially expressed protein. Among the proteins differentially expressed shared by CCC, DCM and IC samples (7 proteins) are Desmin (DESM), Gelsolin precursor (GELS), Lumican (LUM) and Troponin I (TNNI3), identified in spots with increased levels, and Alpha-cardiac actin (ACTC), LIM domain-binding protein 3 (LDB3) and Myosin-7 (MYH7), identified in spots with decreased levels, a pattern consistent with the fetal gene expression profile.

Among proteins that play a role or are regulated by components of the immune system, galectin-3 (LEG3) and proteasome activator complex subunit 1 (PSME1), upregulated by the inflammatory cytokines IFN-gamma and TNF-alpha, show increased levels exclusively in samples from patients with CCC. We also found B-cell related proteins to be upregulated in CCC, like tyrosine-protein kinase BLK (BLK), which plays an important role in the surface immunoglobulin signaling pathway and was also found with increased expression only in CCC samples. Likewise, we found increased protein levels of immunoglobulin (Ig gamma-1 chain C region - IGHG1) in the samples from patients with CCC, DCM and IC when compared to samples from individuals without cardiomyopathies. However, CCC samples showed the highest levels as compared to samples from the other patient groups.

To investigate the role of IFN-gamma and TNF-alpha on cardiomyocyte mitochondrial function, we stimulated the human adult cardiomyocyte cell line AC16 with several concentrations of IFN-gamma and measured the

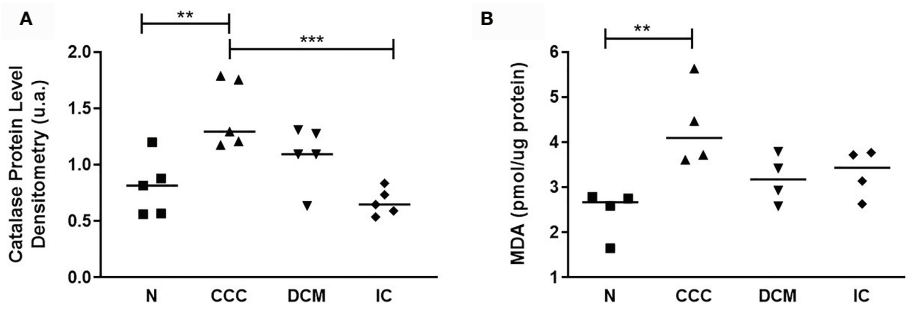

FIGURE 5 | Analysis of antioxidant enzyme Catalase and lipid peroxidation status. **(A)** Catalase protein levels measured by immunoblotting; the densitometric values were normalized by the total protein for each sample (One-Way ANOVA p = 0.0008). **(B)** Malondialdehyde (MDA) production, measured by the thiobarbituric acid reactive substances (TBARS) assay (One-Way ANOVA p = 0.0113). The horizontal lines show statistically significant changes between groups by the Tukey-Kramer test: **p < 0.01; ***p < 0.001.

mitochondrial ΔΨm with supravital fluorescence microscopy. We observed that IFN-gamma impaired the ΔΨm of AC-16 48h after stimulation (**Figure 6**).

DISCUSSION

The proteomic analysis of myocardial tissue revealed that CCC, DCM and IC display a distinct global protein expression profile. Pathway analysis disclosed enrichment in mitochondrial dysfunction, cardiac hypertrophy and fibrosis in the three disease groups. Pathway analysis of proteins differentially expressed in CCC also showed selective enrichment in the CCC group for pathways involved in the fatty acid metabolism and decreased transmembrane potential of mitochondria. CCC patients' myocardium displayed reduced expression of 22 mitochondrial proteins belonging to energy metabolism pathways, as compared to control samples, while IDC and IC displayed 15 and 3, respectively. Significantly, 6 lipid beta-oxidation enzymes were reduced in CCC, while only 2 of them were downregulated in DCM and 1 in IC. To our knowledge, this is the first report on the differential myocardial protein expression profile of multiple cardiomyopathies, including Chagas disease cardiomyopathy. In addition, we found increased levels of malonaldehyde, a sign of oxidative stress and a toxic product of lipid peroxidation, only in CCC samples. Finally, we observed that IFN-gamma treatment of the human cardiomyocyte cell line AC16 induces a dose-dependent reduction of mitochondrial transmembrane potential, providing a possible clue to the inflammatory origin of mitochondrial dysfunction in CCC.

Functional analysis of differentially expressed proteins shows that myocardial samples from patients with CCC display a substantial reduction in levels of proteins involved in several pathways of mitochondrial energy metabolism, particularly in the beta-oxidation pathway. The finding that several enzymes

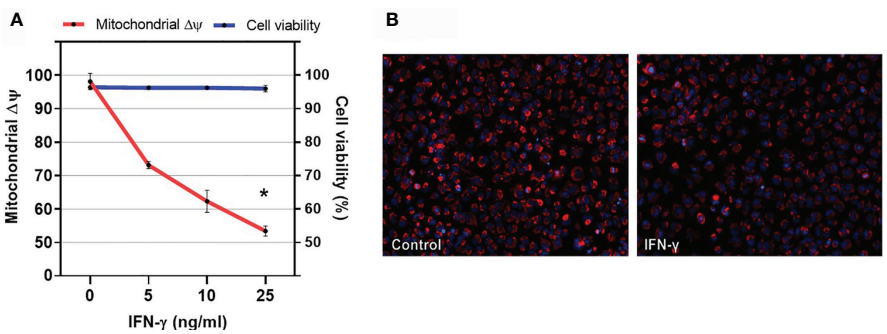

FIGURE 6 | Effect of IFN-gamma on cardiomyocyte mitochondrial membrane potential. **(A)** Human cardiomyocytes AC16 were stimulated with 5, 10 or 25ng/ml of IFN-gamma for 48 hours. Then, cells were stained using 1μM TMRM, 400nM of mitotracker DeepRed, 500ng/ml of PI and 1μM of Hoechst 33342 and micrographs were captured in ImageXpress Micro XLS Widefield High-Content Analysis system at 100x magnification. Fluorescence colocalization of TMRE and mitotracker deepred in live cells (PI negative) was used to calculate mitochondrial ΔΨ. Data are reported as the ratio to not-treated cells. Cell viability is the ratio of the number of live cells (PI-negative) and total cells (PI-negative plus PI-positive cells) x 100. n = 3. *p < 0.05. **(B)** Representative fluorescence microscopy (100x) showing decrease in TMRE fluorescence after incubation with IFN-gamma for 48h.

involved in beta-oxidation are decreased in CCC, while only one is also reduced in DCM suggests that this pathway may be selectively reduced in CCC patients. The finding that the mRNA levels of ACADVL were also decreased in samples from patients with CCC suggests that enzyme levels may be transcriptionally regulated. Very long chain fatty acid dehydrogenase (ACADVL) has activity mainly toward CoA-esters of fatty acids with 16–24 carbons in length (35). In addition, ACADVL catalyzes the major part of palmitoyl-CoA dehydrogenation in many human tissues and cultured cells (36), indicating its central role in the catabolism of long-chain fatty acids. This is clearly reflected by the severe clinical symptoms caused by ACADVL deficiency, such as a high incidence of cardiomyopathy in childhood (37). Patients with ACADVL deficiency may present hypertrophy and dilated cardiomyopathy (38). In addition to the impaired degradation of very long and medium acyl chains, found mainly in CCC samples, we have also observed that other beta-oxidation enzymes involved in degradation of unsaturated fatty acids such as 2,4-dienoyl-CoA reductase (DECR) and 3,2-trans-enoyl-CoA isomerase (D3D2) showed reduced expression in CCC. This reduced expression is shared with DCM and IC, respectively. Activation of NF-κB is most likely to occur in heart tissue from CCC patients, due to the systemic and local expression of IFN-gamma, TNF-alpha and other proinflammatory cytokines (11, 18, 19, 39). Studies showed that activation of nuclear factor NF-κB during cardiac hypertrophy decreases the activity of the protein PPAR (peroxisome proliferator-activated receptor) beta/gamma, leading to a decrease in fatty acid oxidation (40). Furthermore, malate Dehydrogenase (MDHM), exclusively reduced in CCC, is part of the tricarboxylic acid (TCA) cycle. We also found decreased levels of other TCA cycle enzymes, and increased expression of a single TCA enzyme, that were shared with other cardiomyopathies. Studies from our group showed that the gene SERCA Ca^{++} ATPase of sarcoplasmic reticulum (SERCA2), involved in cardiac homeostasis of Ca^{++} was found with reduced expression in the myocardium of patients with CCC (15), possibly indicating a reduction in calcium signaling and excitation/contraction coupling. Studies show that several enzymes of the TCA cycle can be activated by Ca^{++}. Disturbed Ca^{++} homeostasis could lead to the inactivation of dehydrogenases of the TCA cycle by calcium, resulting in a decreased concentration of NADH and hence a reduction in ATP production (41). The finding that several components of complexes I, II, III, and V from the oxidative phosphorylation process showed reduced expression in CCC samples may also contribute to the impairment of ATP production (42). We have also observed reduced expression of several components of the creatine kinase complex, responsible for the translocation of ATP from mitochondria to the myofibrils. Creatine kinase M (KCRM) and mitochondrial creatine kinase (KCRS) showed reduced expression in samples from both CCC and other cardiomyopathies, as previously reported for heart failure (43–45); this finding corroborates previous results from our group (23). Our previous studies also showed that total protein levels (as detected by Immunobloting) and enzymatic activity of KCRM are significantly decreased in CCC myocardium samples as compared to samples from individuals without cardiomyopathies, as well as from DCM and IC patients. Reduction of protein levels of enzymes involved in multiple pathways that lead to ATP production is consistent with an energy deficit in CCC heart tissue. This reduced state of ATP production has been corroborated *in vivo* myocardial ATP flux evaluations (24, 46).

Our finding of increased protein levels of catalase (CATA) only in CCC myocardial samples, together with the reduction in several peroxyredoxins including PRDX6, an IFN-gamma regulated gene, suggests a significant disturbance in the antioxidant system. It is possible that the increased protein level of catalase found in CCC myocardium samples is secondary to a compensatory mechanism for oxidative stress, which could be more intense in CCC than in DCM or IC. Indeed, IFN-gamma, a cytokine that is highly expressed in CCC heart tissue (17, 18, 20) induces expression of NOX2 and increases oxidative stress (47). Increased oxidative stress is intimately involved in the pathogenesis of heart failure. Isocitrate dehydrogenase [NADP] (IDHP), which was found with reduced expression in samples of patients with CCC and DCM, is responsible for the production of NADPH. Indeed, the decrease in the levels of IDHP is related to increased reactive oxygen species, DNA fragmentation, lipid peroxidation, and mitochondrial damage with significant reduction in ATP levels (48). The reduced protein levels of beta-oxidation enzymes involved in degradation of fatty acids may lead to an accumulation of lipid substrates in heart tissue. Given the deficiency in the antioxidant defense system in CCC, it is possible to hypothesize that oxidant conditions prevail in CCC heart tissue, in line with results in experimental *T. cruzi* infection (49–52) which together with our finding of reduced beta-oxidation enzymes could lead to lipid peroxidation.

Our data suggest that CCC myocardium displays signs of reduced mitochondrial activity and energy production. Garg et al. were the first to suggest that myocardial mitochondrial dysfunction and oxidative stress in the pathogenesis of murine models of CCC (reviewed in (53)). Decreased mitochondrial rRNA (15), rDNA (54) and *in vivo* ATP production (24) were observed in CCC myocardium. The IFN-gamma-producing T-cell rich inflammatory profile is a major difference between CCC and DCM; indeed, IFN-gamma is the most highly expressed cytokine in CCC heart tissue (14, 17–19, 55) and the top upstream gene regulator upon pathways analysis in CCC myocardium (20). It is known that IFN-gamma has multiple deleterious effects on cardiomyocyte mitochondria. It induces TNF-alpha and potentiates TNF-alpha-mediated NF-kB signaling, leading to NOS2 production of reactive nitrogen species (RNS) (56, 57). This has been reported to cause mitochondrial fragmentation, disturbance in mitochondrial membrane potential, and reduction of ATP production (58). In addition, IFN-gamma was shown to reduced fatty acid beta-oxidation (59) and oxidative phosphorylation (60), inducing a shift towards glycolysis (61). These factors are probably involved in IFN-gamma-induced cardiomyocyte dysfunction and

apoptosis (62). We hypothesize that many of the mitochondrial energy metabolism changes observed in CCC are locally induced by the high levels of IFN-gamma in CCC myocardium.

IFN-gamma induced proteins like Galectin 3 (LEG3) and Proteasome activator complex subunit 1 - PSME1), found to be upregulated in CCC myocardial tissue, may play a role in the pathology of heart failure and cardiac remodeling; with Galectin-3 showing a stimulatory effect on macrophage migration, fibroblast proliferation and development of fibrosis. Increased levels of Galectin-3 were also found in the hearts of transgenic mice with increased expression of IFN-gamma (63) and mice chronically infected by *T. cruzi*, and shows increased expression in areas of inflammation in CCC myocardium (64). Moreover, mice genetically deficient in Galectin-3 display less myocardial fibrosis at chronic infection (65). Significantly, plasma Galectin-3 levels are a prognostic factor for heart failure (66) and were associated with long-term mortality in CCC (67). PSME1 is the alpha subunit of the immunoproteasome PA28 complex. Significantly, it has been reported that genes encoding the IFN-gamma-induced immunoproteasome subunits display increased expression in CCC heart tissue and the myocardium of *T. cruzi*-infected mice (68). The reduced protein levels of AKT2 (Rac-beta serine/threonine-protein kinase) - which has a role in apoptosis inhibition, through the inhibition of JNK and p38 activation (69) - and the increased protein levels of TR10B (Tumor necrosis factor receptor superfamily member 10B) - a receptor for the apoptosis-inducing ligand TRAIL (TNF-related apoptosis-inducing ligand) - could both facilitate apoptosis (70) and increase susceptibility to oxidative stress.

The involvement of sarcomeric/structural proteins in the pathogenesis of cardiomyopathy is a consequence of the cardiac remodeling and is part of the hypertrophy/embryonic gene expression signature. The finding of 4 structural proteins exclusively down-modulated in CCC may suggest the remodeling is even more intense in CCC than in other cardiomyopathies.

Our study has limitations. The number of samples for the proteomic studies was limited and control samples were significantly younger than patient's samples. This is unavoidable as organ donors tend to be much younger than organ recipients. It thus follows that some of the protein expression changes shared by all cardiomyopathy groups in comparison to organ donor controls could be due to age alone. However, most of the energy metabolism enzyme changes were not shared among the 3 patient groups as compared to organ donor controls.

In summary, proteomic analysis disclosed profound disturbances in several pathways of energy metabolism – including beta-oxidation, tricarboxylic acid cycle, oxidative phosphorylation, and creatine kinases, suggesting a major reduction of mitochondrial energy metabolism which is more significant in CCC than other end-stage dilated cardiomyopathies. In addition, disturbances in the local antioxidant defense system corroborate findings in experimental models and may be related to the active inflammatory process. Oxidative stress-dependent peroxidation of hypothetically accumulated fatty acids as a consequence of decreased levels of beta-oxidation enzymes in CCC might lead to the increased levels of highly toxic molecules such as malonaldehyde (**Figure 7**). Given the high levels of IFN-

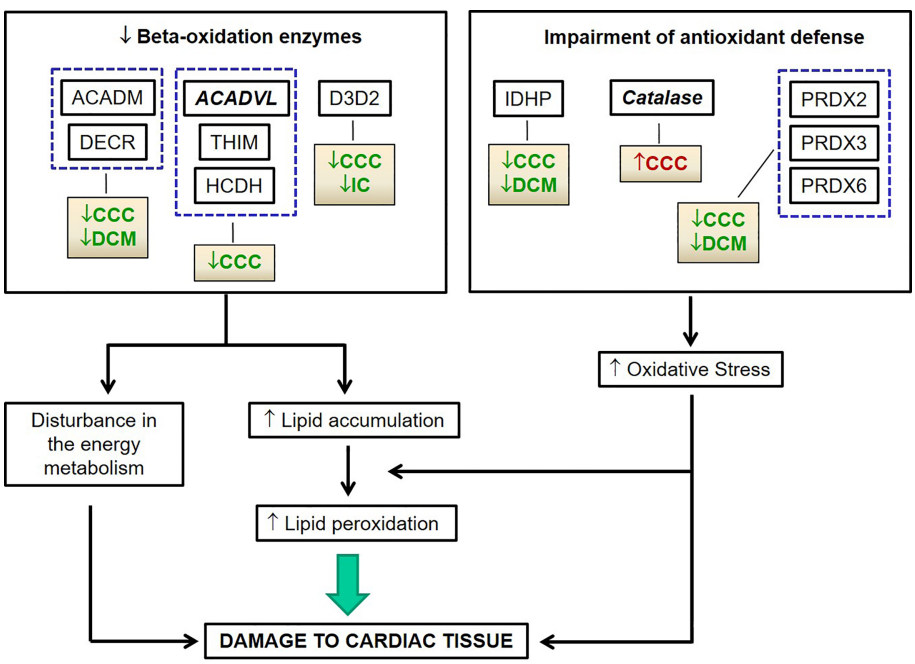

FIGURE 7 | Hypothetical chain of events subsequent to reduced beta-oxidation and oxidative stress related proteins in CCC myocardium leading to cardiac damage.

gamma in CCC heart tissue, we hypothesize that many mitochondrial changes and oxidative stress observed in CCC are due to the continued high expression of this cytokine. This hypothesis is investigated in the back-to-back submitted paper. These factors may play a role in the increased aggressiveness of CCC as compared to other dilated cardiomyopathies and places mitochondrial function as a therapeutic target in Chagas disease. Although anti-cytokine treatment is not an option in Chagas disease due to the risk of reactivation of infection, downstream pathways that promote mitochondrial function are likely therapeutic targets. Indeed, fenofibrate, a PPAR- agonist capable to induce fatty acid beta-oxidation, was able to restore cardiac function in a murine model of Chagas disease (71). Likewise, treatment of chronically *T. cruzi*-infected mice with mitochondria-targeting SIRT1 and/or AMPK agonists SRT1720, resveratrol and metformin reduced myocardial NF-κB transcriptional activity, inflammation and oxidative stress, resulting in beneficial results for restoration of cardiac function (50, 51). Therapy targeting mitochondrial function and energy imbalance should thus in principle be beneficial to restore cardiac function in CCC and other IFN-gamma-dependent inflammatory heart diseases, like viral myocarditis and inflammatory cardiomyopathy of other etiologies and age-related myocardial inflammation and functional decline (72), myocardial infarction (73) and anthracycline antitumor agent cardiotoxicity.

DATA AVAILABILITY STATEMENT

The datasets presented in this study can be found in online repositories. The names of the repository/repositories and accession number(s) can be found in the article/**Supplementary Material**.

ETHICS STATEMENT

The protocol was also approved by the INSERM Internal Review Board and the Brazilian National Ethics in Research Commission (CONEP). The patients/participants provided their written informed consent to participate in this study.

AUTHOR CONTRIBUTIONS

Study design: PT, EC-N, and JK. Phenotype characterization: RS, LB, EB, AF, NS, and PP. Experimental analysis: PT, AD, HL, EN, JS, DL, SB, and AK. Statistical analysis: PT, JS, and EC-N. Manuscript preparation: PT, EC-N, JS, and CC. All authors contributed to the article and approved the submitted version.

FUNDING

This research was supported by the Brazilian Council for Scientific and Technological Development - CNPq and the São Paulo State Research Funding Agency - FAPESP (grant 2013/50302-3). PT was a recipient of a São Paulo State Research Funding Agency - FAPESP fellowship. EC-N and JK are recipients of Brazilian Council for Scientific and Technological Development - CNPq productivity awards 1A. JPSN received a fellowship from Institute MarMaRa. Proteomic analysis was partially performed at and funded by F. Hoffmann-La Roche, Basel, Switzerland. This work was supported by the Institut National de la Santé et de la Recherche Médicale (INSERM); the Aix-Marseille University; the French Agency for Research (Agence Nationale de la Recherche-ANR (grant numbers: "Br-Fr-Chagas", "landscardio"). This project has received funding from the Excellence Initiative of Aix-Marseille University - A*Midex a French "Investissements d'Avenir programme"- Institute MarMaRa AMX-19-IET-007. The funders had no role in study design, data collection and analysis, decision to publish, or preparation of the manuscript.

ACKNOWLEDGMENTS

The authors thank Monique Baron and Eliane Conti Mairena from the University of São Paulo for excellent technical assistance; Daniel Roeder, Anette Schell-Steven, Jens Lamers, Franz Roos, and Michael Foutolakis from Hoffmann-La Roche for valuable advice in experimental design and data analysis for proteomic approach; Camila C. M. Garcia and Marisa H. G. Medeiros from the University of São Paulo for the collaboration in the lipid peroxidation evaluation; and also Miguel Mano (CNC, Portugal) for the usage of Columbus software.

SUPPLEMENTARY MATERIAL

The Supplementary Material for this article can be found online at: https://www.frontiersin.org/articles/10.3389/fimmu.2021.755782/full#supplementary-material

Supplementary Figure 1 | Scheme of the 2D-DIGE approach for the differential proteomic analysis. The approach relies on multiplexing, and simultaneous co-separation of multiple, fluorescently labeled samples, including a pooled internal standard on each gel (Scheme adapted from Ettan DIGE brochure – GE Healthcare).

Supplementary Figure 2 | Representative images from two-dimensional electrophoresis (2D-DIGE) experiments. **(A)** Preparative 2-DE gel used to protein identification by mass spectrometry; **(B)** Representative 2-DE gel of left ventricle myocardial proteins with overlapping images; **(C)** Representative 2-DE gel of left ventricle myocardial proteins displaying each individual fluorescent images (Cy3: DCM, Cy5: CCC, Cy2: Pool).

Supplementary Figure 3 | Volcano plots. The plots display the number of differentially expressed spots ($p<0.01$, t-test) in: **(A)** CCC samples, **(B)** DCM samples and **(C)** IC samples, as compared to individuals without cardiomyopathy. Total number of spots: 683 spots.

Supplementary Figure 4 | Venn diagrams representing the occurrence of spots differentially expressed in common or unique relationships between groups of patients with cardiomyopathy when compared with subjects without cardiomyopathy. Number

of spots with increased **(A)** or decreased **(B)** levels in samples from patients when compared with samples from subjects without cardiomyopathy.

Supplementary Figure 5 | Protein Classification. **(A)** Cellular component classification and **(B)** biological process classification of proteins identified in the proteomic analysis.

Supplementary Figure 6 | Protein and mRNA levels of DECR1 (2,4-dienoyl-CoA reductase 1) in myocardial tissue of CCC, DCM, IC and controls. **(A)** Densitometry measurement of DECR1 protein levels using immunoblot (One-Way ANOVA $p = 0.0011$). **(B)**. DECR1 mRNA levels assessed using real time RT-qPCR (One-Way ANOVA $p = 0.0154$). The horizontal lines show statistically significant changes between groups by the Tukey-Kramer test: *$p < 0.05$; ***$p < 0.001$.

Supplementary Figure 7 | Cartoons depicting energy metabolism related proteins differentially expressed in CCC, DCM and IC myocardium. **(A)** Glycolysis, **(B)** Citric Acid Cycle, **(C)** Oxidative Phosphorylation, **(D)** Creatine Kinase System. Arrows indicate up-regulated (red) or down-regulated (green) expression as compared to control myocardial samples in the proteomic analysis.

Supplementary Figure 8 | Cartoon depicting sarcomeric related proteins differentially expressed in CCC, DCM and IC myocardium. Arrows indicate up-regulated (red) or down-regulated (green) expression as compared to control myocardial samples in the proteomic analysis.

Supplementary Figure 9 | Representative images from Immunoblotting analysis. **(A)** One-dimensional electrophoresis of the samples used for immunoblotting experiments. SDS-PAGE 12.5%, 30µg of proteins, gel stained by "Coomasie Blue Colloidal". **(B)** Representative immunoblotting (Western-blotting) of ACADVL (Very long-chain specific acyl-CoA dehydrogenase), DERC (2,4-dienoyl-CoA reductase 1) and CATA (Catalase) used for densitometry analysis. Relative abundance of a specific protein across the lanes of the blot was given by the normalization to the total amount of protein in each lane.

REFERENCES

1. Libby P, Braunwald E. *Braunwald's Heart Disease : A Textbook of Cardiovascular Medicine*. Philadelphia: Saunders/Elsevier (2008).
2. Bocchi EA, Bestetti RB, Scanavacca MI, Cunha Neto E, Issa VS. Chronic Chagas Heart Disease Management: From Etiology to Cardiomyopathy Treatment. *J Am Coll Cardiol* (2017) 70(12):1510–24. doi: 10.1016/j.jacc.2017.08.004
3. Bestetti RB, Muccillo G. Clinical Course of Chagas' Heart Disease: A Comparison With Dilated Cardiomyopathy. *Int J Cardiol* (1997) 60(2):187–93. doi: 10.1016/S0167-5273(97)00083-1
4. Bocchi EA. Update on Indications and Results of the Surgical Treatment of Heart Failure. *Arq Bras Cardiol* (1994) 63(6):523–30.
5. Mady C, Cardoso RH, Barretto AC, da Luz PL, Bellotti G, Pileggi F. Survival and Predictors of Survival in Patients With Congestive Heart Failure Due to Chagas' Cardiomyopathy. *Circulation* (1994) 90(6):3098–102. doi: 10.1161/01.CIR.90.6.3098
6. Silva CP, Del Carlo CH, Oliveira Junior MT, Scipioni A, Strunz-Cassaro C, Ramirez JA, et al. Why do Patients With Chagasic Cardiomyopathy Have Worse Outcomes Than Those With non-Chagasic Cardiomyopathy? *Arq Bras Cardiol* (2008) 91(6):358–62. doi: 10.1590/S0066-782X2008001800006
7. Bowling J, Walter EA. Recognizing and Meeting the Challenge of Chagas Disease in the USA. *Expert Rev Anti Infect Ther* (2009) 7(10):1223–34. doi: 10.1586/eri.09.107
8. Benatti RD, Al-Kindi SG, Bacal F, Oliveira GH. Heart Transplant Outcomes in Patients With Chagas Cardiomyopathy in the United States. *Clin Transplant* (2018) 32(6):e13279. doi: 10.1111/ctr.13279
9. Morillo CA, Marin-Neto JA, Avezum A, Sosa-Estani S, Rassi AJr., Rosas F, et al. Randomized Trial of Benznidazole for Chronic Chagas' Cardiomyopathy. *N Engl J Med* (2015) 373(14):1295–306. doi: 10.1056/NEJMoa1507574
10. Marin-Neto JA, Cunha-Neto E, Maciel BC, Simoes MV. Pathogenesis of Chronic Chagas Heart Disease. *Circulation* (2007) 115(9):1109–23. doi: 10.1161/CIRCULATIONAHA.106.624296
11. Abel LC, Rizzo LV, Ianni B, Albuquerque F, Bacal F, Carrara D, et al. Chronic Chagas' Disease Cardiomyopathy Patients Display an Increased IFN-Gamma Response to Trypanosoma Cruzi Infection. *J Autoimmun* (2001) 17(1):99–107. doi: 10.1006/jaut.2001.0523
12. Gomes JA, Bahia-Oliveira LM, Rocha MO, Martins-Filho OA, Gazzinelli G, Correa-Oliveira R. Evidence That Development of Severe Cardiomyopathy in Human Chagas' Disease is Due to a Th1-Specific Immune Response. *Infect Immun* (2003) 71(3):1185–93. doi: 10.1128/IAI.71.3.1185-1193.2003
13. Sousa GR, Gomes JA, Fares RC, Damasio MP, Chaves AT, Ferreira KS, et al. Plasma Cytokine Expression is Associated With Cardiac Morbidity in Chagas Disease. *PloS One* (2014) 9(3):e87082. doi: 10.1371/journal.pone.0087082
14. Nogueira LG, Santos RH, Ianni BM, Fiorelli AI, Mairena EC, Benvenuti LA, et al. Myocardial Chemokine Expression and Intensity of Myocarditis in Chagas Cardiomyopathy are Controlled by Polymorphisms in CXCL9 and CXCL10. *PloS Negl Trop Dis* (2012) 6(10):e1867. doi: 10.1371/journal.pntd.0001867
15. Cunha-Neto E, Dzau VJ, Allen PD, Stamatiou D, Benvenutti L, Higuchi ML, et al. Cardiac Gene Expression Profiling Provides Evidence for Cytokinopathy as a Molecular Mechanism in Chagas' Disease Cardiomyopathy. *Am J Pathol* (2005) 167(2):305–13. doi: 10.1016/S0002-9440(10)62976-8
16. Cunha-Neto E, Kalil J. Heart-Infiltrating and Peripheral T Cells in the Pathogenesis of Human Chagas' Disease Cardiomyopathy. *Autoimmunity* (2001) 34(3):187–92. doi: 10.3109/08916930109007383
17. Nogueira LG, Santos RH, Fiorelli AI, Mairena EC, Benvenuti LA, Bocchi EA, et al. Myocardial Gene Expression of T-Bet, GATA-3, Ror-Gammat, FoxP3, and Hallmark Cytokines in Chronic Chagas Disease Cardiomyopathy: An Essentially Unopposed TH1-Type Response. *Mediators Inflammation* (2014) 2014:914326. doi: 10.1155/2014/914326
18. Reis MM, Higuchi Mde L, Benvenuti LA, Aiello VD, Gutierrez PS, Bellotti G, et al. An *in Situ* Quantitative Immunohistochemical Study of Cytokines and IL-2R+ in Chronic Human Chagasic Myocarditis: Correlation With the Presence of Myocardial Trypanosoma Cruzi Antigens. *Clin Immunol Immunopathol* (1997) 83(2):165–72. doi: 10.1006/clin.1997.4335
19. Rocha Rodrigues DB, dos Reis MA, Romano A, Pereira SA, Teixeira Vde P, Tostes SJr., et al. *In Situ* Expression of Regulatory Cytokines by Heart Inflammatory Cells in Chagas' Disease Patients With Heart Failure. *Clin Dev Immunol* (2012) 2012:361730. doi: 10.1155/2012/361730
20. Laugier L, Ferreira LRP, Ferreira FM, Cabantous S, Frade AF, Nunes JP, et al. miRNAs may Play a Major Role in the Control of Gene Expression in Key Pathobiological Processes in Chagas Disease Cardiomyopathy. *PloS Negl Trop Dis* (2020) 14(12):e0008889. doi: 10.1371/journal.pntd.0008889
21. Cunha-Neto E, Coelho V, Guilherme L, Fiorelli A, Stolf N, Kalil J. Autoimmunity in Chagas' Disease. Identification of Cardiac Myosin-B13 Trypanosoma Cruzi Protein Crossreactive T Cell Clones in Heart Lesions of a Chronic Chagas' Cardiomyopathy Patient. *J Clin Invest* (1996) 98(8):1709–12. doi: 10.1172/JCI118969
22. Fonseca SG, Moins-Teisserenc H, Clave E, Ianni B, Nunes VL, Mady C, et al. Identification of Multiple HLA-A*0201-Restricted Cruzipain and FL-160 CD8+ Epitopes Recognized by T Cells From Chronically Trypanosoma Cruzi-Infected Patients. *Microbes Infect* (2005) 7(4):688–97. doi: 10.1016/j.micinf.2005.01.001
23. Teixeira PC, Santos RH, Fiorelli AI, Bilate AM, Benvenuti LA, Stolf NA, et al. Selective Decrease of Components of the Creatine Kinase System and ATP Synthase Complex in Chronic Chagas Disease Cardiomyopathy. *PloS Negl Trop Dis* (2011) 5(6):e1205. doi: 10.1371/journal.pntd.0001205
24. Leme AM, Salemi VM, Parga JR, Ianni BM, Mady C, Weiss RG, et al. Evaluation of the Metabolism of High Energy Phosphates in Patients With Chagas' Disease. *Arq Bras Cardiol* (2010) 95(2):264–70. doi: 10.1590/S0066-782X2010005000099
25. Chevillard C, Nunes JPS, Frade AF, Almeida RR, Pandey RP, Nascimento MS, et al. Disease Tolerance and Pathogen Resistance Genes May Underlie Trypanosoma Cruzi Persistence and Differential Progression to Chagas Disease Cardiomyopathy. *Front Immunol* (2018) 9:2791. doi: 10.3389/fimmu.2018.02791
26. Laugier L, Frade AF, Ferreira FM, Baron MA, Teixeira PC, Cabantous S, et al. Whole-Genome Cardiac DNA Methylation Fingerprint and Gene Expression Analysis Provide New Insights in the Pathogenesis of Chronic Chagas Disease Cardiomyopathy. *Clin Infect Dis* (2017) 65(7):1103–11. doi: 10.1093/cid/cix506

27. Arrell DK, Neverova I, Van Eyk JE. Cardiovascular Proteomics: Evolution and Potential. *Circ Res* (2001) 88(8):763–73. doi: 10.1161/hh0801.090193
28. McGregor E, Dunn MJ. Proteomics of Heart Disease. *Hum Mol Genet* (2003) 12 Spec No 2:R135–44. doi: 10.1093/hmg/ddg278
29. McGregor E, Dunn MJ. Proteomics of the Heart: Unraveling Disease. *Circ Res* (2006) 98(3):309–21. doi: 10.1161/01.RES.0000201280.20709.26
30. Prentice H, Webster KA. Genomic and Proteomic Profiles of Heart Disease. *Trends Cardiovasc Med* (2004) 14(7):282–8. doi: 10.1016/j.tcm.2004.08.001
31. Benjamini Y, Hochberg Y. On the Adaptive Control of the False Discovery Rate in Multiple Testing With Independent Statistics. *J Educ Behav Stat* (2000) 25:60–83. doi: 10.3102/10769986025001060
32. Berndt P, Hobohm U, Langen H. Reliable Automatic Protein Identification From Matrix-Assisted Laser Desorption/Ionization Mass Spectrometric Peptide Fingerprints. *Electrophoresis* (1999) 20(18):3521–6. doi: 10.1002/(SICI)1522-2683(19991201)20:18<3521::AID-ELPS3521>3.0.CO;2-8
33. Schmittgen TD, Livak KJ. Analyzing Real-Time PCR Data by the Comparative C(T) Method. *Nat Protoc* (2008) 3(6):1101–8. doi: 10.1038/nprot.2008.73
34. Esterbauer H, Cheeseman KH. Determination of Aldehydic Lipid Peroxidation Products: Malonaldehyde and 4-Hydroxynonenal. *Methods Enzymol* (1990) 186:407–21. doi: 10.1016/0076-6879(90)86134-H
35. Ghisla S , Thorpe C. Acyl-CoA Dehydrogenases. A Mechanistic Overview. *Eur J Biochem* (2004) 271(3):494–508. doi: 10.1046/j.1432-1033.2003.03946.x
36. Aoyama T, Souri M, Ushikubo S, Kamijo T, Yamaguchi S, Kelley RI, et al. Purification of Human Very-Long-Chain Acyl-Coenzyme A Dehydrogenase and Characterization of its Deficiency in Seven Patients. *J Clin Invest* (1995) 95(6):2465–73. doi: 10.1172/JCI117947
37. Katz S, Landau Y, Pode-Shakked B, Pessach IM, Rubinshtein M, Anikster Y, et al. Cardiac Failure in Very Long Chain Acyl-CoA Dehydrogenase Deficiency Requiring Extracorporeal Membrane Oxygenation (ECMO) Treatment: A Case Report and Review of the Literature. *Mol Genet Metab Rep* (2017) 10:5–7. doi: 10.1016/j.ymgmr.2016.11.008
38. Dyke PC2nd, Konczal L, Bartholomew D, McBride KL, Hoffman TM. Acute Dilated Cardiomyopathy in a Patient With Deficiency of Long-Chain 3-Hydroxyacyl-CoA Dehydrogenase. *Pediatr Cardiol* (2009) 30(4):523–6. doi: 10.1007/s00246-008-9351-8
39. Ferreira RC, Ianni BM, Abel LC, Buck P, Mady C, Kalil J, et al. Increased Plasma Levels of Tumor Necrosis Factor-Alpha in Asymptomatic/"Indeterminate" and Chagas Disease Cardiomyopathy Patients. *Mem Inst Oswaldo Cruz* (2003) 98(3):407–11. doi: 10.1590/S0074-02762003000300021
40. Planavila A, Laguna JC, Vazquez-Carrera M. Nuclear factor-kappaB Activation Leads to Down-Regulation of Fatty Acid Oxidation During Cardiac Hypertrophy. *J Biol Chem* (2005) 280(17):17464–71. doi: 10.1074/jbc.M414220200
41. Denton RM, McCormack JG. Ca2+ as a Second Messenger Within Mitochondria of the Heart and Other Tissues. *Annu Rev Physiol* (1990) 52:451–66. doi: 10.1146/annurev.ph.52.030190.002315
42. Carvajal K, Moreno-Sanchez R. Heart Metabolic Disturbances in Cardiovascular Diseases. *Arch Med Res* (2003) 34(2):89–99. doi: 10.1016/S0188-4409(03)00004-3
43. Brioschi M, Polvani G, Fratto P, Parolari A, Agostoni P, Tremoli E, et al. Redox Proteomics Identification of Oxidatively Modified Myocardial Proteins in Human Heart Failure: Implications for Protein Function. *PloS One* (2012) 7 (5):e35841. doi: 10.1371/journal.pone.0035841
44. Park SJ, Zhang J, Ye Y, Ormaza S, Liang P, Bank AJ, et al. Myocardial Creatine Kinase Expression After Left Ventricular Assist Device Support. *J Am Coll Cardiol* (2002) 39(11):1773–9. doi: 10.1016/S0735-1097(02)01860-0
45. Stride N, Larsen S, Hey-Mogensen M, Sander K, Lund JT, Gustafsson F, et al. Decreased Mitochondrial Oxidative Phosphorylation Capacity in the Human Heart With Left Ventricular Systolic Dysfunction. *Eur J Heart Fail* (2013) 15 (2):150–7. doi: 10.1093/eurjhf/hfs172
46. Betim Paes Leme AM, Salemi VM, Weiss RG, Parga JR, Ianni BM, Mady C, et al. Exercise-Induced Decrease in Myocardial High-Energy Phosphate Metabolites in Patients With Chagas Heart Disease. *J Card Fail* (2013) 19 (7):454–60. doi: 10.1016/j.cardfail.2013.05.008
47. Hodny Z, Reinis M, Hubackova S, Vasicova P, Bartek J. Interferon Gamma/NADPH Oxidase Defense System in Immunity and Cancer. *Oncoimmunology* (2016) 5(2):e1080416. doi: 10.1080/2162402X.2015.1080416
48. Jo SH, Son MK, Koh HJ, Lee SM, Song IH, Kim YO, et al. Control of Mitochondrial Redox Balance and Cellular Defense Against Oxidative Damage by Mitochondrial NADP+-Dependent Isocitrate Dehydrogenase. *J Biol Chem* (2001) 276(19):16168–76. doi: 10.1074/jbc.M010120200
49. Dias PP, Capila RF, do Couto NF, Estrada D, Gadelha FR, Radi R, et al. Cardiomyocyte Oxidants Production may Signal to T. Cruzi Intracellular Development. *PloS Negl Trop Dis* (2017) 11(8):e0005852. doi: 10.1371/journal.pntd.0005852
50. Paiva CN, Medei E, Bozza MT. ROS and Trypanosoma Cruzi: Fuel to Infection, Poison to the Heart. *PloS Pathog* (2018) 14(4):e1006928. doi: 10.1371/journal.ppat.1006928
51. Wan X, Wen JJ, Koo SJ, Liang LY, Garg NJ. SIRT1-PGC1alpha-NFkappaB Pathway of Oxidative and Inflammatory Stress During Trypanosoma Cruzi Infection: Benefits of SIRT1-Targeted Therapy in Improving Heart Function in Chagas Disease. *PloS Pathog* (2016) 12(10):e1005954. doi: 10.1371/journal.ppat.1005954
52. Wen JJ, Dhiman M, Whorton EB, Garg NJ. Tissue-Specific Oxidative Imbalance and Mitochondrial Dysfunction During Trypanosoma Cruzi Infection in Mice. *Microbes Infect* (2008) 10(10-11):1201–9. doi: 10.1016/j.micinf.2008.06.013
53. Lopez M, Tanowitz HB, Garg NJ. Pathogenesis of Chronic Chagas Disease: Macrophages, Mitochondria, and Oxidative Stress. *Curr Clin Microbiol Rep* (2018) 5(1):45–54. doi: 10.1007/s40588-018-0081-2
54. Wan X, Gupta S, Zago MP, Davidson MM, Dousset P, Amoroso A, et al. Defects of mtDNA Replication Impaired Mitochondrial Biogenesis During Trypanosoma Cruzi Infection in Human Cardiomyocytes and Chagasic Patients: The Role of Nrf1/2 and Antioxidant Response. *J Am Heart Assoc* (2012) 1(6):e003855. doi: 10.1161/JAHA.112.003855
55. Ouarhache M, Marquet S, Frade AF, Ferreira AM, Ianni B, Almeida RR, et al. Rare Pathogenic Variants in Mitochondrial and Inflammation-Associated Genes May Lead to Inflammatory Cardiomyopathy in Chagas Disease. *J Clin Immunol* (2021) 41(5):1048–63. doi: 10.1007/s10875-021-01000-y
56. Lee HJ, Oh YK, Rhee M, Lim JY, Hwang JY, Park YS, et al. The Role of STAT1/IRF-1 on Synergistic ROS Production and Loss of Mitochondrial Transmembrane Potential During Hepatic Cell Death Induced by LPS/d-GalN. *J Mol Biol* (2007) 369(4):967–84. doi: 10.1016/j.jmb.2007.03.072
57. Maiti AK, Sharba S, Navabi N, Forsman H, Fernandez HR, Linden SK. IL-4 Protects the Mitochondria Against TNFalpha and IFNgamma Induced Insult During Clearance of Infection With Citrobacter Rodentium and Escherichia Coli. *Sci Rep* (2015) 5:15434. doi: 10.1038/srep15434
58. Buoncervello M, Maccari S, Ascione B, Gambardella L, Marconi M, Spada M, et al. Inflammatory Cytokines Associated With Cancer Growth Induce Mitochondria and Cytoskeleton Alterations in Cardiomyocytes. *J Cell Physiol* (2019) 234(11):20453–68. doi: 10.1002/jcp.28647
59. Ni C, Ma P, Wang R, Lou X, Liu X, Qin Y, et al. Doxorubicin-Induced Cardiotoxicity Involves IFNgamma-Mediated Metabolic Reprogramming in Cardiomyocytes. *J Pathol* (2019) 247(3):320–32. doi: 10.1002/path.5192
60. Van den Bossche J, Baardman J, Otto NA, van der Velden S, Neele AE, van den Berg SM, et al. Mitochondrial Dysfunction Prevents Repolarization of Inflammatory Macrophages. *Cell Rep* (2016) 17(3):684–96. doi: 10.1016/j.celrep.2016.09.008
61. Jessop F, Buntyn R, Schwarz B, Wehrly T, Scott D, Bosio CM. Interferon Gamma Reprograms Host Mitochondrial Metabolism Through Inhibition of Complex II To Control Intracellular Bacterial Replication. *Infect Immun* (2020) 88(2):e00744–19. doi: 10.1128/IAI.00744-19
62. Levick SP, Goldspink PH. Could Interferon-Gamma be a Therapeutic Target for Treating Heart Failure? *Heart Fail Rev* (2014) 19(2):227–36. doi: 10.1007/s10741-013-9393-8
63. Reifenberg K, Lehr HA, Torzewski M, Steige G, Wiese E, Kupper I, et al. Interferon-Gamma Induces Chronic Active Myocarditis and Cardiomyopathy in Transgenic Mice. *Am J Pathol* (2007) 171(2):463–72. doi: 10.2353/ajpath.2007.060906
64. Souza BSF, Silva DN, Carvalho RH, Sampaio GLA, Paredes BD, Aragao Franca L, et al. Association of Cardiac Galectin-3 Expression, Myocarditis, and Fibrosis in Chronic Chagas Disease Cardiomyopathy. *Am J Pathol* (2017) 187(5):1134–46. doi: 10.1016/j.ajpath.2017.01.016
65. Pineda MA, Cuervo H, Fresno M, Soto M, Bonay P. Lack of Galectin-3 Prevents Cardiac Fibrosis and Effective Immune Responses in a Murine Model of Trypanosoma Cruzi Infection. *J Infect Dis* (2015) 212(7):1160–71. doi: 10.1093/infdis/jiv185

66. de Boer RA, Voors AA, Muntendam P, van Gilst WH, van Veldhuisen DJ. Galectin-3: A Novel Mediator of Heart Failure Development and Progression. *Eur J Heart Fail* (2009) 11(9):811–7. doi: 10.1093/eurjhf/hfp097
67. Fernandes F, Moreira CHV, Oliveira LC, Souza-Basqueira M, Ianni BM, Lorenzo CD, et al. Galectin-3 Associated With Severe Forms and Long-Term Mortality in Patients With Chagas Disease. *Arq Bras Cardiol* (2021) 116 (2):248–56. doi: 10.36660/abc.20190403
68. Ersching J, Vasconcelos JR, Ferreira CP, Caetano BC, Machado AV, Bruna-Romero O, et al. The Combined Deficiency of Immunoproteasome Subunits Affects Both the Magnitude and Quality of Pathogen- and Genetic Vaccination-Induced CD8+ T Cell Responses to the Human Protozoan Parasite Trypanosoma Cruzi. *PloS Pathog* (2016) 12(4):e1005593. doi: 10.1371/journal.ppat.1005593
69. Kim MA, Kim HJ, Jee HJ, Kim AJ, Bae YS, Bae SS, et al. Akt2, But Not Akt1, is Required for Cell Survival by Inhibiting Activation of JNK and P38 After UV Irradiation. *Oncogene* (2009) 28(9):1241–7. doi: 10.1038/onc.2008.487
70. Lula JF, Rocha MO, Nunes Mdo C, Ribeiro AL, Teixeira MM, Bahia MT, et al. Plasma Concentrations of Tumour Necrosis Factor-Alpha, Tumour Necrosis Factor-Related Apoptosis-Inducing Ligand, and FasLigand/CD95L in Patients With Chagas Cardiomyopathy Correlate With Left Ventricular Dysfunction. *Eur J Heart Fail* (2009) 11(9):825–31. doi: 10.1093/eurjhf/hfp105
71. Cevey AC, Mirkin GA, Donato M, Rada MJ, Penas FN, Gelpi RJ, et al. Treatment With Fenofibrate Plus a Low Dose of Benznidazole Attenuates Cardiac Dysfunction in Experimental Chagas Disease. *Int J Parasitol Drugs Drug Resist* (2017) 7(3):378–87. doi: 10.1016/j.ijpddr.2017.10.003
72. Ramos GC, van den Berg A, Nunes-Silva V, Weirather J, Peters L, Burkard M, et al. Myocardial Aging as a T-Cell-Mediated Phenomenon. *Proc Natl Acad Sci U.S.A.* (2017) 114(12):E2420–E9. doi: 10.1073/pnas.1621047114
73. Houssari M, Dumesnil A, Tardif V, Kivela R, Pizzinat N, Boukhalfa I, et al. Lymphatic and Immune Cell Cross-Talk Regulates Cardiac Recovery After Experimental Myocardial Infarction. *Arterioscler Thromb Vasc Biol* (2020) 40 (7):1722–37. doi: 10.1161/ATVBAHA.120.314370

Author Disclaimer: The content of this publication, as well the opinions and views expressed herein, was part of a scientific collaboration between the authors and should not be considered, in whole or in parts, as being statements by the company Hoffmann-La Roche.

Conflict of Interest: PT, AD, and EN are current employees of F. Hoffmann-La Roche Ltd and may own company stock.

The remaining authors declare that the research was conducted in the absence of any commercial or financial relationships that could be construed as a potential conflict of interest.

Publisher's Note: All claims expressed in this article are solely those of the authors and do not necessarily represent those of their affiliated organizations, or those of the publisher, the editors and the reviewers. Any product that may be evaluated in this article, or claim that may be made by its manufacturer, is not guaranteed or endorsed by the publisher.

Advantages of publishing in Frontiers

OPEN ACCESS
Articles are free to read for greatest visibility and readership

FAST PUBLICATION
Around 90 days from submission to decision

HIGH QUALITY PEER-REVIEW
Rigorous, collaborative, and constructive peer-review

TRANSPARENT PEER-REVIEW
Editors and reviewers acknowledged by name on published articles

Frontiers
Avenue du Tribunal-Fédéral 34
1005 Lausanne | Switzerland

Visit us: www.frontiersin.org
Contact us: frontiersin.org/about/contact

REPRODUCIBILITY OF RESEARCH
Support open data and methods to enhance research reproducibility

DIGITAL PUBLISHING
Articles designed for optimal readership across devices

FOLLOW US
@frontiersin

IMPACT METRICS
Advanced article metrics track visibility across digital media

EXTENSIVE PROMOTION
Marketing and promotion of impactful research

LOOP RESEARCH NETWORK
Our network increases your article's readership